



NATIONAL TRANSPORTATION
RESEARCH CENTER, INCORPORATED
University Transportation Center

**U32: Vehicle Stability and Dynamics
Longer Combination Vehicles
Final Report**

This project was funded by the NTRCI University Transportation Center under a grant from the U.S. Department of Transportation Research and Innovative Technology Administration (#DTRT-06-G-0043)

The contents of this report reflect the views of the authors, who are responsible for the facts and the accuracy of the information presented herein. This document is disseminated under the sponsorship of the Department of Transportation University Transportation Centers Program, in the interest of information exchange. The U.S. Government assumes no liability for the contents or use thereof.

Doug Pape, Michael Arant, Wayne Brock, Eric Broshears, Caleb Chitwood, Jameson Colbert, Richard Hathaway, Mitchel Keil, Tim LaClair, Jim Patterson, Joseph Petrolino, Collin Pittro, Anthony Spezia, David Wafer

September 2011

Technical Report Documentation Page

1. Report No.	2. Government Accession No.	3. Recipient's Catalog No.		
4. Title and Subtitle U32: Vehicle Stability and Dynamics Longer Combination Vehicles		5. Report Date September 2011		
		6. Performing Organization Code		
7. Author(s) Doug Pape, Michael Arant, Wayne Brock, Eric Broshears, Caleb Chitwood, Jameson Colbert, Richard Hathaway, Mitchel Keil, Tim LaClair, Jim Patterson, Joseph Petrolino, Collin Pittro, Anthony Spezia, David Wafer		8. Performing Organization Report No. NTRCI-50-2011-025		
9. Performing Organization Name and Address National Transportation Research Center, Inc. University Transportation Center 9125 Cross Park Drive Suite #150 Knoxville, TN 37923		10. Work Unit No. (TRAIS)		
		11. Contract or Grant No. RITA Grant – DTRT06G-0043		
12. Sponsoring Agency Name and Address U.S. Department of Transportation Research and Innovative Technology Administration 1200 New Jersey Avenue, SE Washington, DC 20590		13. Type of Report and Period Covered Final Report January – September 2011		
14. Sponsoring Agency Code				
15. Supplementary Notes Special thanks to National Transportation Research Center, Inc., Battelle Memorial Institute, Clemson University, Auburn University, The University of Akron, Hendrickson Suspensions, Bendix Commercial Vehicle Systems, Western Michigan University, Silver Eagle Manufacturing, Oak Ridge National Laboratory, Michelin Americas Research and Development Corporation, Volvo Trucks of America, and Mechanical Simulation Corporation				
16. Abstract <p>This study investigated the safety and stability of longer combination vehicles (LCVs), in particular a triple trailer combination behind a commercial tractor, which has more complicated dynamics than the more common tractor in combination with a single semitrailer. The goal was to measure and model the behavior of LCVs in simple maneuvers. Example maneuvers tested and modeled were single and double lane changes, a gradual lane change, and a constant radius curve.</p> <p>In addition to test track data collection and a brief highway test, two computer models of LCVs were developed. One model is based on TruckSim®, a lumped parameter model widely used for single semitrailer combinations. The other model was built in Adams software, which more explicitly models the geometry of the components of the vehicle, in terms of compliant structural members. Among other results, the models were able to duplicate the experimentally measured rearward amplification behavior that is characteristic of multi-unit combination vehicles.</p>				
17. Key Word LCV, Longer combination vehicle, rearward amplification, offtracking, understeer gradient, heavy duty vehicle, dynamic modeling		18. Distribution Statement No restrictions		
19. Security Class if. (of this report) Unclassified		20. Security Class if. (of this page) Unclassified	21. No. of Pages 444	22. Price

This page intentionally left blank.

Table of Contents

ABBREVIATIONS	XIX
UNITS OF MEASUREMENT	XXI
EXECUTIVE SUMMARY	XXIII
BACKGROUND	XXIII
BRIEF OVERVIEW.....	XXIV
RESEARCH STRATEGY	XXIV
CONCLUSION	XXIV
FUTURE PROGRAM EFFORTS	XXV
CHAPTER 1 – INTRODUCTION AND BACKGROUND	1
1.1 BACKGROUND	1
1.2 PROJECT TEAM	2
1.2.1 Auburn	2
1.2.2 CU-ICAR.....	3
1.2.3 Western Michigan University.....	3
1.2.4 Oak Ridge National Laboratory	3
1.2.5 University of Akron.....	3
1.2.6 Battelle.....	3
1.2.7 Hendrickson Trailer Commercial Vehicle Systems.....	3
1.2.8 Silver Eagle Manufacturing Co.....	3
1.2.9 Volvo Trucks North America	3
1.2.10 Michelin Americas Research and Development Corporation	3
1.2.11 Mechanical Simulation Corporation.....	4
1.2.12 NTRCI	4
1.3 PROJECT DESCRIPTION.....	4
1.4 PROJECT SCHEDULE.....	4
CHAPTER 2 – LITERATURE REVIEW	7
2.1 BACKGROUND OF LONGER COMBINATION VEHICLES	7
2.1.1 Description.....	8
2.1.2 History and Legal Configurations for Heavy-Duty Trucks	9
2.2 DYNAMICS OF LONGER COMBINATION VEHICLES	14
2.2.1 Offtracking	14
2.2.2 Understeer and Oversteer.....	17
2.2.3 Rearward Amplification.....	19
2.3 STABILITY ENHANCEMENTS FOR LONGER COMBINATION VEHICLES	21
2.3.1 Design Variants	22
2.3.2 Electronic Stability Aids.....	23
CHAPTER 3 – TEST PLAN.....	25
3.1 OVERVIEW.....	25
3.2 TEST VEHICLE.....	25
3.3 ON-TRACK MANEUVERS	27
3.3.1 Constant Radius Curve	27
3.3.2 Single Lane Change	28
3.3.3 Gradual Lane Change.....	28
3.3.4 Double Lane Change	28

3.3.5	Impulse Steer	28
3.4	ON-HIGHWAY TESTING.....	29
3.5	METRICS FOR SUCCESSFUL TESTING	30
CHAPTER 4 – ON-TRACK AND ON-HIGHWAY TESTING		31
4.1	SENSORS.....	31
4.2	DATA ACQUISITION.....	37
4.3	HARDWARE INSTALLATION.....	40
4.4	TEST WEEK.....	43
4.5	POST PROCESSING.....	45
4.5.1	Data Handling	46
4.5.2	Data Formatting.....	46
4.5.3	RTK Corrections	48
4.5.4	Data Release	49
CHAPTER 5 – ANALYSIS OF THE TEST TRACK DATA.....		51
5.1	UNDERSTEER CHARACTERISTICS OF UNITS IN THE LCV	51
5.1.1	Understeer Theory	52
5.1.2	Determining the Steer Characteristics of the Tractor	53
5.1.3	Determining the Steer Characteristics of the Trailers and Dollies	56
5.1.4	Understeer Analysis Conclusions	61
5.2	REARWARD AMPLIFICATION OF THE LCV	61
5.2.1	Double Lane Change Event Identification.....	62
5.2.2	Roll Angle Response of Each Axle to Hand Wheel Input	64
5.3	ROLL STEER BEHAVIOR OF THE LCV.....	67
5.3.1	Roll Steer Theory	68
5.3.2	Double Lane Change Axle Steer at Each Axle Location in Response to Hand Wheel Input	68
5.3.3	Conclusions for Roll Angles and Roll Steer in the Double Lane Change	78
CHAPTER 6 – MODELING—RIGID BODY MODEL		81
6.1	MODEL FORMULATION.....	82
6.2	SIMULATION OF TEST TRACK MANEUVERS	84
6.2.1	Single Lane Change Maneuver	84
6.2.2	Gradual Lane Change.....	90
6.2.3	Double Lane Change	91
6.2.4	Constant Radius Maneuver.....	96
6.3	COMPARISON WITH TEST DATA	98
6.3.1	Assessment Overview	99
6.3.2	Test Vehicle Dynamic Center, Nominally Straight Path.....	99
6.3.3	Single Lane Change Articulation Data.....	100
6.3.4	Double Lane Change Articulation Data	107
6.3.5	Comparison Summary	113
6.4	EXAMPLE OF SWEPT SINE ANALYSIS	113
6.4.1	Analysis of Yaw Rate in the Model Data.....	115
CHAPTER 7 – MODELING—COMPLIANT MEMBER MODEL		121
7.1	ADAMS MODEL FORMULATION	121
7.1.1	Tractor	121
7.1.2	Trailer	124
7.1.3	Intermodal Container.....	125
7.1.4	Payload	126
7.1.5	Dolly	127

7.1.6	Other Components of the Adams Model.....	129
7.2	SIMULATION OF TEST TRACK MANEUVERS.....	130
7.2.1	Adams Model Results.....	133
7.2.2	Constant Radius Cornering.....	136
7.2.3	Single Lane Change	145
7.2.4	Double Lane Change	154
7.3	COMPARISON WITH TEST DATA.....	163
7.3.1	Constant Radius Cornering.....	163
7.3.2	Single Lane Change	169
7.3.3	Double Lane Change	176
7.3.4	Comparison Summary	182
7.4	RECOMMENDATIONS FOR CONTINUED MODELING	190
7.4.1	Adams Model Lessons Learned	190
7.4.2	Adams Model Improvements	191
CHAPTER 8 – CONCLUSIONS AND FURTHER RESEARCH.....		195
8.1	CONCLUSIONS.....	195
8.2	FURTHER RESEARCH	196
CHAPTER 9 – REFERENCES.....		199

This page intentionally left blank.

List of Appendices

APPENDIX A - LCV TEST PLAN	A-1
APPENDIX B - LCV INSTRUMENTATION PLAN.....	B-1
APPENDIX C - CHARACTERIZING THE TRIPLE TRAILER COMBINATION AT THE NATIONAL CENTER FOR ASPHALT TECHNOLOGY TEST TRACK AND ONE SEPARATE FEDEX DOLLY AT WMU.....	C-1
APPENDIX D - TRUCKSIM® RELEASE NOTES	D-1
APPENDIX E - ADAMS MODEL RELEASE NOTES	E-1

This page intentionally left blank.

List of Figures

Figure 1-1. Photo. The triple combination in this project's experiments was simulated in two computer models.....	2
Figure 1-2. Chart. Schedule of tasks.....	5
Figure 2-1. Photo. A typical truck tractor in combination with a single semitrailer.....	7
Figure 2-2. Photo. An STAA double has a tractor and two 8.5m (28 ft) semitrailers.....	8
Figure 2-3. Drawing. Outline of a converter dolly.....	9
Figure 2-4. Photo. The dolly connects to the lead trailer by a pintle hitch.....	9
Figure 2-5. Sketch. Configurations of combination vehicles, including LCVs (from FHWA 2004).....	12
Figure 2-6. Map. LCVs may legally move only on the routes identified in this map (from US DOT 2010).....	13
Figure 2-7. Sketch. Low-speed offtracking is the phenomenon when the trailer axle does not turn as sharply as does the tractor (from FHWA 2004).....	15
Figure 2-8. Sketch. In high-speed offtracking, the trailer typically follows a path outside the curve of the tractor's path (from FHWA 2004).....	15
Figure 2-9. Equation. Understeer gradient from measured data.....	17
Figure 2-10. Graph. Simulated response of a double tank trailer combination to a road wheel steer input of 1 degree (from Mallikarjunarao and Fancher 1979).....	20
Figure 2-11. Graph. Rearward amplification of lateral acceleration at the rear trailer of various vehicle configurations as a function of steer input frequency. See Table 2-2 for definitions of the vehicles (from Ervin and Fancher 1984).....	21
Figure 2-12. Sketch. In a "B" train, a fifth wheel is attached to the lead trailer (from Ervin and Fancher 1984).....	22
Figure 2-13. Sketch. A "C" train has two rigid drawbars that prevent the dolly from rotating with respect to the lead trailer (from Ervin and Fancher 1984).....	23
Figure 2-14. Graph. Measured roll response of the rear trailer for a non-RAMS and Trailer-Only RAMS system (from MacAdam et al. 2000).....	24
Figure 3-1. Photo. The test vehicle consisted of one tractor, three semitrailers, and two converter dollies.....	26
Figure 3-2. Drawing. Names of the units of the test vehicle.....	26
Figure 3-3. Photo. The test track has curves of 476 ft (approximately 145 m) radius at the two ends. The straights are 2600 ft (approximately 793 m) long.....	27
Figure 3-4. Map. On-road test route.....	29
Figure 4-1. Diagram. Sensor layout.....	33
Figure 4-2. Chart. Color key to Figure 4-1, along with data connection method and sample rate.....	33
Figure 4-3. Photo. Two models of Celesto string potentiometers were used, the SR1A-62 (left) and the SP1-25 (right).....	34
Figure 4-4. Photo. Oxford RT instruments combine GPS and accelerometer measurements to track the motion of a vehicle.....	35
Figure 4-5. Photo. These two models of inertial measurement units do not include GPS receivers.....	36
Figure 4-6. Photo. A pair of GPS receivers, one manufactured by Novatel and one by u-blox, were mounted on both the tractor and the first trailer.....	36
Figure 4-7. Diagram. Connections between the sensors and the data acquisition system.....	37
Figure 4-8. Diagram. Signals from all sensors were acquired and stored in a central database.....	38
Figure 4-9. Screen shot. An example of an asynchronous file.....	39
Figure 4-10. Photo. Special-purpose signal conditioning circuits for the string pots communicated with the computer via CAN.....	40
Figure 4-11. Table. CAN Message Structure.....	40
Figure 4-12. Photo. These views, looking backward under Trailer 2, show the location of toolbox in which the sensors were mounted (left) and the inside of the toolbox (right).....	41
Figure 4-13. Photo. String Pots measured deflection of the suspension. The red lines in the photos indicate the locations of the two ends of the wire from the string pots.....	41

Figure 4-14. Photo. Dolly-to-trailer articulation angle was measured with a pair of string pots.....	42
Figure 4-15. Photo. Steering input was measured via a string potentiometer with a string wrapped around a plywood wheel on the steering shaft.....	42
Figure 4-16. Diagram. Actual gate layout for the gradual lane change maneuver.....	44
Figure 4-17. Diagram. Actual gate layout for the single lane change maneuver.....	44
Figure 4-18. Diagram. Actual gate layout for the double lane change maneuver.....	44
Figure 4-19. Diagram. Zones for separating data recorded on the curves from data recorded on the straights.....	46
Figure 4-20. Photo. Analysts used the ISO coordinate system, with Y to the left and Z up.....	47
Figure 4-21. Graph. Angular Rate Comparison.....	48
Figure 5-1. Graph. Tractor position north and east for 32 km/h (20 mph) and 64 km/h (40 mph).	51
Figure 5-2. Equation. Ackerman road wheel angle (deg).....	52
Figure 5-3. Equation. Ackerman steer plus the understeer gradient.....	52
Figure 5-4. Equation. Understeer gradient from measured data.....	52
Figure 5-5. Graph. Constant road wheel angle in a curve.....	53
Figure 5-6. Graph. Road wheel angle at 32 km/h (20 mph).....	54
Figure 5-7. Graph. Road wheel angle at 64 km/h (40 mph).....	54
Figure 5-8. Graph. Tractor lateral acceleration vs. understeer gradient (uncorrected for banking).....	56
Figure 5-9. Graph. Tractor lateral acceleration vs. understeer gradient (corrected for banking).....	56
Figure 5-10. Graph. Trailer 2 understeer gradient as a function of banking corrected lateral acceleration.....	60
Figure 5-11. Graph. Trailer 3 understeer gradient vs. lateral acceleration.....	60
Figure 5-12. Graph. Identification of the seven points in the double lane change.....	62
Figure 5-13. Graph. Filtered hand wheel angle at 64 km/h (40 mph).....	63
Figure 5-14. Graph. Unfiltered roll angles measured at separate axle positions at 64 km/h (40 mph).....	64
Figure 5-15. Graph. Roll angle at the steer axle at 64 km/h (40 mph).....	65
Figure 5-16. Graph. Roll angle at the drive axle at 64 km/h (40 mph).....	65
Figure 5-17. Graph. Trailer 1 roll angle (filtered) 64 km/h (40 mph).....	66
Figure 5-18. Graph. Trailer 2 roll angle (filtered) at 64 km/h (40 mph).....	66
Figure 5-19. Graph. Trailer 3 roll angle (filtered) at 64 km/h (40 mph).....	67
Figure 5-20. Equation. Ackerman steer plus two effects contributing to understeer.....	68
Figure 5-21. Graph. Drive axle steer as a function of time in a double lane change.....	69
Figure 5-22. Graph. Trailer axle steer as a function of time in a double lane change.....	69
Figure 5-23. Graph. Unfiltered Steer angle at each axle location at 64 km/h (40 mph).....	70
Figure 5-24. Graph. Unfiltered dolly articulation angle at 64 km/h (40 mph).....	71
Figure 5-25. Graph. Steer axle roll steer (filtered).....	72
Figure 5-26. Graph. Drive axle roll steer angle (filtered).....	72
Figure 5-27. Graph. Trailer 1 roll steer angle (filtered) at 64 km/h (40 mph).....	73
Figure 5-28. Graph. Trailer 2 roll steer angle (filtered) at 64 km/h (40 mph).....	74
Figure 5-29. Graph. Trailer 3 roll steer angle (filtered) at 64 km/h (40 mph).....	74
Figure 5-30. Graph. Dolly 1 articulation angle (filtered) at 64 km/h (40 mph).....	75
Figure 5-31. Graph. Dolly 2 articulation angle (filtered) at 64 km/h (40 mph).....	76
Figure 5-32. Graph. Hand wheel angle and dolly articulation angles at 64 km/h (40 mph).....	76
Figure 5-33. Graph. Hand wheel and roll angles (filtered) at 64 km/h (40 mph).....	77
Figure 5-34. Graph. Relative roll steer angles at each suspension at 64 km/h (40 mph).....	78
Figure 6-1. Screen Capture. Animated output of the TruckSim® model of the LCV test vehicle.....	81
Figure 6-2. Graph. Path of the rear axle of each unit with the hand wheel fixed at straight ahead.....	83
Figure 6-3. Graph. Path of the rear axle of each unit with the hand wheel fixed at straight ahead.....	84
Figure 6-4. Graph. Paths of the rear axles of each unit during a simulated 32 km/h (20 mph) single lane change.....	85
Figure 6-5. Graph. Detail of a portion of Figure 6-4, showing offtracking in a simulated 32 km/h (20 mph) single lane change.....	86
Figure 6-6. Graph. Paths of the rear axles of each unit during a simulated 72 km/h (45 mph) single lane change.....	86

Figure 6-7. Graph. Detail of a portion of Figure 6-6, showing offtracking in a simulated 72 km/h (45 mph) single lane change.....	87
Figure 6-8. Graph. Lateral acceleration at the CG of each unit of the vehicle during a simulated 32 km/h (20 mph) single lane change.....	87
Figure 6-9. Graph. Lateral acceleration at the CG of each unit of the vehicle during a simulated 72 km/h (45 mph) single lane change.....	88
Figure 6-10. Graph. Rearward amplification of lateral acceleration in single lane changes at 32 km/h (20 mph) and 72 km/h (45 mph).....	89
Figure 6-11. Graph. Yaw response of the vehicle for a simulated single lane change at 32 km/h (20 mph).....	89
Figure 6-12. Graph. Yaw of the sprung mass for a simulated 72 km/h (45 mph) single lane change.....	90
Figure 6-13. Graph. Paths of the rear axles of each unit during a simulated 72 km/h (45 mph) gradual lane change.....	90
Figure 6-14. Graph. Paths of the rear axles of each unit during a simulated 32 km/h (20 mph) double lane change.....	91
Figure 6-15. Graph. Detail of Figure 6-14, showing the offtracking at the midpoint of the maneuver.....	92
Figure 6-16. Graph. Detail of Figure 6-14, showing the offtracking near the end point of the maneuver.....	92
Figure 6-17. Graph. Paths of the rear axles of each unit during a simulated 72 km/h (45 mph) double lane change.....	93
Figure 6-18. Graph. Detail of Figure 6-17, showing the offtracking at the midpoint of the maneuver	93
Figure 6-19. Graph. Detail of Figure 6-17, showing the offtracking at the end of the maneuver.....	94
Figure 6-20. Graph. Lateral acceleration at the CG of each unit of the vehicle during a simulated 32 km/h (20 mph) double lane change.....	94
Figure 6-21. Graph. Lateral acceleration at the CG of each unit of the vehicle during a simulated 72 km/h (45 mph) double lane change.....	95
Figure 6-22. Graph. Yaw angle of each unit of the vehicle for a simulated 32 km/h (20 mph) double lane change.....	95
Figure 6-23. Graph. Yaw angle of each unit of the vehicle for a simulated 72 km/h (45 mph) double lane change	96
Figure 6-24. Graph. Lateral acceleration at the CG of each unit of the vehicle during a simulated 32 km/h (20 mph) constant radius curve.....	97
Figure 6-25. Graph. Lateral acceleration at the CG of each unit of the vehicle during a simulated 72 km/h (45 mph) constant radius curve.....	97
Figure 6-26. Graph. Paths of the rear axles of each unit during a simulated 32 km/h (20 mph) constant radius curve.....	98
Figure 6-27. Graph. Paths of the rear axles of each unit during a simulated 72 km/h (45 mph) constant radius curve.....	98
Figure 6-28. Graph. Time history of the measured road wheel angle data that was used to drive the TruckSim® model to produce the following dolly articulation response plots. 72 km/h (45 mph) nominally straight path.....	100
Figure 6-29. Graph. Measured road wheel angle and simulated dolly articulation angles for the nominally straight path.....	100
Figure 6-30. Graph. Simulated and measured articulation angles of Dolly 1 in the nominally straight path.....	100
Figure 6-31. Graph. Simulated and measured articulation angles of Dolly 2 in the nominally straight path.....	100
Figure 6-33. Graph. Simulated and measured articulation angles of Dolly 2 in the (20 mph) single lane change.....	103
Figure 6-34. Graph. Simulated and measured articulation angles of Dolly 1 in the (20 mph) single lane change.....	103
Figure 6-35. Graph. Time history of the measured road wheel angle data that was used to drive the TruckSim® model to produce the dolly articulation response plots in the 40 km/h (25 mph) single lane change.....	104
Figure 6-36. Graph. Simulated and measured articulation angles of Dolly 2.....	104

Figure 6-39. Graph. Simulated and measured articulation angles of Dolly 2.....	105
Figure 6-41. Graph. Time history of the measured road wheel angle data that was used to drive the TruckSim® model to produce the dolly articulation response plots for the 56 km/h (35 mph) single lane change.....	106
Figure 6-42. Graph. Simulated and measured articulation angles of Dolly 2.....	106
Figure 6-44. Graph. Time history of the measured road wheel angle data that was used to drive the TruckSim® model to produce the dolly articulation response plots in the 64 km/h (40 mph) single lane change.....	107
Figure 6-45. Graph. Simulated and measured articulation angles of Dolly 2.....	107
Figure 6-47. Graph. Time history of the measured road wheel angle data that was used to drive the TruckSim® model to produce the dolly articulation response plots in the 32 km/h (20 mph) double lane change.....	109
Figure 6-48. Graph. Simulated and measured articulation angles of Dolly 2.....	109
Figure 6-50. Graph. Time history of the measured road wheel angle data that was used to drive the TruckSim® model to produce the dolly articulation response plots in the 40 km/h (25 mph) double lane change.....	110
Figure 6-51. Graph. Simulated and measured articulation angles of Dolly 2.....	110
Figure 6-53. Graph. Time history of the measured road wheel angle data that was used to drive the TruckSim® model to produce the dolly articulation response plots in the 48 km/h (30 mph) double lane change.....	111
Figure 6-54. Graph. Simulated and measured articulation angles of Dolly 2.....	111
Figure 6-56. Graph. Time history of the measured road wheel angle data that was used to drive the TruckSim® model to produce the dolly articulation response plots in the 56 km/h (35 mph) double lane change.....	112
Figure 6-57. Graph. Simulated and measured articulation angles of Dolly 2.....	112
Figure 6-59. Screen Capture. TruckSim® screen where the swept sine steer input is defined. This is a predefined TruckSim® maneuver. (Mechanical Simulation Corporation 2010).....	114
Figure 6-60. Graph. Simulated trajectory of the test vehicle performing a swept-sine maneuver at 64 km/h (40 mph).....	114
Figure 6-61. Graph. Simulated lateral acceleration of the test vehicle during the proposed swept sine maneuver.....	115
Figure 6-62. Graph. Frequency Response Plot of Yaw Rate Gain with Phase and Coherence Function: Tractor Yaw Rate Gain.....	115
Figure 6-63. Graph. Frequency response plot with phase and coherence function: Trailer 1 yaw rate gain.....	116
Figure 6-64. Graph. Frequency response plot with coherence function: Trailer 2 yaw rate gain.....	117
Figure 6-65. Graph. Frequency response plot with phase and coherence function: Trailer 3 yaw rate gain.....	117
Figure 6-66. Graph. Yaw rate gain of the tractor and three trailers to hand wheel input.....	118
Figure 6-67. Graph. Amplification of the yaw rate of the three trailers to the tractor's yaw rate.....	118
Figure 7-1. Drawing. Adams model of the full vehicle.....	121
Figure 7-2. Drawing. Adams model, tractor left side view.....	122
Figure 7-3. Drawing. Adams Model, Tractor Steer Suspension.....	123
Figure 7-4. Drawing. Adams Model, Trailer Left Side View	124
Figure 7-5. Drawing. Adams model, Hutchison Trailer Suspension.....	125
Figure 7-6. Drawing. Adams Model, Intermodal Container and Payload.....	127
Figure 7-7. Drawing. Adams Model, Dolly Left Side View	128
Figure 7-8. Drawing. Adams Model, Dolly Isometric View	128
Figure 7-9. Screen Shot. Adams Model with Path Graphics	130
Figure 7-10. Graph. Tractor Velocity, Double Lane Change at 56 km/h (35 mph).....	131
Figure 7-11. Graph. Tractor and Trailer Paths, Constant Radius Cornering at 56 km/h (35 mph).....	132
Figure 7-12. Graph. Tractor and Trailer Paths, Single Lane Change at 56 km/h.....	132
Figure 7-13. Graph. Tractor and Trailer Paths, Double Lane Change at 56 km/h (35 mph).....	133
Figure 7-14. Drawing. Graphical representation of offtracking in a constant radius curve.....	135
Figure 7-15. Graph. Adams model example time history.....	136

Figure 7-16. Graph. Steering Input, Constant Radius Cornering at 56 km/h (35 mph).....	137
Figure 7-17. Graph. Path Close-Up, Constant Radius Cornering at 56 km/h (35 mph).....	137
Figure 7-18. Graph. Lateral Acceleration, Constant Radius Cornering at 56 km/h (35 mph).....	138
Figure 7-19. Graph. Roll Angle, Constant Radius Cornering at 56 km/h (35 mph).....	138
Figure 7-20. Graph. Graphical Representation of Offtracking Calculation, Constant Radius Cornering at 56 km/h (35 mph).....	139
Figure 7-21. Graph. Axle Lateral Offtracking, Constant Radius Cornering at 56 km/h (35 mph)	139
Figure 7-22. Graph. Ride Height Change, Constant Radius Cornering at 56 km/h (35 mph).....	140
Figure 7-23. Graph. Dolly Articulation Angle, Constant Radius Cornering at 56 km/h (35 mph).....	140
Figure 7-24. Graph. Lateral Offtracking, Constant Radius Cornering at All Velocities.....	141
Figure 7-25. Graph. Peak Lateral Acceleration, Constant Radius Cornering at All Velocities.....	142
Figure 7-26. Graph. Peak Roll Angle, Constant Radius Cornering at All Velocities.....	142
Figure 7-27. Graph. Peak Driver Side Ride Height Change, Constant Radius Cornering at All Velocities.....	143
Figure 7-28. Graph. Peak Curb Side Ride Height Change, Constant Radius Cornering at All Velocities.....	143
Figure 7-29. Graph. Peak Dolly Articulation Angle, Constant Radius Cornering at All Velocities.....	144
Figure 7-30. Graph. Peak Rearward Amplification, Constant Radius Cornering at All Velocities.....	144
Figure 7-31. Graph. Steering Input, Single Lane Change at 56 km/h (35 mph).....	145
Figure 7-32. Graph. Path Close-Up, Single Lane Change at 56 km/h (35 mph).....	146
Figure 7-33. Graph. Lateral Acceleration, Single Lane Change at 56 km/h (35 mph).....	146
Figure 7-34. Graph. Roll Angle, Single Lane Change at 56 km/h (35 mph).....	147
Figure 7-35. Graph. Graphical Representation of Offtracking Calculation, Single Lane Change at 56 km/h (35 mph).....	147
Figure 7-36. Graph. Axle Lateral Offtracking, Single Lane Change at 56 km/h (35 mph)	148
Figure 7-37. Graph. Ride Height Change, Single Lane Change at 56 km/h (35 mph).....	148
Figure 7-38. Graph. Dolly Articulation Angle, Single Lane Change at 56 km/h (35 mph).....	149
Figure 7-39. Graph. Lateral Offtracking, Single Lane Change at All Velocities.	150
Figure 7-40. Graph. Maximum and Minimum Lateral Acceleration, Single Lane Change at All Velocities.....	150
Figure 7-41. Graph. Maximum and Minimum Axle Roll Angle, Single Lane Change at All Velocities.....	151
Figure 7-42. Graph. Maximum and Minimum Driver Side Ride Height Change, Single Lane Change at All Velocities.....	151
Figure 7-43. Graph. Maximum and Minimum Curb Side Ride Height Change, Single Lane Change at All Velocities.....	152
Figure 7-44. Graph. Maximum and Minimum Dolly Articulation Angle, Single Lane Change at All Velocities.....	152
Figure 7-45. Graph. Rearward Amplification, 1 st Steering Event, Single Lane Change at All Velocities.....	153
Figure 7-46. Graph. Rearward Amplification, second Steering Event, Single Lane Change at All Velocities.....	153
Figure 7-47. Graph. Steering Input, Double Lane Change at 56 km/h (35 mph).....	154
Figure 7-48. Graph. Path Close-Up, Double Lane Change at 56 km/h (35 mph).....	155
Figure 7-49. Graph. Lateral Acceleration, Double Lane Change at 56 km/h (35 mph).	155
Figure 7-50. Graph. Roll Angle, Double Lane Change at 56 km/h (35 mph).....	156
Figure 7-51 - Graphical Representation of Offtracking Calculation, Double Lane Change at 56 km/h (35 mph).	156
Figure 7-52. Graph. Axle Lateral Offtracking, Double Lane Change at 56 km/h (35 mph).....	157
Figure 7-53. Graph. Ride Height Change, Double Lane Change at 56 km/h (35 mph).....	157
Figure 7-54. Graph. Dolly Articulation Angle, Double Lane Change at 56 km/h (35 mph).....	158
Figure 7-55. Graph. Lateral Offtracking, Double Lane Change at All Velocities.	159
Figure 7-56. Graph. Maximum and Minimum Lateral Acceleration, Double Lane Change at All Velocities.....	159
Figure 7-57. Graph. Maximum and Minimum Axle Roll Angle, Double Lane Change at All Velocities.....	160
Figure 7-58. Graph. Maximum and Minimum Driver Side Ride Height Change, Double Lane Change at All Velocities.....	160

Figure 7-59. Graph. Maximum and Minimum Curb Side Ride Height Change, Double Lane Change at All Velocities.....	161
Figure 7-60. Graph. Maximum and Minimum Dolly Articulation Angle, Double Lane Change at All Velocities.....	161
Figure 7-61. Graph. Rearward Amplification, 1 st Steering Event, Double Lane Change at All Velocities.....	162
Figure 7-62 - Rearward Amplification, second Steering Event, Double Lane Change at All Velocities.	162
Figure 7-63. Graph. Model vs. Test, Steer Axle Roll Angle, Constant Radius Cornering at 56 km/h (35 mph).....	163
Figure 7-64. Graph. Model vs. Test, Trailer1 Roll Angle, Constant Radius Cornering at 56 km/h (35 mph).....	164
Figure 7-65. Graph. Model vs. Test, Trailer2 Roll Angle, Constant Radius Cornering at 56 km/h (35 mph).....	164
Figure 7-66. Graph. Model vs. Test, Trailer3 Roll Angle, Constant Radius Cornering at 56 km/h (35 mph).....	165
Figure 7-67. Graph. Model vs. Test, Trailer1D Ride Height Change, Constant Radius Cornering at 56 km/h (35 mph).....	165
Figure 7-68. Graph. Model vs. Test, Trailer2D Ride Height Change, Constant Radius Cornering at 56 km/h (35 mph).....	166
Figure 7-69. Graph. Model vs. Test, Trailer3D Ride Height Change, Constant Radius Cornering at 56 km/h (35 mph).....	166
Figure 7-70. Graph. Model vs. Test, Trailer1C Ride Height Change, Constant Radius Cornering at 56 km/h (35 mph).....	167
Figure 7-71. Graph. Model vs. Test, Trailer2C Ride Height Change, Constant Radius Cornering at 56 km/h (35 mph).....	167
Figure 7-72. Graph. Model vs. Test, Trailer3C Ride Height Change, Constant Radius Cornering at 56 km/h (35 mph).....	168
Figure 7-73. Graph. Model vs. Test, Dolly1 Articulation Angle, Constant Radius Cornering at 56 km/h (35 mph).....	168
Figure 7-74. Graph. Model vs. Test, Dolly2 Articulation Angle, Constant Radius Cornering at 56 km/h (35 mph).....	169
Figure 7-75. Graph. Model vs. Test, Steer Roll Angle, Single Lane Change at 56 km/h (35 mph).....	170
Figure 7-76. Graph. Model vs. Test, Trailer1 Roll Angle, Single Lane Change at 56 km/h (35 mph).....	170
Figure 7-77. Graph. Model vs. Test, Trailer2 Roll Angle, Single Lane Change at 56 km/h (35 mph).....	171
Figure 7-78. Graph. Model vs. Test, Trailer3 Roll Angle, Single Lane Change at 56 km/h (35 mph).....	171
Figure 7-79. Graph. Model vs. Test, Trailer1D Ride Height Change, Single Lane Change at 56 km/h (35 mph).....	172
Figure 7-80. Graph. Model vs. Test, Trailer2D Ride Height Change, Single Lane Change at 56 km/h (35 mph).....	172
Figure 7-81. Graph. Model vs. Test, Trailer3D Ride Height Change, Single Lane Change at 56 km/h (35 mph).....	173
Figure 7-82. Graph. Model vs. Test, Trailer1C Ride Height Change, Single Lane Change at 56 km/h (35 mph).....	173
Figure 7-83. Graph. Model vs. Test, Trailer2C Ride Height Change, Single Lane Change at 56 km/h (35 mph).....	174
Figure 7-84. Graph. Model vs. Test, Trailer3C Ride Height Change, Single Lane Change at 56 km/h (35 mph).....	174
Figure 7-85. Graph. Model vs. Test, Dolly1 Articulation Angle, Single Lane Change at 56 km/h (35 mph).....	175
Figure 7-86. Graph. Model vs. Test, Dolly2 Articulation Angle, Single Lane Change at 56 km/h (35 mph).....	175
Figure 7-87. Graph. Model vs. Test, Steer Axle Roll Angle, Double Lane Change at 56 km/h (35 mph).....	176
Figure 7-88. Graph. Model vs. Test, Trailer1 Roll Angle, Double Lane Change at 56 km/h (35 mph).....	177
Figure 7-89. Graph. Model vs. Test, Trailer2 Roll Angle, Double Lane Change at 56 km/h (35 mph).....	177
Figure 7-90. Graph. Model vs. Test, Trailer3 Roll Angle, Double Lane Change at 56 km/h (35 mph).....	178

Figure 7-91. Graph. Model vs. Test, Trailer1D Ride Height Change, Double Lane Change at 56 km/h (35 mph).....	178
Figure 7-92. Graph. Model vs. Test, Trailer2D Ride Height Change, Double Lane Change at 56 km/h(35 mph).....	179
Figure 7-93. Graph. Model vs. Test, Trailer3D Ride Height Change, Double Lane Change at 56 km/h (35 mph).....	179
Figure 7-94. Graph. Model vs. Test, Trailer1C Ride Height Change, Double Lane Change at 56 km/h (35 mph).....	180
Figure 7-95. Graph. Model vs. Test, Trailer2C Ride Height Change, Double Lane Change at 56 km/h (35 mph).....	180
Figure 7-96. Graph. Model vs. Test, Trailer3C Ride Height Change, Double Lane Change at 56 km/h (35 mph).....	181
Figure 7-97. Graph. Model vs. Test, Dolly1 Articulation Angle, Double Lane Change at 56 km/h (35 mph).....	181
Figure 7-98. Graph. Model vs. Test, Dolly2 Articulation Angle, Double Lane Change at 56 km/h (35 mph).....	182
Figure 7-99. Graph. Simulation vs. Average Test, Suspension Roll Angle, Constant Radius Cornering, 56 km/h (35 mph).....	183
Figure 7-100. Graph. Simulation vs. Average Test, Driver Side Ride Height Change, Constant Radius Cornering, 56 km/h (35 mph).....	183
Figure 7-101. Graph. Simulation vs. Average Test, Curb Side Ride Height Change, Constant Radius Cornering, 56 km/h (35 mph).....	184
Figure 7-102. Graph. Simulation vs. Average Test, Dolly Articulation Angle, Constant Radius Cornering, 56 km/h (35 mph).....	184
Figure 7-103. Graph. Simulation vs. Average Test, Suspension Roll Angle, Single Lange Change, 56 km/h (35 mph).....	185
Figure 7-104. Graph. Simulation vs. Average Test, Driver Side Ride Height Change, Single Lange Change, 56 km/h (35 mph).....	186
Figure 7-105. Graph. Simulation vs. Average Test, Curb Side Ride Height Change, Single Lange Change, 56 km/h (35 mph).....	186
Figure 7-106. Graph. Simulation vs. Average Test, Dolly Articulation Angle, Single Lange Change, 56 km/h (35 mph).....	187
Figure 7-107. Graph. Simulation vs. Average Test, Suspension Roll Angle, Double Lange Change, 56 km/h (35 mph).....	188
Figure 7-108. Graph. Simulation vs. Average Test, Driver Side Ride Height Change, Double Lange Change, 56km/h (35 mph).....	188
Figure 7-109. Graph. Simulation vs. Average Test, Curb Side Ride Height Change, Double Lange Change, 56 km/h (35 mph).....	189
Figure 7-110. Graph. Simulation vs. Average Test, Dolly Articulation Angle, Double Lange Change, 56 km/h (35 mph).....	189
Figure 7-111. Drawing. Container-to-chassis mounting points.....	190
Figure 7-112. Graph. Path close-up, tire comparison, double lane change at 56 km/h (35 mph).....	191

This page intentionally left blank.

List of Tables

Table 2-1. Low-speed offtracking of various LCV configurations in a curve with a radius of 91 m (300 ft), (from Ervin and Fancher 1984, Table 5).....	16
Table 2-2. Legend for Table 2-1, Table 2-3, and Figure 2-11.....	16
Table 2-3. High-speed offtracking of various LCV configurations for a turn radius of 183 m (600 ft) taken at 88.5 km/h (55 mph), from (Ervin and Fancher 1984, Table 7).....	17
Table 2-4. Effect on stability of tractor and trailer steer understeer gradients (Winkler, Ervin 2006).....	18
Table 4-1. Summary of measurements and sensors. The contents of each cell are the brand or model of the sensor used.....	32
Table 4-2. Actual test conditions.....	43
Table 5-1. Tractor understeer gradient analysis.....	55
Table 5-2. Trailer 2 fundamental mechanical dimensions.....	58
Table 5-3. Trailer 2 steer behavior in the constant radius maneuver.....	58
Table 5-4. Trailer 3 fundamental mechanical dimensions.....	59
Table 5-5. Trailer 3 steer behavior in the constant radius maneuver.....	59
Table 5-6. Representative response times for units of the LCV in a 64 km/h double lane change.....	79

This page intentionally left blank.

Abbreviations

Abbreviation or Acronym	Definition
A/D	Analog/digital
Akron	University of Akron
Auburn	Auburn University
a_y	Lateral acceleration
Battelle	Battelle Memorial Institute
CAD	Computer aided design
CAN	Controller area network
CCW	Counterclockwise
CFR	Code of Federal Regulations
CG	Center of gravity
CU-ICAR	Clemson University International Center for Automotive Research
CW	Clockwise
DAS	Data acquisition system
DGPS	Differential global positioning system
DLC	Double lane change
DOT	US Department of Transportation
ESC	Electronic stability control. In this report, ESC is used as a generic term for any electronic system that automatically applies brakes on the tractor or semitrailer to enhance the stability of the vehicle in any way.
FHWA	Federal Highway Administration
FMCSA	Federal Motor Carrier Safety Administration
GPS	Global positioning system
GVW	Gross vehicle weight
Hendrickson	Hendrickson Trailer Commercial Vehicle Systems
IMU	Inertial measurement unit
ISO	International Organization for Standards
LCV	Longer combination vehicle
Michelin	Michelin Americas Research and Development Corporation
MOOS	Mission Oriented Operating Suite
NCAT	National Center for Asphalt Technology
NTRCI	National Transportation Research Center, Inc.
ORNL	Oak Ridge National Laboratory
RAMS	Rearward Amplification Suppression
RT unit	Oxford inertial and GPS measurement system, Model RT2500 or RT 3100
RTK	Real-time kinetics (or kinematics)
SLC	Single lane change
SSH	Secure Shell

Abbreviation or Acronym	Definition
SRT	Static rollover threshold
STAA	Surface Transportation Assistance Act
UTM	Universal Transverse Mercator
Volvo	Volvo Trucks North America
VMT	Vehicle miles traveled
WMU	Western Michigan University

Units of Measurement

Unit	Meaning
deg	degree of angle
deg/s	degree per second
deg/s ²	degree per second squared
g	gravitational unit, 9.8 m/s ²
kg	kilogram
km/h	kilometer per hour
kPa	kilopascal
m	meter
m/s	meter per second
m/s ²	meter per second squared
mm	millimeter
N•m	Newton-meter
N•m/deg	Newton-meter per degree
N•m•s	Newton-meter-second
s	second

This page intentionally left blank.

Executive Summary

This study investigated the safety and stability of longer combination vehicles (LCVs), in particular a triple trailer combination behind a commercial tractor. These trucks have more complicated dynamics than the more common tractor in combination with a single semitrailer. The goal was to measure and model the behavior of LCVs in simple maneuvers. Example maneuvers tested and modeled were single and double lane changes, a gradual lane change, and a constant radius curve. The LCV studied in this project was a tractor, two converter dollies, and a set of three semitrailers, each of which was an intermodal freight container on a chassis.



In addition to test track data collection and a brief highway test, two parallel but independent computer models of LCVs were developed in this project. Among other results, the models were able to duplicate the experimentally measured rearward amplification behavior that is characteristic of multi-unit combination vehicles. “Rearward amplification” is the ratio of lateral motion of the last trailer to the lateral motion of the tractor. It is an important factor in vehicle stability, especially in lane changes or avoidance maneuvers.

Background

Tractors pulling a semitrailer are ubiquitous on the nation’s highways. An LCV can be a pair of trailers where at least one is longer than the 8.53 m (28 ft) pup trailer, or a train of three trailers. While combinations with single semitrailers or a “double” with pup trailers are permitted anywhere on the National Network of highways, LCVs may legally operate only on certain routes in selected states, and most states limit the form of LCVs that may operate. If the use of LCVs is to be expanded, then their safety and stability are among the questions to be addressed.

Brief Overview

This project included experimental and theoretical portions. The experimental portion consisted of a series of planned maneuvers with an LCV triple on the National Center for Asphalt Technology (NCAT) test track at Auburn University. The vehicle was also taken on a drive on public highways. Data from the test track was used to characterize the steering behavior of the tractor and the trailers. The theoretical portion of this project saw the development and use of two models of the test vehicle. Both models were built using measurements of the actual LCV triple used in the testing, and both modeled some of the maneuvers executed at the test track. The models were able to duplicate the rearward amplification behavior that is characteristic of multi-unit combination vehicles.

Research Strategy

A literature review was conducted to provide the current state of the art in the application of LCVs, the dynamic considerations of using LCVs, and methods for dealing with safety and stability when using LCVs. Controlled track testing was performed with an instrumented LCV. Data was collected from inertial measurement units (IMUs), global positioning systems (GPS), and string potentiometers to capture the articulation, body roll, and kinematic data from vehicle components. The goal of the testing was to establish the baseline dynamics of the LCV.

As a complement to the track testing, two independent, computer-based analytical modeling approaches were used to simulate LCV dynamics and behavior. The TruckSim® model was used to model the LCV as a rigid body, whereas the Adams model was used to model the LCV as a system of compliant members. Modeling data was compared with the track test data, with a view to verifying the model results and establishing an outline for future modeling studies in greater depth.

Conclusion

Both models of the LCV triple quantitatively predicted increased rearward amplification of articulation angles. Measurements of all units and visual observations of the third trailer's behavior were consistent with the models' predictions. The amount of rearward amplification and its increase with speed were successfully modeled. The models have been partially verified.

A novel method of using pairs of string potentiometers to measure dolly-to-trailer articulation and roll steer characteristics was proved to be viable. These measurements successfully explained some of the understeer behavior of the trailers.

Future Program Efforts

Based on the research conducted, the following future efforts may provide helpful results:

- A key question is how well an LCV stays in its lane—the effect of low- and high-speed offtracking in steady maneuvers and rearward amplification in dynamic maneuvers. The approach of this project should be used to explore the limits of roll stability, particularly as they depend on loading, suspension condition, and matching between units.
- The LCV used in the current track tests was heavily loaded for pavement testing, and was not representative of the mass and mass distribution of most LCVs in service. Future testing and modeling should be done with a range of loadings and possibly new vehicle dimensions.
- Because all forces on the vehicle are applied through the tires, tire properties are as important to model fidelity as they are to vehicle safety. Tire properties will be key to future efforts, so they must be obtained through dedicated measurements or arrangements with a company owning the information.
- Eventually, the goal of improving stability will entail the application of electronic stability systems to the LCV. The parallel project to study advanced electronic stability control (ESC) can be combined with this project. Models developed in this project can be used to test the algorithms and communication protocols from that project.

Knowledge on the stability of LCVs will be useful to government agencies working to improve the efficiency of freight movement while maintaining the safety of our nation's highways.

This page intentionally left blank.

Chapter 1 – Introduction and Background

As part of its ongoing effort to improve the safety, security, and operational efficiency of heavy commercial vehicles, National Transportation Research Center, Inc. (NTRCI) has begun to investigate the stability of longer combination vehicles (LCVs). The LCV in this study, a triple trailer combination behind a tractor, has more complicated dynamics than the more common tractor in combination with a single semitrailer. The goal of the phase conducted in 2011 was to measure and model the behavior of LCVs in simple maneuvers.

The team executing this work has completed a series of projects for NTRCI on heavy vehicle stability. The team explored the roll stability of a van semitrailer (Knee et al. 2005), a flatbed semitrailer (Pape et al. 2008), and a tank semitrailer (Arant et al. 2009 and LaClair et al. 2010). Another project running concurrently with this one developed algorithms, equipment, and wireless communication protocols for providing electronic stability control (ESC) for multi-unit combination vehicles (Pape et al. 2011).

1.1 Background

Tractors pulling a semitrailer are ubiquitous on the nation’s highways. Tractors pulling a pair of “pup trailers” (8.53 m or 28 ft long semitrailers) are a common way to haul low-density freight and are permitted on the National Network of highways in all 50 states. The term “LCV” refers to a combination of two or more trailers with a gross weight above 36,200 kg (80,000 lb). An LCV can be a pair of trailers where at least one is longer than the 8.5 m (28 ft) trailer, or a train of three pup trailers. The LCV studied in this project was a tractor, two converter dollies, and a set of three trailers, each of which was an intermodal freight container on a chassis.

While combinations with single semitrailers or a “double” with pup trailers are permitted anywhere on the National Network of highways, LCVs may legally operate only on certain routes in selected states, and most states limit the form of LCV that may operate. If the use of LCVs is to be expanded, then their safety and stability are among the questions to be addressed. This project includes experimental and computer simulations of the dynamics of a tractor pulling a “triple” combination. A photograph of the experimental vehicle is shown in Figure 1-1. The combination consists of the tractor, three semitrailers, and two converter dollies.



Figure 1-1. Photo. The triple combination in this project's experiments was simulated in two computer models.

1.2 Project Team

The experiments for this project were conducted at Auburn University National Center for Asphalt Technology (NCAT), which was also responsible for data acquisition. Western Michigan University (WMU) performed the static measurements of the test vehicle. The TruckSim® model was developed by the Clemson University International Center for Automotive Research (CU-ICAR). The Adams model was developed by the University of Akron. Silver Eagle Manufacturing Co. donated equipment for the project and provided valuable advice. More complete descriptions of these and other participating organizations and their roles follow.

1.2.1 Auburn

Auburn University had primary responsibility for conducting the maneuvers on the test track and the highway. The test vehicle and track are regularly used by Auburn's NCAT. Auburn designed and installed the data acquisition equipment on the test vehicle according to needs identified by the team. Auburn was responsible for preparing the data for distribution to the other team members.

1.2.2 CU-ICAR

CU-ICAR led the team in developing the test plan for the on-track and on-highway maneuvers. CU-ICAR conducted its own analysis of the dynamic test data and developed the TruckSim® model. CU-ICAR also contributed to the literature review.

1.2.3 Western Michigan University

WMU, in Kalamazoo, was primarily responsible for measuring the geometric and compliance properties of the test vehicle while it was stationary. WMU also analyzed the data from the test maneuvers.

1.2.4 Oak Ridge National Laboratory

Oak Ridge National Laboratory (ORNL) analyzed the dynamic test data and contributed expertise to many other aspects of the project.

1.2.5 University of Akron

The University of Akron developed one of the two models of the multi-unit combination vehicle. Akron's model was developed in Adams. Akron analyzed the dynamic test data to support its model development.

1.2.6 Battelle

Battelle produced this report, using contributions from the other team members. Battelle contributed to the literature review.

1.2.7 Hendrickson Trailer Commercial Vehicle Systems

Hendrickson contributed expertise to the planning and analysis.

1.2.8 Silver Eagle Manufacturing Co.

Silver Eagle Manufacturing donated one of the converter dollies used in the testing, donated a retrofit kit to modify an existing dolly used by NCAT so both dollies had identical drawbar lengths, and contributed expertise in dolly behavior.

1.2.9 Volvo Trucks North America

Volvo contributed expertise on the trucking industry and a manufacturer's perspective.

1.2.10 Michelin Americas Research and Development Corporation

Michelin Americas Research and Development Corporation donated a full set of new tires for the LCV that was tested. Michelin also supplied knowledge and expertise that was instrumental in building the more accurate simulation models.

1.2.11 Mechanical Simulation Corporation

Mechanical Simulation Corporation (MSC) provided modeling software and preliminary models to aid in the representation of a LCV in the virtual world.

1.2.12 NTRCI

NTRCI staff played an active role in managing the project and coordinating the activities of the numerous contractor teams.

1.3 Project Description

This project included experimental and theoretical portions. The experimental portion consisted of a series of planned maneuvers with an LCV triple on the NCAT test track at Auburn University. The vehicle was also taken on a drive of approximately 1 hour on public highways. Data from the test track was used to characterize the steering behavior of the tractor and the trailers. The theoretical portion of this project saw the development and use of two models of the test vehicle. One model was built in TruckSim®, a commercial package for modeling heavy duty vehicles. The other model was built in Adams, a more generic package for modeling mechanical systems. Both models were built using measurements of the actual LCV triple used in the testing, and both modeled some of the maneuvers executed at the test track. The models were able to duplicate the rearward amplification behavior that is characteristic of multi-unit combination vehicles.

These models describe a particular LCV triple combination that was driven through maneuvers on a test track and a public highway as part of this project. The models begin with its geometry and compliance measured when the vehicle was stationary. The models have been refined following comparison with dynamic data.

The test vehicle drove in a steady-state straight path and constant curvature and executed single and double lane changes on a test track. Limited driving on a highway added further representative conditions for the data. The maneuvers in this phase were not near the limits of stability, so the data is suitable for verifying the models only in everyday conditions. Plans call for the models to be extended in future phases and serve as the basis for evaluating means of improving LCV stability through electronics and design features.

1.4 Project Schedule

This project was conducted in the first nine months of 2011. The three main technical tasks ran in parallel through July 31, 2011. Figure 1-2 is the project schedule. The tasks are identified and their lead organizations are named below the figure.

Tasks	Month of the Project								
	01/11	02/11	03/11	04/11	05/11	06/11	07/11	08/11	09/11
1									
2									
3									
4									
5									
6									
7									
8									
9									
10									
11									

Figure 1-2. Chart. Schedule of tasks.

Task 1: Program Management (NTRCI Lead)

Task 2: Test Plan (CU-ICAR Lead)

Task 3: Partnership Building (NTRCI Lead)

Task 4: Data Acquisition System (Auburn Lead)

Task 5: On-Track Testing (Auburn Lead)

Task 6: On-Highway Testing (Auburn Lead)

Task 7: Multi-Body Vehicle Dynamics Models (Akron and CU-ICAR Lead)

Task 8: Release Notes for the Vehicle Dynamics Models (Akron and CU-ICAR Lead)

Task 9: Vehicle Characterization Testing (WMU Lead)

Task 10: Data Analysis (Battelle Lead)

Task 11: Reporting (Battelle Lead).

This page intentionally left blank.

Chapter 2 – Literature Review

This chapter presents examples of LCVs and motivations for using them. It then explains some of the dynamic considerations they raised and methods for dealing with the dynamics.

2.1 Background of Longer Combination Vehicles

The most common articulated vehicle on U.S. highways is the truck tractor in combination with a semitrailer. The semitrailer could be a dry van (box), as in Figure 2-1, flatbed, refrigerated, tanker, or other trailer design. A tractor pulling two short semitrailers connected by a dolly (Figure 2-2), is used by many carriers, as authorized by the Surface Transportation Assistance Act (STAA). LCVs may have two longer trailers. Or they may have three trailers, which is the topic of this report—the “LCV triple.”



Figure 2-1. Photo. A typical truck tractor in combination with a single semitrailer.



Figure 2-2. Photo. An STAA double has a tractor and two 8.5m (28 ft) semitrailers.

2.1.1 Description

The expression “semi” comes from the proper name of the second unit, which is a semitrailer. Unlike a full trailer, a semitrailer cannot stand on its own but needs to be supported by another vehicle, usually the tractor. In multi-trailer combinations, semitrailers after the first are typically connected (in the U.S.) via a converter dolly, so named because it converts the semitrailer to a full trailer. An outline of a converter dolly is shown in Figure 2-3. The semitrailer behind the dolly is connected to the familiar fifth wheel, as on a tractor. The dolly connects to the trailer ahead of it by a pair of rings known as a pintle hitch, as in Figure 2-4. (Most dollies in service now have rigid mounted fifth wheels and sprung axles, whereas the dolly in the figure and the two dollies used in testing for this project have a rigidly mounted axle and a sprung fifth wheel.)

A fifth wheel allows complete motion in yaw and little resistance to pitch, and it has a measure of stiffness to resist relative roll between the tractor and semitrailer. A pintle hitch allows complete rotation about all three axes.



Figure 2-3. Drawing. Outline of a converter dolly.



Figure 2-4. Photo. The dolly connects to the lead trailer by a pintle hitch.

2.1.2 History and Legal Configurations for Heavy-Duty Trucks

Multiple trailer commercial vehicles have been in continuous operation for more than 100 years (Fancher and Winkler 2007, 607-647). Doubles are permitted on most US interstates but triples are mainly restricted to the western US.

Federal regulation of the nation's heavy duty truck transportation industry prior to 1956 was largely nonexistent, despite the states setting regulations before World War I (FHWA 2000). The result from independent state regulations was that size and weight restrictions became a

patchwork of standards rather than a coherent set of national rules. By 1929, most states regulated truck size dimensions, and today, all states have regulations on public roads for the maximum weight on any single or group of axles; the maximum weight of the entire vehicle; the maximum length, width, and heights of vehicles; and the maximum number of trailers permitted (Transportation Research Board 2002). Federal limits were enacted in 1956 with the passing of the federal-aid highway system. Special permits and grandfather laws in some states do allow trucks exceeding federal standards to continue to operate (NCHRP 2010).

Changes in the quality and capacity of highways, the advancement of vehicle technologies, and the pressing demand for economic efficiency in the transportation of goods and materials have accounted for the evolution of regulations (Transportation Research Board 2002). Improvements in brakes, transmissions, and suspensions responsible for advancing large truck performance, as well as the recent use of sophisticated electronics and information, have allowed for increased size and weight limits in North America, Europe, and Australia (Transportation Research Board 2002).

Current U.S. Federal regulations (23 CFR Part 658) specify size and weight restrictions. Operation of vehicles exceeding the Federal limits can be requested, and the states have the authority to issue permits for this purpose. The STAA (1983) established that combination vehicles consisting of a tractor and two trailing units were permitted for use on interstates and other designated primary highways. States may not limit the length of each trailing unit to less than 8.7 m (28.5 ft) nor impose an overall length limit to these “STAA doubles,” or “twin-trailers.”

The Federal Highway Administration (FHWA) size and weight regulations define a longer combination vehicle (23 CFR 658.5):

As used in this part, *longer combination vehicle* means any combination of a truck tractor and two or more trailers or semitrailers which operates on the Interstate System at a gross vehicle weight greater than 80,000 pounds.

For the purpose of training drivers, The Federal Motor Carrier Safety Administration (FMCSA) has the following definitions (49 CFR 380.105):

- *Longer Combination Vehicle (LCV)* means any combination of a truck-tractor and two or more trailers or semi-trailers, which operate on the National System of Interstate and Defense Highways with a gross vehicle weight (GVW) greater than 36,288 kilograms (80,000 pounds)
- *LCV Double* means an LCV consisting of a truck-tractor in combination with two trailers and/or semi-trailers

- *LCV Triple* means an LCV consisting of a truck-tractor in combination with three trailers and/or semi-trailers.

The LCV “freeze” (STAA 1983 and FHWA 2007), prohibits states that had not permitted the operation of such vehicles prior to June 1991 from doing so in the future (NCHRP 2010).

The three common LCVs found in the U.S. are Rocky Mountain Doubles, Turnpike Doubles, and LCV Triples. Figure 2-5 depicts several common configurations of combination vehicles. Not all configurations of LCV are permitted on all routes. Rocky Mountain Doubles consist of one 12.2 m to 16.2 m (40 ft to 53 ft) trailer and one 8.7 m (28.5 ft) rear trailer, known as a “pup.” These doubles weigh up to 58,513 kg (129,000 lb) (NCHRP 2010). Turnpike Doubles are two 14.6 m (48 ft) trailers with a maximum weight up to 66,678 kg (147,000 lb). Triples consist of three 8.7 m (28.5 ft) trailers at a maximum 58,513 kg (129,000 lb) (NCHRP 2010). By comparison, Canadian Turnpike Double LCVs have two 16.2 m (53 ft) trailers.

Figure 2-6 identifies the routes where LCVs are permitted. They are primarily in western states (NCHRP 2010). LCVs are also permitted for operation on some turnpikes in isolated eastern states, Florida, Indiana, Ohio, New York, and Massachusetts.

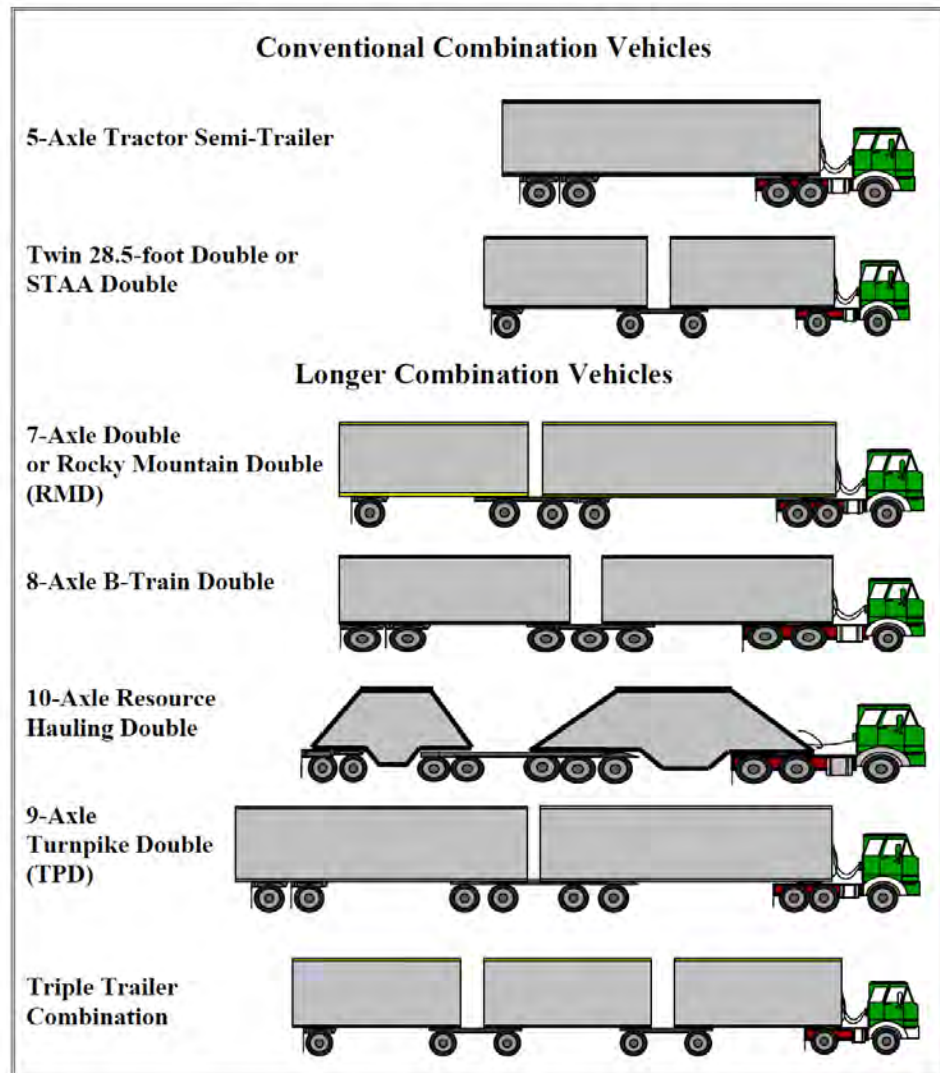


Figure 2-5. Sketch. Configurations of combination vehicles, including LCVs (from FHWA 2004).

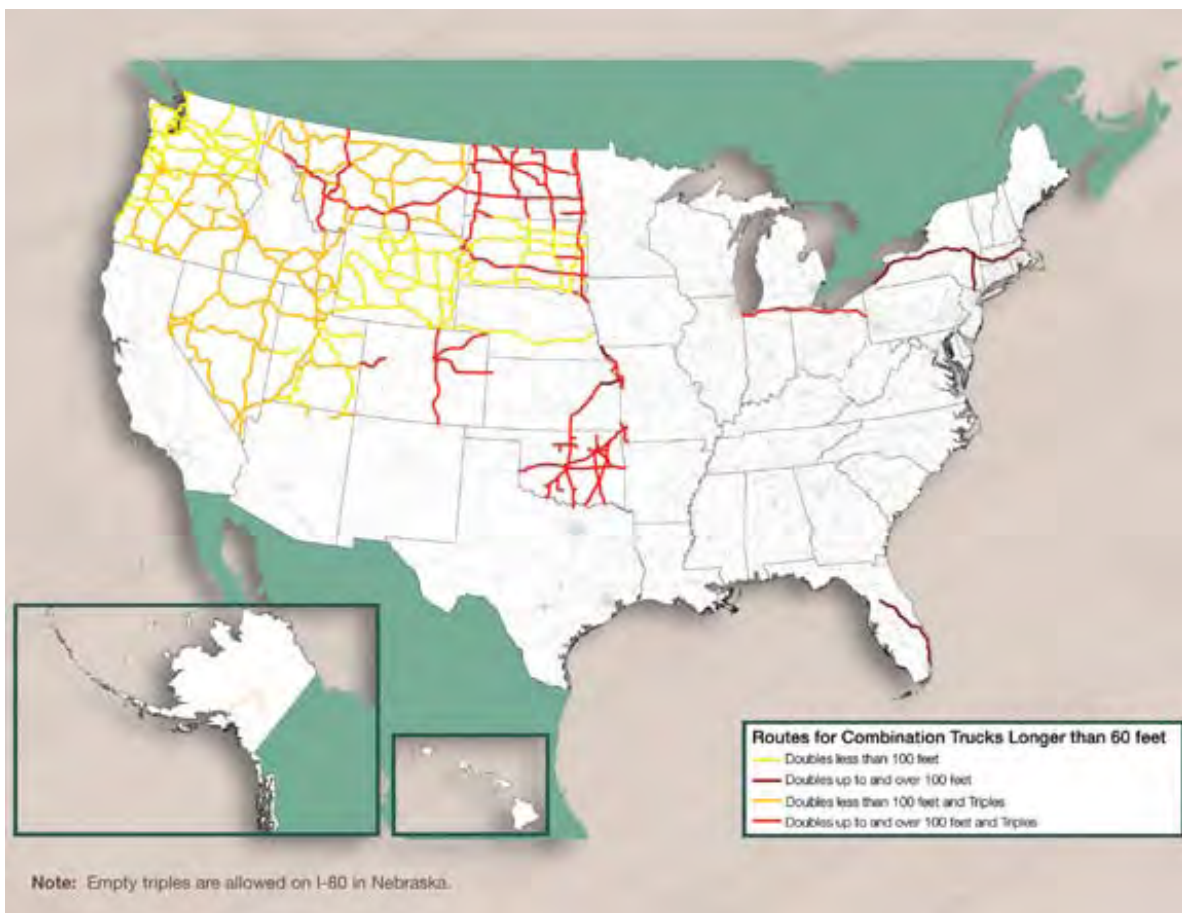


Figure 2-6. Map. LCVs may legally move only on the routes identified in this map (from US DOT 2010).

The benefits sought for using LCVs are primarily productivity and cost. Low density dry freight, particularly in a less-than-truckload package-carrying business, is limited in how much volume can be carried in a single vehicle, rather than by the maximum weight. (In the industry, vehicles for which the payload fills the volume of the trailer(s) before reaching the maximum allowable load are said to “cube out.” In contrast, a load that reaches the maximum permissible weight is said to “weigh out” or “gross out.”) Therefore, the increased cargo volume available in LCVs increases the cargo capacity per tractor (and driver), and for the same loads carried the number of vehicle miles traveled (VMT) is reduced. Carrying more weight also generally results in improved engine efficiency, so the fuel consumed is reduced for the same mass of transported goods with the increase in payload per vehicle. LCVs can permit an increase of 20 to 100 percent increase in cargo capacity (Grislis 2010).

The FHWA’s Comprehensive Truck Size and Weight Study (2000) thoroughly examines the implications of changes to size and weight laws. The study addresses several potential changes in laws regarding LCVs. It notes that nationwide use of LCVs would entail significant infrastructure costs. Bridges would require upgrades to accommodate higher weight, and the

geometric design of curves and intersections would have to be changed. The study synthesizes prior research in safety and stability of LCVs, which is the topic of the present report.

2.2 Dynamics of Longer Combination Vehicles

Two dynamic phenomena pose difficulty in the stability of LCVs: offtracking and rearward amplification. Offtracking means that the last axle of a vehicle does not follow the same path as the steer axle. It is defined as the lateral deviation between the path of the centerline of the front axle and the path of the centerline of another part of the vehicle (ISO 2000). Rearward amplification is a “crack the whip” effect where successive units of the LCV experience a dynamic transient response (lateral position deviations, yaw, lateral accelerations, etc.) more severely than the preceding units in certain maneuvers, with a tendency for the transient response to be amplified at each successive trailer. It is defined as the ratio of a quantity’s maximum amplitude in a trailing unit to its amplitude in the tractor (ISO 2000). Typically, the rearward amplification of the lateral acceleration is calculated, but conceptually any quantity could be considered. Both effects are present in a conventional tractor-semitrailer combination, but they are more pronounced in longer and multi-unit combinations.

These two phenomena are oppositely affected by trailer length. Combinations with longer trailers are less susceptible to rearward amplification. Combinations with shorter trailers are better able to track the path of the tractor. Generally speaking, then, longer trailers are preferable on highways at higher speeds and shorter trailers are preferred for urban environments requiring tight, low-speed turns.

A third phenomenon, mentioned only briefly below, is the propensity of a dolly to jackknife at the pintle hitch if the dolly and following trailer are braked less than the lead unit and subsequently push forward into it.

2.2.1 Offtracking

As conventional LCVs perform constant radius turns at low speeds, the axles of each unit in the vehicle track to the inside of the path followed by the preceding axle (Ervin and Fancher 1984). As shown in Figure 2-7, low-speed offtracking is the reason that truck drivers “square the corner” in urban intersections. At higher speeds, the dynamic effects discussed in Section 2.2.2 take over and the trailer follows a path outside the tractor, as in Figure 2-8. The degree of offtracking depends on the length between the axles and the number of articulation points between the vehicle units (Ervin and Fancher 1984). Greater lengths between the axles, or longer trailers, result in larger offtracking. Offtracking presents maneuverability challenges for tractor-trailers, and the inclusion of additional segments (articulations) in LCVs is a way to minimize offtracking (Fancher and Winkler 2007). Tight highway curves and exit ramps can be a concern because the rearmost trailer can offtrack into the inside edge of the roadway (Ervin and Fancher 1984). Table 2-1 presents the offtracking values simulated for various LCVs on a low-speed exit ramp of a 91.4 m (300 ft) radius. Nomenclature for the combinations is in Table 2-2.

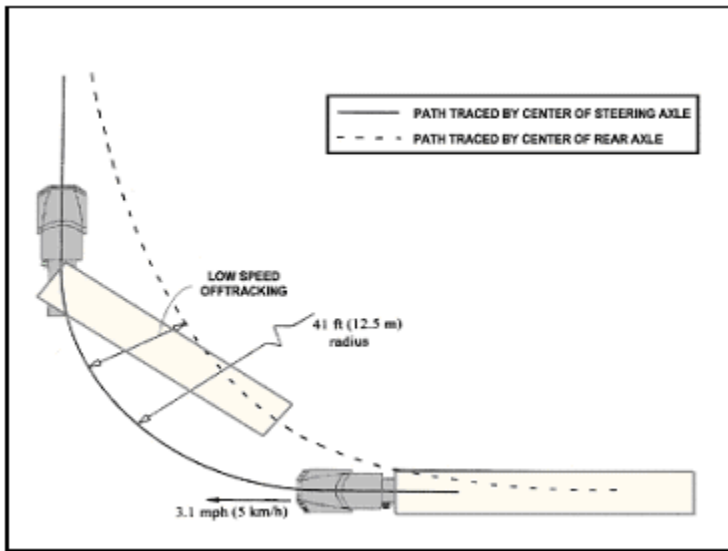


Figure 2-7. Sketch. Low-speed offtracking is the phenomenon when the trailer axle does not turn as sharply as does the tractor (from FHWA 2004).

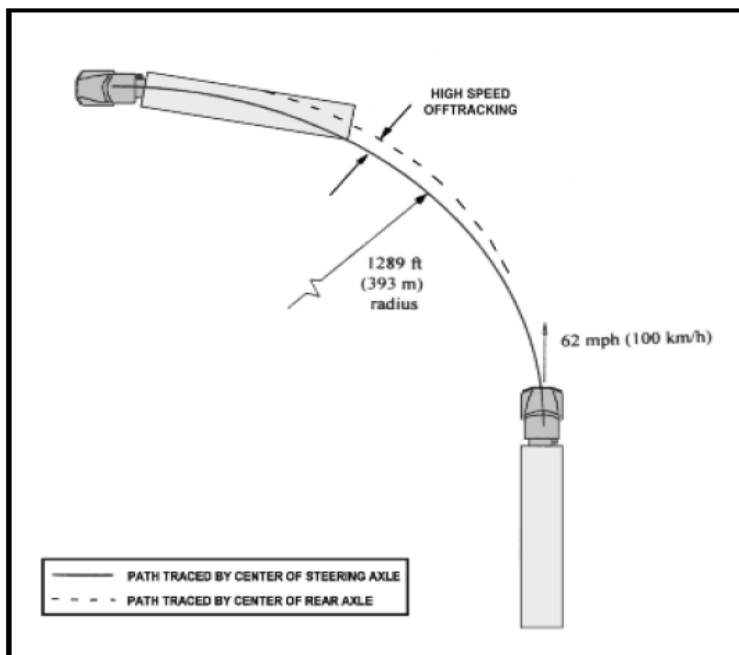


Figure 2-8. Sketch. In high-speed offtracking, the trailer typically follows a path outside the curve of the tractor's path (from FHWA 2004).

Table 2-1. Low-speed offtracking of various LCV configurations in a curve with a radius of 91 m (300 ft), (from Ervin and Fancher 1984, Table 5).

		Offtracking		Maximum Swept Path	
		m	ft	m	ft
1	Double-28	0.61	3.20	2.0	10.5
2	Triple-28	0.88	3.47	2.9	11.4
3	Tr/Semi 48	0.98	3.57	3.2	11.7
4	RMD-45/28	1.04	3.63	3.4	11.9
5	RMD-48/28	1.16	3.75	3.8	12.3
6	TPD-45/45	1.49	4.08	4.9	13.4
7	TPD-48/48	1.71	4.30	5.6	14.1

Table 2-2. Legend for Table 2-1, Table 2-3, and Figure 2-11.

Short Name	Full Name	Semitrailer Lengths (ft)		Semitrailer Lengths (m)	
		first	second	first	second
Tr/Semi-48	Tractor with 48 ft semitrailer	48	--	14.6	--
Double-28	STAA Double	28	28	8.5	8.5
RMD 48/28	Rocky Mountain Double	48	28	14.6	8.5
RMD 45/28	Rocky Mountain Double	45	28	13.7	8.5
TPD 48/48	Turnpike Double	48	48	14.6	14.6
TPD 45/45	Turnpike Double	45	45	13.7	13.7
Triple-28	Triple	28	28	8.5	8.5

The “Swept Path” values indicate the path width needed to pass the entire vehicle, assuming an overall vehicle width of 2.6 m (102 in.) (Ervin, et al. 1984). Compared to the conventional tractor-semitrailer, triple LCVs offtrack moderately less, but Rocky Mountain and Turnpike Double LCVs can experience a 6 to 55 percent increase in low-speed offtracking (Ervin and Fancher 1984).

As LCVs navigate a curve with increasing speed, inside offtracking tends to diminish until a certain point, after which the trailer begins to offtrack to the outside of the turn (Ervin and Fancher 1984). Once again, the magnitude of offtracking is dependent, in part, on the radius of the curve an LCV must travel. The amount of offtracking of the same seven LCV configurations was calculated for a 183 m (600 ft) radius curve taken at 88.5 km/h (55 mph), which is shown in Table 2-3.

Table 2-3. High-speed offtracking of various LCV configurations for a turn radius of 183 m (600 ft) taken at 88.5 km/h (55 mph), from (Ervin and Fancher 1984, Table 7).

		Offtracking	
		m	ft
1	Tr/Semi-48	0.16	0.52
2	TPD 48/48	0.34	1.10
3	TPD 45/45	0.38	1.25
4	RMD 48/28	0.41	1.33
5	Double-28	0.44	1.43
6	RMD 45/28	0.44	1.45
7	Triple-28	0.65	2.13

In this high-speed scenario, all LCVs experienced greater offtracking than the conventional tractor-trailer. The Turnpike Doubles experienced the next least offtracking at 0.34 m and 0.38 m (1.10 ft and 1.25 ft), followed by the Rocky Mountain Doubles at 0.41 m and 0.44 m (1.33 ft and 1.45 ft) and the Triples at 0.65 m (2.13 ft). Generally though, the potential for collisions at high speeds as a result from high-speed offtracking phenomena are considered to be low (Ervin and Fancher 1984).

2.2.2 Understeer and Oversteer

A basic property of a wheeled vehicle's steering capability is its understeer gradient. The under- and oversteer characteristics of a two-axle passenger car are described in introductory textbooks on vehicle dynamics (Gillespie 1992). As shown in Figure 2-9, the understeer gradient is the ratio of the deviation from the purely geometric steering angle to the lateral acceleration. A heavy vehicle with many axles is more complicated to analyze, but it can be expressed as an equivalent two-axle vehicle (Winkler 1998).

$$K = \frac{\left(\delta - \left(\frac{L}{R} \right) \times 57.3 \right)}{a_y}$$

Figure 2-9. Equation. Understeer gradient from measured data.

where

- δ = road wheel angle in degrees,
 - L = tractor wheel base length (steer axle to drive axle centerline)
 - R = turn radius
 - $\frac{v^2}{Rg}$ = lateral acceleration a_y
 - K = understeer gradient (deg/g)
- (The factor 57.3 converts from radians to degrees.)

Each unit of a combination vehicle can be analyzed in a similar manner. The tractor's turn radius is determined by the steer angle of its road wheels. The turn angle of each semitrailer is determined by the articulation angle between the semitrailer and the tractor or dolly on which it rests (Mallikarjunaraao and Fancher 1979).

A vehicle's stability in yaw depends on whether it exhibits understeer (understeer gradient K is positive) or oversteer (K is negative). All passenger car yaw stability systems place priority on avoiding oversteer conditions, as these are the most dangerous for most drivers. The understeer gradient depends on the fore-aft mass distribution, the tires' cornering stiffness, whether body roll induces a steer angle in an otherwise fixed angle, and other properties of the suspension (Gillespie, 1992).

Yaw instability of articulated vehicles is more complicated, as each unit of the vehicle can become unstable in yaw. Moreover, as various units in a combination are loaded and constructed differently, the effects of speed and lateral acceleration on the units' understeer gradients are expected to be different. (Yu, Güvenç et al. 2008), (Zhou, Guo et al. 2008).

Each unit of a conventional tractor-trailer can be understeering or oversteering, so there are four stability combinations relating the behavior of the tractor and the trailer through the articulation of the vehicle (Table 2-4).

Table 2-4. Effect on stability of tractor and trailer steer understeer gradients (Winkler, Ervin 2006).

		Tractor	
		understeer	oversteer
Trailer	understeer	The vehicle is stable. As speed increases, the articulation angle gain (increase in articulation relative to steering input increase) will approach the ratio of the two units' understeer gradients.	As speed increases toward the critical speed, the articulation gain approaches infinity. This results in a jackknife. System is unstable at high speed.
	oversteer	The articulation gain is initially positive but becomes negative and the trailer swings out. This is an unstable arrangement at high speed. However, at low speeds, the articulation gain is positive, making the vehicle drivable.	Response depends on whether the ratio of the understeer gradients is greater or less than the ratio of the wheelbases, and the articulation gain will go to negative or positive infinity. This results in a jackknife or a swing out, though the difference will be hard to tell from the driving perspective. The vehicle is unstable at high speed.

LCVs have yet more complicated stability interactions in yaw, making them difficult to analyze analytically in a general fashion.

2.2.3 Rearward Amplification

The lengths of trailers and the number of articulation points, or number of trailers in combination, affect LCV stability (Ervin and Fancher 1984). Sudden lane changes and avoidance maneuvers can excite the vehicle in a way that leads to rearward amplification. Rearward amplification occurs during sudden steering movements and is usually a concern at speeds greater than 80 km/h (50 mph) (MacAdam et al. 2000). Maneuvers that seem benign at the tractor can, through rearward amplification, cause sufficient lateral acceleration at the second or third trailer to produce a rollover.

Factors that Affect Rearward Amplification

Trailer lengths affect an LCV's stability. The lengths of trailer units tend to be the most significant factor to the risk of rearward amplification. Longer trailers are less susceptible to rearward amplification than short trailers. Rearward amplification is greater with a larger number of trailers. As an example, a triple with 8.5 m (28 ft) trailers will experience greater rearward amplification than a double of 8.5 m (28 ft) trailers or a triple combination using 14.6 m (48 ft) trailers (Ervin and Fancher 1984). Fewer joints, or articulation points, and longer trailers provide greater stability. As in other vehicles, heavy loads and high centers of gravity diminish an LCV's roll stability (Fancher and Winkler 1992).

Obstacle avoidance maneuvers present the potential for rearward amplification in what is often thought of as a "crack of the whip" response. Lateral acceleration in each successive trailer of an LCV becomes amplified more than in the previous trailer. The degree of rearward amplification can also be influenced by the frequency of steering input, locations of pintle hitch connections between trailers, and the ratio between lateral stiffness on the vehicle tires to the weight of the vehicle (Ervin and Fancher 1984).

Figure 2-10 shows the simulated lateral acceleration in a double tank trailer combination as a function of steer frequency. At low frequencies (corresponding to gentle, sweeping maneuvers), all units move together and have the same lateral acceleration. The ratio from one unit to the next is unity; there is no amplification. As the frequency of the steering input rises above about 1 rad/s (0.16 Hz), the response of the tractor and first semitrailer begins to diminish but the response of the dolly and second semitrailer decrease at a lower rate. That means the lateral acceleration of the second semitrailer is more than that of the tractor. At about 3 rad/s (0.48 Hz), the vertical gap in the graph is about its maximum, as indicated by the arrow. The vertical axis on this graph is logarithmic, so vertical distance is indicative of the ratio between two values. The point of maximum gap is the frequency of maximum rearward amplification. When the driver steers at this frequency, the lateral acceleration of the rear of the combination is nearly a factor of two greater than that of the tractor.

While the plot indicates that the magnitude of the lateral acceleration is lower than that generated at a lower frequency steer input, the trend for rearward amplification remains very similar even

in more severe maneuvers and presents a rollover hazard. Since the driver senses only the accelerations generated in the tractor, he may not be aware of an imminent rollover. If the vehicle were traveling at higher speeds or larger steering inputs were used at this same frequency, a similar rearward amplification would still be expected for this frequency, and the greater lateral accelerations at the second trailer could result in a rollover event even if the tractor remains safely below its rollover threshold. Figure 2-11 plots the amplification gain (defined here as the ratio of the lateral acceleration of the rearmost trailing unit to that of the tractor) as a function of frequency, for seven kinds of combination vehicles. As in the example of the double trailer configuration in Figure 2-10, the amplification is uniform at very low frequencies. At a frequency of about 3 rad/s (0.48 Hz), the amplification gain of combinations of two and three 8.5 m (28 ft) trailers is a maximum. Combinations with longer trailers do not experience any gain; the lateral acceleration at the trailer is never more than it is at the tractor.

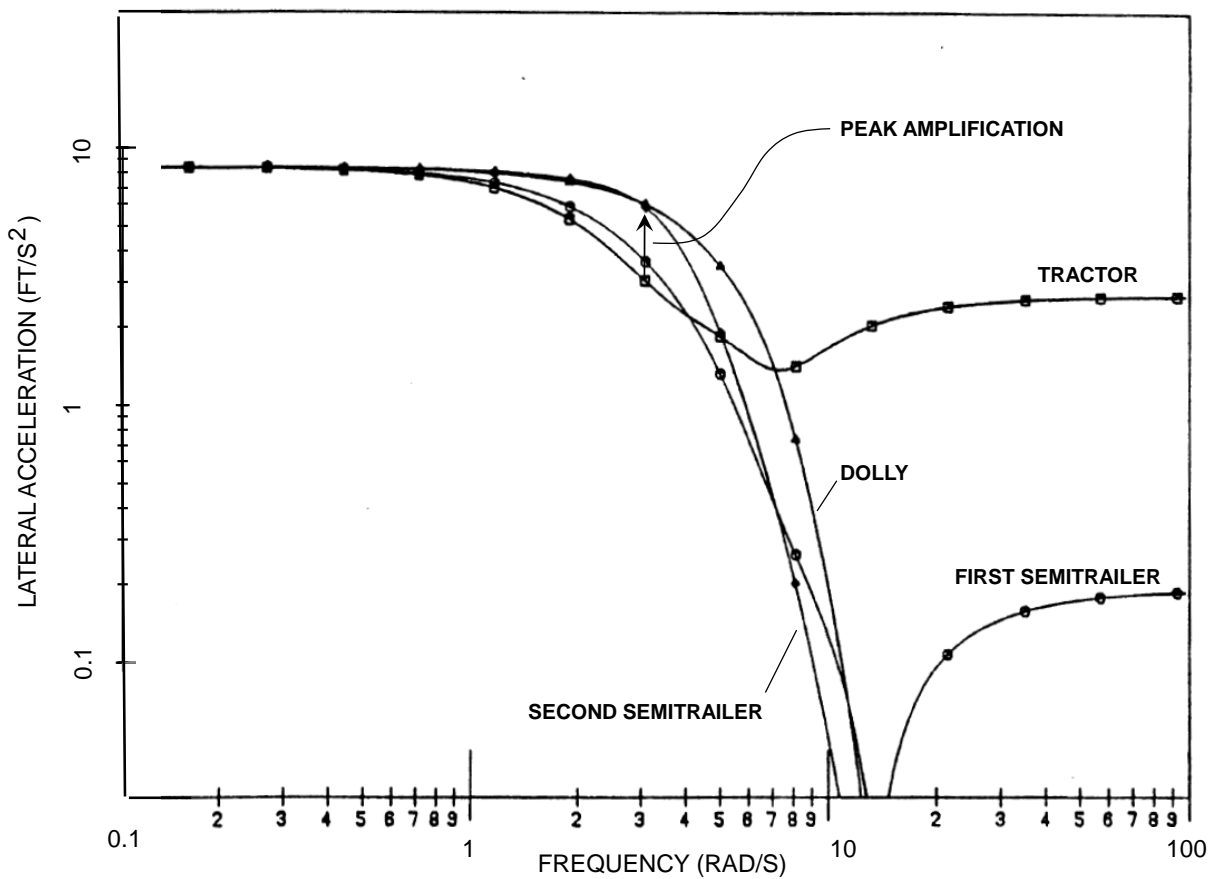


Figure 2-10. Graph. Simulated response of a double tank trailer combination to a road wheel steer input of 1 degree (from Mallikarjunarao and Fancher 1979).

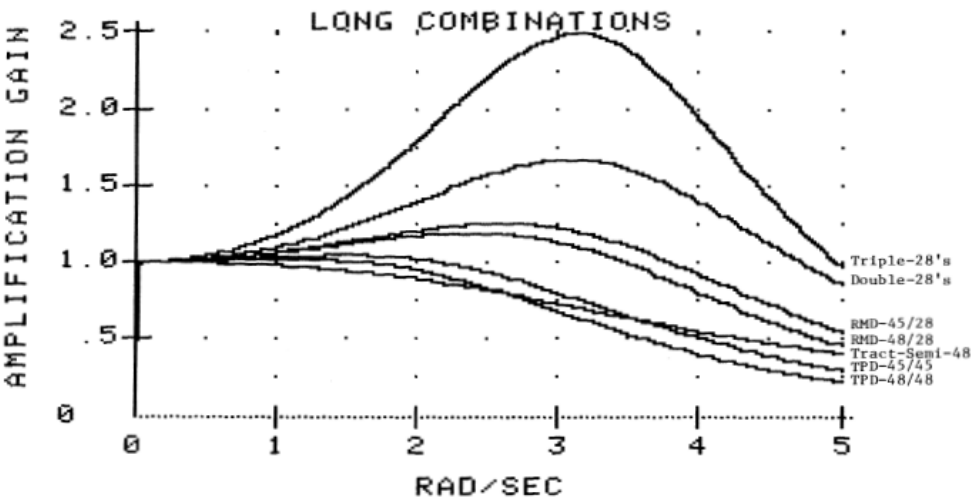


Figure 2-11. Graph. Rearward amplification of lateral acceleration at the rear trailer of various vehicle configurations as a function of steer input frequency. See Table 2-2 for definitions of the vehicles (from Ervin and Fancher 1984).

de Melo (2005) evaluated the stability of a 7-axle B-train tank combination and a 9-axle turnpike double in simulations and testing at speeds from 20 to 90 km/h (12 to 56 mph). Both vehicles were above 50 tonnes (110,000 lb) in configurations more common in Brazil than the U.S. Lateral acceleration at the rear became greater than at the tractor for the B-train at 70 km/h (43 mph) and for the turnpike double at 40 km/h (25 mph). Rearward amplification was significantly greater in the case where the first semitrailer was empty and the second trailer was loaded, with the turnpike double becoming unstable at the higher speeds.

Consequences of Rearward Amplification

Moderate rearward amplification can result in undesirable offtracking and possible encroachment in an adjacent lane, for example during oscillations due to wind or other common road perturbations. The greater hazard of rearward amplification is excessive and unsensed lateral accelerations during maneuvers, which can lead to rollover.

A measure of a vehicle's roll stability is its static rollover threshold (SRT), the maximum degree of steady lateral acceleration that a vehicle can withstand without any of its units rolling over. SRT is measured in gravitational units (Ervin and Fancher 1984). The threshold has been correlated to the real number of rollovers (Ervin and Fancher 1984). A passenger car's SRT is usually greater than 1 g, but a loaded LCV's SRT is less 0.5 g (de Melo 2005). As with other vehicles, an LCV's roll stability is influenced by the height of its center of gravity, track width, suspension design, and tire stiffness.

2.3 Stability Enhancements for Longer Combination Vehicles

A number of modifications and technologies have been examined to improve the stability of trailers and decrease the risk of rollovers and offtracking in turns. Special hitching arrangements

and innovative dollies can be effective in providing greater stability. Electronic stability aids have been demonstrated in research settings.

2.3.1 Design Variants

The vast majority of multi-unit combinations in the U.S. use a dolly like that in Figure 2-3 and Figure 2-4 and are known as an “A-train.” The “B-train” has a fifth wheel mounted at the rear of the lead trailer, as shown in Figure 2-12 (Ervin and Fancher 1984). The C-train has dual drawbars, as shown in Figure 2-13. This eliminates a degree of freedom of motion, which has the advantage of eliminating some vibration modes but also increases the minimum cornering radius.

On a B-train, the lead trailer’s frame extends out the rear of the conventional payload bed, and the fifth wheel and axle assembly are mounted to the end of the rigid frame extension for a direct connection to the succeeding trailer. The design of the B-train provides the following features: The degree of increased offtracking from the addition of another trailer in an LCV is noticeably less (Ervin and Fancher 1984). The B-train, with fewer articulation points, cannot experience dolly jackknife, and articulation instabilities are reduced relative to those of the A-train configuration (Ervin and Fancher 1984). It has significant operational disadvantages because the rigid frame extension prevents trailers from reaching conventional loading docks and trailers cannot be interchanged within a combination.

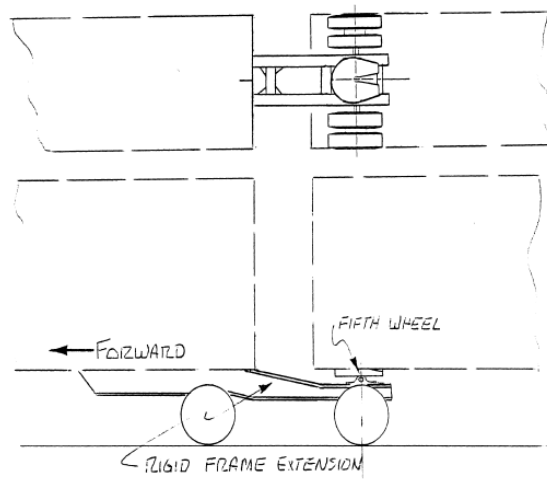


Figure 2-12. Sketch. In a "B" train, a fifth wheel is attached to the lead trailer (from Ervin and Fancher 1984).

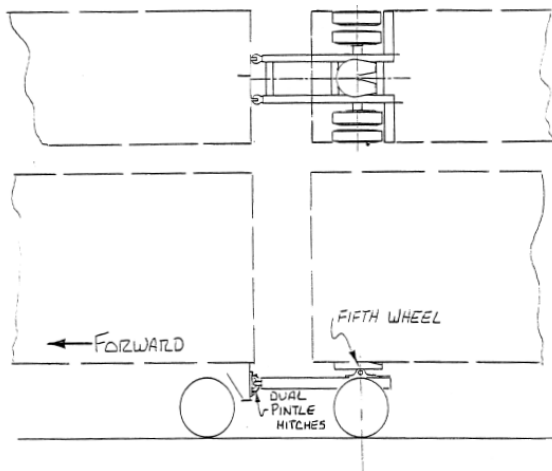


Figure 2-13. Sketch. A "C" train has two rigid drawbars that prevent the dolly from rotating with respect to the lead trailer (from Ervin and Fancher 1984).

The dual-drawbar dolly of the C-train holds greater flexibility over the B-train and in particular can be removed and interchanged (Ervin and Fancher 1984).

Changes to the suspensions of LCV trailers can improve roll stability. Any suspension modification that improves roll stability will help a trailer endure rearward amplification. Wider track and greater auxiliary roll stiffness are common approaches. The inherently large auxiliary roll stiffness of modern air suspensions is a significant improvement over leaf springs, particularly models with significant lash.

2.3.2 *Electronic Stability Aids*

Modern electronic control systems can improve the handling of articulated vehicles. Active trailer steering (He et al. 2010) has been simulated, and selective braking of trailer tires (Ervin et al. 1998 and MacAdam et al. 2000) has been tested in actual vehicles. An ongoing program (Pape et al. 2011) is exploring advanced concepts for stability control in combination vehicles.

He et al. (2010) optimized an algorithm for active trailer steering. Simulations of a low-speed steady curve predicted that offtracking could be reduced by 35 percent. Rearward amplification in a lane change was reduced by 30 percent.

The Rearward Amplification Suppression (RAMS) concept is to apply selective, carefully timed braking to the left and right sides of the trailer and dolly axles to damp excessive yaw motion. The full-vehicle system uses sensor data from throughout the vehicle. The trailer-to-trailer configuration uses only communication between the trailers. Each trailer works independently from one another in the trailer-only application. The trailer-only RAMS system minimizes the dependence on other trailer units (MacAdam et al. 2000).

The RAMS system is enabled when a vehicle is traveling faster than 77 km/h (48 mph). Yaw rate transducers mounted to the trailers provide information to the control algorithm, which in

turn controls the brakes to the individual trailers and dollies. The full-vehicle RAMS uses the tractor steering angle in the control algorithm as well. The RAMS braking system uses diagonal braking across the trailer wheels, which provides both lateral tire forces and braking tire forces for improved stability and control.

The trailer-only RAMS configuration was proven to be greatly effective in reducing rearward amplification in double and triple combinations (MacAdam et al 2000). Figure 2-14 contains the results for a single lane change test of a triple with and without the RAMS system.

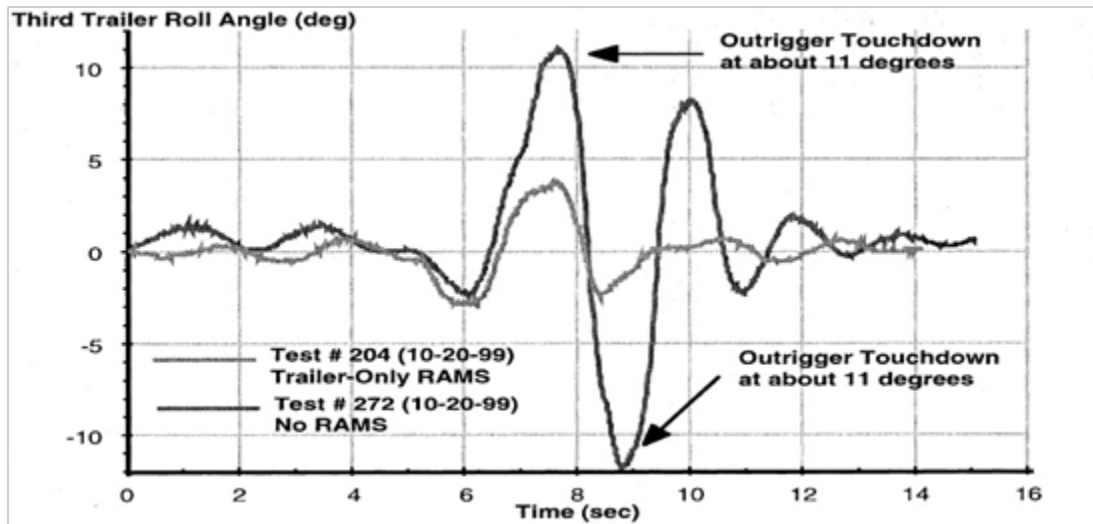


Figure 2-14. Graph. Measured roll response of the rear trailer for a non-RAMS and Trailer-Only RAMS system (from MacAdam et al. 2000).

The more complex full vehicle system was able to provide better stabilization because of its greater number of communication links. None of the RAMS configurations could provide directional stability on very low frictional surfaces such as wet jennite, ice, and snow (MacAdam et al. 2000).

Chapter 3 – Test Plan

This chapter presents the test plan in summary form, summarizing the maneuvers and the reasons for selecting them. The next chapter on data collection presents the tests as they were actually conducted. The complete test plan, as it was written to guide the experiments, is in Appendix A.

The goal of the testing was to observe the behavior of the vehicle in maneuvers that were sufficient to excite its dynamics but did not pose a threat to its stability.

3.1 Overview

The purpose of this testing was to establish the dynamics of an LCV consisting of a tractor and three semitrailers. Testing was carried out at Auburn University’s NCAT test track facility using a vehicle configured for the purpose of testing asphalt. Five testing maneuvers were executed: constant-radius curve, single lane change, gradual lane change, double lane change, and an impulse steer.

The vehicle was instrumented with IMUs and GPS to capture the motion and orientation of the vehicle. String potentiometers were used to capture the articulation, body roll, and kinematic data from the components of the vehicle.

The data from these tests was compared with the predictions of models developed for this research. This test plan was developed to excite responses to driver input appropriate to gauge the behavior of the LCV in sub-limit maneuvers. As a precaution, all maneuvers were limited to produce a lateral acceleration response of no more than 0.2 g, estimated to be one half of the rollover threshold for vehicles of this nature (Winkler et al. 2000).

The goal of the testing was to establish the baseline dynamics of the LCV. The 0.2 g criterion was essential for safety because the test vehicle did not have outriggers and the shoulders of the track were soft.

3.2 Test Vehicle

The NCAT test vehicle was a Freightliner tractor in combination with three Cheetah container chassis carrying loaded 6.1 m (20 ft) shipping containers, pictured in Figure 3-1. The containers were ballasted with concrete roadside barriers. Figure 3-2 is an image of the vehicle as it was modeled in the Adams software for the analysis of Chapter 7. The figure indicates the identifiers for the trailers and dollies.



Figure 3-1. Photo. The test vehicle consisted of one tractor, three semitrailers, and two converter dollies.

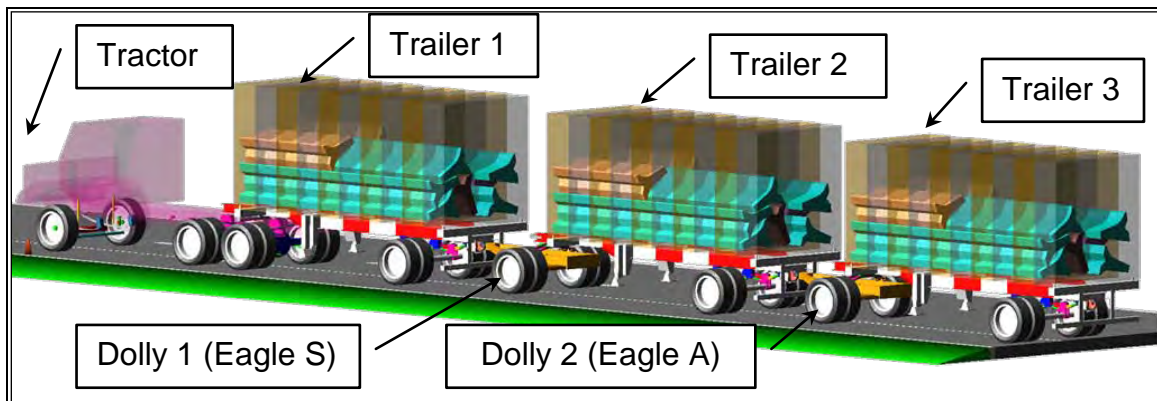


Figure 3-2. Drawing. Names of the units of the test vehicle.

The two converter dollies were manufactured by Silver Eagle Manufacturing. The suspension on these dollies is a pair of transverse leaf springs beneath the fifth wheel and above the frame, which is rigidly mounted on the axle. The Eagle S dolly, behind the first semitrailer, was donated to the project by Silver Eagle. The Eagle A drawbar length was originally greater than 2.4 m (8 ft), while the drawbar of Eagle S was 1.8 m (6 ft). The Eagle S dolly is typical of those in use on the highway, whereas the Eagle A was built specifically for NCAT and is not representative. Eagle A will tend to be more stable due to its extra length. Eagle A had already been in service at Auburn, and its drawbar was shortened to match the new Eagle S, as explained in Appendix C. The Eagle A dolly was in the second dolly position.

Measurements of the vehicle's weight and dimensions are presented in Appendix C.

3.3 *On-Track Maneuvers*

All of the scripted dynamic maneuvers were conducted on the NCAT test track (Figure 3-3). The track is a two-lane oval with a total length of approximately 2.7 km (1.7 mile).

The geometries of the on-track maneuvers were a constant-radius curve, single lane change, gradual lane change, double lane change, and an impulse steer.

The maneuvers were to be carried out in a location on the test track that allowed the vehicle to start the maneuver in a steady-state condition.

The maximum speed permitted on the track is 72 km/h (45 mph), and maneuvers were conducted at or below that limit. The speeds for the single and double lane change were to be determined based on data collected during preliminary testing. Data was to be reviewed after each preliminary run for each maneuver so that limit behavior, as judged by the 0.2 g lateral acceleration limit, was not being approached. Diagrams of the maneuvers as they were originally planned are presented in Appendix A. Diagrams of the maneuvers as they were actually executed are presented in Chapter 4.



Figure 3-3. Photo. The test track has curves of 476 ft (approximately 145 m) radius at the two ends. The straights are 2600 ft (approximately 793 m) long.

3.3.1 *Constant Radius Curve*

This maneuver was to establish the steady-state characteristics of the LCV such as understeer gradients for the tractor and the three semitrailers. The vehicle went through the curved portion of the track at a constant speed while maintaining lane position. The test speeds were to be 32, 40, 48, 56, 64, and 72 km/h (20 to 45 mph). Each test speed was to be repeated 10 times.

3.3.2 Single Lane Change

This maneuver was to establish the transient dynamic behavior of the LCV during a sub-limit obstacle avoidance maneuver. Path deviation and trailer motion settling distances were to be measured with a goal of characterizing the amplification of the trailer motion for each unit in the vehicle. Of interest is the relative position (to tractor) of each trailer in the vehicle, along with yaw rate and lateral acceleration.

The driver was instructed to travel in the right lane of a straight section of track at 72 km/h (45 mph). The driver was to move 3.7 m (12 ft) or one lane to the left over a distance of 46 m (150 ft), while attempting to maintain a constant speed during the maneuver.

3.3.3 Gradual Lane Change

This maneuver was planned to characterize the behavior of an LCV in a gentle, non-evasive lane change at a moderate operational speed. The intent was to collect data to describe the motion of the LCV in a normal operation that is likely to be encountered daily.

The maneuver was identical to the single lane change, except that the transition between lanes was spread over 122 m rather than 46 m (400 ft rather than 150 ft). This maneuver was at the maximum track speed of 72 km/h (45 mph).

3.3.4 Double Lane Change

This maneuver, like the single lane change, was to characterize the transient behavior of the LCV. This test was to establish path deviation and trailer motion settling distances with a goal of determining the amplification characteristics of the trailer motion for each unit in the vehicle. Similar to single lane change, the trajectory relative position (relative to the tractor) of each trailer in the vehicle, along with yaw rate and lateral acceleration, is of interest.

This maneuver, with its dual left-going and right-going inputs, can excite oscillation of the vehicle more easily than the single lane change. Completing this test safely required that the maximum test speed be lower than that of the single lane change. Speeds were selected following the preliminary testing to keep the vehicle well within its stability limit.

The driver was to travel toward the test region of the track in the right lane. Upon reaching the test region, the driver was to proceed into Gate 1 at test speed. Upon exiting Gate 1, while maintaining test speed, the driver was to steer into the left lane toward Gate 2. The driver was to then proceed through Gate 2. After passing through Gate 2, the driver was to steer into the right lane toward Gate 3. The driver was to then pass through Gate 3, maintaining test speed.

3.3.5 Impulse Steer

The goal of this test was to excite the test vehicle with a broad-band input to allow frequency domain analysis. Whereas the lane change maneuvers were somewhat sinusoidal and excited

only a single frequency of the vehicle's response, the impulse was intended to excite many frequencies at once.

The maneuver was to take place in the straight sections of the test track in a location where the vehicle could be excited from a steady-state attitude. The driver was to start the maneuver from the right lane. The driver was to apply a quick 90 deg left steering input to the hand wheel, and then return the hand wheel to center. The driver was to allow the vehicle to proceed without further steering inputs to the left lane, when it would be gradually aligned with the road. The impulse steer maneuver sequence was attempted but not completed. The cab suspension allowed significant oscillation, and the driver was not confident of keeping control of the vehicle if this maneuver were to be repeated at higher speeds. The vehicle itself was not in any danger. The team deferred to the driver's judgment and withdrew the maneuver from the test.

3.4 On-Highway Testing

This portion of the testing was to gather real world data from an LCV operating on public roads at normal highway conditions and speeds. The on-highway testing was conducted on a preselected route according to Alabama State DOT permit. Any lane changes or dynamic events requested by the consortium were to be carried out in safe and legal locations along the route. The trip was planned for mid-day, when traffic was expected to be light to moderate. The route, mapped in Figure 3-4, was determined by NCAT. Directions were:

- NCAT Track to Lee Road 151S-145E-175N-US 280
- Turn right onto US 280E from Lee Road 286 10.5 km (6.5 miles)
- Reverse direction onto US 280W to Lee Road 183 11.4 km (7.1 miles)
- Reverse direction onto US 280E to Lee Road 175 1 km (0.6 miles)
- Return to the NCAT track via Lee County roads.

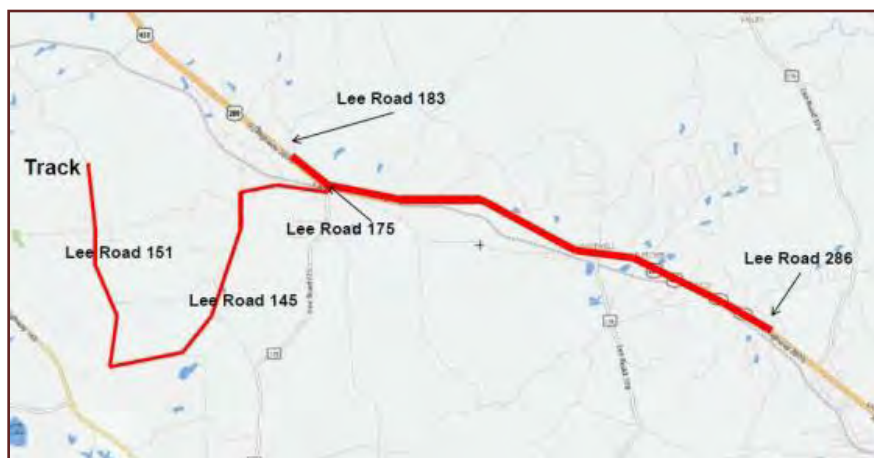


Figure 3-4. Map. On-road test route.

The vehicle was driven from the NCAT test facility to US 280. This allowed the research team to see the vehicle in operation on a public road, in various situations and conditions that were not as controlled as on the test track. Several gradual lane changes were completed at higher speeds than were possible on the test track, and video footage was recorded.

3.5 Metrics for Successful Testing

All tests were to be executed in a manner deemed safe by the driver and test facility management. Path following consistency needed to be demonstrated for the successful completion of these maneuvers. Data was to be reviewed as available or at the end of the testing session to verify that all readings were within range, that the driver was maintaining consistency, and that the data acquisition equipment was functioning properly.

Chapter 4 – On-Track and On-Highway Testing

This chapter addresses the process of instrumenting the test vehicle and collecting the data. The main focus of this task was to execute the test plan of Chapter 3 and collect data necessary for the analysis of the following chapters. This chapter first describes the instruments and data acquisition procedures. It then describes the maneuvers as they were actually executed. Finally, it describes the data processing methods and the lessons learned from the experience.

4.1 Sensors

Sensor selection required the entire team to give input on determining what to measure to ensure that the proper measurements were taken to complete the planned analysis. The method to develop the plan was to decide what to measure, which sensors to use, and where to place the sensors. The complete data acquisition plan is in Appendix B; this chapter begins by summarizing the salient points of the plan. A total of 206 channels were to be recorded. The measurements and the sensors are summarized in Table 4-1. This same information is depicted graphically in Figure 4-1. Figure 4-2 is the color key for the first figure.

Table 4-1. Summary of measurements and sensors.
The contents of each cell are the brand or model of the sensor used.

Unit	Quantity	Vehicle CAN	String Pot	GPS	IMU	GPS and IMU
Tractor	Horizontal and vertical displacement of the steer axle, left side		SP1-25			
	Horizontal and vertical displacement of the steer axle, right side		(SP1-25)			
	Horizontal and vertical displacement of the second drive axle, both sides		SP1-25			
	Steer input at the steer column		SP1-25			
	Steer input, steer kingpin		SP1-25			
	Engine parameters	(X)				
	Three-axis accelerations and angular rates				Memsense	
Trailer 1	Position			Novatel and u-blox		
	Horizontal and vertical displacement of the axle		SP1-25			
	Three-axis accelerations and angular rates				Crossbow	
Trailer 2	Position			Novatel and u-blox		
	Articulation to the leading dolly		SR1A-62			
	Horizontal and vertical displacement of the axle		SP1-25			
	Three-axis accelerations and angular rates					(RT2500)
Trailer 3	Position			Novatel		
	Articulation to the leading dolly		SR1A-62			
	Horizontal and vertical displacement of the axle		SP1-25			
	Three-axis accelerations and angular rates					(RT3100)
	Position			Novatel		

Note: Parentheses in the table indicate measurements that were attempted but, for one reason or another, were unavailable to the analysts.

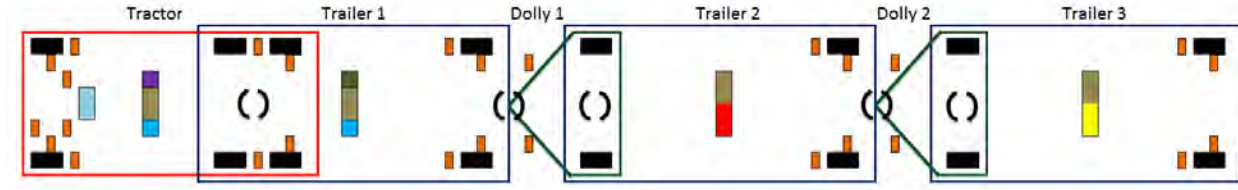


Figure 4-1. Diagram. Sensor layout.

Color	Item Description	Connection Type	Data Rate (Hz)	Color	Item Description	Connection Type	Data Rate (Hz)
Orange	Sting Pot	CAN	100	Purple	MemSense	USB	150
Light Blue	Engine CAN	CAN	100	Dark Green	Crossbow	RS-232	20
Brown	Novatel	RS-232	5	Red	RT-2500	TCP-IP	100
Light Blue	U-Blox	USB	1	Yellow	RT-3100	TCP-IP	100

Figure 4-2. Chart. Color key to Figure 4-1, along with data connection method and sample rate.

The channels that are key to characterizing vehicle dynamics were to be recorded at a nominal sampling rate of 100 Hz. Supplementary channels were sampled at lower rates, as indicated in the table. Section 4.2 explains how each sensor’s data was transmitted to a central computer and every single data point was given a time stamp. While the sampling rate was not exactly 100 Hz and not all channels were sampled simultaneously, an experiment prior to data collection showed that the method reliably provided data at the time indicated in each time stamp.

Each unit of the vehicle had two GPS receivers and an IMU to record position and acceleration, and string potentiometers to measure displacements within the vehicle. The supplemental GPS receivers were to support other Auburn research and to be available as backup data sources for this project. The two GPS and IMUs were separate pieces of equipment on the tractor and Trailer 1; one GPS was integrated with the IMU on Trailers 2 and 3.

String Potentiometers

String potentiometers or “string pots” were used to measure dolly-to-trailer articulation angles, roll steer deflections on the trailers, and steering input. Four were model SR1A-62 shown at the left (Figure 4-3). These weatherproof units have a stroke of 1.58 m (62 in.). They were used in pairs to measure the articulation angle between the trailers and the converter dolly. All other string pots on the vehicle were model SP1-25, at the right in Figure 4-3, with a stroke of 625 mm (25 in.). They were installed to measure axle displacement on the test vehicle. The steering input was also measured with a string pot.

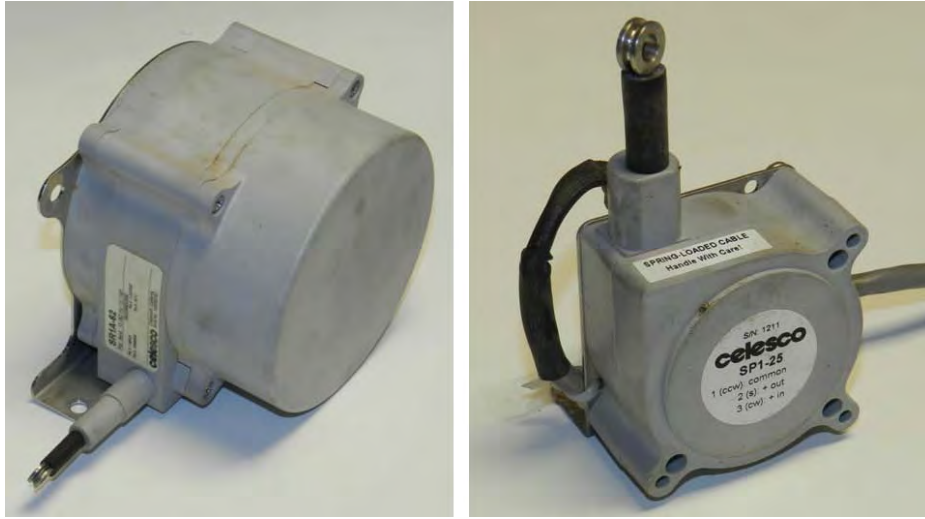


Figure 4-3. Photo. Two models of Celesco string potentiometers were used, the SR1A-62 (left) and the SP1-25 (right).

GPS and IMU

The tractor and the three trailers had GPS receivers and IMU accelerometers. The GPS and IMU functions were integrated in a single instrument on Trailers 2 and 3; the functions were provided by separate sensors on the tractor and Trailer 1.

Oxford RT instruments combine a GPS receiver and an IMU. They combine the information from both sensors using a Kalman filter and output three-dimensional motion and three-dimensional rotation of the vehicle unit on which they are mounted. NTRCI provided one Oxford model RT-3100, and WMU provided a model RT-2500. Photographs of both are in Figure 4-4.



Figure 4-4. Photo. Oxford RT instruments combine GPS and accelerometer measurements to track the motion of a vehicle.

A third IMU was a Crossbow Nav440, and the fourth was a MemSense Nano IMU, both shown in Figure 4-5 and both supplied by Auburn. These two units do not provide the GPS integration as do the Oxford models.



Figure 4-5. Photo. These two models of inertial measurement units do not include GPS receivers.

The Tractor and Trailer 1 had both a u-blox EVK-6H evaluation kit along with a Novatel ProPack-V3, both of which are pictured in Figure 4-6. The second and third trailer both had a Novatel receiver as well as an Oxford RT unit to receive position information. Auburn supplied the supplemental GPS receivers.

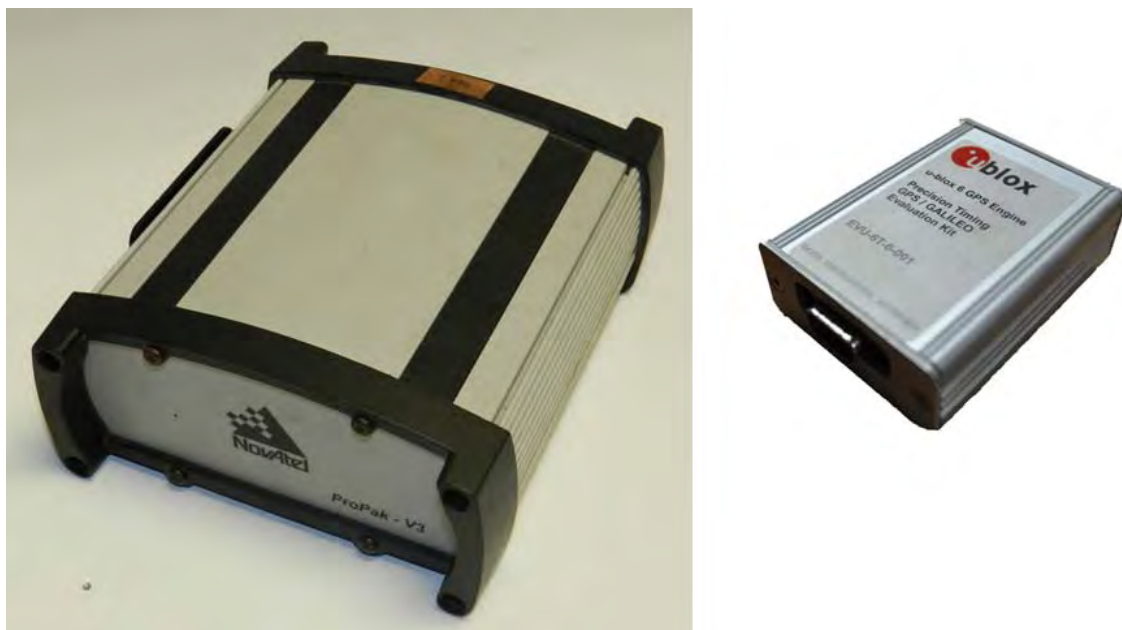


Figure 4-6. Photo. A pair of GPS receivers, one manufactured by Novatel and one by u-blox, were mounted on both the tractor and the first trailer.

4.2 Data Acquisition

The data acquisition system consisted of an industrial computer with the Ubuntu Linux operating system, and a wireless (Wi-Fi) router. The industrial computer ran without a monitor, keyboard, or mouse; a Secure Shell (SSH) connection was used between a separate laptop and the industrial computer for controlling data collection. The wireless router allowed the data collection process to be monitored and controlled via the laptop computer in the truck cab. No data was sent over the wireless link; wireless was only to monitor and control the data acquisition. All data was recorded directly to the industrial computer. The data acquisition process, once started, would not be interrupted by a loss of communication from the laptop in the cab.

The computer interfaced with the instrumentation devices as follows:

- Direct UDP/IP communication with the Oxford RT units over CAT6 Ethernet
- Four serial (RS-232) ports:
 - Three Novatel GPS units on the Tractor and Trailers 1 and 2
 - Trailer 1 IMU (the Crossbow 440)
- Six USB connections:
 - The MemSense AHRS (used as an IMU) A RS232-USB converter for the Novatel GPS on the tractor
 - Two u-blox GPS devices
 - Two USB-to-CAN converters for communicating with the string potentiometers and the tractor computer.

The wiring between the sensors and the computer is shown in Figure 4-7.

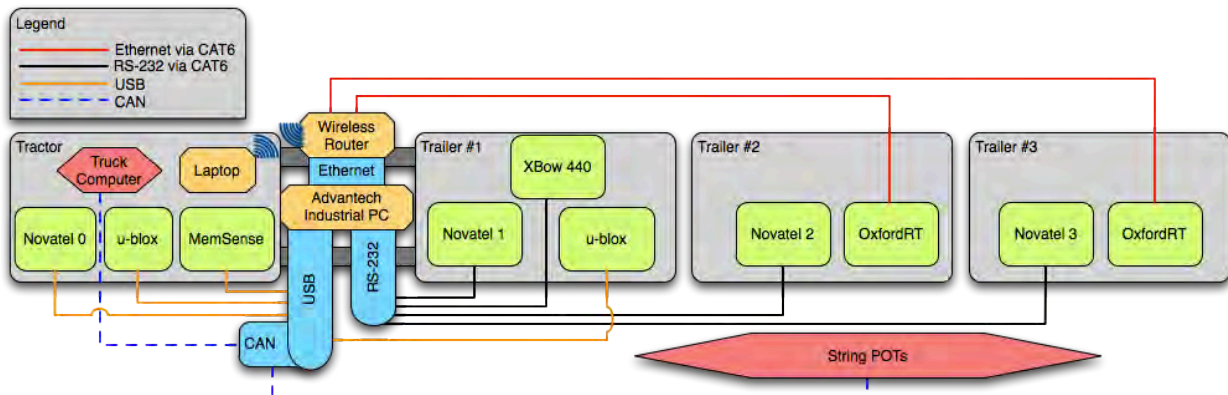


Figure 4-7. Diagram. Connections between the sensors and the data acquisition system.

The Mission Oriented Operating Suite (MOOS) serves as the middleware to communicate all of the sensor data. The MOOS middleware uses a client-server architecture with a centralized database and provides basic tools for Inter-Process Communication via sockets. This allows for viewing the raw data in real time, and logging the data in a standard format. Each sensor had a corresponding process running that would interface with that sensor, format its data, and publish it as separate channels to the MOOS database. The MOOS database holds the latest value from each channel on each sensor and allows other processes to access this data; the structure is shown in Figure 4-8.

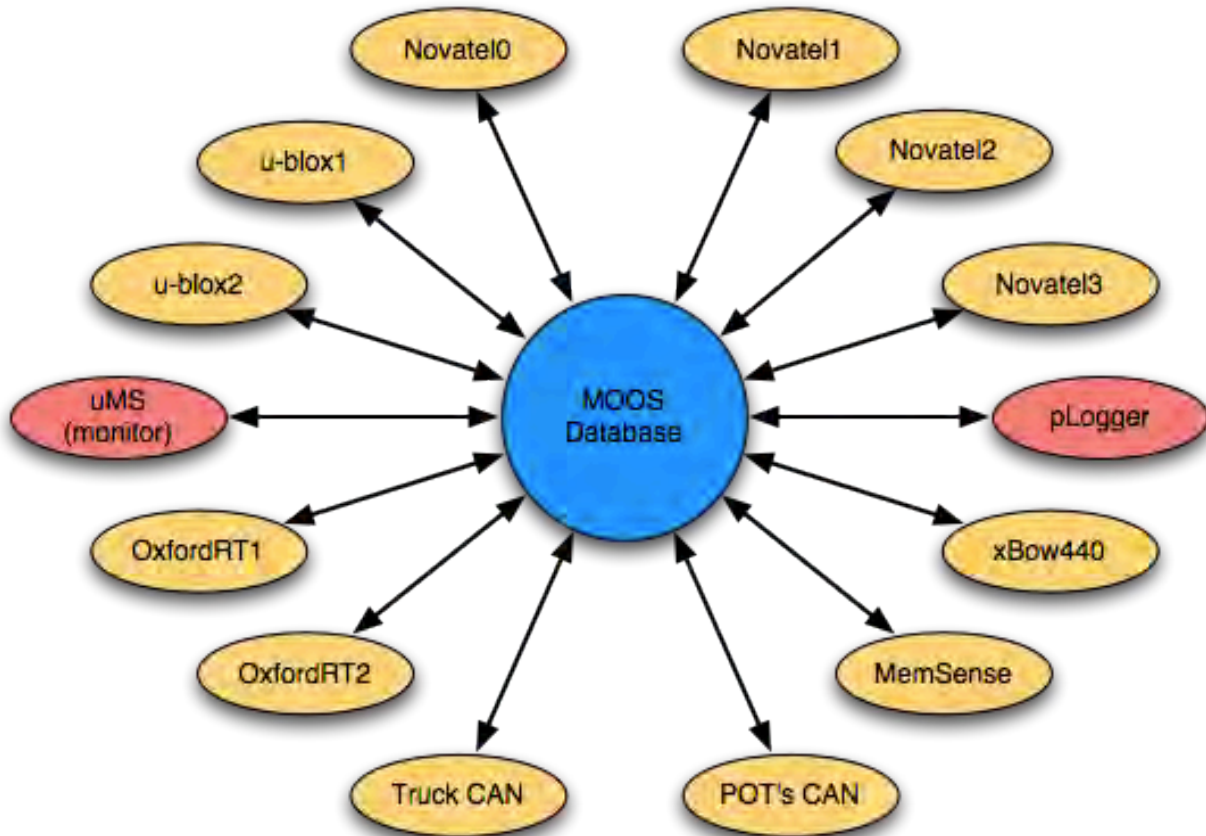


Figure 4-8. Diagram. Signals from all sensors were acquired and stored in a central database.

The MOOS application pLogger was used to log all of the channels. This was done in an asynchronous file format, meaning that the data was recorded whenever it was posted to the database by the sensor. This was done for two reasons: to accurately time-stamp the measurements, and also to accommodate multiple data rates while reducing the workload of the computer. This creates a more accurate time stamp because the measurement is recorded at the time it is posted by the sensor; there is no delay in waiting to get a full message set from all sensors prior to recording. Asynchronous recording enables the system to handle multiple data rates efficiently because the computer is not having to allocate any process power to synchronizing the file. An example of an asynchronous file is shown in Figure 4-9, with the first

column being the time stamp, the second being the physical measurement, the third being the sensor from which the measurement came, and the last being the actual measurement.

2212	1.16	zAngularRateZ_38	gOXTS-RT	0.0006
2213	1.16	zAngularRateY_38	gOXTS-RT	-0.0011
2214	1.16	zAngularRateX_38	gOXTS-RT	0.0023
2215	1.16	zAccelZ_38	gOXTS-RT	0.1471
2216	1.16	zAccelY_38	gOXTS-RT	9.8181
2217	1.16	zAccelX_38	gOXTS-RT	-0.101
2218	1.16	zTime_38	gOXTS-RT	-25.106
2219	1.161	POTS_CAN_613_1	gTruckCanSuspensionPots_pots	43
2220	1.161	POTS_CAN_622_2	gTruckCanSuspensionPots_pots	265
2221	1.161	POTS_CAN_612_1	gTruckCanSuspensionPots_pots	170
2222	1.161	POTS_CAN_621_2	gTruckCanSuspensionPots_pots	204
2223	1.161	POTS_CAN_611_1	gTruckCanSuspensionPots_pots	375
2224	1.161	POTS_CAN_610_1	gTruckCanSuspensionPots_pots	43
2225	1.161	POTS_CAN_620_2	gTruckCanSuspensionPots_pots	265
2226	1.161	POTS_CAN_630_3	gTruckCanSuspensionPots_pots	839
2227	1.162	zGPSSeconds_gNovate12	gNovate12	25618140
2228	1.162	zGPSWeek_gNovate12	gNovate12	163
2229	1.162	zHgtStdDev_gNovate12	gNovate12	4.6626
2230	1.162	zLongStdDev_gNovate12	gNovate12	2.4053
2231	1.162	zLatStdDev_gNovate12	gNovate12	1.6299
2232	1.162	zHeight_gNovate12	gNovate12	185.4075
2233	1.162	zLong_gNovate12	gNovate12	-85.2961
2234	1.162	zLat_gNovate12	gNovate12	32.598
2235	1.162	zSampleTimer_gMemSense	gMemSense	16931
2236	1.162	zMagZ_gMemSense	gMemSense	-0.7923

Figure 4-9. Screen shot. An example of an asynchronous file.

Special-purpose circuits were built to power the string pots, convert their output to digital signals, and transmit the signals to the computer via controller area network (CAN). A total of six CAN boxes were created, each containing the analog-to-digital (A/D) converter and circuit board. One can be seen in Figure 4-10. Three of these boxes were mounted on the tractor, and one each near the axle on each of the semitrailers. Each box conditioned the signal from three, four, or six string pots.



Figure 4-10. Photo. Special-purpose signal conditioning circuits for the string pots communicated with the computer via CAN.

String pots were connected to the CAN boxes via custom cables with DB25 connectors. The cables carried excitation voltage, ground, and the measured signal. At a rate of 100 Hz, the microcontroller in one of the CAN boxes generated a trigger signal to command all CAN boxes, including itself, to sample the string pots and report the measurements to the main computer. In addition, each CAN box sent a status message at 1 Hz. The message set for the string pot CAN bus is presented in Figure 4-11.

POTS_CAN_XXX_X	
	0-5 Channel Number on CAN Box
1-6	CAN Box Number
1:Left Side Steer Axle	
2:Right Side Steer Axle	
3:Drive Axle	
4:Trailer 1 Ride Axle	
5:Trailer 2 Ride Axle	
6:Trailer 3 Ride Axle	
6/7 6:Measurement	
7:Status	

Figure 4-11. Table. CAN Message Structure.

4.3 Hardware Installation

The IMU sensors were mounted as close as possible to the center of gravity (CG) of each unit so that they would report the motion of the CG. Trailer mounted instruments were in modified toolboxes mounted between the frame rails, as in Figure 4-12.



Figure 4-12. Photo. These views, looking backward under Trailer 2, show the location of toolbox in which the sensors were mounted (left) and the inside of the toolbox (right).

The only sensors that were not in the toolboxes were the string pots. They had to be mounted linearly with the axle measurement being recorded. The string pot in the left photo in Figure 4-13 was one of a pair measuring the change in steer angle of the rear axle of a trailer. The string pot in the right photo in Figure 4-13 was one of a pair measuring the roll angle between the frame and the axle of the same axle. Information from these two pairs of string pots was used to determine the roll steer characteristics of the trailer axles. The frame for mounting string pots was constructed of aluminum extrusions, which allowed for adjustability and reproducibility when fabricating all of the mounting brackets for the string pots.



Figure 4-13. Photo. String Pots measured deflection of the suspension. The red lines in the photos indicate the locations of the two ends of the wire from the string pots.

The string pots for dolly articulation were mounted such that the wire ran out of the string pot, through a pulley, and then to a hole that had been drilled into the front cross member of the trailer. This was done to allow the wire of the string pot to travel as closely as possible to tangent with the arc of the tongue of the trailer to give the most accurate measurement; this is illustrated in Figure 4-14.

Steering input was also measured with a string pot. The string pot was mounted on a bracket fixed to the tractor frame, and the string wrapped around a plywood wheel mounted to the steering column, as shown in Figure 4-15. The diameter of the wheel was selected to provide the necessary resolution.

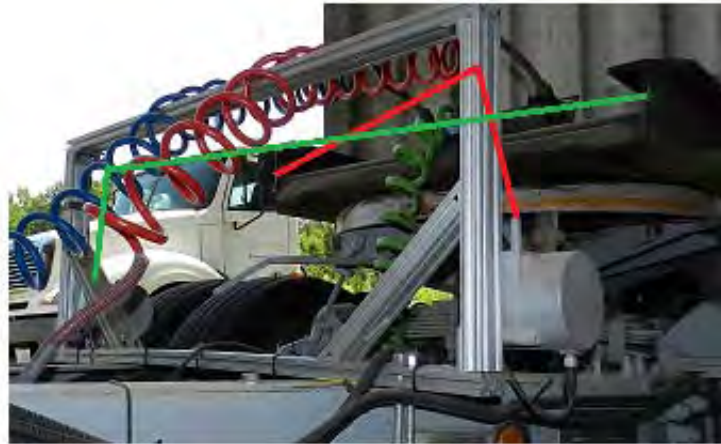


Figure 4-14. Photo. Dolly-to-trailer articulation angle was measured with a pair of string pots.

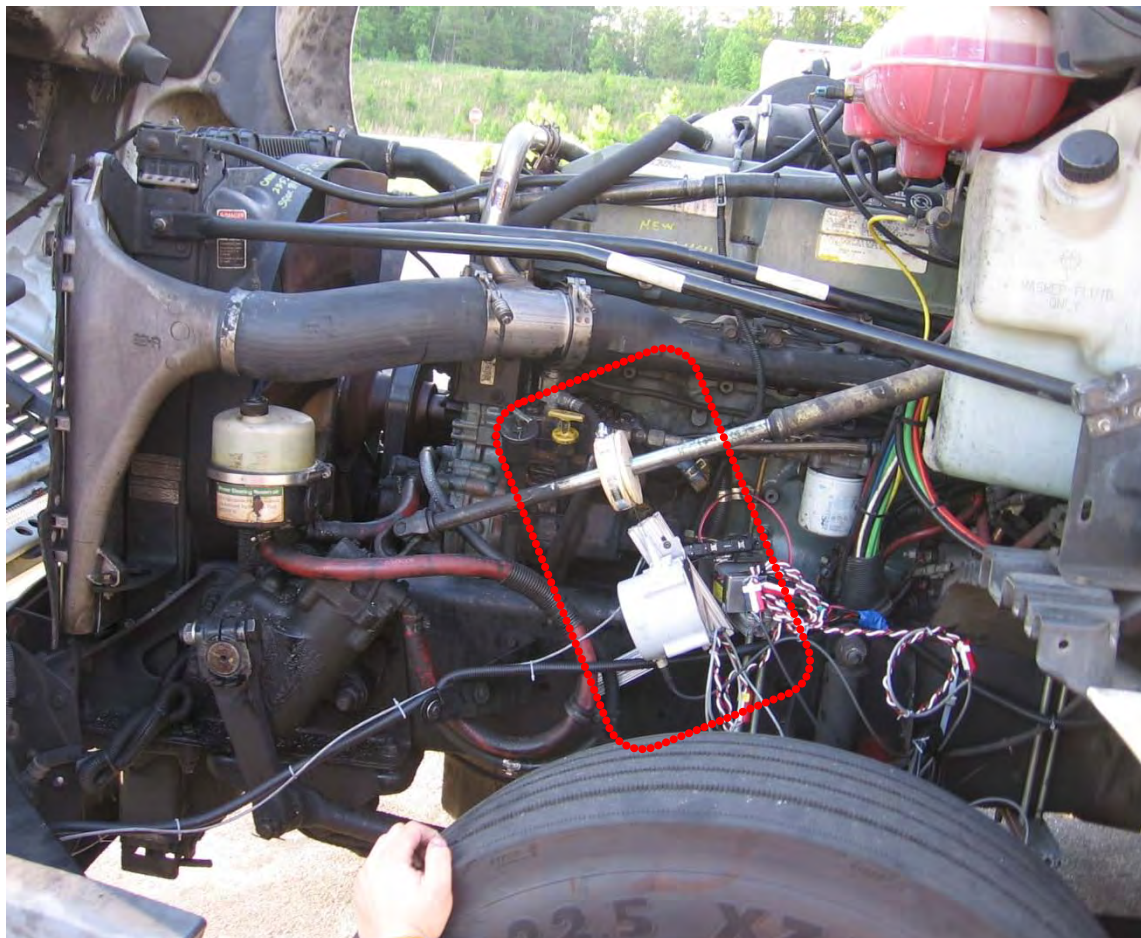


Figure 4-15. Photo. Steering input was measured via a string potentiometer with a string wrapped around a plywood wheel on the steering shaft.

4.4 Test Week

This section chronologically lists the events of the days when the team was at the track for data collection. The test plan (Appendix A) that was developed before the tests, called for a double lane change, a single lane change, constant radius turning, a gradual lane change, and an impulse steer. Along with those maneuvers, the test vehicle was also to be driven on a section of a nearby highway.

Monday

The first steps of the test plan explicitly provided for gentle preliminary maneuvers to proceed incrementally and safely to the test conditions. Gate spacing was adjusted, and the maximum speeds were established. Researchers in a chase car observed the roll behavior of the third trailer during the single and double lane changes. The limit of testing was established when the roll angles and roll rates appeared to be approaching the limit of stability but when the rear tires were still on the pavement. The actual gate spacing used and the maximum speeds of each maneuver are in Table 4-2. Diagrams of the actual gate spacing are Figure 4-16 through Figure 4-18.

Table 4-2. Actual test conditions.

Maneuver	Gate Spacing	Test Speeds
Gradual Lane Change	122 m (400 ft) Figure 4-16	32, 40, 48, 56, 64, 72 km/h (20, 25, 30, 35, 40, 45 mph)
Single Lane Change	61 m (200 ft) Figure 4-17	32, 40, 48, 56, 64 km/h (20, 25, 30, 35, 40 mph)
Double Lane Change	61 m (200 ft) Figure 4-18	32, 40, 48, 56 km/h* (20, 25, 30, 35 mph)
Constant-radius Cornering	--	72 km/h (45 mph)
Impulse Steer	--	32 km/h (20 mph)

* One test of the double lane change at 64 km/h (40 mph) was run.

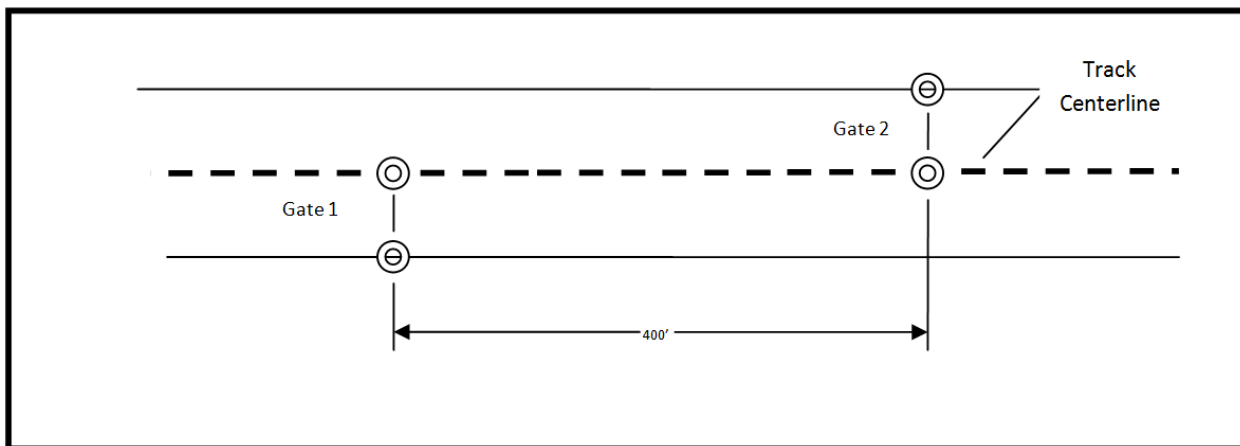


Figure 4-16. Diagram. Actual gate layout for the gradual lane change maneuver

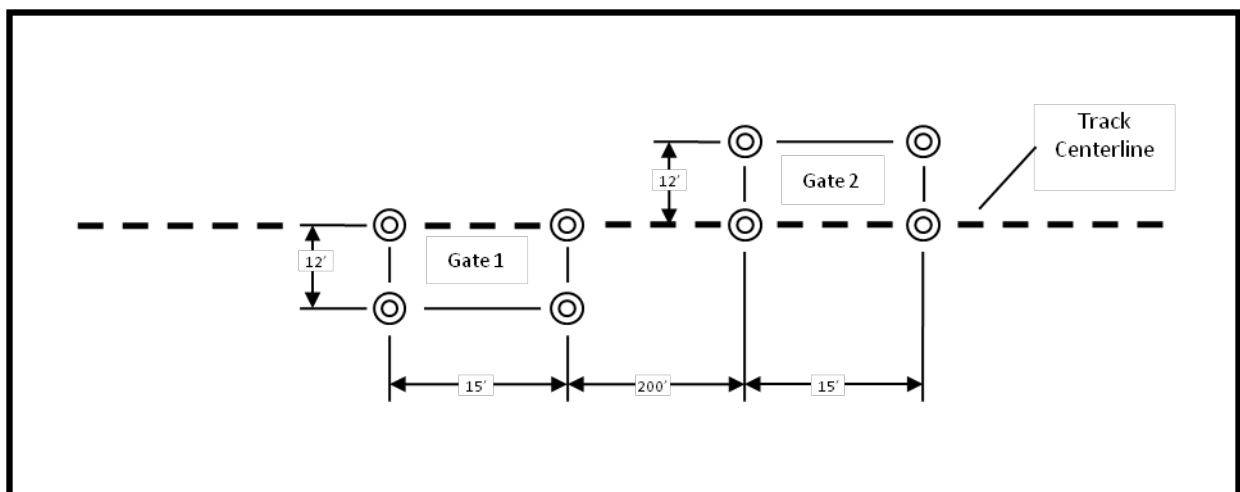


Figure 4-17. Diagram. Actual gate layout for the single lane change maneuver.

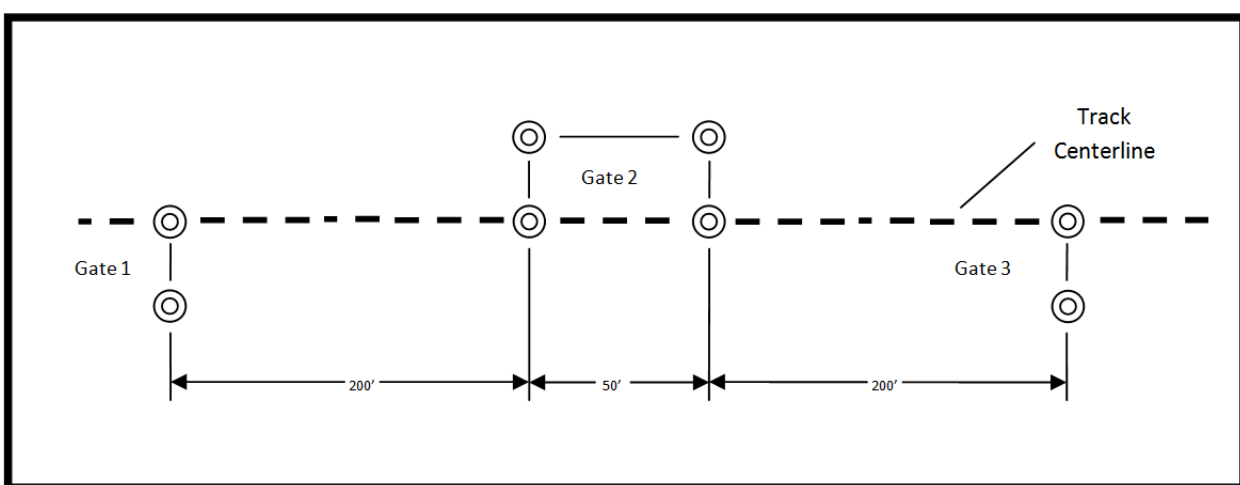


Figure 4-18. Diagram. Actual gate layout for the double lane change maneuver.

Tuesday

Work on the second day focused on calibration of the string pots. The test vehicle was driven through two gradual turns, one to the left and one to the right. After every five degrees of articulation in the dolly, the vehicle was stopped and static data was taken.

The non-synchronous data collection from the CAN bus was tested with a signal generator to measure the degree to which the analog channels were read simultaneously and to verify that the data rate remained consistent. A 1 MHz triangle wave from a signal generator was input, as simulated string pot signals, in two different CAN boxes. When data was sampled at a nominal rate of 100 Hz, even though there was some variation in the time between samples, all channels were recorded with the same time stamp. The recorded signals remained entirely in phase over an extended period, indicating that they were indeed recorded at the time interval indicated by the time stamp. If any time delay was present between the measurements on the separate channels, it was well below the 100 Hz nominal measurement rate.

Wednesday

The on-track maneuvers were completed on Wednesday. Testing began with several runs of single and double lane changes at a slower speed of only 32 km/h (20 mph). The speed was raised in increments of 8 km/h (5 mph) up to the maximum test speeds listed in Table 4-2.

Impulse steer maneuvers were also attempted on Wednesday. The driver quickly turned the hand wheel a quarter turn while driving at 32 km/h (20 mph). The driver had difficulty controlling the vehicle after this input, and the maneuver was not repeated.

Thursday

The first task for Thursday was the final calibration of the string pots and finishing the on-track maneuvers.

The on-highway portion of the testing was conducted according to the plan in Section 3.4. The route was approximately 4 miles down and back on US 280, a four-lane divided road with cross traffic controlled by stop signs, as shown in Figure 3-4. The route from the NCAT track to the highway was along a series of county roads, some of which were unpaved. The test vehicle negotiated the two-lane roads, the intersections, and a grade crossing without incident.

LCV triples are not ordinarily allowed on public roads in Alabama. A permit was obtained from the Alabama Department of Transportation for the on-highway test, and local authorities were notified. NCAT provided two pilot vehicles equipped with the required safety equipment to lead and follow the test vehicle.

4.5 Post Processing

Following the test track and highway maneuvers, the data was downloaded from the collection system and cleansed for distribution to the analysts. This process consisted of four steps:

(1) data handling, (2) data formatting, which included dividing the data runs into singular maneuvers, identifying the maneuver, performing coordinate transformations & unit conversions, and quality checks, (3) real-time kinematic (RTK) corrections, and (4) data release.

4.5.1 Data Handling

The computer that was mounted on the test vehicle recorded every run and stored the data internally. Data was copied daily to a separate storage device for backup. Following the test week, all of the data was then downloaded from the vehicle computer to a more powerful computer for the post-process work. A backup copy was left on the vehicle computer.

4.5.2 Data Formatting

Data recording was more efficient when the recorder ran continuously as the vehicle went around the track, with maneuvers on both the north and south straight segments. Data for each maneuver on the straight or curve was extracted from the larger file following the tests. This was accomplished by defining zones around the track using known GPS coordinates for the track, as shown in Figure 4-19.

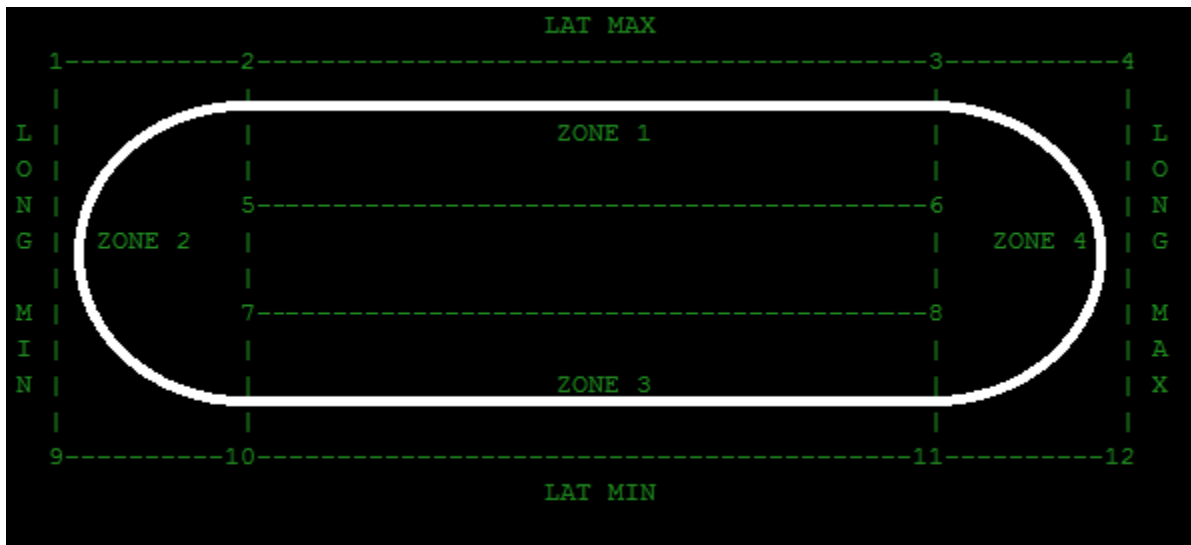


Figure 4-19. Diagram. Zones for separating data recorded on the curves from data recorded on the straights.

A program was written in MATLAB to step through the large files line-by-line to determine the zone, and then to write all of the corresponding data for each zone to a new file. This program was also run against the individual recordings to ensure that all of the files representing a certain maneuver started and stopped at the same geographic point. The speed and maneuver were coded in the individual file names. An example is: “NTRCI_35mph_Dbl_Ln_Chng_R2,” which corresponds to the second running of a 56 km/h (35 mph) double lane change.

The next step was to transform coordinate and convert to engineering units. The analysts chose to use the International Organization for Standards (ISO) vehicle coordinate system with the positive z direction up, as indicated in Figure 4-20.

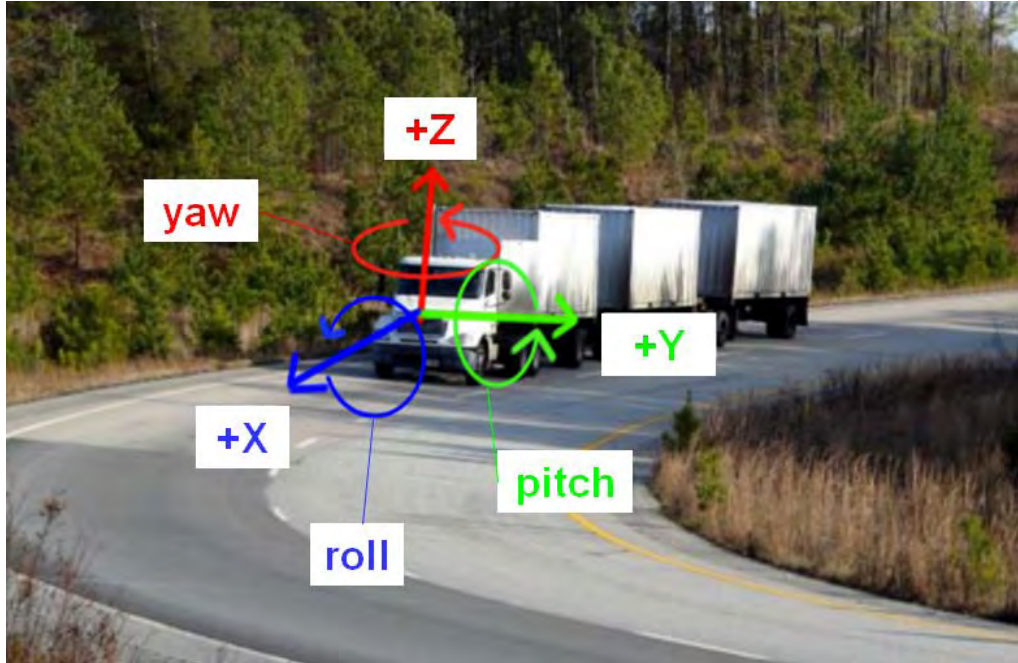


Figure 4-20. Photo. Analysts used the ISO coordinate system, with Y to the left and Z up.

Another Matlab program was written to bring in the data from specific runs and create an overlay plot so that the accelerations of the tractor and three trailers could be compared. Figure 4-21 is the specific case of angular rate about the z-axis in a double lane change. The four IMUs are listed in their order from front to rear in the combination vehicle. The upper graph is the raw data prior to the coordinate transformation, and the lower graph is after the transformation. The lower graph shows the four units of the vehicle yawing in their proper sequence. The data shown is after a 3 Hz low pass Butterworth filter had been applied.

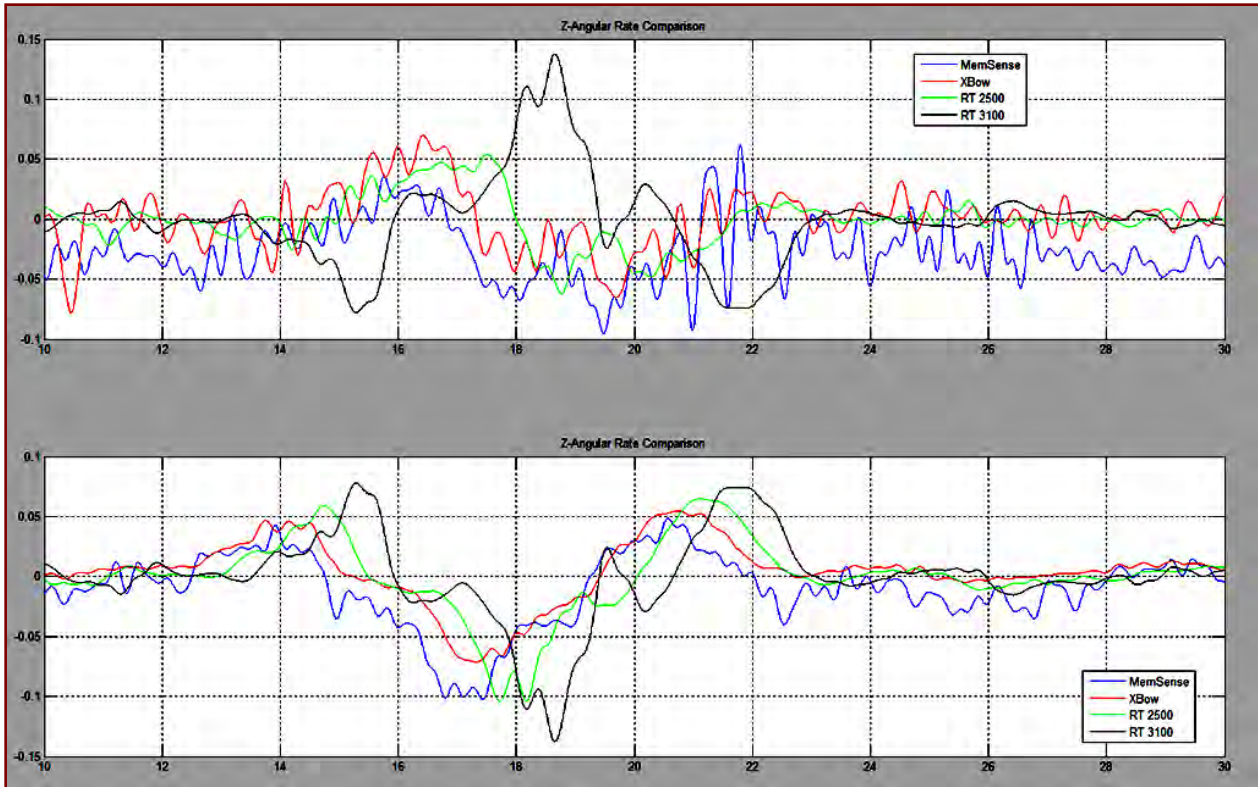


Figure 4-21. Graph. Angular Rate Comparison

After the necessary transforms were confirmed, a program was written in Python to iterate through each file automatically and perform the rotations on the desired channels. The program also converted the latitude and longitude coordinates to Universal Transverse Mercator (UTM) coordinates. This gave the analysts a set of data on the rectilinear positioning of the tractor and trailers relative to an origin point close to the track. This simplified visualization of the data.

4.5.3 RTK Corrections

In order to obtain global positioning coordinates, two GPS receivers were placed on each of the units in the combination. Novatel GPS receivers were on each of the units, while the lower cost alternatives, the u-blox GPS receivers, were on the tractor and first trailer. The second and third trailer both carried an Oxford RT unit, but they were not functioning.

The accuracy of the standard GPS positions that the receivers report is usually on the order of 1 or 2 meters (3 to 6 ft). This error comes from several factors, including atmospheric conditions, which is the largest contributor, as well as satellite and receiver clock biases, and noise in the measurements inside the GPS receiver. As the satellite's signal propagates through the ionosphere and troposphere that surround the Earth, the electron dispersion and humidity can affect the GPS signal.

When several GPS receivers are operating within close proximity (several kilometers), these signal errors become highly correlated. Differential GPS (DGPS) techniques take advantage of this fact and compensate for the correlated errors. DGPS methods can use the pseudorange, the carrier noise measurement, or a combination of both, as explained in Appendix B. RTK systems can take a precise carrier phase measurement and calculate global positions that are equally precise. The RTK system at NCAT uses a static base station with known coordinates near the track and compares its GPS measurements to those of a roving GPS receiver in close proximity.

4.5.4 Data Release

The last step before distribution was a quality check to be performed by Auburn. This was accomplished in parallel with the rotations and conversions. Many data sets were inspected to ensure that the rotations were correct. Throughout that process the data was put through a 3 Hz low-pass Butterworth filter. This enabled Auburn to look at all of the channels for numerous runs to eliminate any major recurring issues in the data. After the data passed this test, it was ready to be distributed to the team for analysis. When the data was downloaded from the PC after the test week, there was 8.2 GB of data; when the data was released to the team, the data to be analyzed was slightly over 32 GB.

The plan for testing identified more than 200 channels to be recorded. A number of experimental challenges encountered in the field caused sensor malfunctions, unexpected noise, and data collection losses, as was indicated in Table 4-1. After the data had been cleansed, checked, and verified, sufficient channels remained to permit limited analysis of the understeer characteristics, offtracking, and rearward amplification. These analyses will be presented in the next three chapters.

This page intentionally left blank.

Chapter 5 – Analysis of the Test Track Data

Understeer characteristics, body roll behavior relative to the axles, and axle steer were examined in the experimental data. Each of these parameters was comparatively analyzed to better understand the amplification trends between units of the LCV train.

5.1 Understeer Characteristics of Units in the LCV

The understeer gradient assesses the ability of the LCV to follow a path defined by the steer angle of the steer axle tires (road wheel angle). If the road wheel angle required is greater than the theoretical or Ackerman angle, the vehicle is said to have understeer. If the road wheel angle required to follow a prescribed radius is less than the Ackerman steer angle, the vehicle is said to have oversteer. The analysis was performed on data collected as the test vehicle passed the curve at the east end of the test track, as shown by GPS data in Figure 5-1.

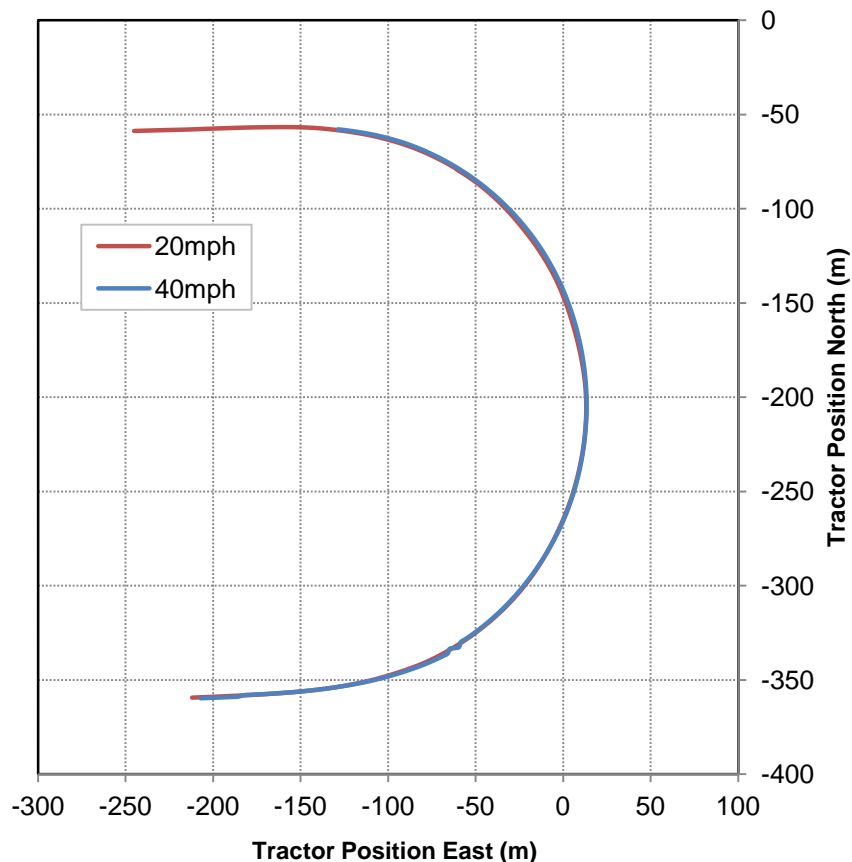


Figure 5-1. Graph. Tractor position north and east for 32 km/h (20 mph) and 64 km/h (40 mph).

5.1.1 Understeer Theory

The “ideal” or Ackerman road wheel angle is as shown in Figure 5-2.

$$\delta = \text{atan}\left(\frac{L}{R}\right) \times \frac{360}{2\pi}$$

Figure 5-2. Equation. Ackerman road wheel angle (deg).

where

- δ = required road wheel angle in degrees,
- L = tractor wheel base length (steer axle to drive axle centerline)
- R = turn radius.

The radius of the curve is usually hundreds of times the length of the vehicle. The angle and its tangent are nearly identical, so the inverse tangent function in oversteer equations is typically omitted for simplicity.

A number of vehicle properties and operational characteristics can cause deviation from this ideal behavior. The understeer adds, or oversteer subtracts, from the required Ackerman road wheel angle, as shown in Figure 5-3. A vehicle with a positive gradient is said to have an understeer condition, and a vehicle with a negative gradient, oversteer. Typically the steer gradient (K) is defined in degrees of steer per unit of lateral acceleration where (a_y) is in gravitational units (g) experienced.

$$\delta = \left(\left(\frac{L}{R} \right) \times 57.3 \right) + K \frac{v^2}{Rg}$$

Figure 5-3. Equation. Ackerman steer plus the understeer gradient.

where

- $\frac{v^2}{Rg}$ = lateral acceleration a_y
- K = understeer gradient (deg/g).

To evaluate the understeer gradient (K), Figure 5-4, data was collected at a variety of speeds in the constant-radius curves of the test track. The curves are banked at 8 deg with a radius of nominally 145 m (476 ft). The actual path radius was obtained from the tractor- and trailer-mounted NOVATEL GPS systems.

$$K = \left(\delta - \left(\frac{L}{R} \right) \times 57.3 \right) \frac{1}{a_y}$$

Figure 5-4. Equation. Understeer gradient from measured data.

5.1.2 Determining the Steer Characteristics of the Tractor

The method used to determine the understeer gradient was to first determine the required Ackerman road wheel steer angle for the constant radius portion of the turn. The turn radius was established using the GPS data for the North position and East position, which was then resolved to a relative position on the track. The continuum of these positions on the track established the turn radius.

The LCV was instrumented with GPS on the tractor and each of the trailers. String potentiometers between the dollies and the trailers provided articulation angle measurement. String potentiometers were also connected to the left and right steer arms of the steer axle to record road wheel angle. For understeer testing, the vehicle recording system recorded data throughout the banked constant radius turns at the East and West ends of the test track.

As indicated in Figure 5-1 the heading directions, East and North, were combined to obtain the radius of the arc in the constant radius maneuver. The path of the vehicles matched this radius very closely. This was verified using a least-squares circular fitting algorithm from the NIST Algorithm Testing System (Shakarji 1998).

Figure 5-5 presents one example of the road wheel angle as the test vehicle drove through the entry spiral, the constant-radius portion, and the exit spiral. To establish the constant radius section, the horizontal asymptote of the collected steer angle was determined to represent the constant radius turn. The blue-colored center section of the plot of Figure 5-5 represents the segment of the turn with the constant radius and nearly constant steer angle.

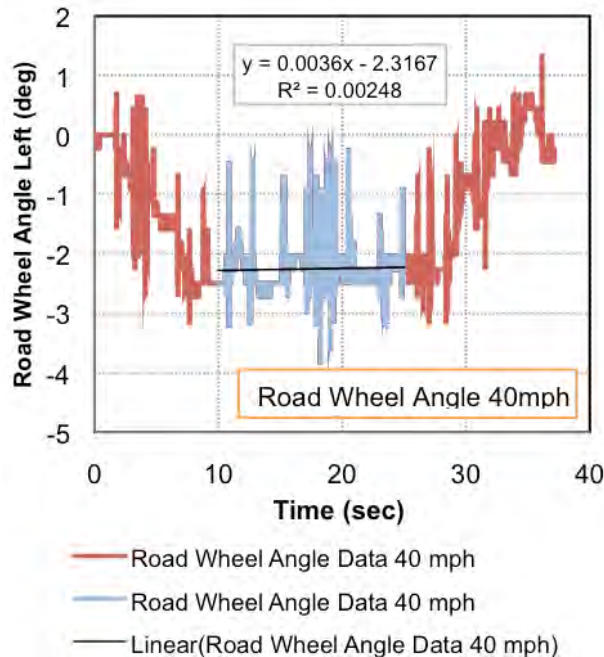


Figure 5-5. Graph. Constant road wheel angle in a curve.

The left road wheel angle was one of the recorded data channels with angles at 32 km/h (20 mph) shown in Figure 5-6 and at 64 km/h (40 mph) shown in Figure 5-7. The center, shaded portion, of the plots is where the measured data was taken as it represented the driver's best effort to maintain constant hand wheel angle. Linear regressions were performed in this region of the plots to determine the average road wheel angle, which represents the road wheel angle necessary to maintain the constant radius turn at each speed. At the lower velocities (Figure 5-6), the driver input to maintain the radius is regular and somewhat periodic, while at the higher velocities (Figure 5-7), the driver corrections are more "as necessary" pulses to the steer input.

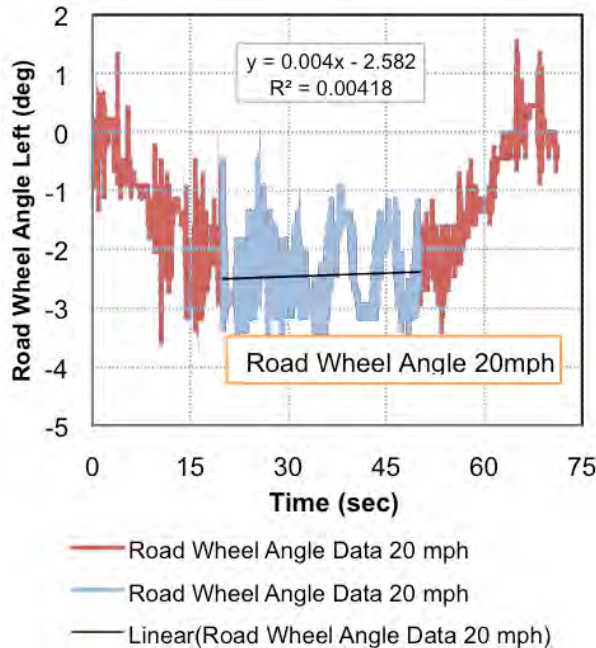


Figure 5-6. Graph. Road wheel angle at 32 km/h (20 mph).

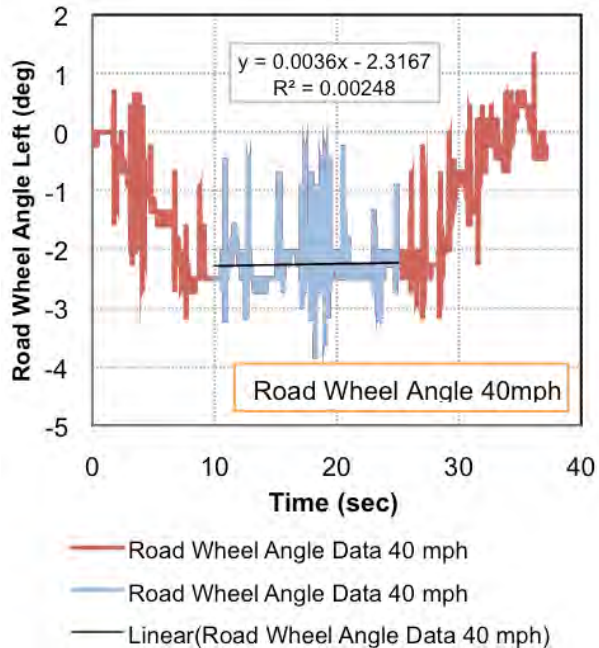


Figure 5-7. Graph. Road wheel angle at 64 km/h (40 mph).

Analysis of the tractor steer in the constant radius turn is presented in Table 5-1. The understeer gradient for the vehicle, based on velocity in the constant radius portion of the turn, is presented in Figure 5-8. Figure 5-9 presents the banking corrected understeer gradient, which is the calculated lateral acceleration minus the component of gravitational acceleration due to the banking acting in the same plane. Figure 5-8 and Figure 5-9 show that the "knee" in the curve occurs at approximately the same point at which the velocity-based lateral acceleration is balanced against the banking-induced gravitational acceleration. The change in slope is potentially a result of the Trailer 1 lateral acceleration vector acting on the tractor, producing either an outward or inward force at the kingpin. The force changing direction at 0.139 g is equivalent to 8 deg banking ($\sin 8^\circ = 0.139$), which in turn changes the slope of the steer gradient. This finding is an observation of only six discrete velocities, and the smoothness of this transition may be different than indicated by the plots. Slight deviations from the calculated knee value were observed, which could be a result of the relatively coarse sampling and noise in the data.

Table 5-1. Tractor understeer gradient analysis.

Speed		Steer input			Calculated and measured turn radius				Calculated steer angle		Acceleration and gradients				
Vehicle Speed (Mph)	Vehicle Speed (Km/h)	Measured road wheel angle inner (deg)	Calculated road wheel angle outer (deg)	Nominal Road wheel angle (deg)	Calculated hand wheel angle (deg)	Calculated "ideal" inner wheel turn radius (m)	Calculated "ideal" outer wheel turn radius (m)	Average radius (m - calculated)	Actual measured Radius (m)	"Ideal" road wheel angle for radius (deg)	Under/Over steer (deg)	Calculated lateral accel (g)	Calculated banking corrected lateral acceleration (g)	Measured lateral acceleration (g) (without roll correction)	Understeer gradient (deg/g)
20	32	2.39	2.35	2.37	48.1	114.3	116.3	115.3	146.3	2.00	0.37	0.056	0.083	0.032	6.66
25	40	2.48	2.43	2.46	49.8	110.2	112.2	111.2	146.5	1.99	0.46	0.087	0.052	0.009	5.30
30	48	2.30	2.26	2.28	46.3	118.7	120.7	119.7	147.0	1.99	0.29	0.125	0.014	0.040	2.33
35	56	2.39	2.35	2.37	48.1	114.1	116.1	115.1	146.5	1.99	0.38	0.170	0.031	0.072	2.21
40	64	2.33	2.29	2.31	47.0	117.0	119.0	118.0	146.6	1.99	0.32	0.222	0.083	0.153	1.44
45	72	2.34	2.30	2.32	47.2	116.5	118.5	117.5	146.1	2.00	0.32	0.282	0.143	0.200	1.14

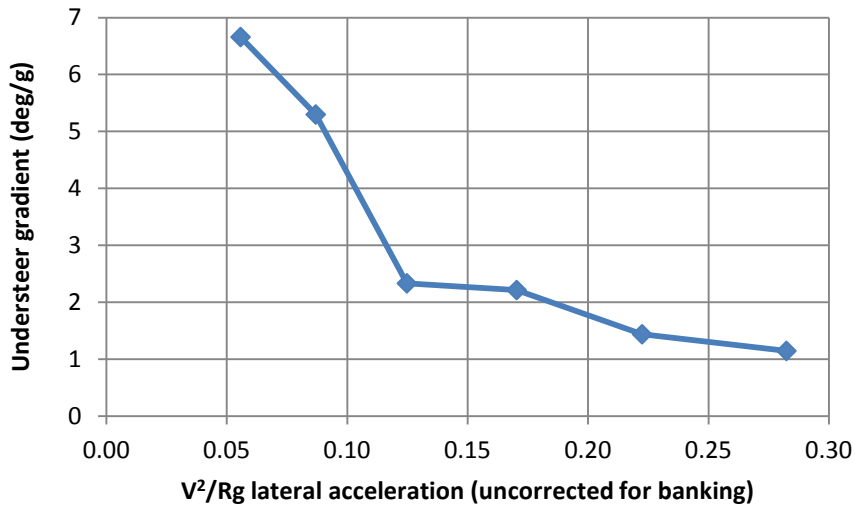


Figure 5-8. Graph. Tractor lateral acceleration vs. understeer gradient (uncorrected for banking).

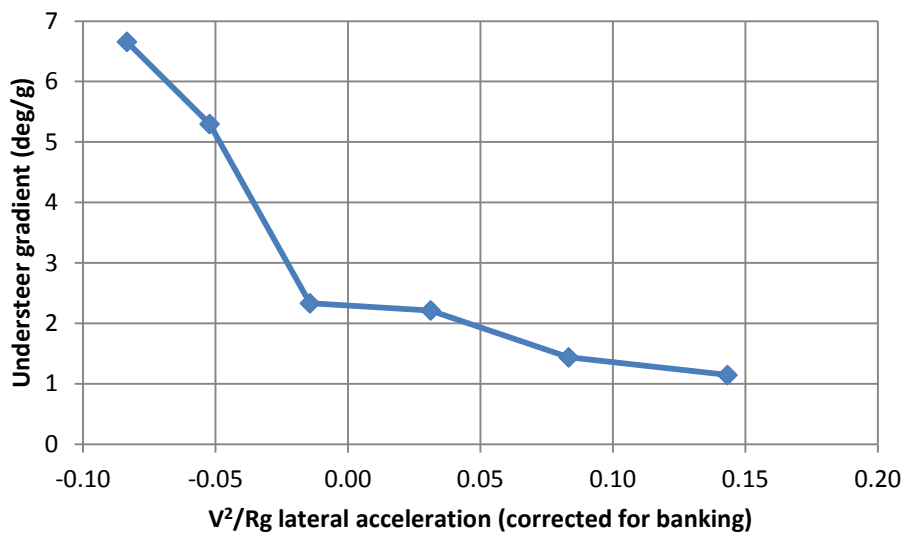


Figure 5-9. Graph. Tractor lateral acceleration vs. understeer gradient (corrected for banking).

5.1.3 Determining the Steer Characteristics of the Trailers and Dollies

The steer characteristics of the trailers are governed by the same equations as those of the tractor. The only difference is that the steer angle δ is not the average road wheel angle but is the articulation angle between the dolly and the semitrailer that it pulls.

By treating the tractor angular orientation to the trailer as the steer input to the trailer, the Ackerman steer angle between the tractor and the trailer is represented by the articulation angle. The steer angle of Trailer 2 can be determined by the Ackermann angle between the first dolly and Trailer 2, and determined similarly for Dolly 2 and Trailer 3.

The steer characteristics of the first trailer could not be analyzed because the data was inadequate.

Table 5-2 presents the dimensional characteristics of Trailer 2. Table 5-3 presents the calculated lateral acceleration and the calculated understeer based on measured vehicle speed, articulation angle, and the trailer's turning radius at the location of the GPS system, which was approximately at the X-Y location of the CG. Table 5-4 and Table 5-5 present similar data for Trailer 3.

Dolly 2 had an 8.3% narrower track than Dolly 1, which resulted in a 17% lower axle roll stiffness contribution from the dolly tires for Dolly 2. This would contribute to potentially greater roll angle for Trailer 3; however, because the dollies' fifth wheels are mounted to a pair of transverse frame-mounted leaf spring with equivalent nominal roll stiffness values for the two dollies, the reduction in roll stiffness at Dolly 1 is less than the 17% predicted by the reduction in axle roll stiffness alone.

Table 5-2. Trailer 2 fundamental mechanical dimensions.

Mechanical Measurement			Dolly 1		Trailer 2		
Trailer 1 Axle – Dolly 1 axle	127 7/8	in.	3248	mm	Dolly track (inner)	64.25	in.
Pintle to Dolly 1 axle	76	in.	1930	mm	Dolly Track (outer)	90 5/8	in.
Kingpin 2 – Trailer 2 axle	209 3/8	in.	5318	mm	Nominal track	77.4	in.
Bank angle	8	deg			Sin	8	= 0.1392

Table 5-3. Trailer 2 steer behavior in the constant radius maneuver.

Vehicle Speed (Mph)	Vehicle speed (Km/h)	Articulation angle and related wheelbase and track changes				Actual Radius @ cg (m)	Theoretical radius @ given articulation angle (m)	Ideal and measured articulation angles, Steer and steer gradients			
		Wheel base change (mm)	Track width change (mm)	Calculated Inner Wheel base (mm)	Calculated Outer Wheelbase (mm)			Measured articulation angle (deg)	"Ideal" articulation angle for radius (deg)	Understeer (deg)	Calculated lateral acceleration (g)
20	32	29.49	1.8	5289	5348	1965	146.00	177.2	1.72	2.09	-0.37
25	40	29.16	1.7	5289	5347	1965	146.12	179.2	1.70	2.08	-0.38
30	48	31.26	2.0	5287	5349	1965	145.60	167.1	1.82	2.09	-0.27
35	56	35.51	2.6	5283	5354	1964	145.64	147.1	2.07	2.09	-0.02
40	64	38.35	3.0	5280	5356	1964	145.66	136.2	2.24	2.09	0.15
45	72	44.03	4.0	5274	5362	1963	145.69	118.6	2.57	2.09	0.48

Table 5-4. Trailer 3 fundamental mechanical dimensions.

Mechanical Measurement				Dolly 2		Trailer 3	
Trailer 2 Axle – Dolly 2 axle	127 7/8	in.	3248	mm	Dolly track (inner)	58	in. 1473 mm
Pintle to Dolly 2 axle	76	in.	1930	mm	Dolly Track (outer)	84 5/8	in. 2149 mm
Kingpin 3 – Trailer 3 axle	209 1/4	in.	5315	mm	Nominal track	71.31	in. 1811 mm

Table 5-5. Trailer 3 steer behavior in the constant radius maneuver.

Speed		Articulation angle and related wheelbase and track changes				Turn radius		Ideal and measured articulation angles, Steer and steer gradients						
Vehicle Speed (Mph)	Vehicle speed (Km/h)	Wheel base change (mm)	Track width change (mm)	Calculated Inner Wheel base (mm)	Calculated Outer Wheelbase (mm)	Track width @ angle (mm)	Actual Radius @ cg (m)	Theoretical radius @ given articulation angle (m)	Measured articulation angle (deg)	Steer angle for radius (deg)	Understeer (deg)	Calculated lateral acceleration (g)	Banking corrected lateral acceleration (g)	Understeer gradient (deg/g)
20	32	26.04	1.5	5289	5341	1810	145.9	184.7	1.65	2.09	-0.44	0.06	-0.083	-7.85
25	40	22.66	1.1	5292	5338	1810	145.9	212.3	1.43	2.09	-0.65	0.09	-0.052	-7.47
30	48	25.37	1.4	5290	5340	1810	145.4	189.6	1.61	2.09	-0.49	0.13	-0.013	-3.87
35	56	23.13	1.2	5292	5338	1810	145.5	208.0	1.46	2.09	-0.63	0.17	0.032	-3.66
40	64	29.41	1.9	5286	5344	1809	145.7	163.5	1.86	2.09	-0.23	0.22	0.084	-1.01
45	72	38.59	3.3	5276	5354	1808	145.6	124.5	2.44	2.09	0.35	0.28	0.144	1.25

Presented in Figure 5-10 is the steer characteristic of Trailer 2 plotted as a function of banking corrected lateral acceleration for Dolly 1 and Trailer 2. Figure 5-10 presents the steer gradient for Trailer 2, while Figure 5-11 presents the steer gradient for Trailer 3. Noise in the instrumentation system, slight differences between trailers, and different dolly track widths (Dolly 1 = 1967 mm (77.44 in.), Dolly 2 = 1811 mm (71.30 in.)) are the most likely contributors to the subtle differences shown between the steer gradients in the constant radius maneuver for Trailer 2 and Trailer 3.

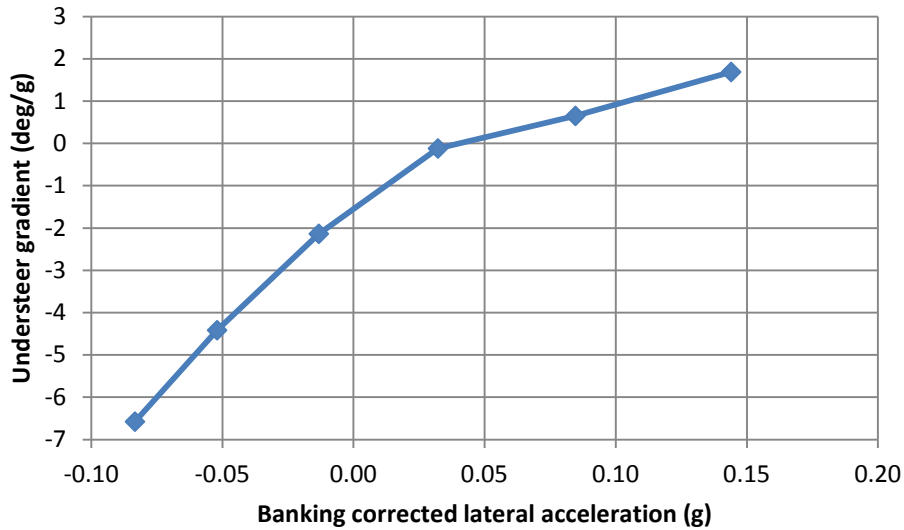


Figure 5-10. Graph. Trailer 2 understeer gradient as a function of banking corrected lateral acceleration.

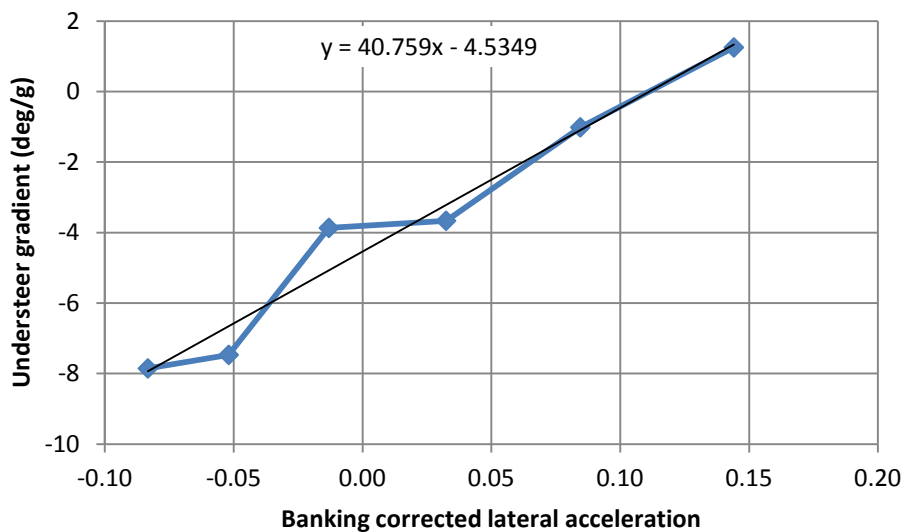


Figure 5-11. Graph. Trailer 3 understeer gradient vs. lateral acceleration.

5.1.4 Understeer Analysis Conclusions

In some ways the data challenged the analysts. The understeer behavior was analyzed in a banked constant radius portion of the track where nominal 8 degree banking was present. The nominal banking was established from track design blueprints and data sheets; however it was not specifically measured. The East and North heading directions obtained from the on-board GPS units were used successfully to obtain the radius that each separate unit of the LCV was following.

The resolution of the on-board GPS units was not precise enough to attain actual articulation angles. Where present, string potentiometer data was used to obtain articulation angles between the dolly and its attached trailer. It was not possible to accurately ascertain the articulation angle between the tractor and Trailer 1 and therefore the steady-state constant radius steer behavior of Trailer 1 was not attainable. It was possible to obtain the steer behavior of the tractor, the steer behavior of Dolly 1 and Trailer 2, and the steer behavior of Dolly 2 and Trailer 3.

The understeer gradient for the tractor was positive for all speeds tested. The gradient did decrease with increasing speed. The gradient also had a more rapid change in value while the lateral accelerations were negative (banking accelerations greater than centripetal accelerations) and a decreased slope once the velocity-based lateral accelerations overcame the slope-based acceleration. This analysis was performed with only six discrete speeds and the aforementioned slope change may be more continuous than is presented in the graphical plots.

The understeer gradients for Trailers 2 and 3 at low velocities were negative, implying oversteer, up to the approximate point where the velocity centripetal acceleration overcame the banking accelerations. This analysis combined the GPS-determined radius that the CG was following and the measured articulation angles. As noted above, Dolly 1 had a 1967 mm track width while Dolly 2 had an 1811 mm track width (8.3% narrower than Dolly 1). This implies that for all roll angles that were positive, understeer was present, whereas for roll angles that were negative, oversteer was present. This conclusion could imply that more of the steer was attributable to the dolly behavior than to the trailer axle and trailer axle tire slip angle behavior; however, more analysis is needed to verify this statement.

5.2 Rearward Amplification of the LCV

Rearward amplification is the tendency for each vehicle unit in the trailer train to exaggerate the yaw motions of the unit that precedes it during a maneuver. Therefore, rearward amplification is defined in terms of peak amplitude of the measured unit divided by the amplitude of the primary or lead unit in the train. In the case of the LCV, the lead unit is the tractor. A rearward amplification greater than one indicates that the following unit experiences a more pronounced response to the input vehicle in the train.

Fancher and Winkler (2007) found that rearward amplification is dependent upon a number of factors including trailer length, tire cornering stiffness, dolly configuration, speed, period of the

maneuver, and load characteristics. One goal of this research was to estimate the rearward amplification of the NCAT triple.

Rearward amplification is typically calculated for lateral acceleration and yaw velocity between the first and last units of a vehicle (ISO 2000). Rearward amplification can be calculated for any motion variable of interest. Rearward amplification was calculated for units' roll angle because roll angle was recorded during the track tests. The roll angles measured were relative roll angles between the body and the axle.

5.2.1 Double Lane Change Event Identification

Figure 5-12 is a plot of the hand wheel angle for the double lane change at 48 km/h (30 mph). The plot clearly indicates seven events in the maneuver, indicated by seven points on the graph. Point 1 is the start of the left steer input to lead the vehicle to the left lane. Point 2 is the maximum steer angle during the lane change. Point 3 shows the time at which the hand wheel angle returns back through zero. Point 4 is the maximum right steer to head the vehicle back to the original (travel) lane. At lower speeds the event had two distinct peaks, as shown in Figure 5-12, which occur due to the time in the left lane at lower speeds. Point 5 is the zero crossover of the left steer maneuver, which is made to restore the vehicle to its original path. Point 6 is the maximum road wheel angle achieved during the return maneuver. Point 7 is the correction to a zero hand wheel angle or a zero crossing. Points 1 to 3 and 5 to 7 correspond to left steer maneuvers. Events 3 to 5 correspond to the right steer maneuver.

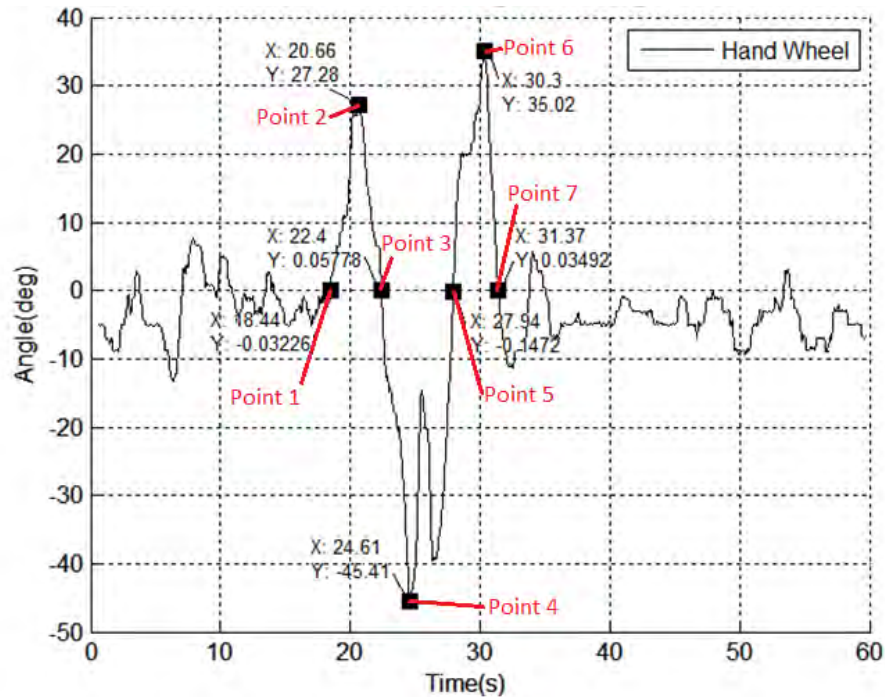


Figure 5-12. Graph. Identification of the seven points in the double lane change.

Filtered hand wheel angle, as shown in Figure 5-13, indicates the magnitude of the input and the time in the event at each of the seven critical comparison points.

Figure 5-14 presents the unfiltered roll angles obtained from string potentiometers mounted between the respective axles and their corresponding frames as measured at the steer, drive, and trailer axles at 64 km/h (40 mph). Plotted with these roll angles is the filtered hand wheel angle, also measured with a string potentiometer, at a ratio of 1/20 for plot scaling. Examination of the plotted response shows the direct response of the roll at the steer axle and the delayed response of the subsequent axles in the vehicle train to the steer input.

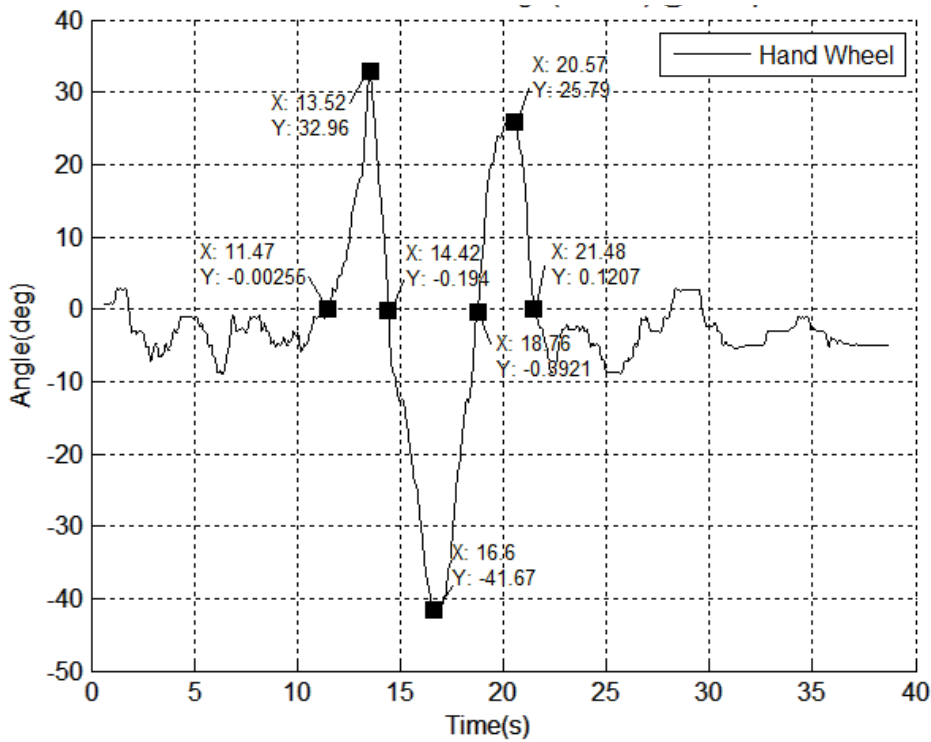


Figure 5-13. Graph. Filtered hand wheel angle at 64 km/h (40 mph).

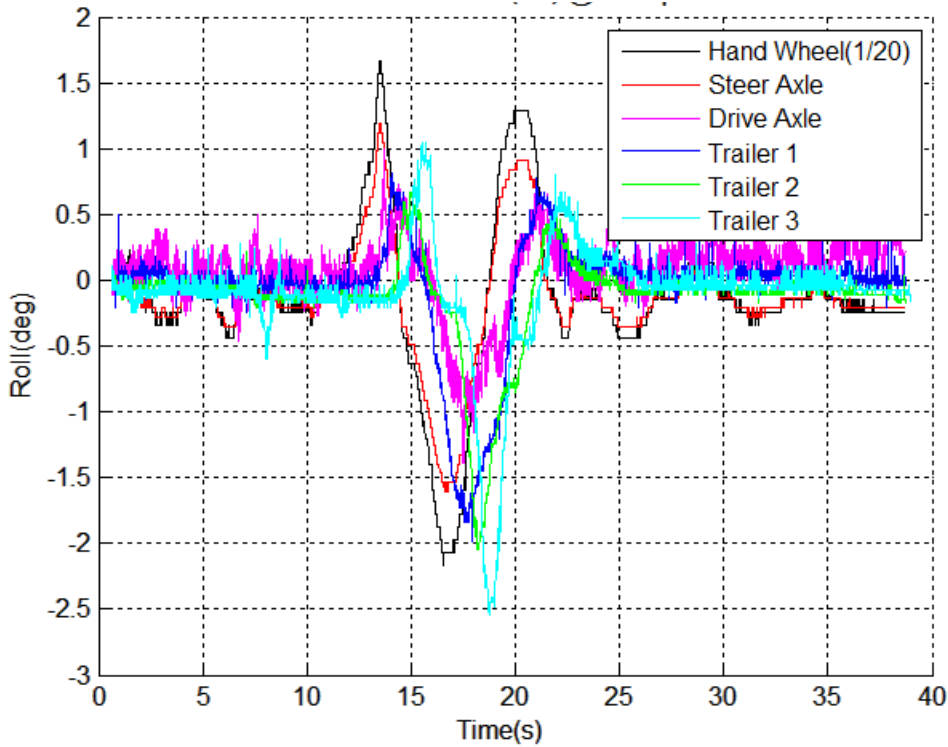


Figure 5-14. Graph. Unfiltered roll angles measured at separate axle positions at 64 km/h (40 mph).

A tenth order, low pass, Butterworth filter was designed and applied using Matlab with a cutoff frequency of 5 Hz. The 5 Hz cutoff frequency was necessary to remove noise in the string potentiometer data. This noise, even though filtered, could have influenced the results. The 5 Hz cutoff frequency was carefully evaluated in an effort to ascertain, and justify, the use of this filter. The only identified system from which data could be lost by the application of the 5 Hz cutoff was the unsprung mass natural frequencies of the tractor and trailer axles. These unsprung frequencies were calculated to approach a 13 Hz limit.

5.2.2 Roll Angle Response of Each Axle to Hand Wheel Input

The filtered roll angle response to the hand wheel input, as measured at the steer axle, is shown in Figure 5-15, with the response at the drive axle indicated in Figure 5-16. The near immediate response of the roll at the steer axle and the delay in the response at the drive axle in the figures is indicative of the torsional deflection of the tractor frame. This tractor had a double-channel frame and would be stiffer in torsion than the typical highway tractor. Presumably the torsional deflection and corresponding delay would be greater on a typical tractor.

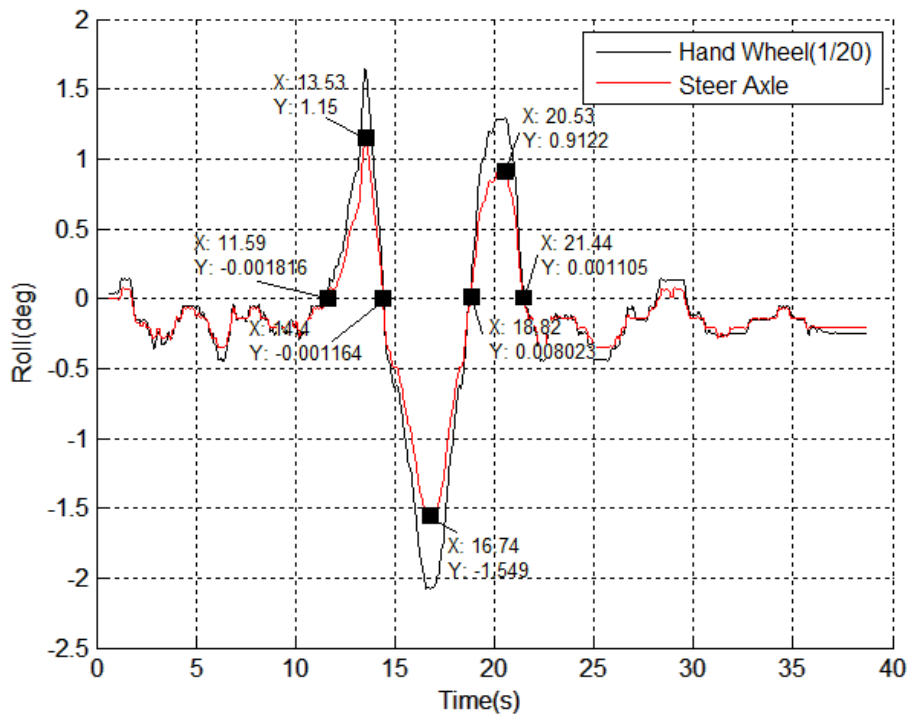


Figure 5-15. Graph. Roll angle at the steer axle at 64 km/h (40 mph).

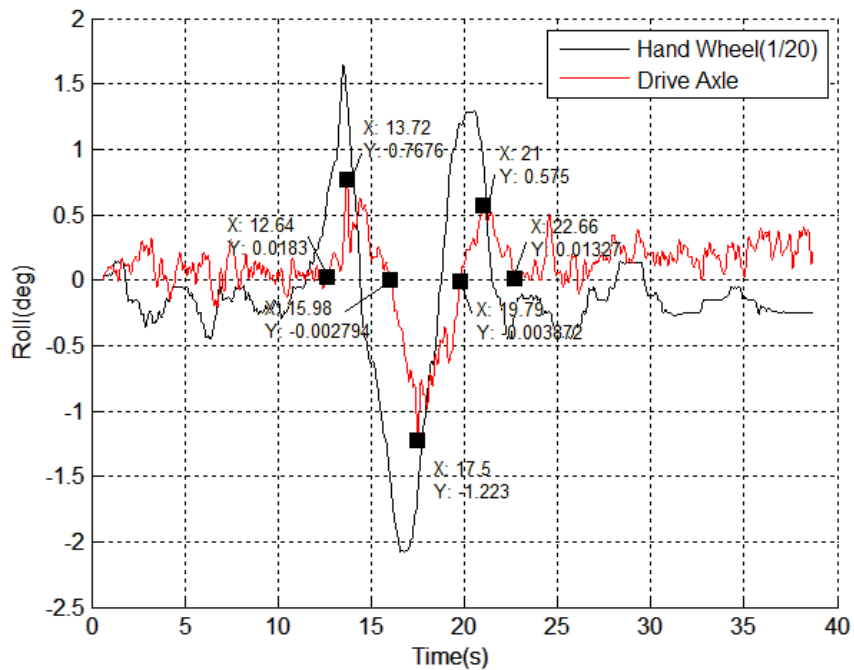


Figure 5-16. Graph. Roll angle at the drive axle at 64 km/h (40 mph).

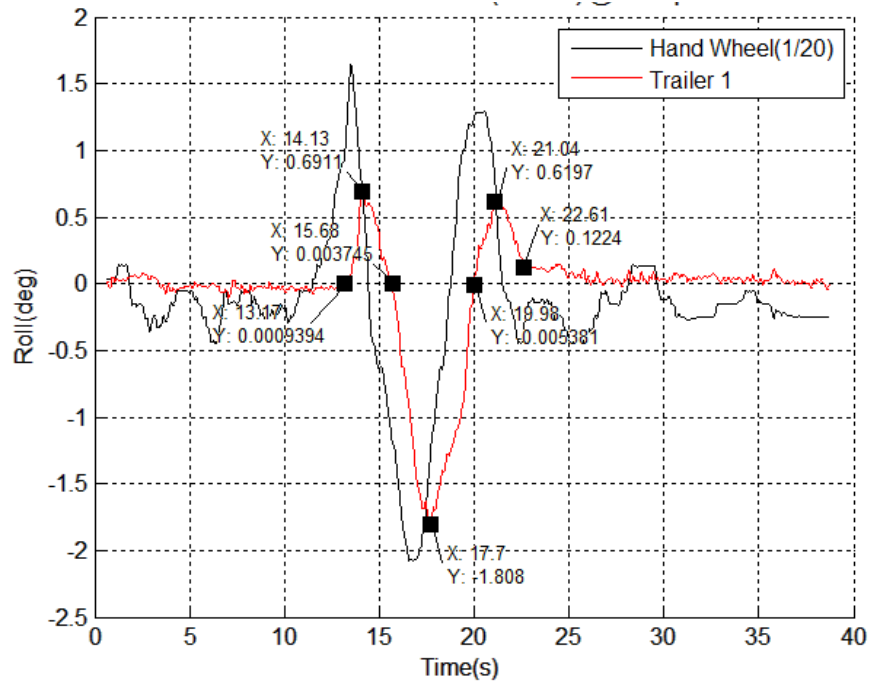


Figure 5-17. Graph. Trailer 1 roll angle (filtered) 64 km/h (40 mph).

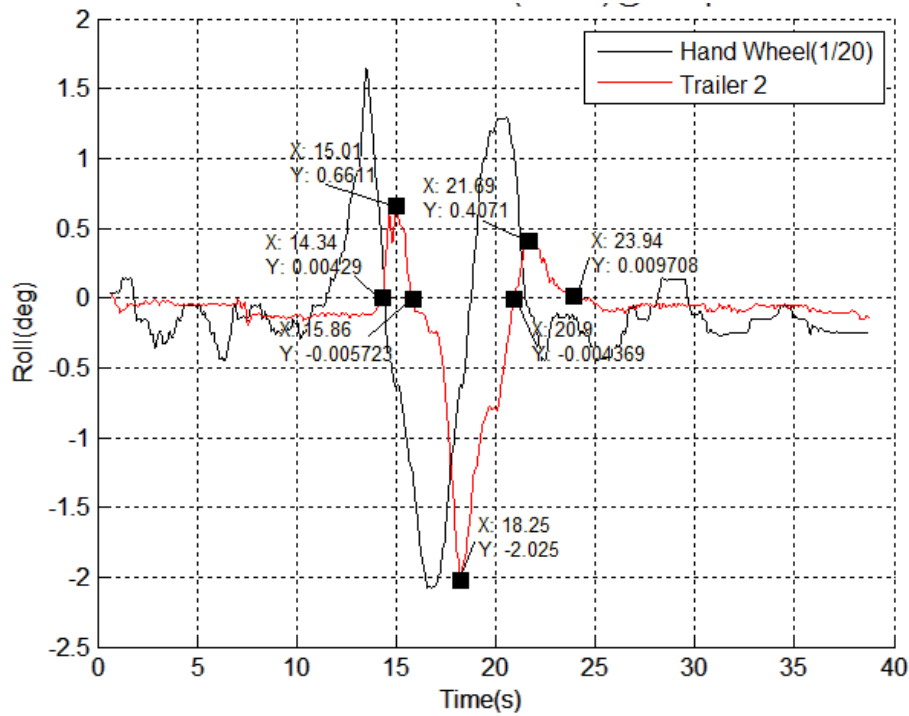


Figure 5-18. Graph. Trailer 2 roll angle (filtered) at 64 km/h (40 mph).

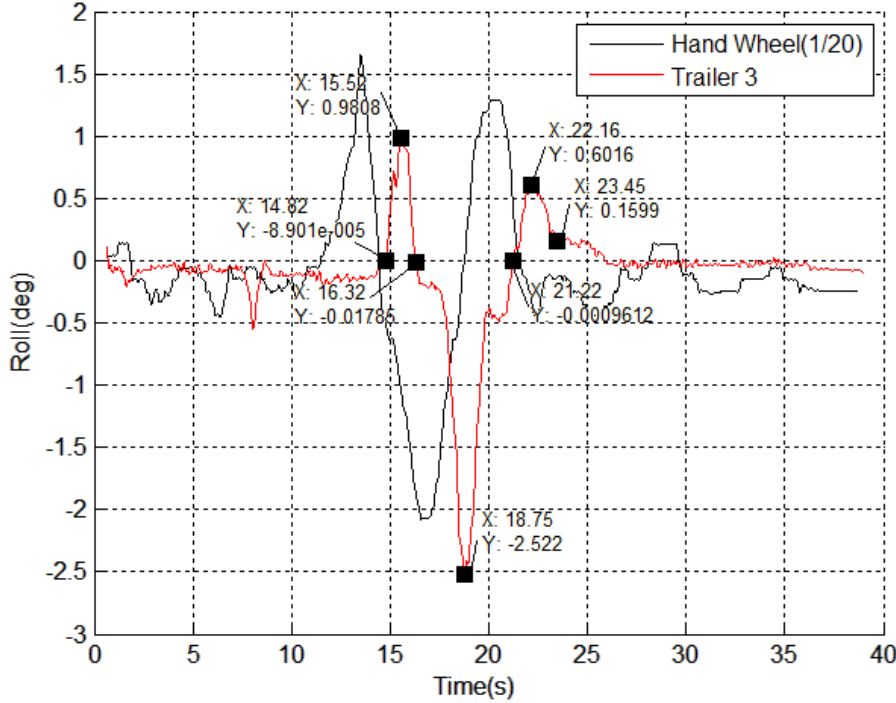


Figure 5-19. Graph. Trailer 3 roll angle (filtered) at 64 km/h (40 mph).

The filtered trailer roll angles during the double lane change at 64 km/h are shown in Figure 5-17, Figure 5-18, and Figure 5-19 for trailers 1, 2, and 3 respectively. The figures indicate that the maximum suspension roll angles during the maneuver are 1.81, 2.02, and 2.52 degrees respectively. These numbers imply a rearward amplification between Trailer 3 and Trailer 1 of 1.4:1. The true roll angle would combine the axle roll with the suspension roll, which produces the total roll angle. The values presented are an average of the repetitive runs of the same maneuver at the same speed, which displayed similar characteristics. The vehicle was steered by a human driver, rather than a robot, so steer input had minor run-to-run deviations. Subjective evaluation of the outliers, based on steer input, forced occasional data sets to be eliminated.

The Trailer 3 values obtained at 64 km/h compare well with previously tested single trailer values for roll angles (LaClair et al. 2010) as the vehicle approached the outer limits in the sub-limit testing. Sublimit tests do not reach the limits of performance, such as wheel liftoff. Visual observation of the third trailer in the train confirmed that the trailer was approaching the outer limits of the envelope.

5.3 Roll Steer Behavior of the LCV

The trailer axle steer adds or subtracts from the required articulation angle, as shown in Figure 5-20. The over- or understeer also affects the offtracking.

5.3.1 Roll Steer Theory

When a vehicle rolls on its suspension during maneuvers, the vehicle axles can rotate about the Z-vertical axis due to the suspension and suspension linkage design. This axle rotation about the Z-axis induces a road wheel angle due to the rolling motion. This is true for wheels on the steered as well as non-steered axles. The steer is a result of the layout of the axle linkage that restrains the axle in the fore/aft direction, which can cause the axles to move in an arc about a real (such as a pivot point) or instant center. See for example Chapter 6 of Gillespie (1992).

The relationship between the amount of axle angular rotation and the amount of steer is primarily a function of the axle linkage system. On the drive and trailer axles, the axle angular rotation directly relates to road wheel steer. On the steer axle, the axle steer indirectly relates to the actual road wheel steer angle. The amount of steer per degree of suspension roll is the roll steer coefficient.

The steer angle required to produce a path curvature is the sum of the Ackerman steer geometry and various effects contributing to understeer (or oversteer). Two of these effects are the cornering stiffness of the tires and their respective loading, and the roll steer characteristics of the axle, as shown in Figure 5-20. The cornering stiffness and the roll steer, in turn, are always a function of the lateral acceleration, which produces both the lateral forces and consequent roll. The portion of the equation in the square brackets is the understeer gradient in Figure 5-4.

$$\delta_{RW} = 57.3 \left(\frac{L}{R} \right) + \left[\left(\frac{W_f}{C_{af}} - \frac{W_r}{C_{ar}} \right) + (E_{\varphi r} - E_{\varphi f}) \bullet K_{\varphi'} \right] \left(\frac{v^2}{R g} \right)$$

Figure 5-20. Equation. Ackerman steer plus two effects contributing to understeer.

where

- δ_{RW} = road wheel steer angle (deg)
 - W_r = weight on the contact patch rear (N)
 - W_f = weight on the contact patch front (N)
 - C_{ar} = cornering stiffness rear tire (N/deg)
 - C_{af} = cornering stiffness front tire (N/deg)
 - $E_{\varphi r}$ = roll induced steer angle of the rear axle (steer deg/deg roll)
 - $E_{\varphi f}$ = roll induced steer angle of the front axle (steer deg/deg roll)
 - K_{φ} = total suspension roll stiffness (deg roll/g)
- (The factor 57.3 converts from radians to degrees.)

5.3.2 Double Lane Change Axle Steer at Each Axle Location in Response to Hand Wheel Input

Figure 5-21 and Figure 5-22 present representative plots of the drive axle steer and trailer axle steer respectively as a function of time in the double lane change. Of the drive axles, only the second drive axle was instrumented to measure steer. Due to the complex loading of the drive axles, the lateral locating links being attached to the frame on opposite frame rails, and the differences in tire slip angle from the first to second drive axles, it may be beneficial in the future

to instrument both drive axles for their individual steer contribution. String potentiometers mounted horizontally, in the same plane as the axle, were used to measure steer, while string potentiometers were mounted between the axle and the frame to measure roll angle. On the instrumented drive axle and the trailer axles, the roll and steer measuring potentiometers were at the same lateral distance from the vehicle centerline for each instrumented axle.

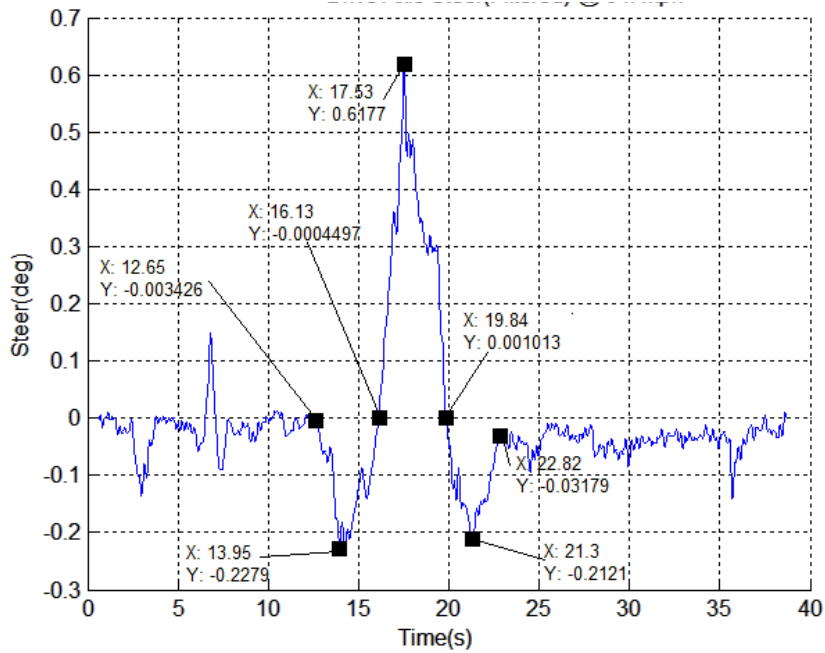


Figure 5-21. Graph. Drive axle steer as a function of time in a double lane change.

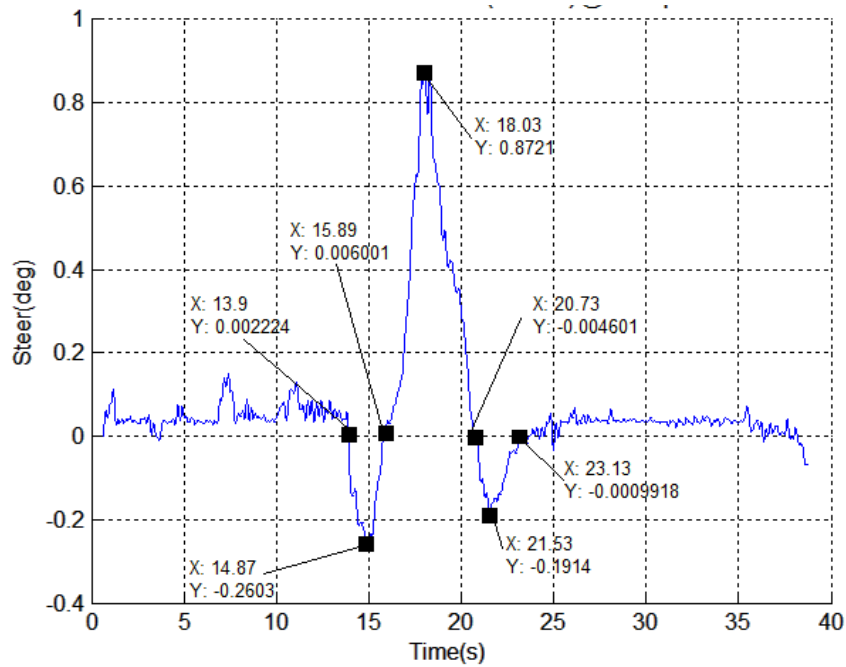


Figure 5-22. Graph. Trailer axle steer as a function of time in a double lane change.

The test vehicle was instrumented with string potentiometers mounted in the horizontal plane on each side of the vehicle at each axle to measure axle position relative to the trailer frame and with vertical string potentiometers to measure vertical axle position and resulting roll angle. The steer and drive axle mountings were aft of the axle, while all trailer axles had the string potentiometers mounted forward of the trailer axles. All the axle string potentiometers were extended to approximately 80% of full extension, which minimized the roll angle influence on string potentiometer extension. Calculation proved that the angular change was within one count resolution of the A/D conversion and hence angle correction was unnecessary.

The roll-induced steer was measured for each of the axles in the vehicle train. Figure 5-23 shows the unfiltered roll induced suspension steer for the steer, drive, and trailer axles at 64 km/h (40 mph). The dollies had suspended fifth wheels and frame mounted axles, which therefore introduced no suspension roll steer, although slip angle effects of the dolly tires would influence the resulting articulation angle.

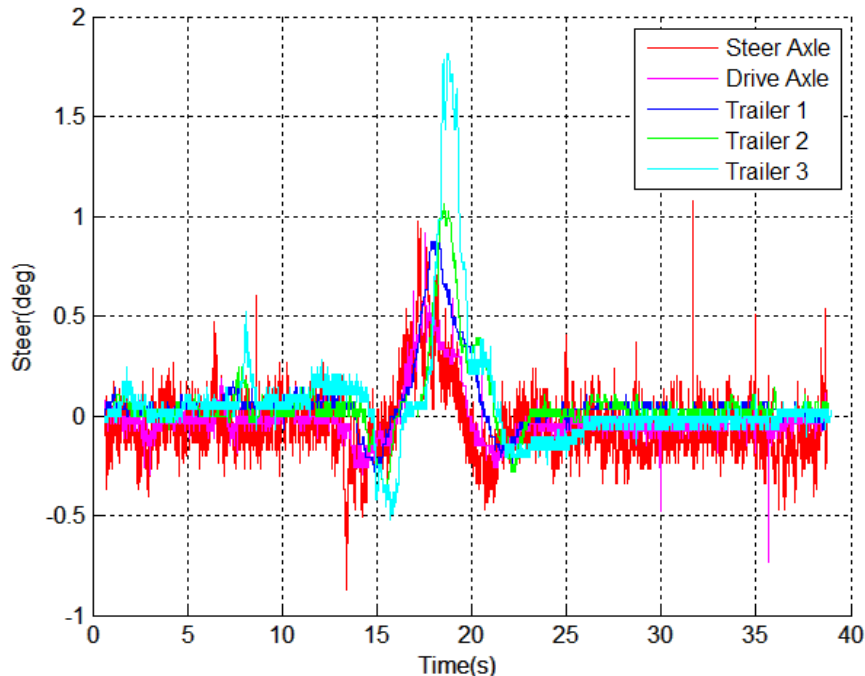


Figure 5-23. Graph. Unfiltered Steer angle at each axle location at 64 km/h (40 mph).

Shown in Figure 5-24 is the unfiltered dolly to trailer articulation angles and the filtered hand wheel angle. For plotting purposes the hand wheel angle is presented at 1/20 its measured value. The time between steer inputs at the hand wheel and the articulation angle response can be noted in the figure, as well as the articulation angle amplitudes.

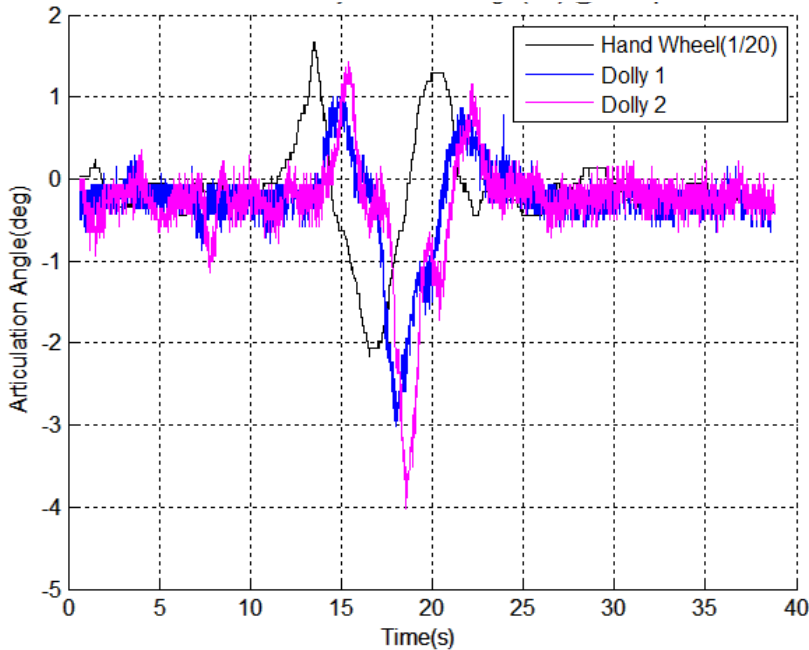


Figure 5-24. Graph. Unfiltered dolly articulation angle at 64 km/h (40 mph).

Steer axle roll steer is shown in Figure 5-25 and drive axle roll steer is shown in Figure 5-26. The result is that the steer axle results in a rotation about the Z-axis, which produces a roll understeer effect requiring increased steer input from the hand wheel (Points 1 to 3 are counterclockwise, or CCW rotation about the Z-axis; points 3 to 5 are clockwise, or CW rotation about the Z-axis; and points 5 to 7 are CCW rotation about the Z-axis with points as indicated in Figure 5-12).

The drive axle geometry produces a rotation of the axle about the Z-axis, which results in a roll oversteer tendency requiring reduced input from the hand wheel (Plot identified points 1 to 3 are CCW rotation about the Z-axis, points 3 to 5 are CW rotation about the Z-axis, and points 5 to 7 are CCW rotation about the Z-axis).

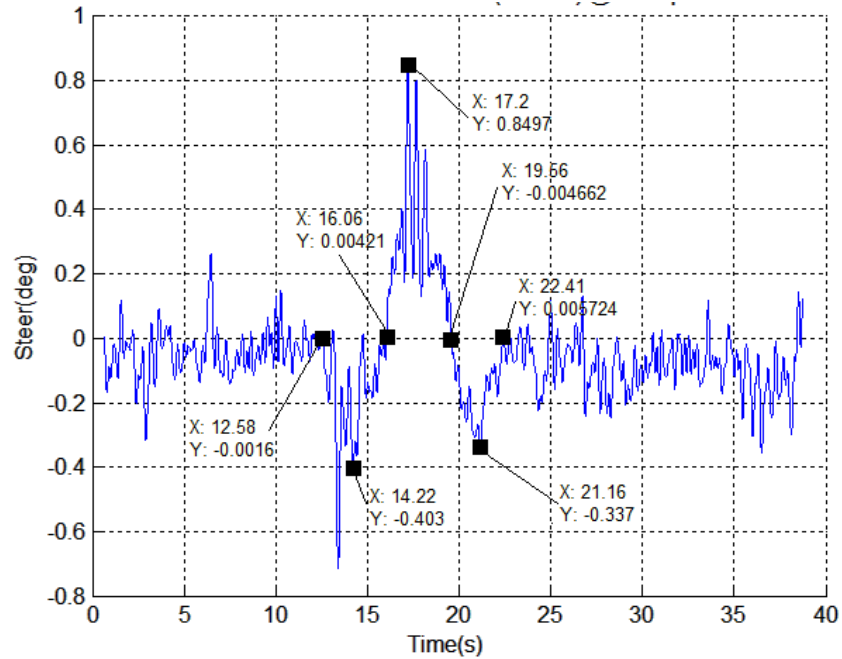


Figure 5-25. Graph. Steer axle roll steer (filtered).

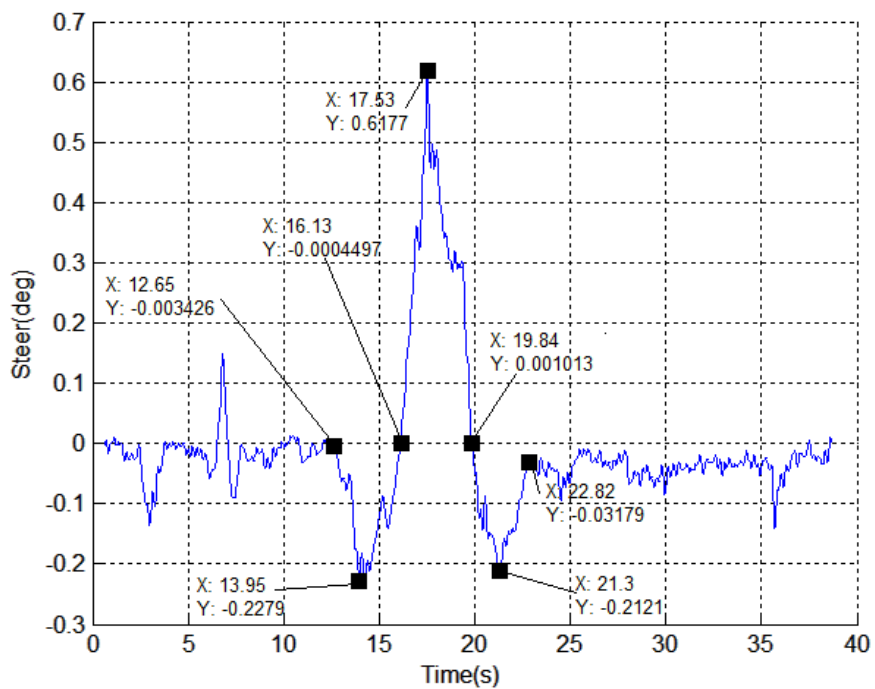


Figure 5-26. Graph. Drive axle roll steer angle (filtered).

Trailer 1 roll steer angle is shown in Figure 5-27. The roll steer produced by the axle angular change results in a direct relationship to steer and results in a roll oversteer condition. Trailer 2 roll steer angle is shown in Figure 5-28 and Trailer 3 roll steer angle is shown in Figure 5-29. The result is that the trailer axle steer on all trailers produces a roll oversteer condition for the trailers, which in turn reduces the articulation angles between the dolly and the following trailer (Plot identified points 1 to 3 are CCW rotation about the Z-axis, points 3 to 5 are CW rotation about the Z-axis, and points 5 to 7 are CCW rotation about the Z-axis).

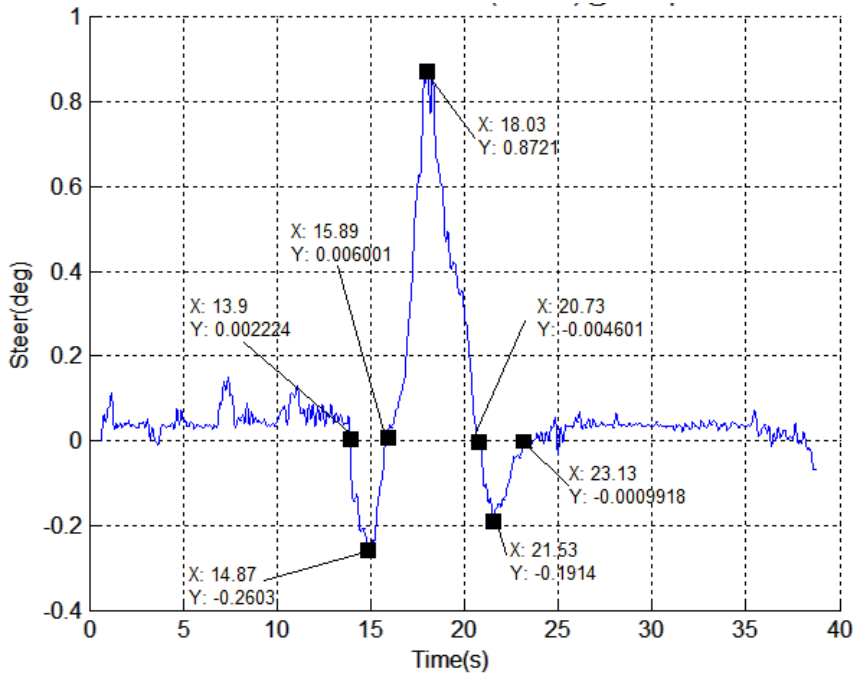


Figure 5-27. Graph. Trailer 1 roll steer angle (filtered) at 64 km/h (40 mph).

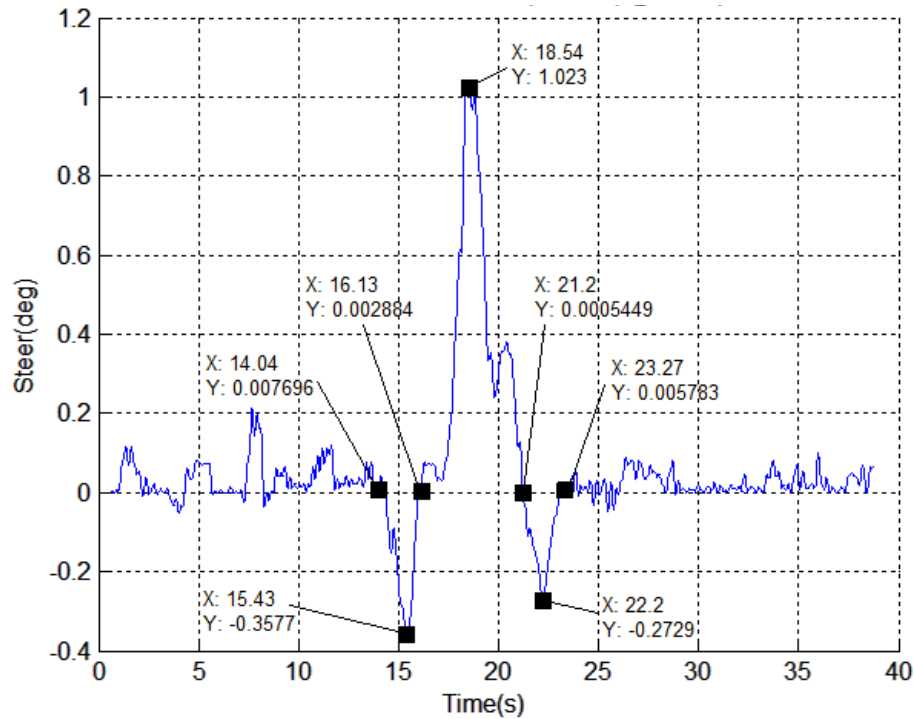


Figure 5-28. Graph. Trailer 2 roll steer angle (filtered) at 64 km/h (40 mph).

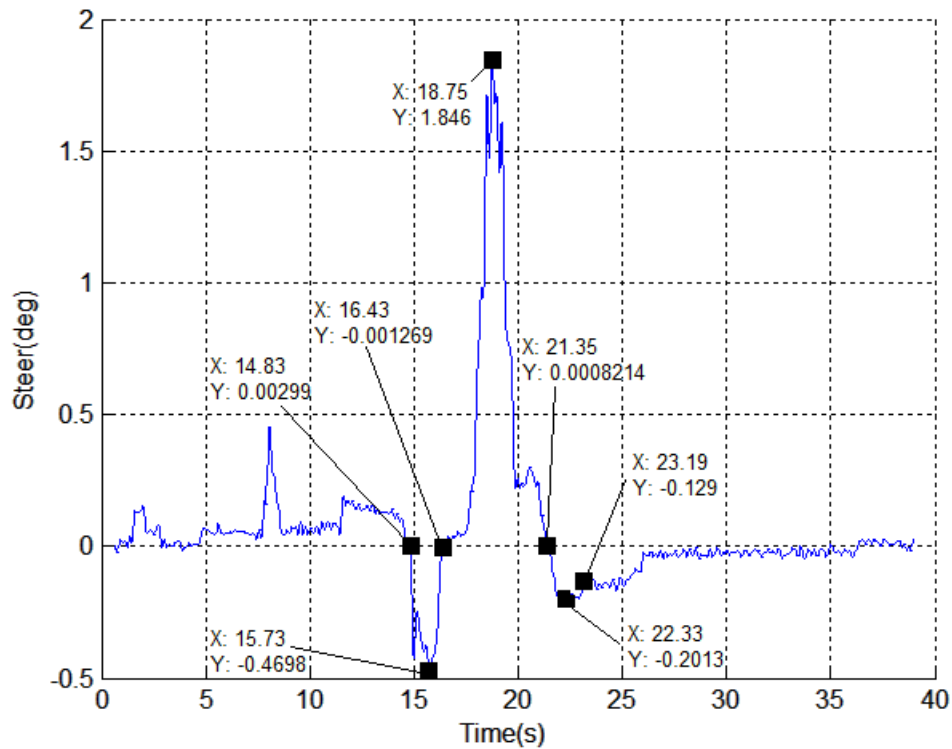


Figure 5-29. Graph. Trailer 3 roll steer angle (filtered) at 64 km/h (40 mph).

The following plots show the relative phasing of the vehicle units in response to the driver steer input. The Dolly 1 and Dolly 2 articulation angles in the double lane change, plotted with the hand wheel angle/20, are shown in Figure 5-30, Figure 5-31, and Figure 5-32 for 64 km/h. Phase delays for the input steer to the dolly articulation response are shown as well as the articulation maximum angle difference.

Hand wheel angle relative to the dolly articulation angles for 64 km/h are shown in Figure 5-32. Considering that the hand wheel to road wheel ratio for the tractor is approximately 20:1, the ratio of the steer input to the tractor and each trailer can be visually compared with values of approximately 2.05, 2.79, and 3.75 degrees indicated from the road wheel, Dolly 1, and Dolly 2 respectively. Dolly 1 indicates a -2.79 degree maximum articulation angle, while Dolly 2 achieves a -3.75 degree maximum articulation angle for a ratio of 1.34 times as great as Dolly 1.

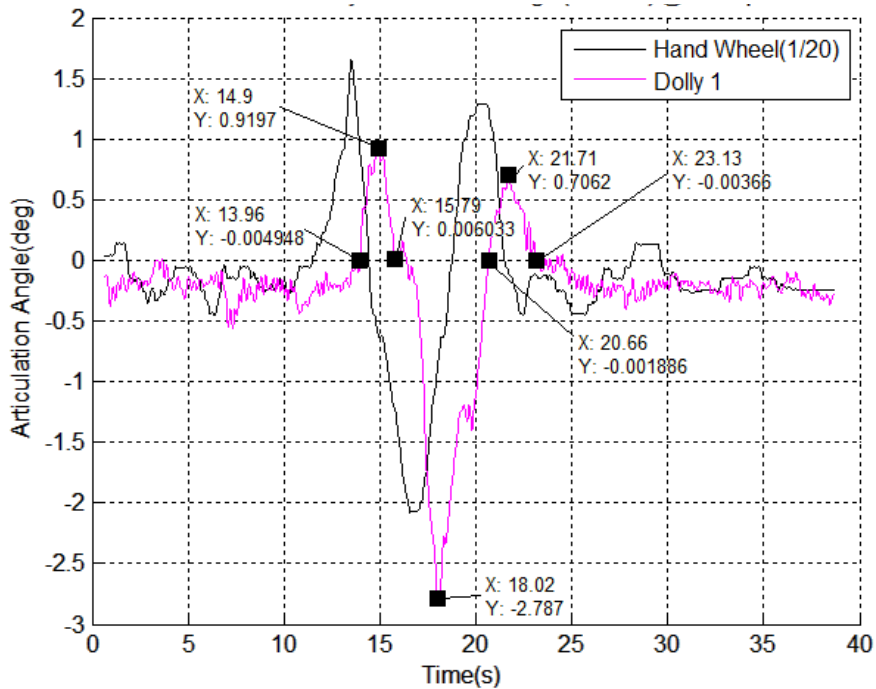


Figure 5-30. Graph. Dolly 1 articulation angle (filtered) at 64 km/h (40 mph).

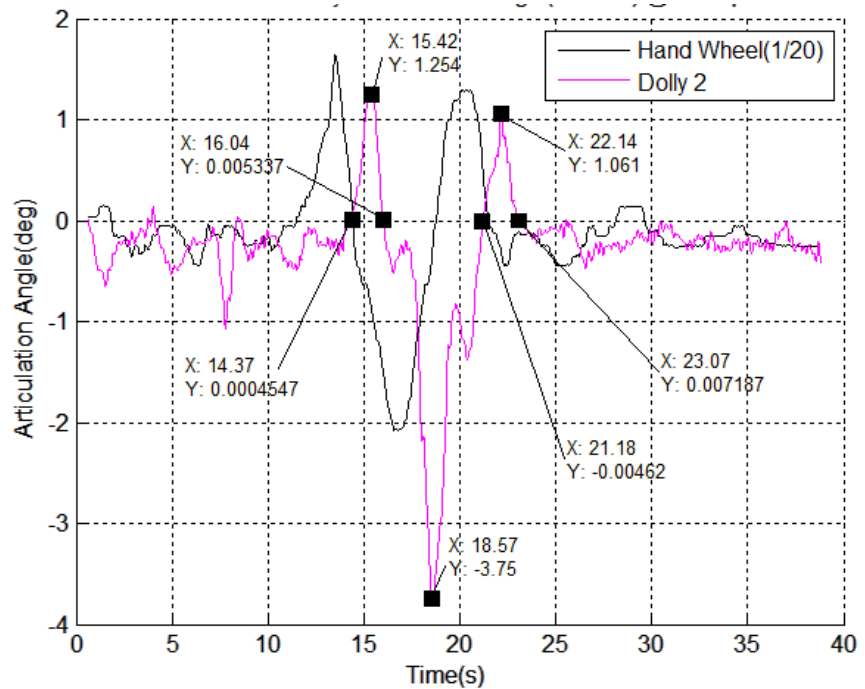


Figure 5-31. Graph. Dolly 2 articulation angle (filtered) at 64 km/h (40 mph).

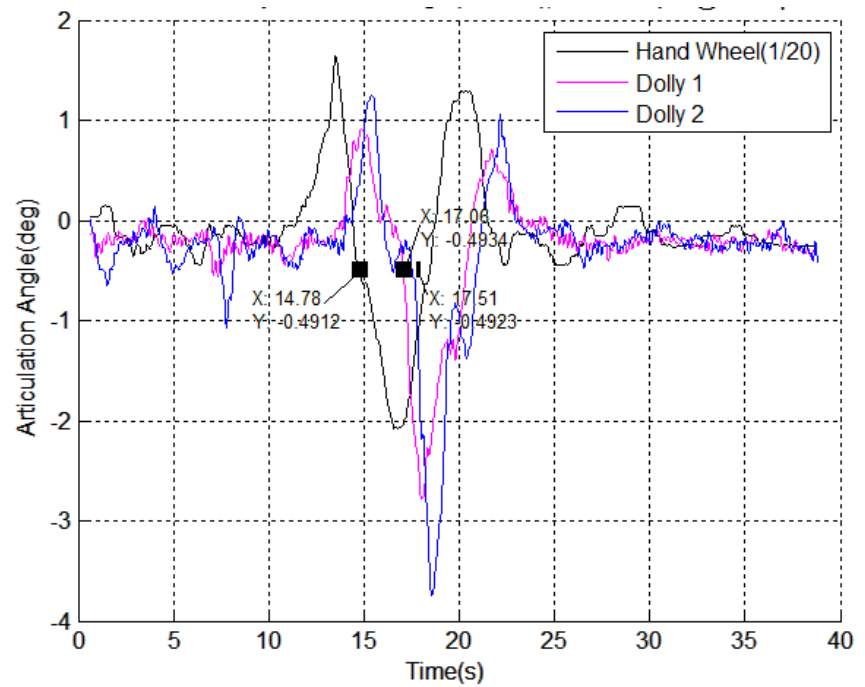


Figure 5-32. Graph. Hand wheel angle and dolly articulation angles at 64 km/h (40 mph).

Roll response to the steer input measured at the different axles in the vehicle train are shown in Figure 5-33.

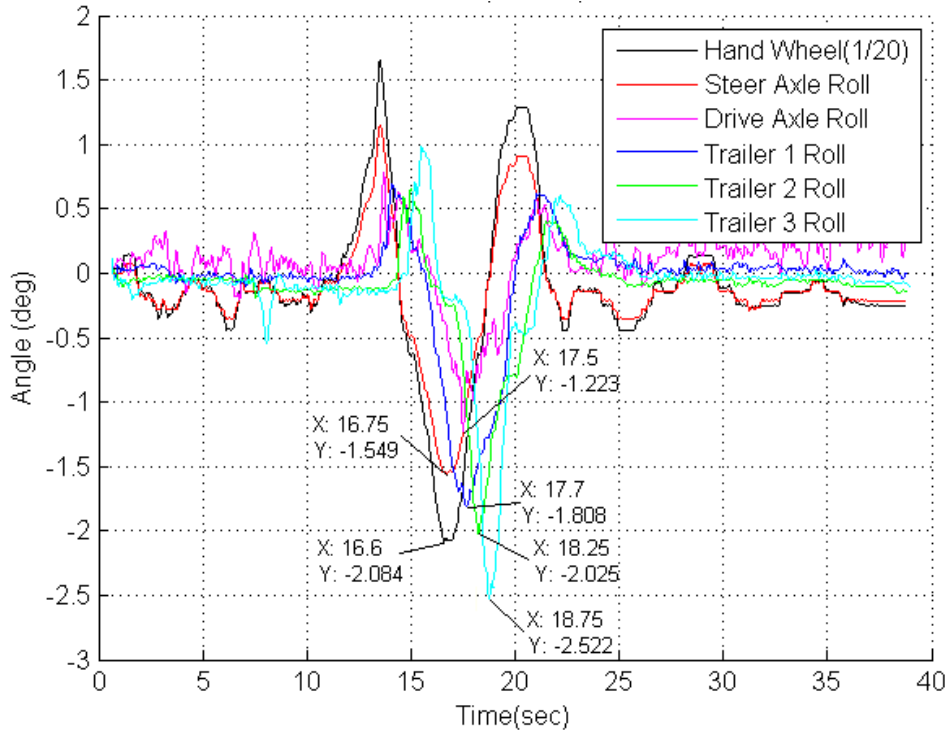


Figure 5-33. Graph. Hand wheel and roll angles (filtered) at 64 km/h (40 mph).

Relative phasing of the roll steer angles are shown in Figure 5-34. Plotted are the axle roll steer values and times, where times are essentially directly related to roll response.

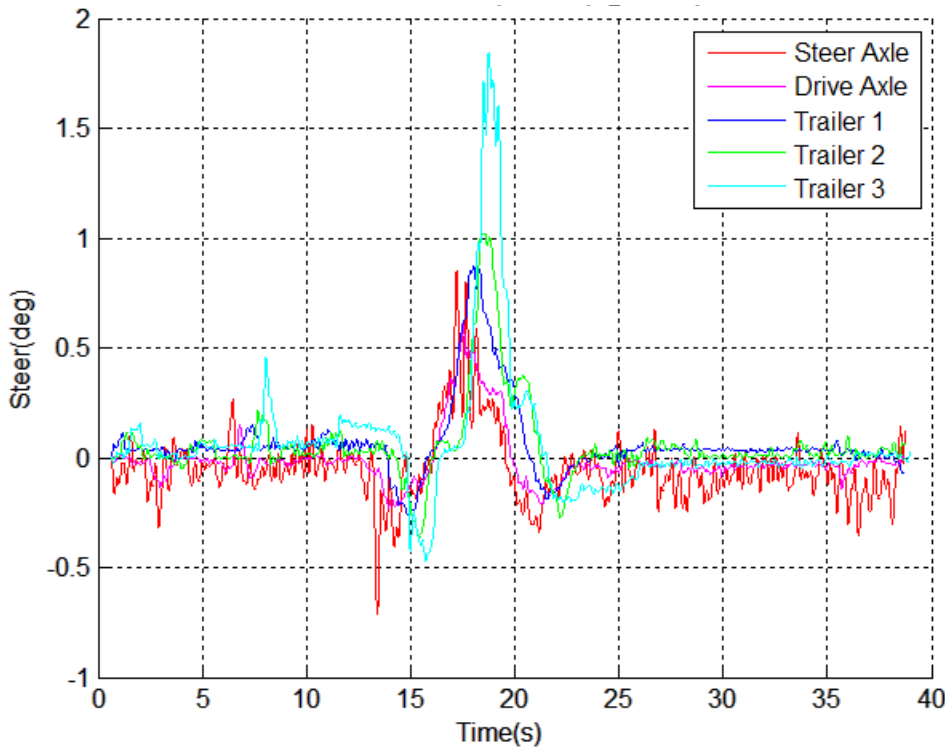


Figure 5-34. Graph. Relative roll steer angles at each suspension at 64 km/h (40 mph).

5.3.3 Conclusions for Roll Angles and Roll Steer in the Double Lane Change

Table 5-6 shows the times at which the identified roll points in the maneuver occurred. These points and the time delay (Δ) that was present between the input, which is the hand wheel steer and the response at each axle location, are indicated. As shown in Table 5-6, the delay between the roll at the steer axle and the roll at the drive axle of the tractor is approximately 1 s for the first point. This indicates a time-dependent twist of the tractor frame induced by a time delay between roll of/at the steer axle and roll of/at the drive axle. Noise in the drive axle string potentiometer measurements and identification of the exact point of zero roll when exiting the maneuver account for the occasional negative signs in the values of Table 5-6.

Table 5-6. Representative response times for units of the LCV in a 64 km/h double lane change.

	Event Time and Time Delay (s)						
	point 1	point 2	point 3	point 4	point 5	point 6	point 7
Hand Wheel (Hw)	11.47	13.52	14.42	16.60	18.76	20.57	21.48
Steer (St)	11.59	13.53	14.40	16.74	18.82	20.53	21.44
Δ St-Hw	0.1	0	0	0.1	0.1	0	0
Drive (Dr)	12.64	13.72	15.98	17.50	19.79	21.00	22.66
Δ Dr-Hw	1.17	0.20	1.56	0.90	1.03	0.43	1.18
Δ Dr-St	1.05	0.19	1.58	0.76	0.97	0.47	1.22
Trailer 1 (Trlr1)	13.17	14.13	15.68	17.70	19.98	21.04	22.61
Δ Trlr1-Hw	1.70	0.61	1.26	1.10	1.22	0.47	1.13
Δ Trlr1-St	1.58	0.60	1.28	0.96	1.16	0.51	1.17
Δ Trlr1-Dr	0.5	0.4	-0.3	0.2	0.2	0.0	0.0
Trailer 2 (Trlr2)	14.34	15.01	15.86	18.25	20.90	21.69	23.94
Δ Trlr2-Hw	2.87	1.49	1.44	1.65	2.14	1.12	2.46
Δ Trlr2-St	2.75	1.48	1.46	1.51	2.08	1.16	2.50
Δ Trlr2-Dr	1.70	1.29	-0.12	0.75	1.11	0.69	1.28
Δ Trlr2-Trlr1	1.17	0.88	0.18	0.55	0.92	0.65	1.33
Trailer 3 (Trlr3)	14.82	15.52	16.32	18.75	21.22	22.16	23.45
Δ Trlr3-Hw	3.35	2.00	1.90	2.15	2.46	1.59	1.97
Δ Trlr3-St	3.23	1.99	1.92	2.01	2.40	1.63	2.01
Δ Trlr3-Dr	2.18	1.80	0.34	1.25	1.43	1.16	0.79
Δ Trlr3-Trlr1	1.65	1.39	0.64	1.05	1.24	1.12	0.84
Δ Trlr3-Trlr2	0.48	0.51	0.46	0.50	0.32	0.47	-0.49

Analysis indicated that the maximum suspension roll angles measured between the frame and the axle during the double lane change were 1.81, 2.02, and 2.52 degrees respectively. These numbers imply a rearward trailer roll angle amplification of 1.4:1 between Trailer 3 and Trailer 1. Roll angle, with multiple trailers of similar design with similar loads, is a reasonable predictor of roll amplification between the trailers. Reliable lateral acceleration data was not attainable from the collected data set, and therefore the standard rearward amplification definition, which is the ratio between lateral acceleration of the tractor and the subsequent units of the vehicle train, was not applicable. Lateral acceleration of each unit needs to be more accurately characterized, identified, and related to track position in future studies.

This page intentionally left blank.

Chapter 6 – Modeling—Rigid Body Model

Two models of the LCV were developed, both using commercial modeling software. The first was a rigid body model in TruckSim®, a package specific to commercial motor vehicles. The second model was in Adams, a general-purpose tool for modeling mechanical systems. The two models were developed separately by different researchers from the project team. This chapter presents the TruckSim® model, and the next chapter presents the Adams model.

TruckSim® allows LCVs to be modeled by entering mass properties and kinematic and compliance data. The package also provides the ability to run modeled vehicles through user-defined tests and output the results in forms varying from tabular data to plots and animations. Data characterizing the vehicle to be modeled is entered into TruckSim® in the form of linear coefficients and tables. For this research, TruckSim® was packaged with custom solvers and models with the capability of simulating the dynamic responses for combination vehicles with up to three trailers.

As installed, TruckSim® contained stable but generic models for LCVs. These generic models were made specific to the characteristics of the NCAT test vehicle by changing component dimension and location, mass property, kinematic, and compliance data. This data was measured and recorded during characterization testing performed and reported by WMU. Figure 6-1 shows a screen capture of the model of the NCAT test vehicle performing a simulated constant radius maneuver.

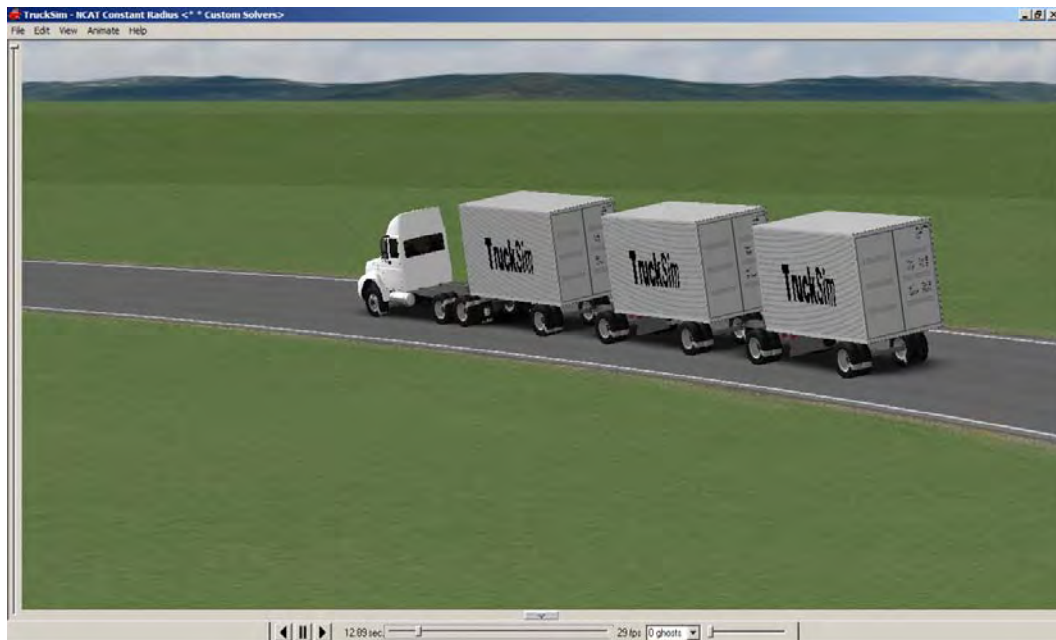


Figure 6-1. Screen Capture. Animated output of the TruckSim® model of the LCV test vehicle.

6.1 Model Formulation

The vehicle was modeled according to the measurements in the Vehicle Characterization Report in Appendix C. Where measurements were not available, the standard parameters in TruckSim® were used or values were estimated. Paths for the closed-loop driver model were developed to duplicate the test maneuvers for checking the model’s function and observing the simulated vehicle’s behavior in ideal conditions. Separately, the steering input to the model was the road wheel angle measured during the actual maneuvers, so that the model’s predictions could be compared with measurements.

Complete details of the TruckSim® model development are in Appendix D.

An LCV should not be expected to move as a single unit in a straight line with zero steer angles in any of the constituent units. The driver must guide the vehicle straight with alternating right and left motions of the hand wheel to compensate for disturbance from wind and road.

Tolerances and wear of the vehicle can cause misalignment to occur, requiring units of the vehicle to maintain a steer angle to keep an apparently steady state straight motion. This can be due to any minor differences between the units such as steering misalignment, steering gear wear, suspension angle misalignment, frame damage, suspension wear, tire inflation variation, road crown, or even bearing drag. Measurement offsets can also be present in the test data as a result of imprecise alignment of sensors, imprecise calibration, or other systematic errors associated with the instrumentation setup. While it is impossible to pinpoint a cause for this behavior in the NCAT test vehicle, it was apparent in the test data. See Figure 6-29 for an example of the dynamic center articulation of the NCAT test vehicle.

Of concern during analysis, and as seen in the model verification section, TruckSim® demonstrates a starting transient behavior that can be mitigated but not completely eliminated. This starting instability causes the simulation to start in a dynamic out-of-line orientation, which settles into a constant angle of articulation between the units of the LCV. This attitude continues for the duration of the simulation.

In all TruckSim® response plots: Unit 1 refers to the tractor, Unit 2 refers to Trailer 1, Unit 3 refers to Dolly 1, Unit 4 refers to Trailer 2, Unit 5 refers to Dolly 2, and Unit 6 refers to Trailer 3. The trajectory plots show the coordinates of the rear axles of each major unit of the LCV (tractor or trailer): Axle 3 is the rear drive axle, Axle 4 is the Trailer 1 axle, Axle 6 is the Trailer 2 axle, and Axle 8 is the Trailer 3 axle.

Open Loop TruckSim® Straight Course

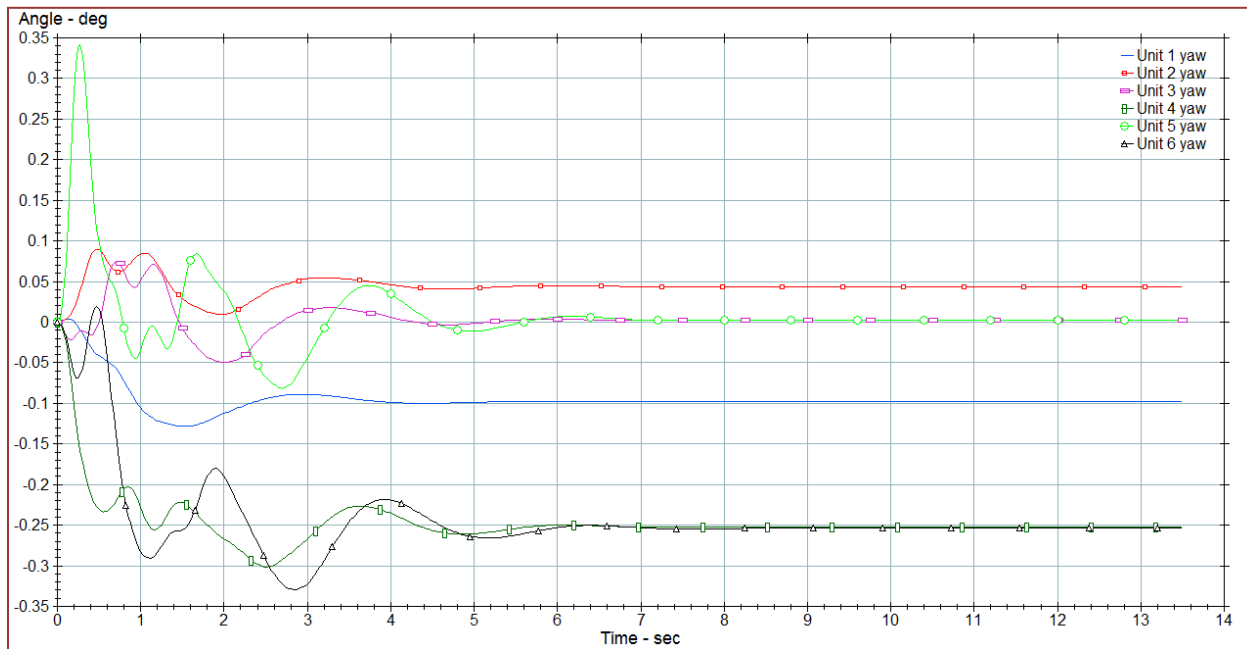


Figure 6-2. Graph. Path of the rear axle of each unit with the hand wheel fixed at straight ahead.

Figure 6-2 shows the yaw angles of each unit in the LCV during an un-steered simulation at 72 km/h (45 mph). This was simulated by setting the model in motion at a constant 72 km/h (45 mph) with an open loop steer controller having no steer angle defined, which is as if the driver takes his hands off the steering wheel while maintaining the constant speed. This simulation was performed in order to demonstrate the stability of the model, but the results also show some interesting characteristics that are relevant to the transient maneuvers presented subsequently.

The results show transient dynamics during the first few seconds. Afterwards, the vehicle stabilizes until a dynamically neutral attitude is achieved, where the yaw angles of each unit maintain a near straight trajectory. This initial oscillation is typical of simulations as the masses “settle” from their initial conditions into equilibrium. Each maneuver begins with a short straight section during which the vehicle simulation is allowed to stabilize before the primary steering inputs begin.

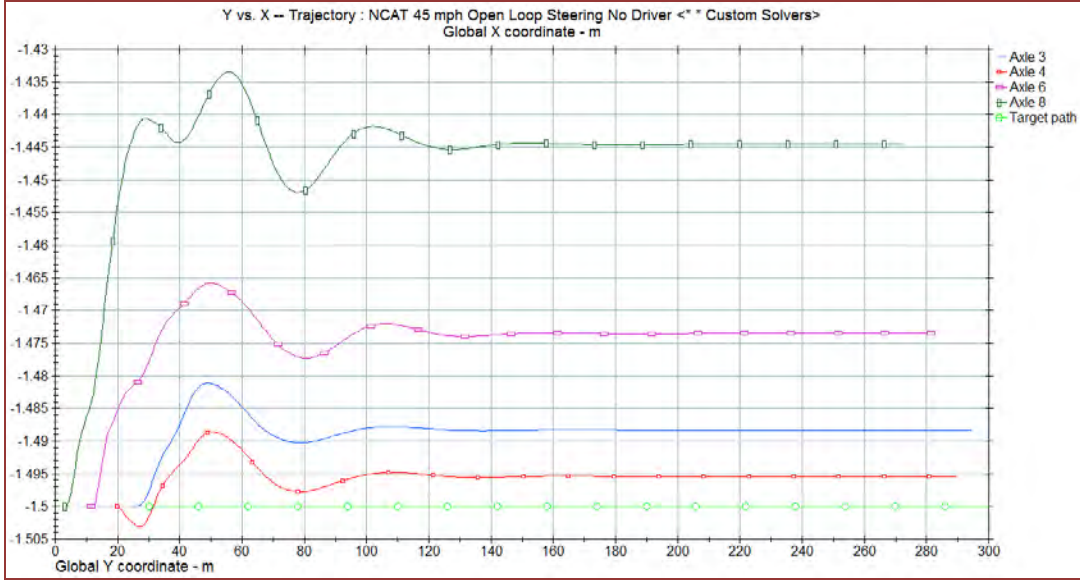


Figure 6-3. Graph. Path of the rear axle of each unit with the hand wheel fixed at straight ahead.

The trajectory of the rear axles of each unit show the same starting transient behavior as seen in the yaw plot in Figure 6-3.

6.2 Simulation of Test Track Maneuvers

To verify the stability of the model, each maneuver that was conducted on the test track as described in Chapter 4 was simulated in TruckSim®. The maneuver setup is documented in Appendix A. Indications of instability would be wild, unexpected, increasing fluctuations or rapid divergence in the simulated response. The model constructed for this research demonstrated none of these characteristics. The figures in this section show the time history lateral acceleration, time history yaw rate, and lateral tracking per station for each of the units completing each of the test plan maneuvers. To ensure stability of the model's operation at the test speeds, each maneuver was simulated at 32 and 72 km/h (20 and 45 mph). The figures contained in the following sections show that the model is stable within the established parameters of the planned test maneuvers at the speeds required by the test plan.

6.2.1 Single Lane Change Maneuver

The path for the single lane change begins with a straight segment to allow unwanted starting transients to settle, as discussed above, and then the vehicle moves 3.5 m (12 ft—one lane) to the left. The path is shown in the first two figures, which are the coordinates of the rear axle of each unit of the simulated vehicle in the horizontal plane. Note in Figure 6-4 (32 km/h, 20 mph) that the final units of the vehicle do not travel as far down the track as the tractor before they begin to move toward the other lane. This is typical low-speed offtracking. The magnitude of the offtracking for the 32 km/h (20 mph) case is about 5 cm. The opposite effect of high-speed offtracking is evident in the 72 km/h (45 mph) figure, where the final trailer travels farther down

the straight path, clearly lagging the response of the more forward units. At the second turn of the maneuver, the paths of the trailing units overshoot (and oscillate two cycles) before returning to their position behind the tractor. This is an example of rearward amplification. The maximum offtracking in the 72 km/h (45 mph) case is on the order of 30 cm, which is much more significant than that observed in the lower speed case.

This behavior is shown in plots of the yaw angle as well. Figure 6-11, yaw angle for the 32 km/h (20 mph) single lane change, shows a decreasing yaw for each successive unit rearward in the vehicle. Since the units follow more closely in the 32 km/h (20 mph) maneuver the yaw response is lower for each unit. For the 72 km/h (45 mph) single lane change maneuver in Figure 6-12,, the lag in response for each following unit causes the respective yaw to increase down the vehicle. Both the simulated yaw angle and lateral acceleration response show that the model exhibits rearward amplification for the higher speed operation. The trailers overshoot as they settle in the left lane between 7 and 8 s in Figure 6-12.

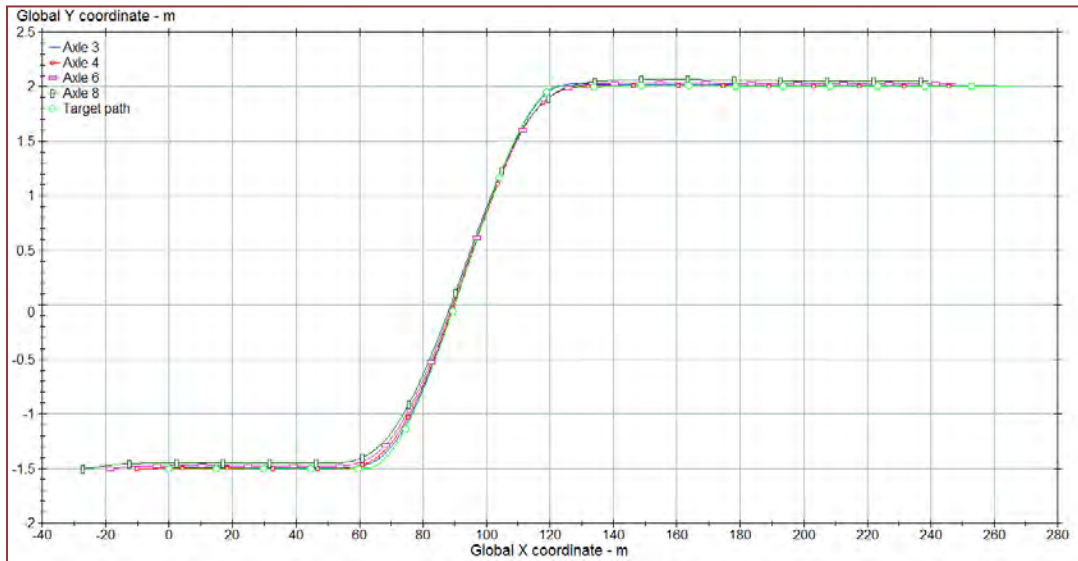


Figure 6-4. Graph. Paths of the rear axles of each unit during a simulated 32 km/h (20 mph) single lane change.

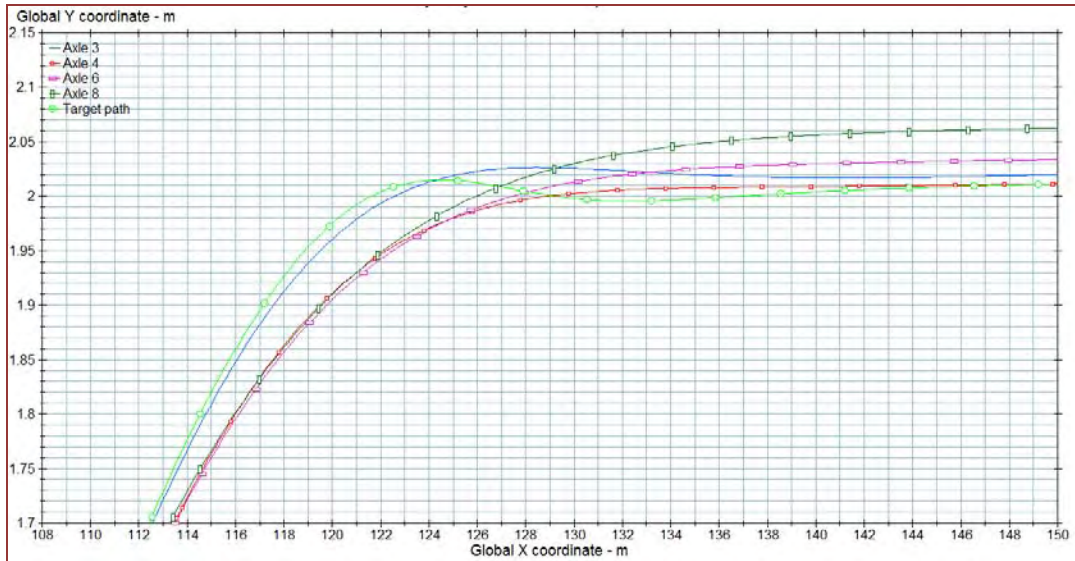


Figure 6-5. Graph. Detail of a portion of Figure 6-4, showing offtracking in a simulated 32 km/h (20 mph) single lane change

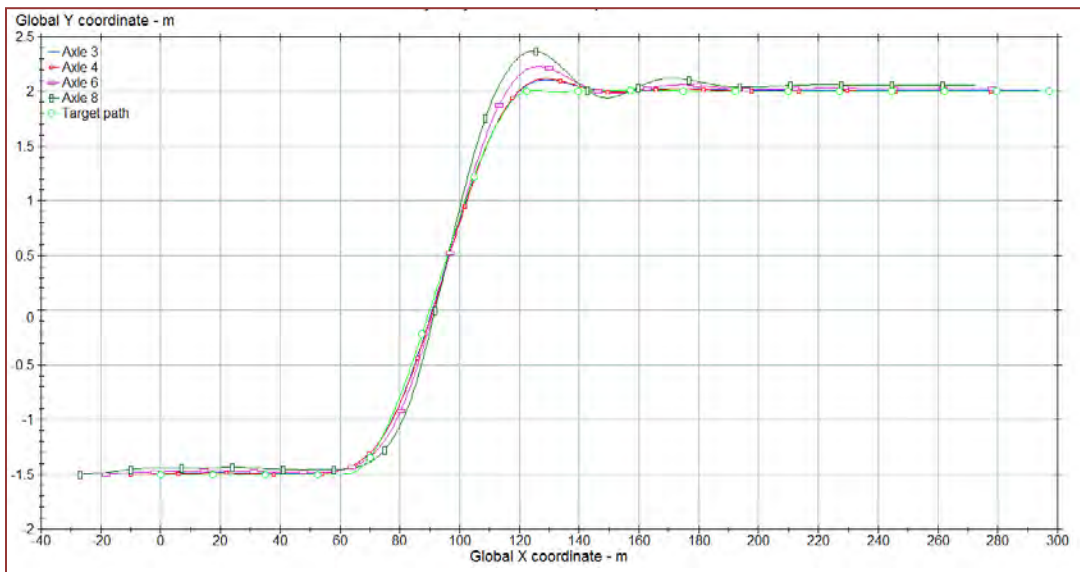


Figure 6-6. Graph. Paths of the rear axles of each unit during a simulated 72 km/h (45 mph) single lane change.

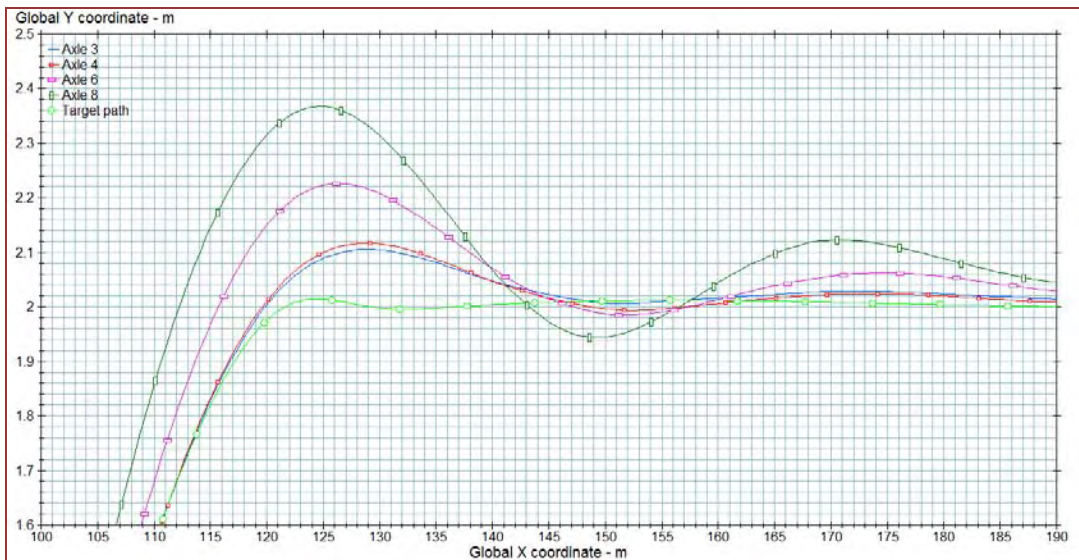


Figure 6-7. Graph. Detail of a portion of Figure 6-6, showing offtracking in a simulated 72 km/h (45 mph) single lane change.

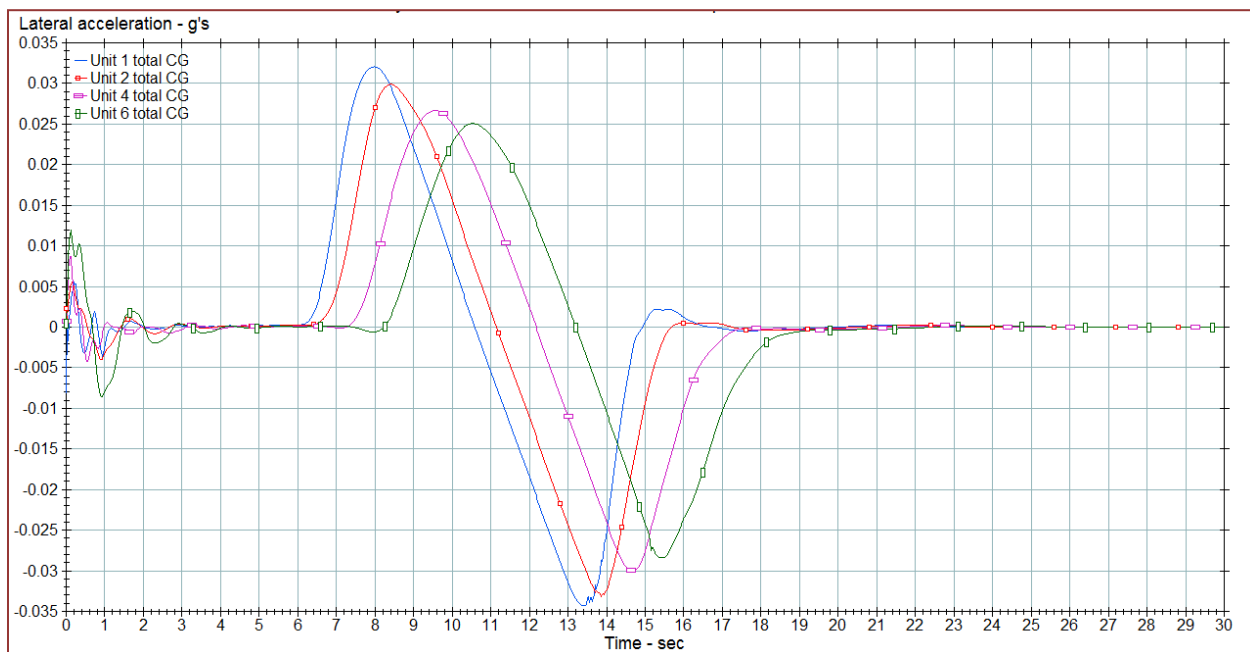


Figure 6-8. Graph. Lateral acceleration at the CG of each unit of the vehicle during a simulated 32 km/h (20 mph) single lane change.

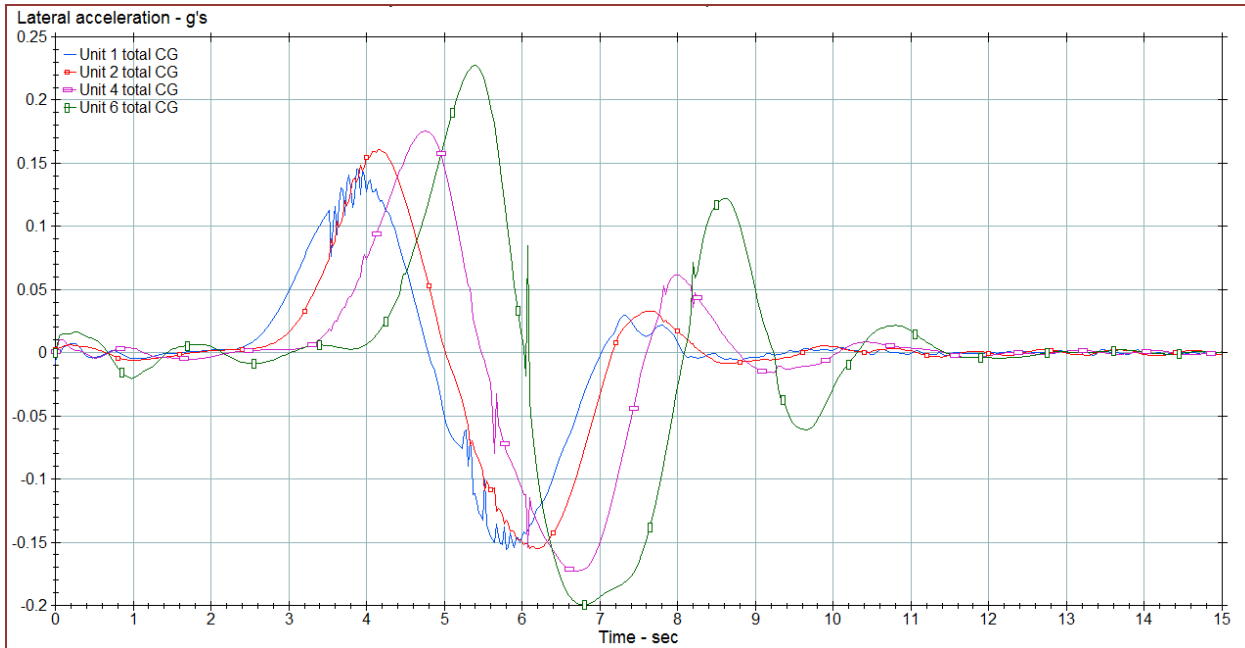


Figure 6-9. Graph. Lateral acceleration at the CG of each unit of the vehicle during a simulated 72 km/h (45 mph) single lane change.

The tractor's lateral acceleration has high-frequency oscillation as it approaches the peaks in Figure 6-9 and again in Figure 6-21, the corresponding double lane change. It could be caused by a numerical instability related to a stick-slip in the tires or suspension.

Figure 6-10 shows how the lateral acceleration changes for the units along the vehicle. The plot shows the ratio of lateral acceleration to the lead unit in the LCV. Completing the lane change at 72 km/h (45 mph), the vehicle showed rearward amplification: each successive trailer toward the rear has a higher peak lateral acceleration. In contrast, at the lower speed of 32 km/h (20 mph), the peak lateral acceleration decreases toward the rear.

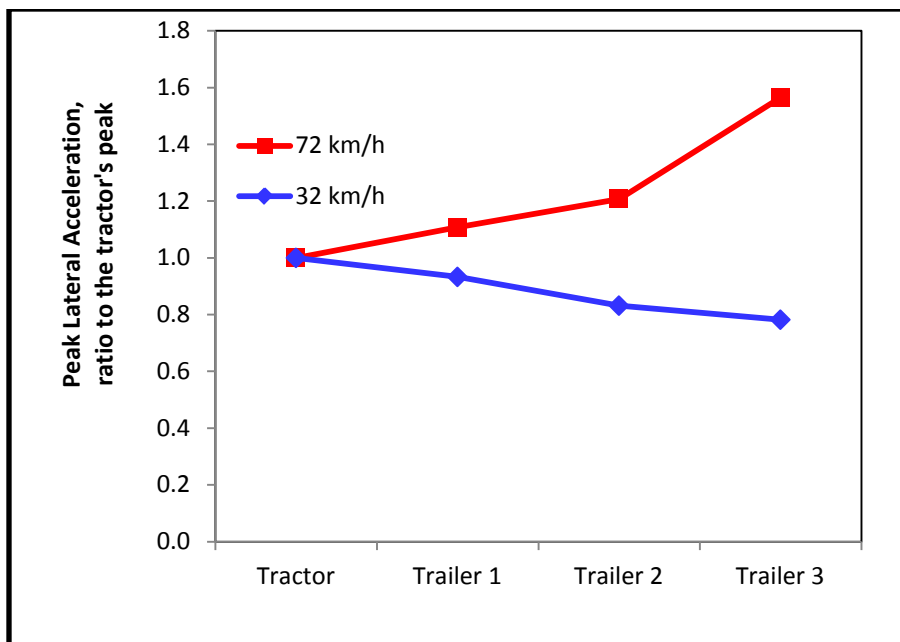


Figure 6-10. Graph. Rearward amplification of lateral acceleration in single lane changes at 32 km/h (20 mph) and 72 km/h (45 mph).

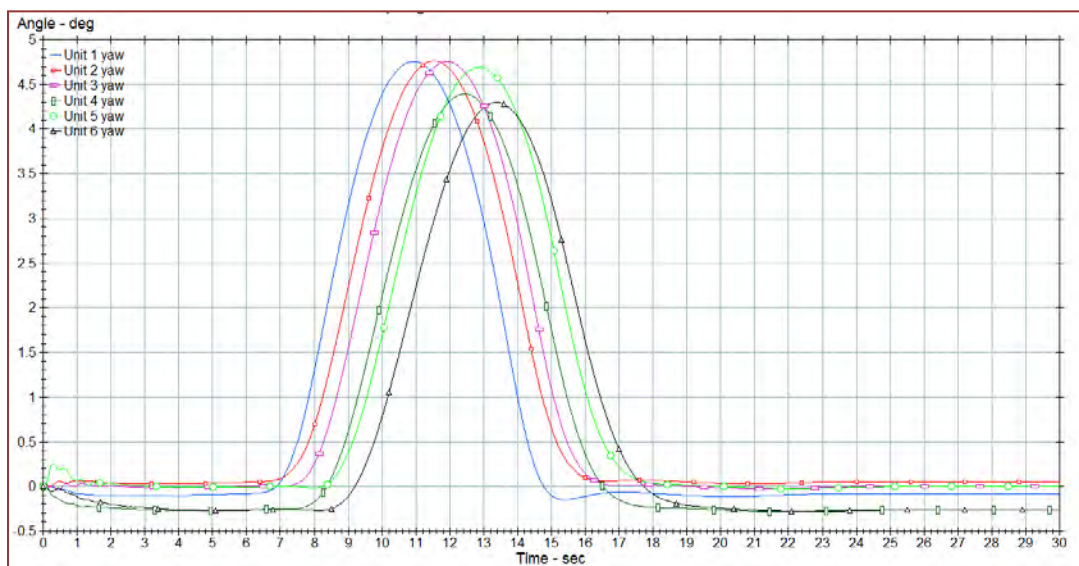


Figure 6-11. Graph. Yaw response of the vehicle for a simulated single lane change at 32 km/h (20 mph).

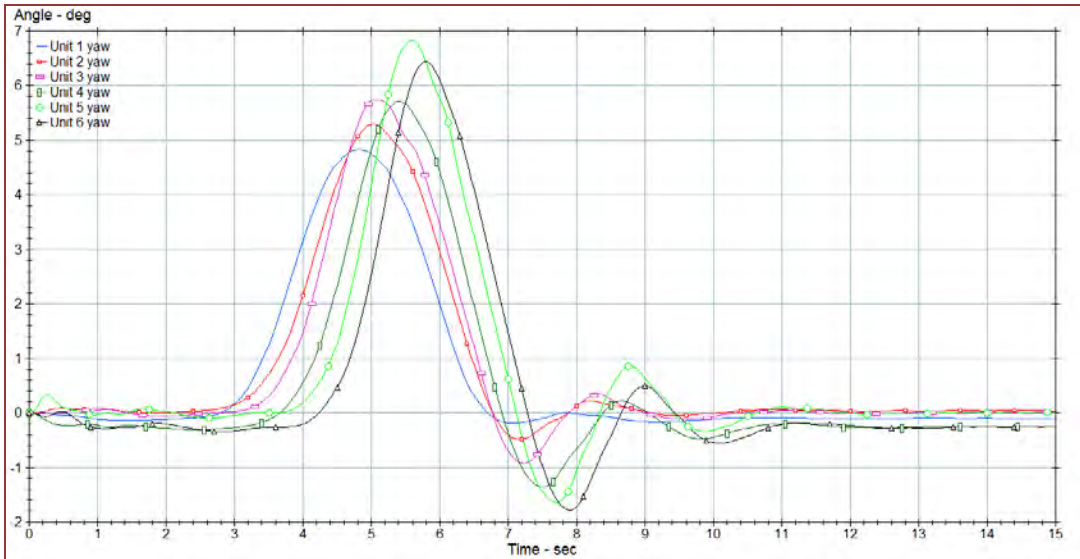


Figure 6-12. Graph. Yaw of the sprung mass for a simulated 72 km/h (45 mph) single lane change.

6.2.2 Gradual Lane Change

The gradual lane change (Figure 6-13) produced a response similar to the shorter, more abrupt single lane change maneuver at 72 km/h (45 mph). The overshoot of Trailer 3 is about 0.2 m in the gradual lane change, less than the 0.4 m simulated in the single lane change. As expected, the oscillation is less in the gradual maneuver, as well.

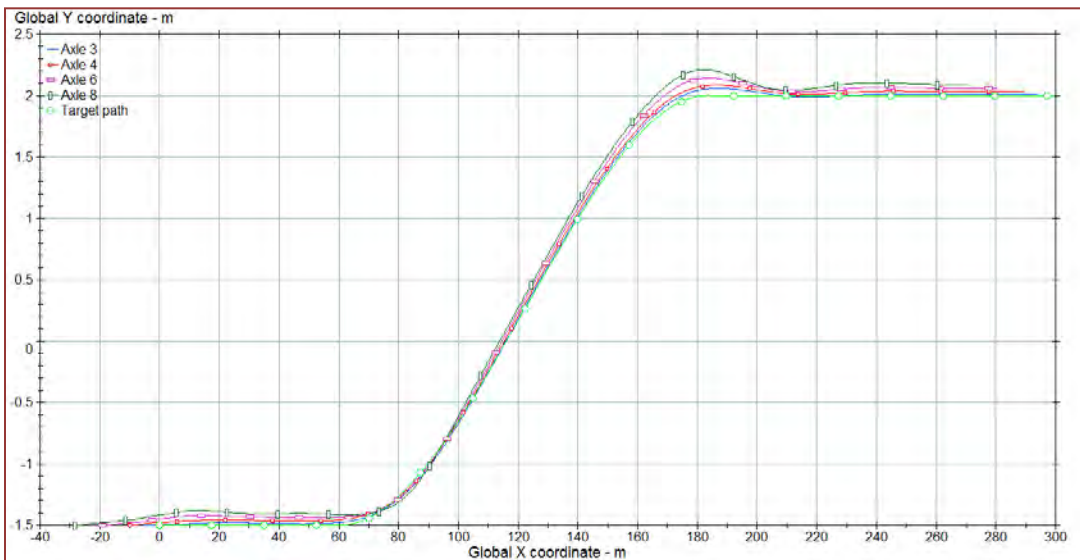


Figure 6-13. Graph. Paths of the rear axles of each unit during a simulated 72 km/h (45 mph) gradual lane change.

6.2.3 Double Lane Change

Corresponding simulations were run for the double lane change. The path for the double lane change begins with a straight segment in the right lane to allow starting transients to settle, and then the vehicle moves 3.5 m (12 ft—one lane) to the left. After traveling 50 ft in the left lane, the vehicle moves back into the right lane (Figure 4-18). Similarly to the single lane change, the path is shown in the first two figures, which are the coordinates of the rear axles of each unit of the simulated vehicle in the horizontal plane. Note in Figure 6-14 (32 km/h, 20 mph) that the final units of the vehicle do not travel as far down the track before they begin to move toward the other lane. This is typical low-speed offtracking. The opposite effect of high-speed offtracking is evident in Figure 6-17 (72 km/h, 45 mph), where the final trailer travels farther down the straight path, clearly lagging the response of the more forward units. As the maneuver ends, the paths of the trailing vehicles overshoot (and oscillate one cycle) before returning to their position behind the tractor. This is rearward amplification.

As with the single lane change, this behavior is shown in plots of the yaw angle as well. In Figure 6-22, the yaw angle for the 32 km/h (20 mph) double lane change shows a decreasing yaw for each successive unit rearward in the vehicle. Since the units follow more closely in the 32 km/h (20 mph) maneuver, the yaw response is lower for each unit. In contrast, in Figure 6-23, the corresponding 72 km/h (45 mph) maneuver shows that the peak yaw angle increases from tractor to Trailer 3. Both yaw angle and lateral acceleration response of the model exhibit rearward amplification at the higher speed. The distance along which the vehicle travels is the same at both speeds, so the frequency content of the steer input is higher at the higher speed.

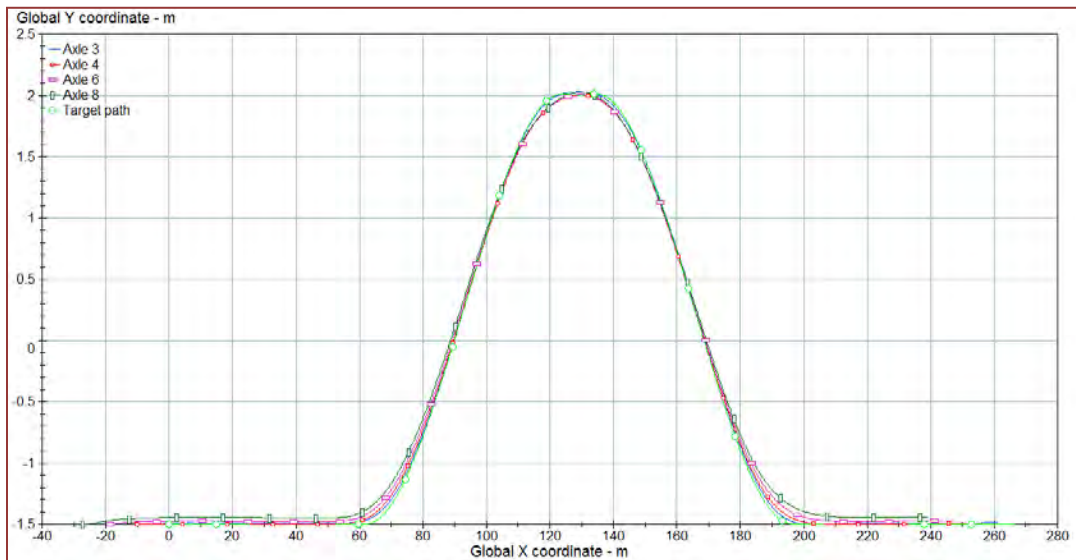


Figure 6-14. Graph. Paths of the rear axles of each unit during a simulated 32 km/h (20 mph) double lane change.

Figure 6-14 shows the path of each unit as it completes the 32 km/h (20 mph) double lane change. Offtracking is evident in the turn out of the right lane, the turn back toward the left lane (Figure 6-15), and the turn back into the right lane (Figure 6-16). Notice that Axle 8 (on Trailer 3) offtracks to the inside on entrance and at the end of the maneuver.

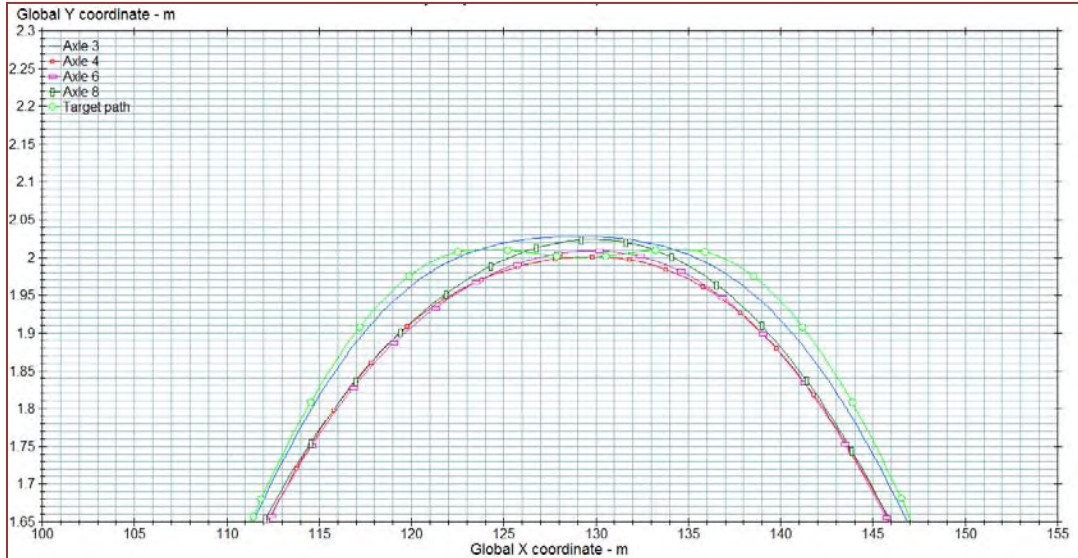


Figure 6-15. Graph. Detail of Figure 6-14, showing the offtracking at the midpoint of the maneuver.

At the mid-point of the maneuver, the tractor tracks outside of all of the other units. Interestingly the other units are in reverse order: Axe 8 (Trailer 3) tracks outside of Axe 6 (Trailer 2), which tracks outside of Axe 4 (Trailer 1). At the end of the maneuver, the rear axle of Trailer 3, followed in order by Trailers 2 and 1, track inside of the tractor.

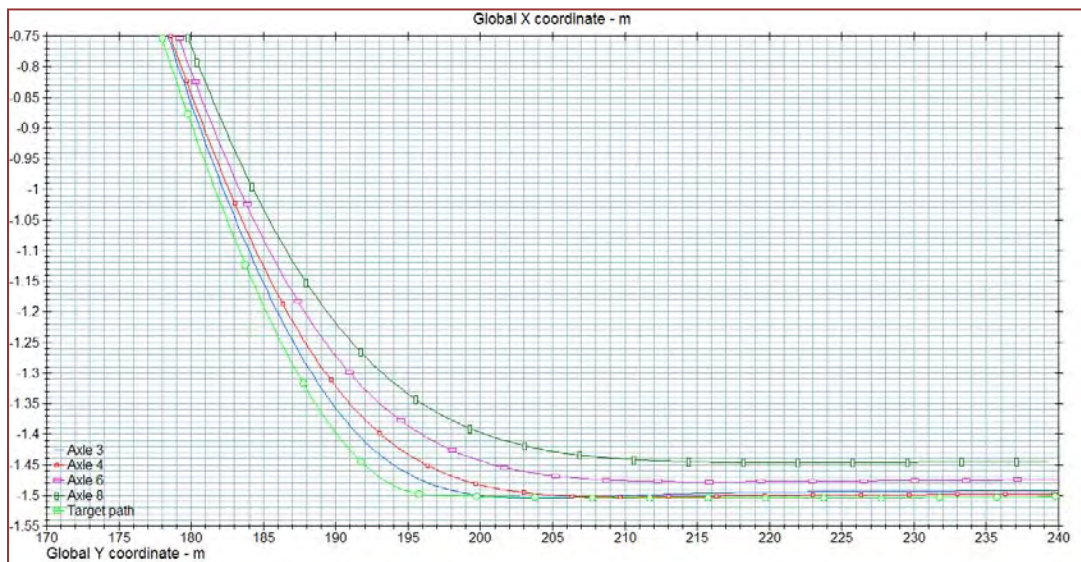


Figure 6-16. Graph. Detail of Figure 6-14, showing the offtracking near the end point of the maneuver.

More severe offtracking is evident in the 72 km/h (20 mph) double lane change in Figure 6-17. Oscillation is noticeable at the end of the maneuver when the vehicle is re-entering the right lane. Axle 8 (Trailer 3) is most severe.

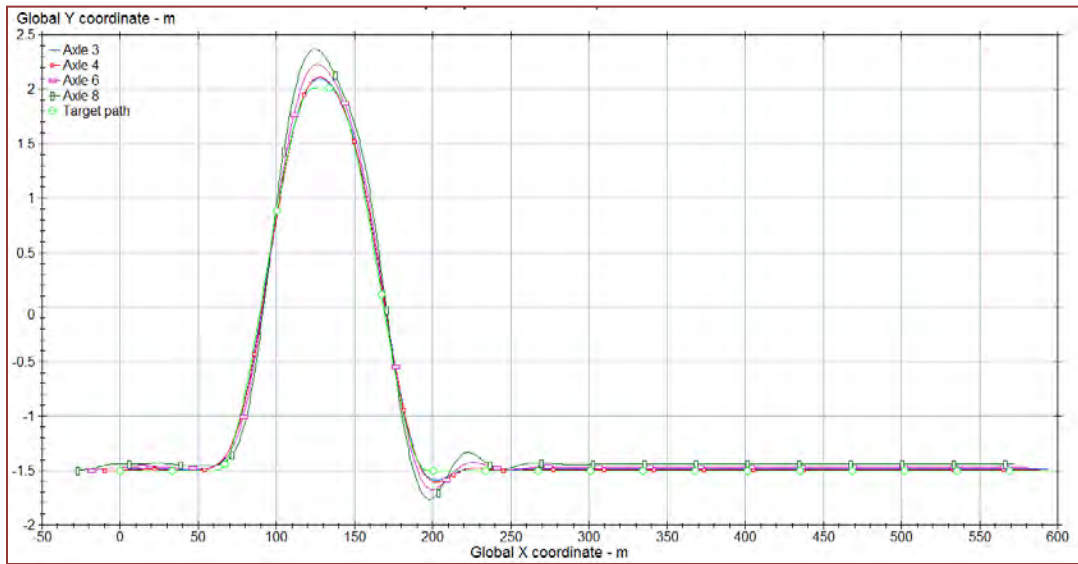


Figure 6-17. Graph. Paths of the rear axles of each unit during a simulated 72 km/h (45 mph) double lane change.

Figure 6-18 shows that the peak offtracking increases from Trailer 1 to Trailer 3, as is expected for the higher speed maneuver.

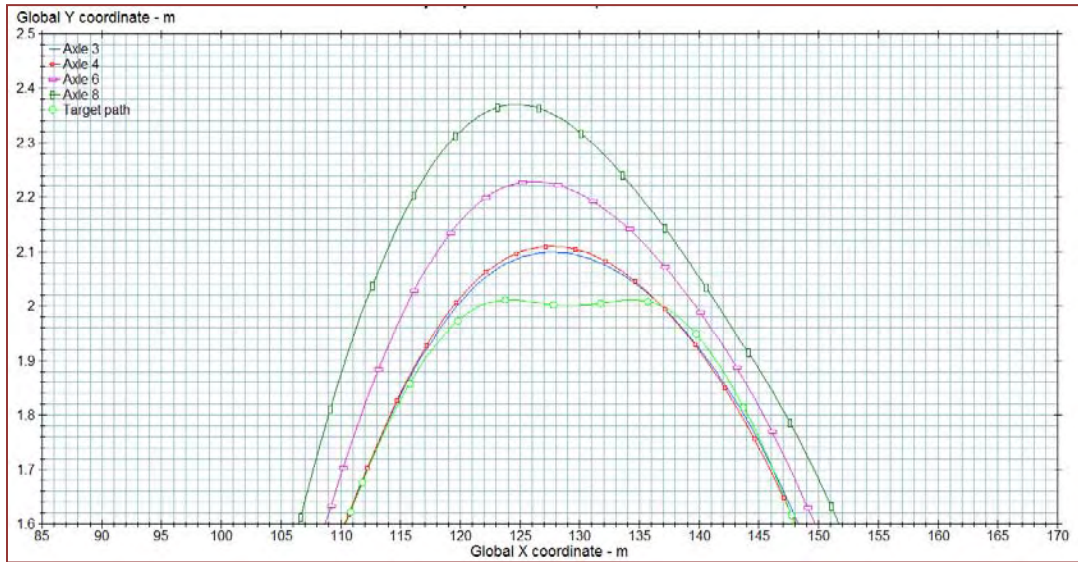


Figure 6-18. Graph. Detail of Figure 6-17, showing the offtracking at the midpoint of the maneuver

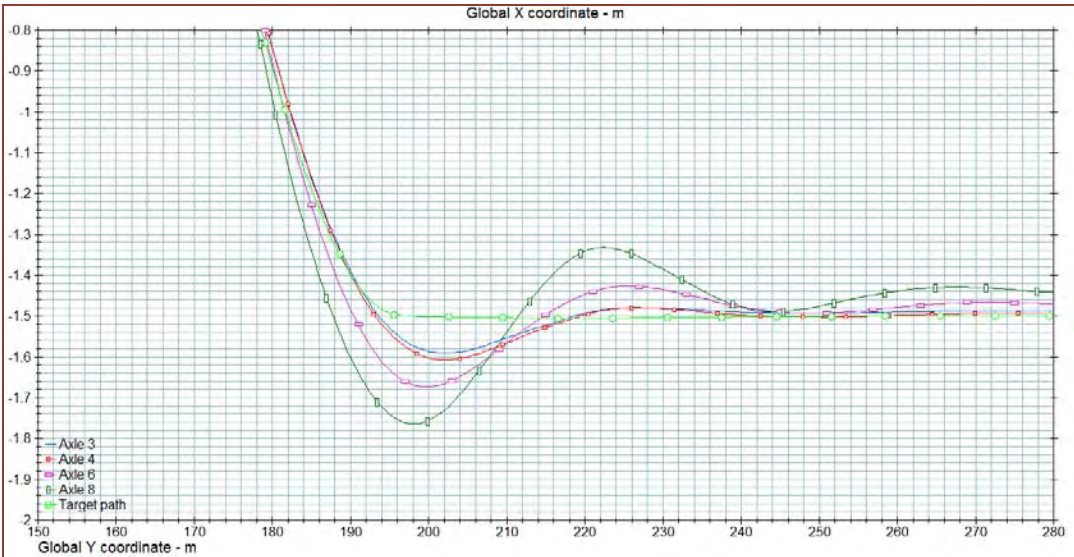


Figure 6-19. Graph. Detail of Figure 6-17, showing the offtracking at the end of the maneuver.

At the maneuver end the order of offtracking is the same as in the maneuver middle. Axle 8 (Trailer 3) tracks out farthest, followed in reverse order up to Axle 3. This follows through the oscillation, as each axle overshoots the path and oscillates back to center.

Consistent with the peak offtracking is the rearward amplification of lateral acceleration in the three trailers. Figure 6-20 and Figure 6-21 are the lateral accelerations of the simulated 32 km/h (20 mph) and 72 km/h (45 mph) double lane change, respectively. Figure 6-22 and Figure 6-23 are the yaw angles for the same two cases. At the lower speed, the response of more rearward trailers is less than that of the tractor; at the higher speed, rearward amplification is evident.

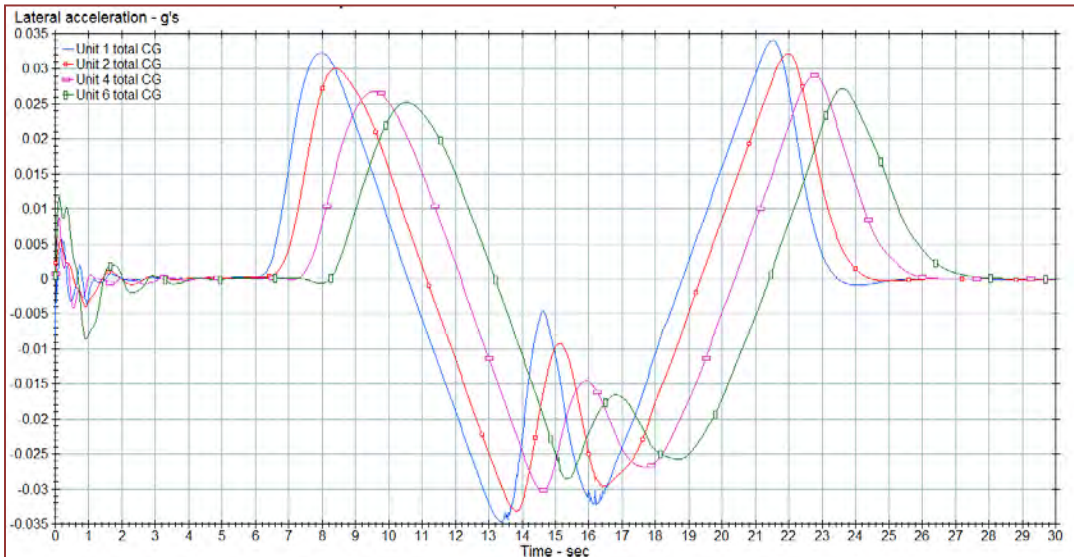


Figure 6-20. Graph. Lateral acceleration at the CG of each unit of the vehicle during a simulated 32 km/h (20 mph) double lane change.

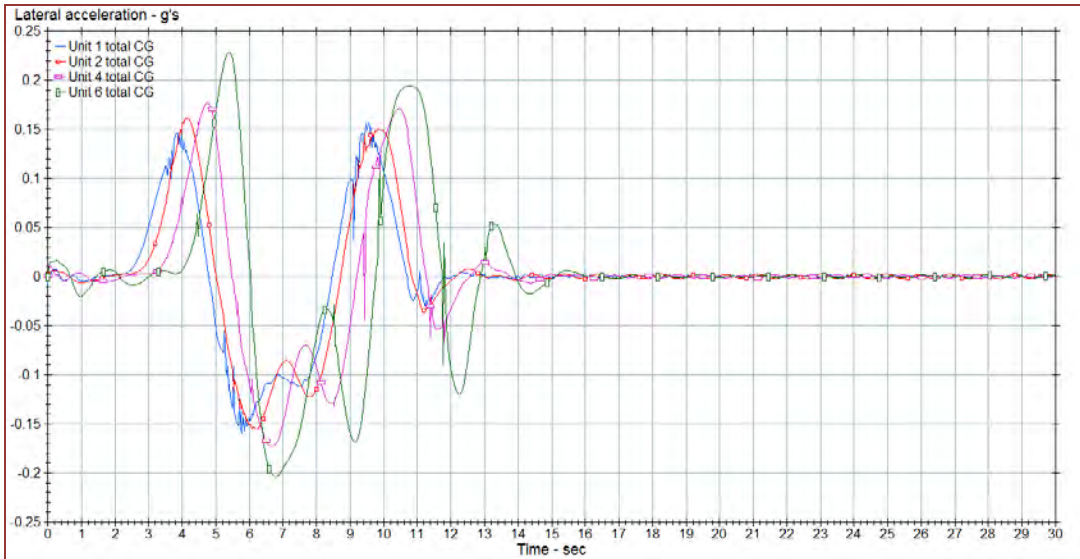


Figure 6-21. Graph. Lateral acceleration at the CG of each unit of the vehicle during a simulated 72 km/h (45 mph) double lane change.

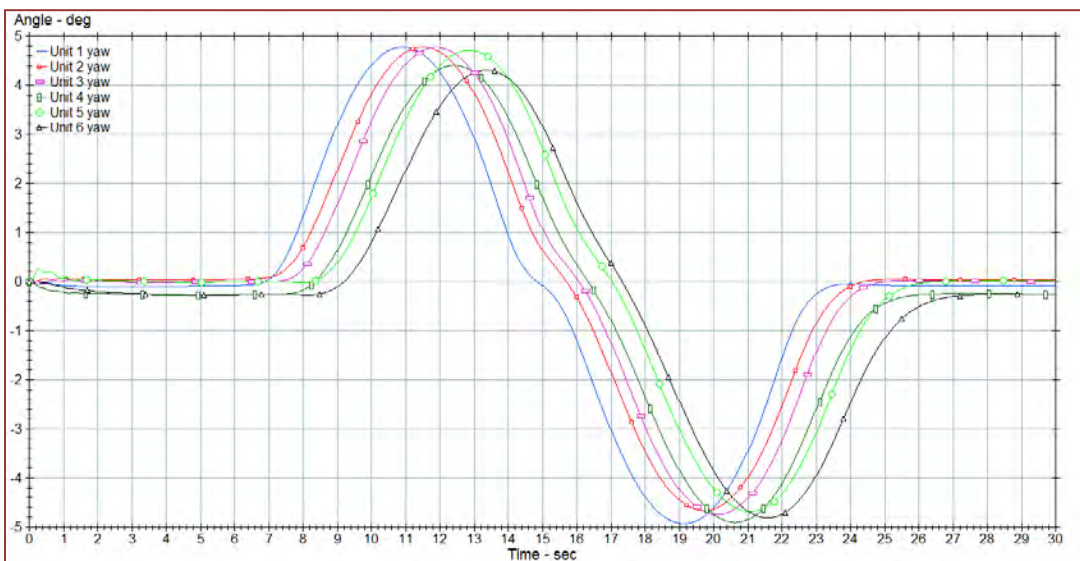


Figure 6-22. Graph. Yaw angle of each unit of the vehicle for a simulated 32 km/h (20 mph) double lane change.

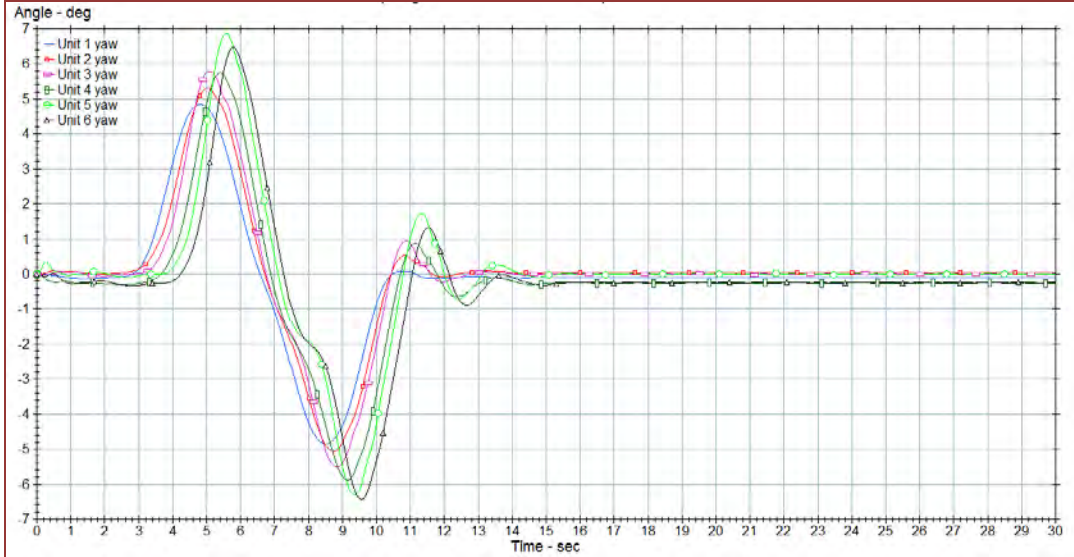


Figure 6-23. Graph. Yaw angle of each unit of the vehicle for a simulated 72 km/h (45 mph) double lane change

6.2.4 Constant Radius Maneuver

This simulation was run on a 146 m (479 ft) radius track with an 8 deg bank. The initial transient lateral acceleration is a combination of the starting transients of the model, the truck climbing onto the track over the bank, and the vehicle accelerating through the gears to the target speed. The simulation of the constant radius maneuver could not be initiated at speed, because the truck entering the track causes instability and failure of the model. A suitable acceleration curve was used until the target speed was reached and the dynamics stabilizes to reach a near steady state behavior.

Figure 6-24 shows the lateral acceleration of the units as the vehicle enters the maneuver. Steady state is reached at about 50 s, but oscillation of the tractor remains. Figure 6-25 shows the acceleration into the same curve at a higher speed.

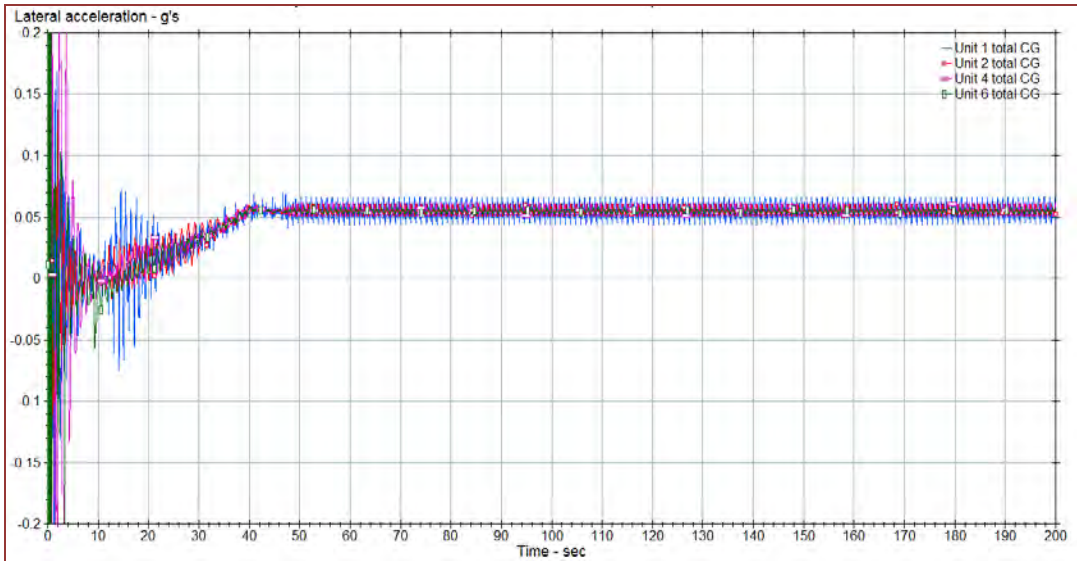


Figure 6-24. Graph. Lateral acceleration at the CG of each unit of the vehicle during a simulated 32 km/h (20 mph) constant radius curve.

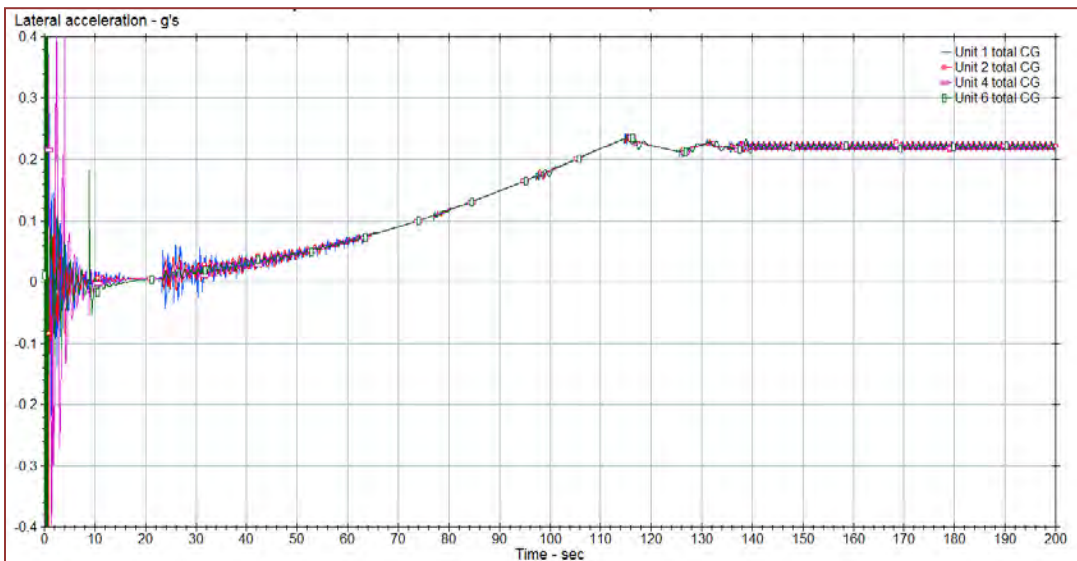


Figure 6-25. Graph. Lateral acceleration at the CG of each unit of the vehicle during a simulated 72 km/h (45 mph) constant radius curve.

Figure 6-26 shows the steady state tracking of the LCV in the constant radius maneuver simulated at 32 km/h (20 mph). All units track to the inside of Axle 3 (rear tractor drive) in order from Trailer 1 to Trailer 3. Axle 8 (Trailer 3) offtracks about 0.55 m from the path of the tractor rear drive axle. The plot shows only 2 meters of travel distance traveled, so that the curvature of the path is barely visible. Figure 6-27 shows the steady state tracking of the LCV in the constant radius maneuver simulated at 72 km/h (45 mph). At the higher speed, the units still track in the same order, but in a significantly tighter pattern. With the superelevation (bank) of the track, the speed of this maneuver is near the theoretical neutral speed at which the

gravitational forces are balanced by the centripetal force. Trailer 3 tracks about 0.02 m inside the tractor.

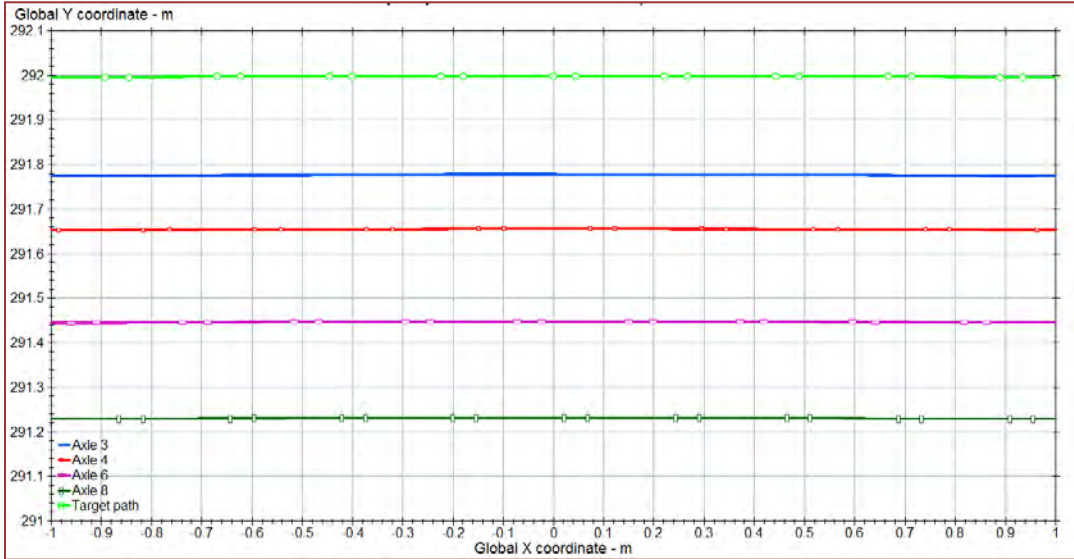


Figure 6-26. Graph. Paths of the rear axles of each unit during a simulated 32 km/h (20 mph) constant radius curve.

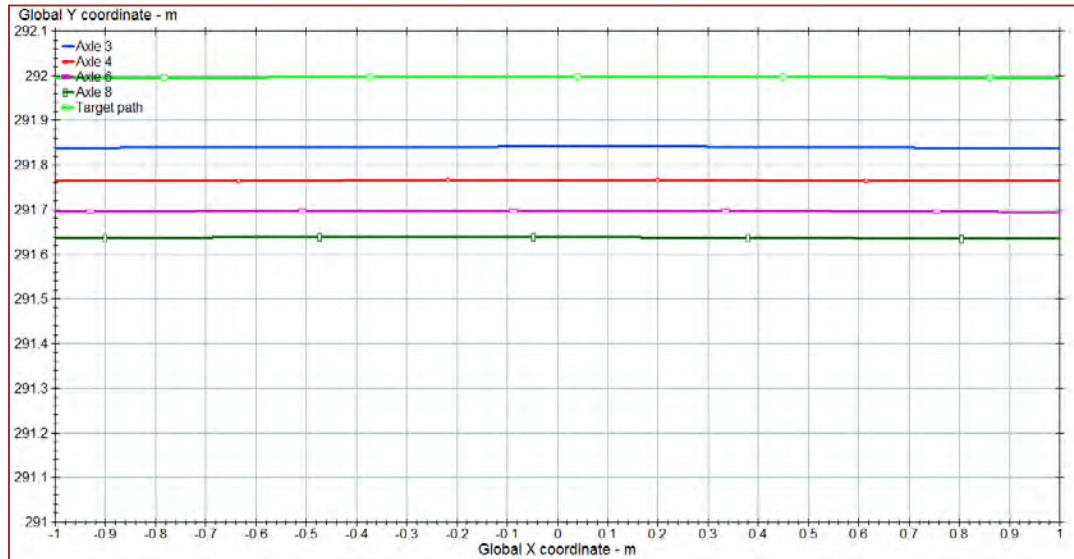


Figure 6-27. Graph. Paths of the rear axles of each unit during a simulated 72 km/h (45 mph) constant radius curve.

6.3 Comparison with Test Data

Predictions of this TruckSim® model were compared with data collected at the test track as in Chapter 4. Road wheel steer angle signals measured at the test track were used as input to the TruckSim® model. The articulation angles at the two dollies that were measured in the same maneuvers were in most cases good matches to the articulation angles predicted by the model.

6.3.1 Assessment Overview

The process began with setting up a simulation in TruckSim® and Simulink™ that loads, calibrates, and filters the string pot data for hand wheel and dolly articulation angles. A Matlab™ script was used to calibrate the hand-wheel angle and dolly articulation data according to the polynomials reported by WMU. The data was then low-pass filtered at 5 Hz using a third-order Butterworth filter to soften the transitions. Finally the hand wheel angle data was interpolated to make a consistently timed 100 Hz signal to pass to TruckSim®. The processed hand wheel steer angle data was imported to TruckSim® and used to “drive” the simulated truck. The simulated dolly articulation angle was exported from TruckSim® and passed to a Matlab™ script for overlay plotting with measured vehicle articulation data. The Matlab™ script allowed an offset to be applied to the TruckSim® data trace to position it over the test data. This was necessary because of offsets in the data, and it was done for each maneuver, so the offset was not necessarily constant from one case to another.

The validation procedure described above was used for the single and double lane change maneuvers because they provided sufficient input to excite the system, and their transients allowed response phasing comparison down the LCV. The straight driving maneuver was used to provide insight into the dynamic center, or the steady state non-zero yaw condition.

The following sections contain sets of figures showing how closely the model resembled the behavior of the test vehicle. After the Nominally Straight path is the single lane change, then the double lane change.

6.3.2 Test Vehicle Dynamic Center, Nominally Straight Path

Figure 6-28 is a portion of the measured road wheel angle as the truck drove an essentially straight path at 72 km/h (45 mph). Figure 6-29 through Figure 6-31 contain plots of dolly articulation data, recorded for the vehicle traveling in a straight line. In the latter two plots, the measured articulation data is overlaid with the simulated articulation data for the modeled vehicle driven by the imported road wheel angle data.

This data illustrates the magnitudes of steering correction and corresponding variations in the dolly articulation angle while following a nominally straight path. Comparing these variations to the transient maneuvers below can provide some insight into what is significant with respect to the steer angle input and the response of the dolly articulation angles.

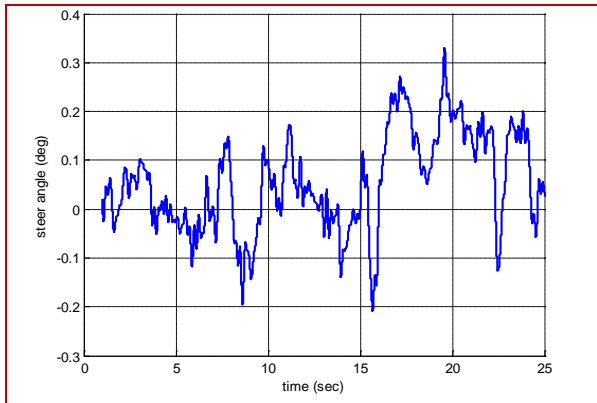


Figure 6-28. Graph. Time history of the measured road wheel angle data that was used to drive the TruckSim® model to produce the following dolly articulation response plots. 72 km/h (45 mph) nominally straight path.

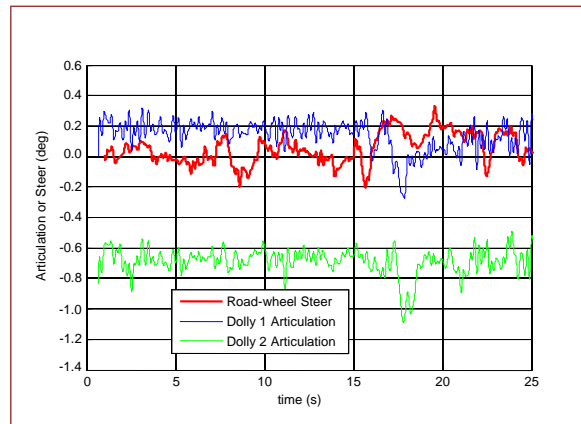


Figure 6-29. Graph. Measured road wheel angle and simulated dolly articulation angles for the nominally straight path.

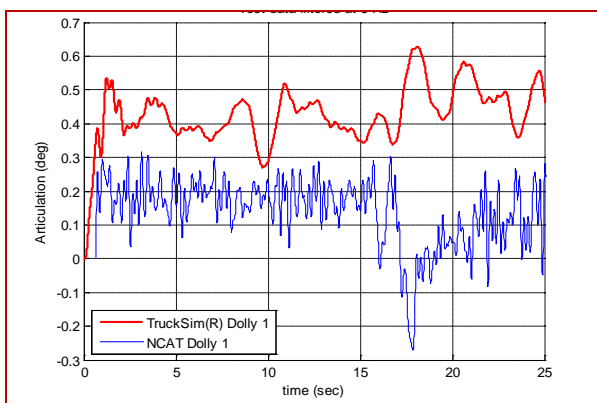


Figure 6-30. Graph. Simulated and measured articulation angles of Dolly 1 in the nominally straight path.

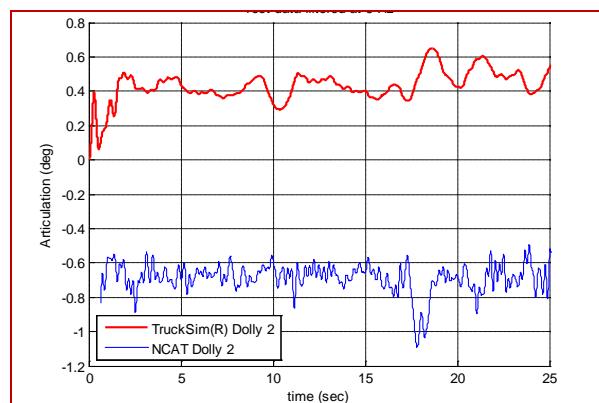


Figure 6-31. Graph. Simulated and measured articulation angles of Dolly 2 in the nominally straight path.

6.3.3 Single Lane Change Articulation Data

Agreement between the simulated single lane change articulation data and the test data recorded during test week is generally reasonable, with the modeled magnitude in articulation angle closely following the measured articulation for the primary turns in the maneuver. There are some notable differences, as outlined in this section. Figures for comparing single lane change test data recorded during test week at NCAT with TruckSim® simulation data are grouped by test speed. Each speed heading begins with a plot of the recorded steer input that was used to generate the simulated output at that speed.

The main steer input for the single lane change consists of an initial turn to the left to move the vehicle to the left lane, followed by a turn to the right to redirect the vehicle along the direction of the lane. For example, in Figure 6-32, the primary steering inputs occur between 10 s and 25 s. The data shows that the driver used some smaller scale corrective steering inputs after the

main maneuver was completed to help reduce oscillations as the vehicle continued its straight path in the left lane, during the time interval from 25 to 70 s. Finally, after traveling nominally straight during that period, the driver begins to steer back to the right lane at 70 s and then begins a left turn into the loop at the end of the test track. The straight and the curve entry are included to show the response of the vehicle in these conditions; they are not strictly a part of the single lane change maneuver.

Figure 6-36 (40 km/h, 25 mph, Dolly 2) and Figure 6-39 (48 km/h, 30 mph, Dolly 2) show the best agreement between simulation data and recorded test data. In Figure 6-36, the magnitude of articulation throughout the maneuver is nearly identical. There is only a slight variation in the phase of the initial positive direction swing of the maneuver, where the simulation data leads the test data by approximately 1 s. In both figures, the magnitudes of articulation throughout the maneuver are nearly identical between the simulation and experiment. The phase of the model response leads that of the test data. This seems to be aggravated by a sudden motion in the hand wheel input (shown in Figure 6-38) at approximately 12 seconds, but the flat spot in the steer input generates a response in the dolly motion that appears in both the model result and the test data at around 17 s. Although the data at first glance appears to be out of phase with the model result, the initial rise in the articulation angle is very well aligned in time, and the difference becomes apparent only following the peak. The magnitude of the predicted dolly articulation seems to drop off more quickly from its peak in most of the maneuvers than what was measured. This could be a result of more friction being present in the real system that prevents the dollies from moving as freely as in the model.

The agreement between measurement and simulation of the single lane change was generally good and better at the lower speeds. Figure 6-42 and Figure 6-43 (56 km/h, 35 mph, Dolly 2 and Dolly 1 respectively) show somewhat greater articulation magnitude differences between simulation and test data. This is also present in the 64 km/h (40 mph) single lane change in Figure 6-45 and Figure 6-46.

In many cases, the measured articulation angle does not return to the same level after the primary turns are complete, as at the beginning of the maneuver. This happens in both the single and double lane changes [e.g., Figure 6-39, Figure 6-46 (64 km/h, 40 mph), after about 13 s, Figure 6-49]. That it happens in some cases and not others argues against hysteresis in the measurement system; a thorough examination of more measurements is necessary to determine what is happening and why the vehicle appears not to return to the same equilibrium after the maneuver.

In general the agreement between the simulation and the test data was better for Dolly 2 than Dolly 1 for all speeds of the single lane change. The model predictions for the articulation angle generally exhibit increased levels of oscillation in response to the small corrective steering inputs that are present following the second turn of the maneuver. This is likely the result of the presence of friction on the vehicle that was not included in the model. In many cases, the test

data also shows a shift in articulation during the straight section after the main maneuver, which could be indicative of hysteresis as a result of friction in the fifth wheel or it could represent an issue with the measurements themselves.

32 km/h (20 mph) Single Lane Change

Simulation and test results for the 32 km/h (20 mph) single lane change (Figure 6-33 and Figure 6-34) differed more significantly than in the higher-speed cases, although the overall trend is still well predicted and the magnitudes of peaks are relatively close. Dolly 2's articulation was similar in phasing but had a poor agreement in magnitude in the negative direction swing, between 60 s and 70 s. The model responded with a much greater magnitude than that which was shown in the test data and the change in articulation angle occurred more quickly from the peaks, as mentioned above. Dolly 1's articulation also showed worse agreement in magnitude for this period than in the other conditions. The simulated data leads the test data throughout. The magnitudes were off for the entire maneuver. (The string pot data was low-pass filtered at 5 Hz to show a clean signal. Agreement in magnitude was better when the data was filtered at 10 Hz. Recording a clean signal in future tests will be important for comparisons.)

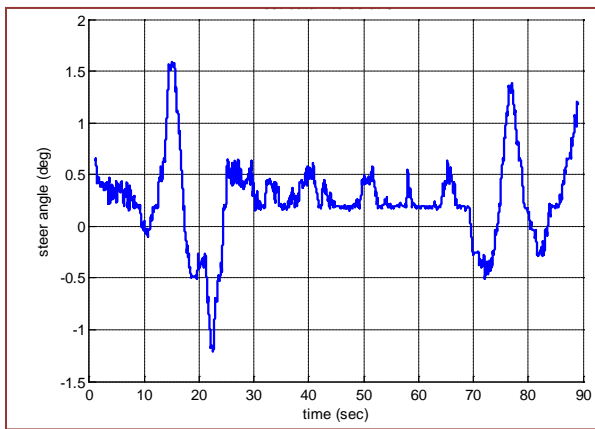


Figure 6-32. Graph. Time history of the measured road wheel angle data that was used to drive the TruckSim® model to produce the following dolly articulation response plots. 32 km/h (20 mph) single lane change.

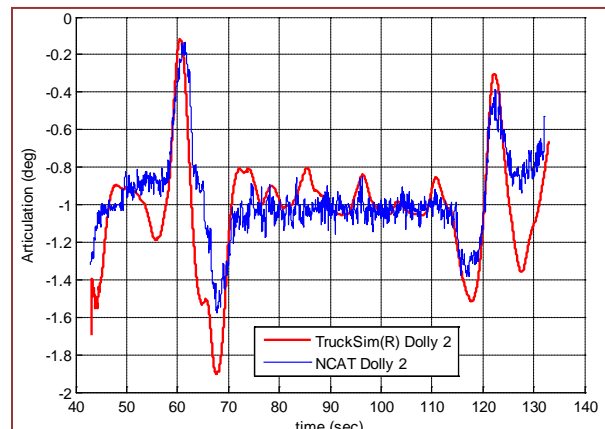


Figure 6-33. Graph. Simulated and measured articulation angles of Dolly 2 in the 32km/h (20 mph) single lane change.

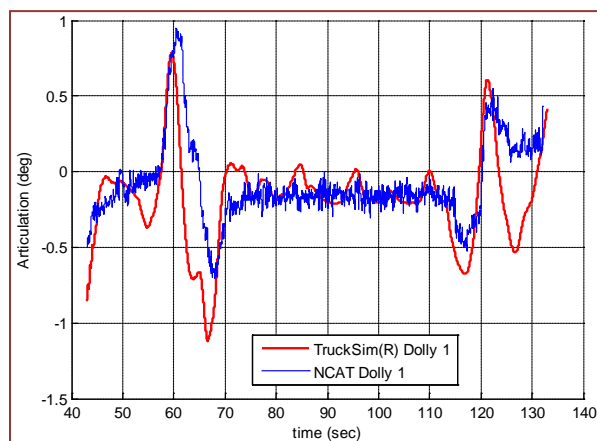


Figure 6-34. Graph. Simulated and measured articulation angles of Dolly 1 in the 32 km/h (20 mph) single lane change.

40 km/h (25 mph) Single Lane Change

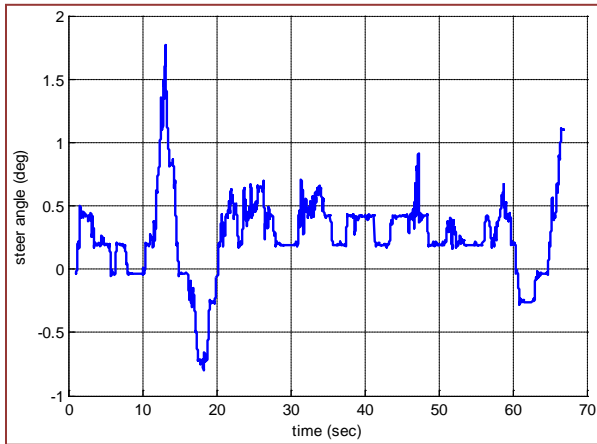


Figure 6-35. Graph. Time history of the measured road wheel angle data that was used to drive the TruckSim® model to produce the dolly articulation response plots in the 40 km/h (25 mph) single lane change.

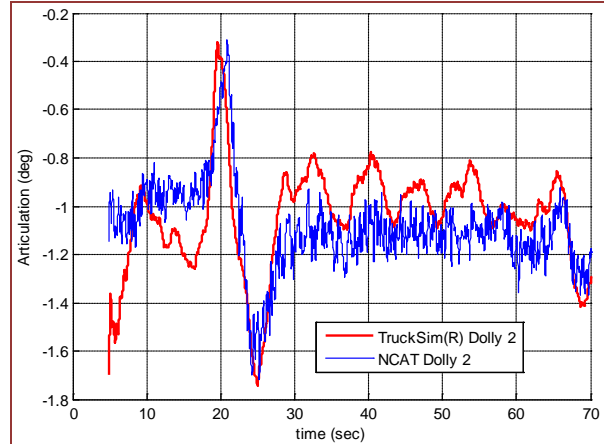


Figure 6-36. Graph. Simulated and measured articulation angles of Dolly 2.

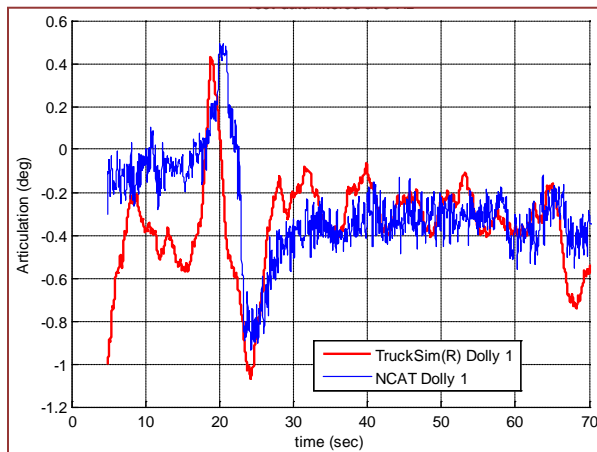


Figure 6-37. Graph. Simulated and measured articulation angles of Dolly 1.

48 km/h (30 mph) Single Lane Change

Dolly 2's articulation in Figure 6-39 shows reasonable agreement between test and simulation data. The shape of the peak articulation in the initial positive motion is slightly wider, suggesting that the dolly dwelled in that position longer than the simulation. This dwell likely carried through to the sudden hand wheel motion at 19 s, causing the difference in magnitude.

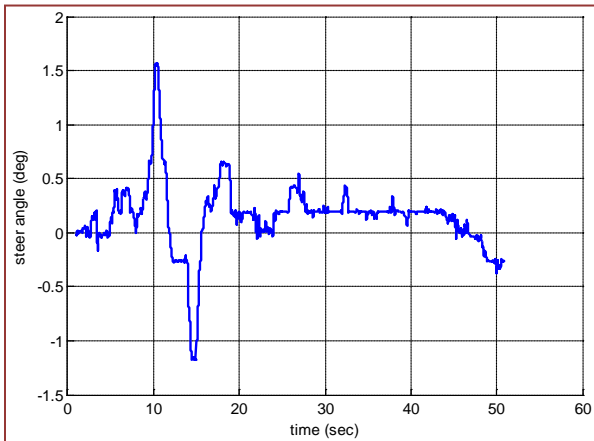


Figure 6-38. Graph. Time history of the measured road wheel angle data that was used to drive the TruckSim® model to produce the dolly articulation response plots in the 48 km/h (30 mph) single lane change.

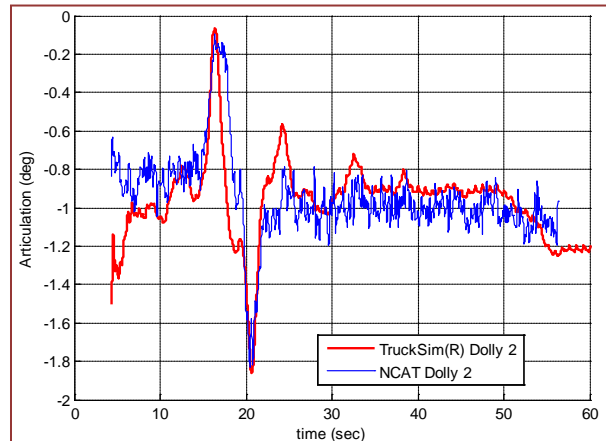


Figure 6-39. Graph. Simulated and measured articulation angles of Dolly 2.

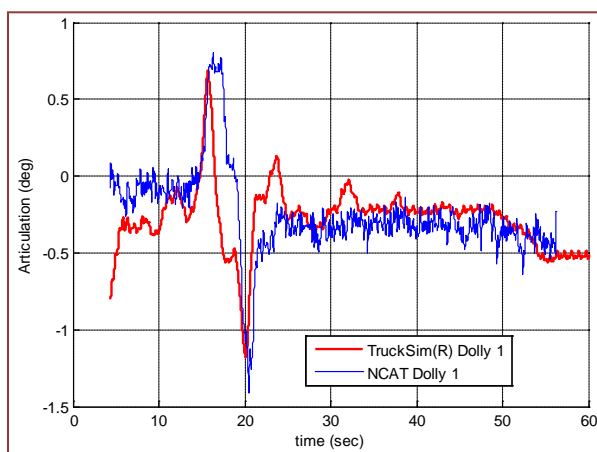


Figure 6-40. Graph. Simulated and measured articulation angles of Dolly 1.

56 km/h (35 mph) Single Lane Change

Figure 6-42 (Dolly 2) shows good agreement between simulation data and recorded test data. The magnitudes of articulation were nearly identical throughout. Once again, the simulated articulation changes more quickly after the maximum articulation is reached, which makes the width of the peak more narrow than the measured data. The rate of change in the articulation angle after a peak is almost always faster in the model than the measurement.

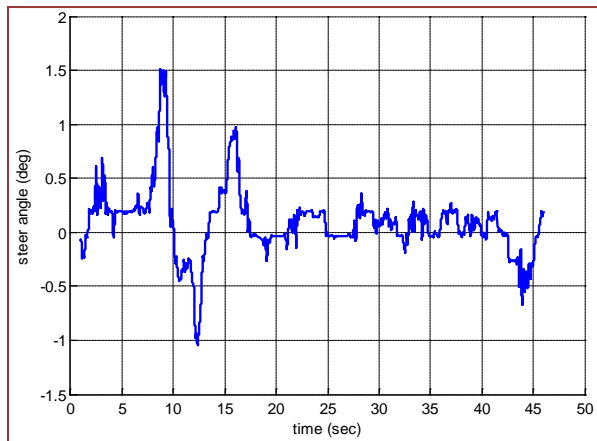


Figure 6-41. Graph. Time history of the measured road wheel angle data that was used to drive the TruckSim® model to produce the dolly articulation response plots for the 56 km/h (35 mph) single lane change.

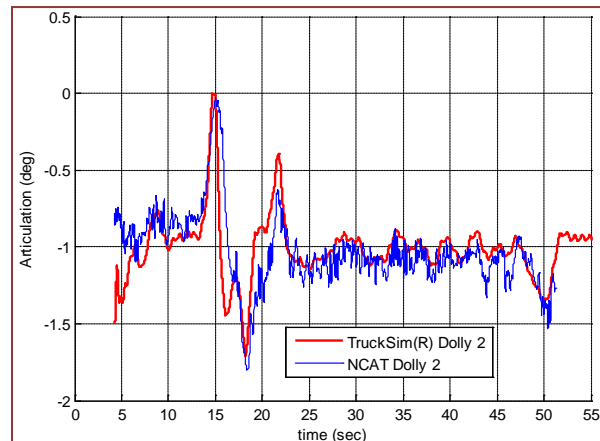


Figure 6-42. Graph. Simulated and measured articulation angles of Dolly 2.

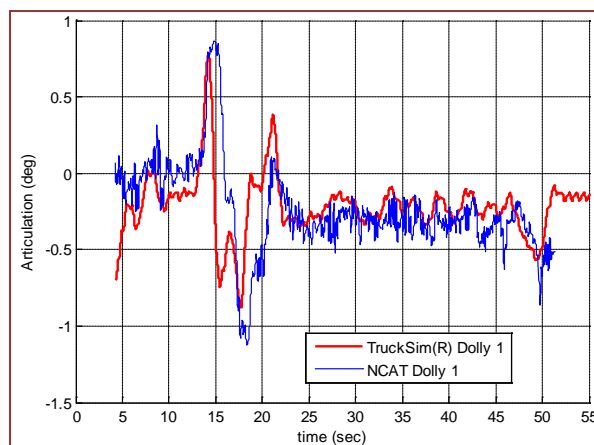


Figure 6-43. Graph. Simulated and measured articulation angles of Dolly 1.

64 km/h (40 mph) Single Lane Change

The discrepancy between test and simulation data is significant after the first half of the lane change and continuing into the straight portion of Figure 6-46 (64 km/h, 40 mph). Differences are noticeable in phasing magnitude and response shape. The poor agreement could possibly be attributed to the typical issues with Dolly 1 being worsened by the effects of speed.

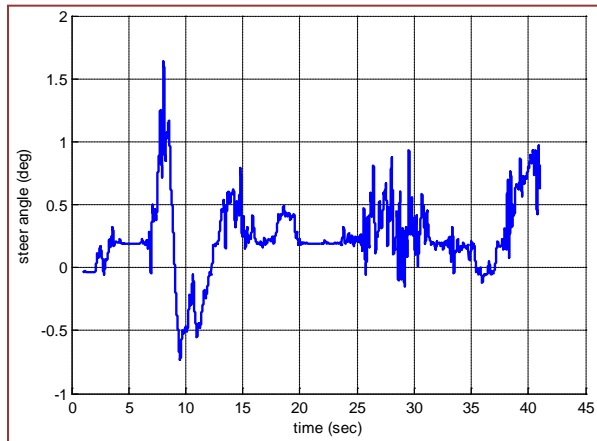


Figure 6-44. Graph. Time history of the measured road wheel angle data that was used to drive the TruckSim® model to produce the dolly articulation response plots in the 64 km/h (40 mph) single lane change.

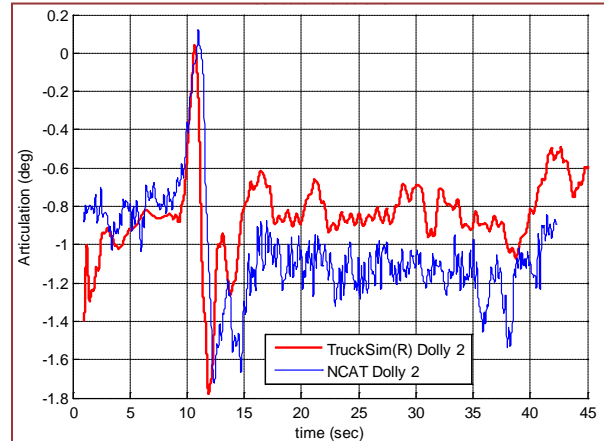


Figure 6-45. Graph. Simulated and measured articulation angles of Dolly 2.

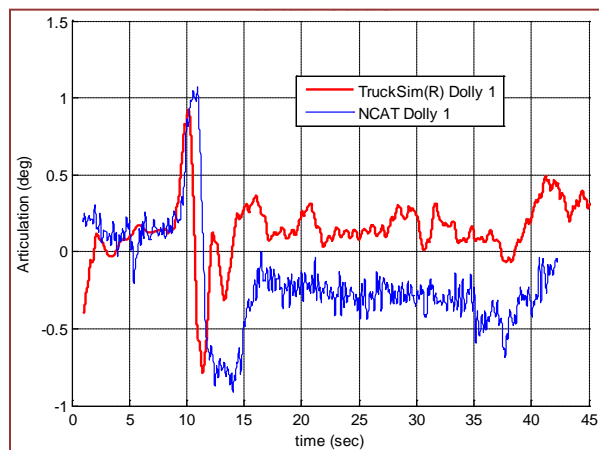


Figure 6-46. Graph. Simulated and measured articulation angles of Dolly 1.

6.3.4 Double Lane Change Articulation Data

All of the simulated lane change articulation data at least roughly resembled the test data recorded at NCAT. Figure 6-47 through Figure 6-58 repeat, for the double lane change, the same pattern that was established for the single lane change. The following sections are grouped

by test speed. There is a plot of the recorded and processed steer input used to drive the model at the beginning of each section.

The model agreement is similar to that for the single lane change maneuver, with reasonable agreement in the magnitude of the predicted articulation angle during the primary turns, but with the modeled articulation angle changing earlier and more rapidly than what occurred on the test vehicle, resulting in narrower peaks and troughs.

The best agreement between test data and simulation data for the double lane change was in Figure 6-48 and Figure 6-49 (32 km/h, 20 mph, Dolly 2 and Dolly 1), and Figure 6-51 (40km/h, 25 mph, Dolly 2). The magnitude of the articulation and phasing align well. At the third major inflection in dolly articulation (where the driver brings the truck back into right lane), the simulated articulation response is higher than that of the recorded test data.

As with the single lane change, in general the agreement between the simulation and the test data was better for Dolly 2 than Dolly 1 in both magnitude and phasing for all test speeds of the double lane change. And, as with the single lane change, the higher speed maneuvers generally show larger differences between the test data and model predictions.

32 km/h (20 mph) Double Lane Change

Figure 6-48 (32 km/h, 20 mph, Dolly 2) shows that test and simulation articulation data for Dolly 2 are in good agreement in phase. The magnitude agrees well for the first portion of the maneuver. At the fourth major inflection at about 75 s, where the driver steers the truck back into the right lane, the simulation has a larger magnitude articulation than the recorded data. Agreement for Dolly 1 was not quite as good.

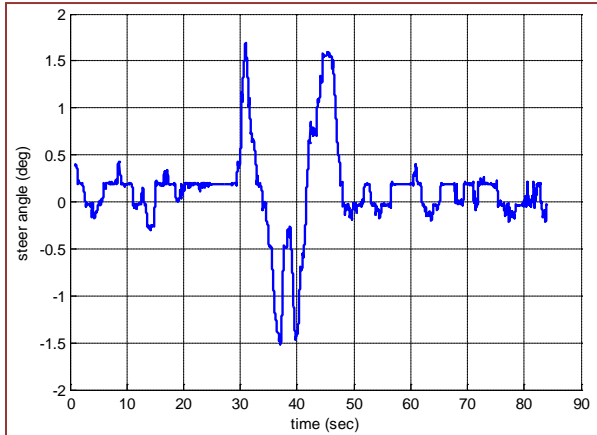


Figure 6-47. Graph. Time history of the measured road wheel angle data that was used to drive the TruckSim® model to produce the dolly articulation response plots in the 32 km/h (20 mph) double lane change.

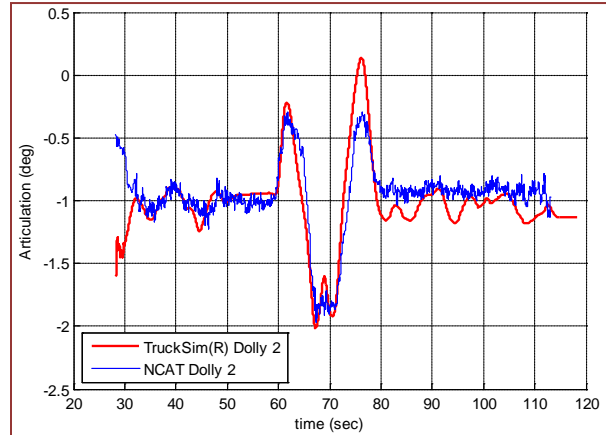


Figure 6-48. Graph. Simulated and measured articulation angles of Dolly 2.

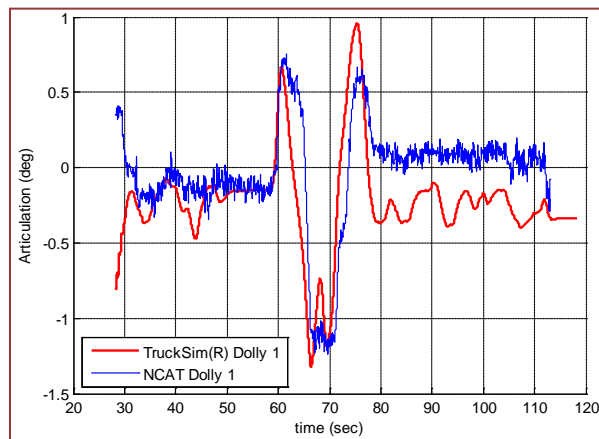


Figure 6-49. Graph. Simulated and measured articulation angles of Dolly 1.

40 km/h (25 mph) Double Lane Change

Figure 6-51 (Dolly 2) shows typical agreement with minor phase lag in the transition from the left lane back to the right (at approximately 35 s).

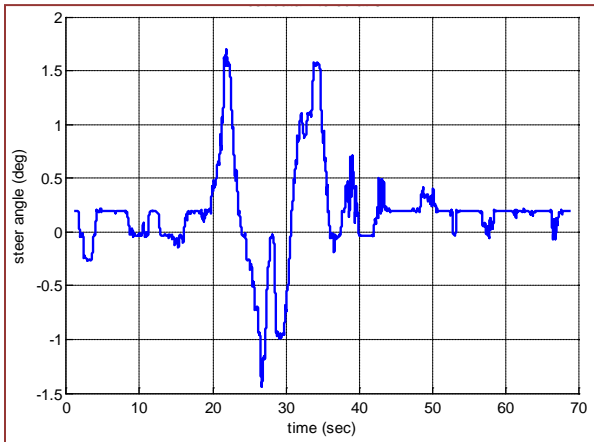


Figure 6-50. Graph. Time history of the measured road wheel angle data that was used to drive the TruckSim® model to produce the dolly articulation response plots in the 40 km/h (25 mph) double lane change.

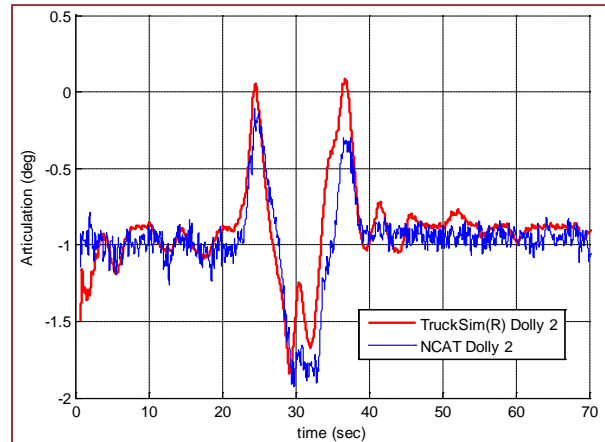


Figure 6-51. Graph. Simulated and measured articulation angles of Dolly 2.

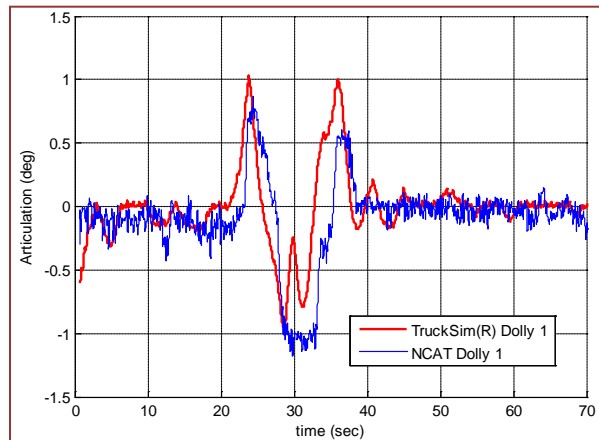


Figure 6-52. Graph. Simulated and measured articulation angles of Dolly 1.

48 km/h (30 mph) Double Lane Change

Figure 6-54 (Dolly 2) also shows good agreement between test data and simulation data. As was the case in some of the single lane change plots, the model tends to lead the vehicle response by 1 s or more. This is possibly exacerbated by a sudden motion in the steer input at approximately 20 s. The shape of the simulated response is similar to that shown for Dolly 2, but the difference in phasing and magnitude is apparent throughout the maneuver.

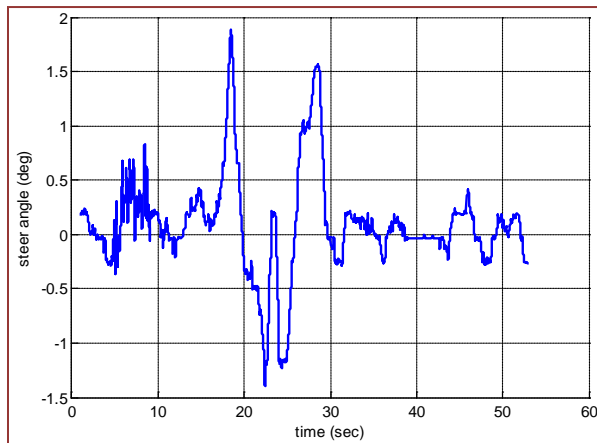


Figure 6-53. Graph. Time history of the measured road wheel angle data that was used to drive the TruckSim® model to produce the dolly articulation response plots in the 48 km/h (30 mph) double lane change.

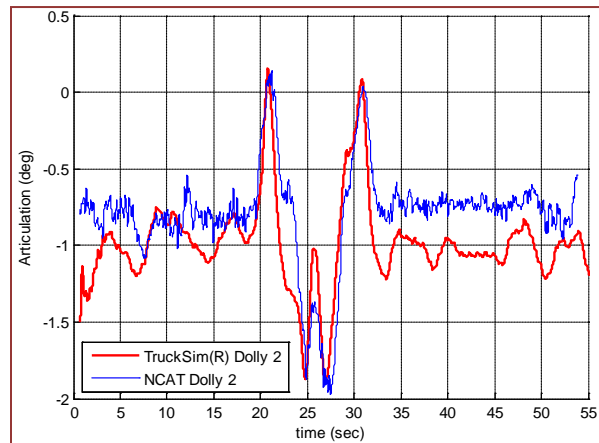


Figure 6-54. Graph. Simulated and measured articulation angles of Dolly 2.

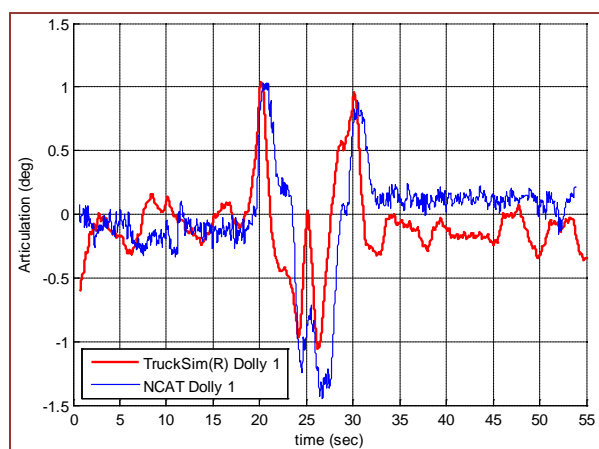


Figure 6-55. Graph. Simulated and measured articulation angles of Dolly 1.

56 km/h (35 mph) Double Lane Change

Figure 6-57 shows a poorer agreement for Dolly 1 than Dolly 2 in Figure 6-58. This is typical and expected.

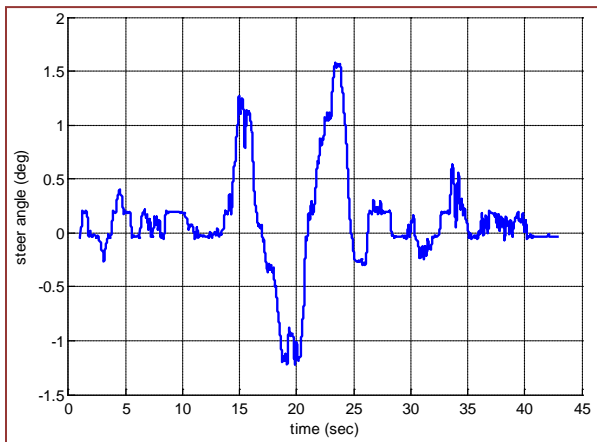


Figure 6-56. Graph. Time history of the measured road wheel angle data that was used to drive the TruckSim® model to produce the dolly articulation response plots in the 56 km/h (35 mph) double lane change.

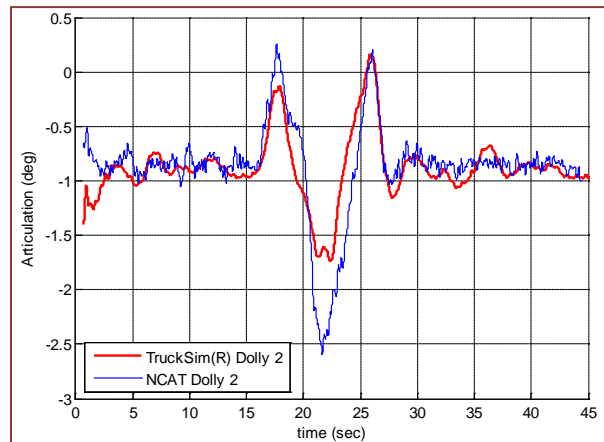


Figure 6-57. Graph. Simulated and measured articulation angles of Dolly 2

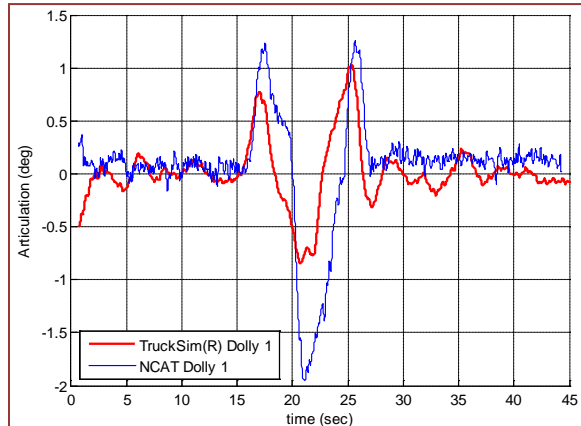


Figure 6-58. Graph. Simulated and measured articulation angles of Dolly 1.

6.3.5 Comparison Summary

Agreement between the test track data and the TruckSim® simulations was qualitatively good in all cases and quantitatively good in most cases. Minor differences were expected and noticed. The model response demonstrated less fidelity to the test data in the faster maneuver speeds. In general, the model response for Dolly 1 demonstrated less fidelity than Dolly 2 at all maneuver speeds.

6.4 Example of Swept Sine Analysis

The responses of each individual unit contribute to the total response of an LCV. The lead trailer drives the following trailer through the dolly. Data from impulse steer and swept-sine steer maneuvers can be analyzed to produce dynamic response characteristics such as natural frequencies, damping ratios, and phase lags of responses to steer input such as yaw rate and lateral acceleration. Lag time for response from unit to unit can be measured from time history based analysis. Unit characteristics such as damping ratio and natural frequency for various responses will be more difficult to assess without a way to decompose the response of each unit in the LCV. Knowledge of the characteristics of each unit could possibly aid analysis of time history data by showing that one unit may be more active than another (if, for example, its yaw rate response was very lightly damped in comparison to another unit). Another trailer may be dull in its response (if it has a highly damped low natural frequency yaw rate response). Rearward amplification can be identified using these techniques as well, as in Figure 2-11 of the literature review. Yaw rate and lateral acceleration gain can potentially be analyzed from the road wheel steer input to trailer yaw or acceleration to establish the amplification characteristics of the vehicle and at which frequencies they occur.

One way to analyze the frequency response of a vehicle is with a swept-sine steer input. The following plots outline the steer input, lateral acceleration, and trajectory estimated for this maneuver. See Figure 6-59 for a TruckSim® plot of the steer input for the maneuver, Figure 6-60 for a graph of the simulated trajectory for the maneuver, and Figure 6-61 for the simulated lateral acceleration.

In the TruckSim® plots in this section, Unit 1 refers to the tractor, Unit 2 refers to Trailer 1, Unit 3 refers to Dolly 1, Unit 4 refers to Trailer 2, Unit 5 refers to Dolly 2, and Unit 6 refers to Trailer 3.

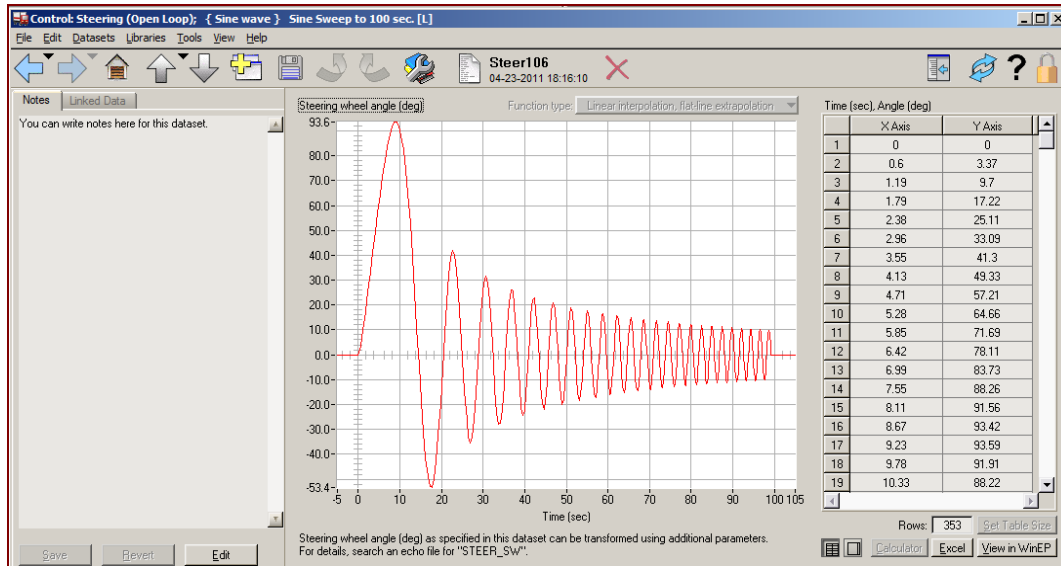


Figure 6-59. Screen Capture. TruckSim® screen where the swept sine steer input is defined. This is a predefined TruckSim® maneuver. (Mechanical Simulation Corporation 2010)

The swept-sine steer input shown in Figure 6-59 covers approximately 0.05 to 0.5 Hz. For actual and future implementation, a steering pattern should be established to include a broader frequency range. A frequency range of 0.05 Hz to 3 Hz should be sufficient, since this covers the range of what is expected to influence the vehicle dynamics up to the normal limits of human steering capabilities.

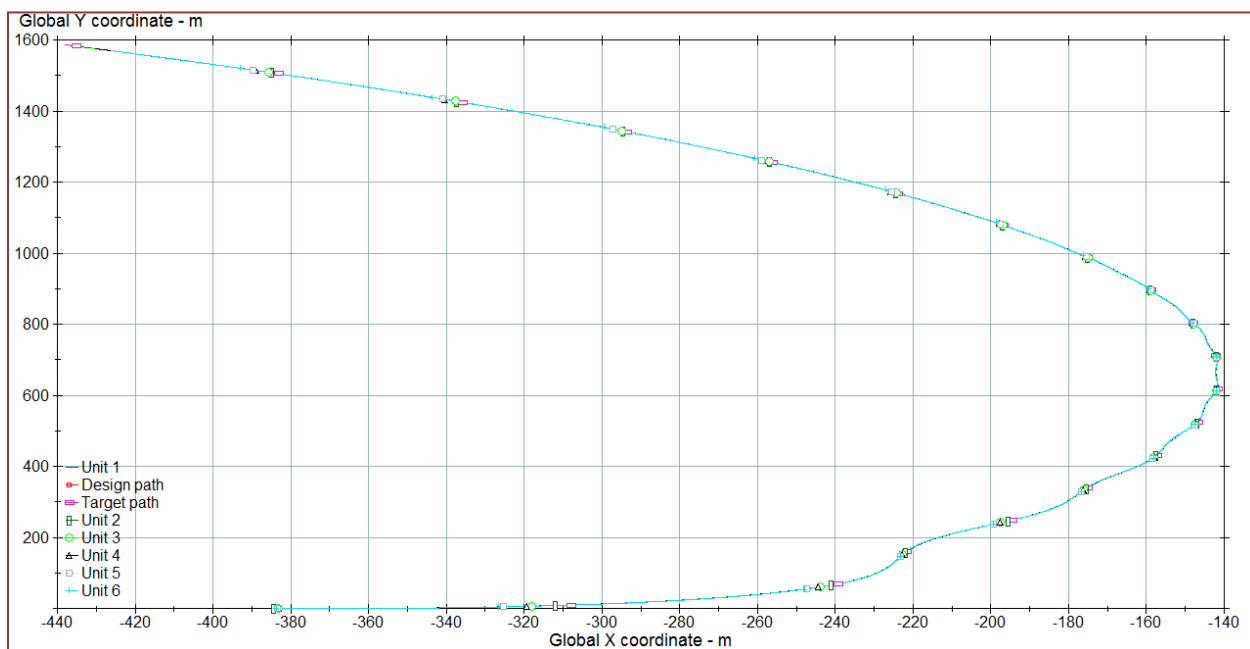


Figure 6-60. Graph. Simulated trajectory of the test vehicle performing a swept-sine maneuver at 64 km/h (40 mph).

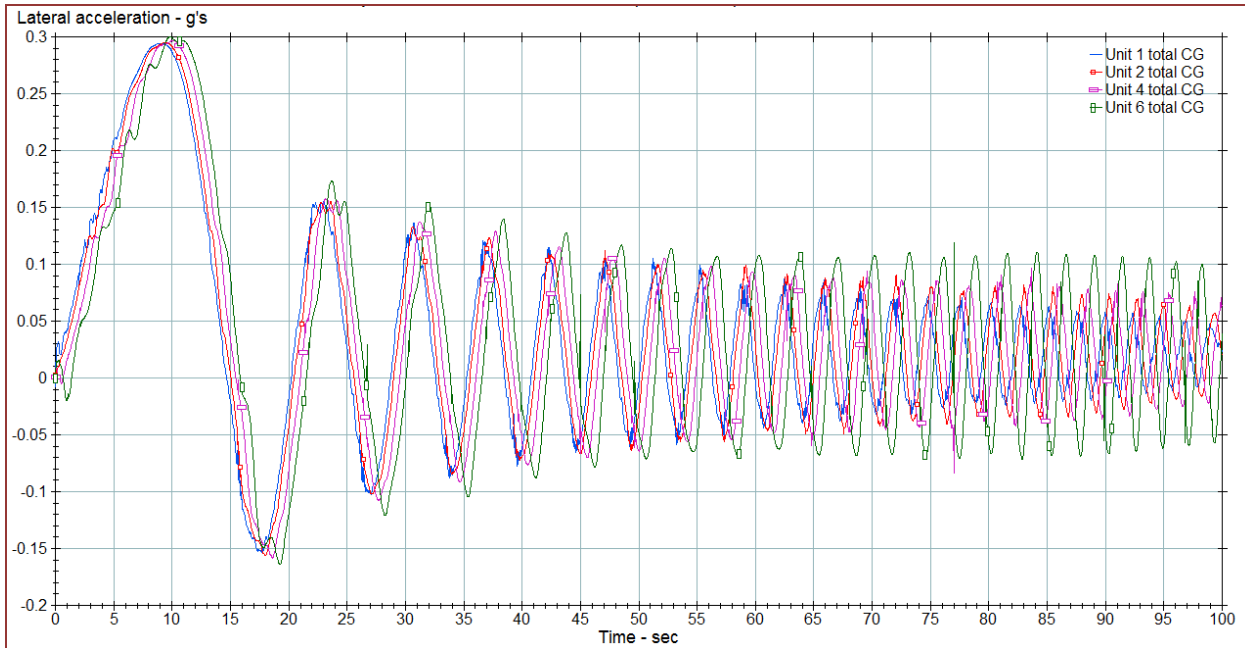


Figure 6-61. Graph. Simulated lateral acceleration of the test vehicle during the proposed swept sine maneuver.

6.4.1 Analysis of Yaw Rate in the Model Data

The yaw rates from the swept sine maneuver simulated in TruckSim[®] were carried through analysis to show how it might be done. The next five figures show this analysis. Figure 6-62 shows the yaw rate gain from the hand-wheel input for the tractor. The change in phase angle is expected as the response starts to lag the input in the higher frequencies.

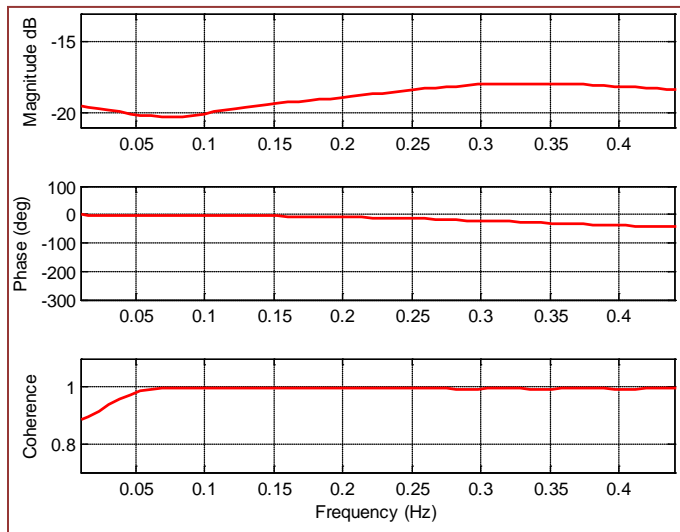
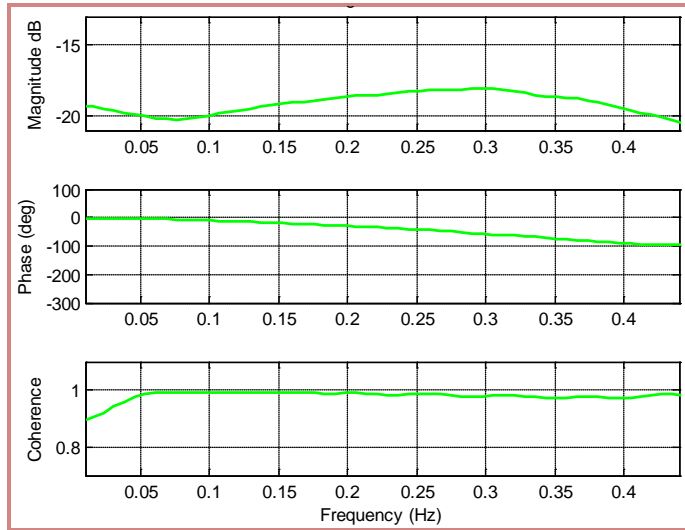


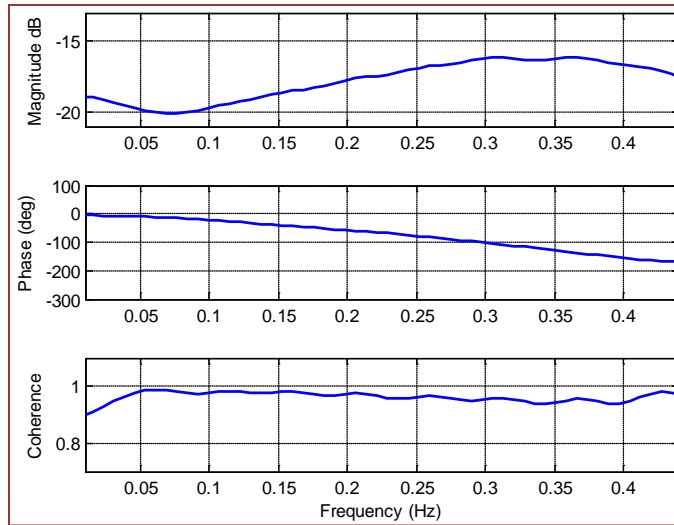
Figure 6-62. Graph. Frequency Response Plot of Yaw Rate Gain with Phase and Coherence Function: Tractor Yaw Rate Gain.

Figure 6-63 shows the yaw rate gain from hand wheel input for Trailer 1. The coherence function is still nearly 1 from 0.05 Hz to almost 0.5 Hz with only slight reduction in coherence from 0.25 Hz to the upper range of the spectrum. Trailer 1 shows a more significant phase change as the response lags the input even greater than for the tractor. The peak yaw rate gain occurs at approximately 0.3 Hz for Trailer 1.



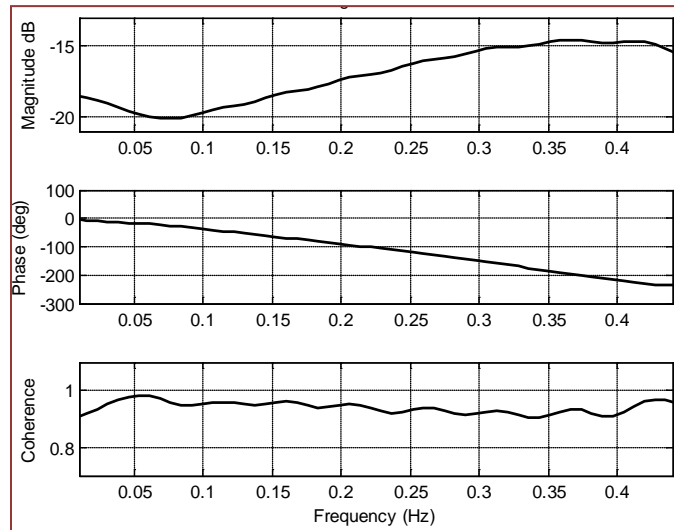
**Figure 6-63. Graph. Frequency response plot with phase and coherence function:
Trailer 1 yaw rate gain.**

Figure 6-64 shows yaw rate gain from hand-wheel input for Trailer 2. The coherence for this transfer function is lower than that of Trailer 1 and the tractor. This is due to other inputs than the hand-wheel causing the yaw response for this trailer. This is the combined effect of the signal passing down the length of the trailer. Since the coherence is calculated from the steer input, the additional responses along the combination (Trailer 1 and Dolly 1) contributing to the response of Trailer 2 reduce the coherence of the second trailer response to the steer input. The maximum yaw rate gain lies between 0.3 and 0.4 Hz.



**Figure 6-64. Graph. Frequency response plot with coherence function:
Trailer 2 yaw rate gain.**

Figure 6-65 shows the yaw rate gain of Trailer 3 from the hand wheel input. The yaw rate gain peaks at above 0.4 Hz. The coherence function is less than the previous units in the combination. This again is likely due to the additive nature of the vehicle response reducing the interdependence between hand wheel input and Trailer 3 yaw rate



**Figure 6-65. Graph. Frequency response plot with phase and coherence function:
Trailer 3 yaw rate gain.**

Figure 6-66 shows an overlay of the yaw rate gains from across the entire LCV model. The magnitudes show clear amplification between units from the tractor-Trailer 1 combination and Trailer 2 and Trailer 3. The spread in the yaw rate gains shows that the amplification increases with the frequency of response. A more abrupt response has a larger amplification. The peaks

of the yaw rate gain of each trailer seem to occur at different frequencies. This suggests that each trailer has a unique damped natural frequency.

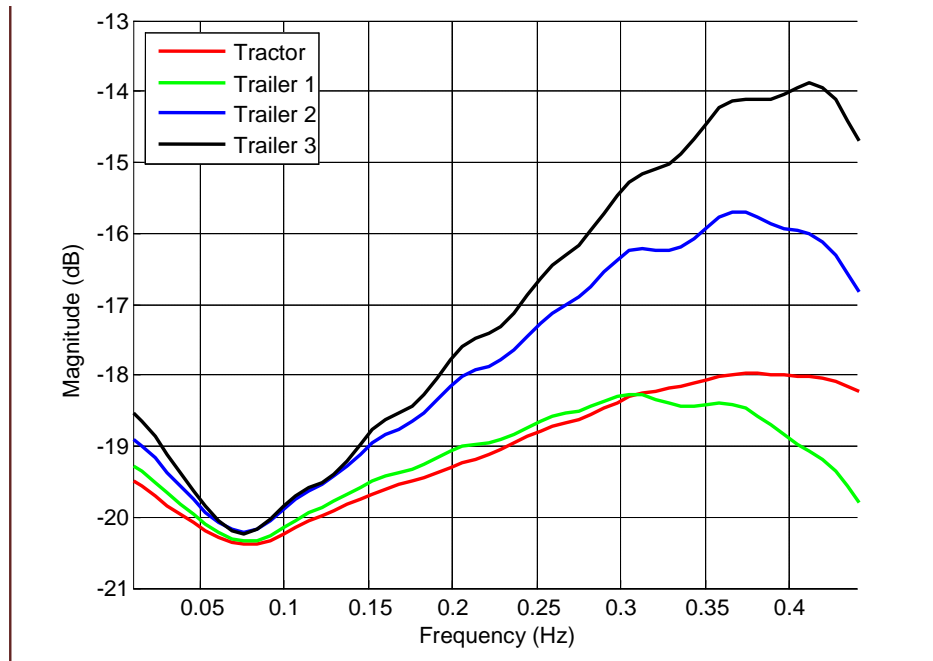


Figure 6-66. Graph. Yaw rate gain of the tractor and three trailers to hand wheel input.

Figure 6-67 contains the same information with a different reference quantity. It shows the ratio of yaw rate gain from tractor to Trailers 1 through 3, i.e., the rearward amplification of the yaw rate. Trailer 1 shows the least amplification in the lower range of the response and shows an attenuated response above 0.28 Hz. Trailer 2 and Trailer 3 exhibit significant rearward amplification, with maximum amplification of about 25% and 50%, respectively.

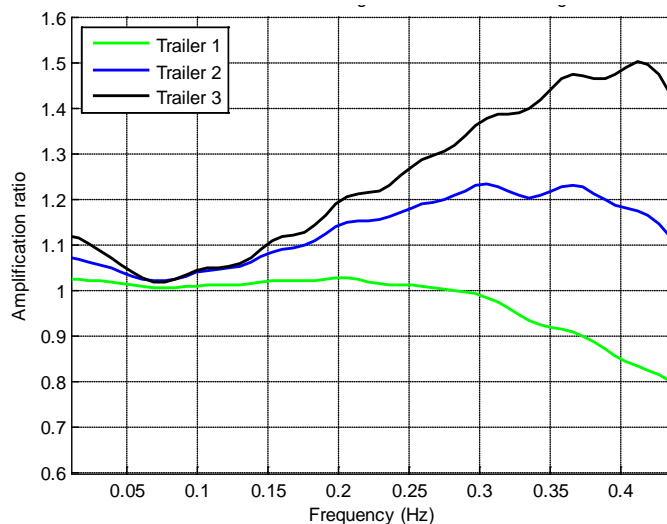


Figure 6-67. Graph. Amplification of the yaw rate of the three trailers to the tractor's yaw rate.

The amplification and hierarchy of response shown in the final two figures show that Trailers 2 and 3 are can be highly excited to hand wheel input above about 0.2 Hz. Trailer 1 behaves differently as the yaw response gain falls below that of the tractor above 0.3 Hz. This is the same effect as in Figure 2-11 of the literature review; the nature of the response in Figure 6-67 is different from the examples in that figure because it is specific to the LCV triple at NCAT. Further study of the interaction of the trailers will lead to a better understanding of this response.

The transfer functions do not have to be confined to relating hand wheel input to dynamic output. Other inputs can be used. Transfer functions from dolly to trailer can potentially be used to analyze individual response characteristics for each trailer explicitly, similarly to what was done with the test data in Chapter 5.

This page intentionally left blank.

Chapter 7 – Modeling—Compliant Member Model

Adams is a general use, multi-body dynamics program, which is designed to allow the development of models of any mechanical system. This is done through the creation of rigid bodies representing the mass and inertia of the components, which can be interconnected by compliant elements. These entities may also have some or all of their degrees of freedom restricted relative to “ground” or each other. The equations of motion for the system are then automatically developed and numerically integrated over a specified time period. Once a simulation is complete, many physical quantities of interest can be plotted, and the behavior of the system visualized through animations.

Some of the program’s advanced capability, applied in the subject LCV model, allows body flexibility, intermittent contact, and nonlinear entities. Although these features make the system more complicated, they also improve its fidelity.

Each unit of the vehicle was required to represent the total system. In addition, each unit may contain any number of subsystems, such as suspensions or steering linkages. Where available, data from the original equipment manufacturer was used to define these entities. Unfortunately, many items were based on estimations due to a lack of information.

7.1 Adams Model Formulation

The vehicle system comprised several dollies and trailers. These units were given a number to aid in their identification, starting with the unit closest to the tractor. This resulted in the naming convention shown in Figure 7-1, which was utilized to organize the model results. Each unit of the vehicle is described below.

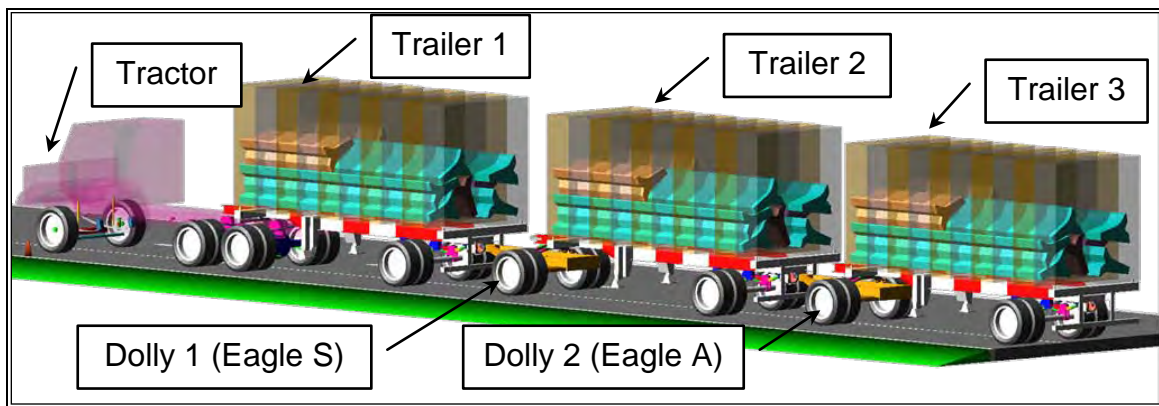


Figure 7-1. Drawing. Adams model of the full vehicle.

7.1.1 Tractor

The tractor used at NCAT was a 6x4 Freightliner with a 4.7 m (186 in.) wheelbase. It incorporated a traditional mechanical spring steer suspension, and a trailing arm air ride suspension at the rear tandem axles. A fifth wheel was located between the tandem axles,

providing a connection to the trailer. This tractor represented a vehicle commonly used for on-highway operations, with the possible exception of its double-rail frame. Its model is in Figure 7-2.

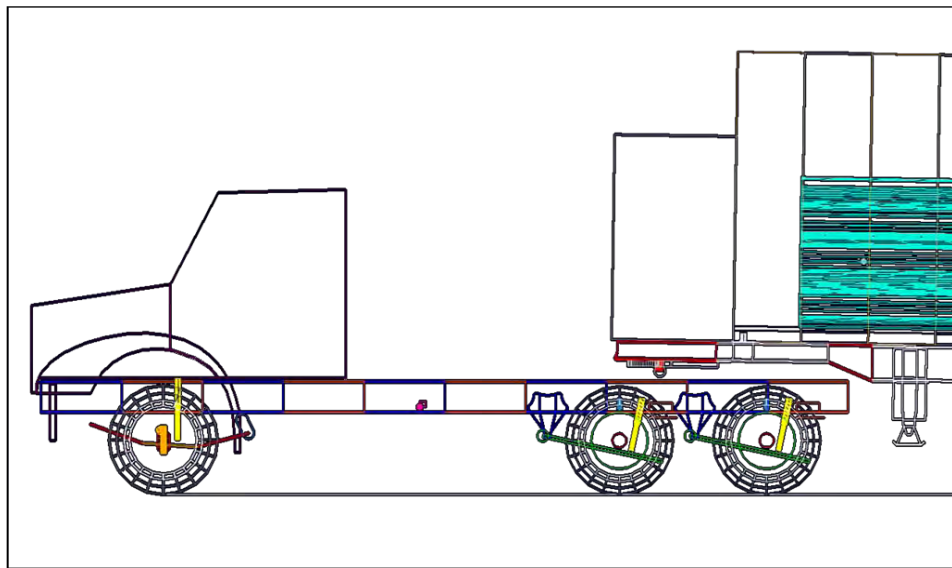


Figure 7-2. Drawing. Adams model, tractor left side view.

Steering System

In order to have the vehicle model “drive” on the test track, a steering system was required that would follow the desired course. Two spindles with kingpins were used to allow rotation of the steer tires, and they were connected via an Adams coupler element. This element enforced an equal and opposite rotation of the spindles, and essentially acted as the tie rod. The steering input was done through a simple “point-follower” algorithm that acted as a simple controller. Parameters exist in the model to tune the capability of this algorithm, and to have the vehicle follow different paths. In addition, the path error could be examined to determine how well the controller matched the desired route, which was stored in an Adams spline element. For this model, the desired paths were the mathematically precise routes defining each event.

Steer Suspension

The model of the tractor steer suspension is in Figure 7-3. The mechanical spring used in the steer axle suspension was created using the SAE three-link method (SAE 1980). This was a simplification that replaced the spring pack with three discrete rigid links. In Adams, these links were connected with joints and bushing elements. The spring rate of this suspension was defined using the measurements made by WMU. The rear of the spring was attached to a shackle, which was then attached to the tractor frame. The forward end of the spring had a traditional eye with bushing configuration. The total mass, center of gravity, and mass moments of inertia of these components were estimated by the Adams software.

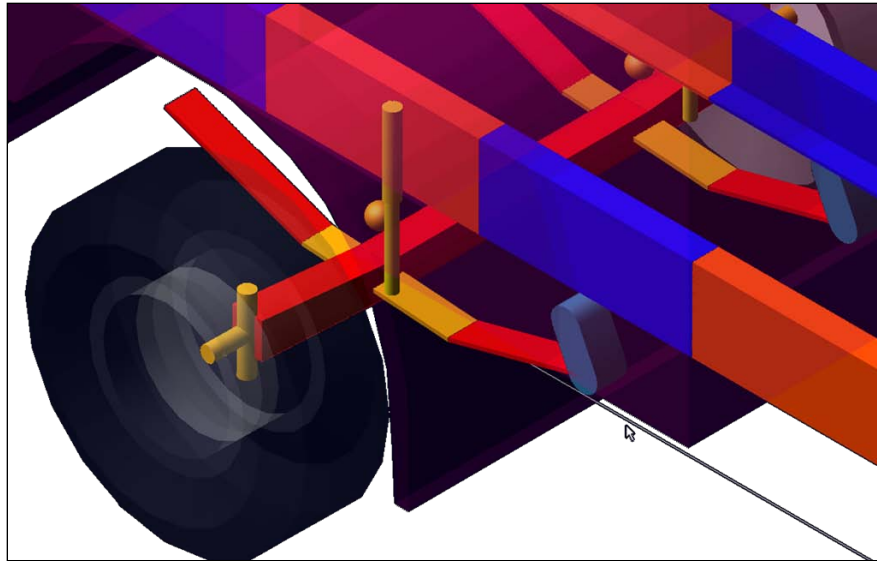


Figure 7-3. Drawing. Adams Model, Tractor Steer Suspension

Drive Suspension

The suspension at the tandem drive axles was a Freightliner “Airliner” trailing arm air suspension. This system incorporated a mechanical spring in combination with an airbag. The spring rate of this suspension was defined using the measurements made by WMU. Shock absorbers were included in the system, as well as transverse torque rods (Panhard Rods) controlling lateral displacement of the axles. There were also bushings at several of the suspension attachment points, with appropriate stiffness and damping coefficients. The stiffness and damping of these entities were estimated. The total mass, CG, and mass moments of inertia were determined from direct measurement, computer aided design (CAD) models, and published data.

Stiffness

The component providing the primary stiffness of the tractor was the ladder type frame. This flexibility could be incorporated in the system, if deemed relevant, through various modeling techniques. For this model, this response was developed by utilizing Adams bushing elements, which were “tuned” to represent the measured torsional stiffness. By specifying “high” values for these elements, a rigid frame condition could be realized.

Fifth Wheel

The fifth wheel allowed two rotational degrees of freedom between the tractor and trailer. This behavior was modeled using simple Adams joint elements. The total mass, CG, and mass moments of inertia were determined from direct measurement, CAD models, and published data.

Velocity Controller

The forward velocity of the vehicle was assigned as an initial condition to all the rigid and flexible bodies in the system. In order to maintain this velocity during the maneuvers, which could cause the vehicle to lose velocity, a rotational force was applied at the tractor drive wheels. The magnitude of the force was monitored by a simple proportional-integral controller. The gain coefficients for the controller terms were determined through trial and error until an acceptable level of control was achieved.

7.1.2 Trailer

Each of the three trailers was a 6.1 m long (20 ft) intermodal container on a chassis manufactured by Cheetah. The chassis were modeled as simple ladder-type frames, with bolster assemblies to attach the containers (Figure 7-4). The 6.1 m (20 ft) nominal size is not as common as the 12.2 m (40 ft) and longer containers; they and the concrete barrier ballast were selected to match the vehicles in the tests. Trailers more typically used in double and triple applications are 8.5 m (28 ft) vans.

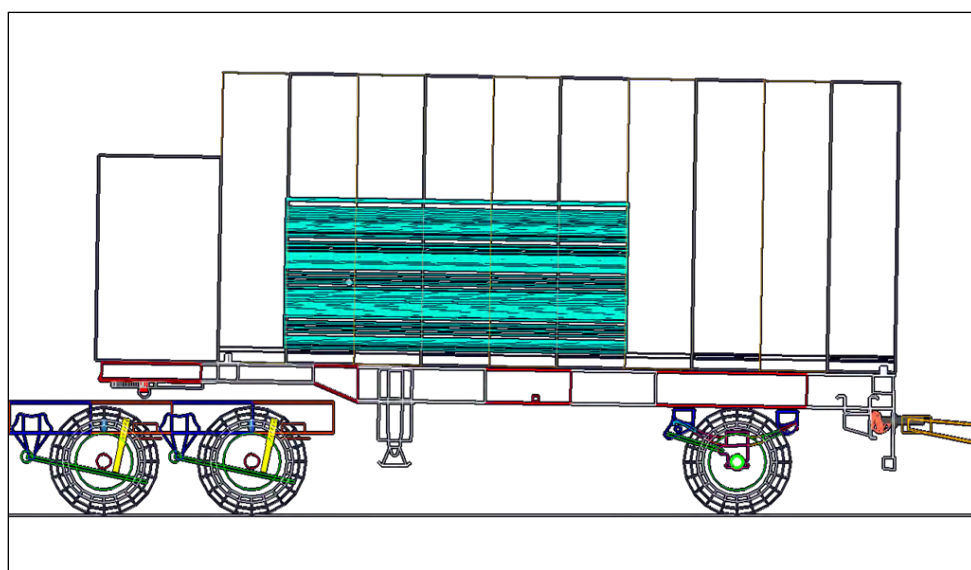


Figure 7-4. Drawing. Adams Model, Trailer Left Side View

Suspension

The trailers employed a common Hutchens mechanical spring suspension, which was represented by the SAE three-link method, as shown in Figure 7-5. The spring rate of this suspension was compared to published data, and adjusted as required. Damping in this type of suspension was supplied through interleaf friction in the spring pack, and friction at the frame hanger cam or slipper surfaces. Longitudinal torque rods provided fore/aft axle control. There were also bushings at several of the suspension attachment points, with approximate stiffness and damping coefficients. The axle tube was represented by an Adams “flex body,” which is a

modal representation. The total mass, CG, and mass moments of inertia were determined from direct measurement, CAD models, and published data.

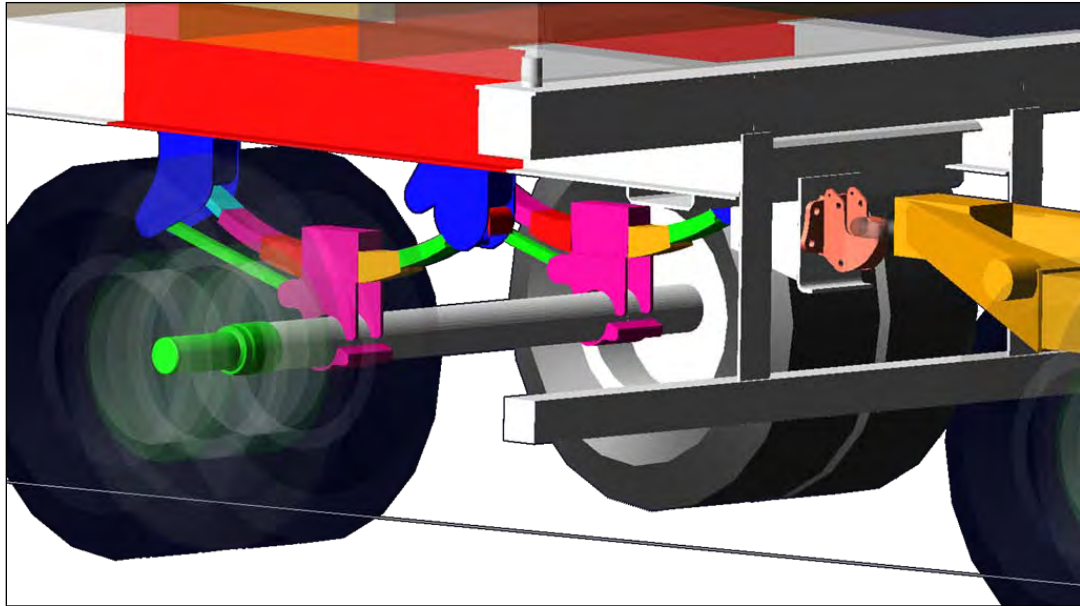


Figure 7-5. Drawing. Adams model, Hutchinson Trailer Suspension

Stiffness

The component providing the primary stiffness of the trailer was the ladder type frame. This flexibility could be incorporated in the system, if deemed relevant, through various modeling techniques. For this model, this response was developed by utilizing Adams bushing elements, which were “tuned” to represent the measured torsion stiffness. By specifying “high” values for these section properties, a rigid frame condition could be realized.

Connectivity

A standard kingpin was used at the forward end of the trailer to mate to the fifth wheel of the preceding unit. At the rear of each trailer, a pintle hook was mounted to allow the attachment of the dolly drawbar eye. For this model, both of these connections were represented by Adams joint entities.

7.1.3 Intermodal Container

Hyundai manufactured the containers used on the vehicle. They comprised a typical trailer type construction of longitudinal and lateral c-channels, corrugated steel sides, and plywood floor.

Stiffness

The component providing the primary stiffness of the intermodal container was the box construction. For this model, this response was developed by utilizing Adams bushing elements,

which were “tuned” to represent the stiffness estimated in an ANSYS finite element model. By specifying “high” values for these elements, a rigid frame condition could be realized.

Connectivity

The container was mounted to the trailer at pins located on the trailer bolster arms. The container did not rest on the frame of the trailer. These connections were modeled with stiff bushing elements, allowing load transfer through each point.

7.1.4 Payload

The intermodal containers were loaded with portions of concrete construction “jersey barriers.” Several of these barriers were stacked in each trailer to develop the required axle loads. The density and location of these entities was adjusted to closely match the static load configuration measured at the test track.

Mass Properties

The total mass, CG, and mass moments of inertia of the rigid bodies comprising the system are required by the Adams program to correctly represent this portion of the system equations of motion. Several sources were utilized in determining these quantities, including direct measurement, CAD models, or published reports. In order to estimate the CG, these components were modeled as 3D solids and assembled in a generic loading configuration.

Connectivity

Representative geometry for the barriers was created in Adams, Figure 7-6, utilizing the generic loading configuration developed in the CAD model. The barrier geometry was attached to the intermodal container, and each other, through Adams bushing elements. These elements were given fairly high stiffness, minimizing relative motion but providing better load distribution.

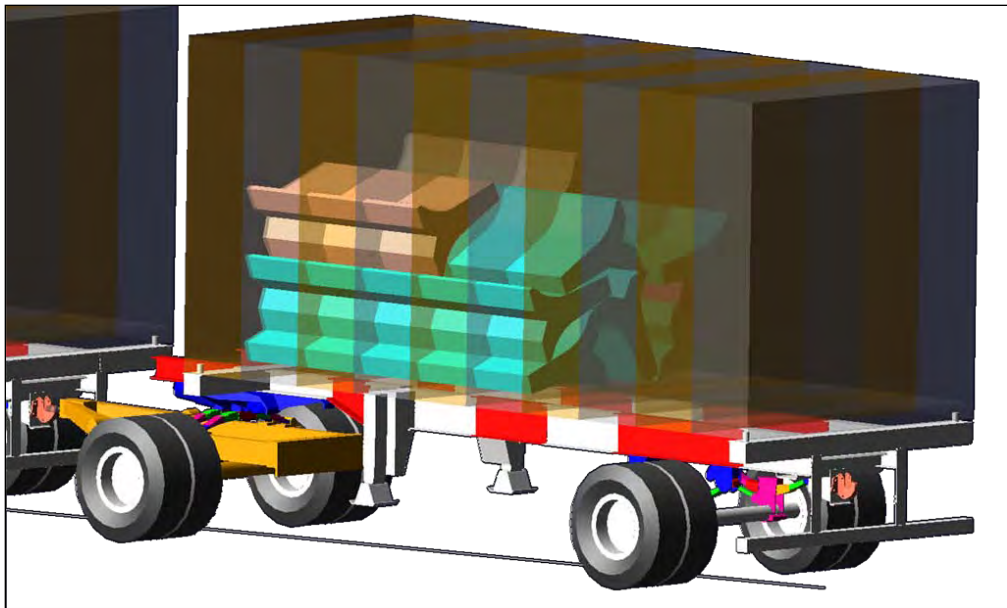


Figure 7-6. Drawing. Adams Model, Intermodal Container and Payload

Hard Points

Specific points on the vehicle were required to correctly locate items such as the CG or suspension mounts. Many of these quantities were determined through direct measurements made on the test vehicle. Others were estimated by creating CAD layouts or from the manufacturer website.

Mass Properties

The total mass, CG, and mass moments of inertia of the rigid bodies comprising the system are required by the Adams program to correctly represent this portion of the system equations of motion. Several sources were utilized in estimating these quantities, including direct measurement, CAD models, and published reports.

7.1.5 Dolly

The vehicle on the tests had two dollies, both by Silver Eagle Manufacturing. Both of the dollies were the “Eagle” model, with the difference between them being the axle track dimension. The dolly located between Trailers 1 and 2 was labeled “Eagle S,” and was delivered new to NCAT for this testing. “Eagle A” was the original dolly used with the system, and was positioned between Trailers 2 and 3. The spring and bushing rates between these units could vary due to their age difference. The Eagle incorporates a fifth wheel style suspension with the axle rigidly mounted to the frame. Silver Eagle Manufacturing provided a CAD model of this unit, which allowed for precise mass properties and hard point locations. The model of the dolly is in Figure 7-7.

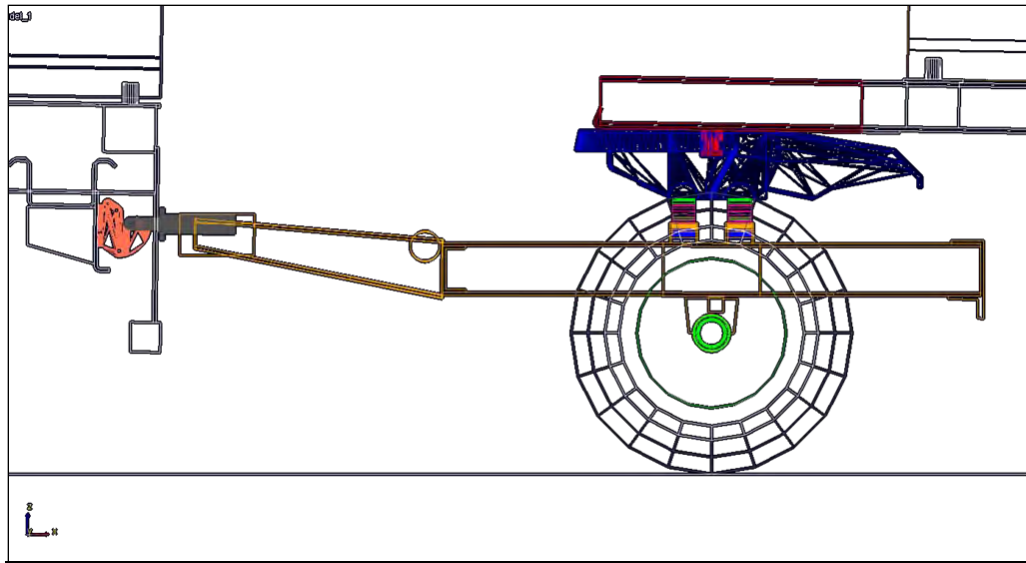


Figure 7-7. Drawing. Adams Model, Dolly Left Side View

Suspension

The Eagle dolly employed a pair of mechanical springs, configured in parallel, to mount the fifth wheel to the dolly frame. Each spring was an assembly composed of several leafs. These were represented using the SAE three-link method, as shown in Figure 7-8. The end of each spring was attached via a large, cylindrical rubber bushing. The spring rate of this suspension was compared to published data, and adjusted as required. Damping in this type of suspension is supplied through interleaf friction in the spring pack. The total mass, CG, and mass moments of inertia were determined from direct measurement, CAD models, and published data.

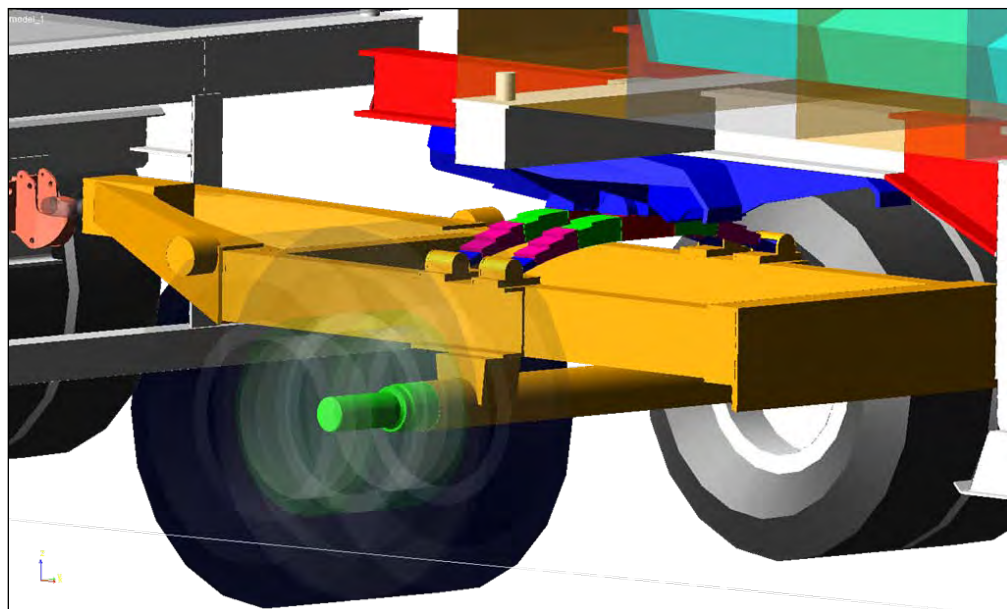


Figure 7-8. Drawing. Adams Model, Dolly Isometric View

Stiffness

The dolly frame and axle were treated as rigid bodies.

Fifth Wheel

The dolly fifth wheel was attached directly to the pair of suspension spring packs. The total mass, CG, and mass moments of inertia were determined from the CAD model.

Connectivity

The drawbar eye, which mates to the pintle hook on the trailer, is attached to the dolly by a pair of bushing elements. These represent the rubber elements in the actual dolly, and use an estimated stiffness and damping.

7.1.6 Other Components of the Adams Model

These are the remaining items needed to construct the model.

Tires

The interface between the vehicle and the road surface was realized through the use of the Adams model tire elements. Many different tire modeling algorithms are available, ranging from those with basic vertical and lateral stiffness coefficients to more sophisticated versions requiring extensive testing and fitting procedures. The method of road surface representation, as well as the intended vehicle events, will determine the appropriate tire model to use. However, with the difficulty in acquiring tire data, often the user is faced with few choices. For this and other reasons, the model was set up with the basic Fiala method tires. This algorithm is acceptable for basic handling maneuvers, and requires a reasonable amount of tire data. For this model, the tires used representative data.

Road

The general shape of the test track is an oval. The two curve sections, constructed with spiral entries and a maximum bank angle of 8 deg, were used for the constant-radius cornering events. For the single and double lane change maneuvers, the straight sections of the track were used. These sections were built with a slight crown. Data provided by NCAT allowed for the creation of a digital model of the road surface. NCAT measured a coefficient of friction of 0.7 for the surface.

For the basic development of the model, a flat road surface was utilized. This simplification allowed for faster model development and debugging. Basic Adams geometric entities were added to the model to give a visual reference to the user, and to verify that the vehicle was properly following the road course (Figure 7-9). These entities did not represent the actual road data used by Adams, and may be different than what was used by the current simulation. This data was completely mathematical in nature, existing in data files and memory during solution.

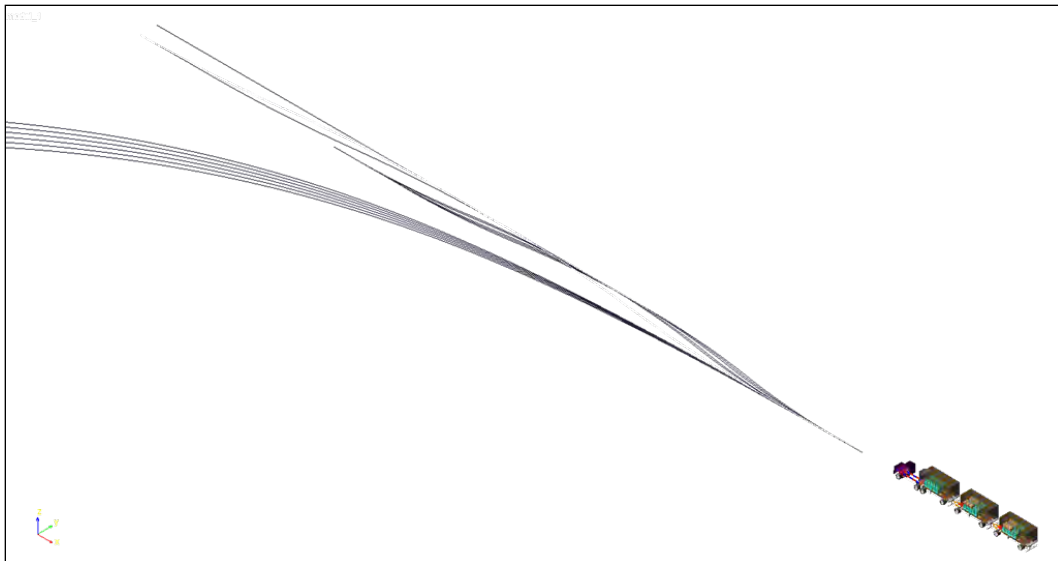


Figure 7-9. Screen Shot. Adams Model with Path Graphics

Preloads

To set the model to correct initial conditions, some preloads may be required. This is of particular importance for maintaining the correct ride height for air suspensions. The model is currently set for the default preloads required for the system as tested at NCAT. If the user requires a different loading configuration, new preloads will need to be determined. This can be an iterative process, although engineering-based initial estimates can minimize the number of iterations required. The velocity of the vehicle is another example of an initial condition that can be changed.

Requests

By default, Adams will generate data for each element within the model relative to the global coordinate system. Requests for any other information can be made by the user. These can be algebraic manipulations of the existing data, transformations to other coordinate systems, or completely new calculations. Many of these custom requests have been created, such as roll angles of various bodies.

7.2 *Simulation of Test Track Maneuvers*

Adams will accept commands that allow the vehicle to simulate various events and maneuvers. For a typical simulation sequence, a static analysis is performed first. This initial solution allows the system to “settle” into an equilibrium condition, and is useful for eliminating transient effects as tires and contact elements engage. A successful static simulation is also an indication of a robust model, as this can be a difficult numerical task. After the static solution, a 1-second simulation of straight driving is executed, which ensures that any remaining transients are damped out, followed by the desired dynamic maneuver. The total time for the simulation is

determined by the speed and path, and includes a few extra seconds to return to steady state. This resulted in total simulation times ranging from 10 to 25 seconds for the total event. The total computer run time for these models was usually under 5 minutes.

After each simulation, the results were given an initial check to verify how well the velocity was maintained and the desired maneuver path was followed. An example of the velocity results for the 56 km/h double lane change is shown in Figure 7-10, which shows that the model velocity is well controlled.

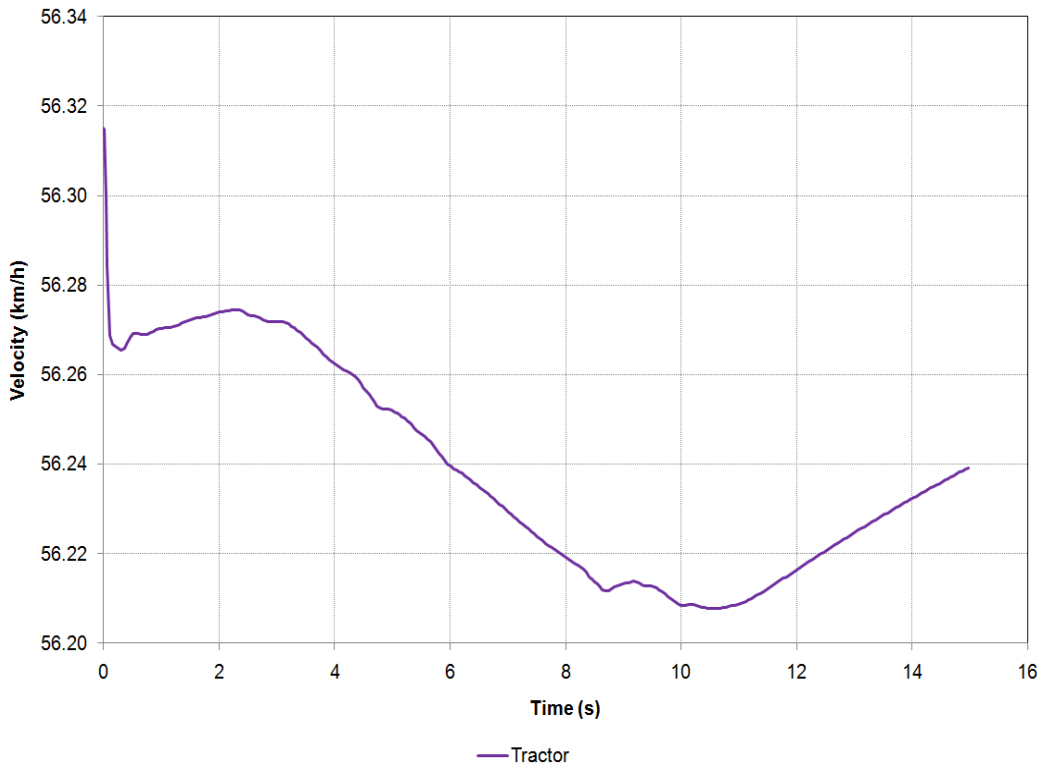


Figure 7-10. Graph. Tractor Velocity, Double Lane Change at 56 km/h (35 mph).

Figure 7-11 through Figure 7-13 show the desired path of the vehicle, as well as the path followed by the CG of the tractor and all three trailers for each event. The dotted line represents the desired path, and the initial trajectory of the vehicle is along the negative x-direction. Again, these plots show that the model is properly following the desired path.

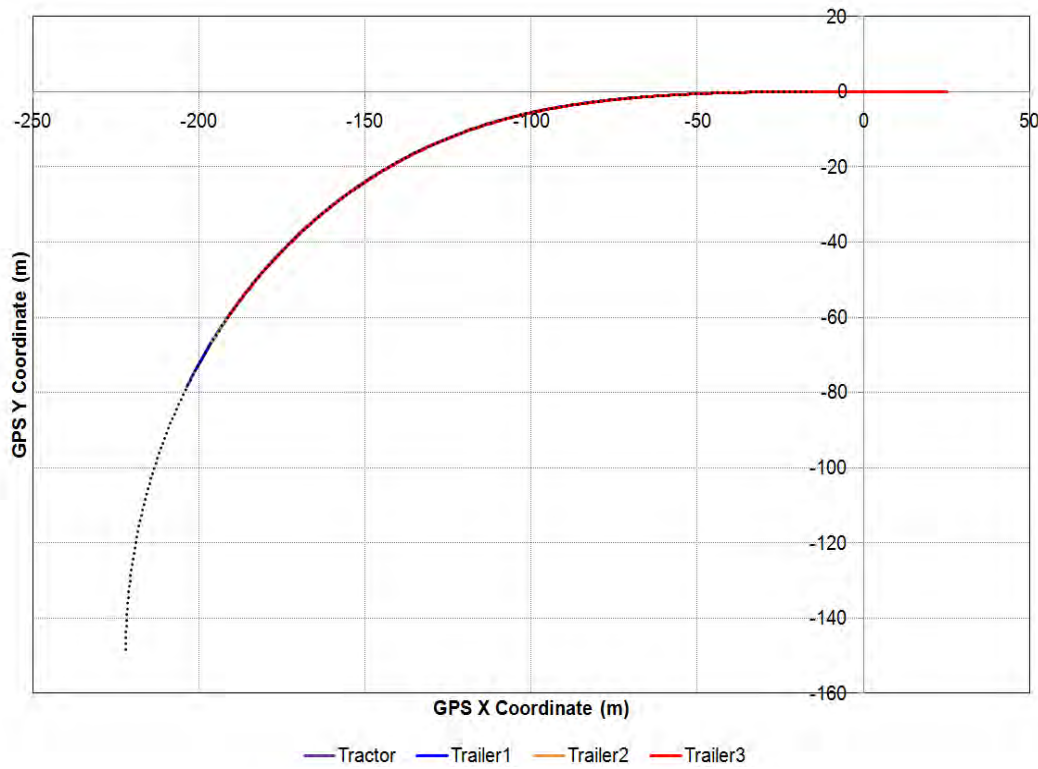


Figure 7-11. Graph. Tractor and Trailer Paths, Constant Radius Cornering at 56 km/h (35 mph).

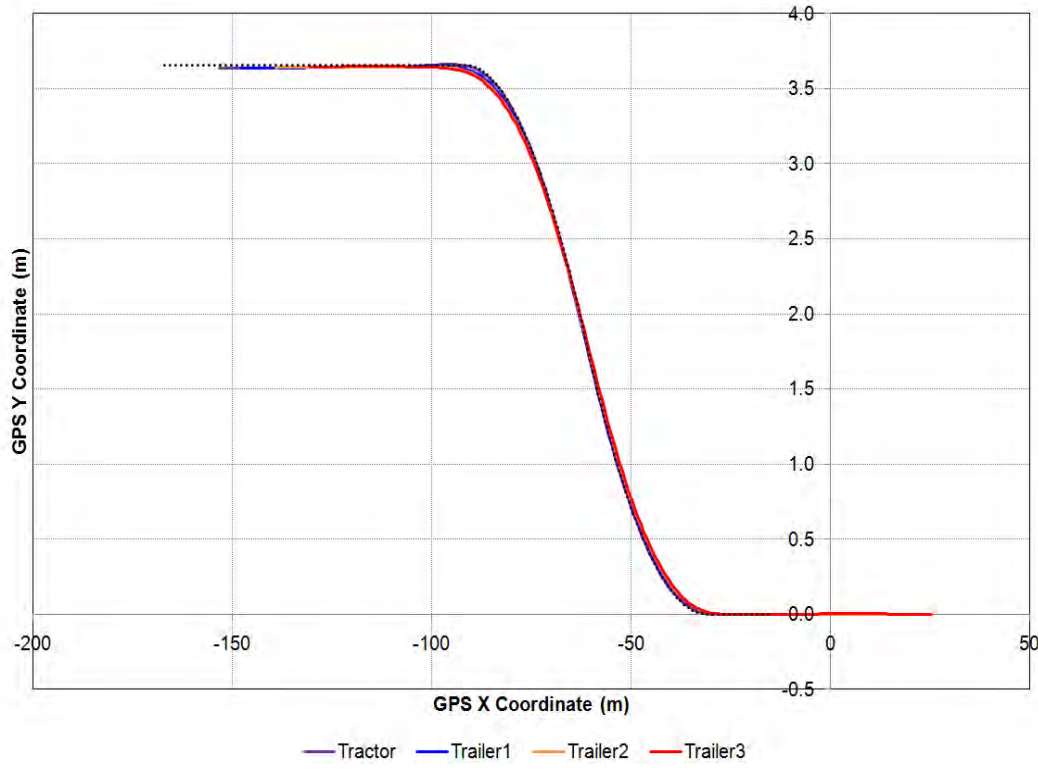


Figure 7-12. Graph. Tractor and Trailer Paths, Single Lane Change at 56 km/h

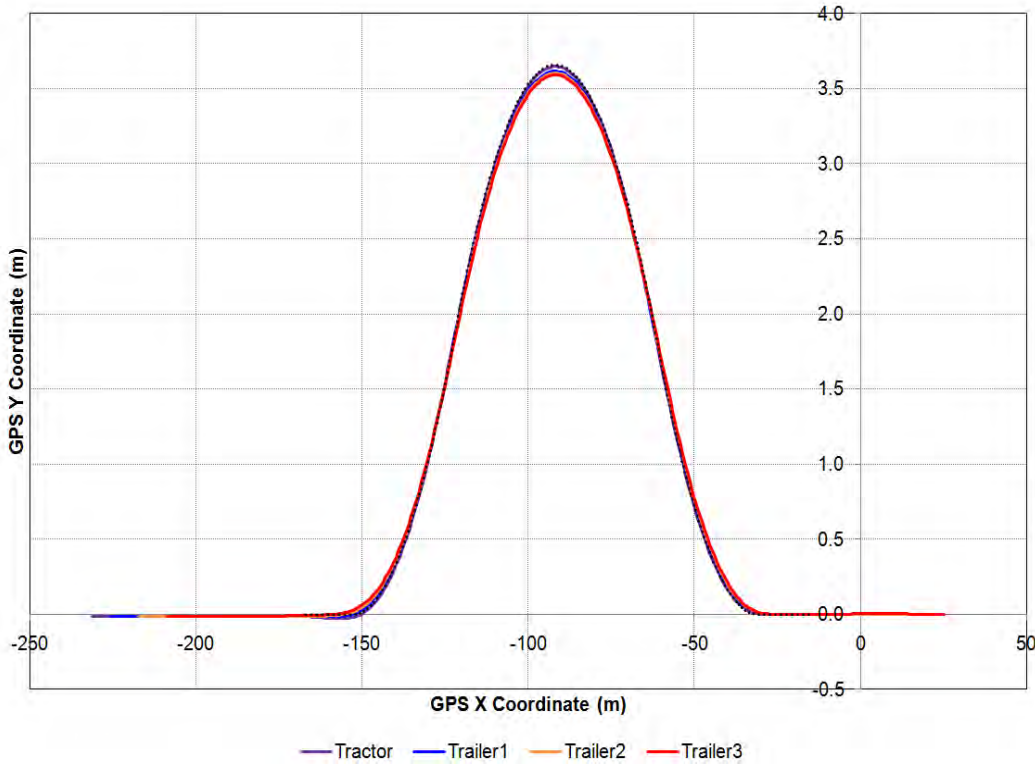


Figure 7-13. Graph. Tractor and Trailer Paths, Double Lane Change at 56 km/h (35 mph).

For convenience, many of the event command sequences are stored in ASCII text files, also referred to as “command files.” These files can be read into Adams, and the program will automatically assign the proper velocity and desired path, and then perform the simulation. Being text files, they can be directly modified to perform variations of the specified maneuver. The model has successfully performed steady-state cornering, and single and double lane change events on a flat road. A tractor-only model has been successfully tested on 3D, finite element mesh generated road surfaces. These events have also been run at various forward velocities ranging from 32 km/h to 72 km/h. Command files exist for all of these events and velocities. See the Adams Model Release Notes in Appendix E for more information.

Each simulation will generate data for every rigid body, flex body, joint, and force within the model. This can result in a large quantity of data output, not all of which may be of interest. Once again, a command file was used, which contains commands that will export quantities deemed important to this phase of the project to an external, comma separated (csv) file. This file could then be opened directly in Excel, where the data could be manipulated further and plotted.

7.2.1 Adams Model Results

With the difficulties experienced with the test data, the bulk of the model comparisons were made by simulating each event for a range of speeds. Several basic quantities were used to assess the sensitivity and capability of the model:

- Rotation angle of the kingpin relative to the steer axle. This is a measure of steering input to the system.
- Lateral acceleration of the tractor and each trailer, measured at the CG.
- Suspension roll angle of the tractor and each trailer. This was calculated by subtracting the axle roll angle from the body roll angle.
- Lateral offtracking of each trailer axle, measured as the distance from the steer axle CG to the CG of the path followed by each axle. See Figure 7-14. The method used, however, was developed as a reasonable approximation to the offtracking, but it is not extremely precise. With strains that develop between the vehicle units during the maneuver, the length to the position of each unit, which is used in the calculation, does not remain constant. Also, the speed of the vehicle during the maneuver can vary somewhat, but the calculation uses a constant speed to determine the time shift between units. Furthermore, the method used does not determine the normal to the path and calculate the distance along that normal, which creates some errors that are greater on a relative basis when the offtracking is small. Nonetheless, these inaccuracies are relatively insignificant and it is more important to characterize the maximum levels of offtracking than the near-zero levels. The approach used allows the offtracking to be approximated in a straightforward manner as a function of time. For the maneuvers simulated with the Adams model, the offtracking did remain almost entirely to the inside of the turns, and the plots presented show the correct trend, but with some discrepancies at the times when minimum offtracking occurs.
- Ride height change of the trailer suspensions. This is the change in distance from the frame to the center of the axle, and was measured on both sides of the vehicle.
- Articulation angle of each dolly with respect to the trailer following it.
- Rearward amplification of each trailer, which is calculated as the ratio of the lateral acceleration at the CG of each trailer to the lateral acceleration at the CG of the tractor.
- GPS coordinates are the position change of the location where each GPS unit was mounted to the vehicle unit.

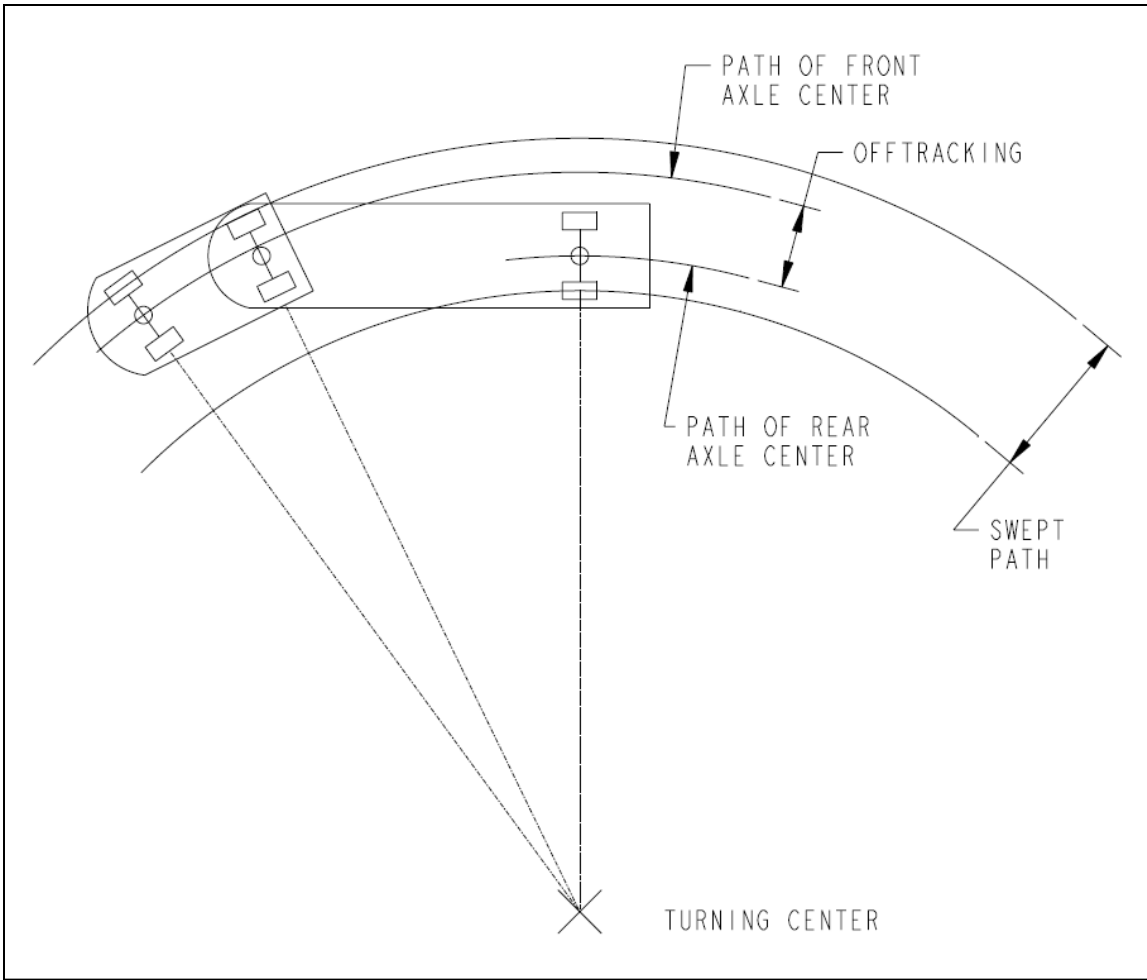


Figure 7-14. Drawing. Graphical representation of offtracking in a constant radius curve.

An Excel spreadsheet was created for each run. These spreadsheets used the result data output by the custom command file described in the previous section, which wrote specific data from the model to a comma separated text file. Once the text file was opened, time history plots were created, and maximum and minimum values were found. Figure 7-15 shows a typical time history from the Adams model, which in this example is lateral acceleration of the trailers in a double lane change. The figure also shows where the maximum and minimum values were determined. The spreadsheet has the capability to express the data in U.S. customary or S.I. units.

In addition, results from the left side of the vehicle, commonly referred to as the “Driver Side,” have a “D” added to its label. Conversely, results from the right side of the vehicle, known as “Curb Side,” have a “C.” Curb side lines are shown as dashed.

In the next sections, example time history results will be shown. These will be from each event, at a speed of 56 km/h. Only results from this velocity are shown here to minimize the number of plots. Maximum and minimum values from each event and all velocities will be shown after the

example time history plots. In these charts, the maximum and minimum values for a particular velocity will be of the same color, but represented with solid or dashed lines.

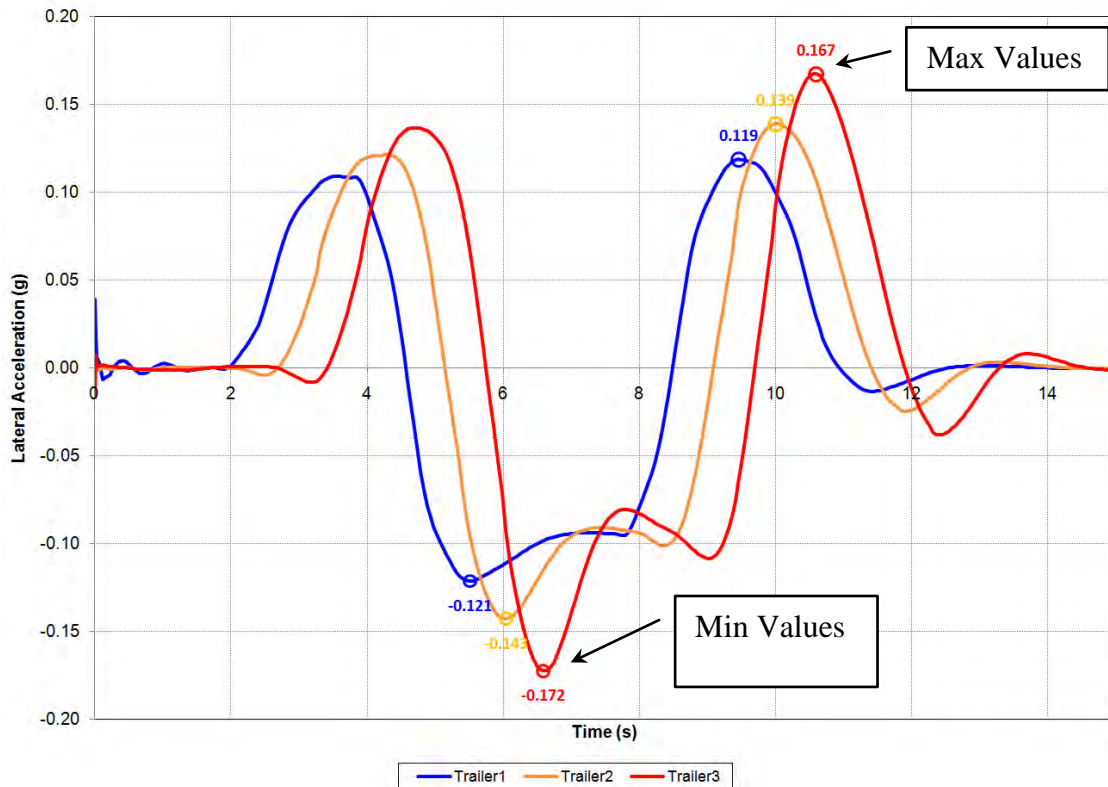


Figure 7-15. Graph. Adams model example time history.

7.2.2 Constant Radius Cornering

Constant radius cornering is a single event maneuver, meaning there is one primary steering input. These simulations were performed using the flat road profile.

Time History

Figure 7-16 through Figure 7-23 show the simulation results for the maneuver at a velocity of 56 km/h (35 mph). These plots show the system reaching a steady state after about 10 seconds, with each trailer reaching a nearly identical lateral acceleration. Suspension Roll Angle and Ride Height Change reached steady state, but not identical values. This could be due to the higher mass of Trailer 1, or the variation in the dolly track dimension. Offtracking is ranked in the order of trailer position.

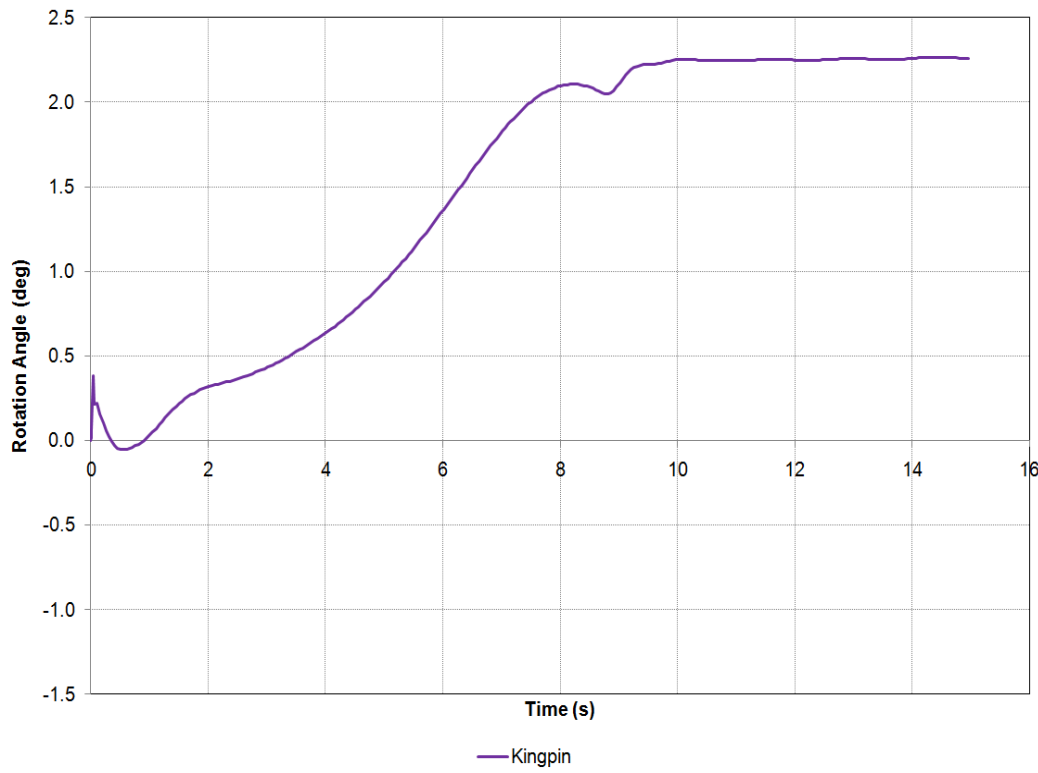


Figure 7-16. Graph. Steering Input, Constant Radius Cornering at 56 km/h (35 mph).

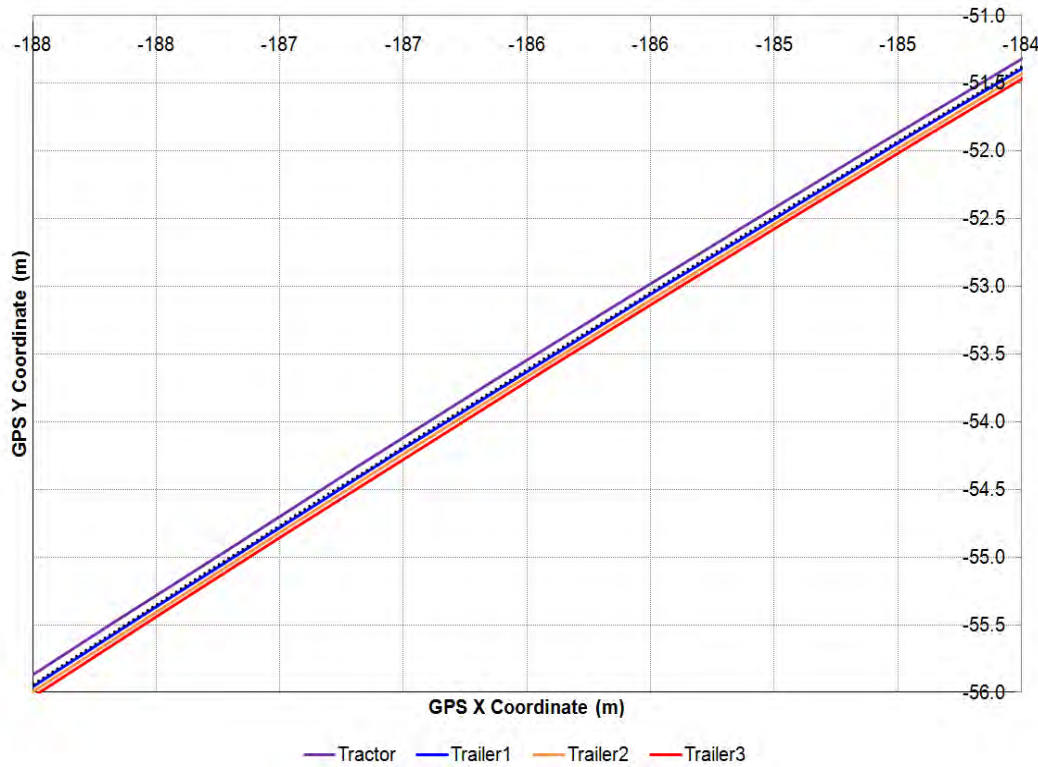


Figure 7-17. Graph. Path Close-Up, Constant Radius Cornering at 56 km/h (35 mph).

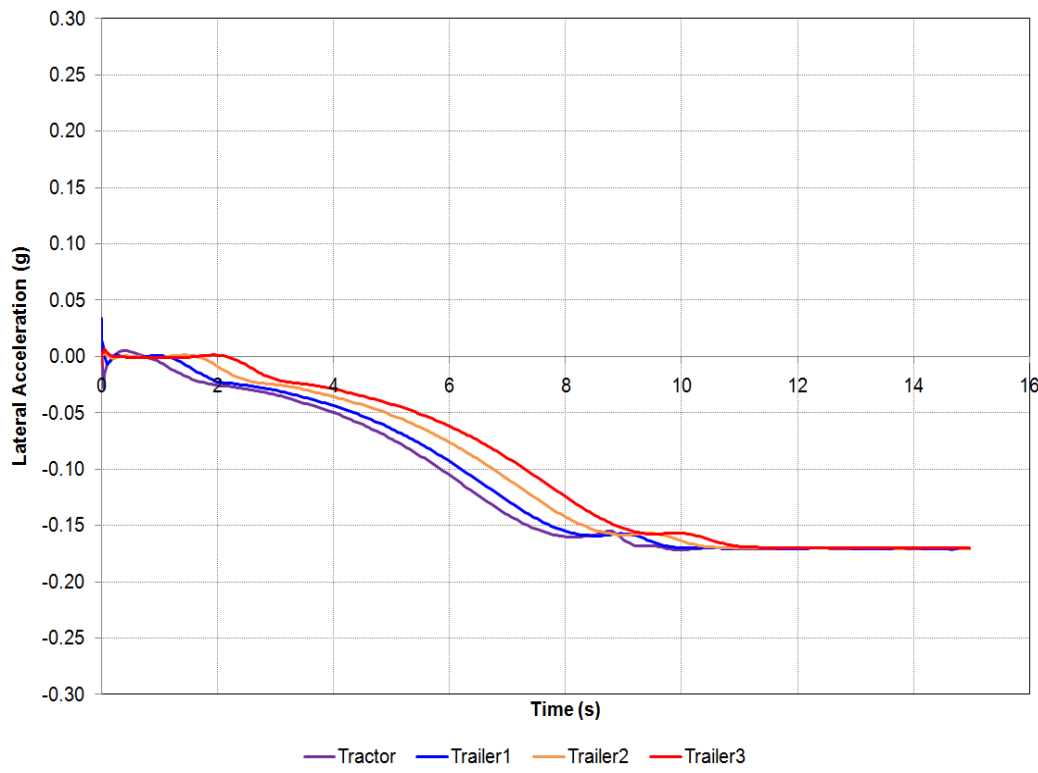


Figure 7-18. Graph. Lateral Acceleration, Constant Radius Cornering at 56 km/h (35 mph).

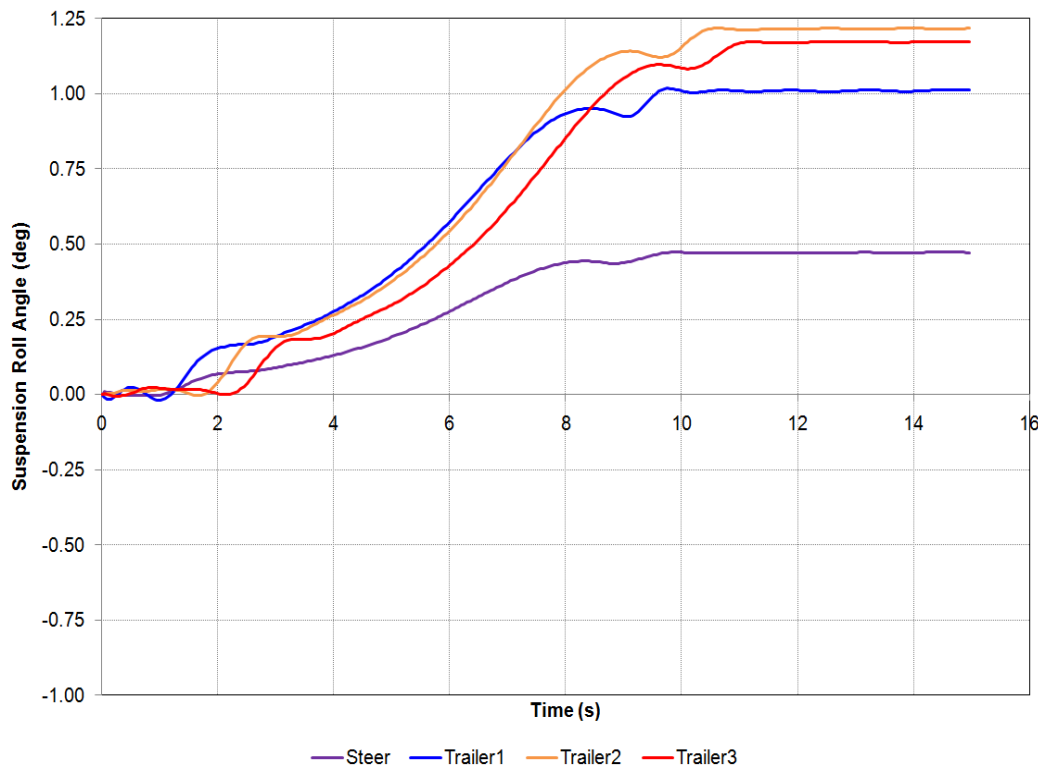


Figure 7-19. Graph. Roll Angle, Constant Radius Cornering at 56 km/h (35 mph).

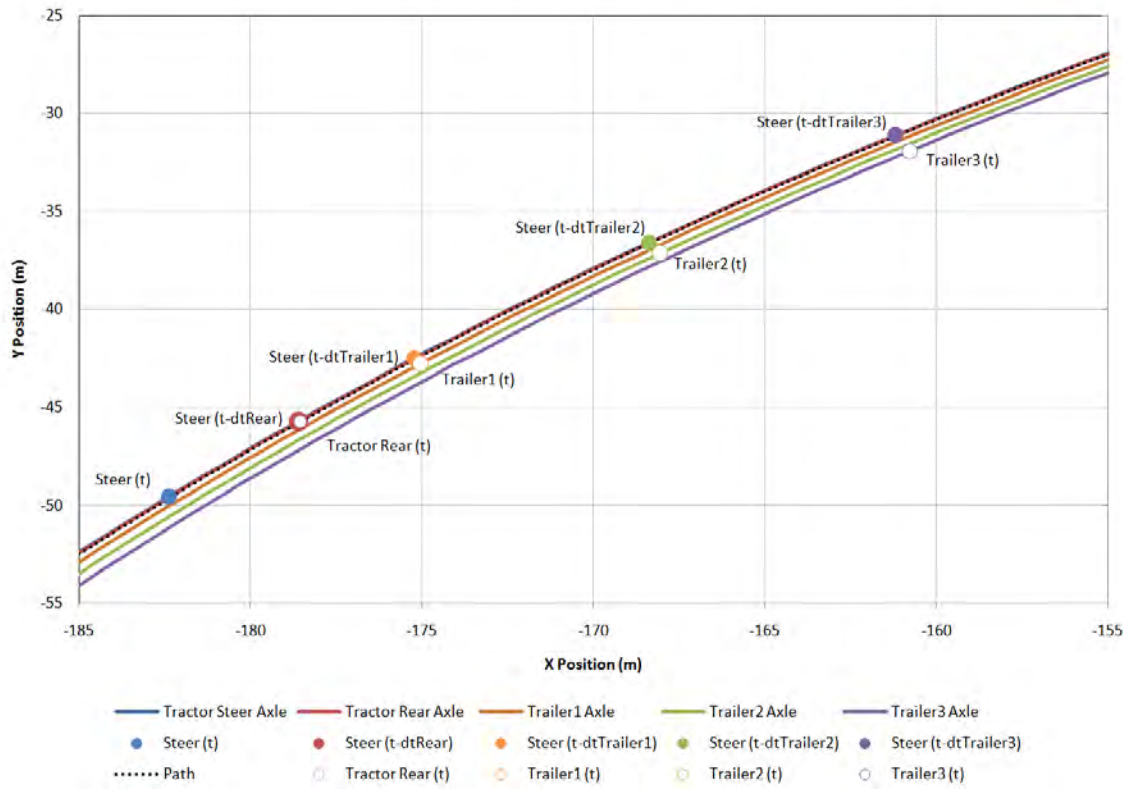


Figure 7-20. Graph. Graphical Representation of Offtracking Calculation, Constant Radius Cornering at 56 km/h (35 mph).

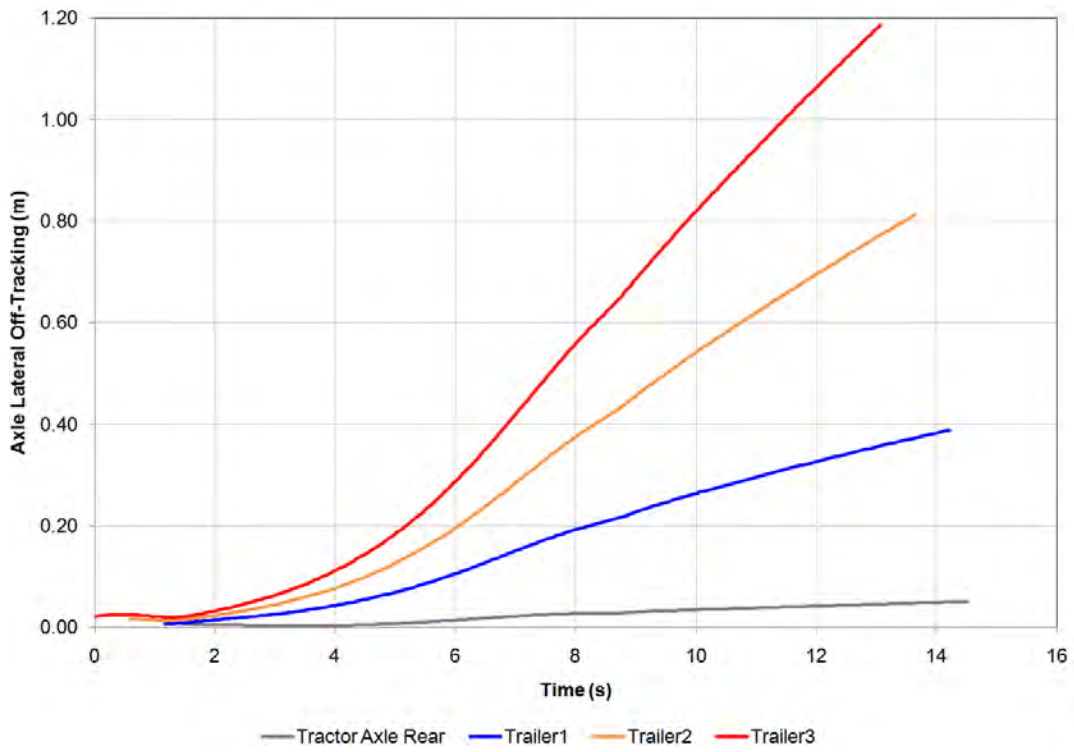


Figure 7-21. Graph. Axle Lateral Offtracking, Constant Radius Cornering at 56 km/h (35 mph).

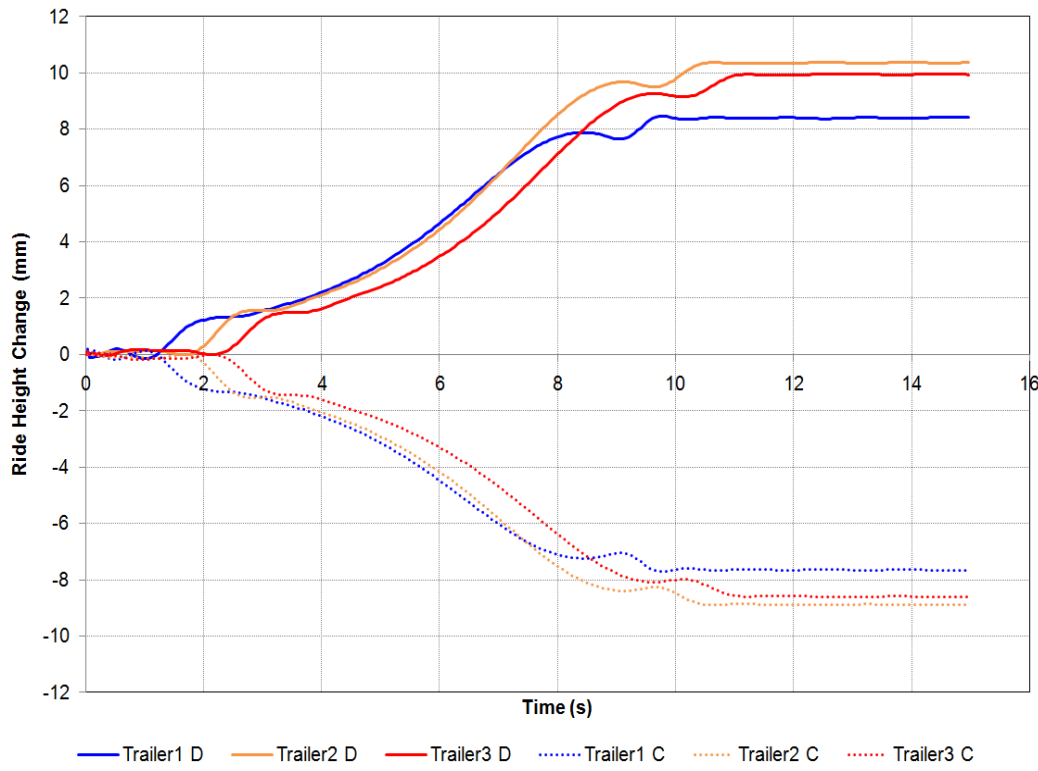


Figure 7-22. Graph. Ride Height Change, Constant Radius Cornering at 56 km/h (35 mph).

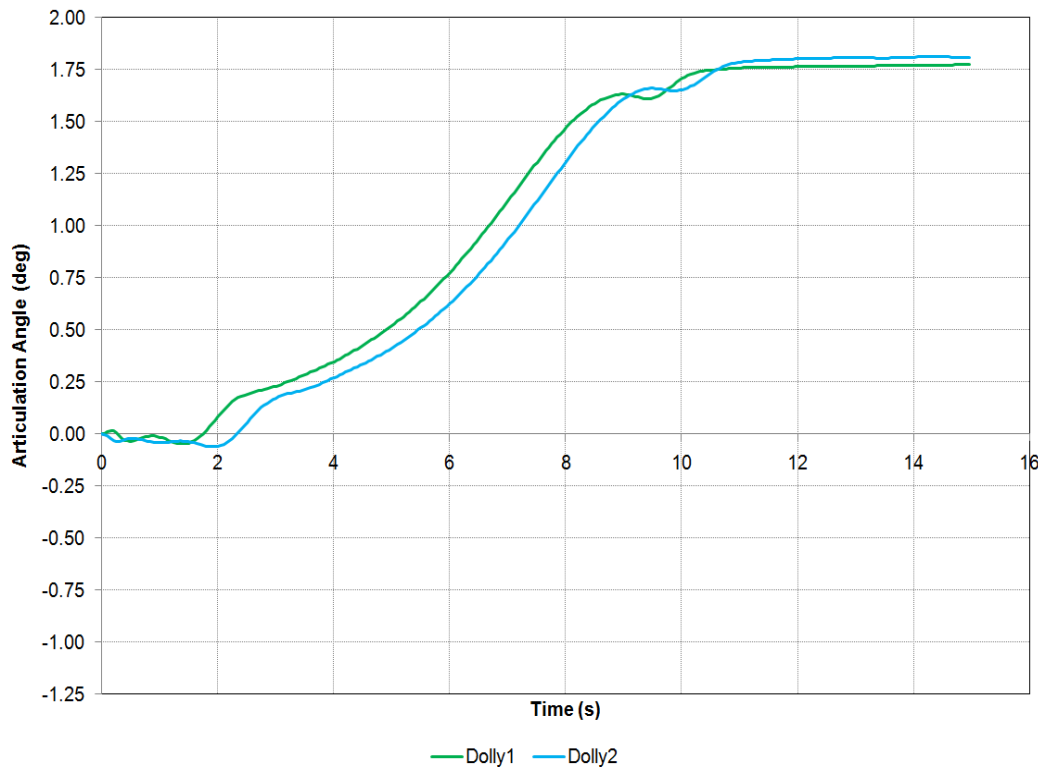


Figure 7-23. Graph. Dolly Articulation Angle, Constant Radius Cornering at 56 km/h (35 mph).

Maximum and Minimum

Maximum and minimum results are shown in Figure 7-24 through Figure 7-30 for velocities ranging from 32 km/h to 72 km/h (20 to 45 mph). The figures show the peak values for the quantity listed, at each speed and for each major unit, for the entire maneuver. These results also show a predictable, steady state behavior. In general, the responses increase proportionally with the forward velocity. The dolly articulation angle axle lateral offtracking show the opposite trend. Rearward amplification is relatively low due to the low velocity and radius of the track curve.

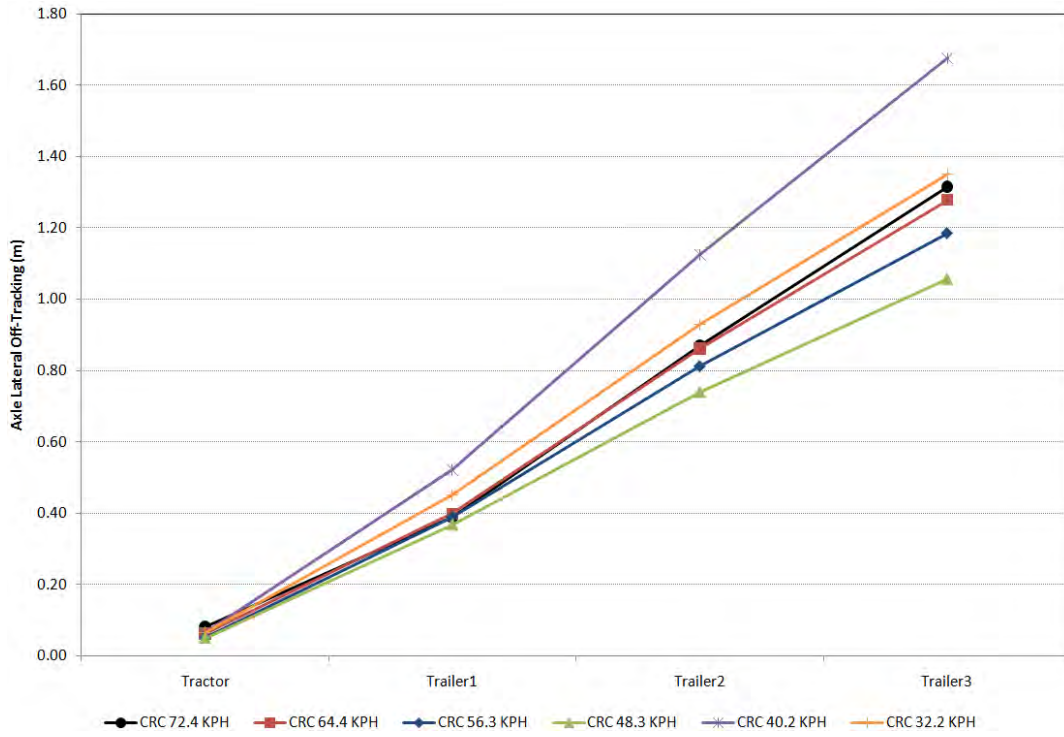


Figure 7-24. Graph. Lateral Offtracking, Constant Radius Cornering at All Velocities.

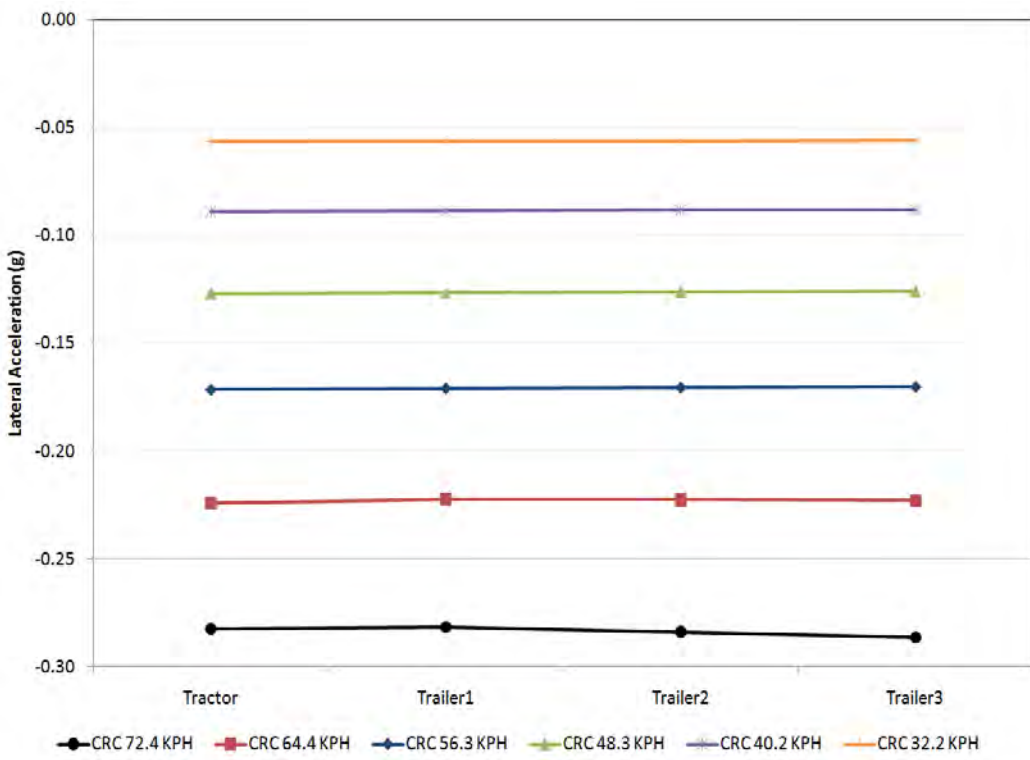


Figure 7-25. Graph. Peak Lateral Acceleration, Constant Radius Cornering at All Velocities.

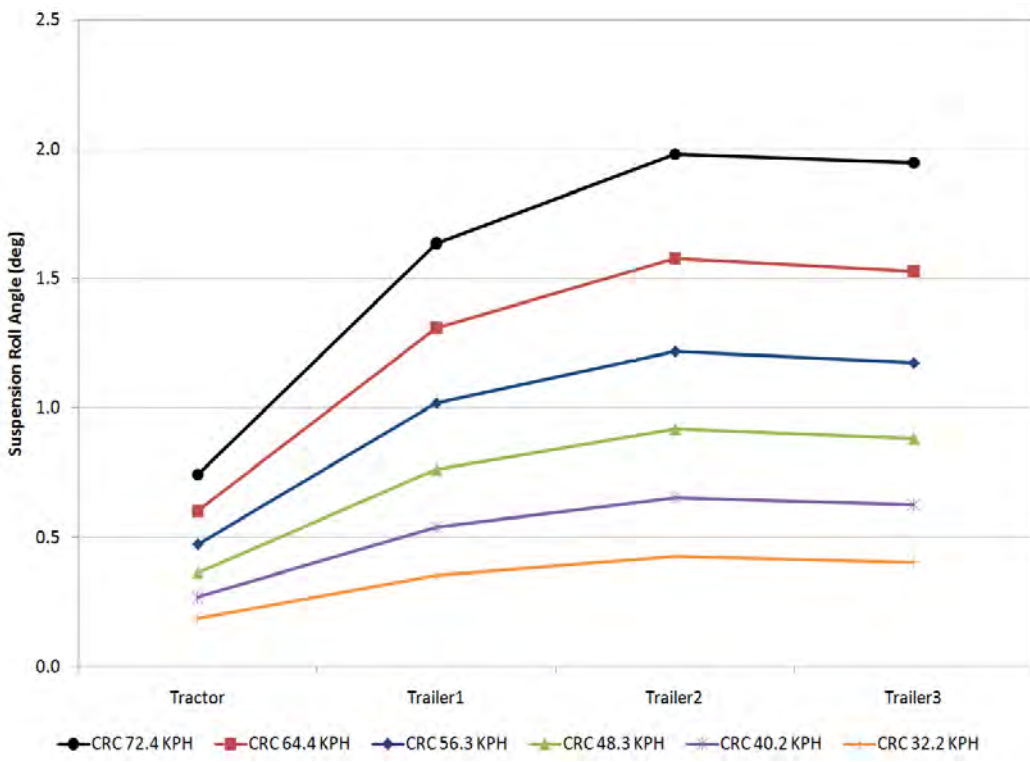


Figure 7-26. Graph. Peak Roll Angle, Constant Radius Cornering at All Velocities.

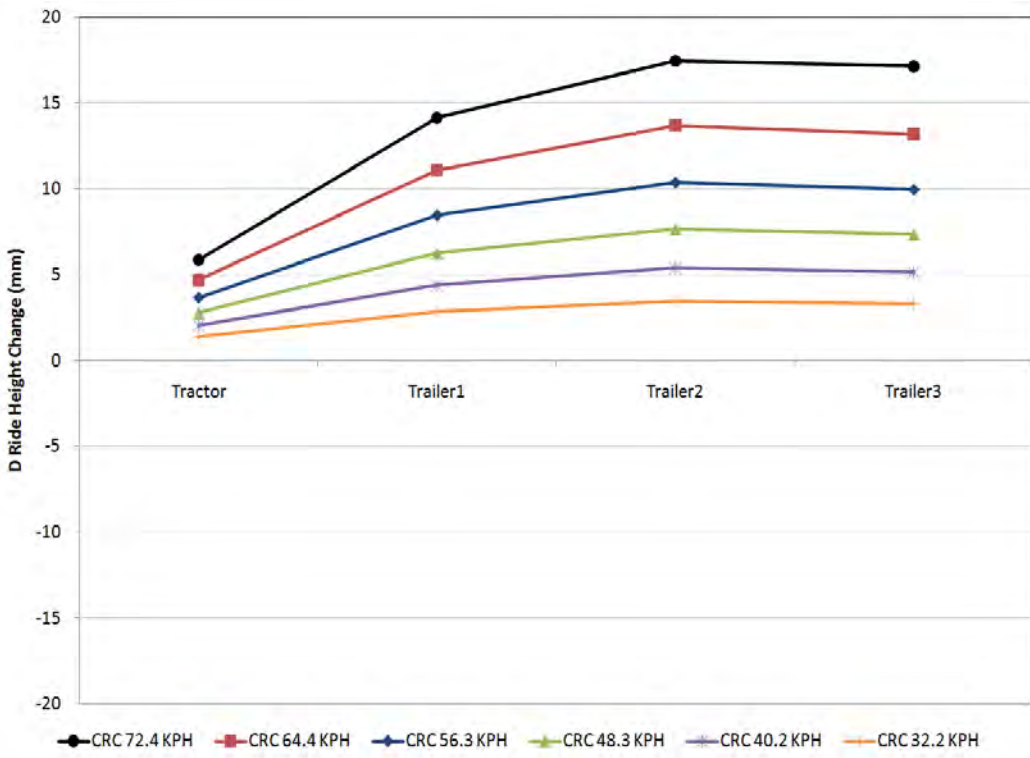


Figure 7-27. Graph. Peak Driver Side Ride Height Change, Constant Radius Cornering at All Velocities.

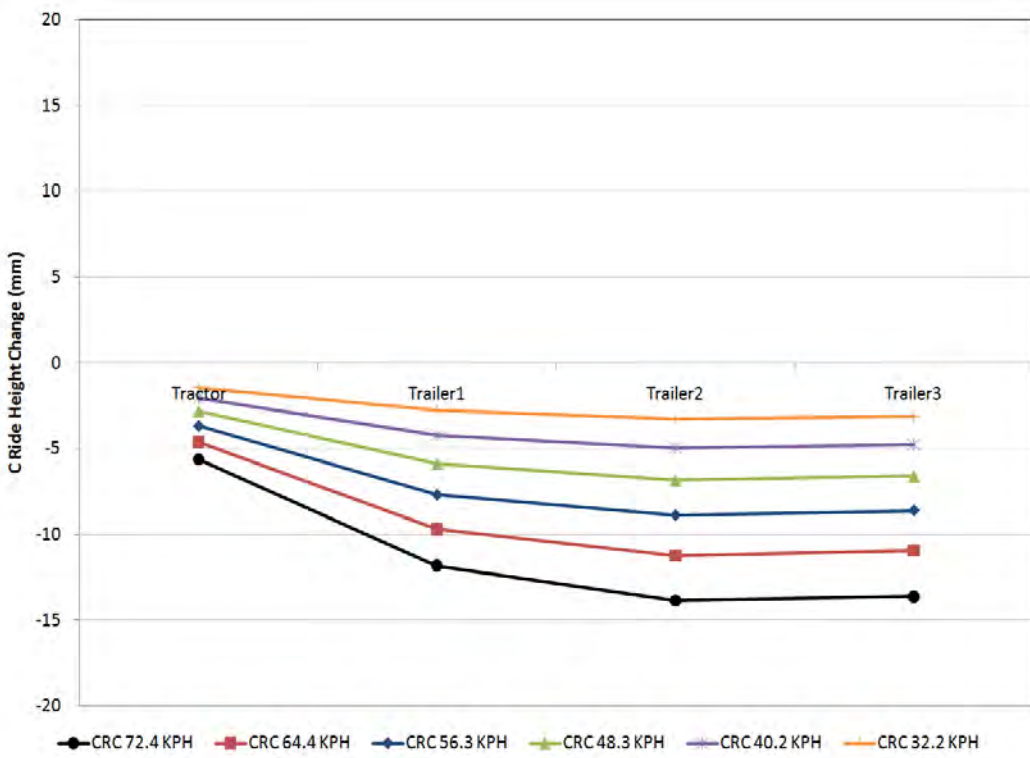


Figure 7-28. Graph. Peak Curb Side Ride Height Change, Constant Radius Cornering at All Velocities.

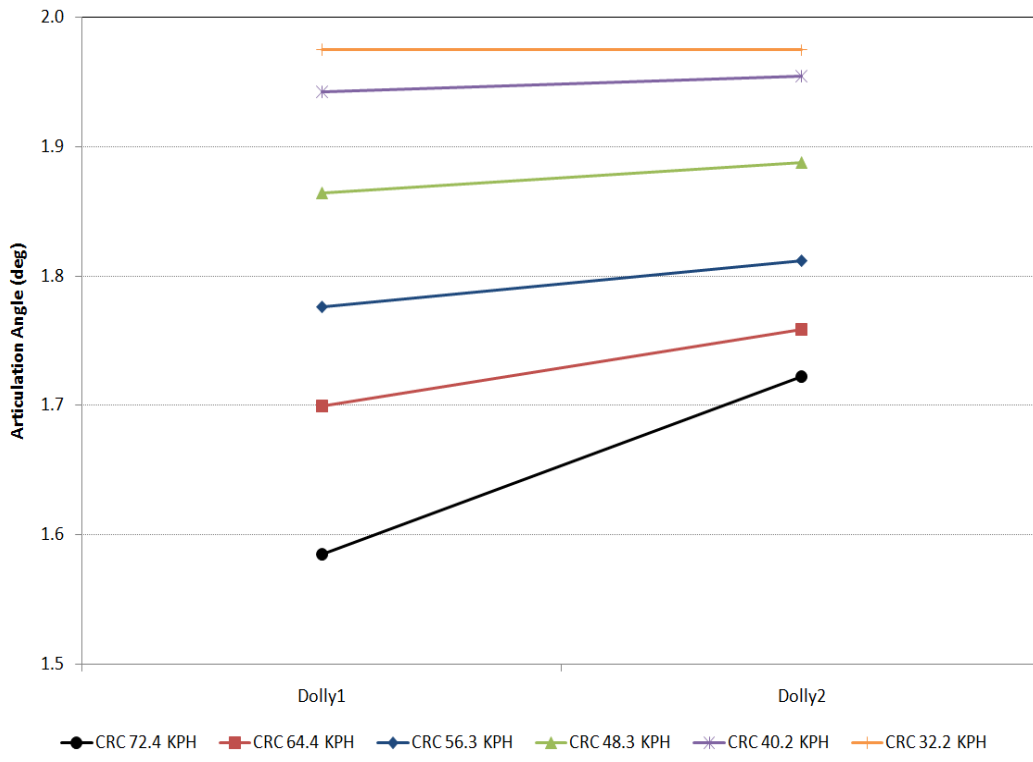


Figure 7-29. Graph. Peak Dolly Articulation Angle, Constant Radius Cornering at All Velocities.

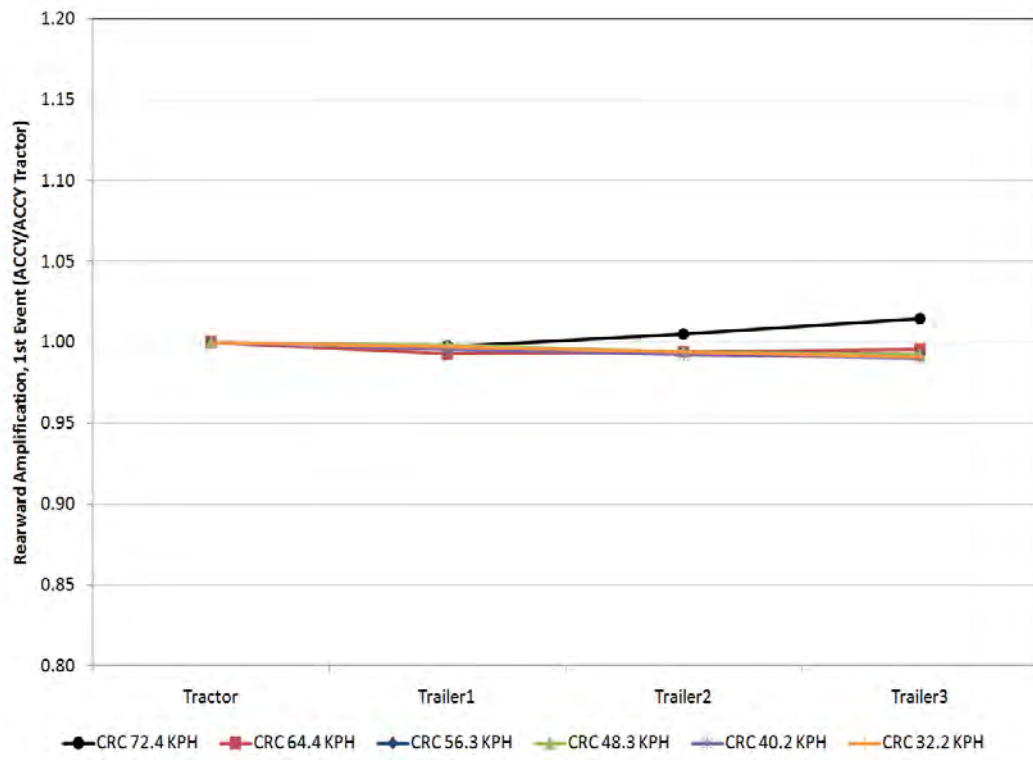


Figure 7-30. Graph. Peak Rearward Amplification, Constant Radius Cornering at All Velocities.

7.2.3 Single Lane Change

The single lane change is a transient, double event maneuver, meaning there are two primary steering inputs. These simulations were performed using the flat road profile.

Time History

Figure 7-31 through Figure 7-38 show the simulation results for the maneuver at a velocity of 56 km/h (35 mph). Many of the time histories show a symmetry between positive and negative peak values. The offtracking is again sorted by trailer position, while lateral acceleration and suspension roll angle reach similar values for each trailer.

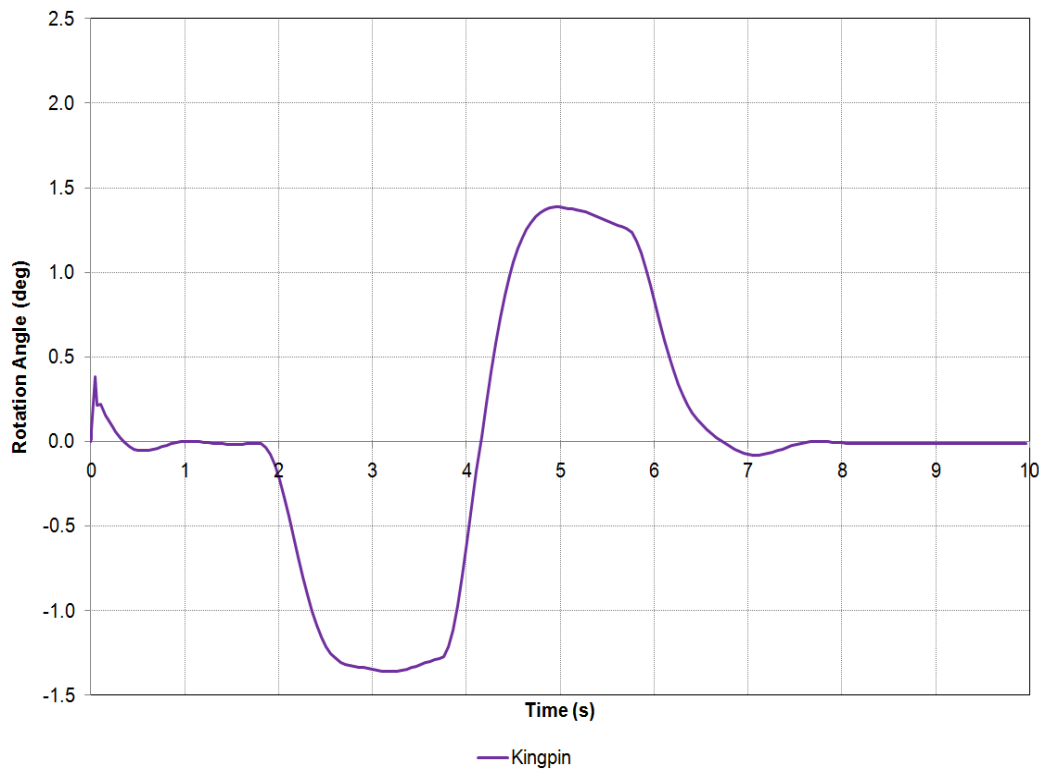


Figure 7-31. Graph. Steering Input, Single Lane Change at 56 km/h (35 mph).

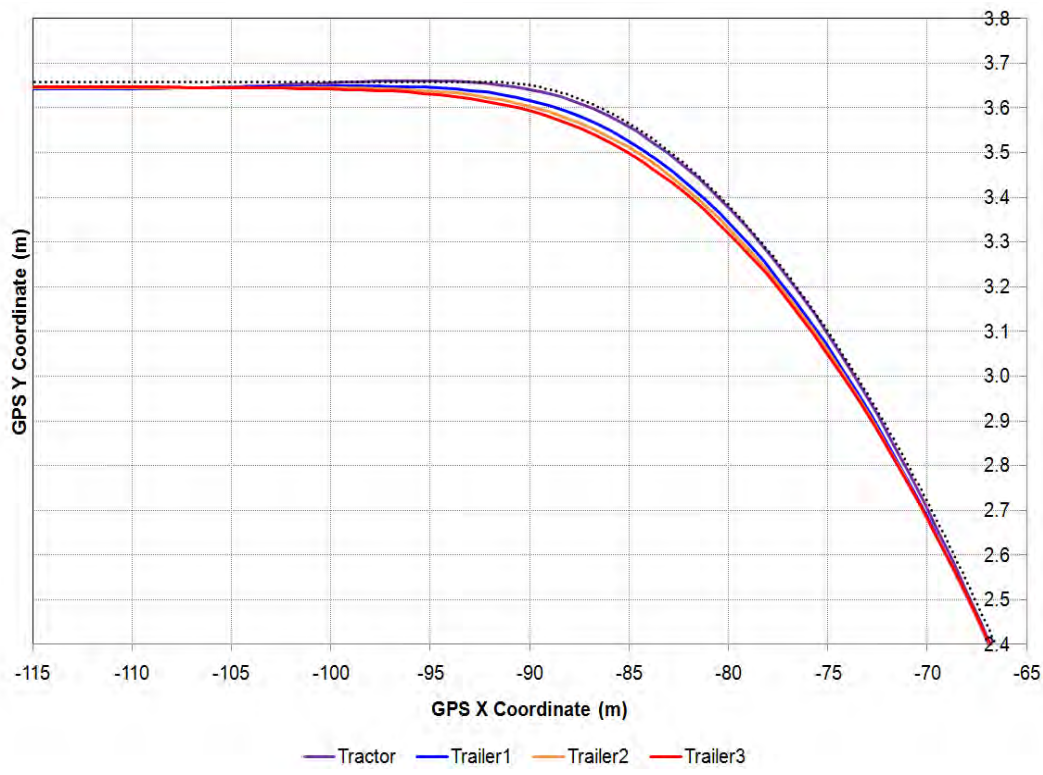


Figure 7-32. Graph. Path Close-Up, Single Lane Change at 56 km/h (35 mph).

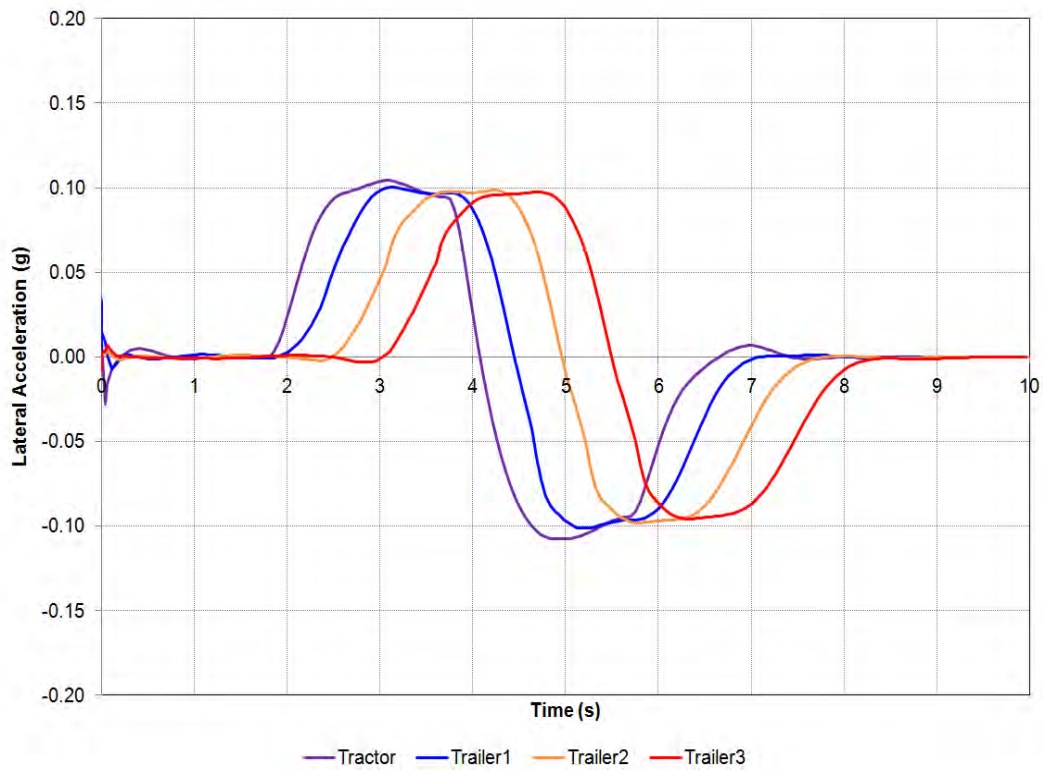


Figure 7-33. Graph. Lateral Acceleration, Single Lane Change at 56 km/h (35 mph).

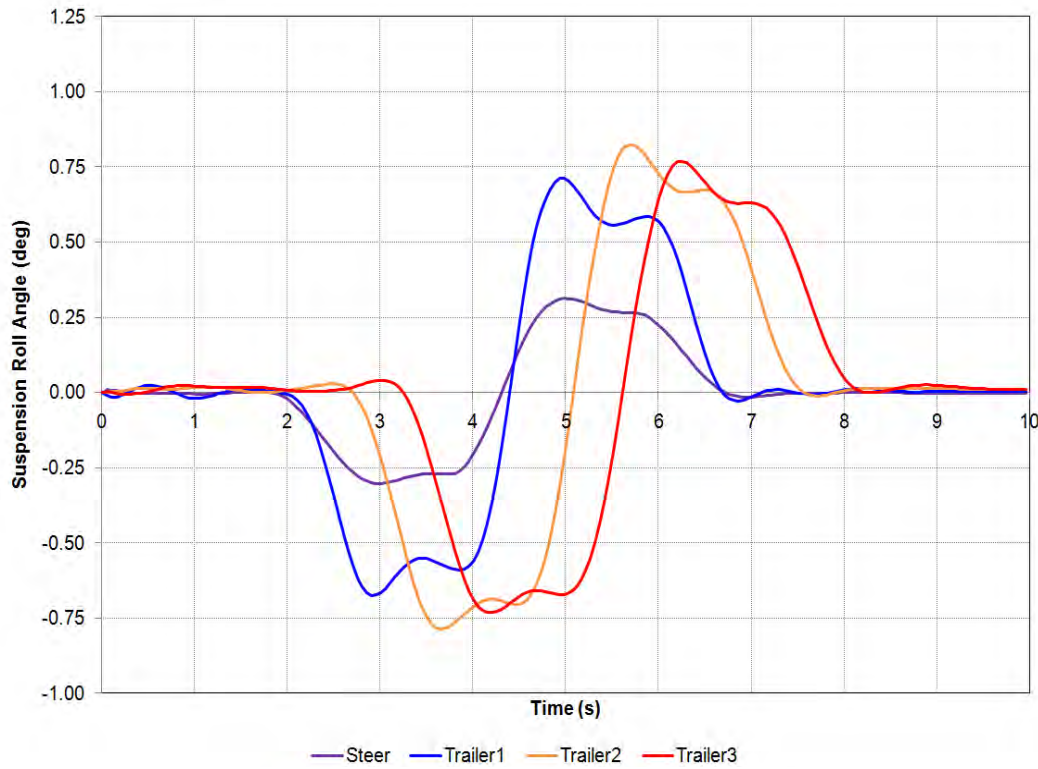


Figure 7-34. Graph. Roll Angle, Single Lane Change at 56 km/h (35 mph).

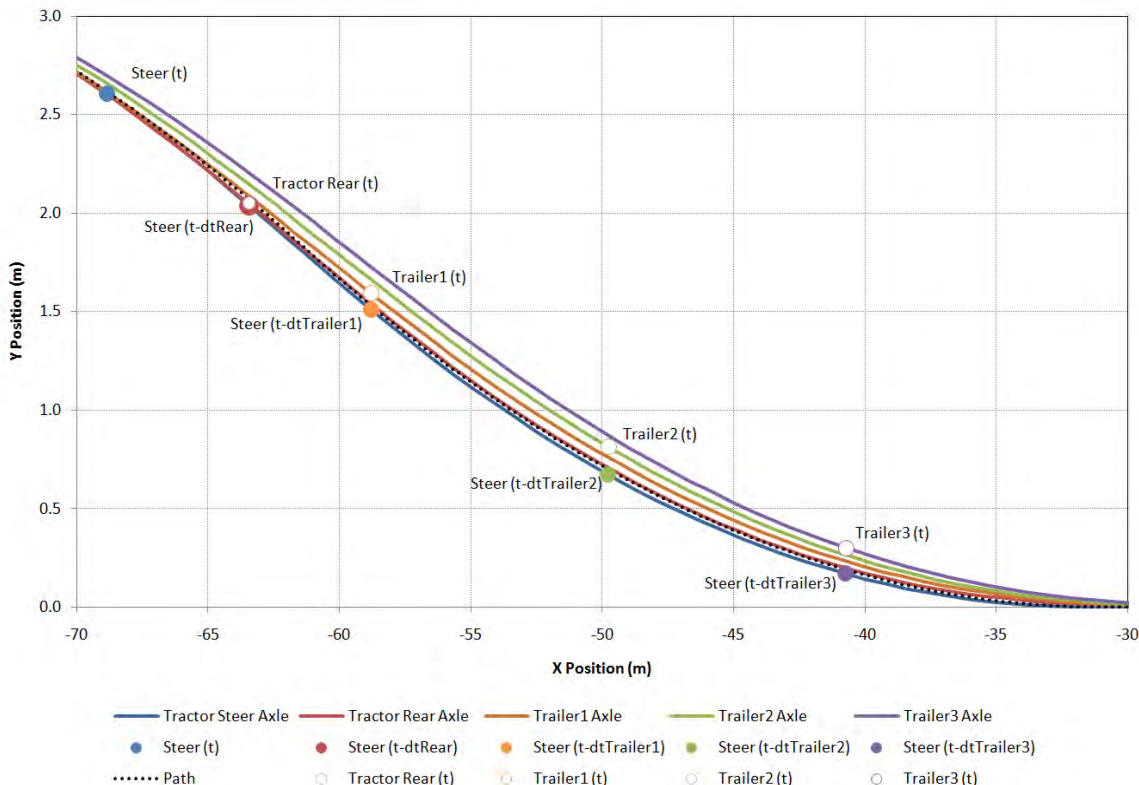


Figure 7-35. Graph. Graphical Representation of Offtracking Calculation, Single Lane Change at 56 km/h (35 mph).

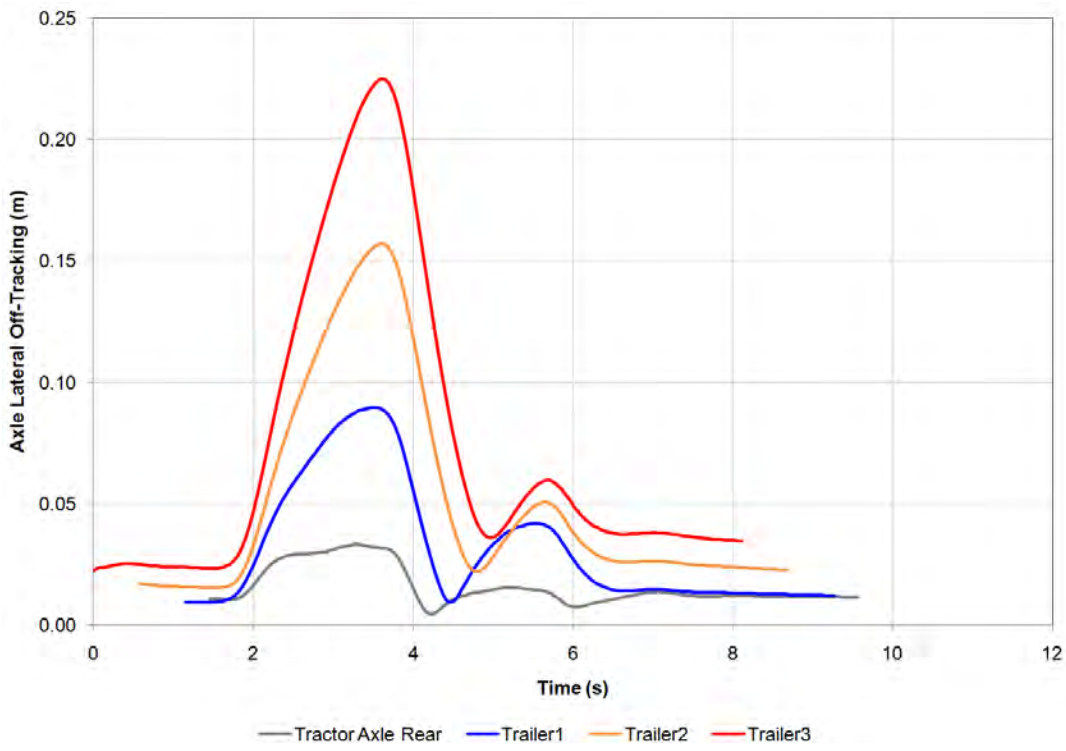


Figure 7-36. Graph. Axle Lateral Offtracking, Single Lane Change at 56 km/h (35 mph).

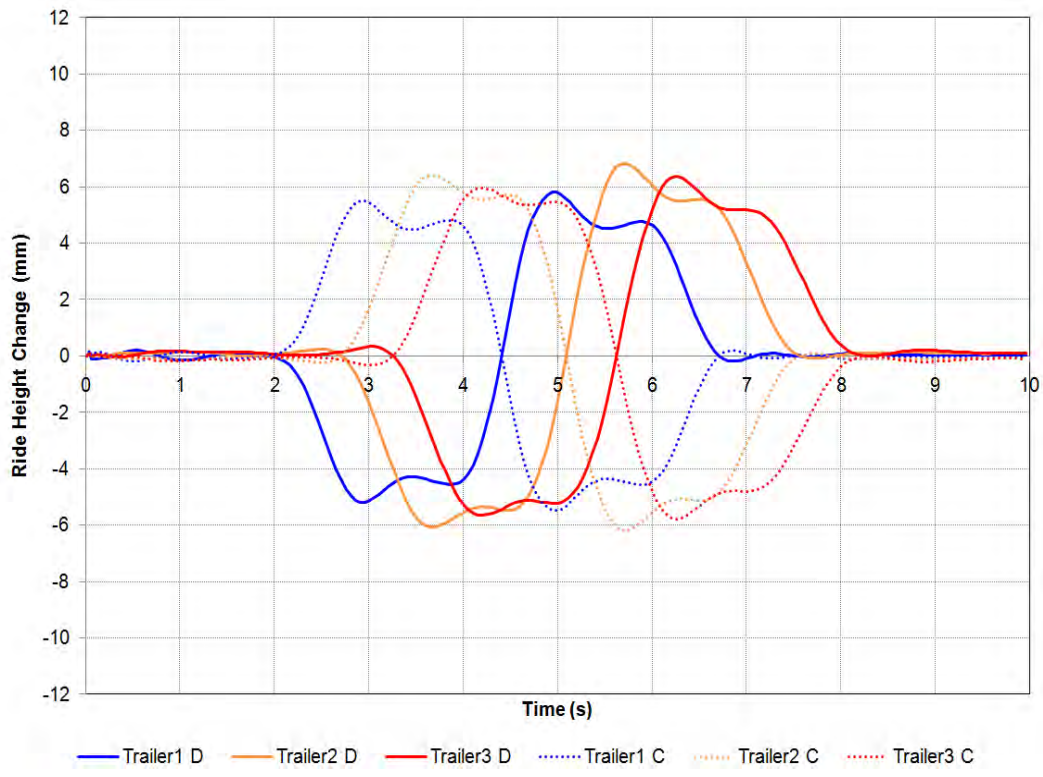


Figure 7-37. Graph. Ride Height Change, Single Lane Change at 56 km/h (35 mph).

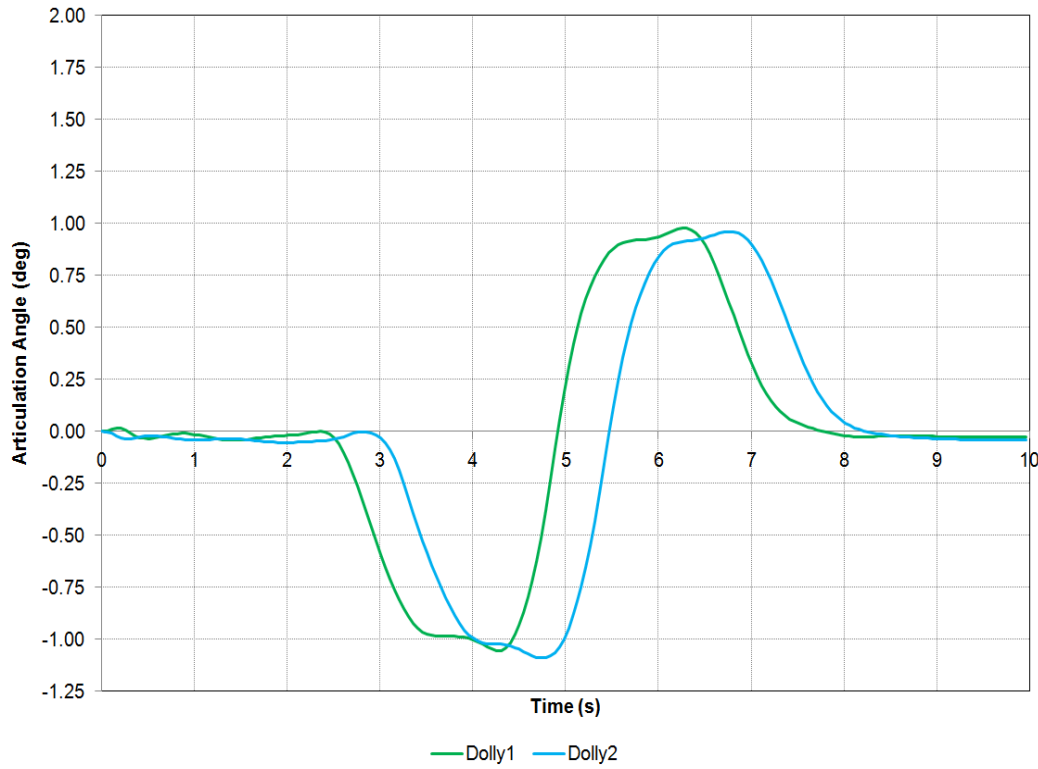


Figure 7-38. Graph. Dolly Articulation Angle, Single Lane Change at 56 km/h (35 mph).

Maximum and Minimum

Figure 7-39 through Figure 7-46 show the model results for velocities ranging from 32 km/h to 72 km/h (20 to 45 mph). These simulations were performed using the flat road profile. The figures show the maximum and minimum values for the quantity listed, at each speed, for the entire maneuver.

In general, the responses increase proportionally with the forward velocity. However, at higher velocities, rearward amplification begins to develop. The data also indicates high and low speed offtracking behavior of the trailers.

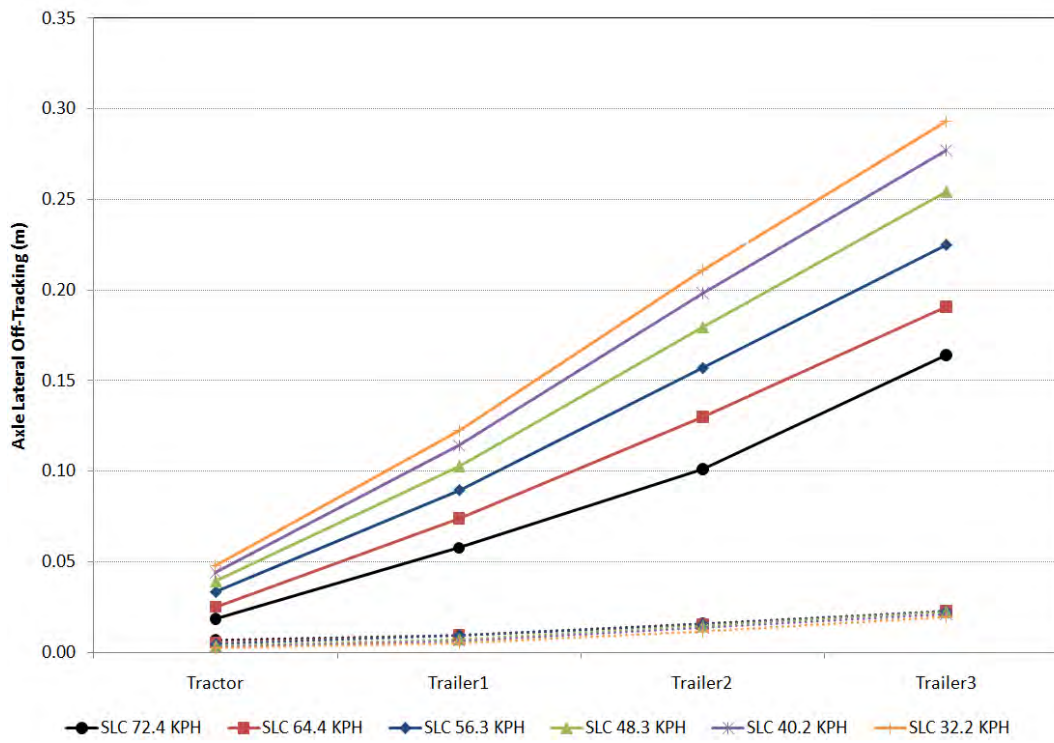


Figure 7-39. Graph. Lateral Offtracking, Single Lane Change at All Velocities.

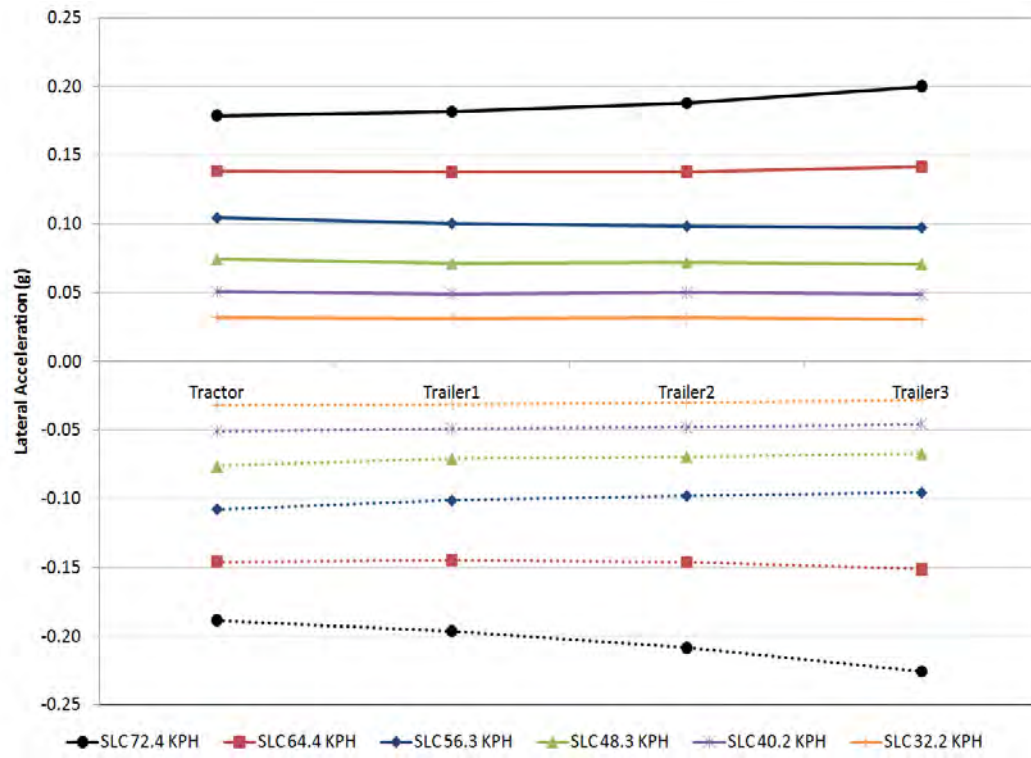


Figure 7-40. Graph. Maximum and Minimum Lateral Acceleration, Single Lane Change at All Velocities.

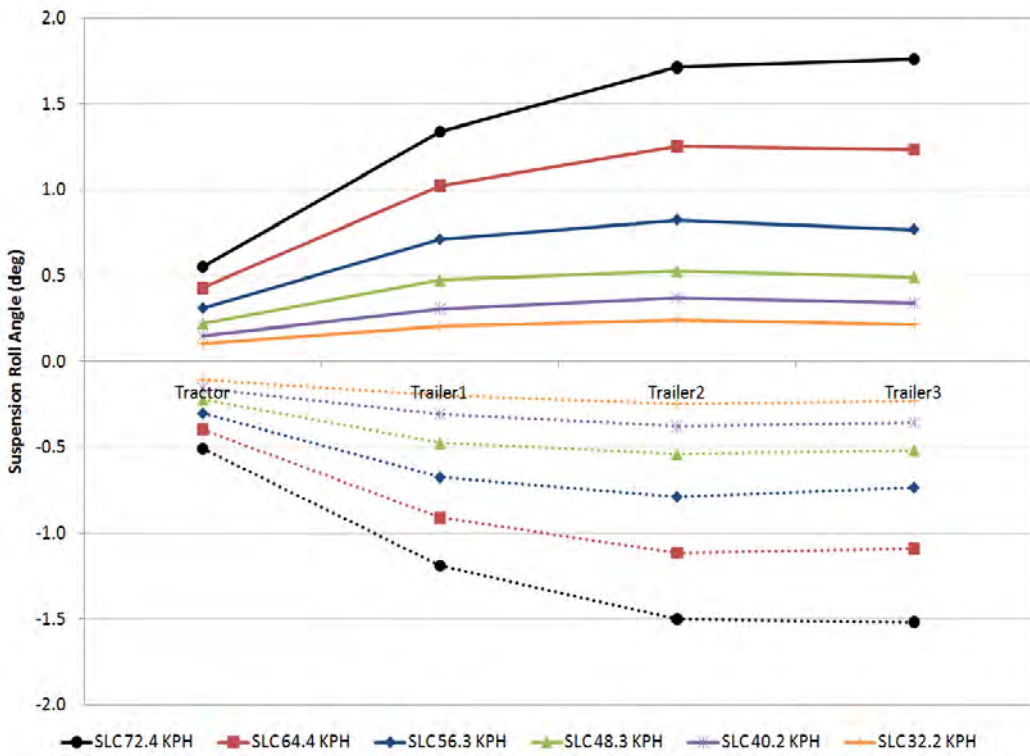


Figure 7-41. Graph. Maximum and Minimum Axle Roll Angle, Single Lane Change at All Velocities.

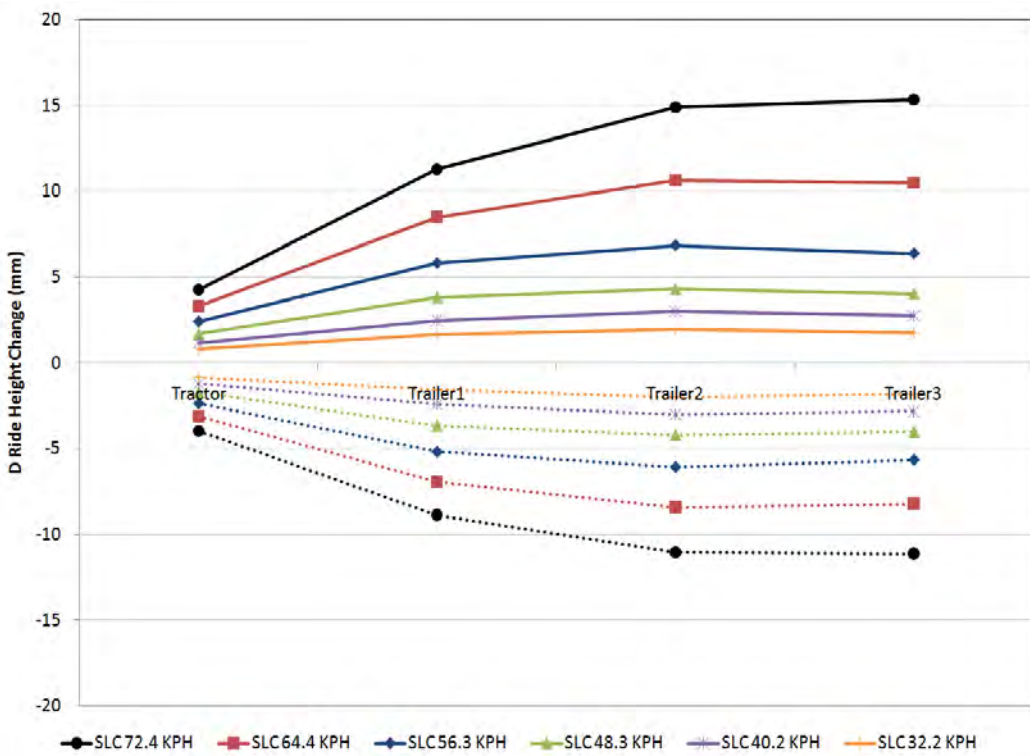


Figure 7-42. Graph. Maximum and Minimum Driver Side Ride Height Change, Single Lane Change at All Velocities.

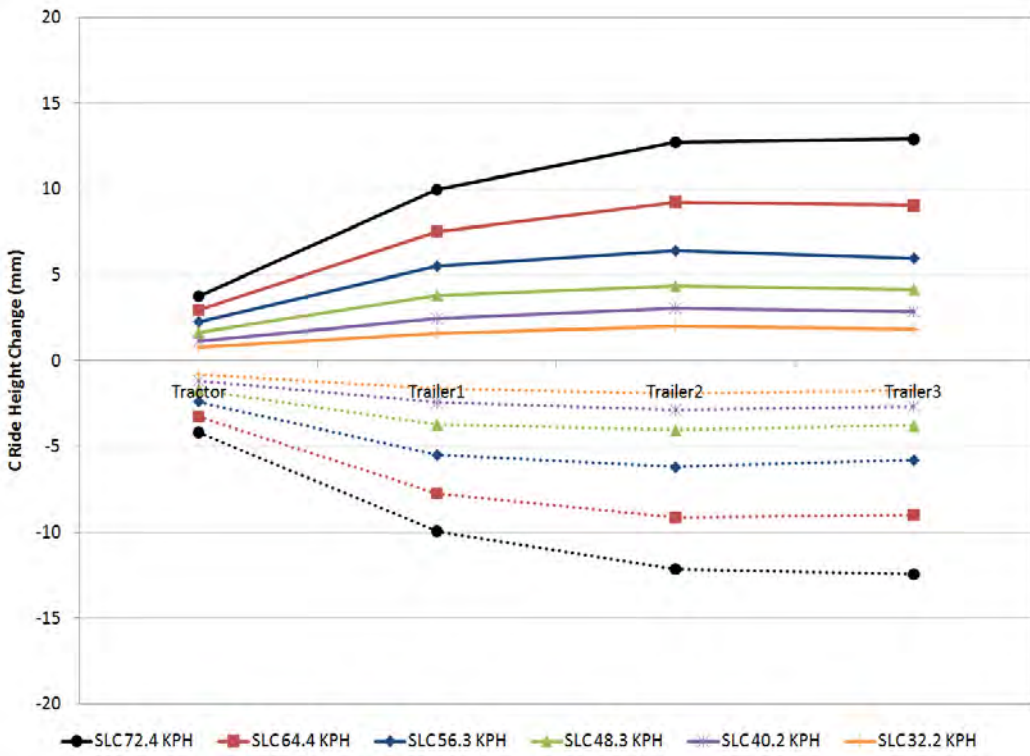


Figure 7-43. Graph. Maximum and Minimum Curb Side Ride Height Change, Single Lane Change at All Velocities.

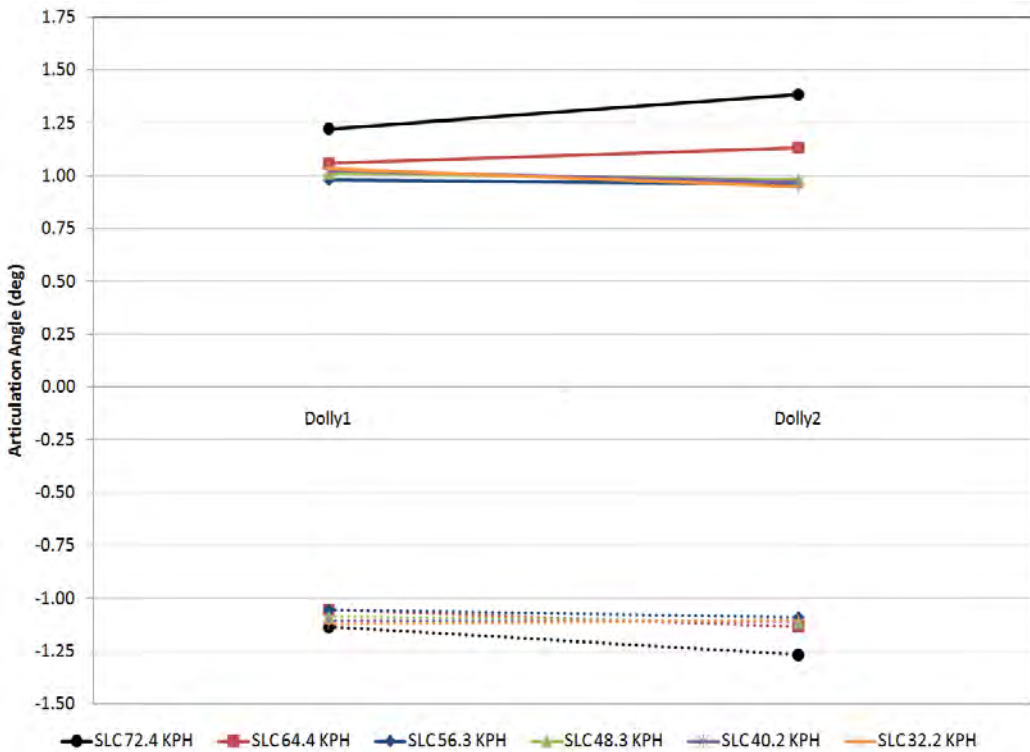


Figure 7-44. Graph. Maximum and Minimum Dolly Articulation Angle, Single Lane Change at All Velocities.

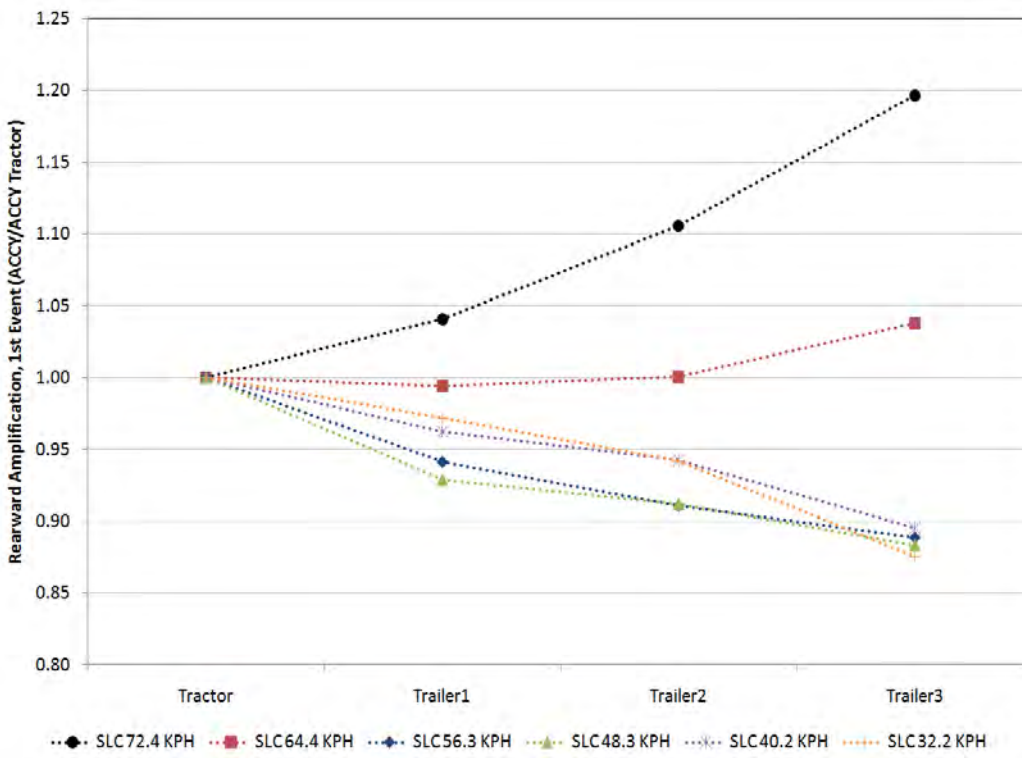


Figure 7-45. Graph. Rearward Amplification, 1st Steering Event, Single Lane Change at All Velocities.

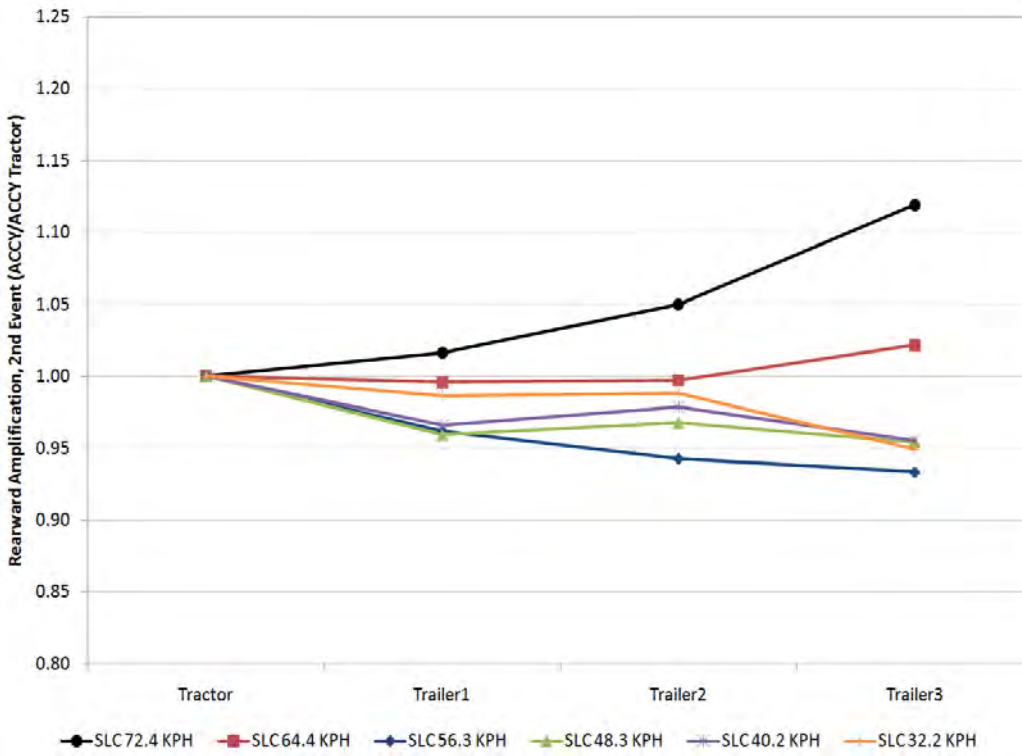


Figure 7-46. Graph. Rearward Amplification, second Steering Event, Single Lane Change at All Velocities.

7.2.4 Double Lane Change

The double lane change event is a transient, triple event maneuver, meaning there are three primary steering inputs. These simulations were performed using the flat road profile.

Time History

Figure 7-47 through Figure 7-54 show the simulation results for the maneuver at a velocity of 56 km/h (35 mph). Many of the time histories show a symmetry between positive and negative values. The offtracking is again sorted by trailer position, while lateral acceleration and roll angle reach similar values for each trailer. Peak values are similar to those found in the single lane change

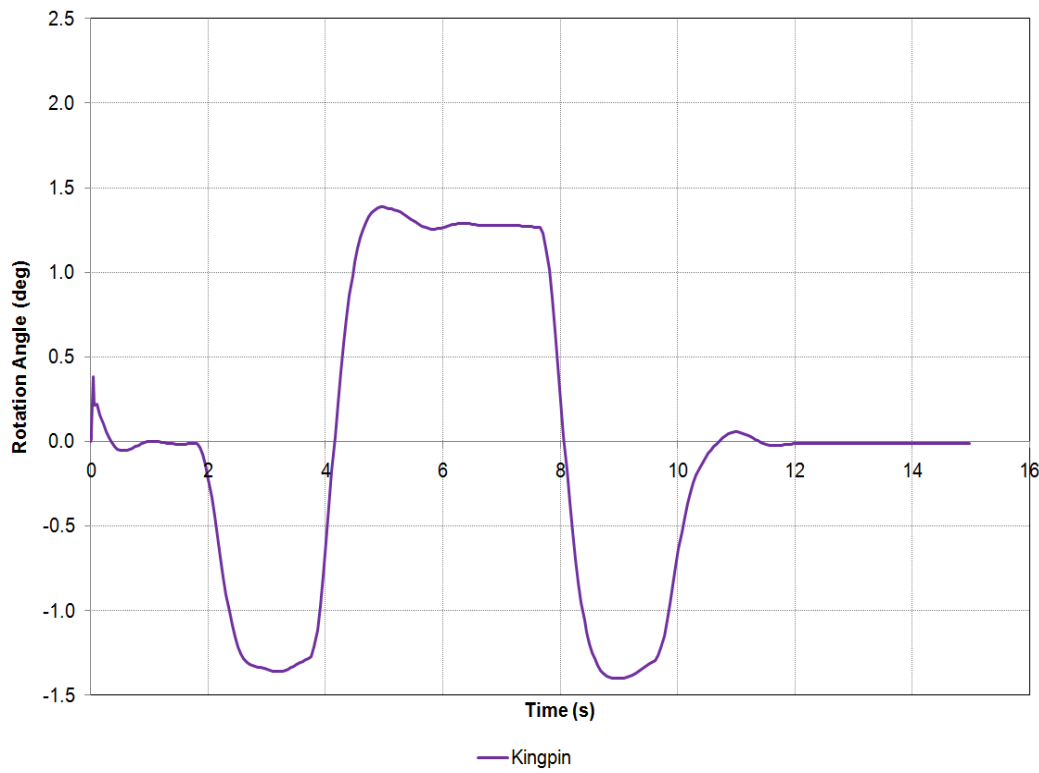


Figure 7-47. Graph. Steering Input, Double Lane Change at 56 km/h (35 mph).

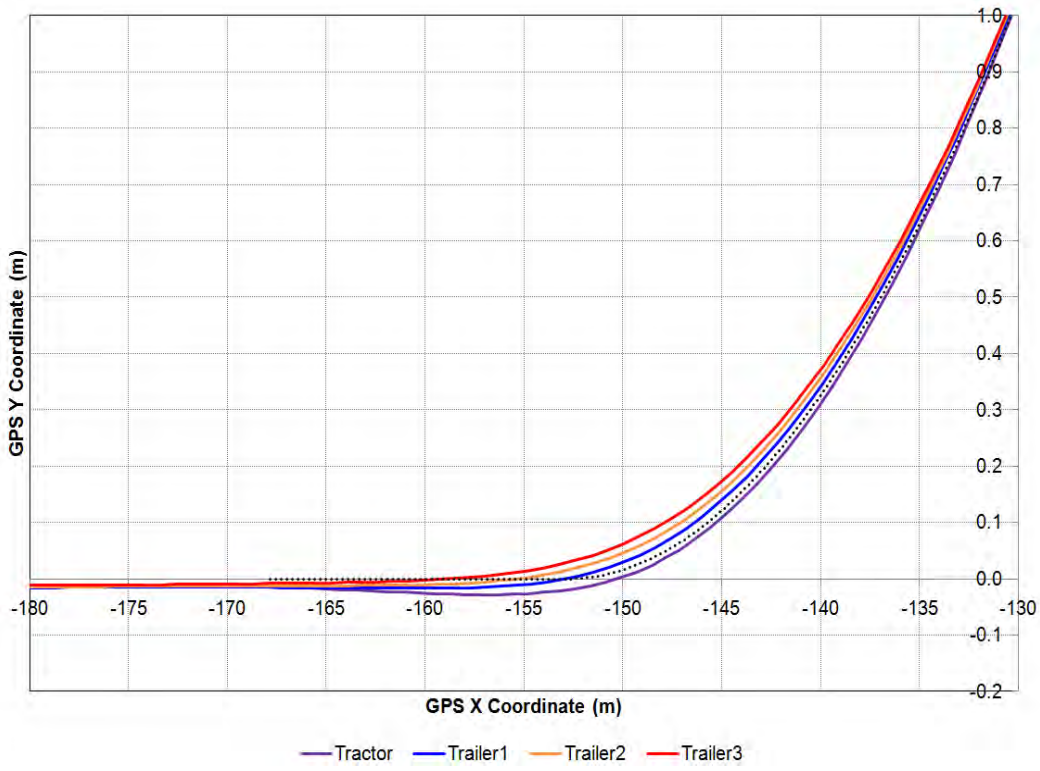


Figure 7-48. Graph. Path Close-Up, Double Lane Change at 56 km/h (35 mph).

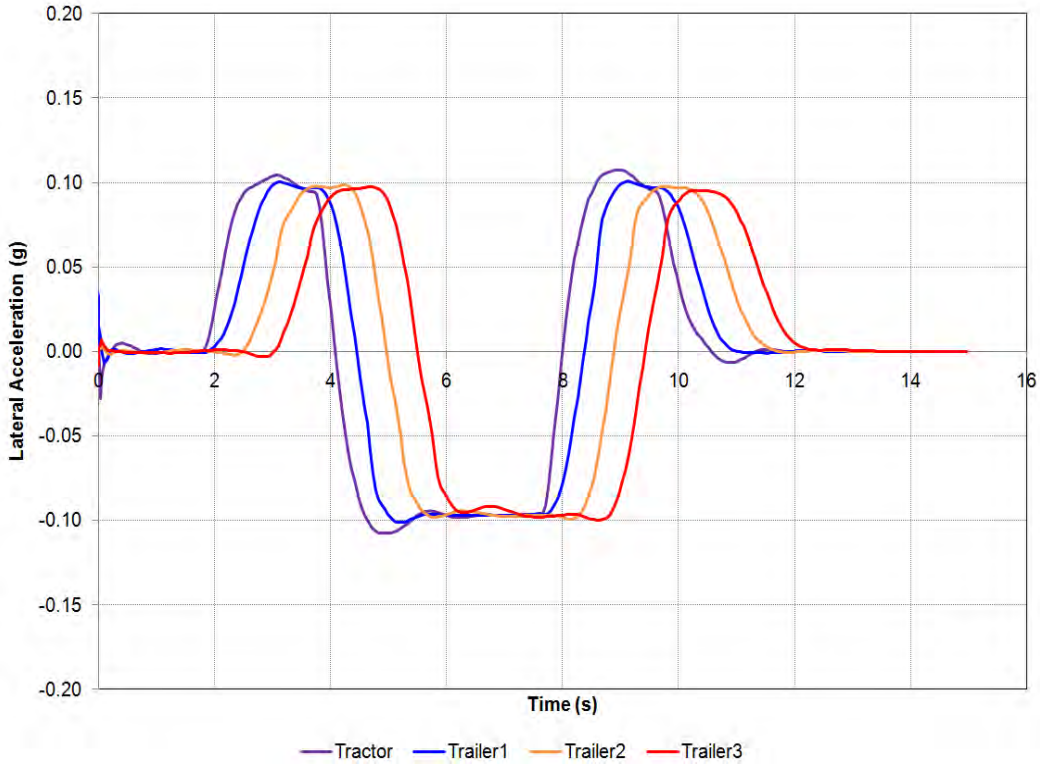


Figure 7-49. Graph. Lateral Acceleration, Double Lane Change at 56 km/h (35 mph).

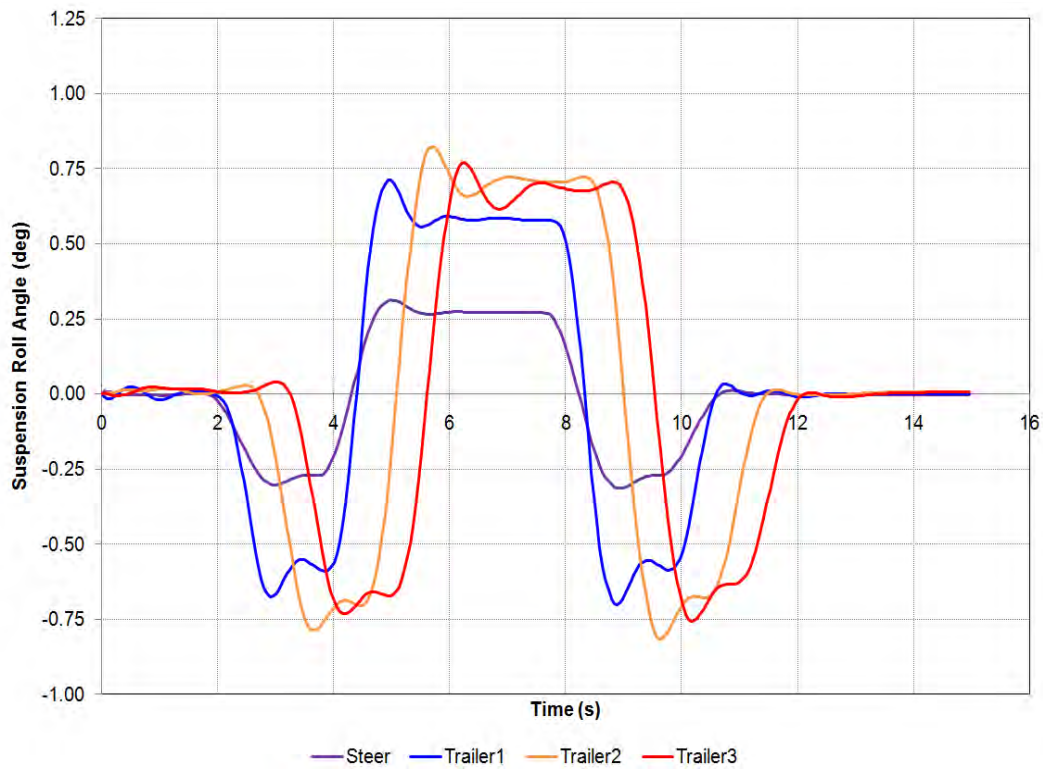


Figure 7-50. Graph. Roll Angle, Double Lane Change at 56 km/h (35 mph).

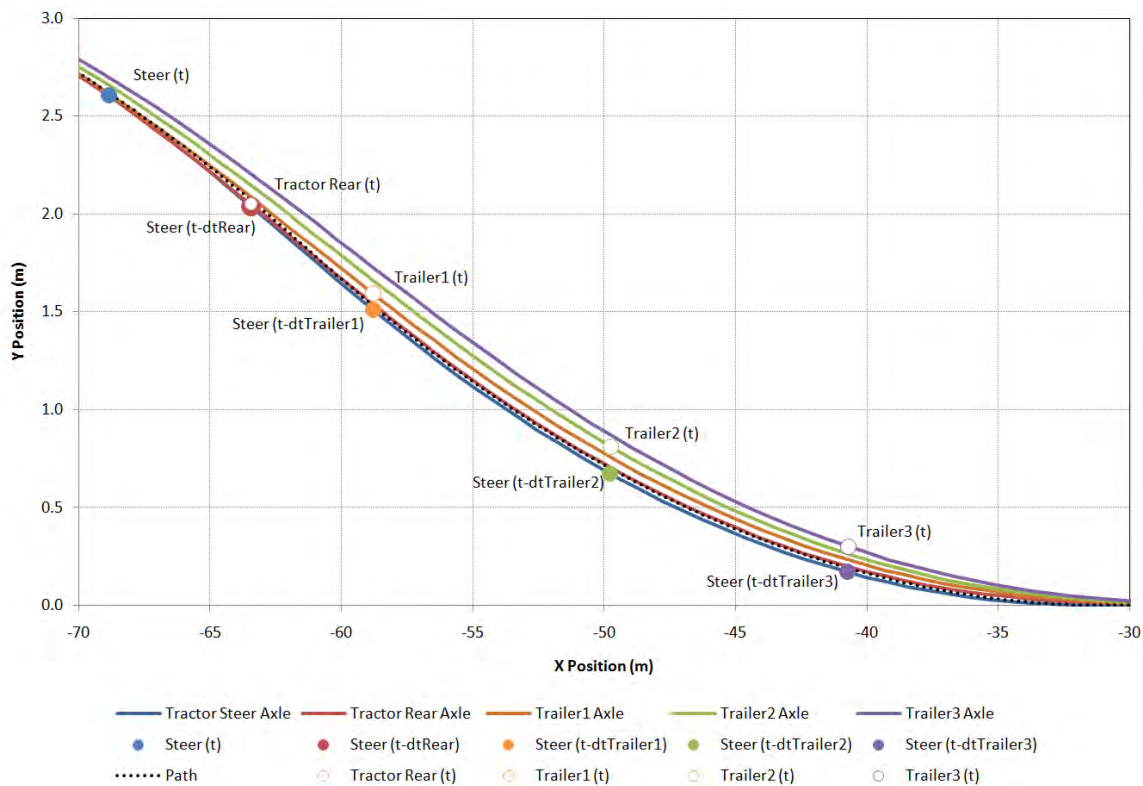


Figure 7-51 - Graphical Representation of Offtracking Calculation, Double Lane Change at 56 km/h (35 mph).

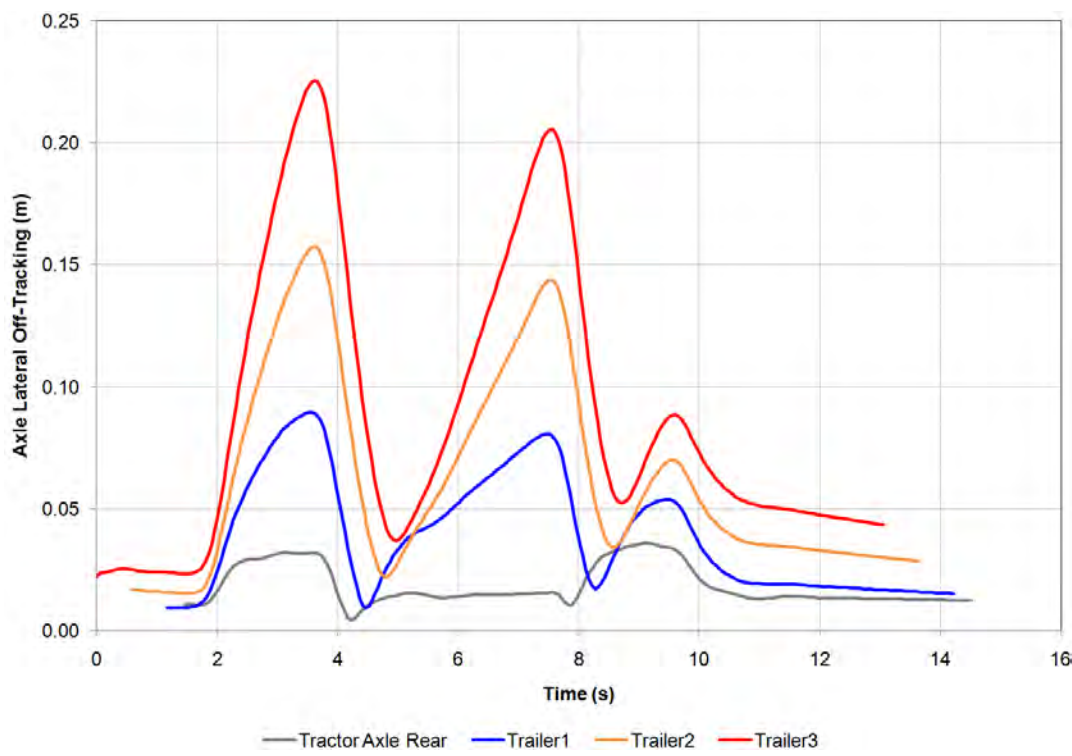


Figure 7-52. Graph. Axle Lateral Offtracking, Double Lane Change at 56 km/h (35 mph).

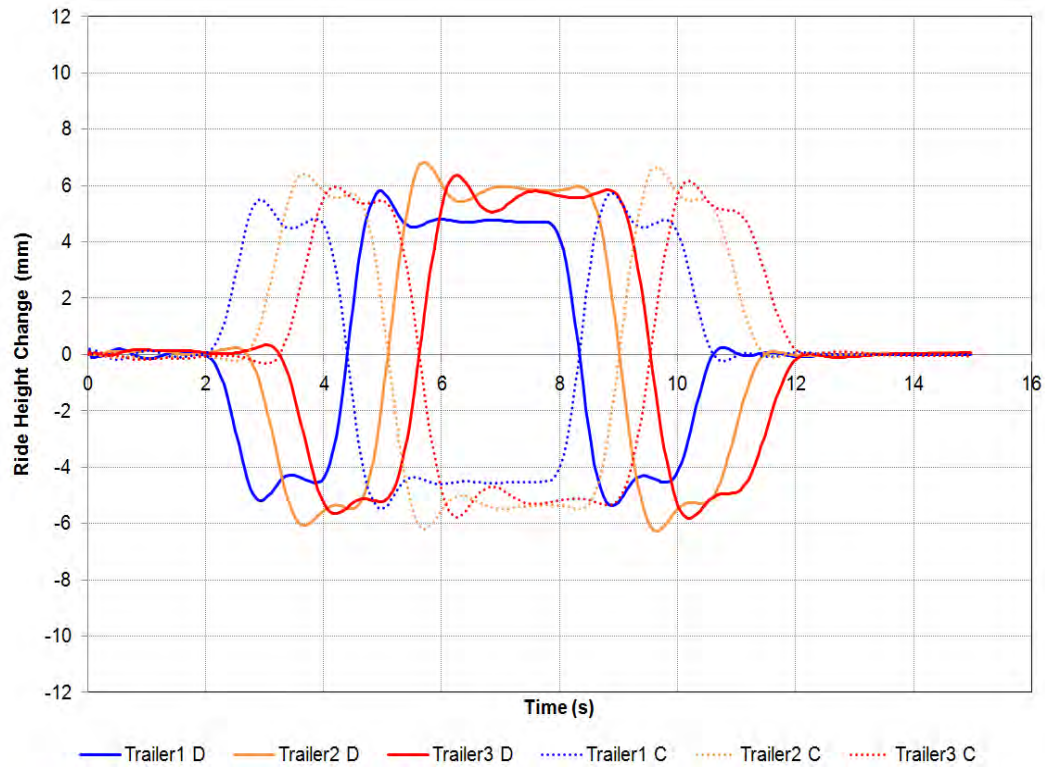


Figure 7-53. Graph. Ride Height Change, Double Lane Change at 56 km/h (35 mph).

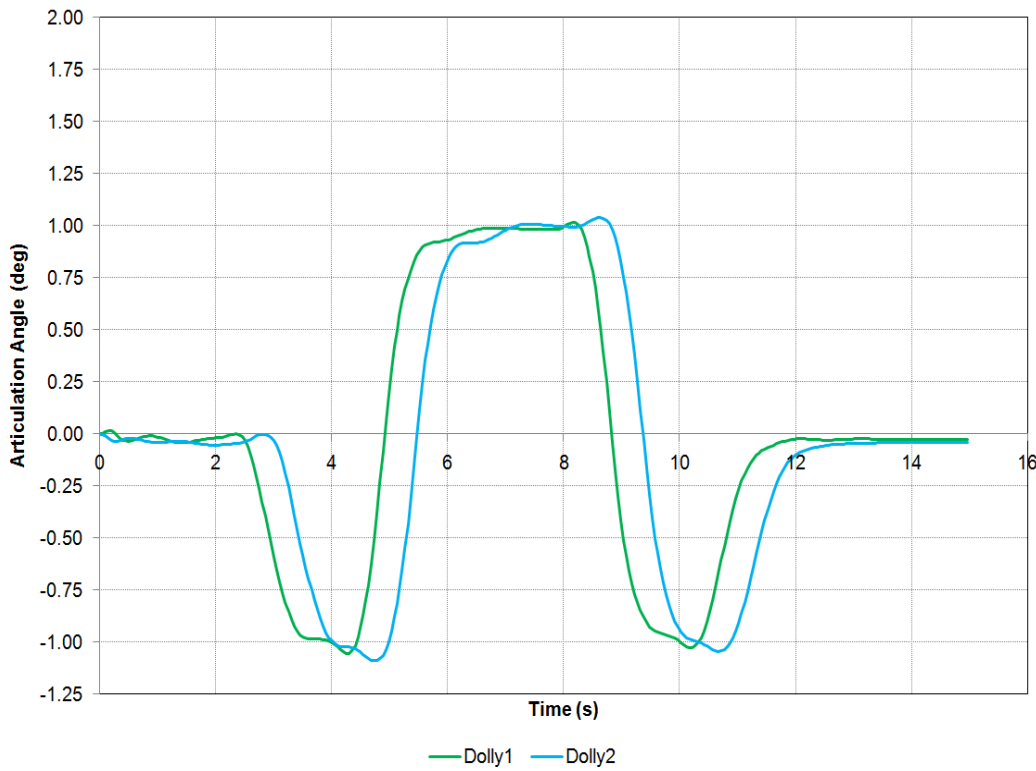


Figure 7-54. Graph. Dolly Articulation Angle, Double Lane Change at 56 km/h (35 mph).

Maximum and Minimum

Figure 7-55 through Figure 7-62 show the model results for at velocities ranging from 32 km/h to 72 km/h (20 to 45 mph). The figures show the maximum and minimum values for the quantity listed, at each speed, for the entire maneuver.

These results show a predictable behavior. In general, the responses increase proportionally with the forward velocity. However, at higher velocities, rearward amplification begins to appear. The data also indicates high and low speed offtracking behavior of the trailers.

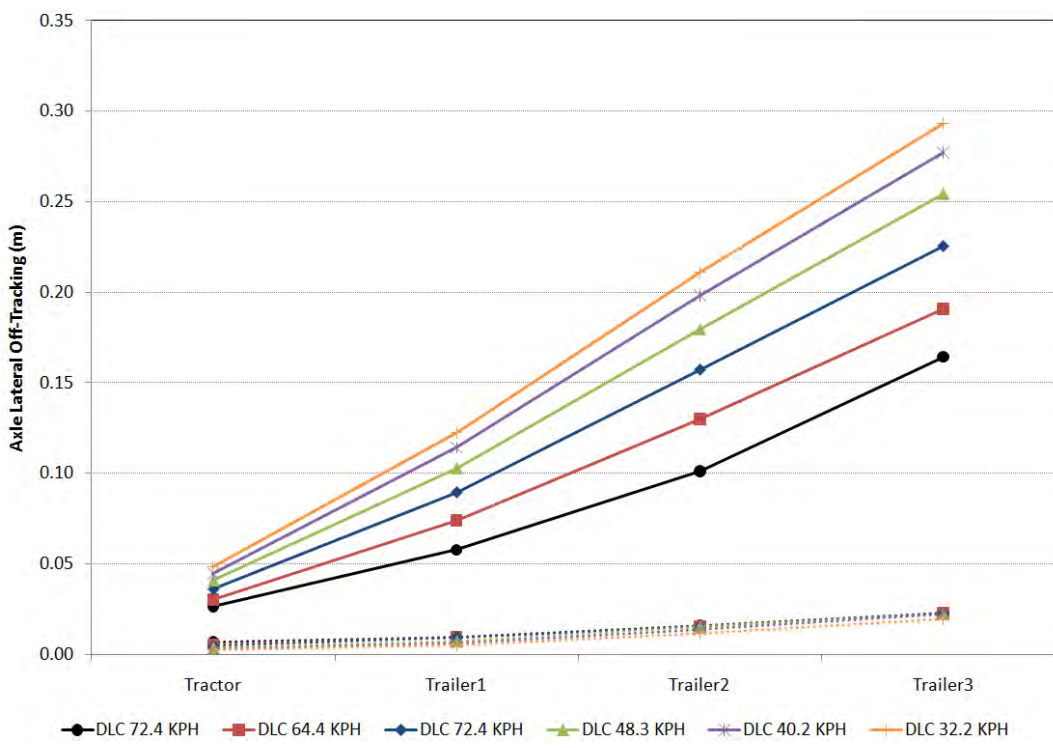


Figure 7-55. Graph. Lateral Offtracking, Double Lane Change at All Velocities.

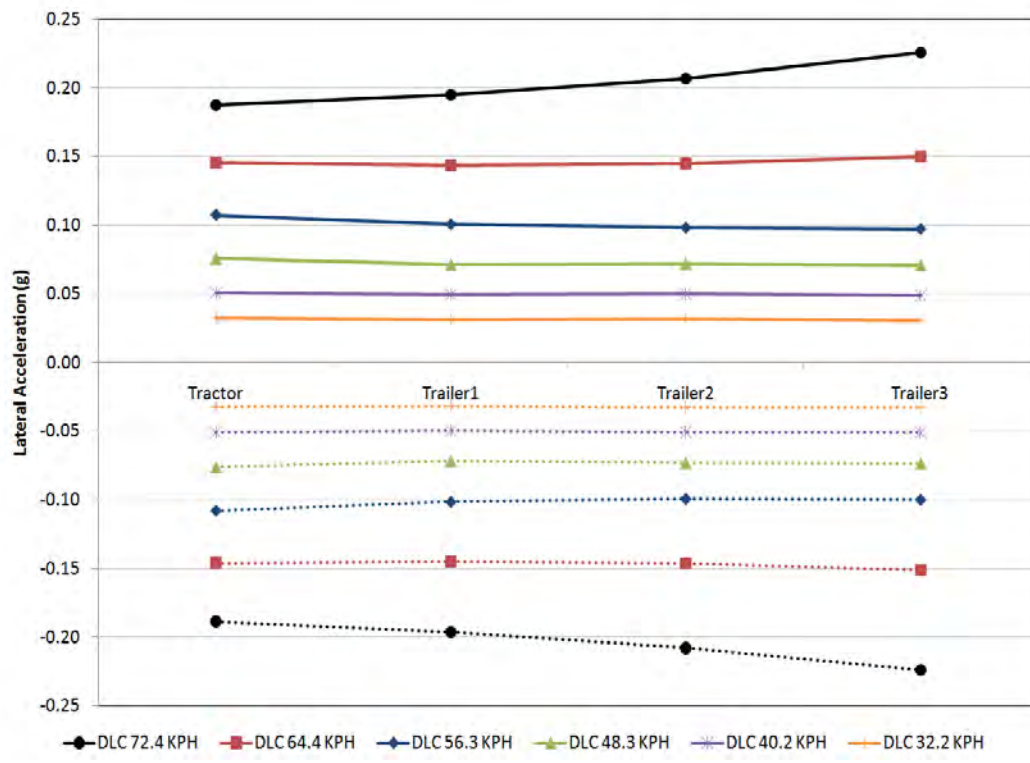


Figure 7-56. Graph. Maximum and Minimum Lateral Acceleration, Double Lane Change at All Velocities.

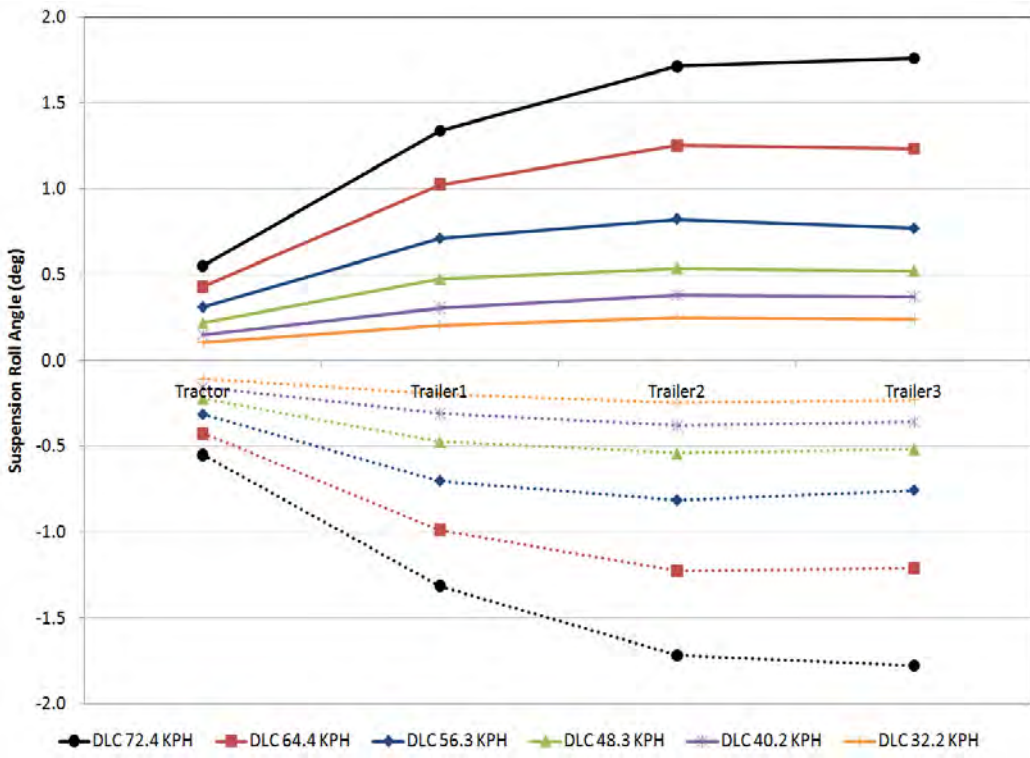


Figure 7-57. Graph. Maximum and Minimum Axle Roll Angle, Double Lane Change at All Velocities.

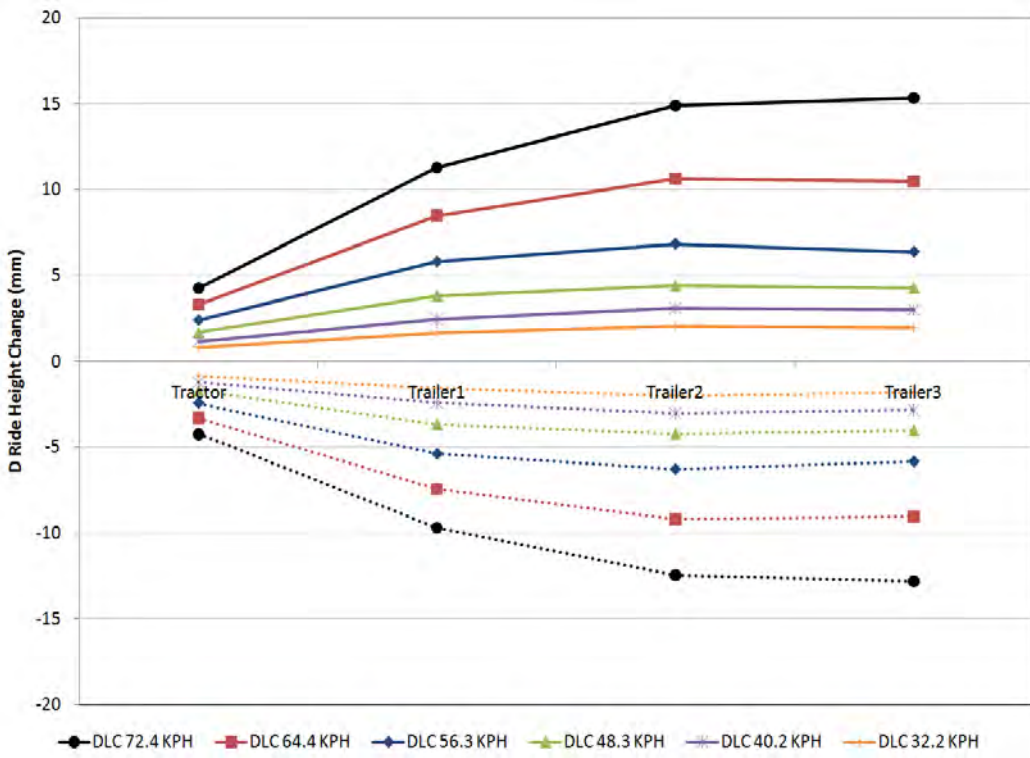


Figure 7-58. Graph. Maximum and Minimum Driver Side Ride Height Change, Double Lane Change at All Velocities.

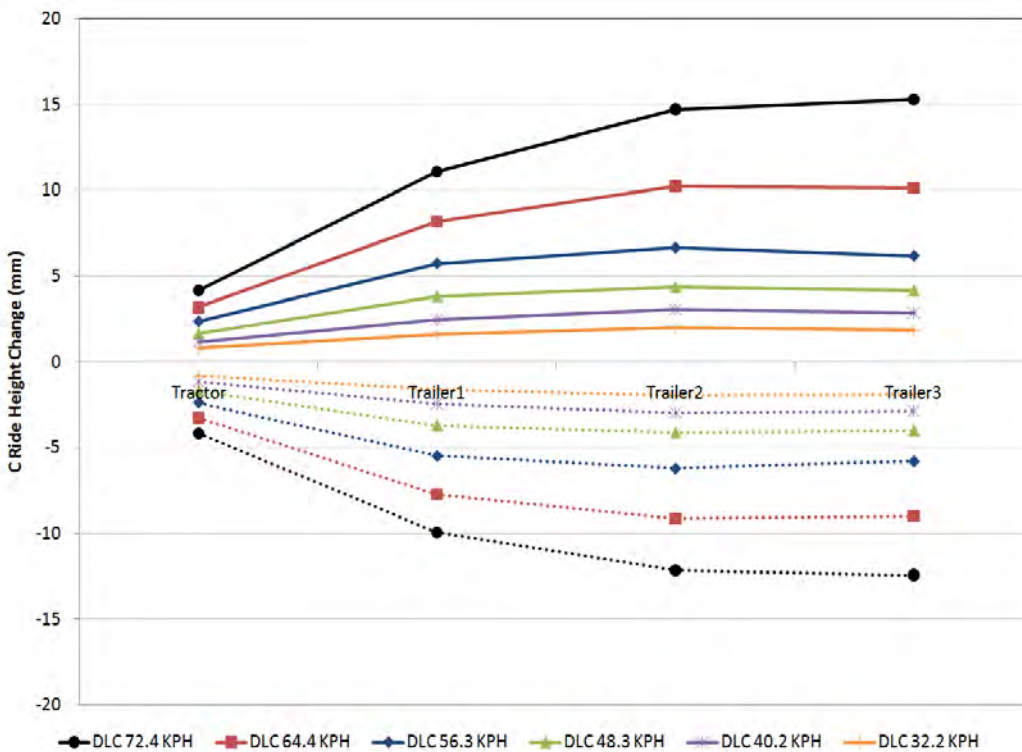


Figure 7-59. Graph. Maximum and Minimum Curb Side Ride Height Change, Double Lane Change at All Velocities.

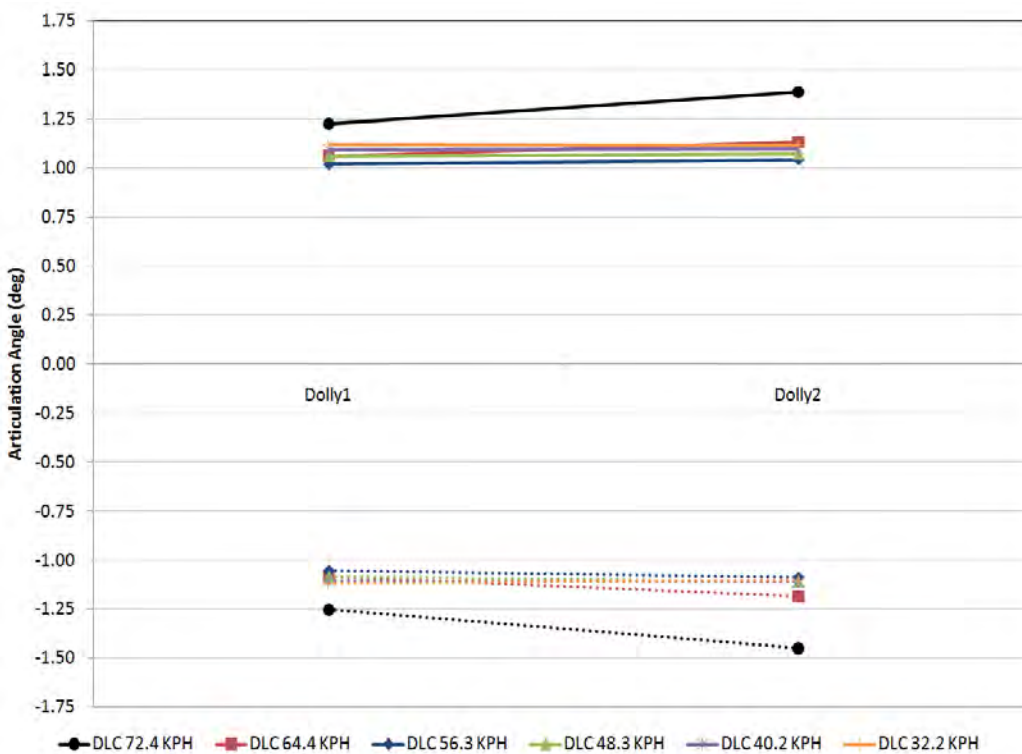


Figure 7-60. Graph. Maximum and Minimum Dolly Articulation Angle, Double Lane Change at All Velocities.

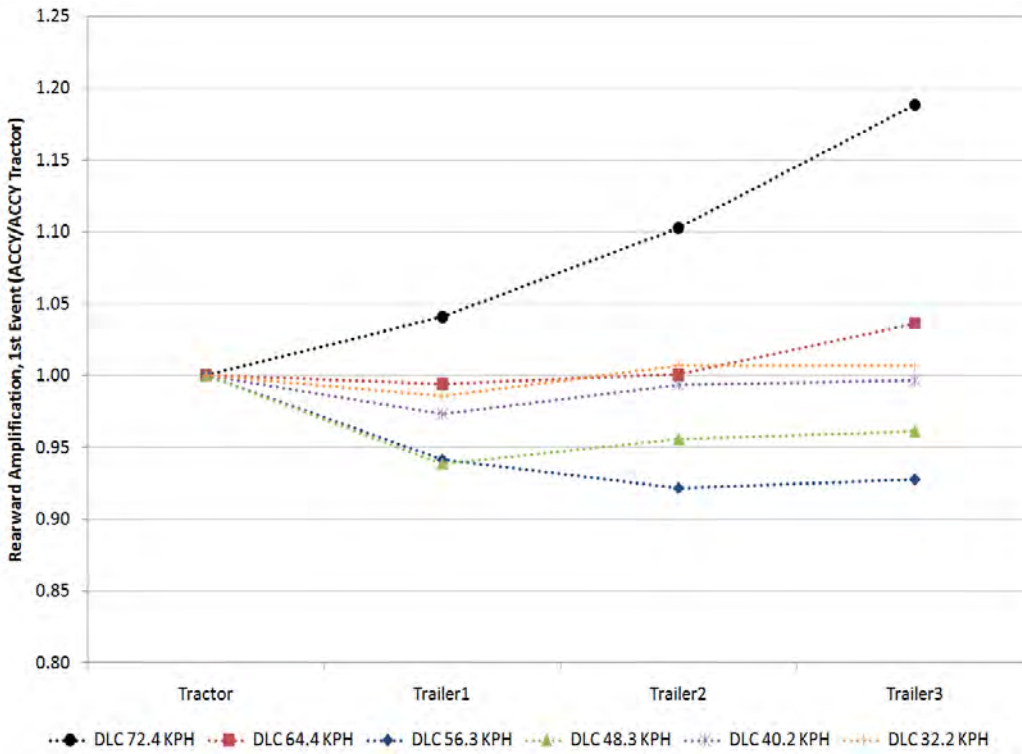


Figure 7-61. Graph. Rearward Amplification, 1st Steering Event, Double Lane Change at All Velocities.

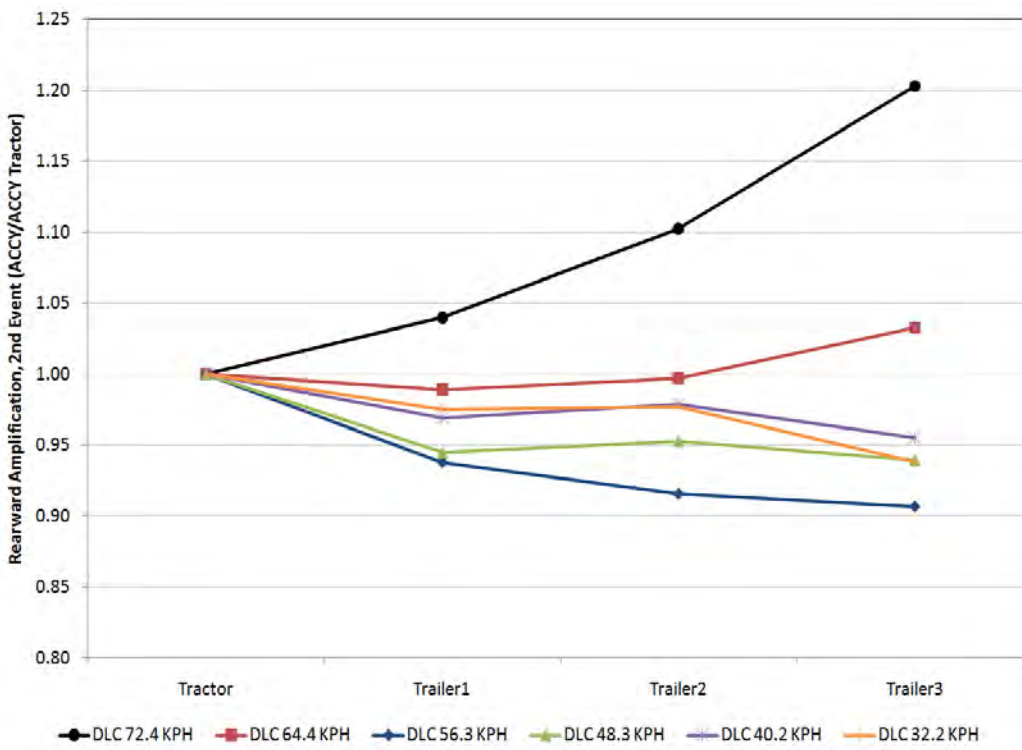


Figure 7-62 - Rearward Amplification, second Steering Event, Double Lane Change at All Velocities.

7.3 Comparison with Test Data

Filtered string potentiometer (string pot) data for each event allowed for a direct comparison of the simulation and physical test results. The figures that follow show up to four different data sets for each event at a velocity of 56 km/h (35 mph). Comparisons are made for suspension roll angle, ride height change, and dolly articulation angle. The plots give an indication of the scatter of the measured data, and show the average of the maximum and minimum values from each run as indicated with the red circle.

The simulation and test show the same general trend in many of the comparison charts. There are, however, sizeable differences in response magnitude, especially in the constant radius cornering event. This could be attributed to lack of a proper road profile, the simple tires, or other estimated system properties.

7.3.1 Constant Radius Cornering

Figure 7-63 through Figure 7-74 show the simulated and measured time histories for the constant radius curve passages.

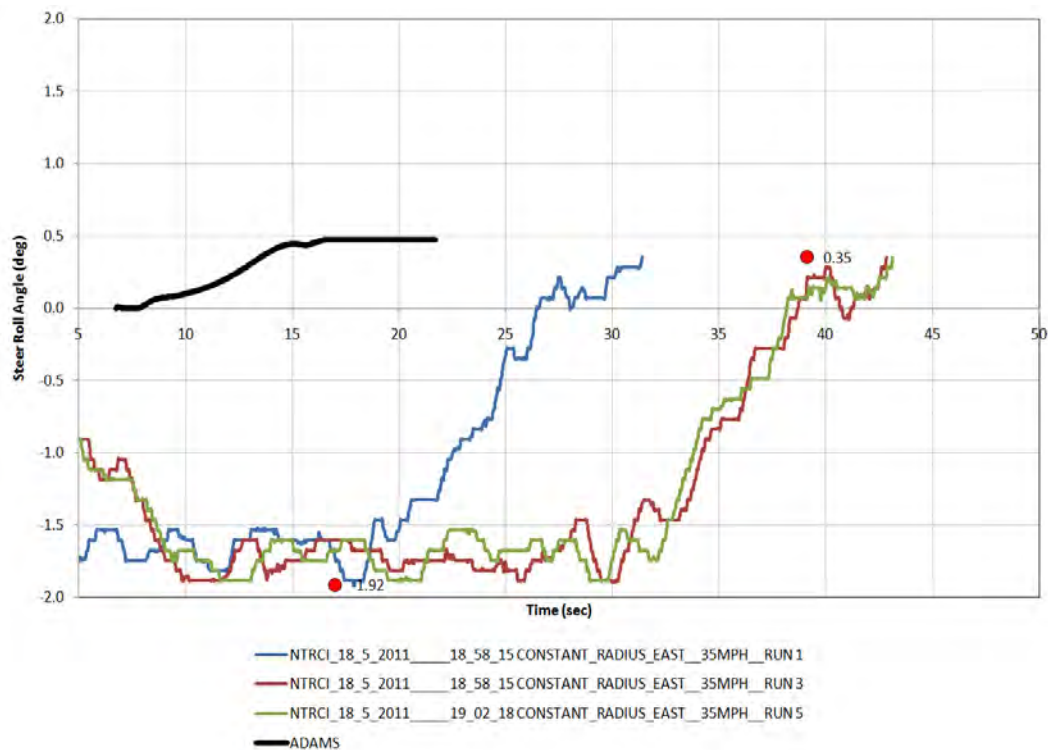


Figure 7-63. Graph. Model vs. Test, Steer Axle Roll Angle, Constant Radius Cornering at 56 km/h (35 mph).

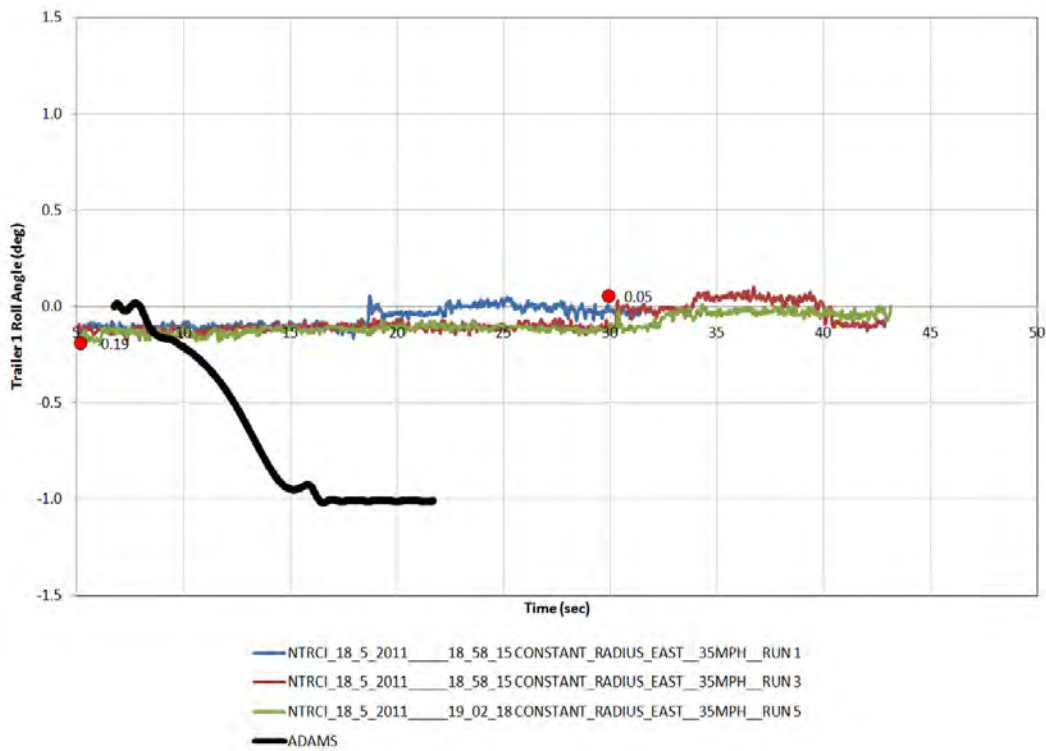


Figure 7-64. Graph. Model vs. Test, Trailer1 Roll Angle, Constant Radius Cornering at 56 km/h (35 mph).

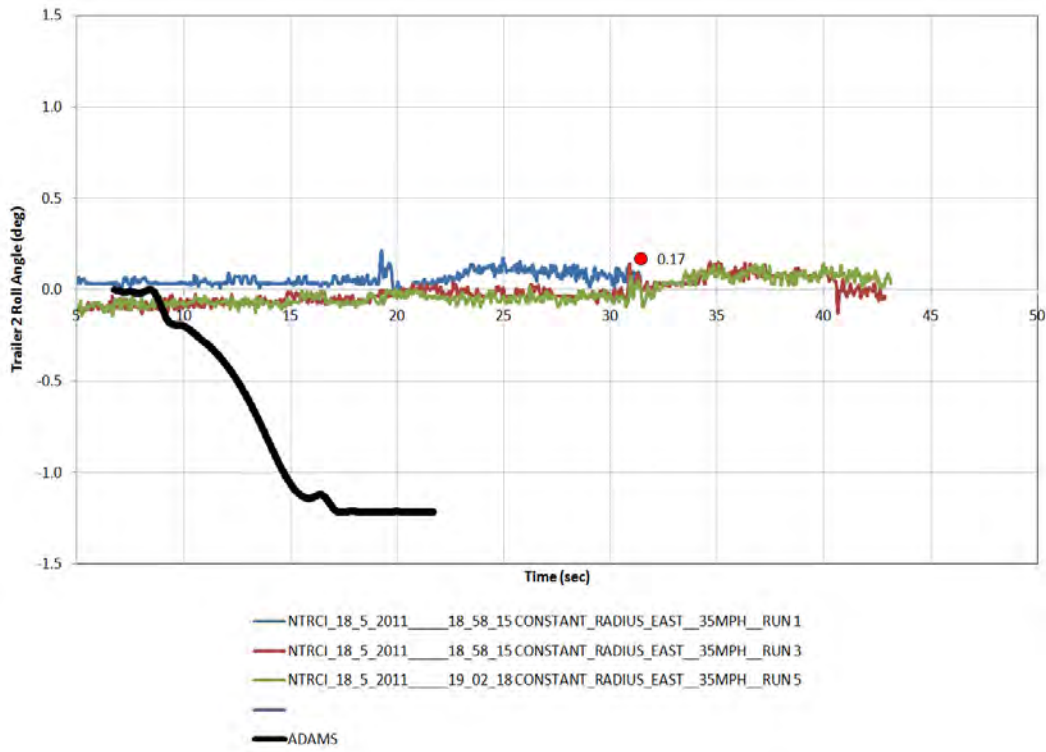


Figure 7-65. Graph. Model vs. Test, Trailer2 Roll Angle, Constant Radius Cornering at 56 km/h (35 mph).

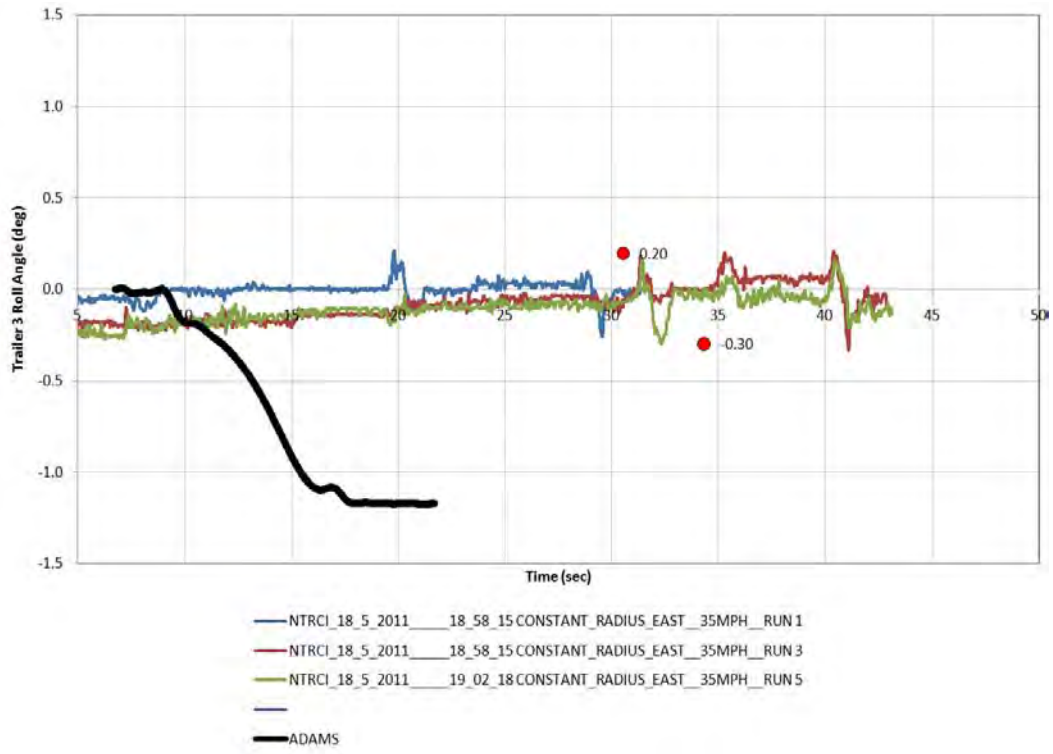


Figure 7-66. Graph. Model vs. Test, Trailer3 Roll Angle, Constant Radius Cornering at 56 km/h (35 mph).

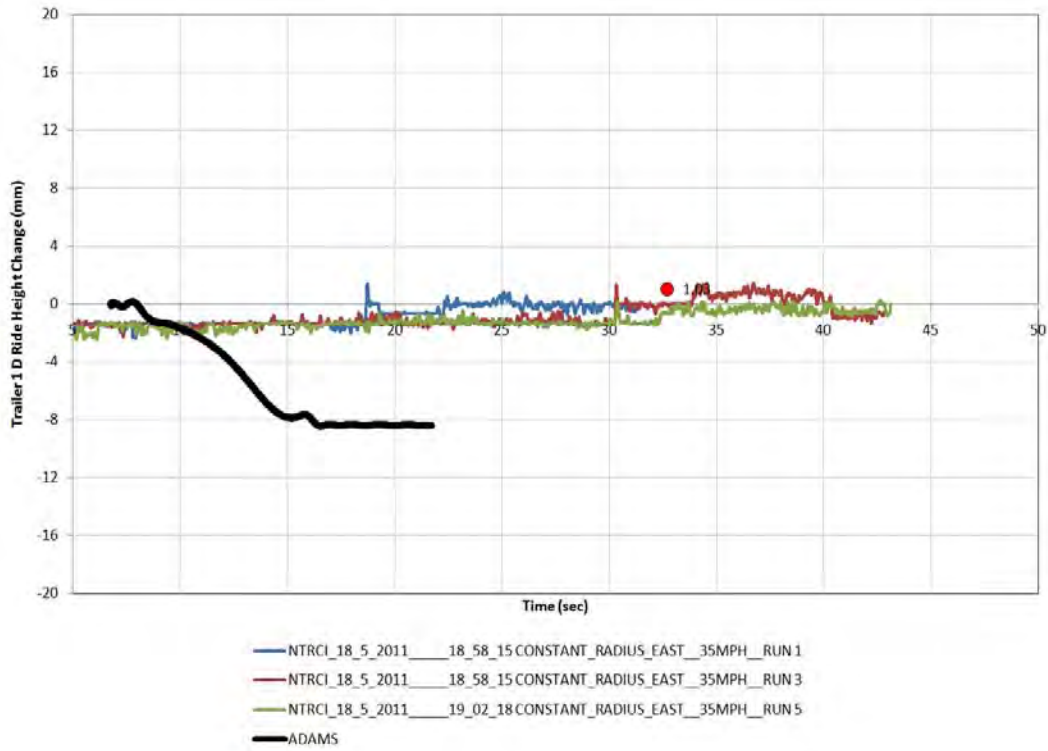


Figure 7-67. Graph. Model vs. Test, Trailer1D Ride Height Change, Constant Radius Cornering at 56 km/h (35 mph).

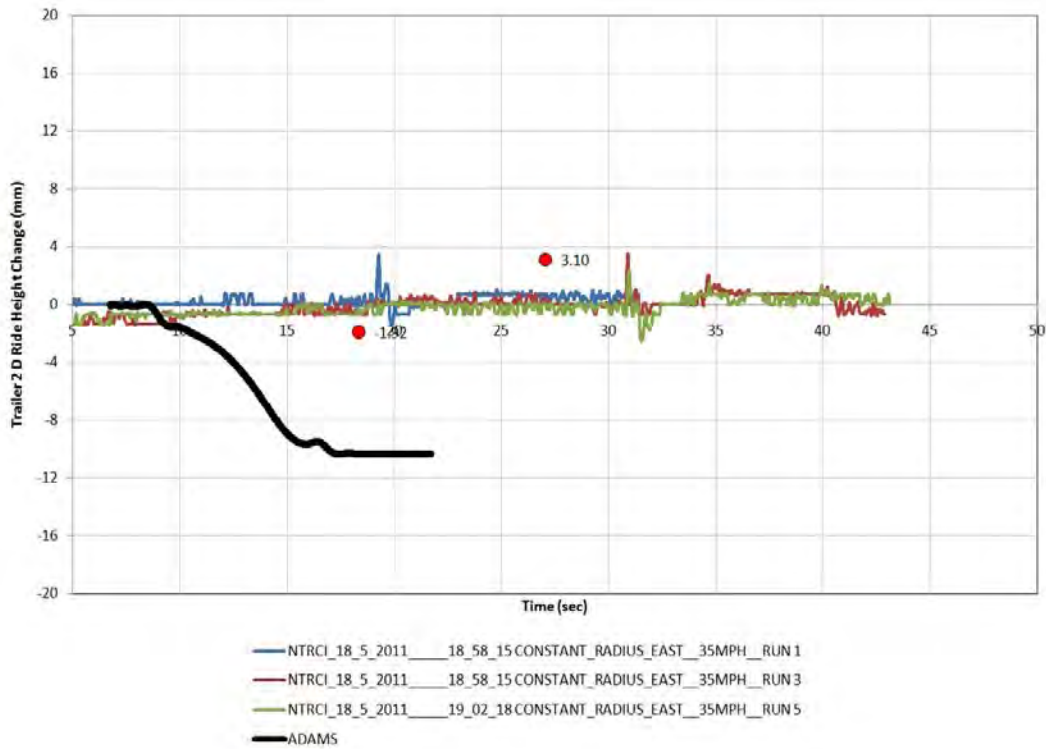


Figure 7-68. Graph. Model vs. Test, Trailer2D Ride Height Change, Constant Radius Cornering at 56 km/h (35 mph).

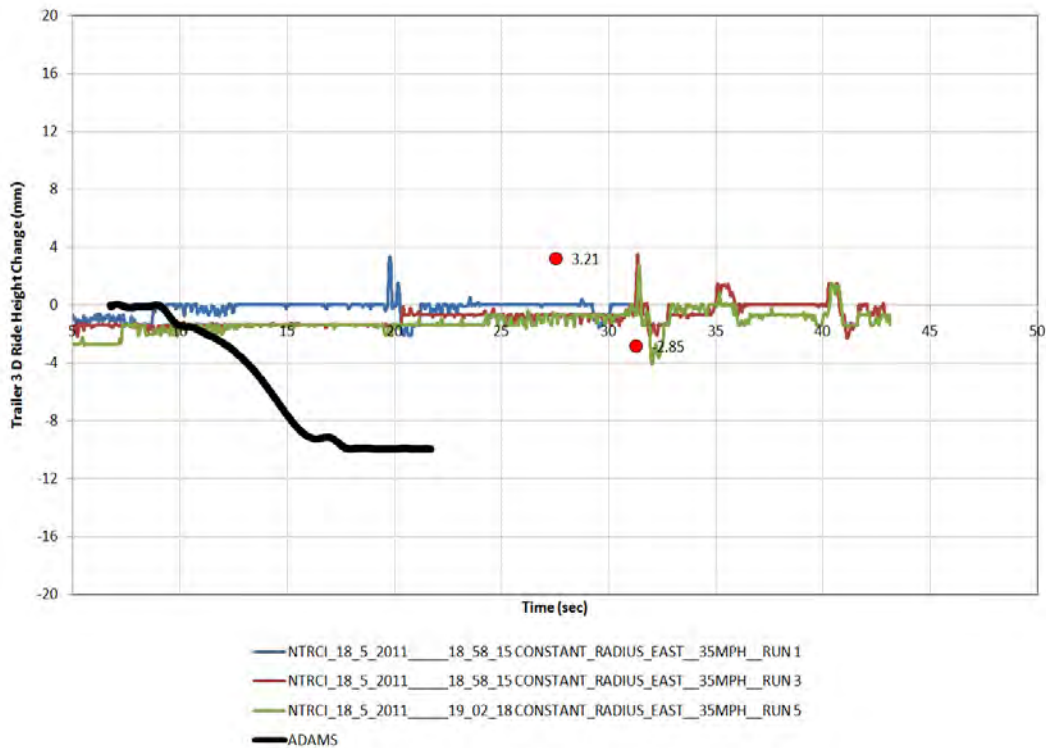


Figure 7-69. Graph. Model vs. Test, Trailer3D Ride Height Change, Constant Radius Cornering at 56 km/h (35 mph).

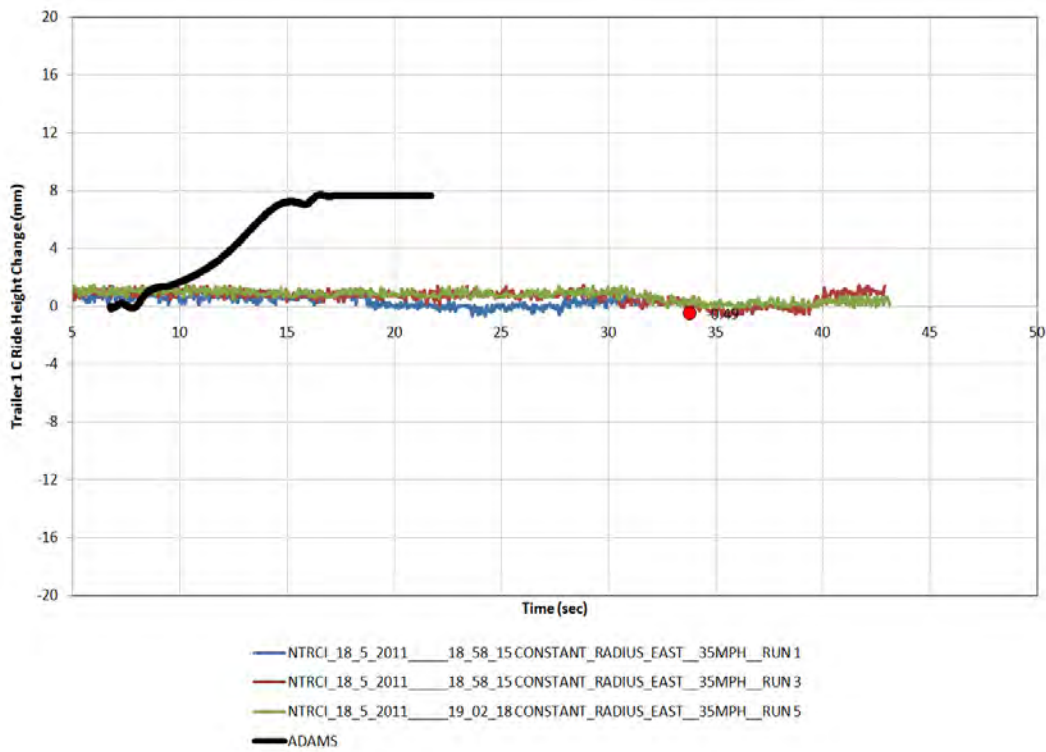


Figure 7-70. Graph. Model vs. Test, Trailer1C Ride Height Change, Constant Radius Cornering at 56 km/h (35 mph).

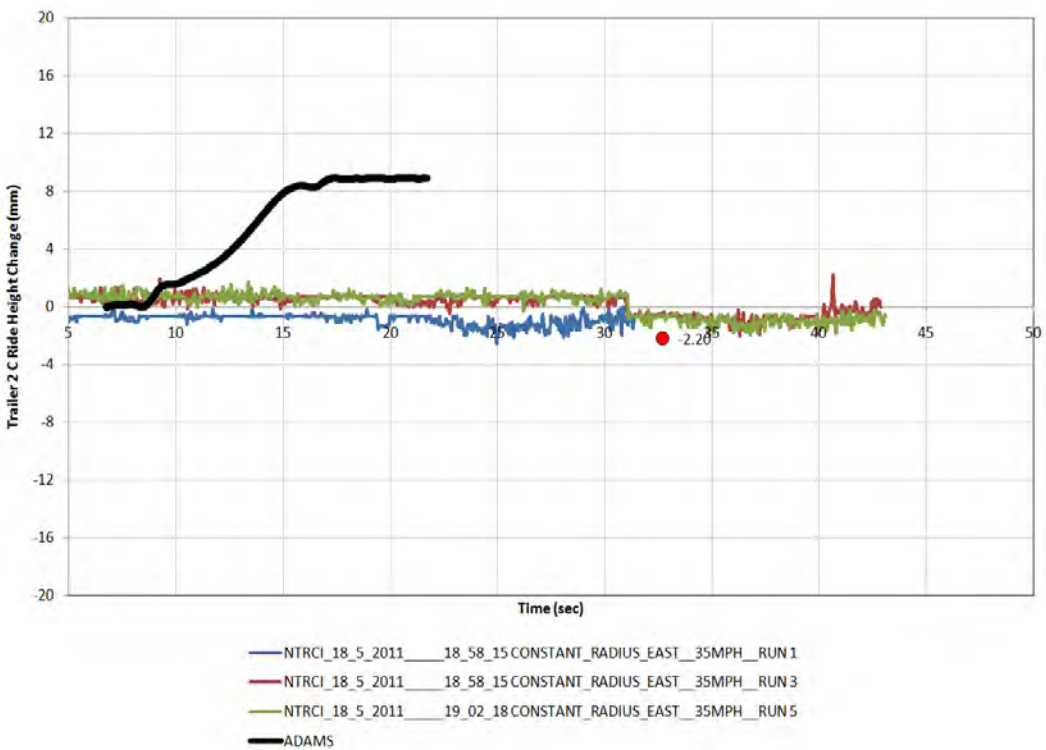


Figure 7-71. Graph. Model vs. Test, Trailer2C Ride Height Change, Constant Radius Cornering at 56 km/h (35 mph).

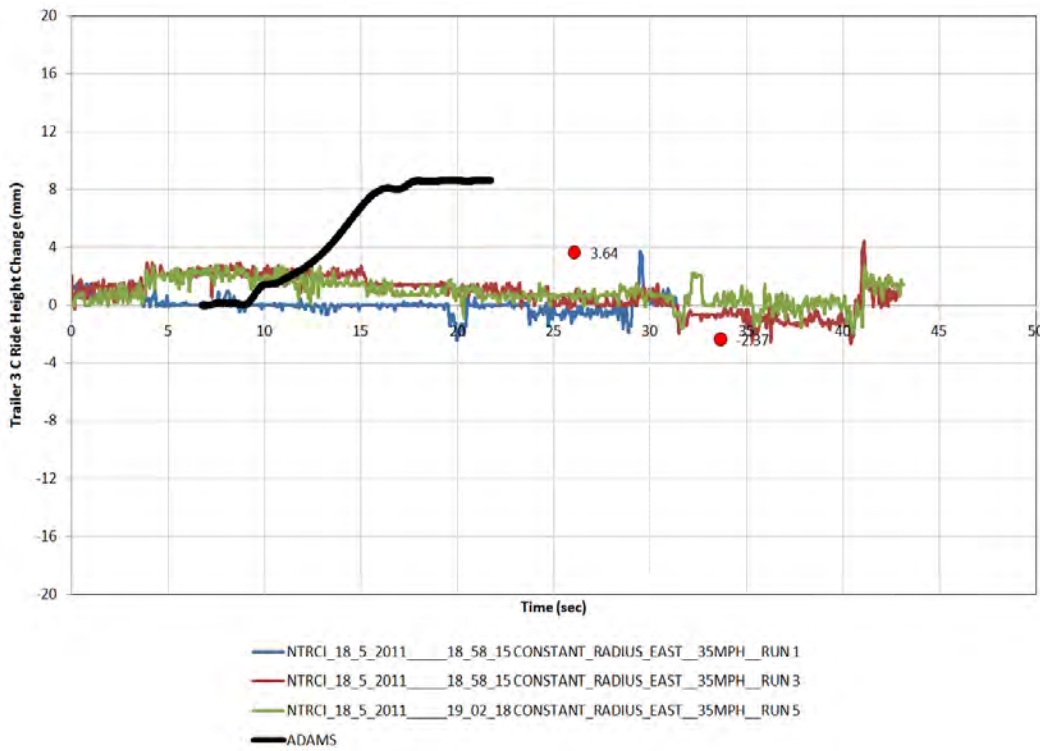


Figure 7-72. Graph. Model vs. Test, Trailer3C Ride Height Change, Constant Radius Cornering at 56 km/h (35 mph).

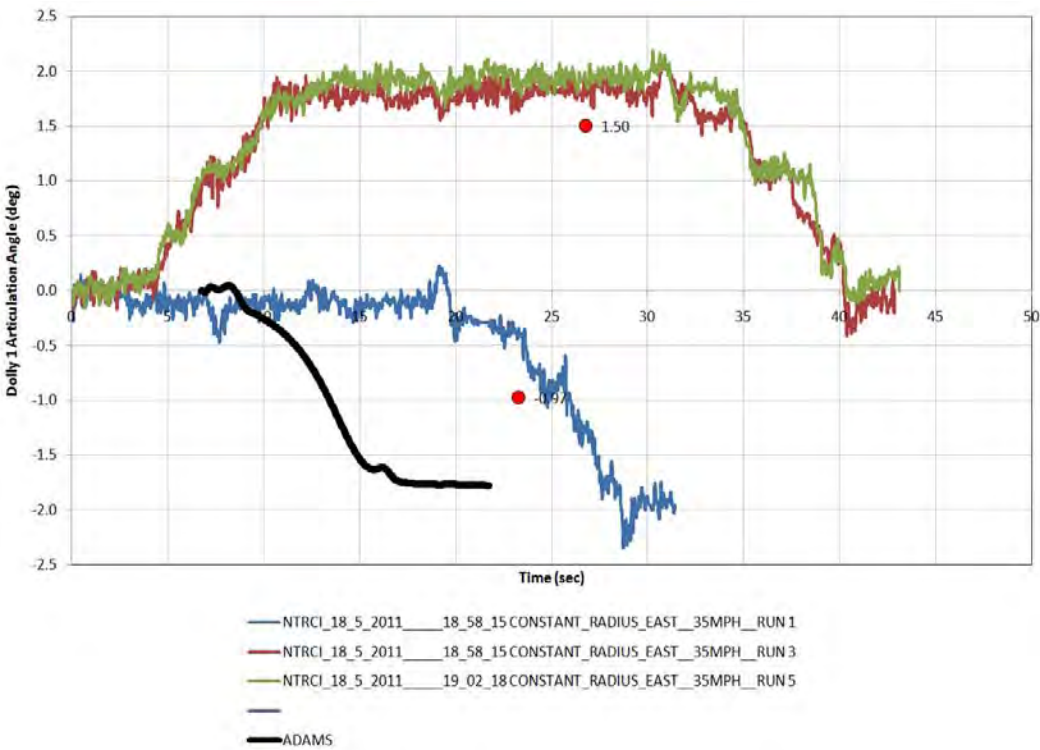


Figure 7-73. Graph. Model vs. Test, Dolly1 Articulation Angle, Constant Radius Cornering at 56 km/h (35 mph).

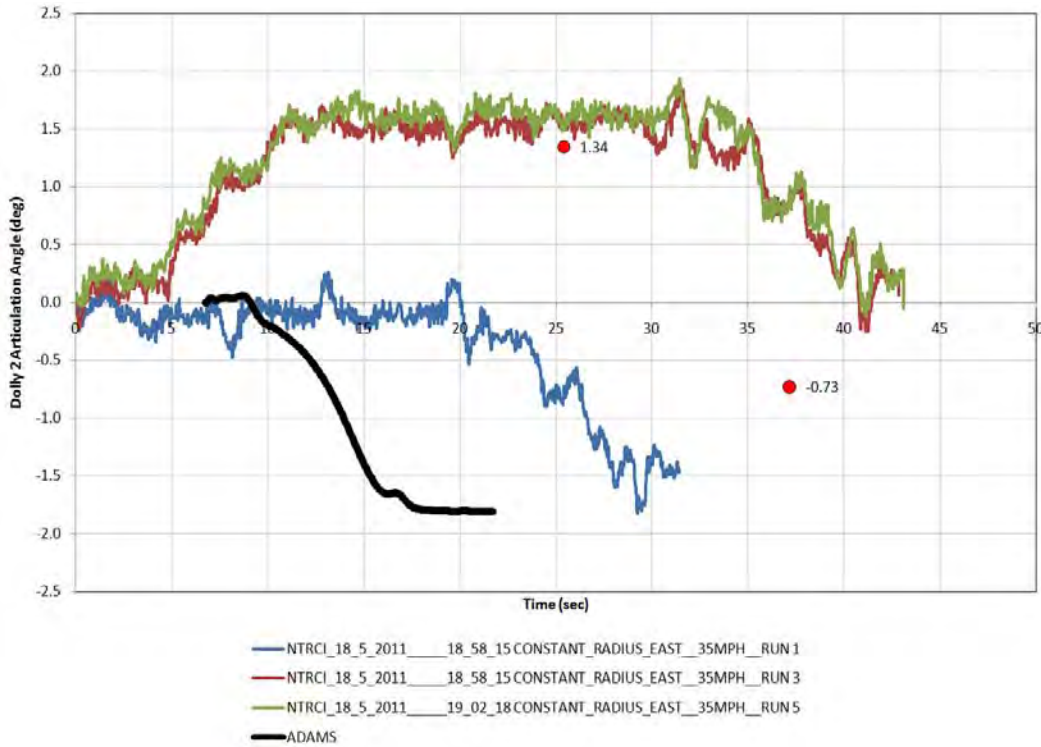


Figure 7-74. Graph. Model vs. Test, Dolly2 Articulation Angle, Constant Radius Cornering at 56 km/h (35 mph).

7.3.2 Single Lane Change

Figure 7-75 through Figure 7-86 show the simulated and measured time histories for the single lane change maneuvers.

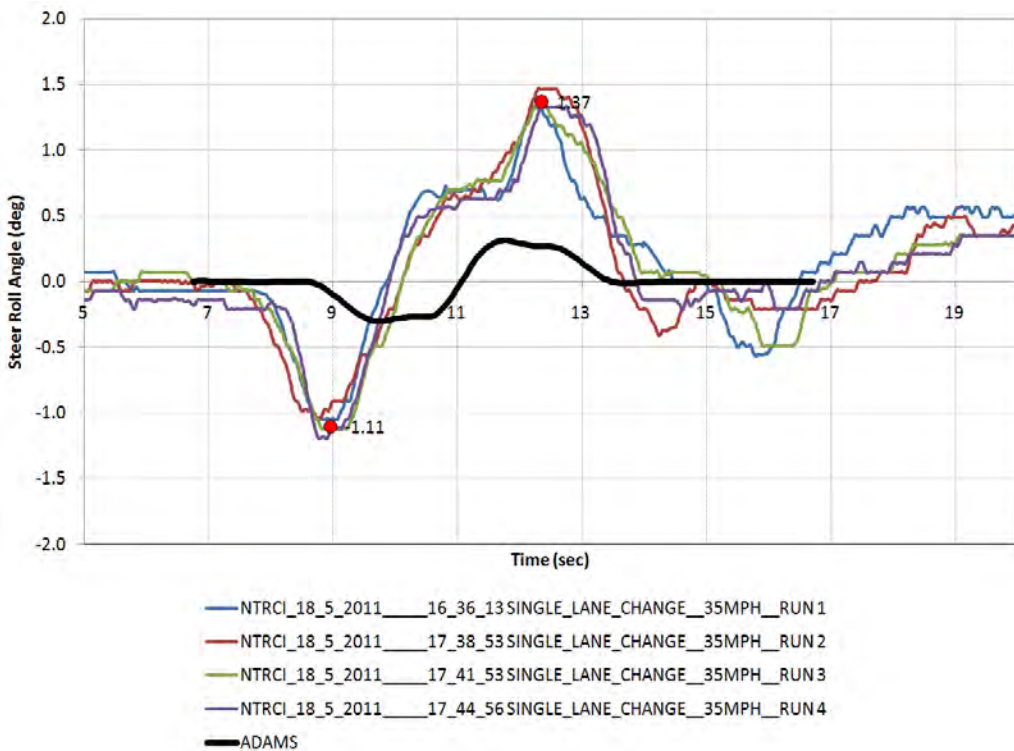


Figure 7-75. Graph. Model vs. Test, Steer Roll Angle, Single Lane Change at 56 km/h (35 mph).

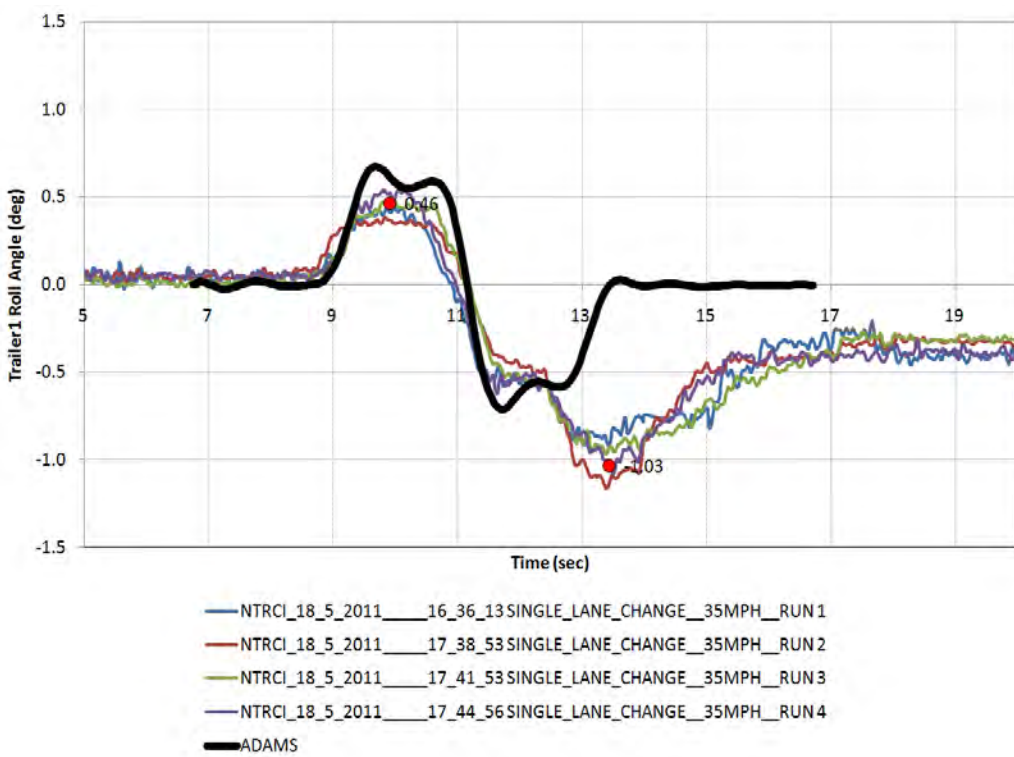


Figure 7-76. Graph. Model vs. Test, Trailer1 Roll Angle, Single Lane Change at 56 km/h (35 mph).

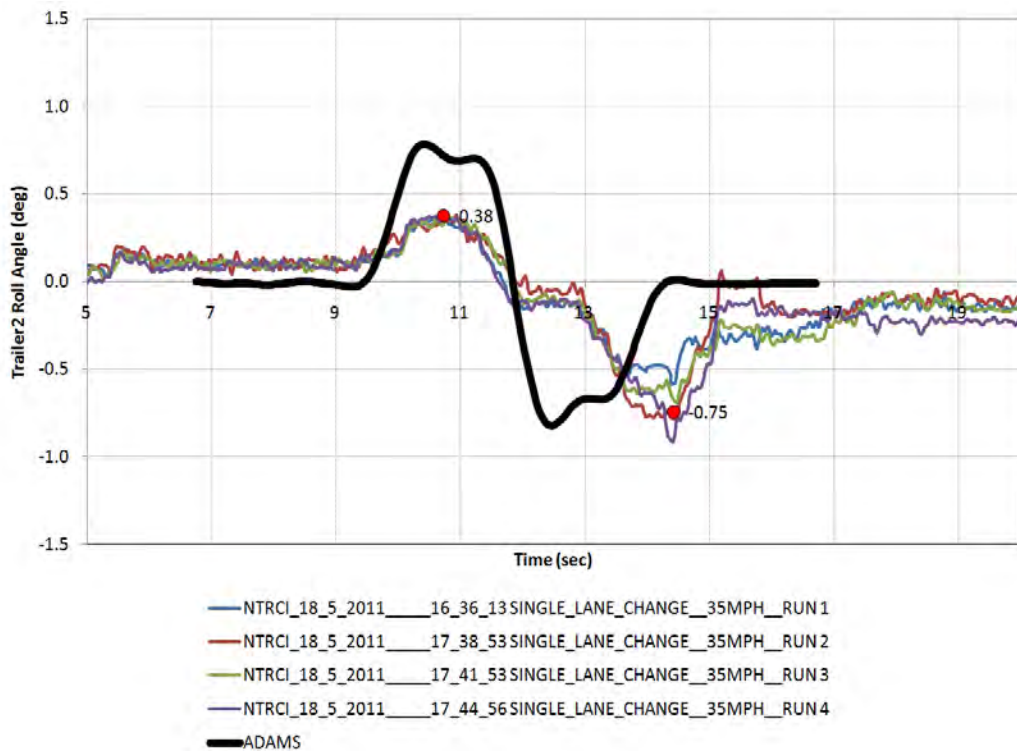


Figure 7-77. Graph. Model vs. Test, Trailer2 Roll Angle, Single Lane Change at 56 km/h (35 mph).

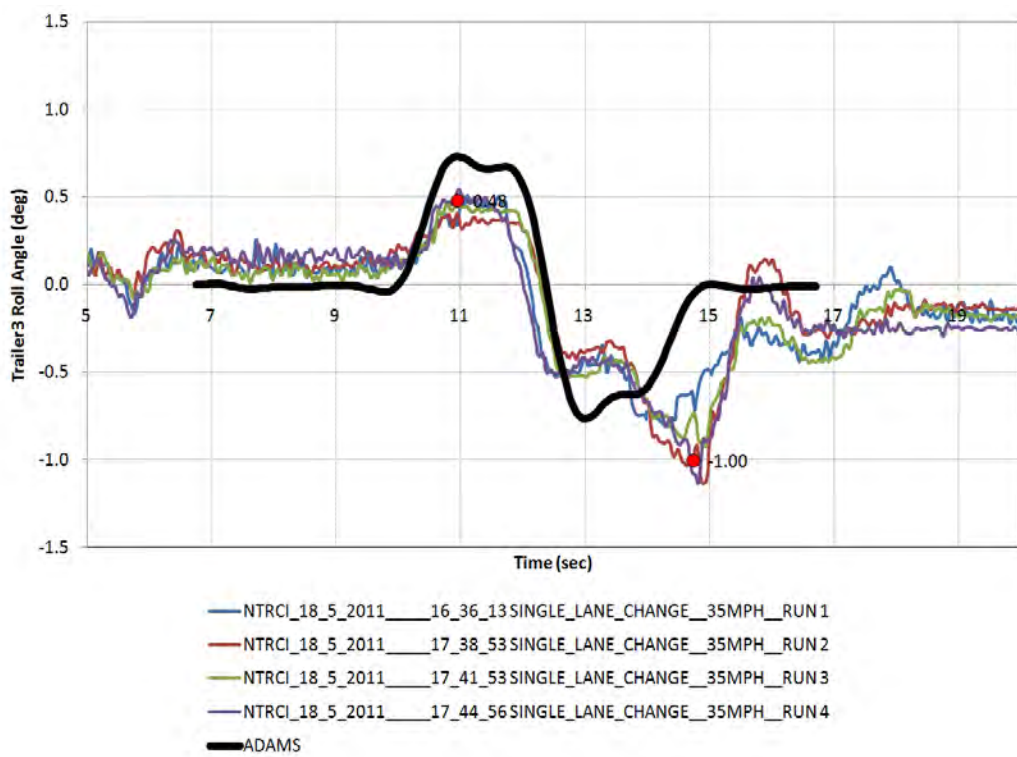


Figure 7-78. Graph. Model vs. Test, Trailer3 Roll Angle, Single Lane Change at 56 km/h (35 mph).

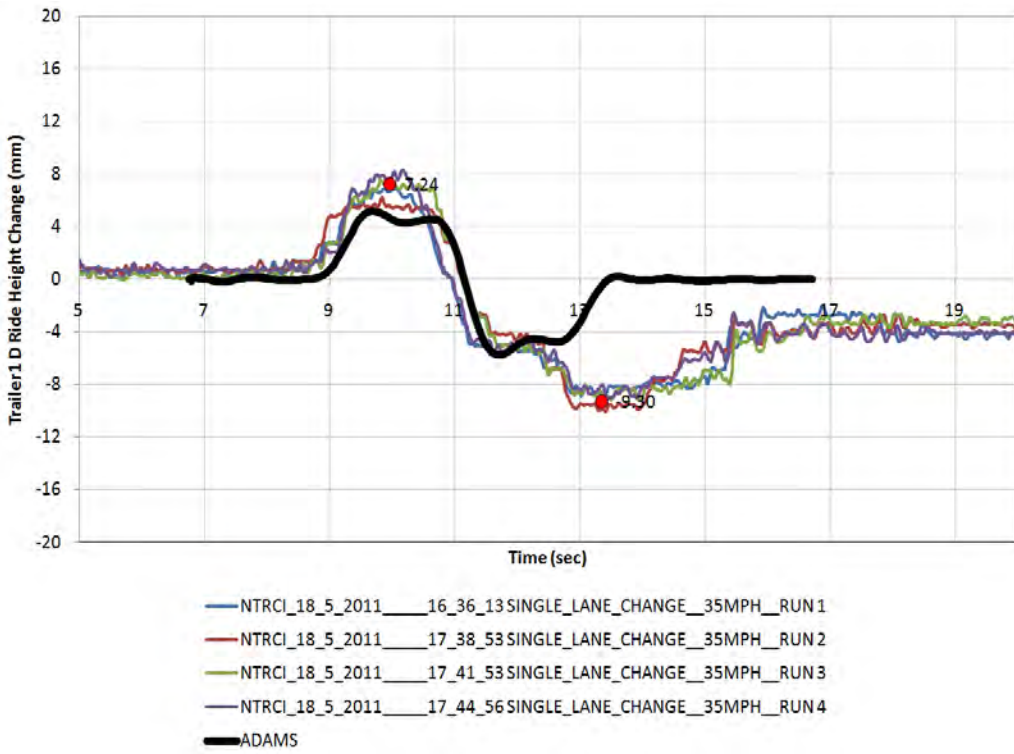


Figure 7-79. Graph. Model vs. Test, Trailer1D Ride Height Change, Single Lane Change at 56 km/h (35 mph).

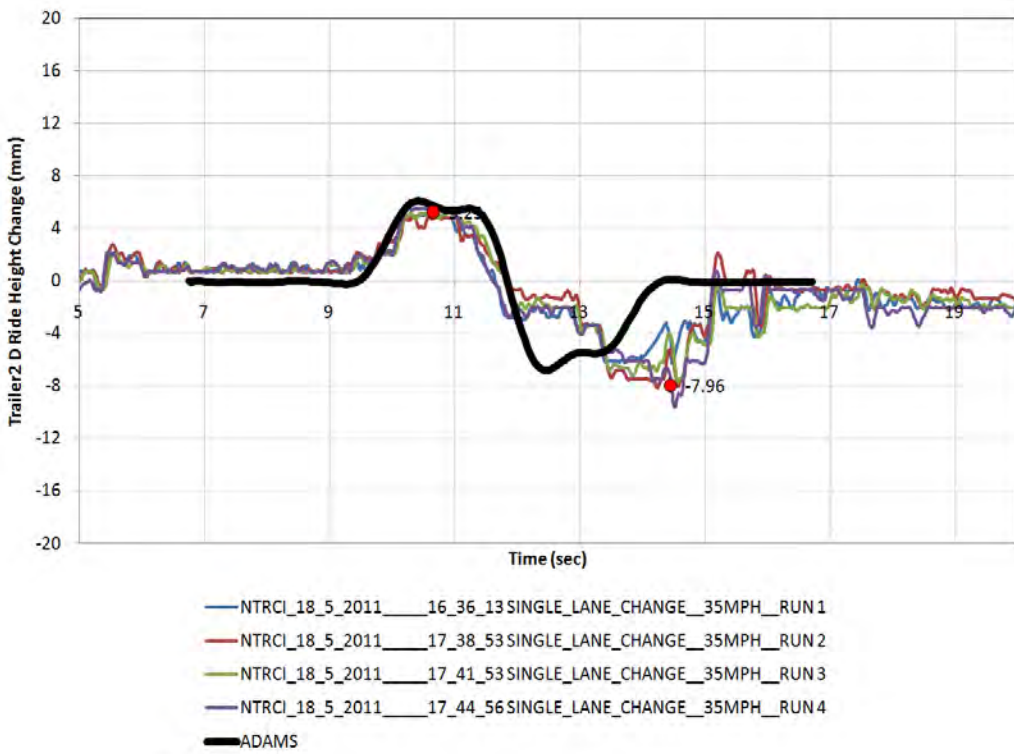


Figure 7-80. Graph. Model vs. Test, Trailer2D Ride Height Change, Single Lane Change at 56 km/h (35 mph).

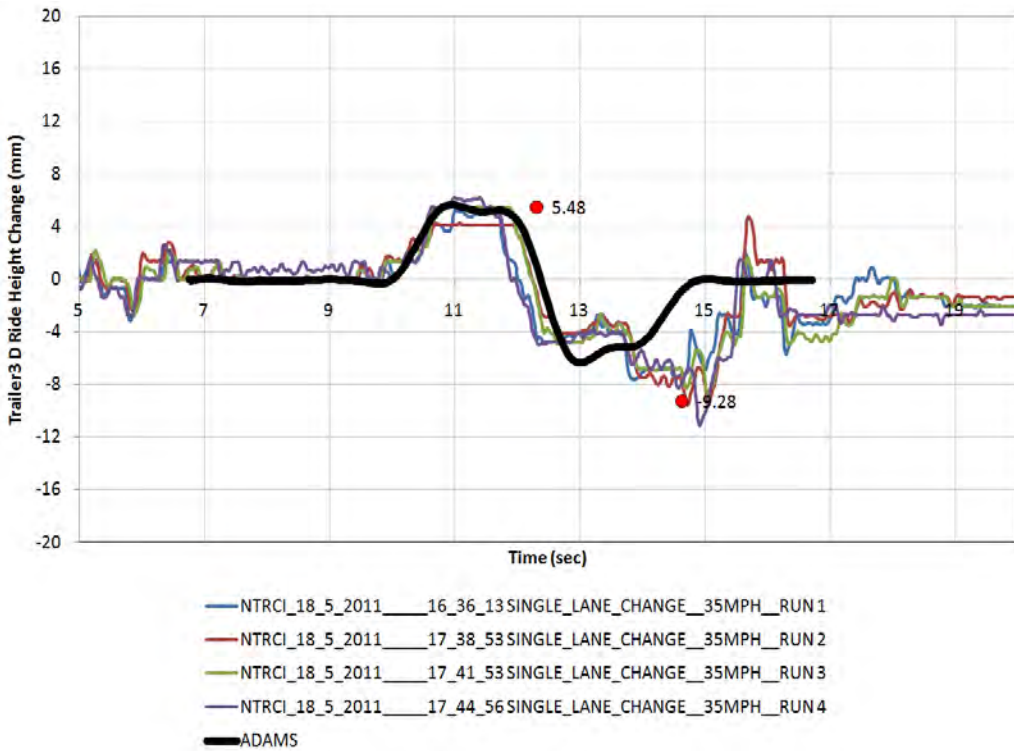


Figure 7-81. Graph. Model vs. Test, Trailer3D Ride Height Change, Single Lane Change at 56 km/h (35 mph).

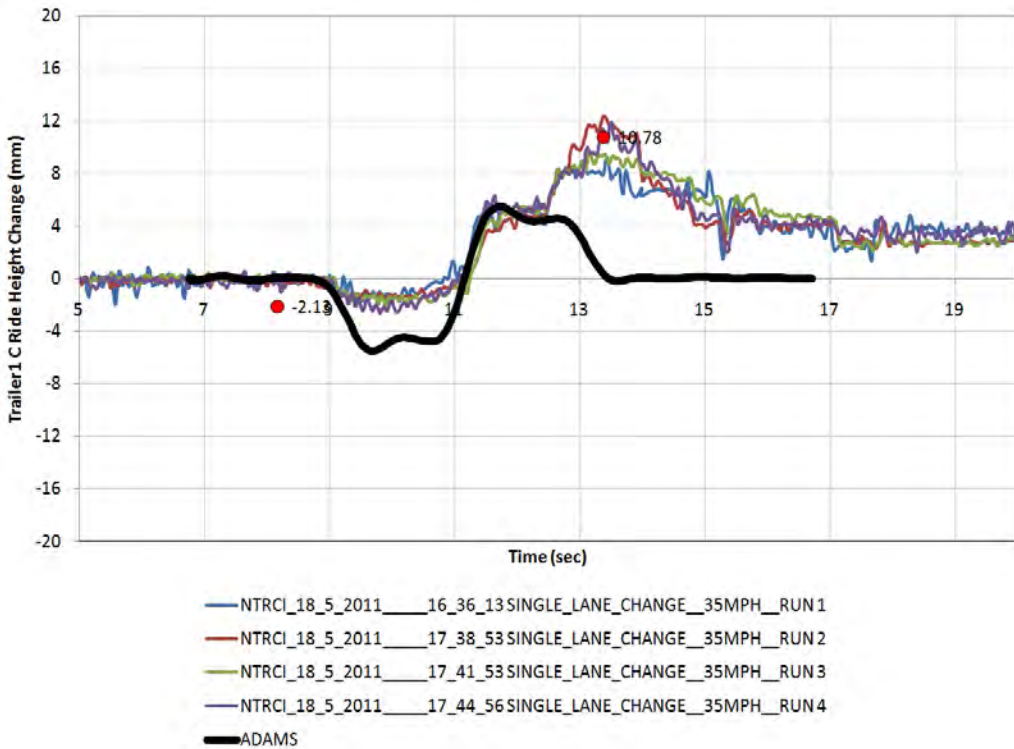


Figure 7-82. Graph. Model vs. Test, Trailer1C Ride Height Change, Single Lane Change at 56 km/h (35 mph).

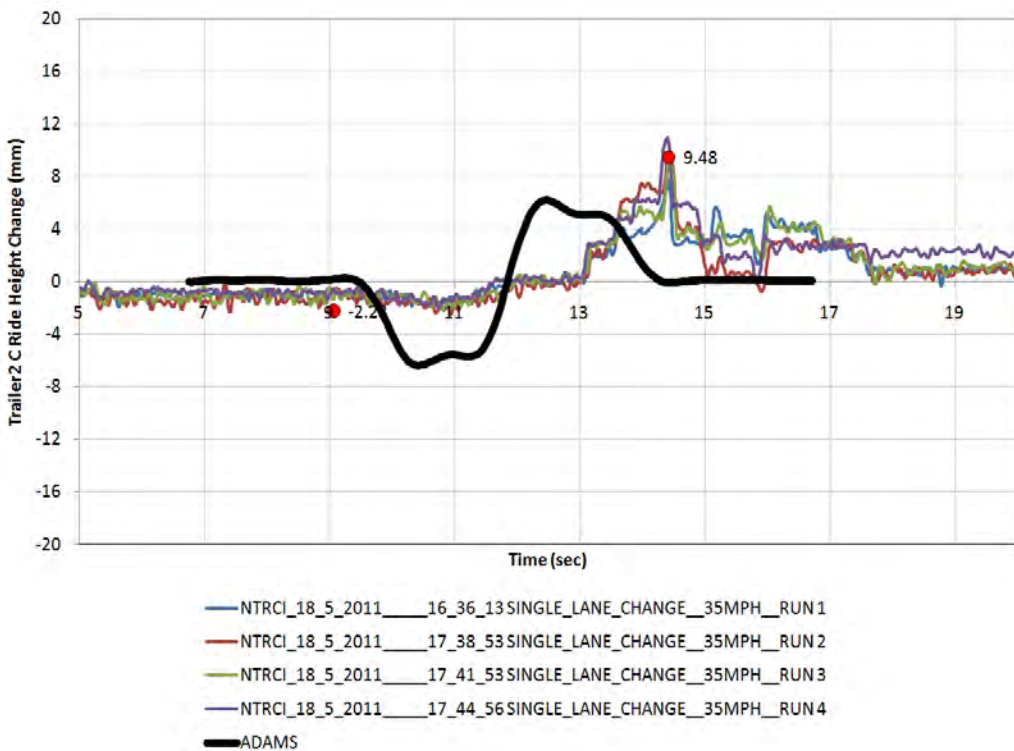


Figure 7-83. Graph. Model vs. Test, Trailer2C Ride Height Change, Single Lane Change at 56 km/h (35 mph).

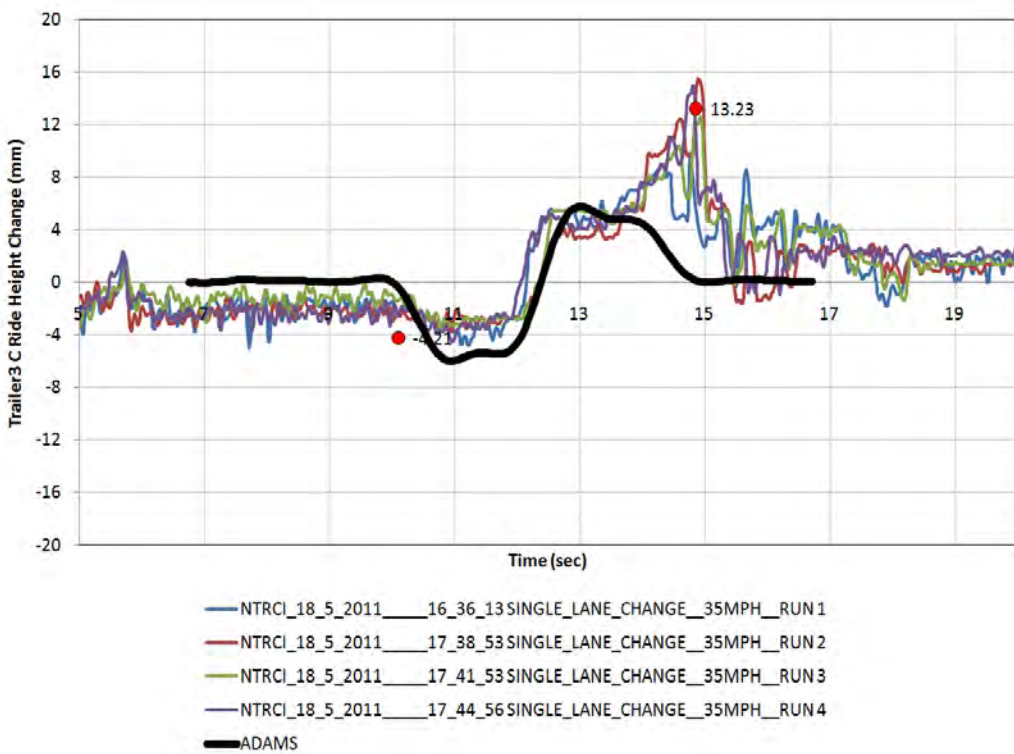


Figure 7-84. Graph. Model vs. Test, Trailer3C Ride Height Change, Single Lane Change at 56 km/h (35 mph).

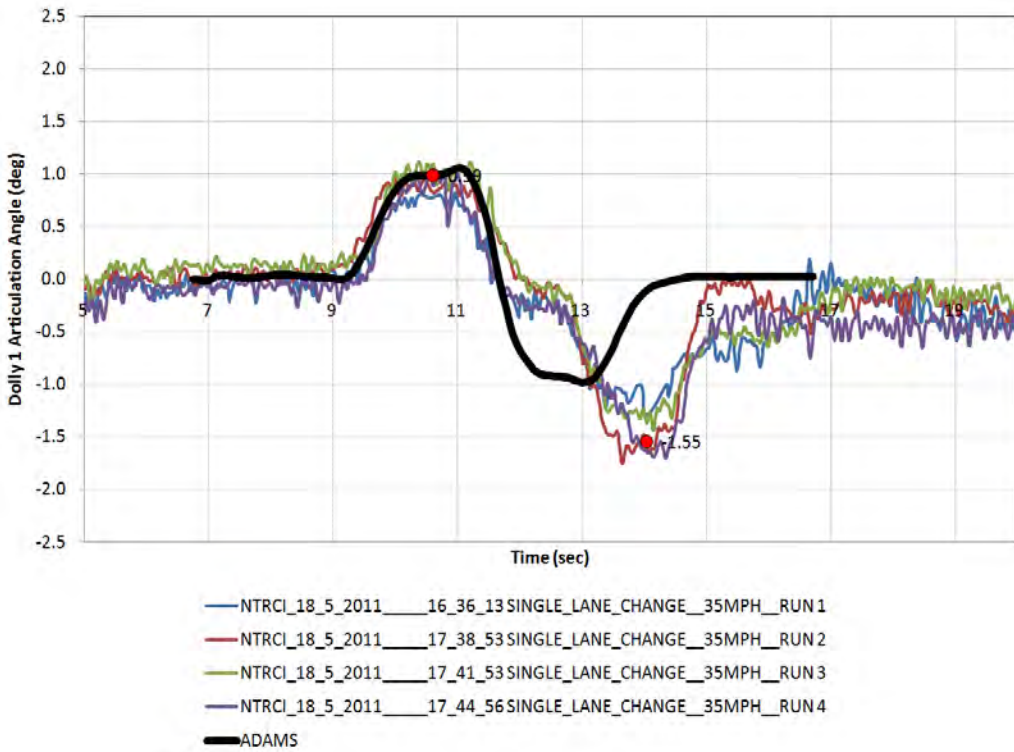


Figure 7-85. Graph. Model vs. Test, Dolly1 Articulation Angle, Single Lane Change at 56 km/h (35 mph).

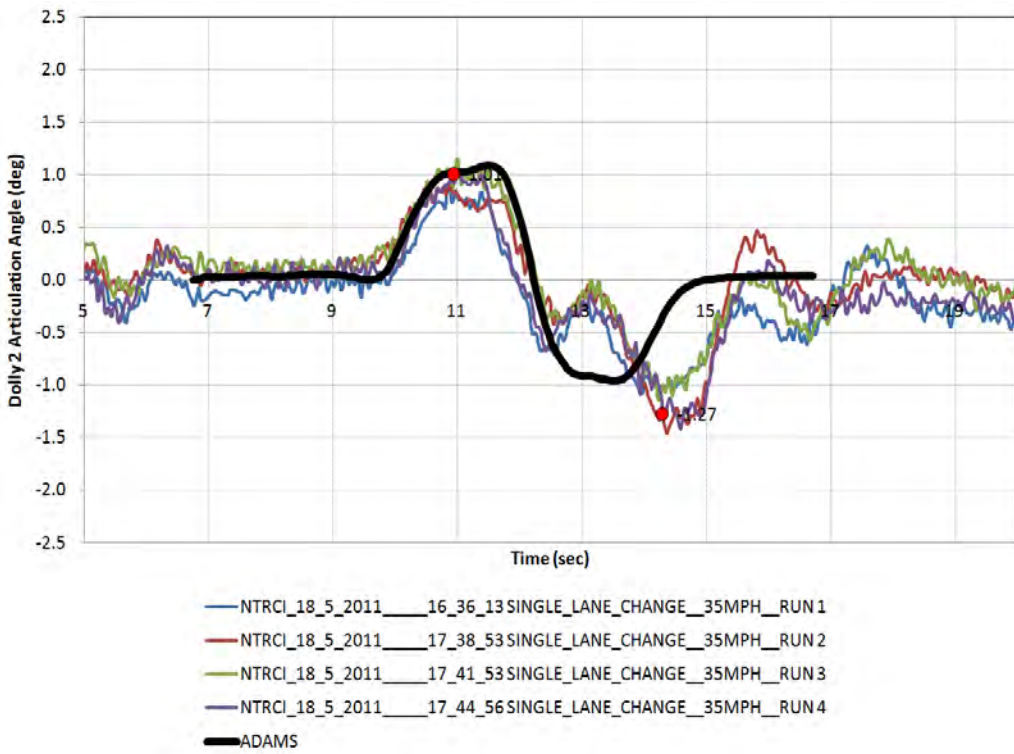


Figure 7-86. Graph. Model vs. Test, Dolly2 Articulation Angle, Single Lane Change at 56 km/h (35 mph).

7.3.3 Double Lane Change

Figure 7-87 through Figure 7-98 show the simulated and measured time histories for the double lane changes.

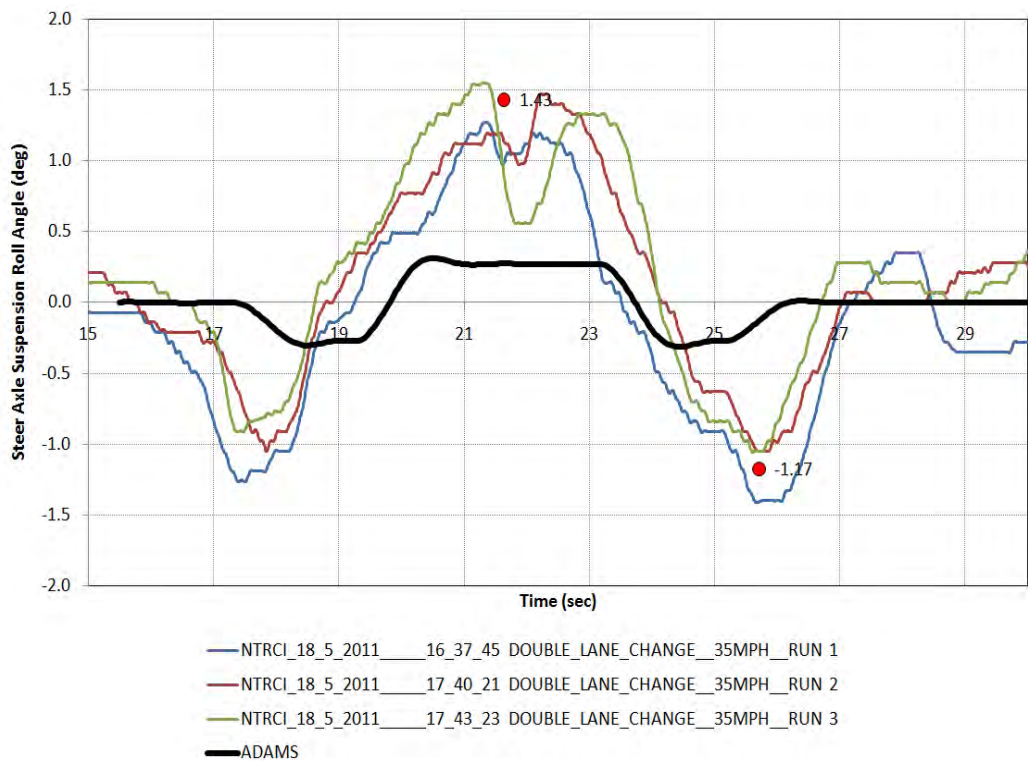


Figure 7-87. Graph. Model vs. Test, Steer Axle Roll Angle, Double Lane Change at 56 km/h (35 mph).

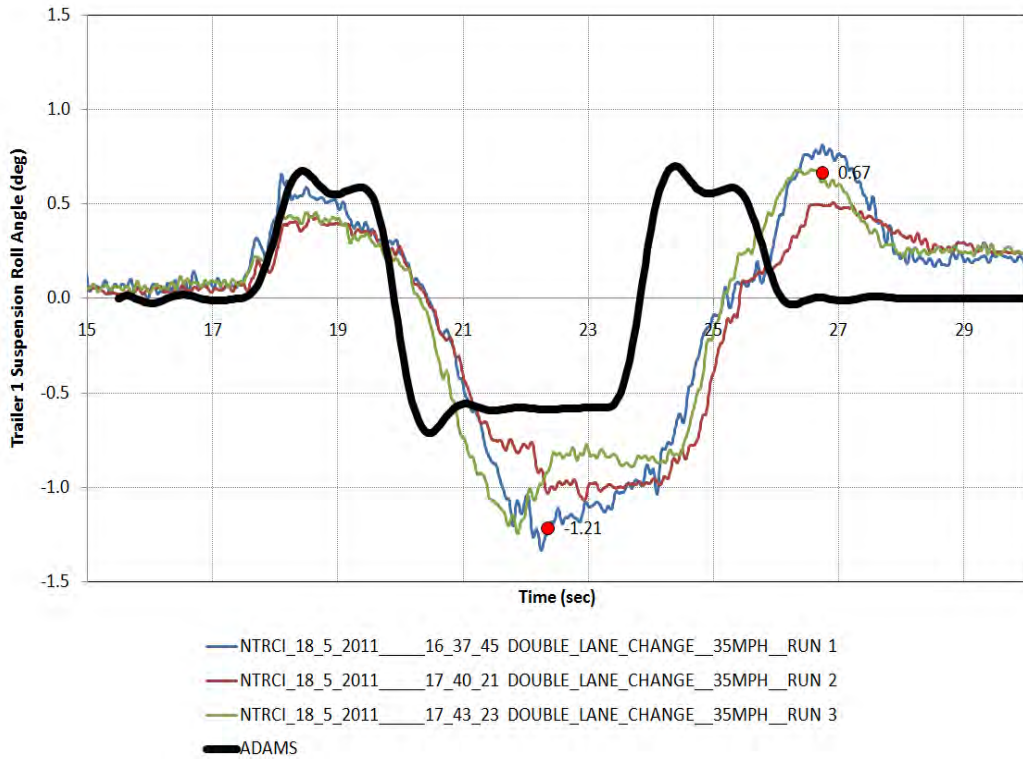


Figure 7-88. Graph. Model vs. Test, Trailer1 Roll Angle, Double Lane Change at 56 km/h (35 mph).

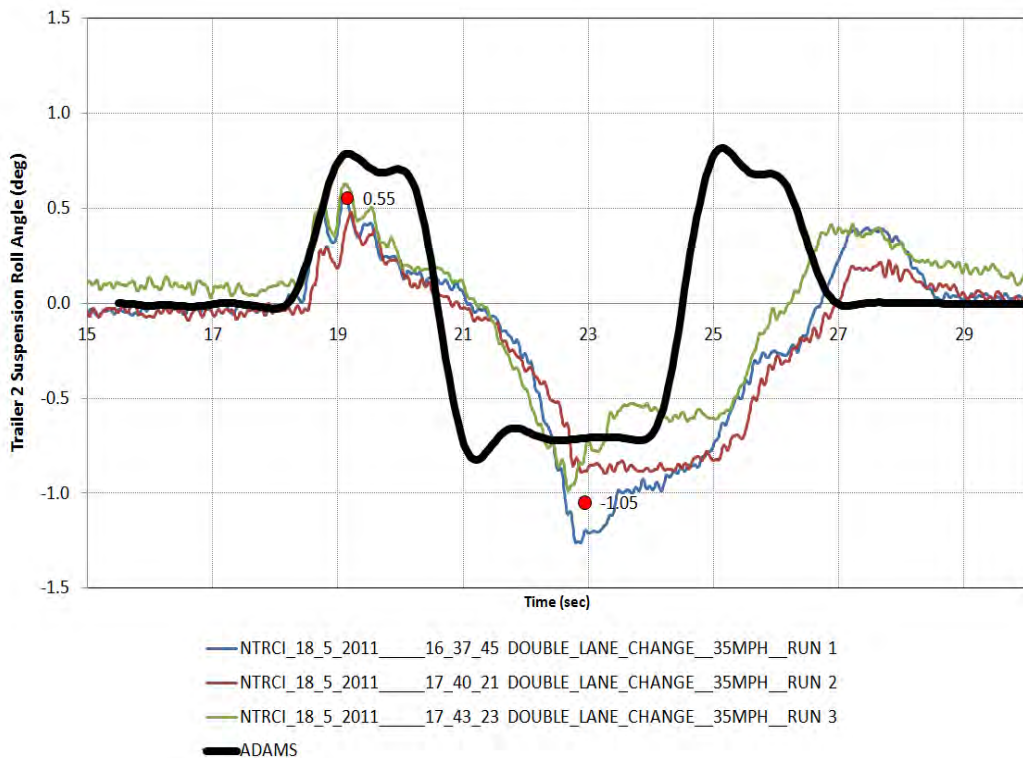


Figure 7-89. Graph. Model vs. Test, Trailer2 Roll Angle, Double Lane Change at 56 km/h (35 mph).

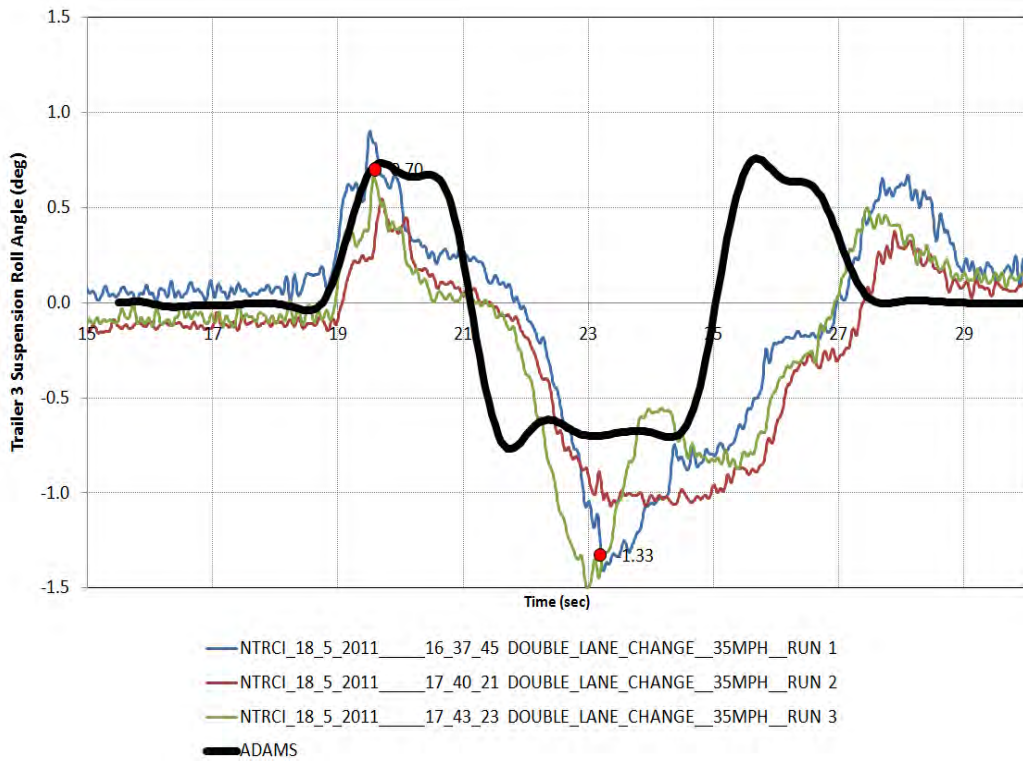


Figure 7-90. Graph. Model vs. Test, Trailer3 Roll Angle, Double Lane Change at 56 km/h (35 mph).

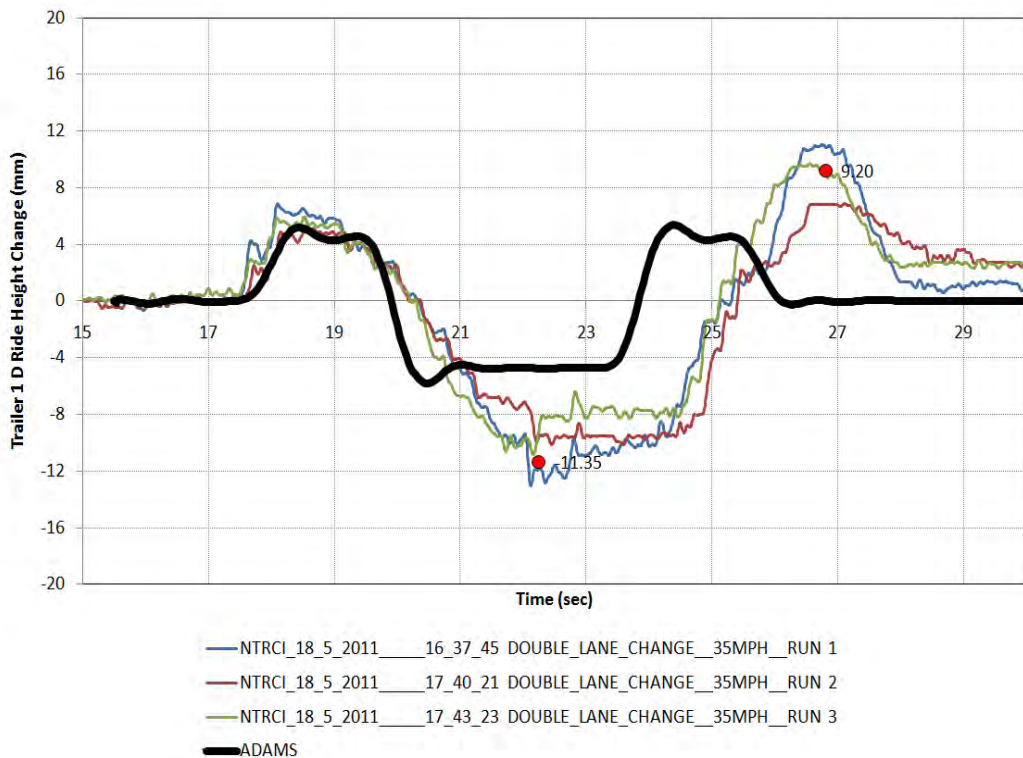


Figure 7-91. Graph. Model vs. Test, Trailer1D Ride Height Change, Double Lane Change at 56 km/h (35 mph).

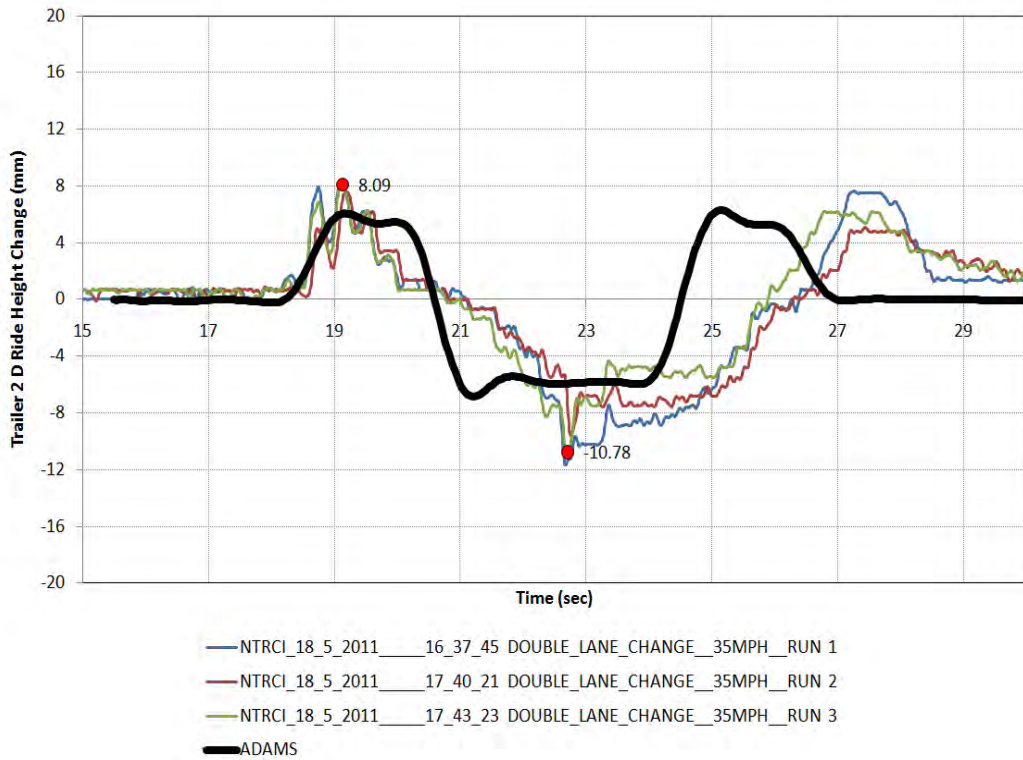


Figure 7-92. Graph. Model vs. Test, Trailer2D Ride Height Change, Double Lane Change at 56 km/h(35 mph).

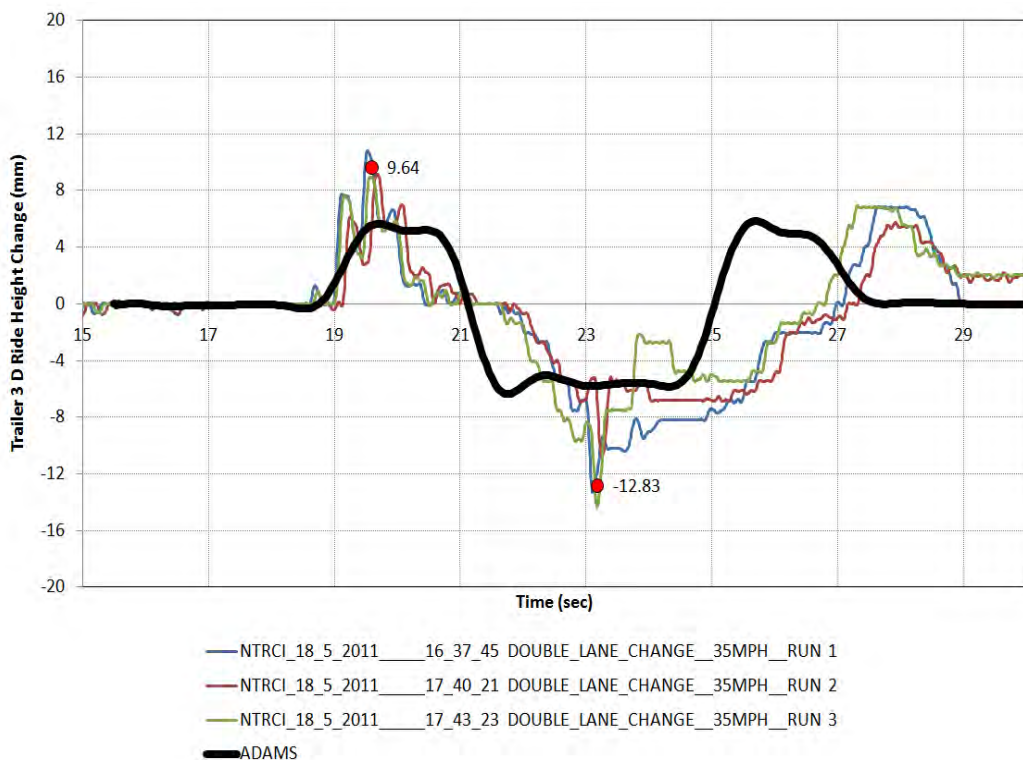


Figure 7-93. Graph. Model vs. Test, Trailer3D Ride Height Change, Double Lane Change at 56 km/h (35 mph).

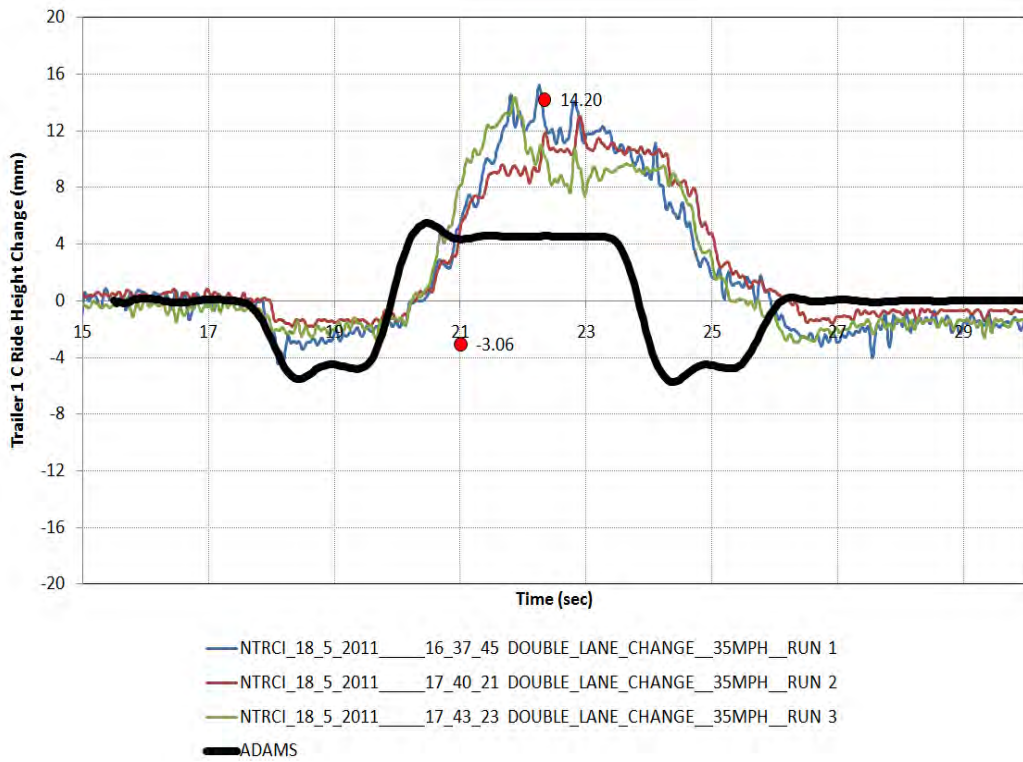


Figure 7-94. Graph. Model vs. Test, Trailer1C Ride Height Change, Double Lane Change at 56 km/h (35 mph).

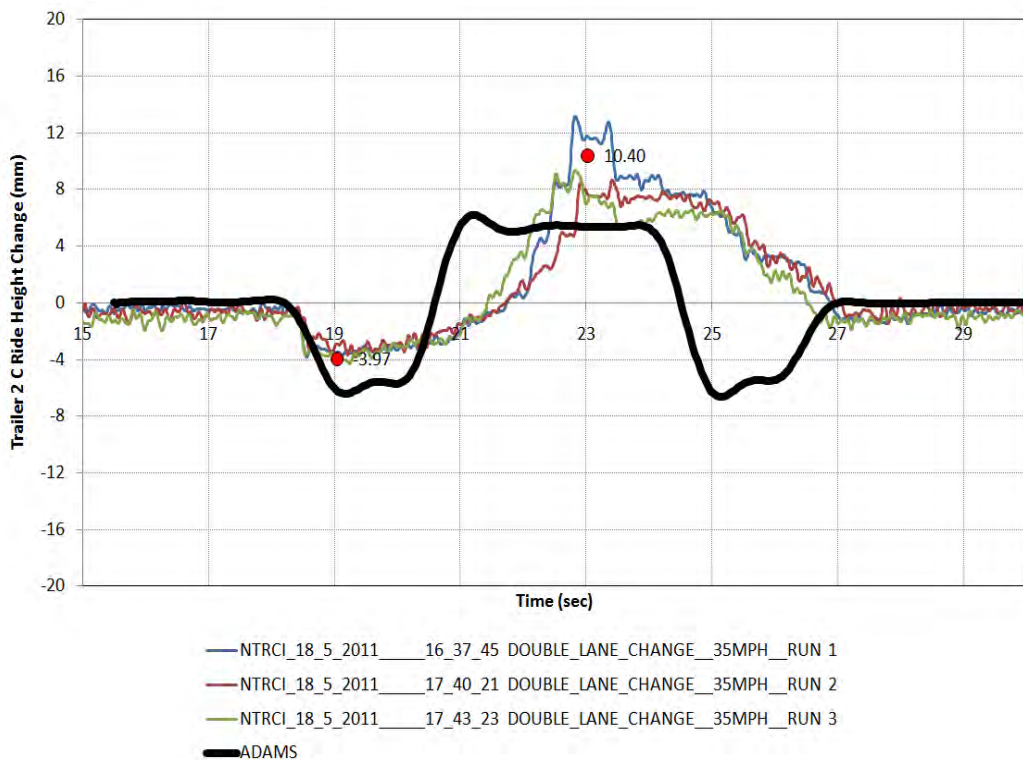


Figure 7-95. Graph. Model vs. Test, Trailer2C Ride Height Change, Double Lane Change at 56 km/h (35 mph).

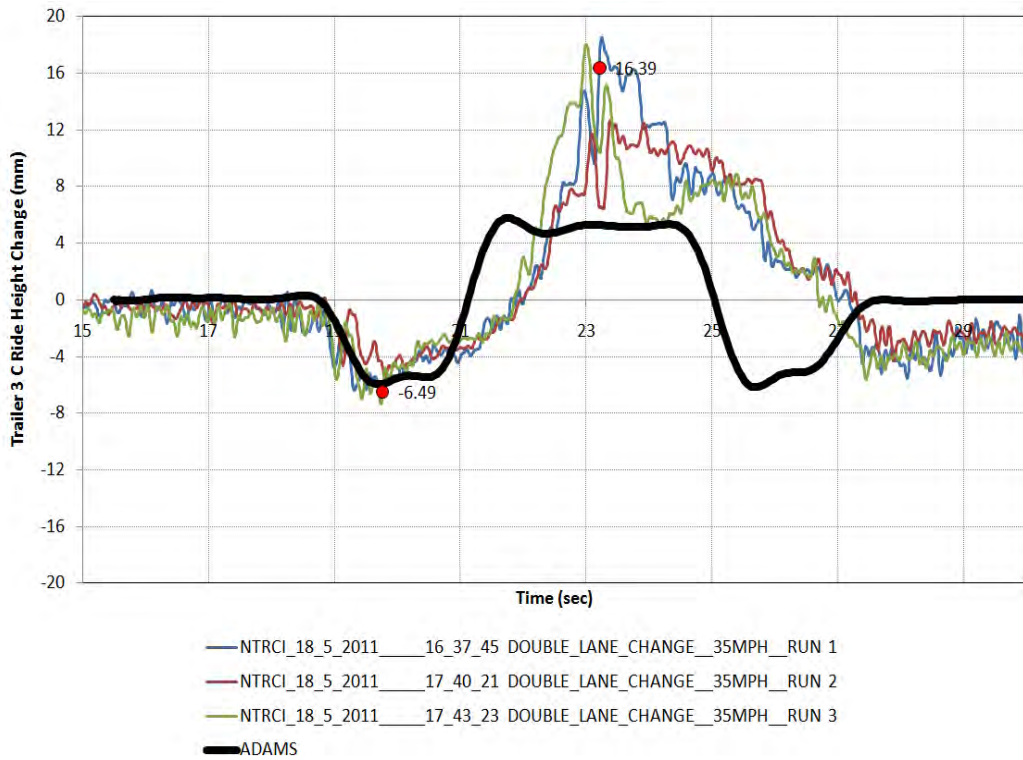


Figure 7-96. Graph. Model vs. Test, Trailer3C Ride Height Change, Double Lane Change at 56 km/h (35 mph).

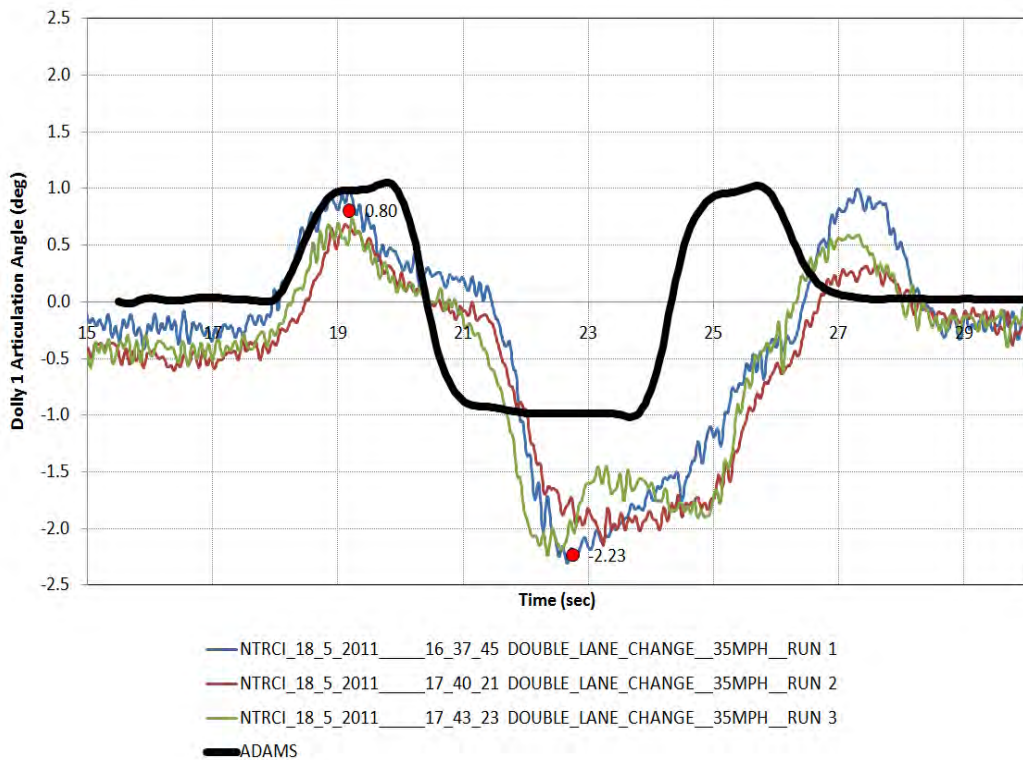


Figure 7-97. Graph. Model vs. Test, Dolly1 Articulation Angle, Double Lane Change at 56 km/h (35 mph).

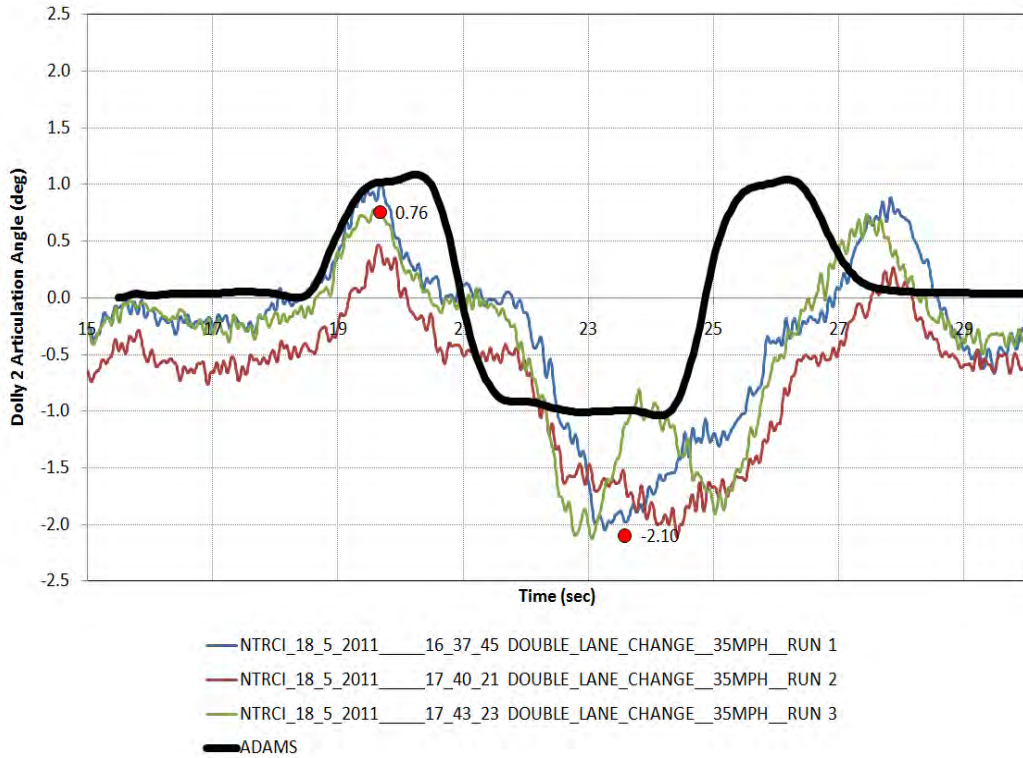


Figure 7-98. Graph. Model vs. Test, Dolly2 Articulation Angle, Double Lane Change at 56 km/h (35 mph).

7.3.4 Comparison Summary

The ranges of the maximum and minimum test values were then used to compare with the model results. The value calculated by the model is indicated with a circle and magnitude label. The range from the test data is shown as a dotted line with a cross bar at each end. These plots indicate where the model results fall relative to the range of values measured in the testing. There are figures for the constant radius cornering, single lane change, and double lane change events at 56 km/h (35 mph).

In general, the simulation results are of the same order of magnitude, and of the same sign, as the test data. In the suspension roll plots, the results suggest that either the tires or the steer suspension are too stiff in the model. This could be attributed to the simple tire algorithm, as well as the estimates for the steer suspension geometry and rates. The model results also tend to exhibit symmetry between maximum and minimum values.

Constant Radius Cornering

Figure 7-99 through Figure 7-102 compare the peak values in the constant radius cornering.

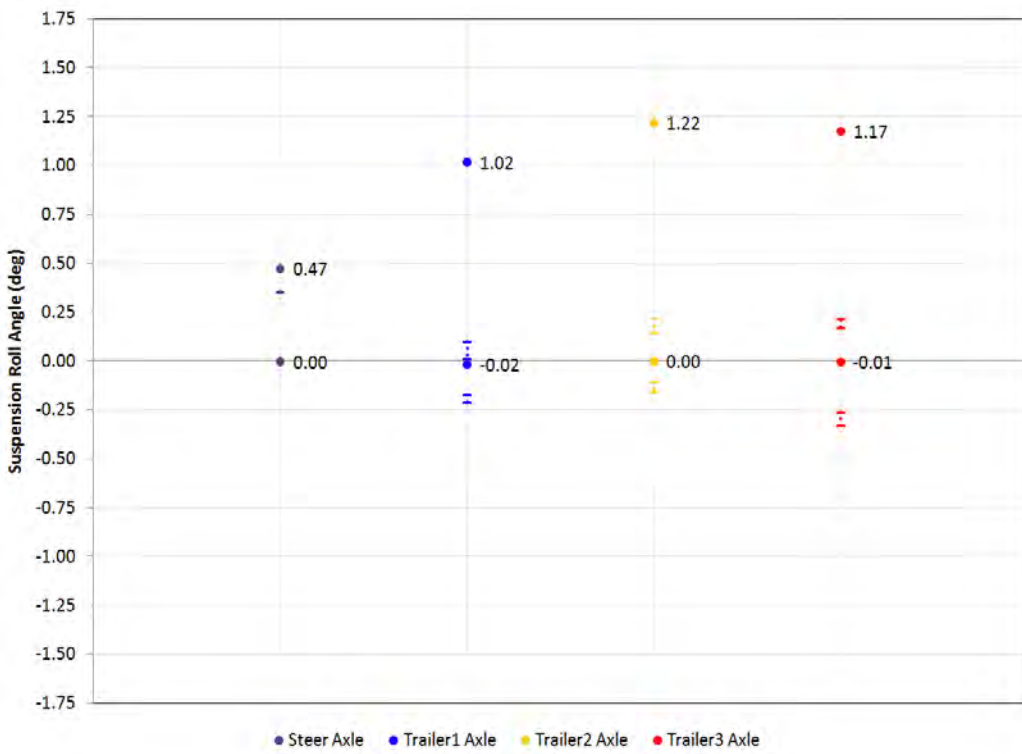


Figure 7-99. Graph. Simulation vs. Average Test, Suspension Roll Angle, Constant Radius Cornering, 56 km/h (35 mph).

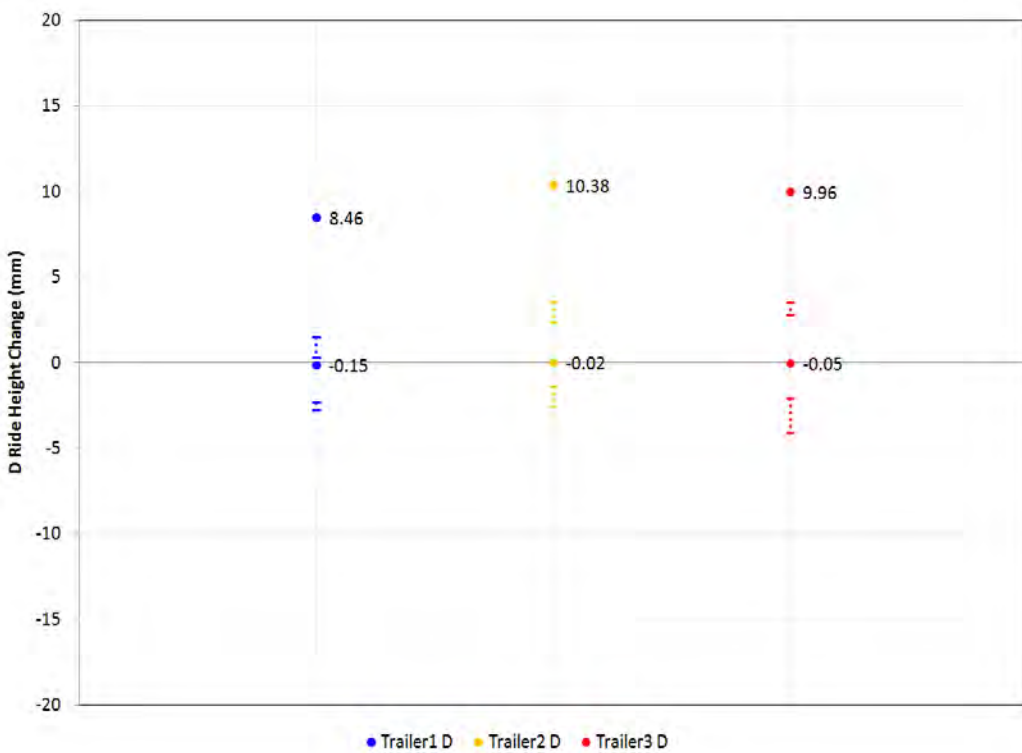


Figure 7-100. Graph. Simulation vs. Average Test, Driver Side Ride Height Change, Constant Radius Cornering, 56 km/h (35 mph).

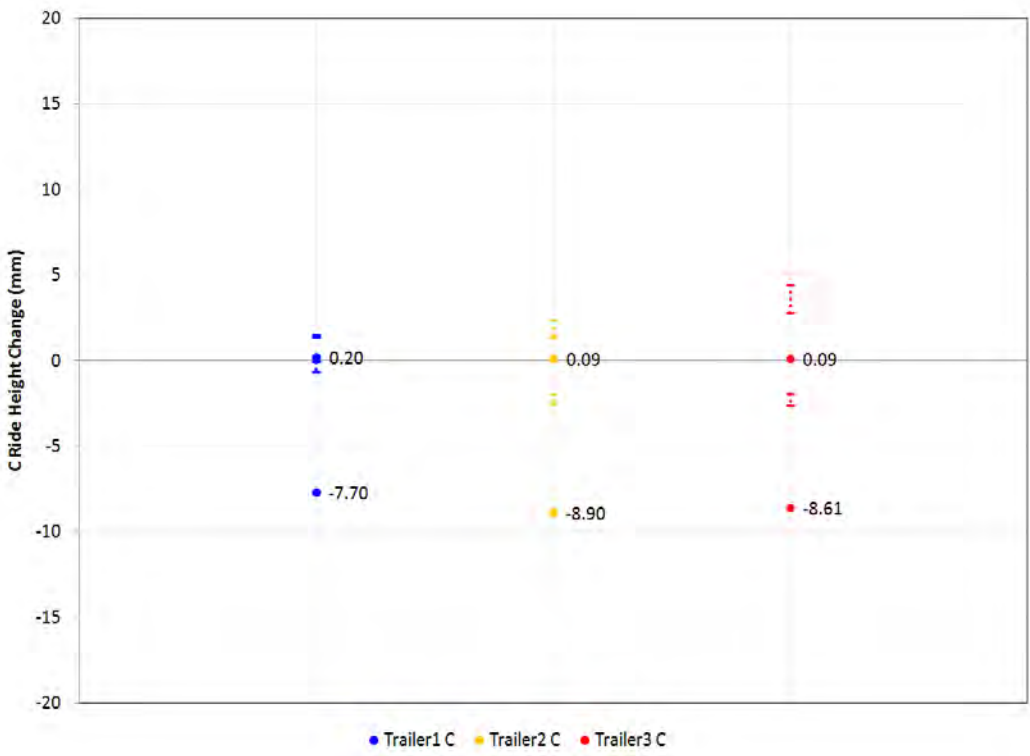


Figure 7-101. Graph. Simulation vs. Average Test, Curb Side Ride Height Change, Constant Radius Cornering, 56 km/h (35 mph).

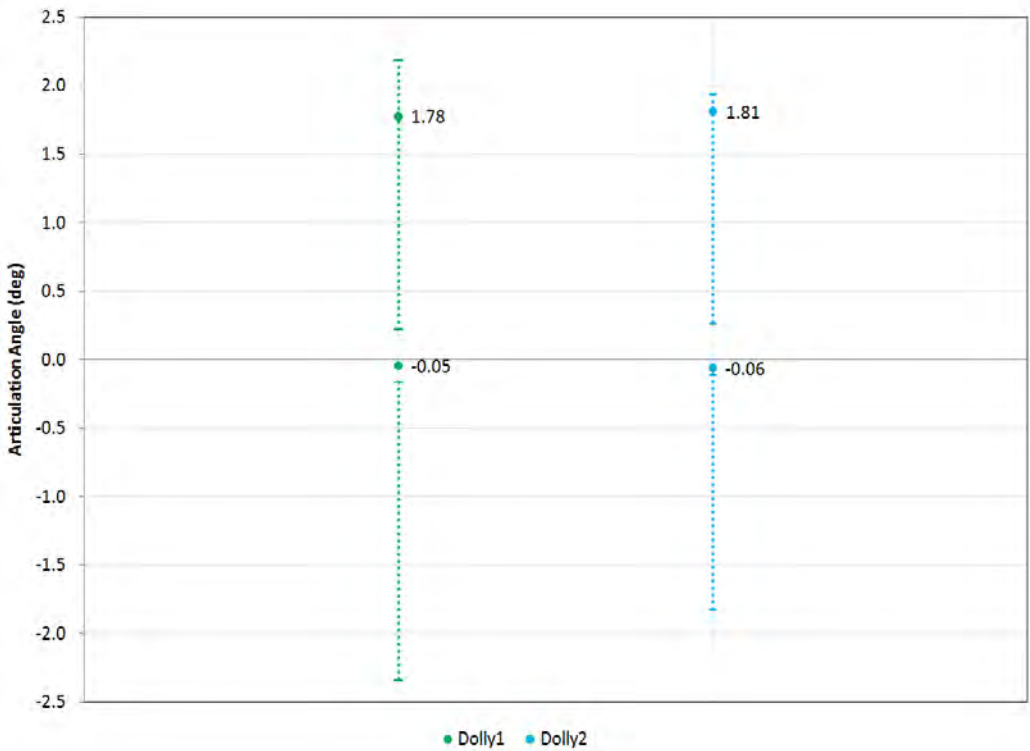


Figure 7-102. Graph. Simulation vs. Average Test, Dolly Articulation Angle, Constant Radius Cornering, 56 km/h (35 mph).

Single Lane Change

Figure 7-103 through Figure 7-106 compare the peak values in the single lane change.

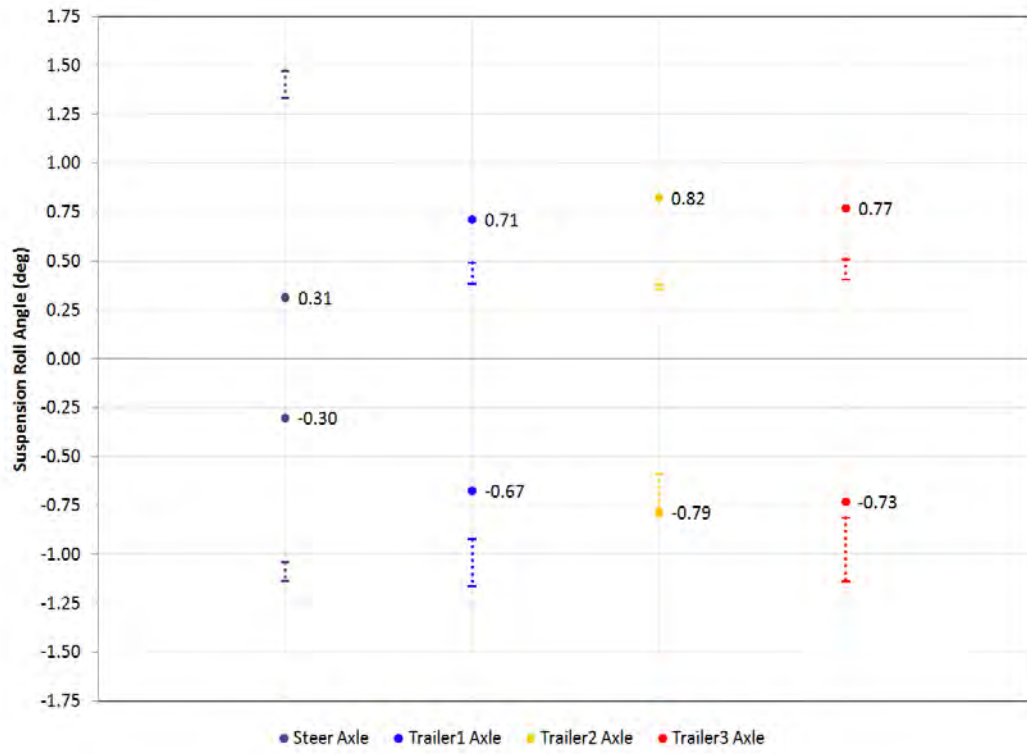


Figure 7-103. Graph. Simulation vs. Average Test, Suspension Roll Angle, Single Lange Change, 56 km/h (35 mph).

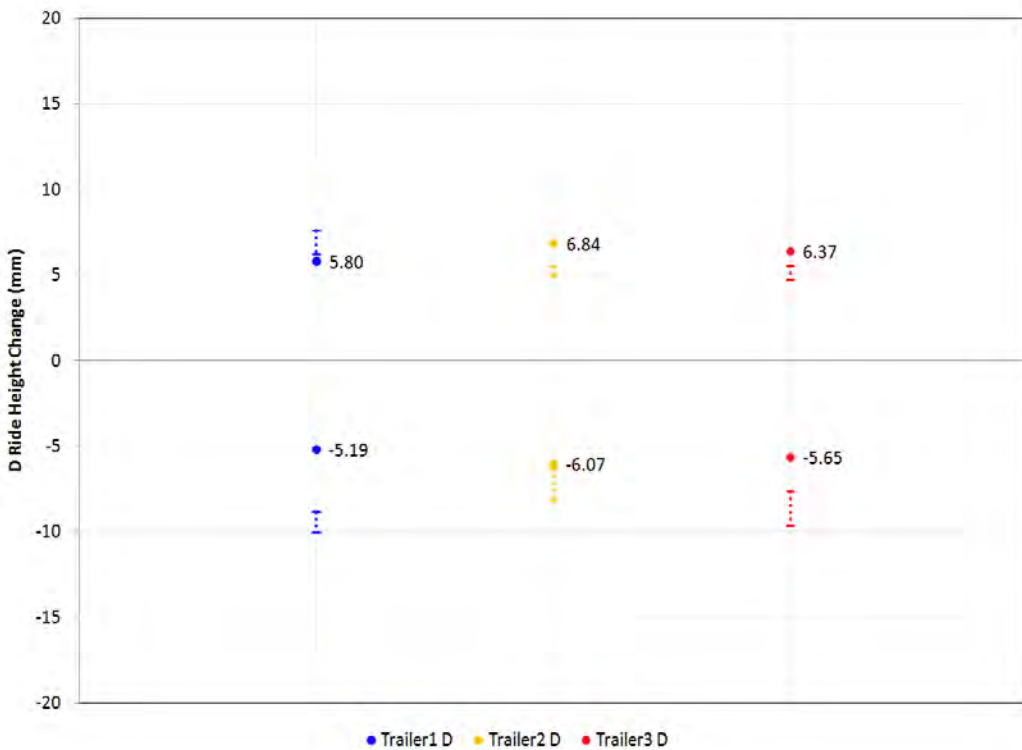


Figure 7-104. Graph. Simulation vs. Average Test, Driver Side Ride Height Change, Single Lane Change, 56 km/h (35 mph).

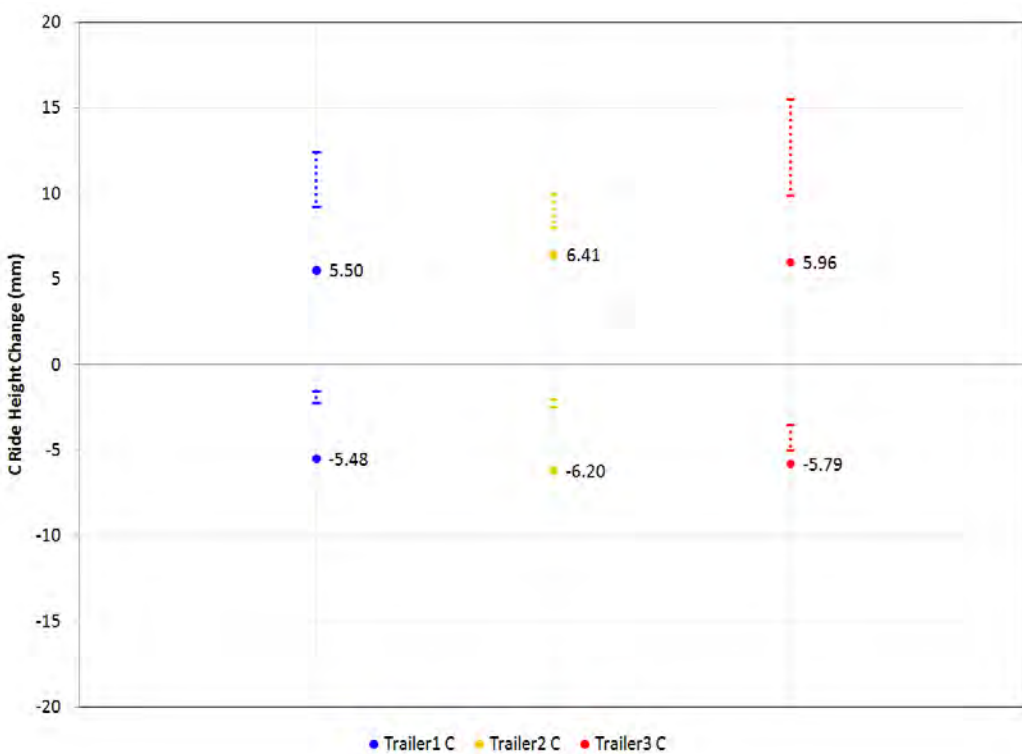


Figure 7-105. Graph. Simulation vs. Average Test, Curb Side Ride Height Change, Single Lane Change, 56 km/h (35 mph).

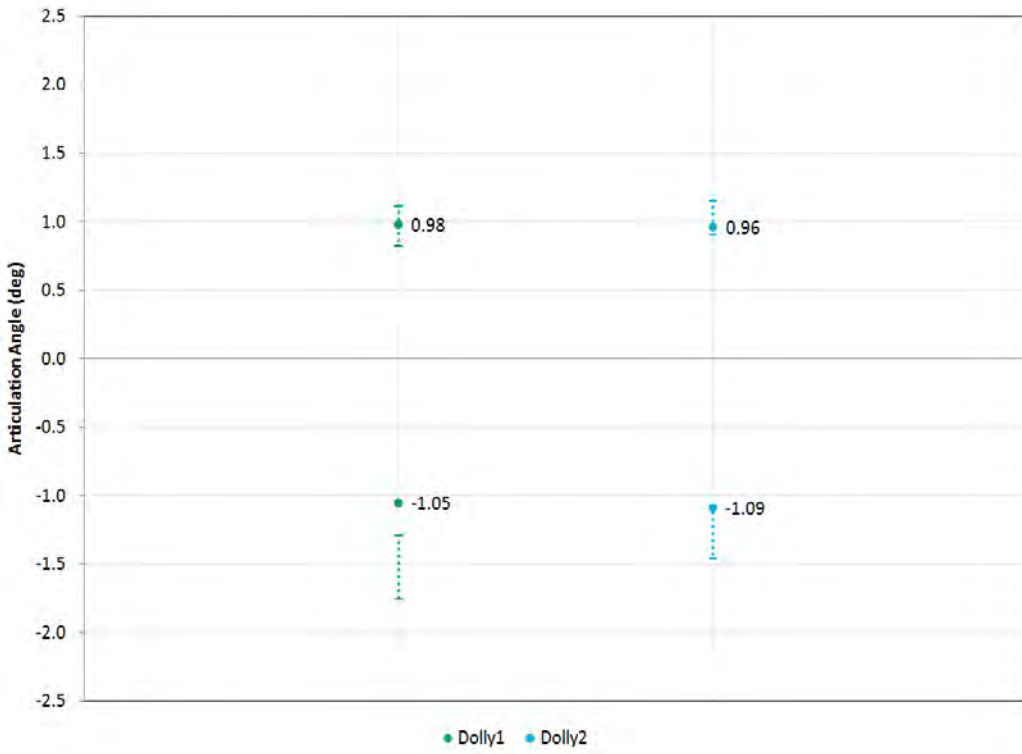


Figure 7-106. Graph. Simulation vs. Average Test, Dolly Articulation Angle, Single Lane Change, 56 km/h (35 mph).

Double Lane Change

Figure 7-107 through Figure 7-110 compare the peak values in the double lane change.

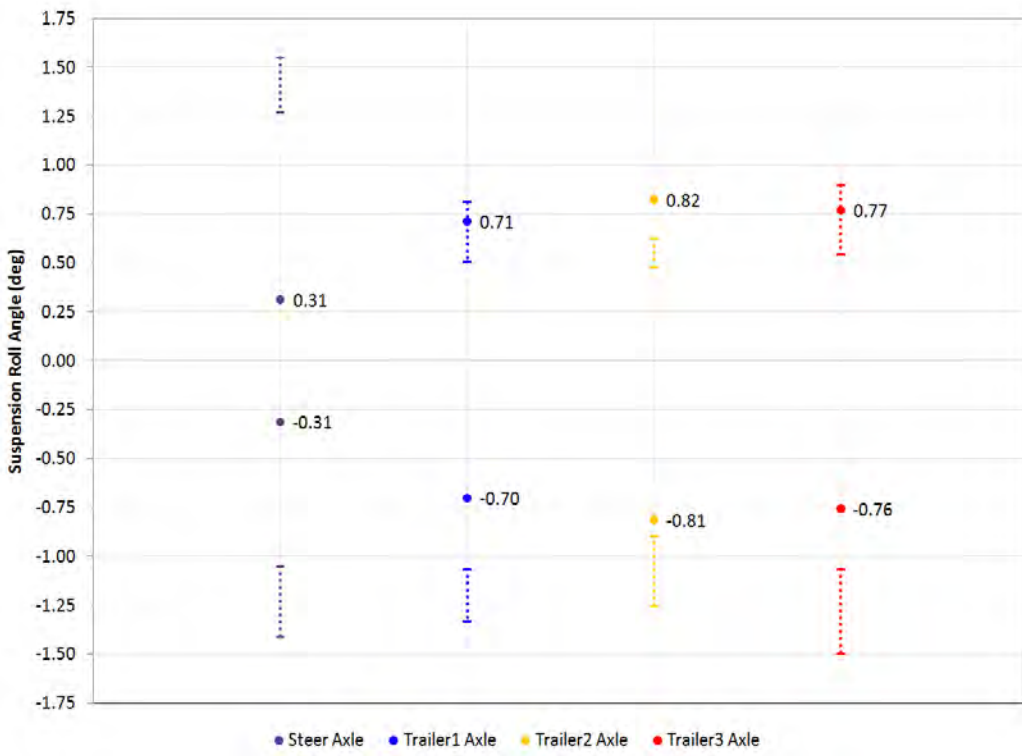


Figure 7-107. Graph. Simulation vs. Average Test, Suspension Roll Angle, Double Lange Change, 56 km/h (35 mph).

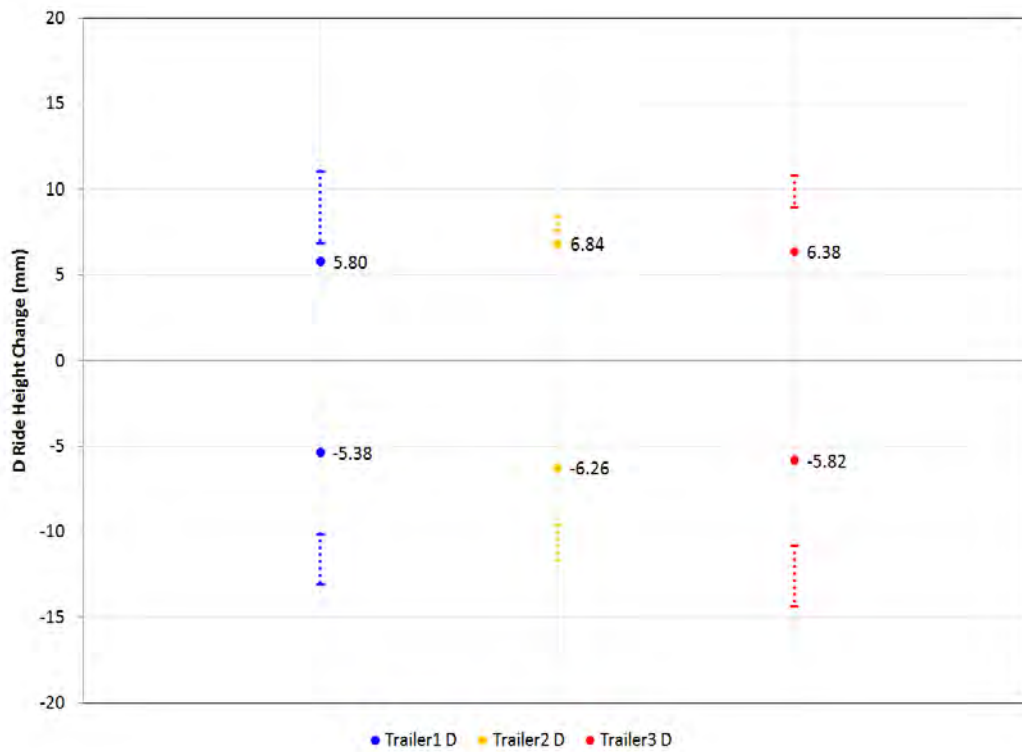


Figure 7-108. Graph. Simulation vs. Average Test, Driver Side Ride Height Change, Double Lange Change, 56km/h (35 mph).

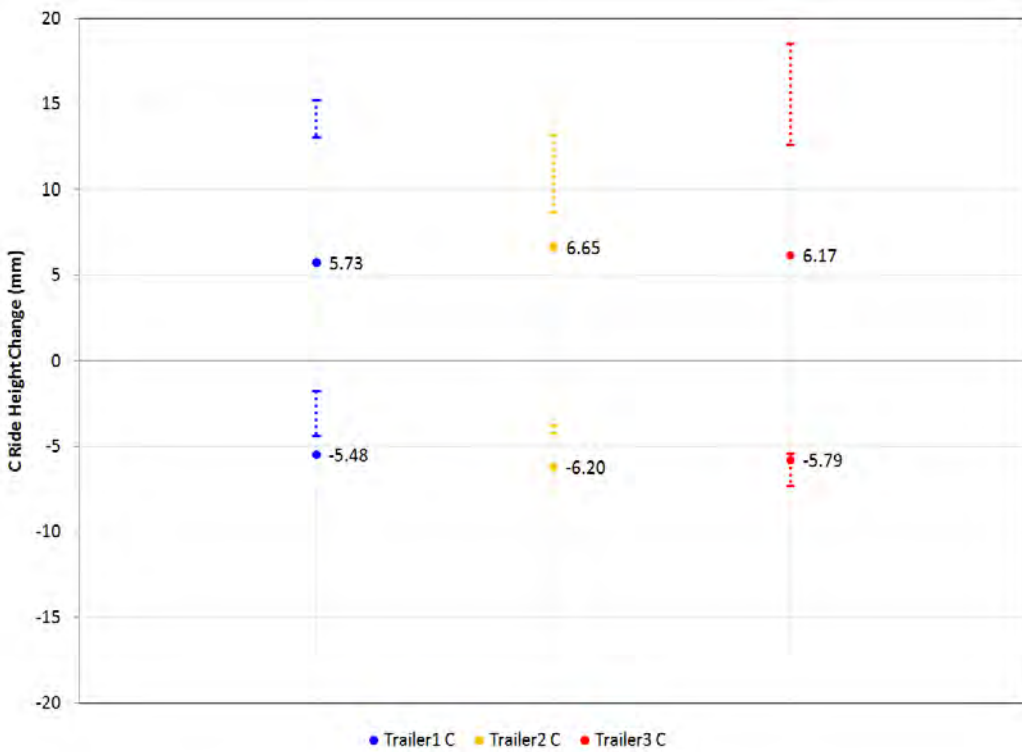


Figure 7-109. Graph. Simulation vs. Average Test, Curb Side Ride Height Change, Double Lange Change, 56 km/h (35 mph).

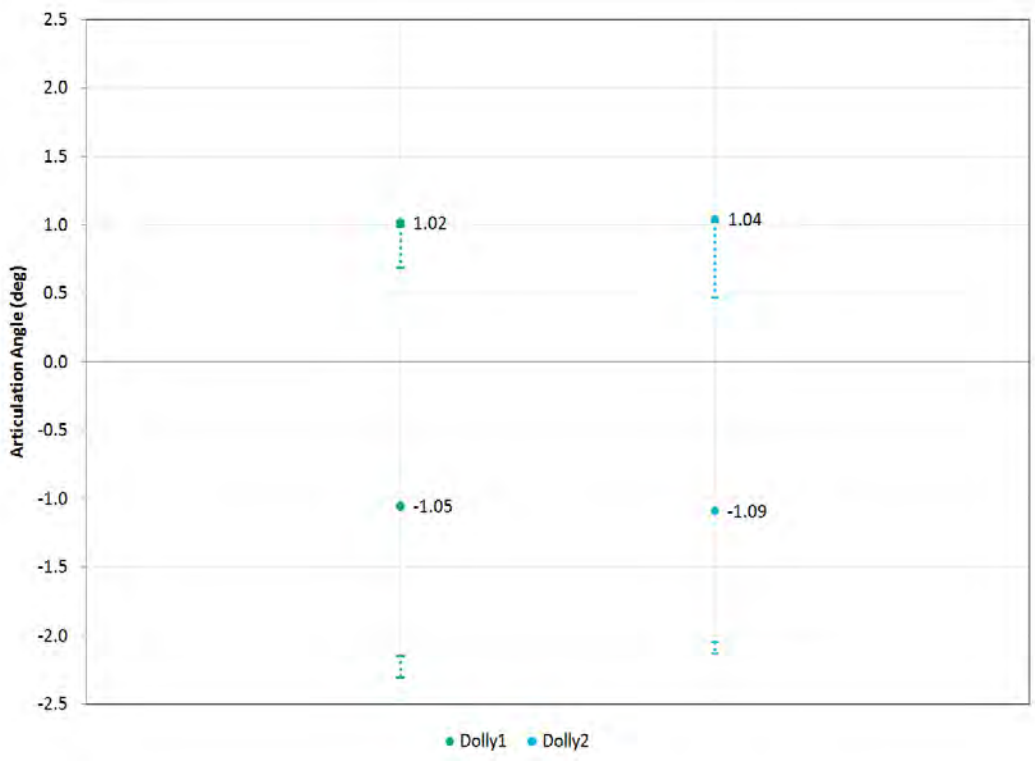


Figure 7-110. Graph. Simulation vs. Average Test, Dolly Articulation Angle, Double Lange Change, 56 km/h (35 mph).

7.4 Recommendations for Continued Modeling

All simulation models are mathematical approximations of the actual physical systems they represent. Simulation models require estimates of the component properties of the individual elements making up the system. As the modeling techniques increase in complexity, such as with the addition of tires or contact elements, the data required become more complex. The quality of the data, and the suitability of the techniques, determined the fidelity of the model.

7.4.1 Adams Model Lessons Learned

For this current effort to generate a partially verified model of the NCAT LCV, many components were built with high-quality data. The three Cheetah trailer chassis and the two Silver Eagle dollies were excellent representations of the mass properties, stiffness, and hard points of these units due to the availability of detailed CAD solid models. Some of these models were supplied by consortium members, while others were created by the participating researchers. In addition, rate curves were available for the spring packs used as suspensions on each of these units, eliminating the need to measure or estimate them.

The payload in each intermodal container was well represented because it was composed of fairly simple geometric shapes. However, properties of the containers themselves were based on estimates as well as measurements. This would introduce errors for the mass, and also make it difficult to estimate any stiffness. This could be an important contributor, because the container is attached to the chassis at discrete points (Figure 7-111), and not distributed along the entire frame. This means that the container, and its payload, are essentially simply supported at the ends of the chassis bolters.

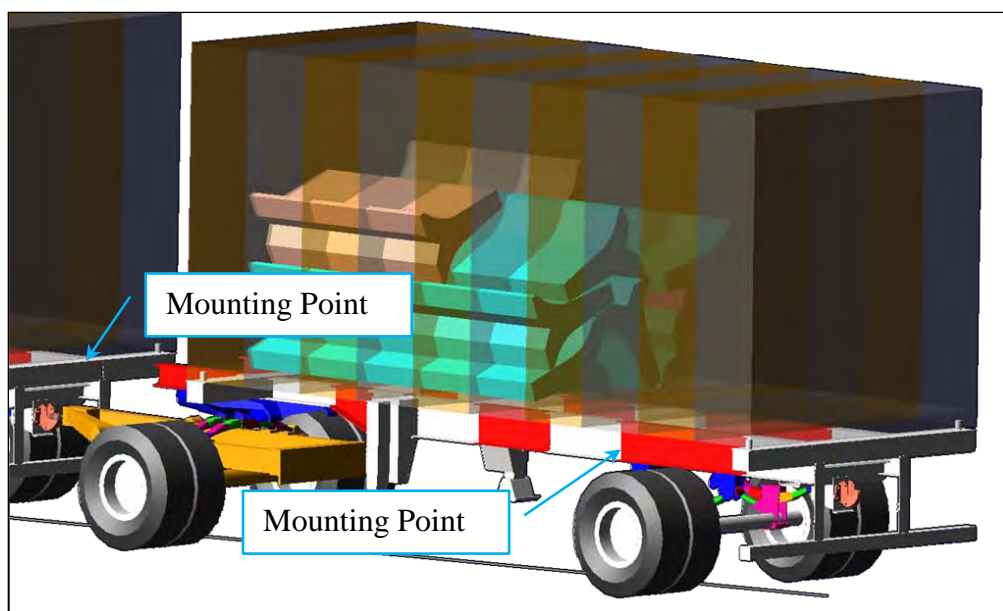


Figure 7-111. Drawing. Container-to-chassis mounting points.

The biggest modeling issues were with respect to the tractor and the tires. All the properties for the tractor were based on field measurements or estimates. Many of the property estimates found in the literature were for tractors that were similar, but not the same make and model. Although the vertical and roll suspension rates were measured trackside, it became difficult to match these rates without additional information, especially relative to unmeasured degrees of freedom. This caused some parameters in the model, such as lateral stiffness, to be broad estimates.

Tire modeling is a complicated endeavor with many different algorithms and levels of behavior available. In addition, many different methods of representing the road are possible.

Unfortunately, data for the tires used on the vehicle was not available, forcing generic data to be used with one of the simplest modeling algorithms. Since the tire-road interaction is the primary source of input to the model, it is difficult to estimate the effect of this simplification. Test simulations with more sophisticated, but proprietary, tire data generated substantially different results. Figure 7-112 compares results between the Fiala tire algorithm used in this model against proprietary Pacejka 2002 data.

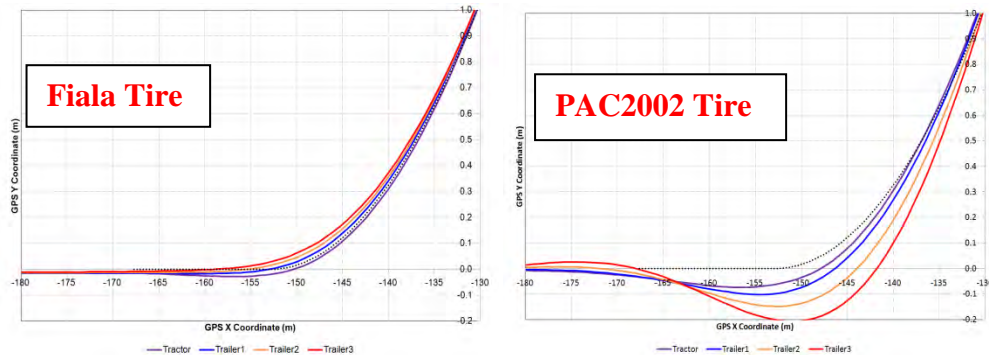


Figure 7-112. Graph. Path close-up, tire comparison, double lane change at 56 km/h (35 mph).

In order to assess the model, the results generated with the simulations need to be compared to the test data. In the future, an initial filtering and averaging effort by more experienced test engineers would be beneficial. This would give a consistent starting point for all subsequent dynamic analysis and modeling correlation work.

7.4.2 Adams Model Improvements

With the current phase of the NTRCI project closing and with the goal of this work being to develop a partially validated model, thoughts of improvements and refinement are in order. Some of the items below are relatively straightforward to implement, while others may prove difficult.

Track Profile Geometry

A 3D model of the test track at NCAT arrived too late to be implemented into the model, but is now available. To be used in Adams, the surfaces representing the track geometry need to be

meshed with a finite element representation. The nodes and elements can then be stored in an Adams tire definition file that is formatted for this method.

Vehicle Path and Velocity Target

The model was simulated using exact mathematical representations of the test track events. It would be straightforward to utilize the actual path of the vehicle. In the same manner, the velocity controller in the model was designed to maintain a constant forward speed. This could also be modified to follow any measured changes in velocity over the course of the event.

Flex Body Springs

The spring leaves representing the tractor, trailer, and dolly spring packs are modeled in a very simple fashion as discretized rigid bodies. Adams also has the ability to utilize modal representations of bodies, which allow for flexibility. In recent releases of the software, the ability of these flex bodies to utilize intermittent contact has been realized, making them useful for modeling the spring leafs and their interaction with cam surfaces on frame brackets, as well as inter-leaf friction. This eliminates the previous modeling simplifications. The drawback to using these elements is their negative impact on solution time due to their computational cost. With the current configuration, the model runs in minutes. If every spring were represented this way, the solution time would jump to hours. Another benefit of having the model solve quickly with a simpler representation is the ability to assess the impact of adding these advanced entities. This allows the user to make an engineering judgment as to the value of this refinement.

Tractor Geometry and Properties

Many properties of the Freightliner tractor were measured, but many others needed to be estimated. Some of the properties which could be improved include:

- Mass, inertia, and CG height
- Force vs. velocity curves for the steer axle and tandem axle shock absorbers
- Free and loaded shapes of the steer suspension spring
- Free and loaded shapes of the tandem suspension spring
- Load vs. height curves at constant pressure for the tandem suspension airbag
- Volume vs. height curves at constant pressure for the tandem suspension airbag
- Tandem suspension spring eye bushing rates
- Transverse torque rod (Panhard) bushing rates.

Tire Properties

The tire is the most complicated element in the model, and the most difficult to represent. It is also the primary source of input to the vehicle, and can have a large effect on the response of the system. This model used the simplest tire algorithm available in Adams, and it was chosen due to a lack of tire data. Developing better tire information should be a top priority for future work with this model.

Vehicle Unit Symmetry

The first trailer unit had a large container filled with concrete at the front. Trailers 1 and 2 had different numbers of jersey barriers. The payload in trailer three was an estimate, as its doors could not be opened. In addition, the two dollies had different track width dimensions, and were of different ages. These are differences that would typically not be considered in a classical analysis of vehicle dynamics, where the configuration of the masses, stiffness, and dimensions would be assumed to be the same. It is difficult to estimate the effect these variations caused, but it could be determined by modifying the current model into a more traditional configuration.

Pintle Hook and Drawbar Eye

The connection at the pintle hooks and drawbar eyes between the dollies and the second and third trailers was modeled by a simple spherical joint. This modeling entity allows three rotational degrees of freedom between the units. It would be possible to use the 3D CAD geometry of these components, along with the Adams solid-to-solid contact capability, to represent a more detailed interaction.

This page intentionally left blank.

Chapter 8 – Conclusions and Further Research

This project represents a step toward establishing a capability of studying the dynamics of LCVs. Behavior in planned maneuvers was measured on a test track, and in natural maneuvers on a public highway. Well-known phenomena of multi-unit combination vehicles were observed and quantified. Methods of sensing the vehicle’s motions during the maneuvers were tested.

Parallel but separate analytical models of LCV triples were built and partially verified with the available test track data. The models reproduced the rearward amplification observed on the test track and its dependence on speed. The models are available for future studies of greater depth to predict the behavior of LCVs in a greater variety of situations.

Research into the behavior of LCV triples will be useful to the National Highway Traffic Safety Administration (NHTSA), the Environmental Protection Agency (EPA), and the Department of Energy (DOE) as they assess the safety implications of LCVs as a means of improving the freight handling efficiency of our nation’s highways.

8.1 Conclusions

The understeer properties of the tractor and trailers in the triple were measured from the constant-radius curves on the banked track. Rearward amplification in roll angle and articulation angle were measured in single and double lane change maneuvers. Roll steer characteristics of the trailers were measured. This partial characterization of the vehicle’s behavior was sufficient to demonstrate the use of string potentiometers in articulation, steer, and roll measurements. The analysis of track data was valuable in the partial verification of the two models.

The brief trip on the public roads took the LCV triple on a four-lane highway with a mix of traffic, curves, and grades. The route between the NCAT track and the state highway included roads in classifications that would not ordinarily see an LCV. At one point, the LCV was simultaneously traversing a railroad grade crossing, climbing a grade, turning right, and beginning to accelerate to a highway speed.

Both models of the LCV triple quantitatively predicted increased rearward amplification of articulation angles. Measurements of all units and visual observations of the third trailer’s behavior were consistent with the models’ predictions. The amount of rearward amplification and its increase with speed were successfully modeled. The models have been partially verified.

Measurements of dolly-to-trailer articulation using a pair of string potentiometers were shown to be viable. Unit-to-unit displacement measurements relying solely on GPS readings require the utmost precision available from GPS. String potentiometers were proven to be a valuable alternative, provided that vibration is handled and that due consideration is given to bandwidth and dynamic range. String potentiometers were also used successfully to measure the roll steer properties of selected axles in the LCV. These measurements proved successful in explaining some of the understeer behavior of the trailers.

8.2 Further Research

The LCV triple used in the testing was selected for its availability. With a tractor, three trailers, and two dollies, it is, at its most basic level, representative of a standard triple. Its behavior was qualitatively representative of what has been observed in prior multi-unit studies, and its movement in the testing was sufficiently well quantified for verifying corresponding characteristics of the two models. However, its primary purpose in testing pavement required that it be highly loaded. Future work will be more generally useful to the trucking industry if test vehicles are loaded with masses and mass distributions more representative of those in service. The mismatch in suspension conditions—some with years of hard experience and one dolly brand new—was an extreme condition but conceivable in normal fleet operations.

The models will need to be adapted to the range of loadings, and possibly new dimensions, of future vehicles. After being adapted to the vehicles of future studies, the models can be used in a phased approach in future studies to predict the behavior of test vehicles. The ensuing experimental work would confirm the models' predictions on, for example, speeds where rearward amplification reaches a certain amplitude. Special test maneuvers can be executed to reproduce behaviors observed in the models.

The two complementary models can be used to predict which properties of the vehicle have the greatest influence on its stability and controllability. These properties should be carefully estimated, either in preliminary quasi-static deflections or in the maneuvers themselves. Sensors can be designed to quantify key properties of the motion. The roll steer string potentiometers used in this project are an example of a specialty sensor that measured an important feature of the dynamic performance.

Because all forces on the vehicle are applied through the tires, their properties are as important to model fidelity as they are to vehicle safety. Both modeling efforts found that their fidelity was best when realistic tire properties were used. Tire properties will be key to future efforts, so they must be obtained through dedicated measurements or arrangements with a company owning the information.

The purpose of this project was to achieve a first step in developing a full modeling capability. Subsequent projects will be directed toward answering the questions of LCV safety and operational efficiency. Primary among these questions will be how well an LCV stays in its lane—the effect of low- and high-speed offtracking in steady maneuvers and rearward amplification in dynamic maneuvers. The limits of roll stability will be explored, particularly as they depend on loading, suspension condition, and matching between units. Continued effort should coordinate with other LCV studies. Trainers of LCV drivers will have tips for the researchers' insight and questions for their study.

A number of effects contribute to a vehicle's understeer characteristics. The roll steer behavior of the dollies was successfully measured in this project. Insufficient tire information was

available to calculate the usually greatest contributor to understeer—the fore-aft balance between mass distribution and tire cornering stiffness. Other possible contributors to the understeer gradient ought to be considered through modeling and also through measurement where justified. This will be especially important where near-limit steering behavior is achieved through extreme rearward amplification.

Eventually, the goal of improving stability will entail the application of electronic stability systems to the LCV. The parallel project to study advanced ESC can be combined with this project. Models developed in this project can be used to test the algorithms and communication protocols from that project.

This page intentionally left blank.

Chapter 9 – References

- Arant, M., S. Nelson, U. Attanayake, R. Hathaway, M. Keil, K. Ro, O. Franzese, H. Knee, T. LaClair, and D. Pape. 2009. U19: Heavy truck rollover characterization (Phase-B) final report. Final report to National Transportation Research Center, Inc., University Transportation Center, Contract No. DTRT06G-0043. Accessed August 2010 at <http://www.ntrci.org/library/U19-Heavy%20Truck%20Rollover%20Characterization%20Phase%20B%201259081915.pdf>
- de Melo, Rubem Penteado. 2005. Lateral stability of long combination vehicles. SAE Paper 2005-01-3992.
- Ervin, R., C. Winkler, P. Fancher, M. Hagan, V. Krishnaswami, H. Zhang, and S. Bogard. 1998. Two active systems for enhancing dynamic stability in heavy truck operations. Final report on Contract No. DTNH22-95-H-07002. Report Number: UMTRI-98-39. Accessed February 2011 at <http://hdl.handle.net/2027.42/1257>
- Ervin, R.D., and P.S. Fancher. 1984. *An Overview of the Dynamic Performance Properties of Long Truck Combinations*. University of Michigan Transportation Research Institute. Special report on Contract No. DTFH61-82-C-00054.
- Fancher, P.S., and C.B. Winkler. 1992. A Methodology for Measuring Rearward Amplification. University of Michigan Transportation Research Institute.
- Fancher, P., and C. Winkler. 2007. Directional performance issues in evaluation and design of articulated heavy vehicles. In *Vehicle System Dynamics*, 607-647. 45:7-8.
- FHWA. 2000. Comprehensive Truck Size and Weight Study Accessed September 2011 at <http://www.fhwa.dot.gov/policy/otps/truck/index.htm>
- FHWA. 2004. The U.S. Department of Transportation's Western Uniformity Scenario Analysis. April 2004. Accessed September 2011. <http://www.fhwa.dot.gov/policy/otps/truck/wusr.pdf>
- FHWA. 2007. S. Code of Federal Regulations, Title 23 (Highways) Part 658 – Truck Size and Weight, Route Designations-Length, Width and Weight Limitations. §5 Definitions. 23 CFR 658.5. U.S. Government Printing Office, Washington, DC.
- FMCSA. July 20, 2004. U.S. Code of Federal Regulations, Title 49 (Transportation), Part 380 Special Training Requirements Subpart A General, §105 Definitions. 49 CFR 380.105. U.S. Government Printing Office, Washington, DC.
- Gillespie, Thomas D. 1992. Fundamentals of Vehicle Dynamics. Warrendale, Pennsylvania: Society of Automotive Engineers.
- Grīslis, Aivis. 2010. Longer combination vehicles and road safety. Transport. 25(3): 336–343. Accessed September 2011 at <http://www.tandfonline.com/doi/abs/10.3846/transport.2010.41>

- He, Yuping, Md Manjurul Islam, and Timothy D. Webster. 2010. *An Integrated Design Method for Articulated Heavy Vehicles with Active Trailer Steering Systems*. SAE International.
- ISO. 2000. Road vehicles—heavy commercial vehicle combinations and articulated buses—lateral stability test methods. ISO 14791:2000(E)
- Knee, H.E., G. Capps, O. Franzese, P. Pollock, D. Coleman, I. Janajreh, S. Haas, N. Frey, E.H. Law, E. Johnson, J. Petrolino, and D. Rice. 2005. Heavy truck rollover characterization: New-generation single tires vs. standard duals. Paper presented at the Truck and Bus Safety and Security Symposium, November 14-16, in Alexandria, Virginia.
- LaClair, T., H. Knee, O. Franzese, M. Arant, R. Hathaway, M. Keil, D. Pape, and Dale Rhoda. 2010. U24 Heavy Truck Rollover (Phase C). Final report to National Transportation Research Center, Inc.; University Transportation Center, Contract No. DTRT06G-0043. Accessed February 2011 at
http://www.ntrci.org/library/U24_Heavy_Truck_Rollover_Phase_C_FINAL_1288900197.pdf
- MacAdam, C., M. Hagan, P. Fancher, C. Winkler, R. Ervin, J. Zhou, and S. Bogard. 2000. *Rearward Amplification Suppression (RAMS)*. Final report on Contract No. DTFH61-96-C-00038.
- Mallikarjunarao, C., and P.S. Fancher, 1979. Tank trailer stability analysis. University of Michigan Transportation Research Institute. Report No. UM-HSRI-79-100.
<http://hdl.handle.net/2027.42/496>
- Mechanical Simulation Corporation. 2010. *TruckSim®*. 912 N Main St., Ann Arbor, MI.
- NCHRP. 2010. *Review of Canadian Experience with the Regulation of Large Commercial Motor Vehicles*. Report 671. Transportation Research Board.
- Pape, D., M. Arant, D. Hall, S. Nelson, J. Petrolino, O. Franzese, H. Knee, N. Wood, S. Yeakel, R. Hathaway, M. Keil, and P. Pollock. 2008. U02: Heavy truck rollover characterization (Phase-A) final report. Final report to National Transportation Research Center, Inc.; University Transportation Center, Contract No. DTRT06G-0043. Accessed August 2010 at
http://www.ntrci.org/library/U02- Heavy_Truck_Rollover_Characterization_Phase_A_1239_201531.pdf.
- Pape, D., M. Arant, W. Brock, D. Delorenzis, T. LaClair, A. Lim, J. Petrolino, and A. Spezia. 2011. U31: Vehicle Stability and Dynamics Electronic Stability Control Final Report. To National Transportation Research Center, Inc.; University Transportation Center, Contract No. DTRT-06-G-0043. U.S. Department of Transportation Research and Innovative Technology Administration.
- Shakarji, Craig M. 1998. Least-Squares Fitting Algorithms of the NIST Algorithm Testing System. Journal of Research of the National Institute of Standards and Technology, Volume 103, Number 6.

SAE International. 1980. Manual on design and application of leaf springs. HS-788. Warrendale, PA: SAE International.

STAA (Jan 6, 1983). Surface Transportation Efficiency Act. Public Law 97-424. Currently codified at:

- 23 USC 127 (d) Longer Combination Vehicles
- 49 USC 31111 (b) General Limitations. (doubles permitted)

Transportation Research Board Executive Committee. 2002. Regulation of Weights, Lengths, and Widths of Commercial Motor Vehicles. Special Report 267.

U.S. DOT. (U.S. Department of Transportation, Federal Highway Administration, Office of Freight Management and Operations). 2010. Freight Facts and Figures. Special compilation by the Freight Operations and Technology Team. Accessed September 2011 at http://ops.fhwa.dot.gov/freight/freight_analysis/nat_freight_stats/docs/10factsfigures/figure3_4.htm

Winkler, Christopher B. 1998. Simplified analysis of the steady-state turning of complex vehicles. Vehicle System Dynamics 29:141-180.

Winkler, Christopher B., Daniel Blower, Robert D. Ervin, and Rao M. Chalasani. 2000. Rollover of Heavy Commercial Vehicles. Warrendale, PA: Society of Automotive Engineers, Inc.

Yu, H., Güvenç, L., and Özgüler, Ü. 2008. Heavy duty vehicle rollover detection and active roll control. Vehicle System Dynamics 46 (6): 451-70.

Zhou, S., Guo, L., and Zhang, S. 2008. Vehicle yaw stability control and its integration with roll stability control. Chinese Control and Decision Conference.

This page intentionally left blank.

Appendix A:

LCV Test Plan

This page intentionally left blank.

Table of Contents

A-1. OVERVIEW	A-1
A-2. TEST VEHICLE	A-1
A-3. INSTRUMENTATION & MEASUREMENT	A-2
A-3.1. Vehicle Motion to be Recorded (Subject to Available Instrumentation).....	A-2
A-4. MANEUVERS	A-4
A-4.1. Constant Radius Turn.....	A-4
A-4.1.1. Background	A-4
A-4.1.2. Maneuver	A-4
A-4.1.3. Metrics for Successful Test	A-4
A-4.2. Impulse Steer	A-4
A-4.2.1. Background	A-4
A-4.2.2. Maneuver	A-5
A-4.2.3. Metrics for Successful Test	A-5
A-4.3. Single Lane Change	A-5
A-4.3.1. Background	A-5
A-4.3.2. Setup: Gate Location Single Lane Change	A-5
A-4.3.3. Maneuver	A-6
A-4.3.4. Metrics for Successful Test	A-6
A-4.4. Gradual Lane Change.....	A-7
A-4.4.1. Background	A-7
A-4.4.2. Setup: Gate Location and Speed for Single Lane Change	A-7
A-4.4.3. Maneuver	A-7
A-4.4.4. Metrics for Successful Test	A-8
A-4.5. Double Lane Change.....	A-8
A-4.5.1. Background	A-8
A-4.5.2. Setup: Gate Location Double Lane Change	A-8
A-4.5.3. Maneuver	A-9
A-4.5.4. Metrics for Successful Test	A-9
A-4.6. On Highway Testing	A-10
A-4.6.1. Background	A-10
A-4.6.2. Setup	A-10
A-4.6.3. Maneuvers	A-10
A-4.6.4. Metrics for Successful Test	A-10
A-5. PRELIMINARY TESTING	A-11
A-5.1.1. Background	A-11
A-5.1.2. Procedure.....	A-11
A-6. TEST SESSION ORDER.....	A-12
A-7. TEST SCHEDULING	A-12
WORKS CITED	A-14

List of Tables

Table A-1. Test Week daily scheduling overview.....	A-12
Table A-2. Detailed hourly test schedule.....	A-12

List of Figures

Figure A-1. Diagram. The test track gate location for the single lane change maneuver.....	A-6
Figure A-2. Diagram. The test track gate location for the high speed lane change.....	A-7
Figure A-3. Diagram. The test track gate location for the double lane change maneuver.	A-9
Figure A-4. Map. The approved on-road test route as established by NCAT officials.	A-10

A-1. Overview

The purpose of this testing is to gather data to establish the dynamics of a longer combination vehicle (LCV) consisting of a tractor three semitrailers. Testing is to be carried out at Auburn University's NCAT test track facility using a vehicle configured for asphalt testing purposes. Five testing maneuvers are proposed: Single Lane Change, Gradual Lane Change, Double Lane Change, Impulse Steer and Constant Radius Turn.

The goal of this testing is to attempt to capture the following vehicle responses in multiple excitation domains:

- 1) Roll angle per lateral acceleration
- 2) Yaw rate per lateral acceleration of tractor and trailers
- 3) Path deviation error per trailer referenced to the tractor
- 4) Lateral acceleration per steer angle
- 5) Yaw rate per steer angle
- 6) Lateral acceleration per trailer
- 7) Lateral acceleration of the tractor
- 8) Yaw rate per trailer
- 9) Yaw rate of the tractor
- 10) Roll angle per trailer
- 11) Roll angle of the tractor
- 12) Understeer gradient of the tractor and trailers
- 13) Trailer motion damping time and distance

These responses will then be analyzed to characterize the behavior of the longer combination vehicle, in particular the amplification of the response along the units of the vehicle toward the third trailer.

A-2. Test Vehicle

Of the test fleet at NCAT, the most appropriate combination for testing purposes consists of a Freightliner tractors entrained with three Cheetah container chassis carrying loaded 6.1 m (20 ft) shipping containers. The trailers are to be connected with similar style converter dollies. These dollies are manufactured by Eagle Manufacturing. The fifth-wheel on both dollies is suspended from the frame with two transverse leaf springs. The designations for the two dollies are "Eagle S" and "Eagle A". The Eagle S dolly is supplied by Silver Eagle Manufacturing. The Eagle A dolly is an Auburn owned dolly that is being converted to match the new Eagle S. The Eagle S dolly is to be located in the first dolly position in the vehicle. The Eagle A dolly is to be located in the second dolly position in the vehicle.

The gross weight of the vehicle is stated to be 70,500 kg (155,000 lb) and will be measured before the testing session. Wheel loads will be recorded for documentation and modeling

purposes. The presence ESC or ABS equipment shall be noted for each unit. No reconfiguration of the vehicle between testing maneuvers should be necessary to complete all testing.

Michelin will supply the tires for the project's test vehicle. Michelin will make proprietary force moment data available for use by a limited number of participants this project. The steer tires are to be the XZA model inflated to 115 psi (7.9 bar). The drive tires are to be the XDA model inflated to 103 psi (7.1 bar). The trailer tires are to be the XT1 model inflated to 103 psi (7.1 bar). All inflation pressures are at operating temperature.

The vehicles will be warmed up through regular test track activity prior to the start of the consortium's test day. The tire pressures are to be checked warm and set to the above stated temperatures. While the tire pressure check is carried out, the data acquisition system will be inspected. The vehicle will perform two laps with the data acquisition system running. The data collected during the two laps is to be checked to verify acquisition equipment operation.

A-3. Instrumentation & Measurement

The data will be collected at 100 Hz and reviewed after testing is completed for the day. Data is to be reviewed periodically during the day to assure proper instrumentation function. Based on the availability of equipment the vehicle shall be instrumented to collect data describing the following motions and distances.

A-3.1. Vehicle Motion to be Recorded (Subject to Available Instrumentation)

Inertial Measurement

1. Yaw Rate, Tractor.....VBox or Crossbow
2. Yaw Rate, Trailer 1.....VBox or Crossbow
3. Yaw Rate, Trailer 2.....RT 2500
4. Yaw Rate, Trailer 3.....RT 3100
5. Roll Rate, Tractor.....VBox or Crossbow
6. Roll Rate, Trailer 1.....VBox or Crossbow
7. Roll Rate, Trailer 2.....RT 2500
8. Roll Rate, Trailer 3.....RT 3100
9. Lat. Acceleration, Tractor.....VBox or Crossbow
10. Lat. Acceleration, Trailer 1.....VBox or Crossbow
11. Lat. Acceleration, Trailer 2.....RT 2500
12. Lat. Acceleration, Trailer 3.....RT 3100
13. Pitch Rate, Tractor.....VBox or Crossbow
14. Pitch Rate, Trailer 1.....VBox or Crossbow
15. Pitch Rate, Trailer 2.....RT 2500
16. Pitch Rate, Trailer 3.....RT 3100
17. Global Position & Orientation, Tractor.....Vbox or Crossbow
18. Global Position & Orientation, Trailer 1.....Vbox or Crossbow
19. Global Position & Orientation, Trailer 2.....RT2500

- 20. Global Position & Orientation, Trailer 3.....RT3100
- 21. Angle, Hand Wheel.....String Pot
- 22. Angle, Right Steer Road Wheel.....String Pot
- 23. Angle, Left Steer Road Wheel.....String Pot
- 24. Angle, Eagle S dolly Yaw to Trailer 2.....String Pot
- 25. Angle, Eagle A dolly Yaw to Trailer 3.....String Pot

Vertical Distance to Frame

- 26. Distance, Frame to Steer Axle Right.....String Pot
- 27. Distance, Frame to Steer Axle Left.....String Pot
- 28. Distance, Frame to Rear Drive Axle Right.....String Pot
- 29. Distance, Frame to Rear Drive Axle Left.....String Pot
- 30. Distance, Trailer 1 Frame to Trailer 1 Axle Right.....String Pot
- 31. Distance, Trailer 1 Frame to Trailer 1 Axle Left.....String Pot
- 32. Distance, Trailer 2 Frame to Trailer 2 Axle Right.....String Pot
- 33. Distance, Trailer 2 Frame to Trailer 2 Axle Left.....String Pot
- 34. Distance, Trailer 3 Frame to Trailer 3 Axle Right.....String Pot
- 35. Distance, Trailer 3 Frame to Trailer 3 Axle Left.....String Pot

Longitudinal Position To Frame Reference Point

- 36. Distance, Steer Axle to Frame Right.....String Pot
- 37. Distance, Steer Axle to Frame Left.....String Pot
- 38. Distance, Front Drive Axle to Frame Right.....String Pot
- 39. Distance, Front Drive Axle to Frame Left.....String Pot
- 40. Distance, Rear Drive Axle to Frame Right.....String Pot
- 41. Distance, Rear Drive Axle to Frame Left.....String Pot
- 42. Distance, Trailer 1 Frame to Trailer 1 Axle Right.....String Pot
- 43. Distance, Trailer 1 Frame to Trailer 1 Axle LeftString Pot
- 44. Distance, Trailer 2 Frame to Trailer 2 Axle Right.....String Pot
- 45. Distance, Trailer 2 Frame to Trailer 2 Axle Left.....String Pot
- 46. Distance, Trailer 3 Frame to Trailer 3 Axle Right.....String Pot
- 47. Distance, Trailer 3 Frame to Trailer 3 Axle Left.....String Pot

The above list is represented desired measurements. The actual list is to be determined by the availability of instrumentation equipment.

For each measured axle of the vehicle, two string pots are to attach vertically from the frame to the axle (one on each side equidistant from the vehicle centerline, perpendicular to the ground) and two are to attach horizontally from a reference point on the frame (one on each side equidistant from the vehicle centerline, parallel to the ground, with the potentiometer on a fabricated bracket). The two strings pots if possible are to be perpendicular to one another in the x-z plane (longitudinal and vertical) at stationary ride height. These are included as an attempt to capture kinematic data during the constant speed maneuver in order the characterize roll steer in lieu of K&C data for TruckSim Modeling.

A-4. Maneuvers

A-4.1. Constant Radius Turn

A-4.1.1. Background

The goal of this test is to establish the steady-state characteristics of the LCV such as understeer gradient for the tractor and the three trailers. Subject to instrumentation availability, measurement of roll steer characteristics of the trailers and converter dollies will also be attempted. Due to the spiral radius nature of the curved sections of the test track, for analysis purposes, the radius of curvature of the trucks motion will be determined from the GPS data. Data will also be collected in the straight portions of the track to characterize the vehicle response while maintaining lane position on a straight road.

A-4.1.2. Maneuver

The driver is to negotiate the curved portion of the track at a constant speed while maintaining lane position consistency. The test speeds are to be 25, 30, 35, 40, and 45 mph. Each test speed is to be repeated 10 times to insure sufficient data is collected. The drivers are to maintain test speed for the entire track length during this test for each of the five test speeds. Selection of the lane (inside or outside) is to be left to NCAT staff. The driver is to maintain the selected lane throughout the maneuver.

A-4.1.3. Metrics for Successful Test

This test will be executed in a manner deemed safe by the driver and test facility management. Data should be reviewed when possible at the end of the testing session to insure that all readings are within range, that the driver is maintaining consistency and that the data acquisition equipment is functioning properly. If the data is to be deemed un-useable the testing should be repeated at earliest convenience. Successful Constant Radius Turn test data will be judged by:

- 1) Consistent speed
- 2) Consistent road wheel steer angle variation
- 3) Consistent Lateral Accelerations between like-speed runs
- 4) Consistent Yaw Rate between like speed runs
- 5) Consistent Vehicle Attitude throughout the maneuver

A-4.2. Impulse Steer

A-4.2.1. Background

The goal of this test is excite the test vehicle with a broad band input so as to utilize frequency domain based analysis techniques of the response.

A-4.2.2. Maneuver

The maneuver is to take place in the straight sections of the test track in a location where the vehicle can be excited from a steady-state attitude. The driver is to start the maneuver from the right lane. The maneuver is initiated by imparting a quick 90 deg left steering input then immediately returning the wheel to centered position. The driver is to allow the vehicle to proceed to the left lane without further steering inputs. Once the tractor is in the left lane, the driver is to steer the vehicle straight into the lane. Then change back to the outside lane. The maneuver is to be performed during the constant radius turn test for each of the test runs.

A-4.2.3. Metrics for Successful Test

This test will be executed in a manner deemed safe by the driver and test facility management. Data should be reviewed when possible at the end of the testing session to insure that all readings are within range, that the driver is maintaining consistency and that the data acquisition equipment is functioning properly. If the data is to be deemed un-useable the testing should be repeated at earliest convenience.

A-4.3. Single Lane Change

A-4.3.1. Background

This maneuver is to establish the transient dynamic behavior of the LCV during an obstacle avoidance style maneuver. By performing this maneuver, path deviation and trailer motion settling distances are to be measured with a goal of characterizing the amplification of the trailer motion for each unit in the vehicle. Of interest is the relative position (to tractor) of each trailer in the vehicle, along with yaw rate and lateral acceleration.

A-4.3.2. Setup: Gate Location Single Lane Change

The gate location for the single lane change is a modification of the maneuver from HTRC Phases 1&2 testing. The original maneuver spanned the equivalent of a three-lane roadway. The initial gate location for the single lane change is essentially the gate set up from the HTRC Phase 1&2 testing with the center lane removed. See Figure A-1 (NTRCI 2005). The gates should be arranged in a portion of the test track where the vehicle can enter Gate 1 in a steady-state, zero-yaw attitude. Preliminary testing will be performed to determine the feasibility of the gate location and test speeds. If it is determined that the gates cannot be navigated consistently at the maximum safe test speed, the gate arrangement should be modified. The gates will be laid out in a manner that insures safety while testing. If NCAT determines that slight modification of the gate design will yield better results or more efficient testing, they may change the gate arrangement with the advisement of project partners. See Section 6, Preliminary Testing.

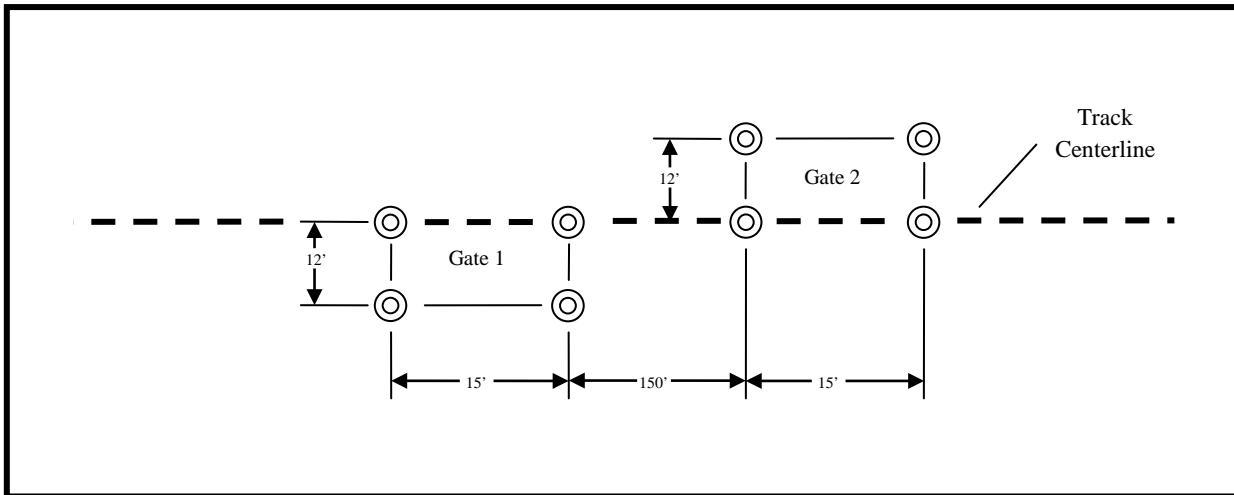


Figure A-1. Diagram. The test track gate location for the single lane change maneuver

A-4.3.3. *Maneuver*

The driver will travel toward the test region of the track in the right lane. Upon reaching the test region, the driver will proceed into Gate 1 at a constant speed. Upon exiting Gate 1, while maintaining speed the driver will steer into the left lane toward Gate 2. The driver will then proceed through Gate 2 maintaining constant test speed. The driver will decide how to negotiate the gates while maintaining the vehicle path within the gate markers. Negotiating the gates consistently will help insure that sufficient data will be collected during the test series.

Considering the loaded condition of the vehicle, the lack of previous test data and to insure consistent speed throughout the maneuver, test speeds shall be determined by preliminary testing.

For the single lane change, three test speeds shall be determined in preliminary testing. During the single lane change test series, each test speed should be repeated a minimum of 10 times to insure that sufficient data had been collected. If the resulting data indicates difficulty in maintaining consistent tractor path at a given speed, an additional 10 runs at that speed will be required.

A-4.3.4. *Metrics for Successful Test*

This test will be executed in a manner deemed safe by the driver and test facility management. Path following consistency must be demonstrated for the successful completion of this maneuver. Data should be reviewed as available or at the end of the testing session to verify that all readings are within range, that the driver is maintaining consistency and that the data acquisition equipment is functioning properly. If the data is to be deemed un-useable, the testing should be repeated at the earliest convenience.

A-4.4. Gradual Lane Change

A-4.4.1. Background

This maneuver is to establish the behavior of an LCV in a gentle, non-evasive style lane change at higher test speeds. The intent is to collect data to describe the motion of the LCV in normal operation that is likely to be encountered daily.

A-4.4.2. Setup: Gate Location and Speed for Single Lane Change

The gates should be arranged in a portion of the test track where the vehicle can enter Gate 1 in a steady-state, zero-yaw attitude. The gates shall be initially set up as in Figure A-2. Feasibility of the gate location will be determined during preliminary testing. If it is determined that the gates cannot be navigated consistently at test speed, the gate arrangement should be modified. The gates will be laid out in a manner that insures safety while testing. If during preliminary testing, NCAT determines that slight modification the gate design will yield better results or more efficient testing, they may change the gate arrangement with the advisement of the project partners. See section 6, Preliminary Testing.

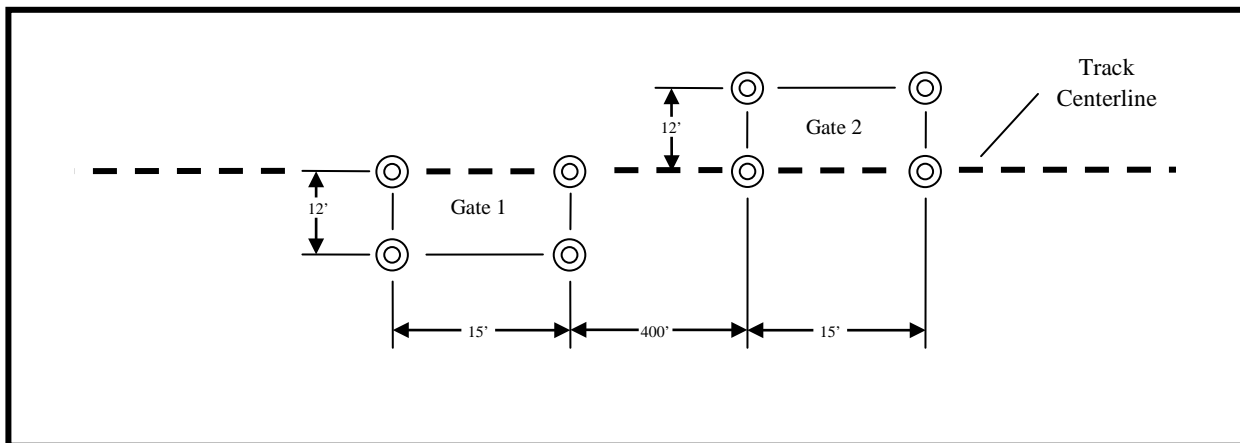


Figure A-2. Diagram. The test track gate location for the high speed lane change.

A-4.4.3. Maneuver

The driver will travel toward the test region of the track in the right lane. The test speed is to be 45 mph. Upon reaching the test region, the driver will proceed into Gate 1 at a constant speed. Upon exiting Gate 1, while maintaining speed the driver will steer into the left lane toward Gate 2. The driver will then proceed through Gate 2 maintaining constant test speed. The driver will decide how to negotiate the gates while maintaining the vehicle path within the gate markers. Negotiating the gates consistently will help insure that sufficient data will be collected during the test series.

Considering the loaded condition of the vehicle, the lack of previous test data and to insure consistency throughout the maneuver, the feasibility of the 45 mph test speed will be determined by preliminary testing.

During the high speed lane change test session, the maneuver will be repeated a minimum of 10 times to insure that sufficient data had been collected. If the resulting data indicates difficulty in maintaining consistent tractor path at a given speed, an additional 10 runs will be required.

A-4.4.4. Metrics for Successful Test

This test will be executed in a manner deemed safe by the driver and test facility management. Path following consistency must be demonstrated for the successful completion of this maneuver. Data should be reviewed as available or at the end of the testing session to verify that all readings are within range, that the driver is maintaining consistency and that the data acquisition equipment is functioning properly. If the data is to be deemed un-useable, the testing should be repeated at the earliest convenience.

A-4.5. Double Lane Change

A-4.5.1. Background

This maneuver, like the single lane change, is to establish the transient behavior of the LCV. Completing this test safely will require that lower test speeds than those used in previous lane change maneuvers. This test is to establish path deviation and trailer motion settling distances with a goal of determining the amplification characteristics of the trailer motion for each unit in the vehicle. Similar to single lane change, relative position (to tractor) of each trailer in the vehicle, along with yaw rate and lateral acceleration is of interest.

A-4.5.2. Setup: Gate Location Double Lane Change

The gate location for the double lane change is a mirror of the single lane change about Gate 2. See Figure A-3. As with the single lane change, the gates should be arranged in a portion of the test track where the vehicle can enter Gate 1 in a steady-state, zero-yaw attitude. The feasibility of the gate location will be determined during preliminary testing. If it is determined that the gates cannot be navigated consistently at the maximum safe test speed, the gate arrangement should be modified. The gates will be laid out in a manner that insures safety while testing. If NCAT determines that slight modification the gate design will yield better results or more efficient testing, they may change the gate arrangement with the advisement of the project partners. See section 6, Preliminary Testing

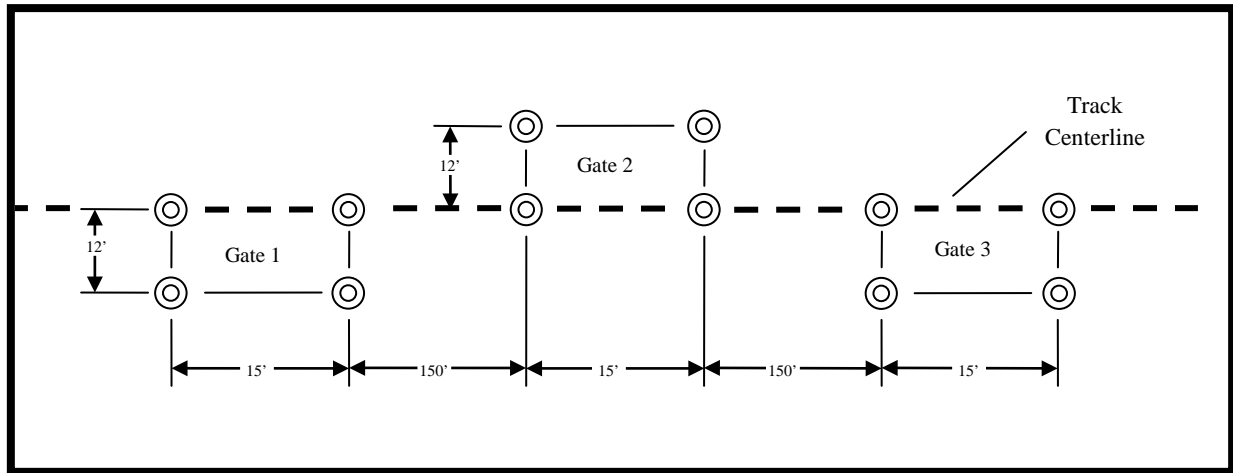


Figure A-3. Diagram. The test track gate location for the double lane change maneuver.

A-4.5.3. *Maneuver*

The driver will travel toward the test region of the track in the right lane. Upon reaching the test region, the driver will proceed into Gate 1 at test speed. Upon exiting Gate 1, while maintaining test speed, the driver will steer into the left lane toward Gate 2. The driver will then proceed through Gate 2. After passing through Gate 2, the driver will steer into the right lane toward Gate 3. The driver will then pass through Gate 3, maintaining test speed. The driver will decide how to negotiate the gates while maintaining the vehicle path within the gate markers. Negotiating the gates consistently will insure that sufficient data is collected during the test series. Test speeds will be determined during preliminary testing as in the single lane change maneuver.

As with the single lane change, three test speeds shall be determined in preliminary testing. During the double lane change test series, each test speed should be repeated a minimum of 10 times to insure that sufficient data had been collected. If the resulting data indicates difficulty in maintaining consistent tractor path at a given speed, an additional 10 runs at that speed will be required.

A-4.5.4. *Metrics for Successful Test*

This test will be executed in a manner deemed safe by the driver and test facility management. Path following consistency must be demonstrated for the successful completion of this maneuver. Data should be reviewed as available or after each testing session to verify that all readings are within range, that the driver is maintaining consistency and that the data acquisition equipment is functioning properly. If the data is to be deemed un-useable the testing should be repeated at earliest convenience.

A-4.6. On Highway Testing

A-4.6.1. Background

This portion of the testing is to gather real world data from a LCV operating on public roads at normal highway speeds. Due to the unknown nature of traffic and road conditions, this portion of the test maneuvers cannot be strictly defined.

A-4.6.2. Setup

NCAT is to obtain permission from Alabama transportation authorities to operate the test vehicle on public roads. The route determined by NCAT is as follows (See the map in Figure A-4):

- Track to Lee Road 151S-145E-175N-US 280
- Right US 280E to Lee Road 286 (6.5 miles)
- Reverse, US 280W to Lee Road 183 (7.1 miles)
- Reverse, US 280E to Lee Road 175 (0.6 miles)

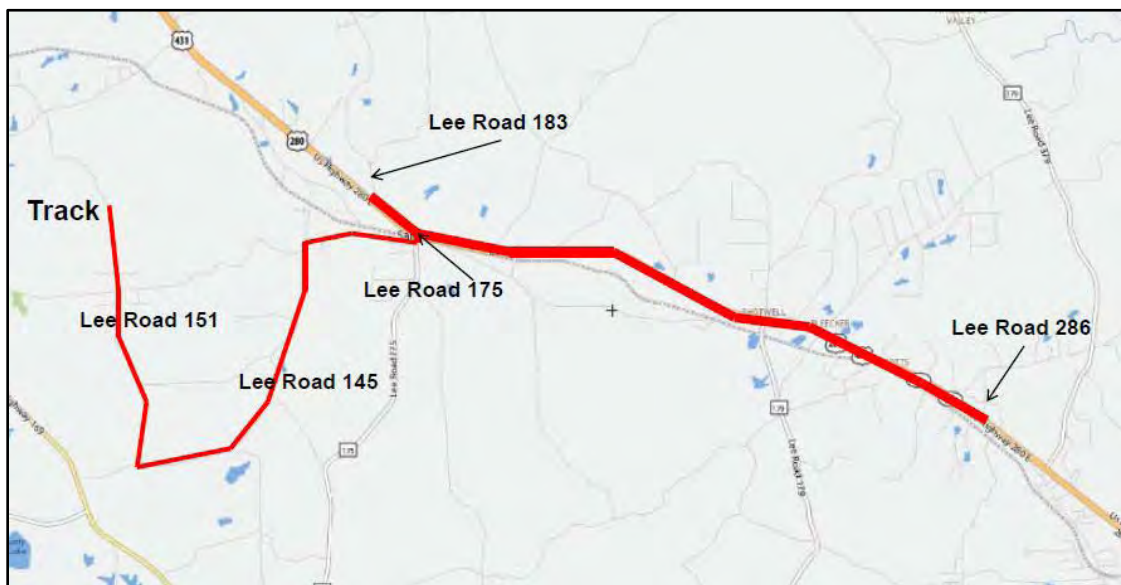


Figure A-4. Map. The approved on-road test route as established by NCAT officials.

A-4.6.3. Maneuvers

Lane changes are to be performed when safe and legal to do so at the discretion of the driver preferably at speeds greater than 45 mph. The lane start and stop time is to be marked in such a way as to facilitate data analysis. If possible, video of the vehicle traversing the test route is to be taken to help characterize the road features during the maneuvers.

A-4.6.4. Metrics for Successful Test

Testing will be conducted in a safe and legal manner. Completion of the test loop with collected data will constitute success.

A-5. Preliminary Testing

A-5.1.1. *Background*

The nature of this research is to establish the baseline dynamics for further LCV testing. As the equipment and its behavior on the test track is unknown, it is necessary to conduct preliminary testing to establish the test parameters for the aforementioned lane change maneuvers.

A-5.1.2. *Procedure*

- **Lane Change Start Location:** To establish the start location of the lane change region, trailer motion data recorded at 45-50 mph will be analyzed to find the point that is the minimum distance from the spiral exits where trailer yaw is negligible. One test vehicle length after this point is to be used as the start point for the lane change maneuvers. This is to apply to all lane changes as well as the impulse steer test.
- **Single and Double Lane Change Test Speeds:** To establish safe test speeds, the gates will be laid out as stated in the maneuver descriptions above. The vehicles will be driven through the gates starting at 5 mph and incremented each time at 5 mph. Data will be collected during these runs and analyzed after each successive pass. The lateral acceleration of any trailer is not to exceed 0.2g (1/2 rollover threshold estimate). If this lateral acceleration is reached, then the previous run speed is to be used as the maximum test speed for the maneuver. If after analysis, it is determined by the testers and other attendant research partners that 0.2g lateral acceleration is inappropriate as a cutoff, a new acceleration shall be established. Each run is to be monitored visually. If excessive body roll or any other indication should suggest that limit dynamics are being approached, no faster speed shall be attempted and the previous run speed is to be used as the maximum test speed. This is to apply to single and double lane changes.
- **High Speed Lane Change Test Speed:** The test speed for the high speed lane change is 45 mph. The maneuver shall be completed during preliminary testing. As with the Single Lane Change and Double Lane Change, the data collected will be analyzed between runs. If the lateral acceleration of any trailer does not exceed 0.2g (1/2 rollover threshold estimate) and no objectionable vehicle behavior is observed by the testers or attendant research partners, 45 mph shall be the test speed for the Gradual Lane Change maneuver.
- **Gate Location:** If it is believed by the testers and other attendant research partners that the gate location is restricting the testing speed and proper excitation of the test vehicle, the gates are to be spaced further apart noting that longer gate spacing and higher test speed increases the magnitude of the dynamics and brings the test vehicle closer to limit behavior. If the gate spacing is determined to be of a length that it is limiting the excitation of the test vehicle, the gates may be shortened. The gate spacing and location is to be established in such a way that insures safe testing. This applies to all lane change maneuvers.

A-6. Test Session Order

The Gradual Lane Change maneuver will be completed twice for each lap around the test track. Since this is a higher speed test, to avoid speed conflicts with other test maneuvers, the Gradual Lane Change must be performed during a separate test session from all other maneuvers.

The Double Lane Change and Single Lane Change maneuvers are to be run successively during one test session, by completing one of each maneuver for each lap around the test track. The single lane change maneuver is to be completed on one straight and the double lane change is to be completed on the opposite straight.

It is believed, due to the size of the vehicle and the track layout, that the Double Lane Change safe test speed will be lower than the single lane change safe test speed so the curved portions of the track will be used to adjust the test speed for the next maneuver. As this is, performing the two lane change maneuvers sequentially will prevent the concurrent performance of the Constant Radius Turn maneuver as the vehicle speed will be in transition through the curved portion of the track. To avoid speed conflicts the Constant Radius Turn testing should be completed during a separate testing session from the other maneuvers. The Impulse Steer Maneuver will be complete while the vehicle is in the straight sections of track between the constant radius maneuvers.

A-7. Test Scheduling

The test schedules presented in this document are tentative and subject to change. Adjustment to the following schedule may be made to accommodate the regular NCAT testing occurring simultaneously.

Table A-1. Test Week daily scheduling overview.

Day	Testing Activity
Monday, May 16 th	Preliminary Lane Change Testing / Gradual Lane Change
Tuesday, May 17 th	Constant Speed Turns / Impulse Steer
Wednesday, May 18 th	Single and Double Lane Change
Thursday, May 19 th	Overflow, On-road Testing, Meetings
Friday, May 20 th	Meetings, Depart

Table A-2. Detailed hourly test schedule

Monday	
7:00	Arrive at NCAT. Test Week Kickoff Meeting. Review of Test Plan and Day's Planned Activities
8:00	Tire Pressure Check. Acquisition Check
9:00	Constant Radius Turn/Impulse Steer Trial
10:00	Track Setup for Gradual Lane Change: Trail Run
11:00	Gradual Lane Change Testing. End of Test Data Check
12:00	Single Lane Change Trial: Maneuver Start Location, Test Speeds and Gate Location

13:00	Lunch
14:00	Track Adjustment for Lane Change Trials
15:00	Single Lane Change Trial: Maneuver Start Location, Test Speeds and Gate Location
16:00	Double Lane Change Trial: Maneuver Start Location, Test Speeds and Gate Location
17:00	Double Lane Change Trial: Maneuver Start Location, Test Speeds and Gate Location
18:00	Establish Lane Change Parameters. End of Day Data Review. Equipment and Vehicle Inspection
19:00	Depart NCAT
Tuesday	
7:00	Arrive at NCAT. Review of day's planned activities
8:00	Tire Pressure Check. Acquisition Check
9:00	Constant Radius Turn/Impulse Steer Testing
10:00	Constant Radius Turn/Impulse Steer Testing. Hourly Data Check
11:00	Constant Radius Turn/Impulse Steer Testing. Hourly Data Check
12:00	Constant Radius Turn/Impulse Steer Testing. Hourly Data Check
13:00	Lunch
14:00	Constant Radius Turn/Impulse Steer Testing. Hourly Data Check
15:00	Constant Radius Turn/Impulse Steer Testing. Hourly Data Check
16:00	Constant Radius Turn/Impulse Steer Testing. Hourly Data Check
17:00	End of Test Data Review. Equipment and Vehicle Inspection
18:00	Track Setup for Lane Changes
19:00	Depart NCAT
Wednesday	
7:00	Arrive at NCAT. Review of day's planned activities
8:00	Tire Pressure Check. Acquisition Check
9:00	Single and Double Lane Change Testing
10:00	Single and Double Lane Change Testing. Hourly Data Check
11:00	Single and Double Lane Change Testing. Hourly Data Check
12:00	Single and Double Lane Change Testing. Hourly Data Check
13:00	Lunch
14:00	Single and Double Lane Change Testing. Hourly Data Check
15:00	Single and Double Lane Change Testing. Hourly Data Check
16:00	Single and Double Lane Change Testing. Hourly Data Check
17:00	Single and Double Lane Change Testing. Hourly Data Check
18:00	End of Test Data Review. Equipment and Vehicle Inspection
19:00	Depart NCAT
Thursday	
7:00	Arrive at NCAT. Review of day's planned activities
8:00	Tire Pressure Check. Acquisition Check
9:00	On-Road Testing
10:00	Post Route Data Check

11:00	On-Road Testing
12:00	Post Route/End of Test Data Check
13:00	Lunch
14:00	Test Overflow/Analysis Review Meeting
15:00	Test Overflow/Analysis Review Meeting
16:00	Test Overflow/Analysis Review Meeting
17:00	Test Overflow/Analysis Review Meeting
18:00	Test Overflow/Analysis Review Meeting
19:00	Depart NCAT
Friday	
7:00	Arrive at NCAT. Review of day's planned activities
8:00	Analysis Review Meeting
9:00	Analysis Review Meeting
10:00	Analysis Review Meeting
11:00	Analysis Review Meeting
12:00	Adjourn Test Week

Works Cited

NTRCI . *Truck Rollover Characterization for Class 8 Tractor-Trailers Utilizing Standard Dual Tires and New Generation Single Tires*. Oak Ridge, TN: NTRCI, 2005.

Appendix B:

LCV Instrumentation Plan

This page intentionally left blank.

Table of Contents

B-1. OVERVIEW	B-1
B-2. TEST VEHICLE.....	B-1
B-3. MEASUREMENTS & INSTRUMENTATION	B-2
B-3.1. POSITION MEASUREMENTS	B-10
B-3.1.1. Global Positioning System (GPS).....	B-10
B-3.1.2. Dynamic Base Real Time Kinematic.....	B-12
B-3.2. INERTIAL MEASUREMENTS.....	B-15
B-3.3. DISPLACEMENT MEASUREMENT	B-19
B-3.4. CAN MESSAGES.....	B-21
B-4. INSTRUMENTATION MOUNTING.....	B-22
B-5. DATA ACQUISITION	B-26
B-5.1. SENSOR WIRING	B-26
B-5.2. SENSOR INTERFACING	B-27
B-5.3. DATA LOGGING.....	B-28
B-6. QUALITY ASSURANCE	B-29

List of Tables

Table B-1. Complete list of measurements to be taken.....	B-3
Table B-2. MemSense Nano specifications.....	B-16
Table B-3. Crossbow Nav440 specifications	B-18
Table B-4. Specifications of the Oxford RT IMU and GPS receivers.....	B-19

List of Figures

Figure B-1. Photo. NCAT test vehicle turning from one county road to another during the on-highway testing	B-2
Figure B-2. Photo. Two GPS receivers, the Novatel (left) and u-blox (right).....	B-10
Figure B-3. Photo. The GPS base station is near the southeast corner of the NCAT track.....	B-11
Figure B-4. Equation. Pseudorange (above) and carrier phase (below) measurements.....	B-12
Figure B-5. Equation. Single differenced measurements of pseudorange (above) and carrier phase (below).....	B-13
Figure B-6. Equation. Double differenced pseudorange measurement.....	B-13
Figure B-7. Equation. Double differenced carrier phase measurement.....	B-14
Figure B-8. Equation. Estimate of the relative position vector (RPV).....	B-14
Figure B-9. Equation. Least squares estimate of the RPV.	B-15
Figure B-10. Photo. Vehicle coordinates.....	B-15
Figure B-11. Photo. MemSense Nano IMU.....	B-16
Figure B-12. Photo. Crossbow Nav440.....	B-17
Figure B-13. Photo. Oxford RT 2500.	B-18
Figure B-14. Photo. Oxford RT 3100.	B-19
Figure B-15. Sketch. Axle deflection diagram.	B-20
Figure B-16. Photo. Celesco string pots.....	B-20
Figure B-17. Diagram. Connections between the CAN boxes and the data collection computer.	B-21
Figure B-18. Photo. CAN box.	B-22
Figure B-19. Diagram. CAN message structure.	B-22
Figure B-20. Photo. Computer mounting.	B-23
Figure B-21. Photo. String pot mounting.	B-23
Figure B-22. Photo. Sensor protection.	B-24
Figure B-23. Photo. Can box mounting.	B-24
Figure B-24. Photo. Articulation pot mounting.	B-25
Figure B-25. Photo. Steer axle displacement mounting.	B-25
Figure B-26. Photo. Steering angle mounting.	B-25
Figure B-27. Photo. Antenna mounting.	B-26
Figure B-28. Diagram. Instrument wiring on the test vehicle.	B-27
Figure B-29. Diagram. MOOS Architecture.	B-28
Figure B-30. Screen Shot. Asynchronous file example.	B-29

This page intentionally left blank.

B-1. Overview

The scope of this appendix is to describe the process of developing and implementing a data acquisition system (DAQ) for use on the LCV triple test vehicle. The purpose of this system is to instrument the vehicle with a multitude of sensors and record data coming from those. These measurements will facilitate the group capturing the desired vehicle responses laid out in the test plan, which are

- 1) Roll angle per lateral acceleration
- 2) Yaw rate per lateral acceleration of tractor and trailers
- 3) Path deviation error per trailer referenced to the tractor
- 4) Lateral acceleration per steer angle
- 5) Yaw rate per steer angle
- 6) Lateral acceleration per trailer
- 7) Lateral acceleration of the tractor
- 8) Yaw rate per trailer
- 9) Yaw rate of the tractor
- 10) Roll angle per trailer
- 11) Roll angle of the tractor
- 12) Understeer gradient of the tractor and trailers
- 13) Trailer motion damping time and distance

The above characteristics can be separated into four groups

- 1) Position Measurements
- 2) Inertial Measurements
- 3) Displacement Measurements
- 4) CAN Messages

B-2. Test Vehicle

The test vehicle is shown in Figure B-1. It consists of a Freightliner tractor in combination with three Cheetah container chassis carrying loaded 6.1-m (20-ft) intermodal shipping containers. At the time of the kick-off meeting, the vehicle was outfitted with two converter dollies both made by Silver Eagle Manufacturing. Prior to the test week Silver Eagle provided a more traditional converter dolly along with a conversion kit for one of the two currently in use at NCAT. This allowed for the vehicle to be outfitted with a pair of dollies that more closely represent those used with triple trailers in service.



Figure B-1. Photo. NCAT test vehicle turning from one county road to another during the on-highway testing.

B-3. Measurements & Instrumentation

In this section desired measurements along with the selection of the appropriate sensor will be detailed. The focus of this task was to achieve all the required measurements with as few sensors as possible. In order to obtain the list of vehicle responses listed above, an extensive list of physical measurements needed to be taken. That list reached a total of 206 channels. A full list of those channels is in Table B-1, along with a description of the measurement. The list is in order of the measurement in correspondence to its location on the triple-trailer; those measurements closest to the front of the tractor are listed first.

Table B-1. Complete list of measurements to be taken.

Channel	Device Type	Reported Channel Name	Location of Device in LCV	Type of Measurement	Reported Units
1	Vehicle CAN	EngineRPM	Tractor Engine	Engine RPM	RPM
2	Vehicle CAN	Driver_Demand_Perc_Torque	Tractor Engine	Requested Percentage of Torque	%
3	Vehicle CAN	Actual_Engine_Perc_Torque	Tractor Engine	Actual Percentage of Torque	%
4	Vehicle CAN	Wheel_based_vehicle_speed_mph	Tractor Engine	Vehicle Speed	MPH
5	Vehicle CAN	Accelerator_pedal_position	Tractor Engine	Displacement of Pedal	Meters
6	Vehicle CAN	Perc_load_at_current_speed	Tractor Engine	Current Percentage of Max Load	%
7	Vehicle CAN	TurboCharger1_speed	Tractor Engine	Turbocharger RPM	RPM
8	Vehicle CAN	Engine_coolant_temp	Tractor Engine	Temperature of Engine Coolant	°C
9	Vehicle CAN	Fuel_rate	Tractor Engine	Current Fuel Rate of Engine	GPH
10	Vehicle CAN	Instantaneous_fuel_economy	Tractor Engine	Current Fuel Economy of Engine	MPG
11	Vehicle CAN	Average_fuel_economy	Tractor Engine	Average Fuel Economy	MPG
12	Vehicle CAN	Throttle_position	Tractor Engine	Displacement of Engine Throttle	Meters
13	String Pot U1	POTS_CAN_710_1	Tractor - CAN Unit 1 -Steer Axle - Left Side	Status Check	None
14	String Pot U1	POTS_CAN_613_1	Tractor - Steering Shaft	Rotation of Steering Shaft	A/D Counts
15	String Pot U1	POTS_CAN_610_1	Tractor - Steer Axle - Left Side	Vertical Movement of Axle	A/D Counts
16	String Pot U1	POTS_CAN_611_1	Tractor - Steer Axle - Left Side	Longitudinal Deflection of Axle	A/D Counts
17	String Pot U1	POTS_CAN_612_1	Tractor - Steering Kingpin - Left Side	Movement of Kingpin	A/D Counts
18	String Pot U2	POTS_CAN_720_2	Tractor - CAN Unit 2 - Steer Axle - Right Side	Status Check	None
19	String Pot U2	POTS_CAN_620_2	Tractor - Steer Axle - Right Side	Vertical Movement of Axle	A/D Counts
20	String Pot U2	POTS_CAN_621_2	Tractor - Steer Axle - Right Side	Longitudinal Deflection of Axle	A/D Counts
21	String Pot U2	POTS_CAN_622_2	Tractor - Steering Kingpin - Right Side	Movement of Kingpin	A/D Counts
22	MemSense	zAccelZ_gMemSense	Tractor	Acceleration	m/s^2
23	MemSense	zAccelY_gMemSense	Tractor	Acceleration	m/s^2
24	MemSense	zAccelX_gMemSense	Tractor	Acceleration	m/s^2
25	MemSense	zGyroZ_gMemSense	Tractor	Angular Rate	Rad/sec
26	MemSense	zGyroY_gMemSense	Tractor	Angular Rate	Rad/sec
27	MemSense	zGyroX_gMemSense	Tractor	Angular Rate	Rad/sec
28	MemSense	zMagX_gMemSense	Tractor	Magnotometer	Gauss

<u>Channel</u>	<u>Device Type</u>	<u>Reported Channel Name</u>	<u>Location of Device in LCV</u>	<u>Type of Measurement</u>	<u>Reported Units</u>
29	MemSense	zMagY_gMemSense	Tractor	Magnotometer	Gauss
30	MemSense	zMagZ_gMemSense	Tractor	Magnotometer	Gauss
31	MemSense	zSampleTimer_gMemSense	Tractor	Sample Timer	N/A
32	MemSense	zTempGyroX_gMemSense	Tractor	Temperature of Gyro	°C
33	MemSense	zTempGyroY_gMemSense	Tractor	Temperature of Gyro	°C
34	MemSense	zTempGyroZ_gMemSense	Tractor	Temperature of Gyro	°C
35	Novatel	zAdrL1_gNovatel0	Tractor	Carrier Phase Mesurement	L1 Cycles
36	Novatel	zAdrL2_gNovatel0	Tractor	Carrier Phase Mesurement	L2 Cycles
37	Novatel	zCnoL1_gNovatel0	Tractor	Carrier to Noise Ratio	dB-Hz
38	Novatel	zCnoL2_gNovatel0	Tractor	Carrier to Noise Ratio	dB-Hz
39	Novatel	zCourse_gNovatel0	Tractor	Course Over Ground	Radians
40	Novatel	zDopL1_gNovatel0	Tractor	Doplar	Hz
41	Novatel	zDopL2_gNovatel0	Tractor	Doplar	Hz
42	Novatel	zGPSSeconds_gNovatel0	Tractor	Milliseconds into GPS week	milliseconds
43	Novatel	zGPSWeek_gNovatel0	Tractor	GPS Week	Week #
44	Novatel	zHeight_gNovatel0	Tractor	Elevation	Meters
45	Novatel	zHgtStdDev_gNovatel0	Tractor	Height Standard Deviation	Meters
46	Novatel	zHorizSpeed_gNovatel0	Tractor	Horizontal Speed	M/S
47	Novatel	zEast_gNovatel0	Tractor	Position	Meters
48	Novatel	zLatStdDev_gNovatel0	Tractor	Latitude Stadard Deviation	Meters
49	Novatel	zNorth_gNovatel0	Tractor	Position	Meters
50	Novatel	zLongStdDev_gNovatel0	Tractor	Longitude Standard Deviation	Meters
51	Novatel	zNumSats_gNovatel0	Tractor	Number of Satellites	N/A
52	Novatel	zPsrL1_gNovatel0	Tractor	Pseudo Range	Meters
53	Novatel	zPsrL2_gNovatel0	Tractor	Pseudo Range	Meters
54	Novatel	zVertVel_gNovatel0	Tractor	Vertical Velocity	m/s
55	u-blox 1	ecefVX_gUblox1	Tractor	ECEF Velocity X-direction	cm/s
56	u-blox 1	ecefVY_gUblox1	Tractor	ECEF Velocity Y-direction	cm/s
57	u-blox 1	ecefVZ_gUblox1	Tractor	ECEF Velocity Z-direction	cm/s
58	u-blox 1	ecefX_gUblox1	Tractor	ECEF Position X-direction	cm
59	u-blox 1	ecefY_gUblox1	Tractor	ECEF Position Y-direction	cm

<u>Channel</u>	<u>Device Type</u>	<u>Reported Channel Name</u>	<u>Location of Device in LCV</u>	<u>Type of Measurement</u>	<u>Reported Units</u>
60	u-blox 1	ecefZ_gUblox1	Tractor	ECEF Position Z-direction	cm
61	u-blox 1	iTOW_gUblox1	Tractor	Time Of Week	milleseconds
62	u-blox 1	pAcc_gUblox1	Tractor	Position Accuracy	cm
63	u-blox 1	pDop_gUblox1	Tractor	Position Delusion of Precision	N/A
64	u-blox 1	sAcc_gUblox1	Tractor	Velocity Accuracy	cm/s
65	u-blox 1	week_gUblox1	Tractor	GPS Week	Week #
66	u-blox 1	zAdrL1_gUblox1	Tractor	Carrier Phase Mesurement	L1 Cycles
67	u-blox 1	zCnoL1_gUblox1	Tractor	Carrier to Noise Ratio	dB-Hz
68	u-blox 1	zDopL1_gUblox1	Tractor	Doplar	Hz
69	u-blox 1	zPsrL1_gUblox1	Tractor	Pseudo Range	Meters
70	String Pot U3	POTS_CAN_730_3	Tractor - CAN Unit 3 - Rear Drive Axle	Status Check	None
71	String Pot U3	POTS_CAN_630_3	Tractor - Rear Drive Axle - Left side	Vertical Movement of Axle	A/D Counts
72	String Pot U3	POTS_CAN_632_3	Tractor - Rear Drive Axle - Left side	Horizontail Deflection of Axle	A/D Counts
73	String Pot U3	POTS_CAN_631_3	Tractor - Rear Drive Axle - Right side	Vertical Movement of Axle	A/D Counts
74	String Pot U3	POTS_CAN_633_3	Tractor - Rear Drive Axle - Right side	Horizontal Deflection of Axle	A/D Counts
75	Cross-bow	zAccelZ_gXbow440	Trailer 1	Acceleration	m/s^2
76	Cross-bow	zAccelY_gXbow440	Trailer 1	Acceleration	m/s^2
77	Cross-bow	zAccelX_gXbow440	Trailer 1	Acceleration	m/s^2
78	Cross-bow	zGyroZ_gXbow440	Trailer 1	Angular Rate	Rad/sec
79	Cross-bow	zGyroY_gXbow440	Trailer 1	Angular Rate	Rad/sec
80	Cross-bow	zGyroX_gXbow440	Trailer 1	Angular Rate	Rad/sec
81	Novatel	zAdrL1_gNovatel1	Trailer 1	Carrier Phase Mesurement	L1 Cycles
82	Novatel	zAdrL2_gNovatel1	Trailer 1	Carrier Phase Mesurement	L2 Cycles
83	Novatel	zCnoL1_gNovatel1	Trailer 1	Carrier to Noise Ratio	dB-Hz
84	Novatel	zCnoL2_gNovatel1	Trailer 1	Carrier to Noise Ratio	dB-Hz
85	Novatel	zCourse_gNovatel1	Trailer 1	Course Over Ground	Radians
86	Novatel	zDopL1_gNovatel1	Trailer 1	Doplar	Hz
87	Novatel	zDopL2_gNovatel1	Trailer 1	Doplar	Hz
88	Novatel	zGPSSeconds_gNovatel1	Trailer 1	Milliseconds into GPS week	milleseconds
89	Novatel	zGPSWeek_gNovatel1	Trailer 1	GPS Week	Week #
90	Novatel	zHeight_gNovatel1	Trailer 1	Elevation	Meters

<u>Channel</u>	<u>Device Type</u>	<u>Reported Channel Name</u>	<u>Location of Device in LCV</u>	<u>Type of Measurement</u>	<u>Reported Units</u>
91	Novatel	zHgtStdDev_gNovatel1	Trailer 1	Height Standard Deviation	Meters
92	Novatel	zHorizSpeed_gNovatel1	Trailer 1	Horizontal Speed	M/S
93	Novatel	zEast_gNovatel1	Trailer 1	Position	Meters
94	Novatel	zLatStdDev_gNovatel1	Trailer 1	Latitude Standard Deviation	Meters
95	Novatel	zNorth_gNovatel1	Trailer 1	Position	Meters
96	Novatel	zLongStdDev_gNovatel1	Trailer 1	Longitude Standard Deviation	Meters
97	Novatel	zNumSats_gNovatel1	Trailer 1	Number of Satellites	N/A
98	Novatel	zPsrL1_gNovatel1	Trailer 1	Pseudo Range	Meters
99	Novatel	zPsrL2_gNovatel1	Trailer 1	Pseudo Range	Meters
100	Novatel	zVertVel_gNovatel1	Trailer 1	Vertical Velocity	m/s
101	u-blox 2	ecefVX_gUblox2	Trailer 1	ECEF Velocity X-direction	cm/s
102	u-blox 2	ecefVY_gUblox2	Trailer 1	ECEF Velocity Y-direction	cm/s
103	u-blox 2	ecefVZ_gUblox2	Trailer 1	ECEF Velocity Z-direction	cm/s
104	u-blox 2	ecefX_gUblox2	Trailer 1	ECEF Position X-direction	cm
105	u-blox 2	ecefY_gUblox2	Trailer 1	ECEF Position Y-direction	cm
106	u-blox 2	ecefZ_gUblox2	Trailer 1	ECEF Position Z-direction	cm
107	u-blox 2	iTOW_gUblox2	Trailer 1	Time Of Week	milliseconds
108	u-blox 2	pAcc_gUblox2	Trailer 1	Position Accuracy	cm
109	u-blox 2	pDop_gUblox2	Trailer 1	Position Delusion of Precision	N/A
110	u-blox 2	sAcc_gUblox2	Trailer 1	Velocity Accuracy	cm/s
111	u-blox 2	week_gUblox2	Trailer 1	GPS Week	Week #
112	u-blox 2	zAdrL1_gUblox2	Trailer 1	Carrier Phase Mesurement	L1 Cycles
113	u-blox 2	zCnoL1_gUblox2	Trailer 1	Carrier to Noise Ratio	dB-Hz
114	u-blox 2	zDopL1_gUblox2	Trailer 1	Doplar	Hz
115	u-blox 2	zPsrL1_gUblox2	Trailer 1	Pseudo Range	Meters
116	String Pot U4	POTS_CAN_740_4	Trailer 1 - CAN Unit 4 - Trailer 1	Status Check	None
117	String Pot U4	POTS_CAN_640_4	Trailer 1 Axle - Left Side	Horizontail Deflection of Axle	A/D Counts
118	String Pot U4	POTS_CAN_642_4	Trailer 1 Axle - Left Side	Vertical Movement of Axle	A/D Counts
119	String Pot U4	POTS_CAN_641_4	Trailer 1 Axle - Right Side	Horizontail Deflection of Axle	A/D Counts
120	String Pot U4	POTS_CAN_643_4	Trailer 1 Axle - Right Side	Vertical Movement of Axle	A/D Counts
121	String Pot U4	POTS_CAN_645_4	Dolly 1 at Left Side of Trailer 2	Fifth Wheel Articulation	A/D Counts

<u>Channel</u>	<u>Device Type</u>	<u>Reported Channel Name</u>	<u>Location of Device in LCV</u>	<u>Type of Measurement</u>	<u>Reported Units</u>
122	String Pot U4	POTS_CAN_644_4	Dolly 1 at Right Side of Trailer 2	Fifth Wheel Articulation	A/D Counts
123	Novatel	zAdrl1_gNovatel2	Trailer 2	Carrier Phase Mesurement	L1 Cycles
124	Novatel	zAdrl2_gNovatel2	Trailer 2	Carrier Phase Mesurement	L2 Cycles
125	Novatel	zCnol1_gNovatel2	Trailer 2	Carrier to Noise Ratio	dB-Hz
126	Novatel	zCnol2_gNovatel2	Trailer 2	Carrier to Noise Ratio	dB-Hz
127	Novatel	zCourse_gNovatel2	Trailer 2	Course Over Ground	Radians
128	Novatel	zDopl1_gNovatel2	Trailer 2	Doplar	Hz
129	Novatel	zDopl2_gNovatel2	Trailer 2	Doplar	Hz
130	Novatel	zGPSSeconds_gNovatel2	Trailer 2	Milliseconds into GPS week	milleseconds
131	Novatel	zGPSWeek_gNovatel2	Trailer 2	GPS Week	Week #
132	Novatel	zHeight_gNovatel2	Trailer 2	Elevation	Meters
133	Novatel	zHgtStdDev_gNovatel2	Trailer 2	Height Standard Deviation	Meters
134	Novatel	zHorizSpeed_gNovatel2	Trailer 2	Horizontal Speed	M/S
135	Novatel	zEast_gNovatel2	Trailer 2	Position	Meters
136	Novatel	zLatStdDev_gNovatel2	Trailer 2	Latitude Stadard Deviation	Meters
137	Novatel	zNorth_gNovatel2	Trailer 2	Position	Meters
138	Novatel	zLongStdDev_gNovatel2	Trailer 2	Longitude Standard Deviation	Meters
139	Novatel	zNumSats_gNovatel2	Trailer 2	Number of Satellites	N/A
140	Novatel	zPsrL1_gNovatel2	Trailer 2	Psuedo Range	Meters
141	Novatel	zPsrL2_gNovatel2	Trailer 2	Psuedo Range	Meters
142	Novatel	zVertVel_gNovatel2	Trailer 2	Vertical Velocity	m/s
143	RT 2500	zAccelY_38	Trailer 2	Acceleration	m/s^2
144	RT 2500	zAccelZ_38	Trailer 2	Acceleration	m/s^2
145	RT 2500	zAccelX_38	Trailer 2	Acceleration	m/s^2
146	RT 2500	zAltitude_38	Trailer 2	Elevation	Meters
147	RT 2500	zAngularRateY_38	Trailer 2	Angular Rate	Rad/sec
148	RT 2500	zAngularRateZ_38	Trailer 2	Angular Rate	Rad/sec
149	RT 2500	zAngularRateX_38	Trailer 2	Angular Rate	Rad/sec
150	RT 2500	zDownVel_38	Trailer 2	Vertical Velocity	m/s
151	RT 2500	zEastVel_38	Trailer 2	East Velocity	m/s
152	RT 2500	zHeading_38	Trailer 2	Heading Angle	Radians

<u>Channel</u>	<u>Device Type</u>	<u>Reported Channel Name</u>	<u>Location of Device in LCV</u>	<u>Type of Measurement</u>	<u>Reported Units</u>
153	RT 2500	zEast_38	Trailer 2	Position	Meters
154	RT 2500	zNorth_38	Trailer 2	Position	Meters
155	RT 2500	zNorthVel_38	Trailer 2	North Velocity	m/s
156	RT 2500	zPitch_38	Trailer 2	Angle of Pitch	Radians
157	RT 2500	zRoll_38	Trailer 2	Angle of Roll	Radians
158	RT 2500	zTime_38	Trailer 2	GPS_Time	N/A
159	String Pot U5	POTS_CAN_750_5	Trailer 2 - CAN Unit 5 - Trailer 2	Status Check	None
160	String Pot U5	POTS_CAN_650_5	Trailer 2 Axle - Left Side	Horizontail Deflection of Axle	A/D Counts
161	String Pot U5	POTS_CAN_652_5	Trailer 2 Axle - Left Side	Vertical Movement of Axle	A/D Counts
162	String Pot U5	POTS_CAN_651_5	Trailer 2 Axle - Right Side	Horizontail Deflection of Axle	A/D Counts
163	String Pot U5	POTS_CAN_653_5	Trailer 2 Axle - Right Side	Vertical Movement of Axle	A/D Counts
164	String Pot U5	POTS_CAN_655_5	Dolly 2 at Left Side of Trailer 3	Fifth Wheel Articulation	A/D Counts
165	String Pot U5	POTS_CAN_654_5	Dolly 2 at Right Side of Trailer 3	Fifth Wheel Articulation	A/D Counts
166	Novatel	zAdrl1_gNovatel3	Trailer 3	Carrier Phase Mesurement	L1 Cycles
167	Novatel	zAdrl2_gNovatel3	Trailer 3	Carrier Phase Mesurement	L2 Cycles
168	Novatel	zCnoL1_gNovatel3	Trailer 3	Carrier to Noise Ratio	dB-Hz
169	Novatel	zCnoL2_gNovatel3	Trailer 3	Carrier to Noise Ratio	dB-Hz
170	Novatel	zCourse_gNovatel3	Trailer 3	Course Over Ground	Radians
171	Novatel	zDopL1_gNovatel3	Trailer 3	Doplar	Hz
172	Novatel	zDopL2_gNovatel3	Trailer 3	Doplar	Hz
173	Novatel	zGPSSeconds_gNovatel3	Trailer 3	Milliseconds into GPS week	milliseconds
174	Novatel	zGPSWeek_gNovatel3	Trailer 3	GPS Week	Week #
175	Novatel	zHeight_gNovatel3	Trailer 3	Elevation	Meters
176	Novatel	zHgtStdDev_gNovatel3	Trailer 3	Height Standard Deviation	Meters
177	Novatel	zHorizSpeed_gNovatel3	Trailer 3	Horizontal Speed	M/S
178	Novatel	zEast_gNovatel3	Trailer 3	Position	Meters
179	Novatel	zLatStdDev_gNovatel3	Trailer 3	Latitude Stadard Deviation	Meters
180	Novatel	zNorth_gNovatel3	Trailer 3	Position	Meters
181	Novatel	zLongStdDev_gNovatel3	Trailer 3	Longitude Standard Deviation	Meters
182	Novatel	zNumSats_gNovatel3	Trailer 3	Number of Satellites	N/A
183	Novatel	zPsrL1_gNovatel3	Trailer 3	Psuedo Range	Meters

<u>Channel</u>	<u>Device Type</u>	<u>Reported Channel Name</u>	<u>Location of Device in LCV</u>	<u>Type of Measurement</u>	<u>Reported Units</u>
184	Novatel	zPsrL2_gNovatel3	Trailer 3	Pseudo Range	Meters
185	Novatel	zVertVel_gNovatel3	Trailer 3	Vertical Velocity	m/s
186	RT 3000	zAccelX_42	Trailer 3	Acceleration	m/s^2
187	RT 3000	zAccelY_42	Trailer 3	Acceleration	m/s^2
188	RT 3000	zAccelZ_42	Trailer 3	Acceleration	m/s^2
189	RT 3000	zAltitude_42	Trailer 3	Elevation	Meters
190	RT 3000	zAngularRateX_42	Trailer 3	Angular Rate	Rad/sec
191	RT 3000	zAngularRateY_42	Trailer 3	Angular Rate	Rad/sec
192	RT 3000	zAngularRateZ_42	Trailer 3	Angular Rate	Rad/sec
193	RT 3000	zDownVel_42	Trailer 3	Vertical Velocity	m/s
194	RT 3000	zEastVel_42	Trailer 3	East Velocity	m/s
195	RT 3000	zHeading_42	Trailer 3	Heading Angle	Radians
196	RT 3000	zEast_42	Trailer 3	Position	Meters
197	RT 3000	zNorth_42	Trailer 3	Position	Meters
198	RT 3000	zNorthVel_42	Trailer 3	North Velocity	m/s
199	RT 3000	zPitch_42	Trailer 3	Angle of Pitch	Radians
200	RT 3000	zRoll_42	Trailer 3	Angle of Roll	Radians
201	RT 3000	zTime_42	Trailer 3	GPS_Time	N/A
202	String Pot U6	POTS_CAN_760_6	Trailer 3 - CAN Unit 6 - Trailer 3	Status Check	None
203	String Pot U6	POTS_CAN_660_6	Trailer 3 Axle - Left Side	Horizontail Deflection of Axle	A/D Counts
204	String Pot U6	POTS_CAN_662_6	Trailer 3 Axle - Left Side	Vertical Movement of Axle	A/D Counts
205	String Pot U6	POTS_CAN_661_6	Trailer 3 Axle - Right Side	Horizontail Deflection of Axle	A/D Counts
206	String Pot U6	POTS_CAN_663_6	Trailer 3 Axle - Right Side	Vertical Movement of Axle	A/D Counts

B-3.1. Position Measurements

More than half of the channels, 124 of the 206 total, were of vehicle position. The reason for the high number is for Auburn to complete the intended tasks of providing centimeter level accuracy for position versus the normal meter level accuracy. In order to achieve this Auburn will instrument both the tractor and trailers with GPS receivers in addition to any other equipment to ensure the correct measurements are received. The Tractor is to have both a u-blox EVK-6H evaluation kit pictured in Figure B-2 along with a Novatel ProPack-V3 also shown in Figure B-2. This package will then be repeated for the first trailer. The second and third trailer will be instrumented with a Novatel receiver as well as the Oxford unit to receive position information.

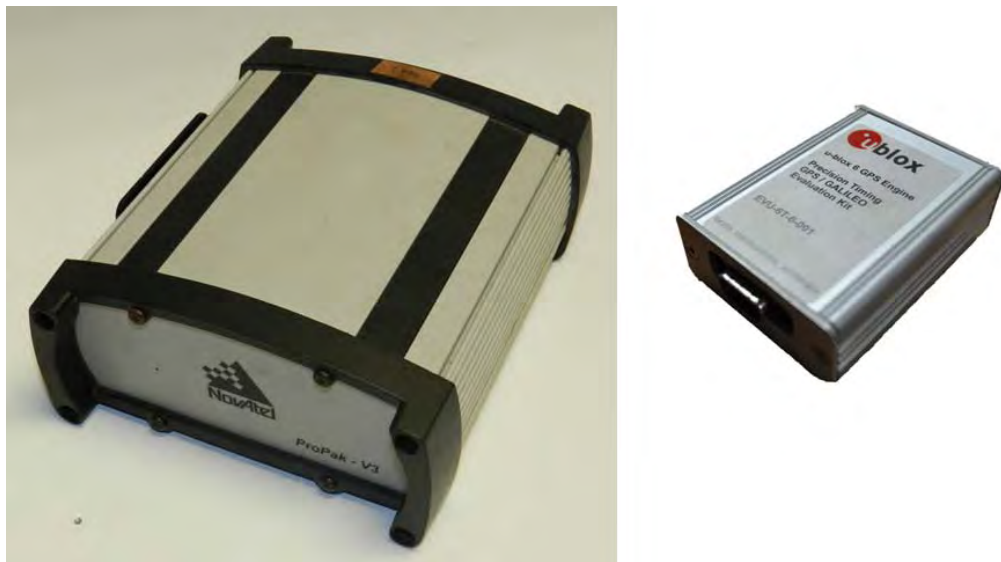


Figure B-2. Photo. Two GPS receivers, the Novatel (left) and u-blox (right).

B-3.1.1. Global Positioning System (GPS)

In this project, several GPS receivers will be placed on each of the units in the LCV. Differential GPS (DGPS) techniques are used to limit the position errors of the standard GPS solutions. When GPS receivers are operating in close proximity, DGPS can take advantage of the error sources that are common to the receivers. The errors introduced by the ionosphere and stratosphere are highly correlated for receivers operating within several kilometers. After DGPS correction, the individual satellite clock errors are also nearly identical. Using a method called Single Differencing (SD), two separate receiver's measurements are differenced to reduce the errors that are common to both receivers. DGPS methods can either use just the pseudorange, just the carrier phase measurement, or a combination of both.

The GPS carrier phase measurement is the accumulation of cycles of the GPS carrier sinusoidal from the time of the signal acquisition by the receiver to the current time. Using this phase shift instead of the pseudorange can result in a much more accurate result on the order of millimeters,

as opposed to meters; but even this measurement contains an ever-changing ambiguous number of carrier cycles which must be resolved. If this carrier phase integer ambiguity can be estimated accurately, the relative position vector (RPV) between multiple GPS receivers can be estimated on the order of centimeters.

Real time kinematic (RTK) systems take advantage of the accurately estimated carrier phase measurement to calculate equally precise global position estimates. This is done by comparing the measurements from a static GPS base station with known coordinates to the measurements of a dynamic receiver operating in close proximity. For this project, the static base station was located on the hill on the southern end of the track shown in Figure B-3, and the dynamic receivers were the tractor and second trailer which both had the required radio modem for RTK corrections. The base station sends signals to the dynamic receiver that includes measurements such as its position, pseudorange, and carrier phase measurements, and with this information the RPV between the static base station and the dynamic receiver can be estimated. The RPV can then be added to the global position of the base station to give the global position solution for the dynamic receiver. Though this method can accurately estimate the global position of the dynamic rover receiver, it does require that rover to be within a close proximity of the static base station.



Figure B-3. Photo. The GPS base station is near the southeast corner of the NCAT track.

The longer combination vehicle scenario offers a unique opportunity to employ these same techniques, but without requiring the static base station. The accuracy of the global position is not the ultimate goal, but just the relative location between the RTK corrected positions and the normal GPS receivers. Again, in this project the first and third trailer will have the required radio modem for communication with the base station for RTK corrections, so the goal is to find the RPVs to the first and third trailers. So in this case, the vehicles with the RTK corrections are treated as the static base station, and the other vehicles' positions are estimated relative to the

RTK corrected positions. In doing this the global position accuracy is lost, but the accuracy of the RPV is retained. This method has come to be known as Dynamic base RTK (DRTK). The important GPS measurements and the RPV estimation algorithms will be briefly discussed.

B-3.1.2. *Dynamic Base Real Time Kinematic*

To understand the DRTK algorithm, it is pertinent to first understand the relevant GPS measurements. The previously mentioned pseudorange and carrier phase measurements are expressed algebraically as in Figure B-4.

$$\begin{aligned}\rho_a^s &= r_a^s + cdt_a + cdt^s + T_a^s + I_a^s + M_a^s + v_a^s \\ \phi_a^s &= r_a^s + cdt_a + cdt^s + T_a^s - I_a^s + \lambda N_a^s + M_a^s + v_a^s\end{aligned}$$

Figure B-4. Equation. Pseudorange (above) and carrier phase (below) measurements.

Where,

ρ_a^s	is the measured pseudorange between receiver a and satellite s
ϕ_a^s	is the measured carrier phase between receiver a and satellite s
r_a^s	is the true range between receiver a and satellite s
c	is the speed of light
dt_a	is the receiver clock bias
dt^s	is the satellite clock bias
T_a^s	is the tropospheric delay between receiver a and satellite s
I_a^s	is the ionospheric delay between receiver a and satellite s
λ	is the carrier wavelength ($L1 = 0.1902$ m or $L2 = 0.2442$ m)
N_a^s	is the carrier integer ambiguity between receiver a and satellite s
M_a^s	is the multipath error
v_a^s	is the measurement noise

The earth's atmosphere can introduce delays to the GPS signal. One interesting detail to note is that the atmosphere affects the code based pseudorange and the carrier based phase measurements differently. Though the magnitudes of the errors are the same when they are expressed in units of length, the code is delayed which increases the measured pseudorange and the carrier phase is advanced which decreases the phase measurement. Assuming that the multi-path errors are small enough to deem negligible, the ionospheric error and the carrier integer ambiguity are the dominant sources of the difference in the two measurements.

Single Difference (SD)

Single differencing can help mitigate these common errors between receivers. This is accomplished by taking the pseudorange and carrier phase measurements from two receivers and

finding the difference between the two. The single differenced pseudorange and carrier phase are calculated by subtracting the measurements of receiver one to a satellite from the measurements of receiver two to the same satellite. By doing this, the single difference pseudorange and carrier phase measurements can be computed for each satellite that is common to both receivers. Satellite clock errors are removed in this process, and the ionospheric and tropospheric errors are significantly reduced and the residual atmospheric errors are small enough that they can be lumped in with the receiver's measurement noise. After the single differencing process, the pseudorange measurement is a function of the distance between the two receivers, the relative clock bias between the receivers, and the noise of increased variance. The carrier phase measurement after single differencing is a function of all the terms that the single differenced pseudorange measurement is a function of, as well as an additional term that refers to the carrier phase ambiguities for each of the receivers. The equations describing the single differenced pseudorange and carrier phase measurements are expressed in Figure B-5.

$$\Delta \rho_{ab}^s = r_{ab}^s + cdt_{ab} + v_{ab}^s$$

$$\Delta \phi_{ab}^s = r_{ab}^s + cdt_{ab} + \lambda N_{ab}^s + v_{ab}^s$$

Figure B-5. Equation. Single differenced measurements of pseudorange (above) and carrier phase (below).

Note that the subscript *ab* denotes the relative measurements between receiver *a* and receiver *b*. In this derivation, multi-path errors are assumed to be small enough to be deemed negligible. Multi-path errors become of importance in more urban-rich environments where the GPS signal is relayed off of the surrounding buildings and architecture.

Double Difference (DD)

As seen from the equations, the single differenced pseudorange and carrier phase measurements still contain the clock bias relative between the receivers. Removing this relative clock bias term is of importance and can be done so through double differencing. The process for double differencing begins by choosing one of the computed single differenced measurements and setting that as the base measurement. The measurement corresponding to the closest satellite is usually chosen to be the base measurement. This value is subtracted from the single differenced measurements of the other visible satellites to the respective receiver. This effectively removes the receiver clock bias term from the single differenced equations. The double differenced pseudorange is now a function of just the relative position between the two receivers and the measurement noise, and is expressed mathematically in Figure B-6.

$$\Delta \Delta \rho_{ab}^{st} = r_{ab}^{st} + v_{ab}^{st}$$

Figure B-6. Equation. Double differenced pseudorange measurement.

Similar to the single differenced carrier phase measurement, the double differenced carrier phase measurement also contains the relative position and measurement noise term as well as the additional relative carrier phase ambiguity term, and is expressed as in Figure B-7.

$$\Delta\Delta\phi_{ab}^{st} = r_{ab}^{st} + \lambda N_{ab}^{st} + v_{ab}^{st}$$

Figure B-7. Equation. Double differenced carrier phase measurement.

Algorithm

Using DRTK to estimate the RPV between two different receivers is a multi-stage process. The carrier phase ambiguities are first estimated as floating point values. Fixed integer estimates of the ambiguities are then computed. The fixed integer estimate is then subtracted from the double differenced carrier phase measurement and the RPV is estimated. The entire process entails the use of a Kalman filter for the floating point ambiguity estimation, the LAMBDA method for ambiguity integer fixing, and lastly the use of the least squares method to estimate the relative position vector.

Least Squares Method for RPV Estimation

The last step in the DRTK process is to estimate the RPV between two separate GPS receivers. The first two steps of the DRTK process provide the best available estimation of the double differenced carrier phase ambiguities. Under ideal conditions, the fixed integer estimates are successfully calculated with the LAMBDA method, but the RPV is estimated regardless. The RPV estimate is thereby designated as either a high-precision (HPRPV) estimate in which the fixed integer estimates are available or a low-precision (LPRPV) in which the floating point estimates must be used. Regardless of the precision of the ambiguity estimation, the solution procedure is the same. The equation in Figure B-8 is the RPV estimate as derived from the previous equations.

$$\Delta\Delta\phi_{ab} - \lambda \Delta\Delta N_{ab} = \Delta u_a r_{ab} + v_{ab}$$

Figure B-8. Equation. Estimate of the relative position vector (RPV).

Note that the Δ before the unit vector indicates that the base unit vector has been subtracted to form the correct geometry and that the satellite notation has been removed for clarity. The least squares method is used to estimate the RPV as shown in Figure B-9.

$$r_{ab} = (\Delta u_a^T \Delta u_a)^{-1} \Delta u_a^T (\Delta \Delta \phi_{ab} - \lambda \Delta \Delta N_{ab})$$

Figure B-9. Equation. Least squares estimate of the RPV.

B-3.2. Inertial Measurements

Inertial measurements require the use of accelerometers and gyroscopes. Inertial measurement units (IMUs) contain three accelerometers and three gyroscopes internally aligned in such a fashion to be allowed six degrees of freedom. The output that this six-axis IMU gives is usually in terms of yaw, pitch, and roll. When placed near the center of gravity of a vehicle, this data can be translated into the yaw, pitch, and roll of the vehicle illustrated in Figure B-10.

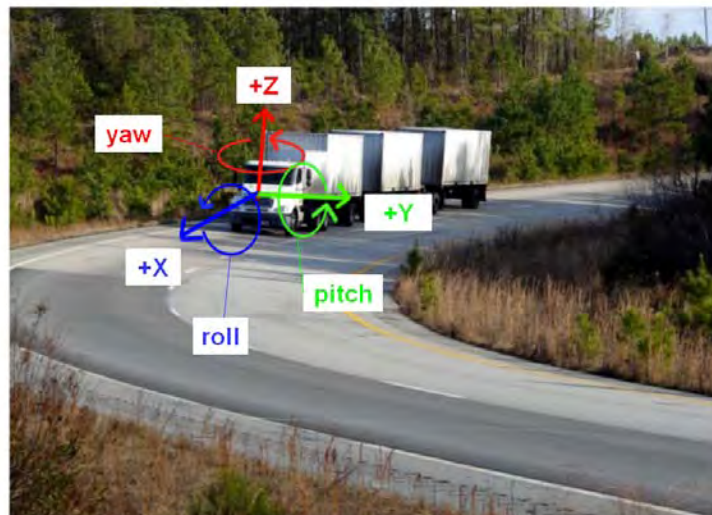


Figure B-10. Photo. Vehicle coordinates.

Like most sensors, the quality of the IMU depends on its price. Several quality IMUs were borrowed for this project from various sources. An IMU was mounted on each of the units in the combination. A MemSense IMU was obtained by Auburn University to be mounted on the tractor. Being much lower in price than the other sensors, the MemSense offers exceptional quality for its price. The MemSense is shown in Figure B-11 along with its technical specifications in Table B-2.



Figure B-11. Photo. MemSense Nano IMU.

Table B-2. MemSense Nano specifications.

Acceleration	NA02			NA05			NA10			g mg % of FS	0 to 70 °C Maximum Typical (Maximum) Typical (Maximum), 1 σ See Equation 1 on page 9 -3dB point	
	± 2	± 5	± 10	± 30	± 30	± 30	± 0.4 (± 1.0)	± 0.4 (± 1.0)	± 0.4 (± 1.0)			
Dynamic Range	± 2	± 5	± 10	± 30	± 30	± 30	± 0.4 (± 1.0)	± 0.4 (± 1.0)	± 0.4 (± 1.0)	g mg % of FS	0 to 70 °C Maximum Typical (Maximum) Typical (Maximum), 1 σ See Equation 1 on page 9 -3dB point	
Offset	±30	±30	±30	±30	±30	±30	0.6 (0.8)	1.1 (1.3)	2.1 (2.8)	mg		
Nonlinearity	± 0.4 (± 1.0)	± 0.4 (± 1.0)	± 0.4 (± 1.0)	± 0.4 (± 1.0)	± 0.4 (± 1.0)	± 0.4 (± 1.0)	0.6 (0.8)	1.1 (1.3)	2.1 (2.8)	% of FS		
Noise	0.6 (0.8)	1.1 (1.3)	2.1 (2.8)	2.2888x10 ⁻⁴	2.2888x10 ⁻⁴	4.5776x10 ⁻⁴	9.1553x10 ⁻⁵	2.2888x10 ⁻⁴	4.5776x10 ⁻⁴	g/bit		
Digital Sensitivity	9.1553x10 ⁻⁵	2.2888x10 ⁻⁴	4.5776x10 ⁻⁴	50	50	50	50	50	50	Hz		
Bandwidth ¹	50	50	50	50	50	50	50	50	50			
Angular Rate	-0150F050			-0300F050			-0600F050			°/s °/s %	0 to 70 °C Maximum Maximum Best fit straight line Typical (Maximum), 1 σ See Equation 1 on page 9 -3dB point	
	± 150	± 300	± 600	± 1200	± 1200	± 1200	± 150	± 300	± 600	°/s °/s %		
Dynamic Range	± 150	± 300	± 600	± 1200	± 1200	± 1200	± 1.5	± 1.5	± 1.5	°/s °/s %	0 to 70 °C Maximum Maximum Best fit straight line	
Offset	+/-1.5	+/-1.5	+/-1.5	+/-1.5	+/-1.5	+/-1.5	+/-1	+/-1	+/-1	°/s °/s %		
Cross-Axis Sensitivity	+/-1	+/-1	+/-1	+/-1	+/-1	+/-1	0.1	0.1	0.1	°/s °/s %		
Nonlinearity	0.1	0.1	0.1	0.1	0.1	0.1	0.36 (0.95)	0.56 (0.95)	0.56 (0.95)	°/s °/s %		
Noise	0.36 (0.95)	0.56 (0.95)	0.56 (0.95)	0.56 (0.95)	0.56 (0.95)	0.56 (0.95)	6.8664x10 ⁻³	1.3733x10 ⁻²	2.7465x10 ⁻²	5.4932x10 ⁻²	Hz	
Digital Sensitivity	6.8664x10 ⁻³	1.3733x10 ⁻²	2.7465x10 ⁻²	5.4932x10 ⁻²	50	50	50	50	50	Hz		
Bandwidth ¹	50	50	50	50	50	50	50	50	50			

The Crossbow NAV 440, shown in Figure B-12 is a higher-end IMU that has been consistently reliable for Auburn. Table B-3 shows its technical specifications. The CrossBow was provided by Auburn University.



Figure B-12. Photo. Crossbow Nav440.

Table B-3. Crossbow Nav440 specifications.

PERFORMANCE	
Position/Velocity	
Position Accuracy	<3.0 m CEP
1PPS Accuracy	±50 ns
Heading	
Accuracy	<1.0° rms (magnetic) <0.75° rms (with GPS aiding)
Attitude	
Range: Roll, Pitch	±180°, ±90°
Accuracy	<0.4°
Angular Rate	
Range: Roll, Pitch, Yaw	±200°
Bias Stability in run	<10°/hr
Bias Stability over temp	<0.02°/sec
Acceleration	
Input Range	±4 g or ±10 g
Bias Stability in run	<1 mg
Bias Stability over temp	<4 mg

The Oxford RT-2500 Inertial and GPS Navigation System, shown in Figure B-13 includes three angular rate sensors (gyroscopes), three servo-grade accelerometers, the GPS receiver and all the required processing in one very compact box. The internal processing includes the strap-down algorithms (using a WGS-84 earth model), Kalman filtering and in-flight alignment algorithms. The internal Pentium-class processor runs the QNX real-time operating system to ensure that the outputs are always delivered on time the technical specifications can be seen in Table B-4. The Oxford RT-2500 unit was provided by Western Michigan University.



Figure B-13. Photo. Oxford RT 2500.

The Oxford RT-3100, shown in Figure B-14 is similar to the Oxford RT-2500 model, but promises a little better accuracy in its measurements. Its technical specifications can be seen in Table B-4. The Oxford RT-3100 unit was provided by NTRCI.



Figure B-14. Photo. Oxford RT 3100.

Table B-4. Specifications of the Oxford RT IMU and GPS receivers.

Quantity	unit	RT2500	RT3100
Positioning Accuracy (SBAS)	m	2.0 SBAS	0.6
Positioning Accuracy (DGPS)	m	--	0.4
Velocity Accuracy	km/h rms	0.2	0.1
Heading	deg standard deviation	0.3	0.1
Roll and Pitch	deg standard deviation	0.15	0.05
Acceleration Linearity	% standard deviation	0.01	0.01
Angular Rate Bias	deg/s standard deviation	0.02	0.01

B-3.3. Displacement Measurement

Several of the desired characteristics have to do with vehicle roll and understeer tendencies. In order to fully capture those characteristics it is necessary to understand what the axle of the vehicle is doing at the time of the maneuver. In order to capture this, the group decided to use string potentiometers (string pots) to measure the linear displacement of each axle in three

dimensions. A diagram to show how this was to be achieved is shown below in Figure B-15. Combining the string pot measurements with the IMUs and GPS measurements the desired characteristic values can be obtained.

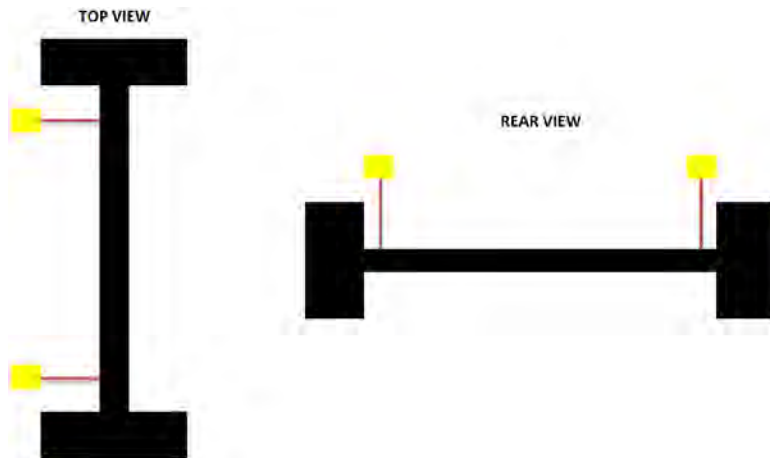


Figure B-15. Sketch. Axle deflection diagram.

A total of 26 string pots will be needed. Western Michigan has on hand fourteen string pots that can be leant for the project, it was decided that any other string pots would be purchased from the same manufacture for similarity across the LCV. Western Michigan will loan ten Celeesco model SP1-25 which are a 625-mm (25-in.) transducer and additionally four model SR1A-62 String Pots which are a 1.575-m (62-in.) weather-resistant model. Both models are shown below in Figure B-16. In order to fulfill the need of the project Auburn will purchase an additional fourteen model SP1-25 String Pots, two of which will be spares.

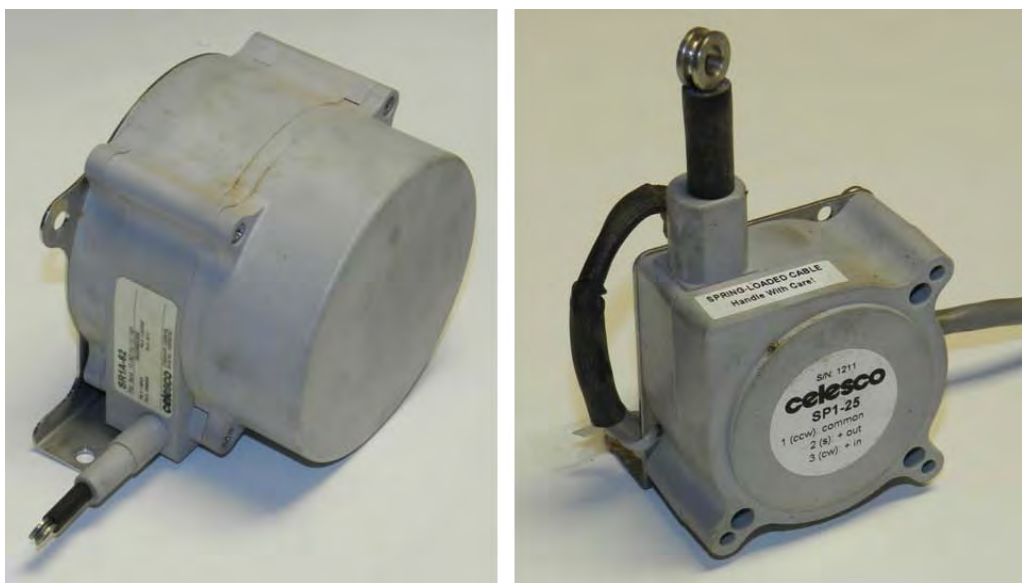


Figure B-16. Photo. Celeesco string pots.

Most of the sensors in this project have internal signal conditioning and output a digital signal. Auburn will need to build signal conditioning, including an analog-to-digital (A/D) converter, for the string pots. Auburn will determine the location and number of the CAN boxes with A/D converters. The string pots are to be connected to an A/D converter, which will convert the signal to digital and then send the message over a Controller Area Network (CAN) network similar to that which is found on most production vehicles. The main driving force behind this is controllability, with Auburn designing and implementing the system all of the inner workings will be known making any possible troubleshooting easily accomplished. A diagram of the system is in Figure B-17.

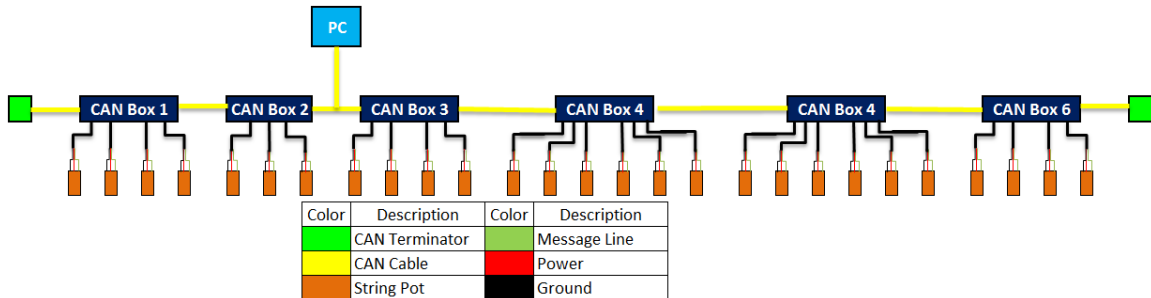


Figure B-17. Diagram. Connections between the CAN boxes and the data collection computer.

B-3.4. CAN Messages

The final group of measurements is CAN messages. This is the same type of network that is standard on vehicles today in order for microcontrollers and devices to communicate with each other within a vehicle without a host computer. The LCV will contain two separate CAN buses, one that is already there from the factory and one that will be created for the string pots. The factory installed CAN network is in accordance with the SAE J1939 standard. Using the SAE J1939 message list, Auburn will tap into the network and log the messages. A list of the messages to be recorded is in Table B-2.

The second network is to be created and installed by Auburn for use with the string pots and their associated A/D converters. This path was chosen for multiple reasons; the main two being complete control over design and to lower line noise on the string pots by placing the A/D converter close to the string pots themselves. The idea of having complete control over the network is the most critical part of the whole process this will allow Auburn to not only develop its own message set that would not interfere with any other CAN network. An added benefit is that it enables Auburn to have extensive knowledge of the system so that in the event something goes wrong it will take less time to diagnose and resolve the issue. There are a total of six CAN boxes to be created each containing the A/D and circuit board; one of these can be seen in Figure B-18.



Figure B-18. Photo. CAN box.

Each string pot is to be connected to the CAN box by a custom DB25 connector that is wired to provide power and ground to each string pot as well as a line for the message. In order to collect the measurements from the string pots, each A/D will have to be polled; this is to be achieved by setting up one of the CAN boxes to send out a message on the CAN bus at 100 Hz. The message set used for the string pots is relatively straightforward; each A/D will send out a status message every second to alert the computer if something is not working. The message set for the String Post CAN-bus can be seen in Figure B-19.

POTS_CAN_XXX_X	
	0-5 Channel Number on CAN Box
1-6	CAN Box Number
1:Left Side Steer Axle	
2:Right Side Steer Axle	
3:Drive Axle	
4:Trailer 1 Ride Axle	
5:Trailer 2 Ride Axle	
6:Trailer 3 Ride Axle	
6/7	6:Measurement
	7:Status

Figure B-19. Diagram. CAN message structure.

B-4. Instrumentation Mounting

All of these mounting brackets are to be fabricated and manufactured in the GAVLAB shop out at the NCAT facility. With the three trailers being nearly identical, the mounting boxes and brackets required will be fairly similar. Several sensors will need to be mounted in the tractor's

engine compartment. This includes the similar string pot set up around the axle, along with two string pots for vertical and horizontal displacement of the kingpin, and a large string pot for the angular rotation of the steering shaft. Behind the tractor cab a toolbox with the main CPU will be mounted. This box is where the CAN-bus will be inputted into the industrial computer for data acquisition and processing. Below, in Figure B-20 pictures of the actual toolbox that was on the tractor can be seen. This box contained the industrial computer, which will handle all of the data acquisition.

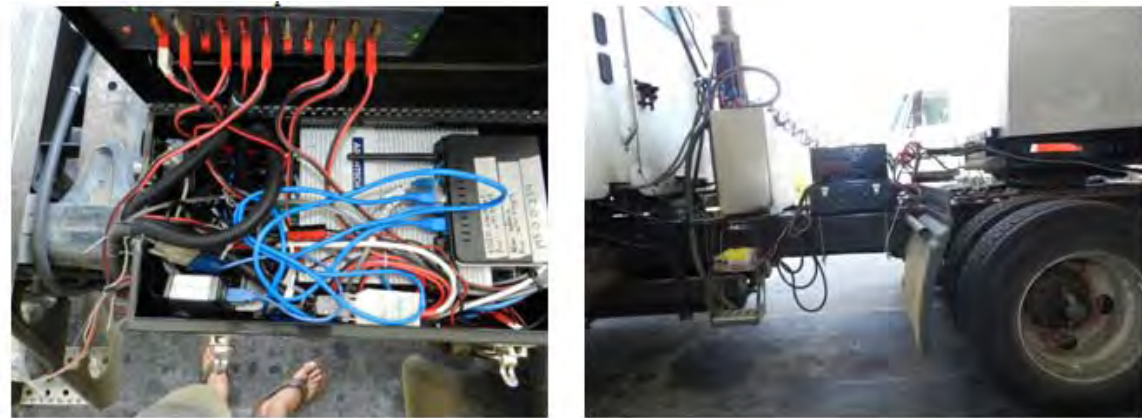


Figure B-20. Photo. Computer mounting.

To measure the axle displacements, string potentiometers are to be used. One string pot will be mounted directly above the axle and another string pot was mounted directly horizontal to the axle. This was done to maximize the displacements and get the best results. Figure B-21 shows these brackets mounted on the LCV.



Figure B-21. Photo. String pot mounting.

Similar to the toolbox mounted directly behind the cab of the tractor, other toolboxes were to be mounted under each of the trailers. Figure B-22 demonstrates how they were mounted; a close-up shows the power and serial cables going into and coming out of the box.



Figure B-22. Photo. Sensor protection.

As described above each of the string pots were connected to a CAN-box that contained the A/D converter. These A/D converters could handle six string pot inputs, and they output their data into the CAN bus that run alongside the trailer combination. Figure B-23 below shows one of these A/D converter boxes.



Figure B-23. Photo. CAN box mounting.

To calculate the articulation angle, the longer string pots are to be mounted on the dolly and attached to the successive trailer. They will be crisscrossed in an attempt to get as linear of a measurement as possible and to maximize the displacement. Figure B-24 shows the actual mounting on the LCV.



Figure B-24. Photo. Articulation pot mounting.

The tractor's engine compartment not only is less conducive to taking measurements it also requires more of them. The displacement of the kingpin on both sides requires two more string pots; additionally measuring the angular displacement of the steering shaft will require an additional string pot. The axle deflection string pots can be seen in Figure B-25 and the steering shaft in Figure B-26.



Figure B-25. Photo. Steer axle displacement mounting.

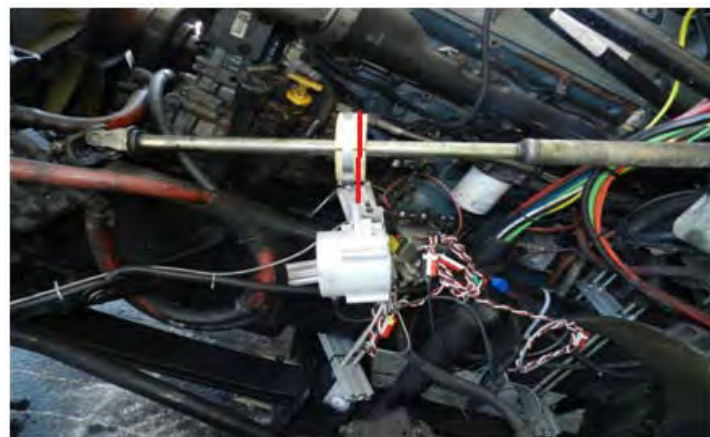


Figure B-26. Photo. Steering angle mounting.

Each of the GPS receivers requires antennas to be mounted on top of its respective trailer. Shown in Figure B-27 are the patch antenna on the center of the trailer roof for the u-blox, and the larger antenna on the side of the trailer roof for the Novatel.



Figure B-27. Photo. Antenna mounting.

B-5. Data Acquisition

The test vehicle will be equipped with numerous sensors that need to be interfaced with various communication methods. To facilitate this complex data collection with the maximum control over the process, a custom data collection system will be developed. The system is to consist of an industrial computer with Ubuntu Linux operating system and a wireless (WiFi) router. The Industrial computer will run without a monitor, keyboard, or mouse and will connect to the Oxford RT units via the router on an Ethernet network connection. The wireless router allows the data collection process to be monitored and controlled via a laptop computer in the truck cab. It should be noted that no data will be sent over the wireless link it is only to monitor and control the data acquisition. All data will be recorded directly to the industrial PC and the data acquisition process, once started, will not be interrupted by a loss of communication from the laptop in the cab.

B-5.1. *Sensor Wiring*

In addition to the direct UDP/IP communication with the Oxford RT units over CAT6 Ethernet, the computer has four serial (RS-232) ports for three of the Novatel GPS receivers and the Trailer 1 IMU, the Crossbow 440, six USB connections from: the Microstrain AHRS (used as an IMU), a RS232-USB converter for the Novatel GPS on the truck, two from the u-blox GPS devices, and two from the USB-to-CAN converters for communicating with the string potentiometers and the truck computer. The wiring between the sensors and the computer can be seen in Figure B-28.

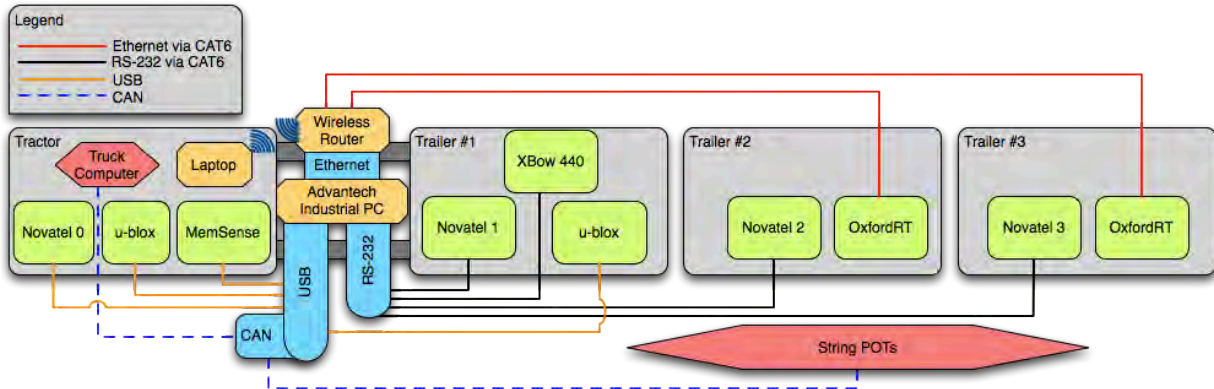


Figure B-28. Diagram. Instrument wiring on the test vehicle.

B-5.2. Sensor Interfacing

Code will be written to receive and interpret the data from each sensor. Before the project started, the lab already had code to interface with the Novatels, and the Crossbow. The new sensors that had to be interfaced were the MemSense IMU, the u-blox GPS units, and the Oxford RT units. The code for all of the sensor interfaces is going to be written in C++ and run on the embedded Linux computer on the tractor. The middleware used to communicate all of the sensor data between processes is called Mission Oriented Operating Suite (MOOS). This middleware uses client-server architecture with a centralized database and provides basic tools for Inter-Process Communication via sockets. This allows for viewing the raw data in real time, and logging the data in a standard format. Each sensor will have a corresponding process running that will interface with that sensor, format its data, and publish it as separate channels to the MOOS database. The MOOS database holds the latest value from each channel on each sensor and allows other processes to access this data. An illustration of this interface process can be seen in Figure B-29.

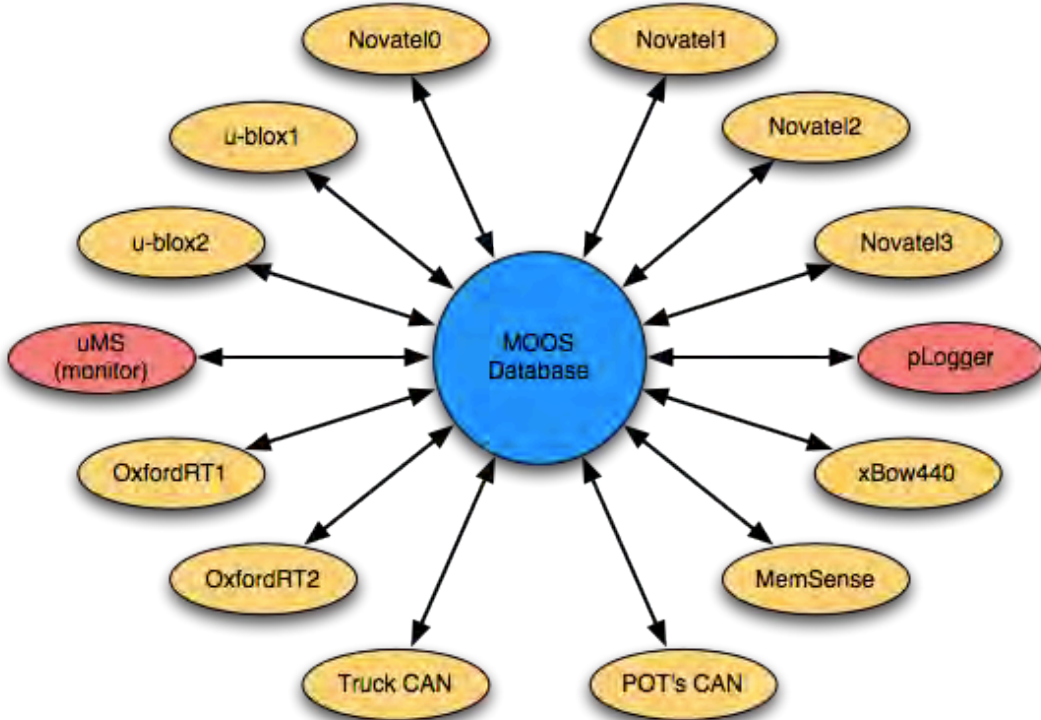


Figure B-29. Diagram. MOOS Architecture.

B-5.3. Data Logging

Using the laptop in the cab of the truck, the logging will be started and stopped via Secure Shell (SSH). Additionally, the data can be monitored using MOOS's uMS utility which shows the latest values for each of the sensors in a table. The MOOS utility pLogger connects to the MOOS database and records all changes to all channels to an asynchronous log format. This preserves the data in its raw form with its original timestamps taken by the sensor interface process. This is more difficult to process than synchronous data logs, but provides more accurate timing information. An example of the file format can be seen in Figure B-30.

2212	1.16	zAngularRateZ_38	gOXTS-RT	0.0006
2213	1.16	zAngularRateY_38	gOXTS-RT	-0.0011
2214	1.16	zAngularRateX_38	gOXTS-RT	0.0023
2215	1.16	zAccelZ_38	gOXTS-RT	0.1471
2216	1.16	zAccelY_38	gOXTS-RT	9.8181
2217	1.16	zAccelX_38	gOXTS-RT	-0.101
2218	1.16	zTime_38	gOXTS-RT	-25.106
2219	1.161	POTS_CAN_613_1	gTruckCanSuspensionPots_pots	43
2220	1.161	POTS_CAN_622_2	gTruckCanSuspensionPots_pots	265
2221	1.161	POTS_CAN_612_1	gTruckCanSuspensionPots_pots	170
2222	1.161	POTS_CAN_621_2	gTruckCanSuspensionPots_pots	204
2223	1.161	POTS_CAN_611_1	gTruckCanSuspensionPots_pots	375
2224	1.161	POTS_CAN_610_1	gTruckCanSuspensionPots_pots	43
2225	1.161	POTS_CAN_620_2	gTruckCanSuspensionPots_pots	265
2226	1.161	POTS_CAN_630_3	gTruckCanSuspensionPots_pots	839
2227	1.162	zGPSSeconds_gNovate12	gNovate12	25618140
2228	1.162	zGPSWeek_gNovate12	gNovate12	163
2229	1.162	zHgtStdDev_gNovate12	gNovate12	4.6626
2230	1.162	zLongStdDev_gNovate12	gNovate12	2.4053
2231	1.162	zLatStdDev_gNovate12	gNovate12	1.6299
2232	1.162	zHeight_gNovate12	gNovate12	185.4075
2233	1.162	zLong_gNovate12	gNovate12	-85.2961
2234	1.162	zLat_gNovate12	gNovate12	32.598
2235	1.162	zSampleTimer_gMemSense	gMemSense	16931
2236	1.162	zMagZ_gMemSense	gMemSense	-0.7923

Figure B-30. Screen Shot. Asynchronous file example.

B-6. Quality Assurance

The purpose of this section is to discuss the measures that both Auburn and the group as a whole will take to ensure the quality of the data while at NCAT for the test week. This was divided into two main tasks; maneuver recording and trackside quality checks. Both of these tasks will be done simultaneously during the test week to ensure a record is kept of everything that is done. During testing, the data acquisition system software to log all of the data was initialized before and stopped after each maneuver. This allowed each run to be logged and stored in a more organized manner.

Each run will initially be logged using a time stamp, and example of this would be "NTRCI_19_5_2011____10_26_13". This title corresponds to the run that was conducted on May 19th, 2011 at approximately 10:26:13 AM. A note will be written to track which maneuver is performed at which time in an effort to sync it up with the logged data later. The titles of each run will later be changed to reflect the respective maneuver performed during the time corresponding to the previous title. For example, "NTRCI_35mph_Dbl_Ln_Chng_R2" corresponds to the second run of the 35 mph double lane change maneuver.

One of the practices used in quality assurance will be a trackside quality check. This means that at any point in the test week, the group will have the ability to look at any of the data for any of the previously recorded runs. This is to be accomplished by using code written for use on a previous phase of testing.

This page intentionally left blank.

Appendix C:

**Characterizing the Triple Trailer Combination
at the National Center for Asphalt Technology
Test Track and One Separate FedEx Dolly at WMU**

This page intentionally left blank.

Table of Contents

C-1	PROCESS.....	C-1
C-2	OVERALL DESCRIPTION OF THE VEHICLE	C-6
C-2.1	BASIC DIMENSIONAL PARAMETERS FOR THE LONGER COMBINATION VEHICLE (LCV)	C-7
C-2.2	FREIGHTLINER TRACTOR CHASSIS	C-14
C-2.2.1	Summary Tractor Information provided by NCAT	C-14
C-2.2.2	2004 Freightliner Front Steer Axle.....	C-14
C-2.2.3	Pitman Arm, Drag Link, Steer Arm and Linkage	C-16
C-2.2.4	Drive Axle Characteristics.....	C-23
C-2.2.5	Steer Axle Measured Spring Ride Rates and Roll Rates.....	C-28
C-2.2.6	Tractor Frame Geometry and Stiffness.....	C-31
C-2.3	TRAILER 1.....	C-33
C-2.3.1	Concrete Compartment Characteristics	C-33
C-2.3.2	Configuration and Cargo.....	C-38
C-2.4	TRAILER 2	C-39
C-2.4.1	Additional Ballast Characteristics	C-41
C-2.4.2	Resulting Load Transfer to Kingpin and Rear Axle.....	C-42
C-2.5	TRAILER 3	C-43
C-2.5.1	Configuration and Ballast.....	C-43
C-2.5.2	Trailer Suspension	45
C-2.5.3	Trailer Torsional Stiffness	C-50
C-2.6	EAGLE DOLLY (NCAT AND FEDEX).....	C-50
C-2.6.1	Pintle Hook, Eye and Drawbar Assembly.....	C-55
C-2.6.2	Fifth Wheel, Fifth Wheel Mounting and Transverse Leaf Characteristics	C-57
C-2.6.3	Pitch and Roll Stiffness of the Unloaded FedEx Dolly.....	C-63
C-2.6.4	Bounce and Roll Stiffness of the Loaded NCAT Eagle Dolly.....	C-65
C-2.6.5	Weight Distribution WMU FedEx Dolly	C-66
C-2.6.6	Dolly Ballast System	C-68
C-2.7	FALCON DOLLY OF THE NCAT TRAIN (NOT USED IN TRACK TESTING)	C-69
C-2.7.1	Pintle Hook, Eye and Drawbar Assembly.....	C-72
C-2.7.2	Fifth Wheel, Fifth wheel mounting and Leaf Spring Characteristics	C-74
C-3	REALIZING A SOLID MODEL OF THE FEDEX EAGLE DOLLY.....	C-75
C-3.1	METHODOLOGY.....	C-75
C-3.2	BILL OF MATERIALS	C-79
C-4	DETAILED DIMENSIONS OF THE TEST VEHICLE.....	C-82

List of Tables

Table C-1. Partial equipment list.....	C-1
Table C-2. Characteristic parameters that will assist in modeling.....	C-2
Table C-3. Tractor and trailer 1 of the LCV train.....	C-9
Table C-4. Dolly 1 and trailer 2 of the LCV train.....	C-11
Table C-5. Dolly 2 (Falcon) and Trailer 3 of the LCV train.	C-13
Table C-6. Basic steer axle related dimensions.....	C-15
Table C-7. Obtained steering ratios from measured angles.	C-17
Table C-8. Equivalent wheelbase calculation (2004 Freightliner).....	C-19
Table C-9. Basic drive axle dimensional properties.	C-24
Table C-10. Drive axle steer coefficients (separated by axle and roll direction).	C-28
Table C-11. Concrete compartment characteristics (calculated weights and volumes).	C-35
Table C-12. Compartment center of gravity measures from the kingpin.....	C-35
Table C-13. Ballast characteristics Trailer 1 (calculated weight and volume).	C-37
Table C-14. Additional ballast center of gravity measured form the kingpin Trailer 1.....	C-37
Table C-15. Combined center of gravity of compartment and ballast Trailer 1.	C-37
Table C-16. Ballast and compartment weight transfer to kingpin and rear axle Trailer 1.....	C-38
Table C-17. Ballast characteristics Trailer 2 (calculated weight and volume).	C-42
Table C-18. Additional ballast center of gravity measured form the kingpin Trailer 2.....	C-42
Table C-19. Ballast weight transfer to kingpin and rear axle Trailer 2.....	C-42
Table C-20. Measured spring stiffness, Trailer 1.....	C-47
Table C-21. Measured roll stiffness, Trailer 1.	C-48
Table C-22. Measured roll steer, Trailer 1.	C-49
Table C-23. Trailer frame and container torsional stiffness.	C-50
Table C-24. Dolly (VIN) Vehicle Identification numbers.....	C-51
Table C-25. NCAT (before it was shortened) and FedEx Eagle dolly fundamental measurement differences.	C-54
Table C-26. Pintle eye dimensional characteristics (FedEx).....	C-57
Table C-27. Basic Leaf Spring Parameters (NCAT vs. FedEx).....	C-61
Table C-28. Eagle Dolly transverse leaf characteristics.....	C-66
Table C-29. Calculated weight distributions.	C-67
Table C-30. Measured weight properties.	C-68
Table C-31. Basic Falcon dolly dimensional properties.....	C-70
Table C-32. Pintle eye dimensional characteristics (Falcon).....	C-74
Table C-33. Detailed Dimensions.	C-83

List of Figures

Figure C-1. Photo. The complete test vehicle at NCAT.....	C-6
Figure C-2. Drawing. Names of the units of the test vehicle.....	C-6
Figure C-3. Diagram.Schematic of the Freightliner dual axle tractor coupled to the first Cheetah chassis.....	C-8
Figure C-4. Diagram.Schematic showing the Eagle A dolly coupled to the second Cheetah chassis. Note: This drawing shows the drawbar length of 96 in. (2438 mm), as it was originally measured. The drawbar was shortened to nominally 72 in. (1829 mm) for the test, to match Eagle S. This dolly was positioned between Trailer 2 and Trailer 3 during the track and highway testing.	C-10
Figure C-5. Diagram. Schematic of the Falcon dolly coupled to the third Cheetah Chassis.....	C-12
Figure C-6. Photo. Left front corner viewed rearward.....	C-15
Figure C-7. Photo. Left front corner showing bump rubber and damper location.....	C-15
Figure C-8. Photo. Left front damper orientation.....	C-16
Figure C-9. Photo. Pitman arm and gearbox.....	C-16
Figure C-10. Photo. Pitman arm.....	C-16
Figure C-11. Photo. Tie rod.	C-17
Figure C-12. Graph. Experimentally measured steer properties.	C-18
Figure C-13. Graph. Calculated 100% Ackerman using the nominal wheelbase (4.763 m).....	C-20
Figure C-14. Graph. Calculated 100% Ackerman characteristics using the equivalent wheelbase (5.102 m).	C-20
Figure C-15. String potentiometer for axle steer measurement.	C-20
Figure C-16. Axle angle measurement potentiometer positioning.	C-20
Figure C-17. Photo. Steer axle height sensor(s).	C-21
Figure C-18. Photo. Tie rod roll steer measurement sensor.	C-21
Figure C-19. Graph. Steer axle roll angle change as a function of roll angle (rotation about Z-axis)....	C-22
Figure C-20. Graph. Steer axle angle change as a function of suspension roll angle plotted as its understeer tendency.	C-22
Figure C-21. Graph. Road wheel steer relative to the steer axle as a function of suspension roll angle.	C-23
Figure C-22. Photo. Drive axle leaf spring front mount.	C-24
Figure C-23. Photo. Drive axle underslung leaf spring mount with damper mounting.	C-24
Figure C-24. Photo. Drive axle leaf spring elements (forward of axle centerline).	C-25
Figure C-25. Photo. Rear Drive axle air bag.	C-25
Figure C-26. Photo. Rear Drive axle air bag and leaf (1 rear view).	C-25
Figure C-27. Photo. Rear Air bag and leaf (2-bottom view).	C-25
Figure C-28. Photo. Drive axle height sensing for roll steer and roll stiffness measurement.	C-26
Figure C-29. Graph. Drive axle roll steer.	C-26

Figure C-30. Photo. Drive axle 2 panhard bar axle connection.....	C-27
Figure C-31. Photo. Drive axle 2 panhard bar frame connection (right frame rail).....	C-27
Figure C-32. Graph. Linear fit of drive axle steer vs. roll angle for CW and CCW roll angles.....	C-27
Figure C-33. Graph. Third order polynomial fit of drive axle roll steer.....	C-28
Figure C-34. Graph. Steer axle vertical spring rate (raw data and linear fit). Measurements (boxes) and linear fit (line).	C-29
Figure C-35. Graph. Measured steer axle vertical spring rates (raw data and linear fits).....	C-29
Figure C-36. Graph. Steer axle roll stiffness with linear regression in the linear region, data and a linear fit.	C-30
Figure C-37. Graph. Body roll stiffness (raw data and Polynomial fit).....	C-30
Figure C-38. Photo. Lower frame flange.	C-31
Figure C-39. Photo. Vertical frame flange with outside to outside dimension displayed.	C-31
Figure C-40. Graph. Torsional Stiffness as Recorded Electronically.....	C-32
Figure C-41. Graph. Tractor torsional stiffness (raw data and polynomial fit).	C-32
Figure C-42. Graph. Comparison of full electronic recording and hand recorded validation data (hand data included tire deflection).....	C-33
Figure C-43. Photo. Trailer 1; concrete filled bulkhead.	C-34
Figure C-44. Photo. Trailer 1; concrete filled bulkhead.	C-34
Figure C-45. Diagram. Trailer 1 schematic for center of gravity calculations.	C-36
Figure C-46. Photo. Highway barrier stacking for trailer ballast, Trailer 1.....	C-36
Figure C-47. Photo. Highway barrier ballast, Trailer 1.....	C-36
Figure C-48. Photo. Interior roof construction, Trailer 1.....	C-38
Figure C-49. Photo. Interior side construction and damage caused by fire, Trailer 1.....	C-38
Figure C-50. Photo. Container box ribs, Trailer 1.....	C-39
Figure C-51. Photo. Fire damage to floor, Trailer 1.	C-39
Figure C-52. Photo. Passenger side view, Trailer 2.	C-39
Figure C-53. Photo. Dolly and trailer configuration, Trailer 2.....	C-39
Figure C-54. Photo. Left front interior corner of container, Trailer 2.....	C-40
Figure C-55. Photo. Left rear interior corner of container, Trailer 2.	C-40
Figure C-56. Photo. Cargo box door, Trailer 2.....	C-40
Figure C-57. Photo. Back rear driver side wall, Trailer 2.	C-40
Figure C-58. Photo. Door configuration, Trailer 2.....	C-41
Figure C-59. Photo. Left side view, Trailer 2.	C-41
Figure C-60. Photo. Highway barrier stacking for trailer ballast, Trailer 2.....	C-41
Figure C-61. Photo. Highway barrier ballast, Trailer 2.....	C-41
Figure C-62. Photo. Trailer 3 rear view.	C-43
Figure C-63. Photo.Trailer 3 door configuration.....	C-43
Figure C-64. Photo. Trailer 3 driver side view.....	C-43
Figure C-65. Photo. Trailer 3 passenger side view.	C-43
Figure C-66. Photo. Dolly and Trailer 3 configurations.	C-44
Figure C-67. Photo. Trailer 3 cargo box attached as designed.	C-44
Figure C-68. Photo. Trailer 3 exterior wall damage.	C-44

Figure C-69. Photo. Falcon dolly and Trailer 3 connection.....	C-44
Figure C-70. Photo. Under carriage view of the Hutchens suspension.....	C-45
Figure C-71. Photo. Right side suspension (front view) showing the fixed-length trailing arm.....	C-45
Figure C-72. Photo. Left side suspension (front view) showing the adjustable-length trailing arm.....	C-45
Figure C-73. Photo. Right side rear trailing arm mounting.....	C-45
Figure C-74. Photo. Right side front trailing arm mounting.....	C-46
Figure C-75. Photo. Right side trailing arm mount and spring height	C-46
Figure C-76. Photo. Right side three leaf spring with mounting brackets displayed.....	C-46
Figure C-77. Photo. Right side rear spring bracket showing clearance.....	C-46
Figure C-78. Graph. Trailer 1 Spring stiffness (Cheetah Chassis).....	C-47
Figure C-79. Graph. Trailer 1 Roll stiffness (Polynomial fit and Linear fit in the linear region).....	C-48
Figure C-80. Graph. Trailer 1 axle roll steer (Cheetah Chassis).....	C-49
Figure C-81. Graph. Torsional Stiffness, Trailer 2.....	C-50
Figure C-82. Photo. Eagle dolly in the NCAT train.....	C-51
Figure C-83. Diagram. FedEx dolly.....	C-52
Figure C-84. Diagram. NCAT Eagle Dolly as measured before it was shortened.....	C-53
Figure C-85. Photo. NCAT dolly drawbar length and attachment.....	C-54
Figure C-86. Photo. NCAT dolly showing attachment connection.....	C-54
Figure C-87. Photo. The pintle hook and eye connection (NCAT).....	C-55
Figure C-88. Photo. Drawbar showing the horizontal orientation of the drawbar and frame (NCAT).....	C-55
Figure C-89. Photo. Top view of the drawbar of the FedEx dolly.....	C-55
Figure C-90. Photo. Rubber mounted pintle eye containment housing with visible retention plates on the FedEx dolly.....	C-56
Figure C-91. Photo. Retention showing 2.5-in. tubular threaded bolt on the FedEx dolly.....	C-56
Figure C-92. Photo. Pintle eye retention nut (FedEx).....	C-56
Figure C-93. Equation. Empirical relation for estimating the elastic modulus of rubber.....	C-57
Figure C-94. Photo. Fifth wheel on the FedEx dolly.....	C-58
Figure C-95. Photo. NCAT Eagle dolly transverse leaf spring.....	C-59
Figure C-96. Photo. NCAT Eagle dolly.....	C-59
Figure C-97. Photo. Mounting system viewed from beneath the FedEx dolly.....	C-59
Figure C-98. Photo. Eagle dolly dual transverse leaf spring spacing (NCAT).....	C-60
Figure C-99. Photo. Leaf Spring rubber end mountings (FedEx).....	C-60
Figure C-100. Photo. Leaf Spring rubber ends mounting (FedEx).....	C-60
Figure C-101. Graph. Silver Eagle-Eagle Dolly Spring specifications.....	C-60
Figure C-102. Graph. Digitized Silver Eagle vertical spring rate.....	C-62
Figure C-103. Photo. Load transfer bracket (FedEx).....	C-63
Figure C-104. Photo. Load transfer bracket (FedEx).....	C-63
Figure C-105. Photo. Load transfer bracket (FedEx).....	C-63
Figure C-106. Photo. Load transfer bracket assembly bottom (FedEx).....	C-63
Figure C-107. Graph. Pitch stiffness of the fifth wheel on the unloaded FedEx dolly.....	C-64
Figure C-108. Graph. Graph. Roll stiffness of the fifth wheel on the unloaded FedEx dolly.....	C-64

Figure C-109. Graph. Vertical spring rate of the fifth wheel on the NCAT Eagle dolly.....	C-65
Figure C-110. Graph. Roll stiffness of the fifth wheel on the loaded NCAT Eagle dolly.....	C-65
Figure C-111. Diagram. FedEx dolly dimensions.....	C-67
Figure C-112. Photo. Weighing the FedEx dolly (axle weights only).....	C-68
Figure C-113. Photo. Weighing the FedEx dolly (tongue weight only).....	C-68
Figure C-114. Diagram. FedEx ballast weight located behind the axle centerline.	C-69
Figure C-115. Photo. FedEx dolly ballast system.	C-69
Figure C-116. Photo. NCAT Eagle Dolly ballast system.	C-69
Figure C-117. Photo. Falcon dolly in the NCAT train.....	C-70
Figure C-118. Diagram. Basic dimensions of Falcon dolly.....	C-71
Figure C-119. Photo. Falcon dolly frame showing flange widths.....	C-72
Figure C-120. Photo. Falcon Dolly frame and flange widths.....	C-72
Figure C-121. Photo. Leaf spring outset from frame rail.	C-72
Figure C-122. Photo. Falcon dolly undercarriage (from front).	C-72
Figure C-123. Photo. Falcon drawbar pintle hook and eye connection.....	C-73
Figure C-124. Photo. Drawbar taper to pintle hook.	C-73
Figure C-125. Photo. Top view Falcon pintle and drawbar.....	C-73
Figure C-126. Photo. Pintle hook and mounting.....	C-74
Figure C-127. Photo. Pintle drawbar extension location and mounting.....	C-74
Figure C-128. Photo. Leaf spring and axle assembly.....	C-74
Figure C-129. Photo. Falcon dolly leaf spring with adjustable trailing arm shown.....	C-74
Figure C-130. Photo. Falcon dolly leaf spring and axle assembly as viewed from rear.....	C-75
Figure C-131. Photo. Leaf spring forward end mount with trailing arm.....	C-75
Figure C-132. Diagram. ATOS scan data automatically transformed into the project using coded reference point markers.....	C-76
Figure C-133. Diagram. Reference point markers shown in green, scan data in red, positive surfaces in grey, and negative surfaces in teal.....	C-76
Figure C-134. Diagram. A post processed point cloud is shown on the left. The resulting polygon mesh with blue edges is shown center and the surface representation on the right.	C-77
Figure C-135. Diagram. Progressive removal of unnecessary points from the mesh to reduce file size.....	C-77
Figure C-136. Illustration. Pro/ENGINEER CAD rendering of the Eagle dolly.....	C-78
Figure C-137. Diagram. CAD assembly imported into the ATOS scan data for model verification.	C-78
Figure C-138. Diagram. CAD model surface deviation to ATOS scan data.....	C-79
Figure C-139. Diagram. Dolly assembly.....	C-79
Figure C-140. Diagram. Dolly frame assembly.....	C-80
Figure C-141. Diagram. Rotating pintle hook assembly.....	C-80
Figure C-142. Diagram. Axle mounting assembly.	C-81
Figure C-143. Diagram. Sprung fifth wheel assembly.....	C-81
Figure C-144. Diagram. Air tank assembly.	C-82
Figure C-145. Diagram. Dual wheel assembly.....	C-82

C-1. Process

Initially procedures for characterizing the National Center for Asphalt Technology (NCAT) trailer train were outlined. A team visited NCAT for the physical measurements three months before the maneuvers.

Prior to the visit a team from Western Michigan University (WMU) developed a test plan, calibrated equipment, and built fixtures for the testing. A simplified list of the equipment used during the characterization effort is shown in Table C-1.

Table C-1. Partial equipment list.

Item	Quantity	Device
1	2	25000 lb load cells
2	6	0-25 inch string potentiometers
3	6	0-62.5 inch string potentiometers (weatherproof)
4	5	0-12 inch string potentiometers
5	1	Mechanical height probe mechanism
5	2	Bridge Amplifiers
6	2	Analog to digital interface cards
7	1	10 inch 9 foot long I beam with stands
8	1	6 inch 83 inch long I beam
9	2	20,000 lb bottle jacks
10	1	Digital inclinometer
11	1	Dial inclinometer
12	3	Power supplies
13	4	Laptop computers
14	3	Dial indicators
		Miscellaneous measuring equipment
		Miscellaneous tools
		Miscellaneous transducer wire

Table C-2. Characteristic parameters that will assist in modeling.

	The characteristics below identify parameters that will assist in modeling and identify the planned approach to obtaining the values. In each case we will "Plot to verify" at the site. All will be done on a "best effort" basis. Safety, available equipment and accuracy will govern to what extent the desired values can be obtained. In some cases the obtained values will be used to validate model obtained values and/or identify differences.		
Value	Procedure	Equipment	Comment
	<i>Note: on axles with air suspension disconnect height control valve</i>		
Wheelbase and track width of every unit in the train	<ol style="list-style-type: none"> 1) Measure all X-axis locations of every unit in the Longer combination vehicle train. 2) Measure center-to-center distances between all tires of each axle set. 	<ul style="list-style-type: none"> • Tape measures and plumb bobs. (WMU) 	
Tire Rolling radius	<ol style="list-style-type: none"> 1) Measure axle centerline to the ground at each axle 	<ul style="list-style-type: none"> • Special fixture (WMU) 	
CG X-Y location of Tractor and basic weight at each axle (connected to train and independent of train)	<ol style="list-style-type: none"> 1) Tractor fueled (or measure fuel and location). Place scales under steer axle tires and drive axle tires of tractor and scales under first trailer axle. Measure and record all scale weights. Verify drive axle spacing and wheelbase 2) Lower landing gear of Trailer 1 and remove all weight from fifth wheel. Record unladen tractor weights (Steer and drives). Lower Trailer 1 onto fifth wheel. Re-record all weights. 	<ul style="list-style-type: none"> • Drive on scales (NCAT) <ul style="list-style-type: none"> ◦ 2-steer axles scales ◦ 2- front dr. axle scales ◦ 2-rear drive axle scales ◦ 2-trailer axle scales 	Could reduce the number of scales by assuming symmetry or measuring each axle separately.
CG of each separate trailer X-Y location and weight at each axle	<ol style="list-style-type: none"> 1) Place scales under drive axle tires of tractor and scales under first trailer axle. Measure and record all scale weights. Measure steer axle to kingpin and kingpin to Trailer 1 axle. 2) Move scales to Dolly 1 and Trailer 2 axle. Measure and record all scale weights. Measure Dolly 1 kingpin to Trailer 2 axle. Measure Trailer Axle 1 to Dolly 1 distance. 3) Move scales to Dolly 2 and Trailer 3 axle. Measure and record all scale weights. Measure Dolly 2 kingpin to Trailer 3 axle. Measure Trailer axle 2 to Dolly 1 distance. 	<ul style="list-style-type: none"> • Drive on Scales (NCAT) • Tape measures (WMU) 	
Suspension Roll Stiffness-trailer	<ol style="list-style-type: none"> 1) Place truck scales under trailer tires. Measure static weight. 2) Attach string pots between frame and axle. Zero readouts. 3) Place HD Screw jacks under frame and remove approx 5000 lb from axle weight. Measure and record jack spacing, string pot spacing, initial frame angle and scale weights each side. 4) Put one turn in and one turn out of jacks. Record string pot displacement and scales weights. 5) Repeat as is possible. 	<ul style="list-style-type: none"> • Drive on scales (NCAT) • String pots (WMU) • Screw type jack stands (WMU) • Tape measures (WMU) • Digital angle finder (WMU) 	

Suspension Roll Stiffness-tractor	<p>Not entirely certain.</p> <ol style="list-style-type: none"> 1) Steer axle can be obtained as above for trailer while removing only 2000 lb. 2) Drive axle can be obtained in similar manner if the trailer can be disconnected or trailer raised so fifth wheel "floats". 	<ul style="list-style-type: none"> • Drive on scales (NCAT) • String pots (WMU) • Screw type jack stands (WMU) • Tape measures (WMU) • Digital angle finder (WMU) • 25, 000 lb load cells with amplifiers (WMU) 	
Tire radial stiffness	<ol style="list-style-type: none"> 1) Place truck scales under tires. Measure static weight. 2) Attach dial indicator between wheel and ground. 3) Place HD Screw jacks under frame and remove approx 1000 lb. 4) Measure and record scale weights each side and dial indicator reading. 5) Add another turn to screw jacks. Repeat as is possible. 	<ul style="list-style-type: none"> • Dial indicators (WMU) • Screw jacks (WMU) • Drive on scales (NCAT) • Air or hydraulic jacks (NCAT) 	
Trailer Vertical suspension stiffness	<ol style="list-style-type: none"> 1) Place truck scales under tires. Measure static weight. 2) Attach string pots between frame and axle. Zero readouts. 3) Place HD Screw jacks under frame and remove approx 1000 lb equally from each wheel load. 4) Measure and record jack spacing, string pot spacing, initial frame height and scale weights each side. 5) One turn in of both jacks (decreasing jack height 1/8 in.). 6) Record string pot displacement and scales weights. 7) Repeat as is possible. 8) Measure wheel track (inner and outer) 9) Measure gap in any overload springs 	<ul style="list-style-type: none"> • String pots (WMU) • Screw jacks (WMU) • Drive on scales (NCAT) • 25,000 lb load cells with amplifiers (WMU) • String pots (WMU) 	The rate obtained will be in one direction only (unloading). Should be able to extrapolate as long as overload springs are not in contact.
Tractor Dr axle -Vertical suspension stiffness	<ol style="list-style-type: none"> 1) Place truck scales under tires. Measure static weight. 2) Disconnect ride height sensor. Attach string pots between frame and axle. Zero readouts. 3) Measure and record initial frame height and scale weights each side. 4) Using trailer landing gear remove approximately 1000 lb from fifth wheel load. 5) Record string pot displacement and scales weights. 6) Repeat as is possible. 	<ul style="list-style-type: none"> • String pots (WMU) • Trailer landing gear • Drive on scales (NCAT) • 25,000 lb load cells (WMU) 	

Tractor Steer axle –Vertical suspension stiffness	<ol style="list-style-type: none"> 1) Place truck scales under tires. Measure static weight. 2) Disconnect ride height sensor. Attach string pots between frame and axle. Zero readouts. 3) Measure and record initial frame height and scale weights each side. 4) Using heavy duty screw jacks raise the frame to remove approx 1000 lb from steer axle. 5) Record string pot displacement and scales weights. 6) Repeat as is possible. 	<ul style="list-style-type: none"> • String pots (WMU) • Trailer landing gear • Drive on scales (NCAT) 	
Auxiliary roll stiffness	From vertical suspension stiffness calculate the spring related suspension roll stiffness. Take difference of Suspension roll stiffness and Spring related roll stiffness.		Calculated from measured values
Roll steer-Trailer axles	<ol style="list-style-type: none"> 1) Same setup as suspension roll stiffness. 2) Add two string pots either forward or rearward of axle or add bar to tire and measure actual change in angle of tire. 3) Zero and proceed as did in roll stiffness measurement. 	<ul style="list-style-type: none"> • String pots for height (WMU) • Screw type jack stands (WMU) • Tape measures (WMU) • String pots for steer with spanner (WMU) • Digital angle finder (WMU) • Horizontal angle finder (WMU) 	
Roll steer-Truck drive axles	<p>Not certain.</p> <ol style="list-style-type: none"> 1) If we can disconnect trailer then procedure will mimic the trailer axle procedure with the screw jacks providing the angular displacement 2) The string pots measuring angle and steer. 	<ul style="list-style-type: none"> • String pots for height ((WMU)) • Screw type jack stands (WMU) • Tape measures (WMU) • String pots for steer with spanner (WMU) • Digital angle finder (WMU) • Horizontal angle protractor (WMU) 	

Steer axle steering gain and Ackerman	<ol style="list-style-type: none"> 1) Measure static toe 2) Wrap string pot around steering shaft (or affix to pitman arm). 3) Connect string pot to steering arm at spindle (alternatively to roadwheel). 4) Place low friction surfaces beneath tires to allow steering. 5) Calibrate with physical measurement. 6) Put steer input into handwheel and measure roadwheel angle. 7) Verify at extreme with physical measurement. 8) Reproduce on opposite wheel in same direction (preferably steering to the left) 9) Repeat steering to right to allow ackerman assessment. 	<ul style="list-style-type: none"> • 5 string pots (WMU) • Low friction turn plates (?? NCAT turn plates?, or homemade) • Horizontal angle protractor (WMU) • Digital angle finder (WMU) 	Most interested in values up to 180 deg of handwheel input. Up to about 8 deg of roadwheel angle. Need to run engine for power assist while measuring.
Roll center heights of each suspension	<ol style="list-style-type: none"> 1) Measure spring hanger heights, spindle centerline and spring axle mount height of steer axle 2) Measure panhard bar heights at frame and at axle for each drive axle 3) Measure spring hanger heights, axle centerline and spring axle mount height of steer axle. 	<ul style="list-style-type: none"> • Tape measures (WMU) 	This will generate what will be approximate roll center heights. Force based roll center heights as obtained in K&C will not be possible.

C-2. Overall Description of the Vehicle

The vehicle consisted of one truck tractor, three semitrailers, and two converter dollies. The tractor was a 6x4 (two drive axle) Freightliner. The three semitrailers were each a Cheetah chassis with a 20-ft (6.1-m) intermodal container. The first trailer was modified by the addition of an extra compartment on the front for ballast. The second and third trailers were essentially identical.



Figure C-1. Photo. The complete test vehicle at NCAT.

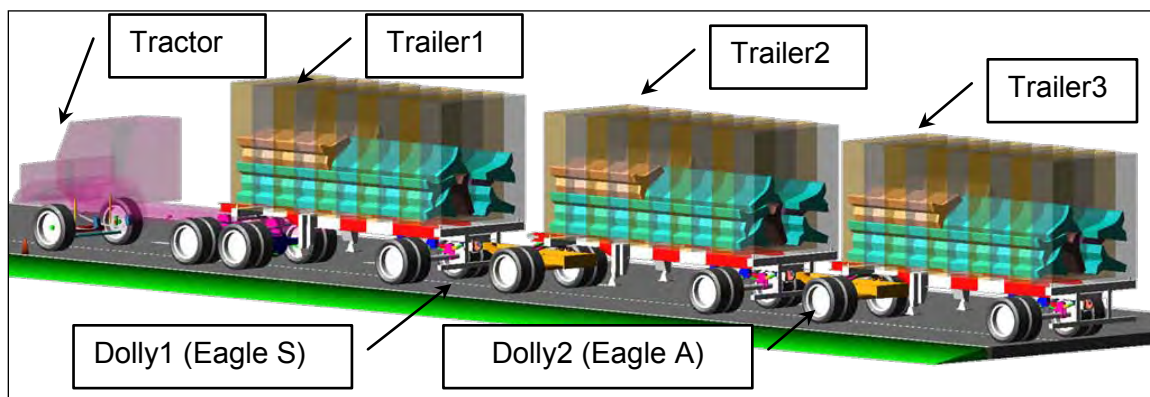


Figure C-2. Drawing. Names of the units of the test vehicle.

Four converter dollies were used in the project. All were manufactured by NTRCI partner Silver Eagle Manufacturing. One of the four was modified, so a total of five dollies appear in this appendix:

- (Original long drawbar) Eagle Dolly. This dolly had been in use at NCAT before this project. It was characterized for this appendix. Before the track testing, its drawbar was

shortened from 2438 mm (96 in.) to 1829 mm (72 in.), to be closer to the size of item (c) on this list

- b) (Modifed) Eagle Dolly. Referred to as Dolly 2 or Eagle A in the main text of this report, it was behind the second trailer during the track testing and on-highway testing. This is the same unit as item (a) on this list, but it has been shortened.
- c) (New) Eagle Dolly. This new dolly was donated to the project by Silver Eagle Manufacturing. Referred to as Dolly 1 or Eagle S in the main text of this report, it was behind the first trailer during the track testing and on-highway testing.
- d) Falcon Dolly. This dolly had been in use by PAVE before this project. It had been modified from its original construction. Its measurements appear in this appendix, but it was not used in the testing on the track or on the highway.
- e) FedEx Dolly. This is an Eagle model dolly made available to the project by FedEx. It differs in many respects from item (c) on this list, as will be noted in C-2.6. It had a wide track, wider frame rail spacing and different pintle hook support system.

In this appendix, the term “Dolly 2” refers to the dolly between the second and third semitrailers, which was item (b) on this list.

C-2.1 Basic Dimensional Parameters for the Longer Combination Vehicle (LCV)

The NCAT triple train consisted of a Freightliner tractor connected to a Cheetah chassis with a modified and weighted cargo container. Connected to the first Cheetah chassis was a Silver Eagle- Eagle model dolly, which was coupled to a second Cheetah chassis. To the second Cheetah chassis was mounted a second weighted container. This second container was primarily weighted with concrete highway barriers. To the second Cheetah chassis with container was coupled a Silver Eagle Falcon model dolly, which appeared to be a non-standard dolly. The Falcon dolly was then coupled to a third Cheetah chassis, to which was mounted a third weighted container.

Figure C-1 displays a simple schematic of the first two vehicles in the train. Accompanying the schematic are the basic width and length properties of the two vehicles. Table C-3 provides additional measurement values for the tractor and the first trailer in the train. Figure C-4 is a schematic of the next two elements in the train, which are the Eagle dolly and the second Cheetah chassis with its container. Table C-4 provides additional measurement values for the Eagle dolly coupled to the second trailer in the train. Figure C-5 outlines the properties of the final two elements in the vehicle train, which are the Falcon dolly coupled to the final Cheetah chassis onto which was mounted the third container box. Table C-5 provides additional measurements for the Falcon dolly coupled to the third trailer in the train.

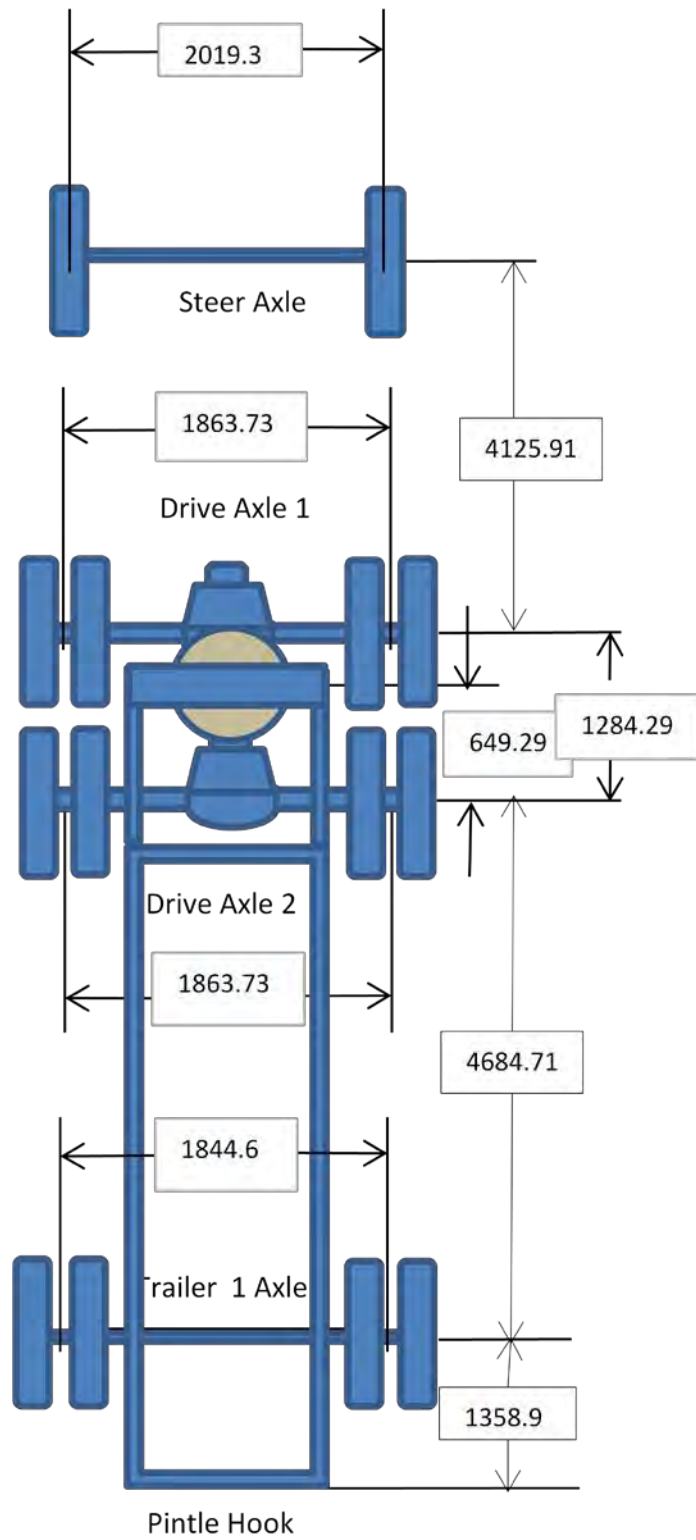


Figure C-3. Diagram.Schematic of the Freightliner dual axle tractor coupled to the first Cheetah chassis.

Table C-3. Tractor and trailer 1 of the LCV train.

Tractor and Trailer Component Locations								
LCV Geometry		Note: Origin for all measurements is the center of the front bumper of the tractor						
		X-axis		Y-axis		Z-axis		comments
Tractor		in	mm	in	mm	in	mm	
front bumper		0	0.0	0	0	0	0	
steer axle	40 1/16	1017.6		0	0			
Steer Axle ground Clearance						10 3/8	263.525	From ground to bottom of axle, axle has a beam drop
steer axle track width				79 1/2	2019.3			
drive axle 1	202 1/2	5143.5		0	0	18 1/2	469.9	
drive axle 1 track width				73 3/8	1863.7			
drive axle 2	253 1/16	6427.8		0	0	18 1/2	469.9	
drive axle 2 track width				73 3/8	1863.7			
fifth wheel Center	227 1/2	5778.5		0	0	46 1/2	1181.1	
rear of tractor	273	6934.2		0	0			
Trailer 1								
King pin	227 1/2	5778.5		0	0	46 1/2	1181.1	Height is to king-pin platform which rests on the fifth wheel
front of container	253 1/2	6438.9		96	2438.4			y-axis is container width and z
landing gear	314 1/2	7988.3		66	1676.4	12 3/4	323.85	y-axis is outside to outside
trailer 1 axle	437 1/2	11112.5		0	0	18 1/2	469.9	
trailer axle 1 track width				72 5/8	1844.7			
rear of trailer	491	12471.4		96	2438.4	39 1/4	996.95	y-axis denotes bumper width
pintle hook	491	12471.4		0	0	30 1/2	774.7	to center of lower jaw
Cargo Container 1								
length	228	5791.2			0			
width				96	2438.4			
box height					0	102	2590.8	
volume (in^3)	2232576							
side wall thickness	0.093	2.4						Best measurement

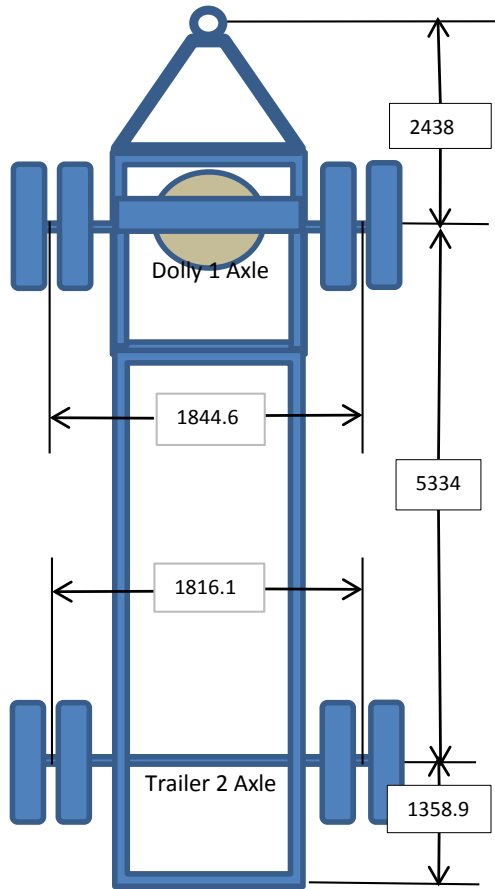


Figure C-4. Diagram.Schematic showing the Eagle A dolly coupled to the second Cheetah chassis. Note: This drawing shows the drawbar length of 96 in. (2438 mm), as it was originally measured. The drawbar was shortened to nominally 72 in. (1829 mm) for the test, to match Eagle S. This dolly was positioned between Trailer 2 and Trailer 3 during the track and highway testing.

Table C-4. Dolly 1 and trailer 2 of the LCV train.

Tractor Trailer Component Locations – Eagle dolly, Trailer 2								
LCV Geometry		Note: Origin for all measurements is the center of the front bumper of the tractor						
		X-axis		Y-axis		Z-axis		comments
		in.	mm	in.	mm	in.	mm	
	pintle eye	491	12471.4	0	0	30 1/2	774.7	
	fifth wheel attachment	584 5/8	14849.5	0	0	42 7/16	1077.9	
	dolly axle	584 5/8	14849.5		0	18 5/16	465.1	
	dolly track width			72 5/8	1844.7			
	rear of dolly	618 5/8	15713.1	37 1/2	952.5			
	Trailer 2							
	king pin	584 5/8	14849.5					
	front of container	610 5/8	15509.9	96	2438.4	46.5	1181.1	Height is to king-pin platform which rests on the fifth wheel
	landing gear	671 5/8	17059.3	33.5	850.9	18	457.2	y-axis denotes length
	trailer 2 axle	794 5/8	20183.5	0	0	18.5	469.9	
	trailer 2 track width			71.5	1816.1			
	rear of trailer	848 1/8	21542.4	96	2438.4	39.25	996.95	y-axis denotes width of trailer
	pintle hook	848 1/8	21542.4	0	0	30.5	774.7	
	Cargo Container 2							
	length	228	5791.2					
	width			96	2438.4			
	height off frame					102	2590.8	
	volume (in^3)	2232576						
	side wall thickness	0.093	2.36					Best measurement

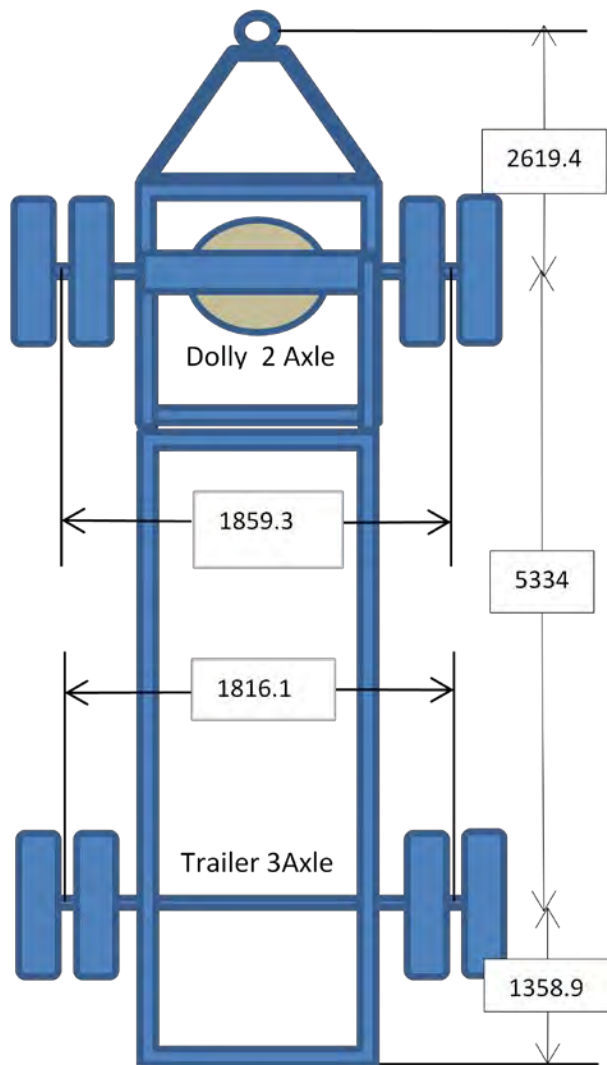


Figure C-5. Diagram. Schematic of the Falcon dolly coupled to the third Cheetah Chassis.

Table C-5. Dolly 2 (Falcon) and Trailer 3 of the LCV train.

Tractor Trailer Component Locations – Falcon Dolly and Trailer 3									
LCV Geometry		Note: Origin for all measurements is the center of the front bumper of the tractor							
		X-axis		Y-axis		Z-axis		comments	
		X-axis		Y-axis		Z-axis			
		in.	mm	in.	mm	in.	mm		
Dolly 2 (Falcon)									
pintle eye	848 1/8	21542.4	0	0	30.5	774.7			
dolly axle	951 1/4	24161.8	0	0	18.5	469.9			
fifth wheel/ Kingpin centerpoint	952 3/8	24190.3	0	0	43	1092.2			
dolly track width			73.2	1859.28					
rear of dolly	978 1/2	24853.9	0	0	20.8	528.32			
Trailer 3									
king pin	952 3/8	24190.3	0	0	30.5	774.7			
front of container	978 3/8	24850.7	96	2438.4	46.5	1181.1	y-axis denotes width		
landing gear	1039 3/8	26400.1	33.5	850.9	18	457.2			
trailer 3 axle	1162 3/8	29524.3	85	2159	18.5	469.9	y-axis denotes width		
trailer 3 track width			72.3	1836.4					
rear of trailer	1215.875	30883.2	96	2438.4	39.3	998.22			
pintle hook	1181	29997.4	0	0	30.5	774.7			
Cargo Container 3									
length	228	5791.2							
width			96	2438.4					
height					102	2590.8			
volume (in. ³)	2232576								
side wall thickness	0.093	2.36					Best measurement		

C-2.2 Freightliner Tractor Chassis

ID tractor: 2004 Freightliner “Day cab design”

VIN: IFUJ86CK44LM93888

C-2.2.1 Summary Tractor Information provided by NCAT

- Model Year – 2004
- GVW – 52,000
- Engine – Minimum 14.0 Liter 435HP @ 2100 RPM 1650 LB/FT Torque
- Transmission – Eaton Fuller RTOC-16909A
- Transmission – Convert transmission to 13-speed at 500,000 miles (Provide total price for parts and labor as a separate line item)
- Front Axle – Dana Spicer E-1200I 3.5” Drop Front Axle rated at 12,000 LB
- Front Brakes – Dana Spicer 15 x 4L ES LMS Extended Lube front brakes
- Front Suspension – 12,000 LB Taper-Leaf
- Rear Axle – Dana Spicer DSH40 rated at 40,000 LB
- Rear Axle Ratio – 3.70
- Main Driveline – Dana Spicer SPL250HD
- Inter-axle Driveline – Dana Spicer SPL170 XL
- Inter-axle Lockout – To include indicator light
- Rear Brakes – Dana Spicer 16.5x7L LMS extended lube
- Rear Suspension – Airliner 40,000 LB extra duty
- Rear Shock Absorbers – Both axles
- Wheelbase – 187”
- Frame – 7/16” x 3-11/16” x 11-1/8” steel frame with a ¼” full C-Channel frame reinforcement with a minimum RBM rating 3,432,000 lbf-in per rail
- Frame Overhang – Minimum of 57 inches
- Clear Frame Rails 30” back of cab for cab guard mounting
- Air Slide fifth Wheel – 24” with a vertical load capacity of 70,000 lbs and a trailing load capacity of 200,000 lbs
- Fuel Tank – 100-gallon aluminum right hand mounted fuel tank
- Front Tires – 275/80R 22.5 14 PLY Michelin XZA2
- Front Wheels – Aluminum 10-Hub Pilot
- Rear Tires – 275/80R 22.5 14 PLY Michelin XDA H/T
- Rear Wheels – 10-Hub Pilot 5-hand steel wheels
- Cab – Minimum of 120” conventional cab
- Cab Mounts – Air ride

C-2.2.2 2004 Freightliner Front Steer Axle

The front steer axle is of a Dana Spicer design with a 3.5 inch drop and is rated at 12,000 lb. capacity. The steer axle uses two longitudinal leaf springs with a rear spring shackle to allow for longitudinal expansion as the spring is compressed. Each side is designed with two leafs forward

of the axle and one leaf connecting between the axle and the shackle. A limited number of defining characteristics are shown in Table C-6.

Table C-6. Basic steer axle related dimensions.

Component	Component Dimension	
	inch	mm
Steer axle track width	79.5	2019
Outside to outside tire span	89	2261
Leaf spring span	35 1/8	838
Individual leaf width	3 7/8	98.4
Frame rail spacing (outside-outside)	34 1/2	876
Pitman arm length	10 ¾	273
Drag Link length	32 ¼	819
Tie rod length	66 7/16	1688
Steer arm length at wheel		
Kingpin-kingpin	69	1753
Bump stop span	34 1/4	876
Bump stop to frame clearance	2.5	6.35

Shown in Figure C-6 and Figure C-7 are steer axle damper locations and orientations. The steer axle dampers are essentially vertical with a rearward positioning to the axle centerline. Note the bump stop location.



Figure C-6. Photo. Left front corner viewed rearward.



Figure C-7. Photo. Left front corner showing bump rubber and damper location.



Figure C-8. Photo. Left front damper orientation.

C-2.2.3 Pitman Arm, Drag Link, Steer Arm and Linkage

The recirculating ball steering gear (Figure C-9) drives a 273 mm pitman arm (Figure C-10) to change the rotational motion of the hand wheel to linear translation. Through a drag link, steer arms, and tie rod (Figure C-11), the system produces an overall ratio of 20.3:1 between the hand wheel and the road wheel. The experimentally obtained ratios are shown in Figure C-12 and in Table C-7. The graph shows the effective ratio due to the Ackerman relationships.



Figure C-9. Photo. Pitman arm and gearbox.



Figure C-10. Photo. Pitman arm.



Figure C-11. Photo. Tie rod.

C-2.2.3.1 Ackerman Steer Behavior

The steer characteristics of the steer axle tires were measured. Plotted in Figure C-12 is the experimentally measured steer behavior. Plotted in Figure C-13 and Figure C-14 are the calculated 100% Ackerman values for the tractor using the nominal wheelbase (steer axle to centerline of the drive axles) and the equivalent wheelbase (steer axle to the theoretical centerline based on tire cornering stiffness and drive axle spacing).

The overall steering ratio, hand wheel to road wheel, was determined to be 20.3:1 as shown in Table C-7.

Table C-7. Obtained steering ratios from measured angles.

	Regression		Ratio	
Inside	0.0527	X	18.975	:1
Outside	0.0461	X	21.692	:1
Average			20.3	:1

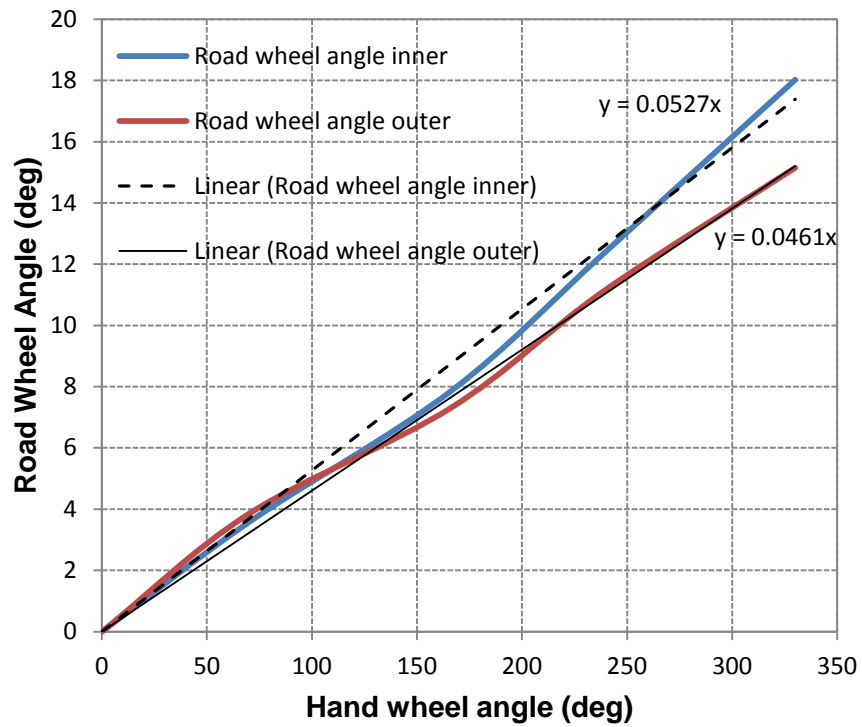


Figure C-12. Graph. Experimentally measured steer properties.

The percentage Ackerman is a function of the wheelbase. The wheelbase can be explained in a variety of ways where the customary definition is the longitudinal measurement between the steer axle and the centerline between the two drive axles, which is herein referred to as “nominal wheelbase.” A second definition is the longitudinal distance between the steer axle and the rotation center between the two drive axles, which takes into account the cornering stiffness of the tires and the axle spacing and which is herein referred to as “equivalent wheelbase.” Table C-8 presents the equivalent wheelbase calculation and demonstrates a wheelbase that is approximately 0.340 m (13.37 inches) longer than the measured nominal wheelbase. Since percentage Ackerman is influenced by the wheelbase, both are presented.

Table C-8. Equivalent wheelbase calculation (2004 Freightliner).

Equivalent Wheelbase		
Steer Axle to Drive Axle 1 spacing	4.115 m	162.0 in
Steer Axle to Drive Axle 2 spacing	5.410 m	213.0 in
Number of Drive axles	2	
Steer axle to average of Dr Axle positions	4.763 m	187.500 in
Length rearmost drive axle to rear drive Axle center (delta)	0.6475 m ²	25.492 in
Tandem factor (T) =	0.419 m ²	649.8 in ²
Cornering Stiffness of Steer tires	3500 N/deg	785 lb/deg
	200550 N/rad	44976 lb/rad
Number of Tires on Steer axle	2	
Number of Tires per drive axle	4	
Cornering Stiffness Drive Tires	2500 N/deg	561 lb/deg
	143250 N/rad	32125 lb/rad
Cornering stiffness factor =	3.857	3.857
T/I ² =	0.018485	0.018485
Equivalent Wheelbase	5.102 m	200.9 in
L _{equiv} -L _{cust} =	0.340 m	13.37 in

Figure C-13 and Figure C-14 present the calculated relationship between the hand wheel angle and the road wheel angle for both the nominal and the equivalent wheelbase cases. The steer characteristic measured for the tractor is close to true Ackerman geometry.

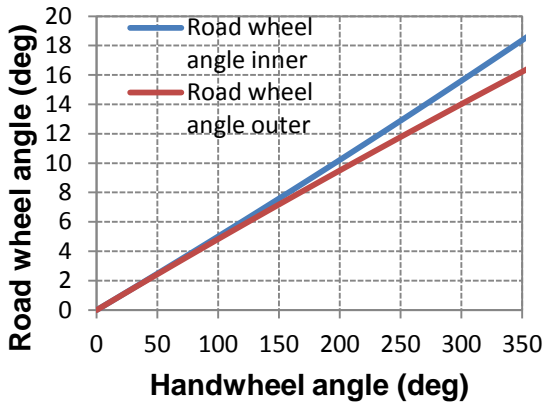


Figure C-13. Graph. Calculated 100% Ackerman using the nominal wheelbase (4.763 m).

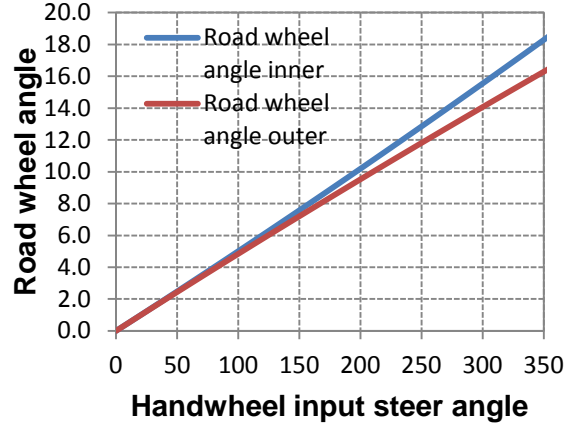


Figure C-14. Graph. Calculated 100% Ackerman characteristics using the equivalent wheelbase (5.102 m).

C-2.2.3.2 Steer Axle Roll Steer Behavior

Roll steer of the front axle was measured in two steps. The first step involved determining the axle angle change, relative to the longitudinal axis of the vehicle, as a function of roll angle, as shown in Figure C-15 and Figure C-16. The plots for these measurements are presented in Figure C-19 and Figure C-20.



Figure C-15. String potentiometer for axle steer measurement.



Figure C-16. Axle angle measurement potentiometer positioning.

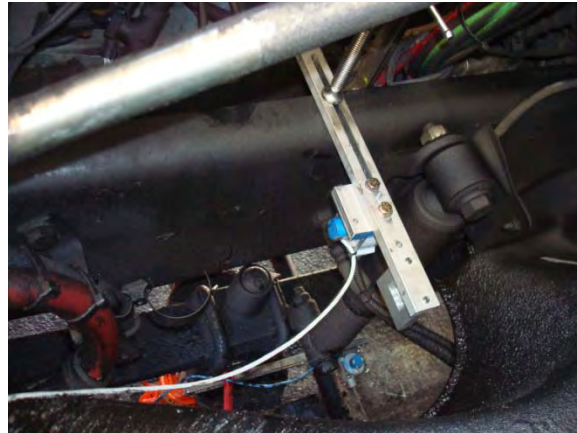


Figure C-17. Photo. Steer axle height sensor(s).

The second step was to determine the tire angle change relative to the axle as a function of roll angle. These two measurements (axle angle change – Figure C-16 and road wheel angle change relative to the axle – Figure C-18) were then combined to establish the total roll steer of the steer axle. To establish the values, the axle was independently drooped left and right where droop left can be interpreted as clockwise roll (CWR) and droop right can be interpreted as counter clockwise roll (CCWR). The axle was drooped by adjusting the jack height screws.



Figure C-18. Photo. Tie rod roll steer measurement sensor.

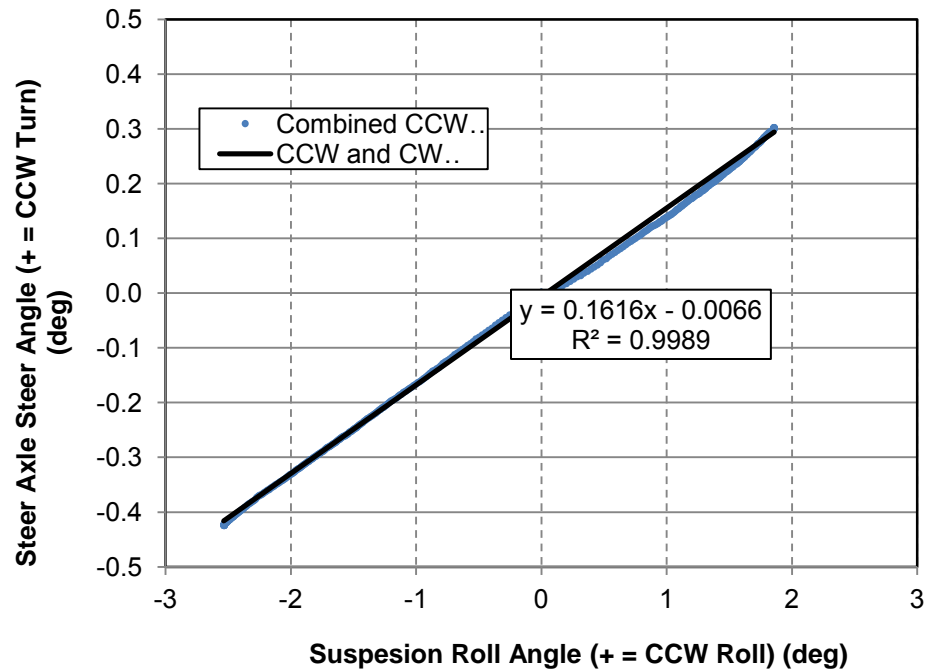


Figure C-19. Graph. Steer axle roll angle change as a function of roll angle (rotation about Z-axis).

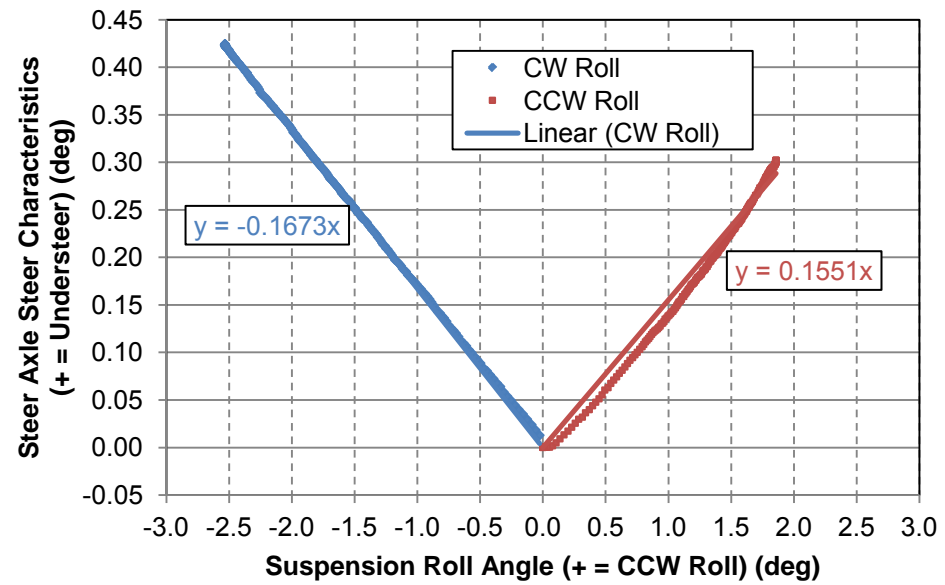


Figure C-20. Graph. Steer axle angle change as a function of suspension roll angle plotted as its understeer tendency.

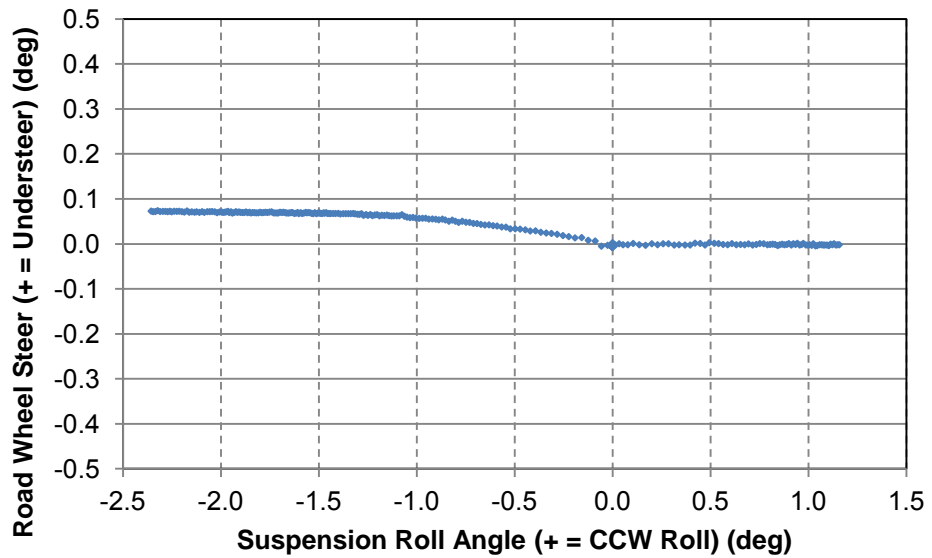


Figure C-21. Graph. Road wheel steer relative to the steer axle as a function of suspension roll angle.

Figure C-21 indicates that additional understeer is added as the left side goes through droop with little effect when the right side experiences droop.

C-2.2.4 Drive Axle Characteristics

The drive axles are Dana Spicer DSH40 axles rated at 40,000 LB for the pair. The air suspension is the Airliner design with basic parameters defined in Table C-9.

Table C-9. Basic drive axle dimensional properties.

Drive Axle Component	Component dimension	
	inch	mm
Drive axle track width	72 1/4	1835
Air bag span	31	787
Frame rail spacing (outside-outside)	34 1/2	876
Leaf spring span	40 1/2	1029
Outside tire to outside tire (bulge-bulge)	95	2413
Spring hanger to axle centerline (longitudinal)	31	787
Air bag to axle centerline (longitudinal)	13	330
Kinematic motion ratio of airbags	1.42 :1	
Axle bump stop spacing	46	1168
Damper to axle centerline distance	4 1/2	114
Damper inclination angle (rearward at top)	80 deg	
Kinematic motion ratio of dampers	1.13:1	

Figure C-22, Figure C-23, and Figure C-24 present the drive axle mounting system and configuration. Figure C-25, Figure C-26, and Figure C-27 show the airbag mounting and the airbag to leaf spring interface. Figure C-27 shows the angled lower leaf spring through which the airbag imparts its deflection characteristics.



Figure C-22. Photo. Drive axle leaf spring front mount.



Figure C-23. Photo. Drive axle underslung leaf spring mount with damper mounting.



Figure C-24. Photo. Drive axle leaf spring elements (forward of axle centerline).



Figure C-25. Photo. Rear Drive axle air bag.



Figure C-26. Photo. Rear Drive axle air bag and leaf (1 rear view).



Figure C-27. Photo. Rear Air bag and leaf (2-bottom view).

C-2.2.4.1 Drive axle Roll Steer Behavior

Drive axle roll steer was measured using a pair of string potentiometers mounted between the frame rails and the axle for height and roll measurement, as shown in Figure C-28. An additional pair of string potentiometers were mounted aft of the axle in the horizontal plane. The horizontal string potentiometers were used to measure longitudinal and angular change of the axle in the range of travel. The rearmost drive axle (drive axle 2) was used for measurement. The results of the angular change with roll angle are plotted in Figure C-29.



Figure C-28. Photo. Drive axle height sensing for roll steer and roll stiffness measurement.

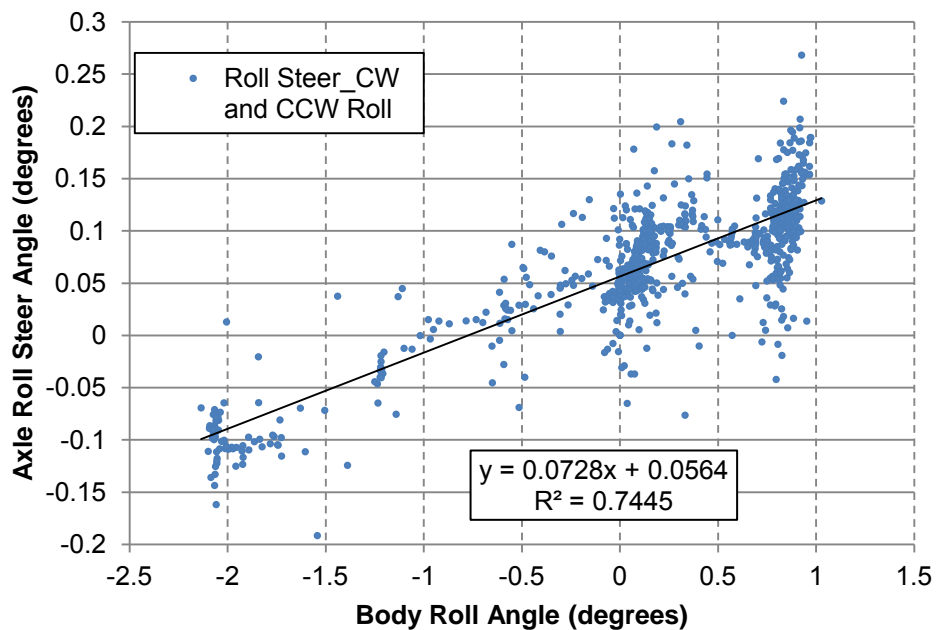


Figure C-29. Graph. Drive axle roll steer.

Figure C-32 separates the displacements in clockwise (CW) and counter clockwise (CCW) roll to show that; 1) each produces a roll understeer and 2) there exists some asymmetry between CW and CCW roll. This asymmetry is the result of the panhard rod orientation. On the second drive axle, which was the measured axle, the panhard rod connects between the left side of the drive axle housing and the right frame rail, as shown in Figure C-30 and Figure C-31. Conversely the first drive axle has its panhard rod connected to the left frame rail.



Figure C-30. Photo. Drive axle 2 panhard bar axle connection.



Figure C-31. Photo. Drive axle 2 panhard bar frame connection (right frame rail).

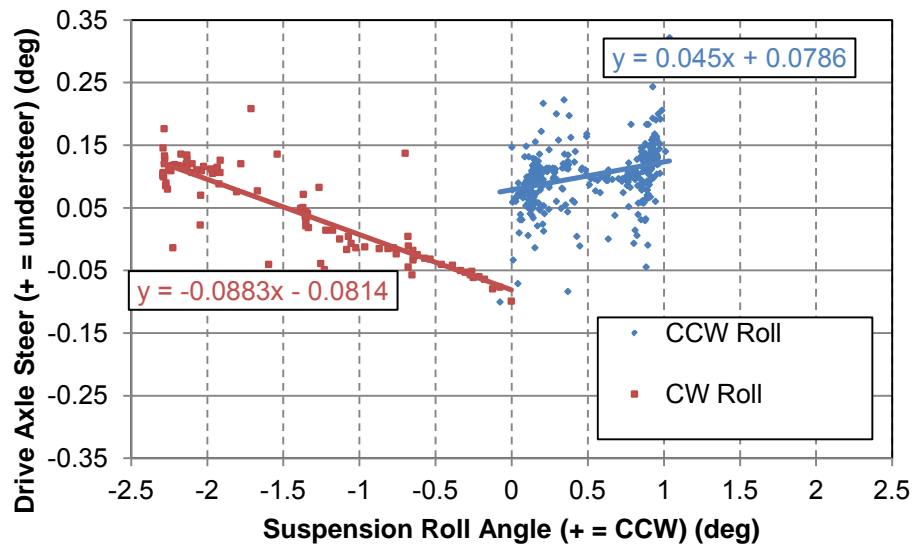


Figure C-32. Graph. Linear fit of drive axle steer vs. roll angle for CW and CCW roll angles.

The different panhard directions between the first drive axle (left frame rail) and the second drive axle (right frame rail) basically cause the first drive axle to have a similar response with the asymmetries reversed, as indicated in Table C-10. The drive axle geometry primarily demonstrates understeer.

**Table C-10. Drive axle steer coefficients
(separated by axle and roll direction).**

Drive axle 2 linear steer characteristics		
	Steer coefficient	
CW roll	-0.0883	Deg/deg
CCW roll	0.045	Deg/deg
Drive axle 1 steer characteristics (est.)		
CW roll	-0.045	Deg/deg
CCW roll	0.0883	Deg/deg

Figure C-33 presents a polynomial fit of the drive axle steer for Axle 2.

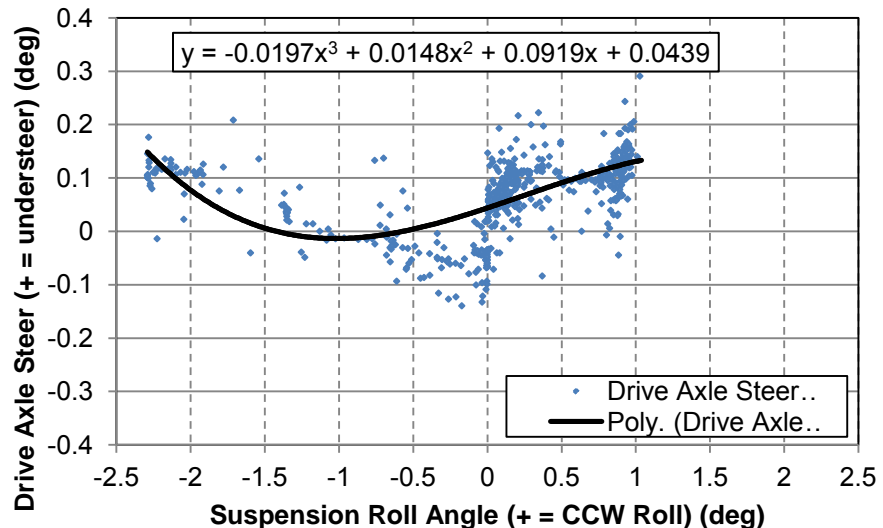


Figure C-33. Graph. Third order polynomial fit of drive axle roll steer.

C-2.2.5 Steer Axle Measured Spring Ride Rates and Roll Rates

To evaluate the steer axle suspension vertical and roll stiffness, the tractor frame was supported with rigid supports. Hydraulic jacks acting through loads cells were accurately spaced under the suspension springs and the deflection and roll properties of the axle were measured against displacement measured through string potentiometers. The vertical suspension results are plotted in Figure C-34 and Figure C-35. Figure C-37 and Figure C-37 present the axle roll stiffness as linear and polynomial regressions.

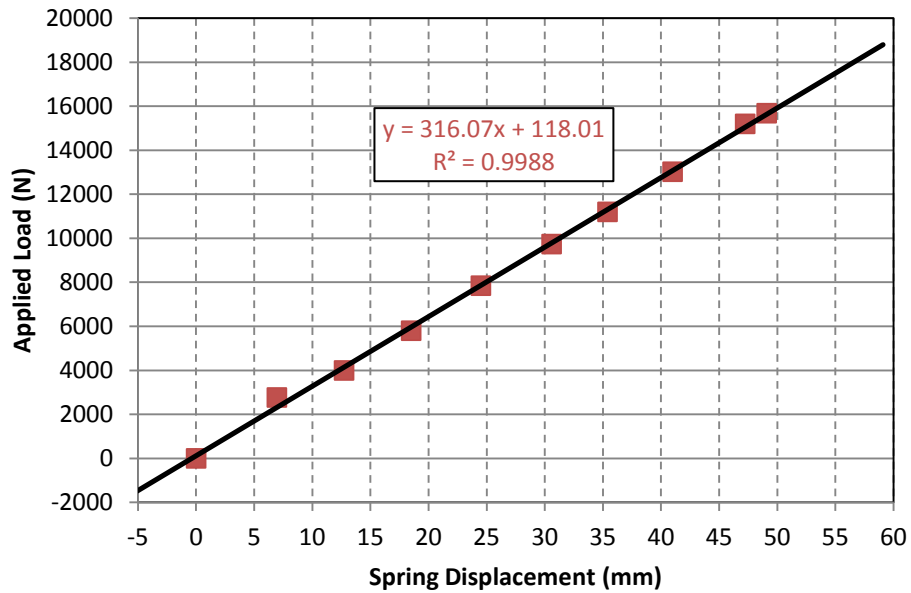


Figure C-34. Graph. Steer axle vertical spring rate (raw data and linear fit). Measurements (boxes) and linear fit (line).

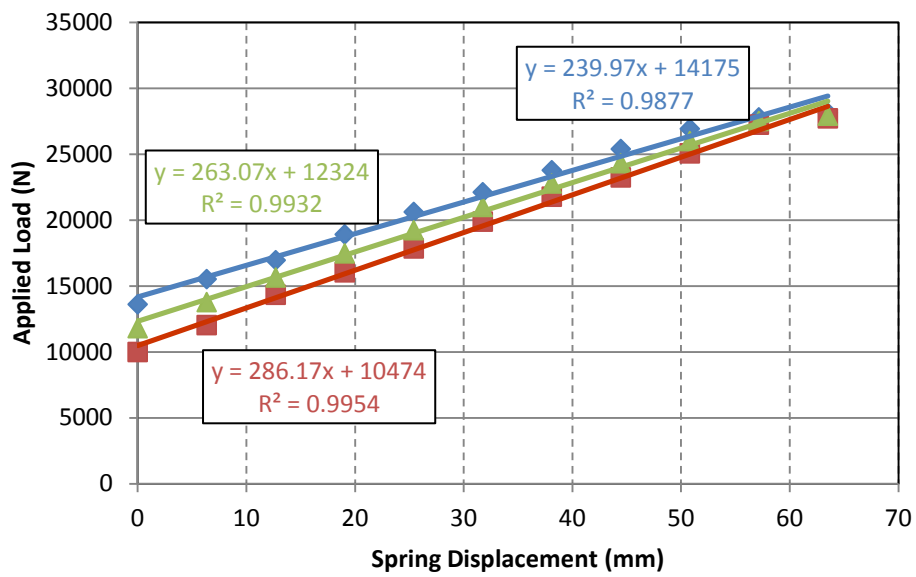


Figure C-35. Graph. Measured steer axle vertical spring rates (raw data and linear fits).

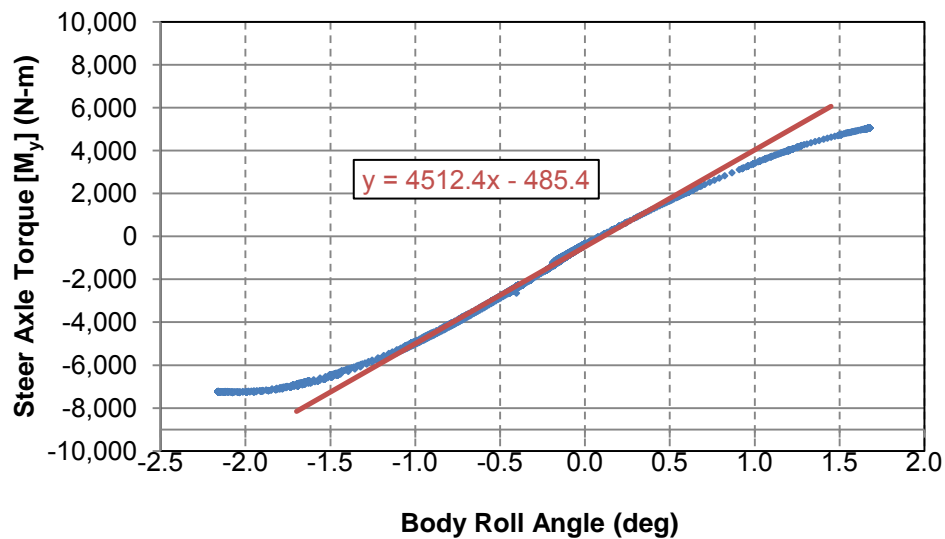


Figure C-36. Graph. Steer axle roll stiffness with linear regression in the linear region, data and a linear fit.

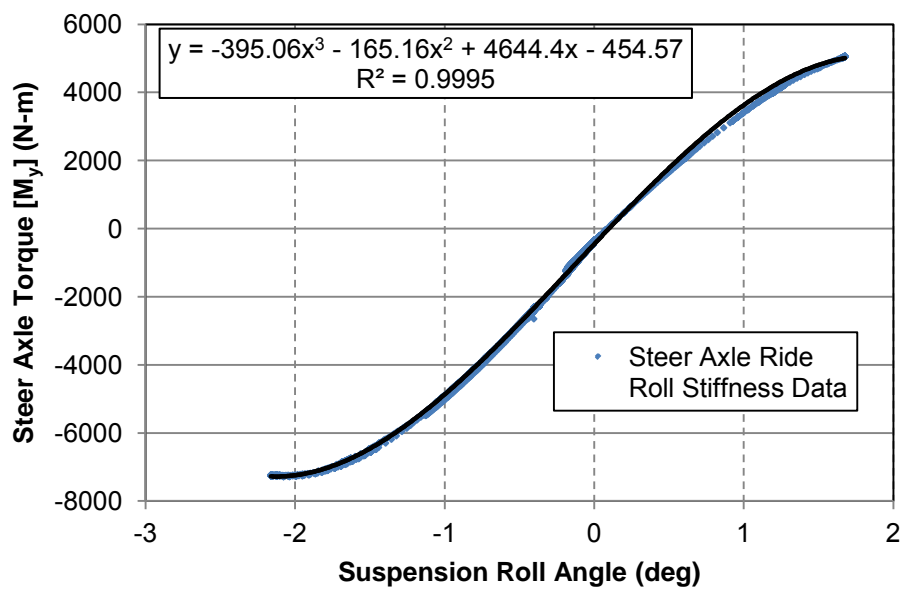


Figure C-37. Graph. Body roll stiffness (raw data and Polynomial fit).

C-2.2.6 Tractor Frame Geometry and Stiffness

The Freightliner chassis is a double wall frame structure, as shown in Figure C-38 and Figure C-39. Figure C-39 displays the frame section thickness and the outside-outside frame rail spacing. The tractor frame is described in the Freightliner supplied information as follows: Frame – 7/16" x 3-11/16" x 11-1/8" steel frame with a 1/4" full C-Channel frame reinforcement with a minimum RBM (resistance to bending moment) rating 3,432,000 lbf-in. per rail.



Figure C-38. Photo. Lower frame flange.



Figure C-39. Photo. Vertical frame flange with outside to outside dimension displayed.

C-2.2.6.1 Tractor Frame Torsional Stiffness

The tractor frame was analyzed by raising and supporting the frame between drive axle 1 and drive axle 2 to establish the rear rigid points. The steer axle was blocked between the axle and the frame, directly over the leaf springs. Loads cells and heavy duty hydraulic jacks were placed under the steer axle, and string potentiometers were connected between the tractor frame and ground. Displacement was introduced, in opposite directions on each side of the vehicle, to introduce a torque at the steer axle, which was directly imparted to the frame. Both physical measurement of the displacement and electronic monitoring were used to assure valid results.

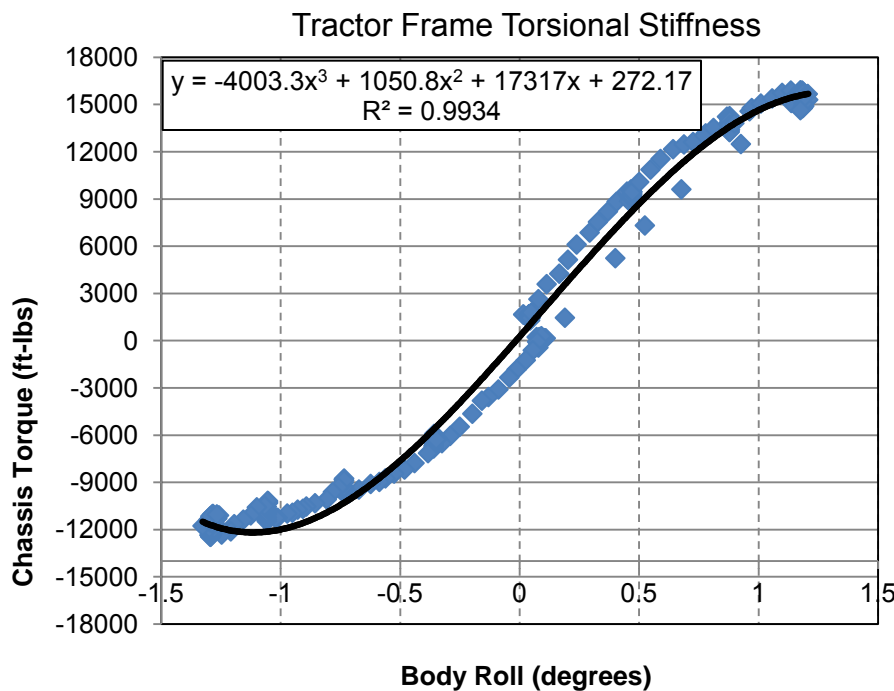


Figure C-40. Graph. Torsional Stiffness as Recorded Electronically.

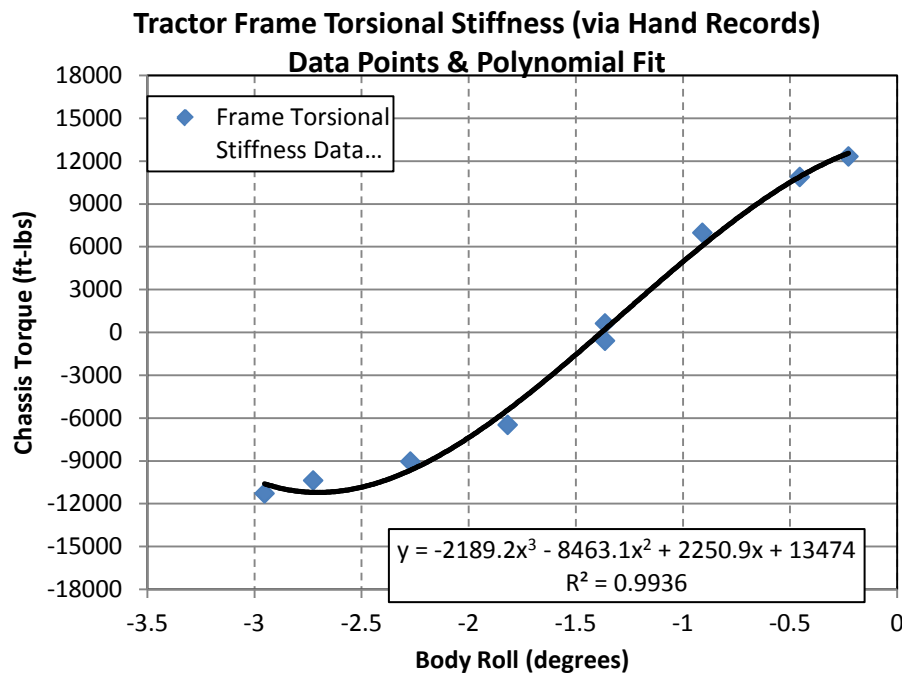


Figure C-41. Graph. Tractor torsional stiffness (raw data and polynomial fit).

**Frame Torsional Stiffness Data, electronic vs.
Hand Records (Frame + Tire Torsional Stiffness) Data**

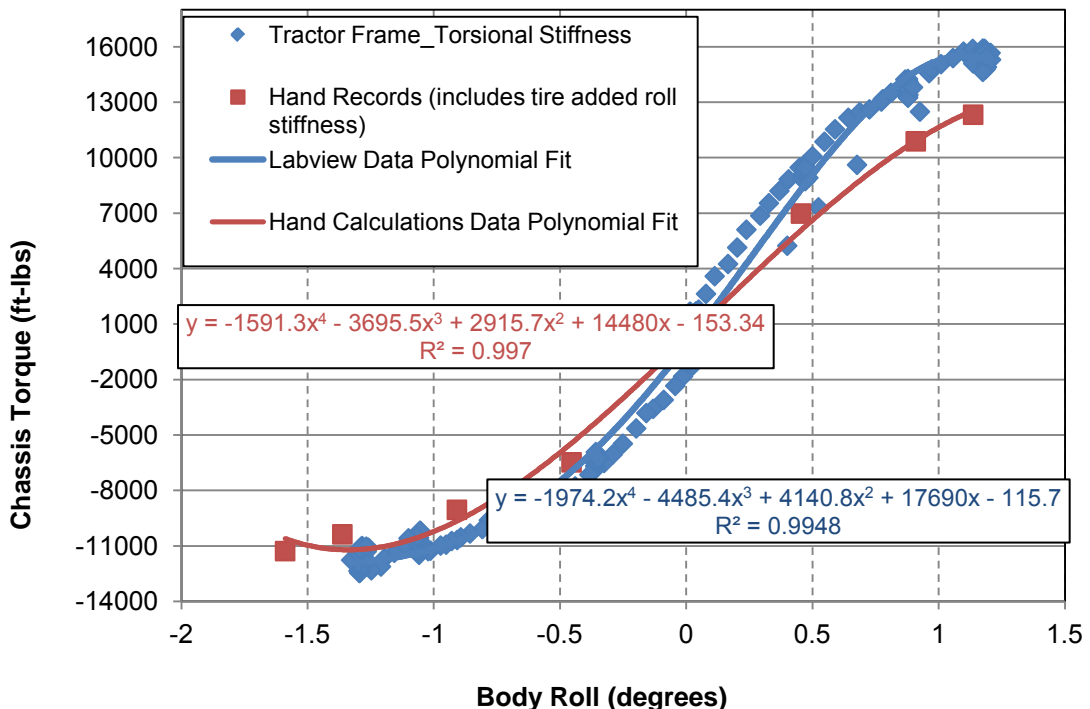


Figure C-42. Graph. Comparison of full electronic recording and hand recorded validation data (hand data included tire deflection).

C-2.3 Trailer 1

VIN: 5EFISC23X5B760932

C-2.3.1 Concrete Compartment Characteristics

Trailer 1 is directly coupled to the tractor fifth wheel. This particular trailer has a welded compartment mounted to the front of the container box, as shown in Figure C-43 and Figure C-44. The compartment is constructed of 9.53 mm (3/8 in.) thick steel and is welded to the container as well as welded to the container chassis.



Figure C-43. Photo. Trailer 1; concrete filled bulkhead.



Figure C-44. Photo. Trailer 1; concrete filled bulkhead.

From a top view the compartment is trapezoidal in shape with a width of 2438 mm at the container interface and a width of 1219 mm at the most forward location. The compartment extends beyond the front of the container a distance of 1092 mm. The compartment has an 1829 mm (72 in) height and is concrete filled to a depth of 1676 mm (66 in). The measured dimensions, calculated volumes, and calculated weights are shown in Table C-11.

Table C-11. Concrete compartment characteristics (calculated weights and volumes).

Concrete Compartment Characteristics											
X dimension				Y dimension				Z dimension			
1092	mm	43	in	1219	mm	48	in	1829	mm	72	in
				2438	mm	96	in	1676	mm	66	in
Steel plate thickness								Material volumes			
Steel plate thickness			9.53	mm	0.375	in	0.13	m ³	7641	in ³	Volume of steel
							3.35	m ³	204336	in ³	Volume of concrete
							3.47	m ³	211977	in ³	Estimated total volume
Material densities (estimated)								Material weights			
Steel density		7700	kg/m ³	0.284	lbs/in ³		964	kg	2170.0	lbs	Weight of steel
Concrete density		2160	kg/m ³	0.078	lbs/in ³		7233	kg	15889.2	lbs	Weight of concrete
							8197	kg	18059.2	lbs	Estimated total weight

The location of the center of gravity of the concrete compartment measured from the top of the frame rail at the kingpin location is shown in Table C-12 and Figure C-45.

Table C-12. Compartment center of gravity measures from the kingpin.

CG Characteristics Concrete Compartment (measured from the top of the frame rail @ kingpin location)											
X dimension				Y dimension				Z dimension			
216	mm	8.5	in	0	mm	0	in	775	mm	30.5	in
175	mm	6.9	in	0	mm	0	in	838	mm	33.0	in
180	mm	7.1	in	0	mm	0	in	831	mm	32.7	in
											Estimated CG Comp.

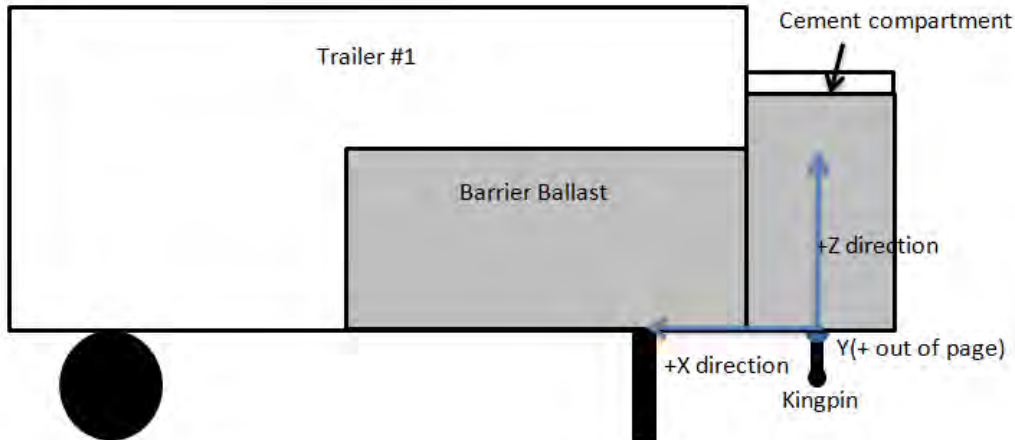


Figure C-45. Diagram. Trailer 1 schematic for center of gravity calculations.

C-2.3.1.1 Additional Ballast Characteristics

Additional ballast, made up of concrete highway barriers, was placed within the container box as shown in Figure C-46 and Figure C-47.



Figure C-46. Photo. Highway barrier stacking for trailer ballast, Trailer 1.



Figure C-47. Photo. Highway barrier ballast, Trailer 1.

The ballast measured dimension, calculated volume, and estimated weight are shown in Table C-13.

Table C-13. Ballast characteristics Trailer 1 (calculated weight and volume).

Ballast Characteristics Trailer 1											
X dimension (Height)			Y dimension (Width)			Z dimension (Length)					
813	mm	32	in	610	mm	24	in	3048	mm	120	in
Cross section area						Material volume					
Cross section area	0.17	m ²		268.4	in ²		0.53	m ³	32208	in ³	Volume of 1 barrier
Number of barriers						Material weights					
Number of barriers				7	units		1996	kg	4400	lbs	Weight of 1 barrier
							13971	kg	30800	lbs	Ballast total weight

The estimated location of the center of gravity of the ballast measured from the top of the frame rail at the kingpin location is shown in Table C-14.

Table C-14. Additional ballast center of gravity measured form the kingpin Trailer 1.

CG Additional Ballast Trailer 1 (measured from the top of the frame rail @ kingpin location)											
X dimension				Y dimension			Z dimension				
2642	mm	104	in	-729	mm	-28.7	in	236	mm	9.3	in
2642	mm	104	in	-511	mm	-20.1	in	1118	mm	44.0	in
2642	mm	104	in	729	mm	28.7	in	236	mm	9.3	in
2642	mm	104	in	0	mm	0.0	in	532	mm	20.9	in
2642	mm	104	in	305	mm	12.0	in	1118	mm	44.0	in
2642	mm	104	in	-917	mm	-36.1	in	660	mm	26.0	in
2642	mm	104	in	917	mm	36.1	in	660	mm	26.0	in
2642	mm	104	in	-30	mm	-1.2	in	653	mm	25.7	in
											Estimated CG Ballast

C-2.3.1.2 Combined Ballast and Concrete Compartment Characteristics

The estimated location of the center of gravity of Trailer 1, accounting for both the concrete compartment and ballast, is shown in Table C-15.

Table C-15. Combined center of gravity of compartment and ballast Trailer 1.

CG Characteristics Trailer 1 (measured from the top of the frame rail @ kingpin location)											
X dimension				Y dimension			Z dimension				
180	mm	7.1	in	0	mm	0.0	in	831	mm	32.7	in
2642	mm	104.0	in	0	mm	-1.2	in	653	mm	25.7	in
1732	mm	68.2	in	-19	mm	-0.76	in	719	mm	28.3	in
											Estimated CG Trailer 1

C-2.3.1.3 Resulting Load Transfer to Kingpin and Rear Axle

The resulting weight transfer from the concrete compartment and ballast to the kingpin and rear axle are shown in Table C-16 .

Table C-16. Ballast and compartment weight transfer to kingpin and rear axle Trailer 1.

Weight Transfer to Kingpin and Rear Axle from Ballast and Compartment of Trailer 1				
Total weight of Trailer 1	22167	kg	48859	lbs
CG location X dimension	1732	mm	68.2	in
Total distance kingpin to rear axle X dimension	4601	mm	181.1	in
Weight transfer to kingpin	13820	kg	30468	lbs
Weight transfer to rear axle	8342	kg	18391	lbs

C-2.3.2 Configuration and Cargo

Trailer 1 is the same as Trailer 2 and Trailer 3 in construction barring the concrete compartment at the front. Trailer 1 has fire damage, which has caused floor ribs to displace or droop down at the outer edges of the cargo box and a portion of the plywood floor is burned away. See Figure C-48 to Figure C-51.



Figure C-48. Photo. Interior roof construction, Trailer 1.



Figure C-49. Photo. Interior side construction and damage caused by fire, Trailer 1.

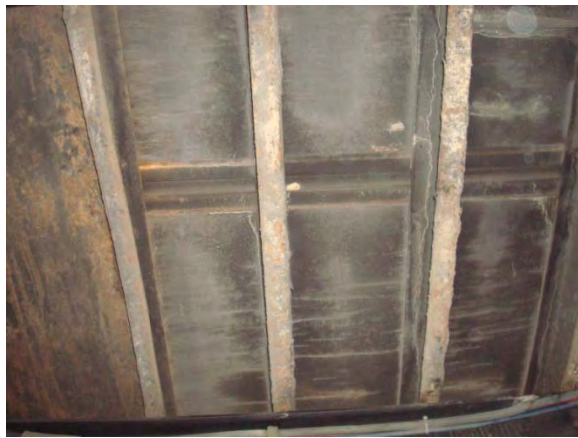


Figure C-50. Photo. Container box ribs, Trailer 1.



Figure C-51. Photo. Fire damage to floor, Trailer 1.

C-2.4 Trailer 2

VIN: 5EFISC2365B760930

Trailer 2 is connected to the Eagle dolly that is connected to the pintle hook of Trailer 1. Trailer 2 differs from Trailer 1 as it has no concrete compartment located at the front. See Figure C-52 and Figure C-53.



Figure C-52. Photo. Passenger side view, Trailer 2.



Figure C-53. Photo. Dolly and trailer configuration, Trailer 2.

Interior and exterior configurations of Trailer 2 are shown in Figure C-54 to Figure C-59.



Figure C-54. Photo. Left front interior corner of container, Trailer 2.



Figure C-55. Photo. Left rear interior corner of container, Trailer 2.



Figure C-56. Photo. Cargo box door, Trailer 2.



Figure C-57. Photo. Back rear driver side wall, Trailer 2.



Figure C-58. Photo. Door configuration, Trailer 2.



Figure C-59. Photo. Left side view, Trailer 2.

C-2.4.1 Additional Ballast Characteristics

Additional ballast has been added to Trailer 2, made up of concrete highway barriers within the container box, which are shown in Figure C-60 and Figure C-61.



Figure C-60. Photo. Highway barrier stacking for trailer ballast, Trailer 2.



Figure C-61. Photo. Highway barrier ballast, Trailer 2.

The ballast measured dimensions, calculated volumes and calculated weights are shown in Table C-17.

Table C-17. Ballast characteristics Trailer 2 (calculated weight and volume).

Ballast Characteristics Trailer 2												
X dimension (Height)			Y dimension (Width)				Z dimension (Length)					
813	mm	32	in	610	mm	24	in	3048	mm	120	in	1 Barrier
Cross section area							Material volume					
Cross section area	0.17	m ²		268.4	in ²		0.53	m ³	32208	in ³	Volume of 1 barrier	
Number of barriers							Material weights					
Number of barriers				7	units		1996	kg	4400	lbs	Weight of 1 barrier	
Half barriers				2	units		15966	kg	35200	lbs	Ballast total weight	

The location of the center of gravity of the ballast, measured from the kingpin, is shown in Table C-18.

Table C-18. Additional ballast center of gravity measured form the kingpin Trailer 2.

CG Additional Ballast Trailer 2 (from the top of the frame rail @ kingpin location)												
X dimension			Y dimension				Z dimension					
2743	mm	108.0	in	-460	mm	-18.1	in	1092	mm	43.0	in	CG Block 5
2743	mm	108.0	in	-845	mm	-33.3	in	737	mm	29.0	in	CG Block 6
3023	mm	119.0	in	568	mm	22.4	in	991	mm	39.0	in	CG Block 13
2743	mm	108.0	in	625	mm	24.6	in	381	mm	15.0	in	CG Block 15
2743	mm	108.0	in	-67	mm	-2.7	in	686	mm	27.0	in	CG Block 17
2743	mm	108.0	in	-728	mm	-28.7	in	381	mm	15.0	in	CG Block 18
2743	mm	108.0	in	799	mm	31.5	in	737	mm	29.0	in	CG Block unmarked
1664	mm	65.5	in	381	mm	15.0	in	1397	mm	55.0	in	CG Block short 1
1664	mm	65.5	in	-845	mm	-33.3	in	1397	mm	55.0	in	CG Block short 2
2320	mm	91.3	in	-43	mm	-1.7	in	595	mm	23.4	in	Estimated CG Ballast

C-2.4.2 Resulting Load Transfer to Kingpin and Rear Axle

The resulting load transfer from the ballast to the rear axle and kingpin are shown in Table C-19.

Table C-19. Ballast weight transfer to kingpin and rear axle Trailer 2.

Weight Transfer to Kingpin and Rear Axle from Ballast Trailer 2					
Total weight of ballast Trailer 1		15966	kg	35200	lbs
CG location X dimension		2320	mm	91.34	in
Total distance kingpin to rear axle X dimension		4601	mm	181.13	in
Weight transfer to kingpin		7914	kg	17448	lbs
Weight transfer to rear axle		8052	kg	17752	lbs

C-2.5 Trailer 3

VIN: 5EFISC2385B760931

C-2.5.1 Configuration and Ballast

The dimensions of Trailer 3 are nearly identical to Trailer 2. See Figure C-62 to Figure C-63 for Trailer 3 external configuration. This specific trailer could not be opened due to safety concerns. Therefore, data on the ballast load stacking configuration could not be collected.



Figure C-62. Photo. Trailer 3 rear view.



Figure C-63. Photo.Trailer 3 door configuration.



Figure C-64. Photo. Trailer 3 driver side view.



Figure C-65. Photo. Trailer 3 passenger side view.



Figure C-66. Photo. Dolly and Trailer 3 configurations.



Figure C-67. Photo. Trailer 3 cargo box attached as designed.



Figure C-68. Photo. Trailer 3 exterior wall damage.



Figure C-69. Photo. Falcon dolly and Trailer 3 connection.

C-2.5.2 Trailer Suspension

A Hutchens suspension (Hutchens Industries) is installed under all three of the Cheetah Chassis to which the container boxes are mounted. This suspension is shown in Figure C-70 through Figure C-77.



Figure C-70. Photo. Under carriage view of the Hutchens suspension.



Figure C-71. Photo. Right side suspension (front view) showing the fixed-length trailing arm.

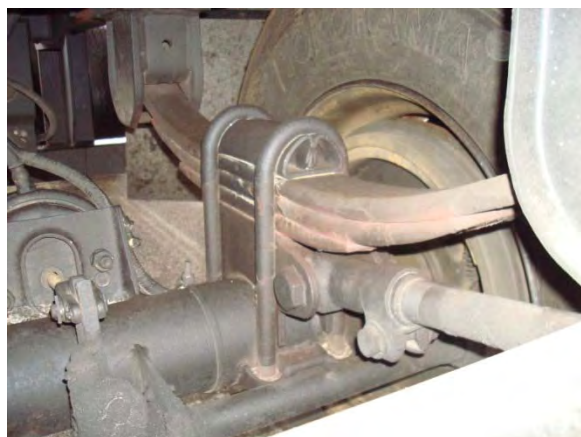


Figure C-72. Photo. Left side suspension (front view) showing the adjustable-length trailing arm.

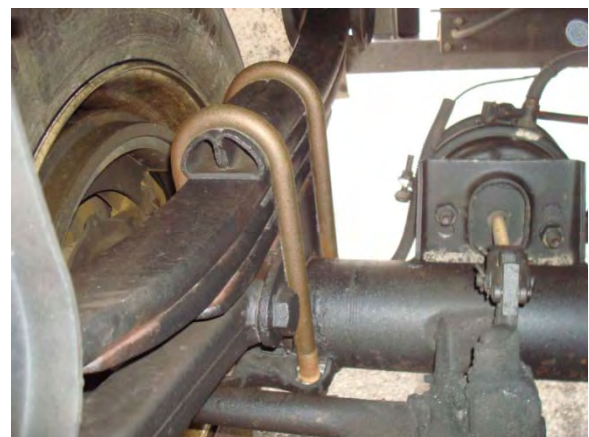


Figure C-73. Photo. Right side rear trailing arm mounting.



Figure C-74. Photo. Right side front trailing arm mounting.



Figure C-75. Photo. Right side trailing arm mount and spring height



Figure C-76. Photo. Right side three leaf spring with mounting brackets displayed.



Figure C-77. Photo. Right side rear spring bracket showing clearance.

The measured suspension characteristics are presented in Figure C-78 through Figure C-80. These characteristics were measured on Trailer 1 only. The trailer chassis torsional stiffness was measured on Trailer 2 and is presented in Figure C-81.

C-2.5.2.1 Trailer Vertical Spring Stiffness

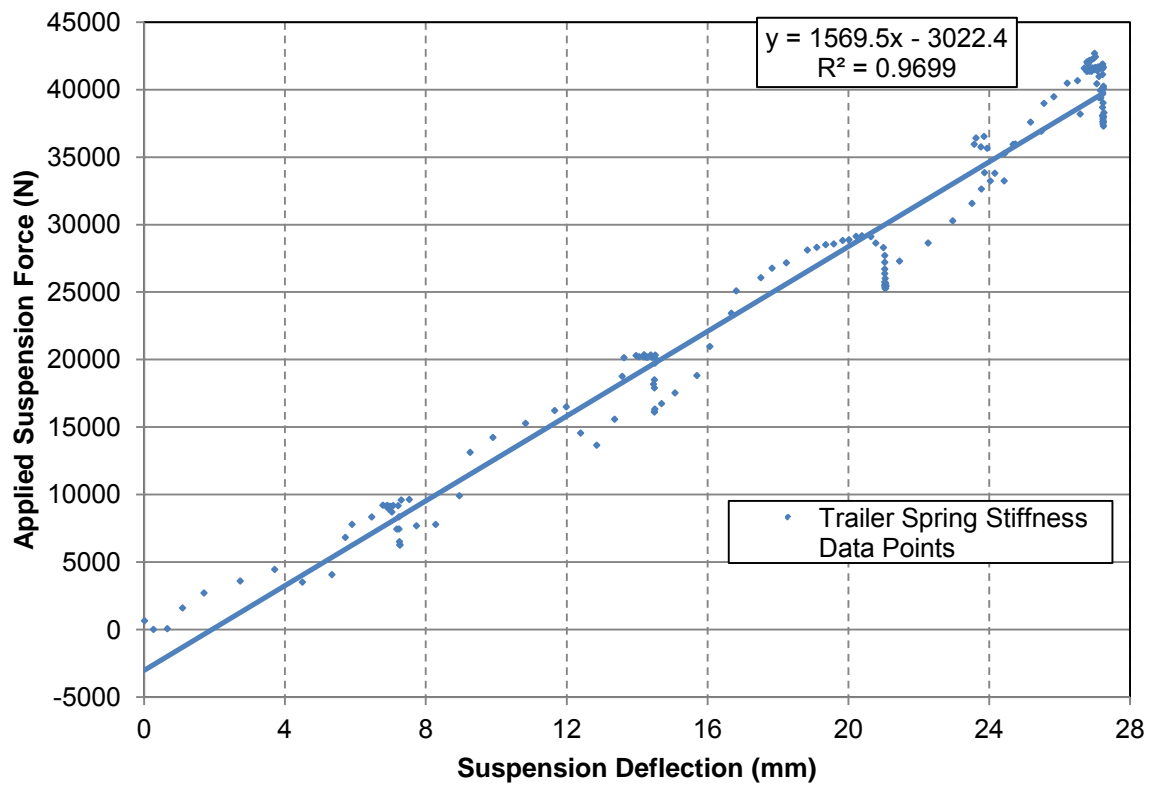


Figure C-78. Graph. Trailer 1 Spring stiffness (Cheetah Chassis).

Table C-20. Measured spring stiffness, Trailer 1.

Cheetah Chassis with Hutchens Suspension Spring Stiffness Data		
Spring stiffness	1569.5	N/mm

C-2.5.2.2 Trailer Roll Stiffness

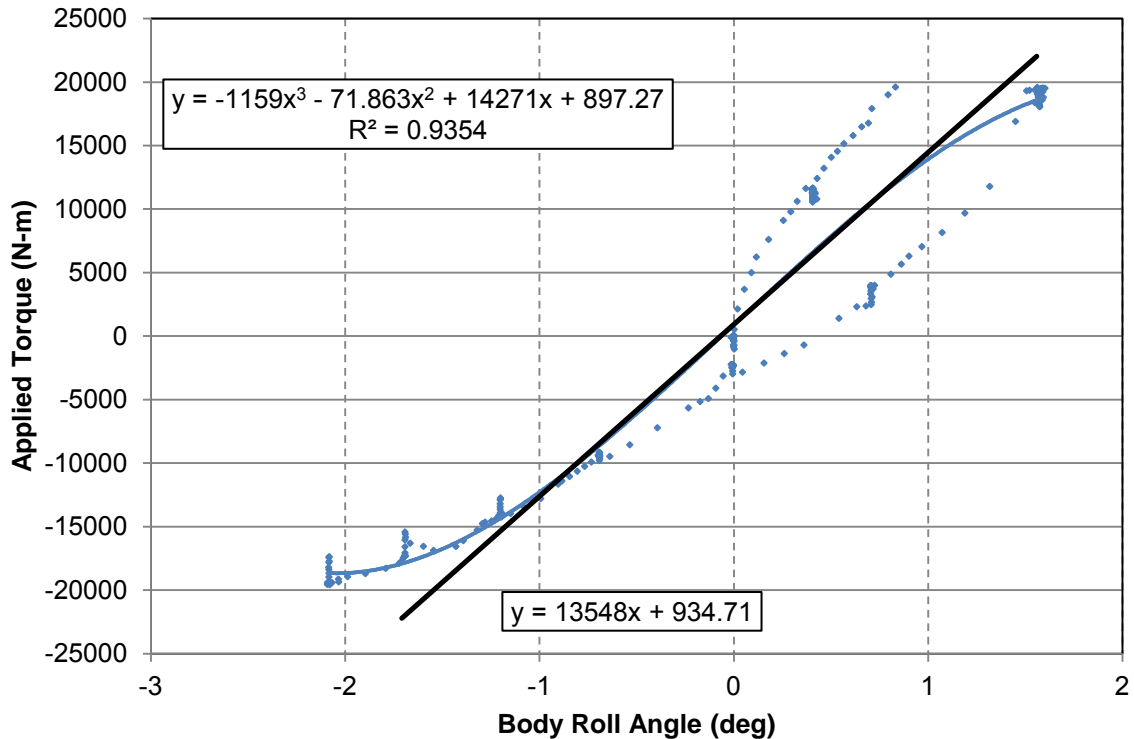


Figure C-79. Graph. Trailer 1 Roll stiffness (Polynomial fit and Linear fit in the linear region).

Table C-21. Measured roll stiffness, Trailer 1.

Cheetah Chassis with Hutchens Suspension Roll Stiffness Data		
Roll stiffness	13548	N-m/deg

C-2.5.2.3 Trailer Roll Steer

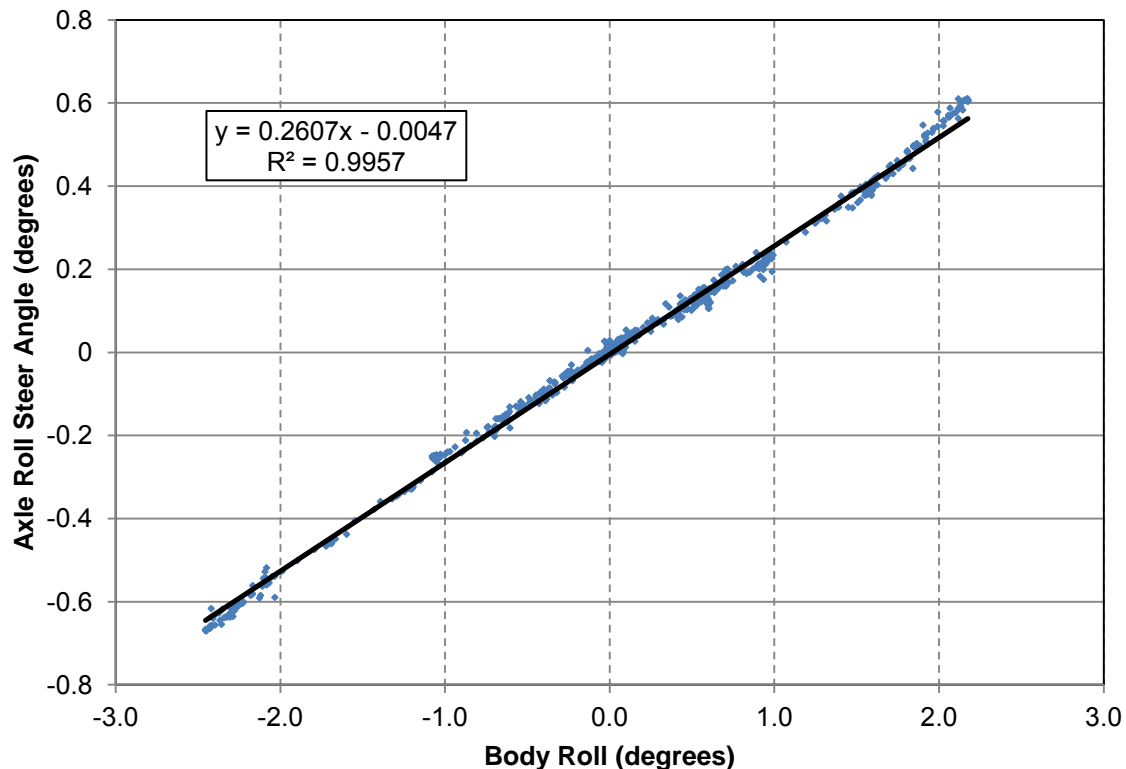


Figure C-80. Graph. Trailer 1 axle roll steer (Cheetah Chassis).

Table C-22. Measured roll steer, Trailer 1.

Cheetah Chassis with Hutchens Suspension Roll Steer Characteristics		
Trailer 1		
Axle roll steer	0.2607	deg/deg

C-2.5.3 Trailer Torsional Stiffness

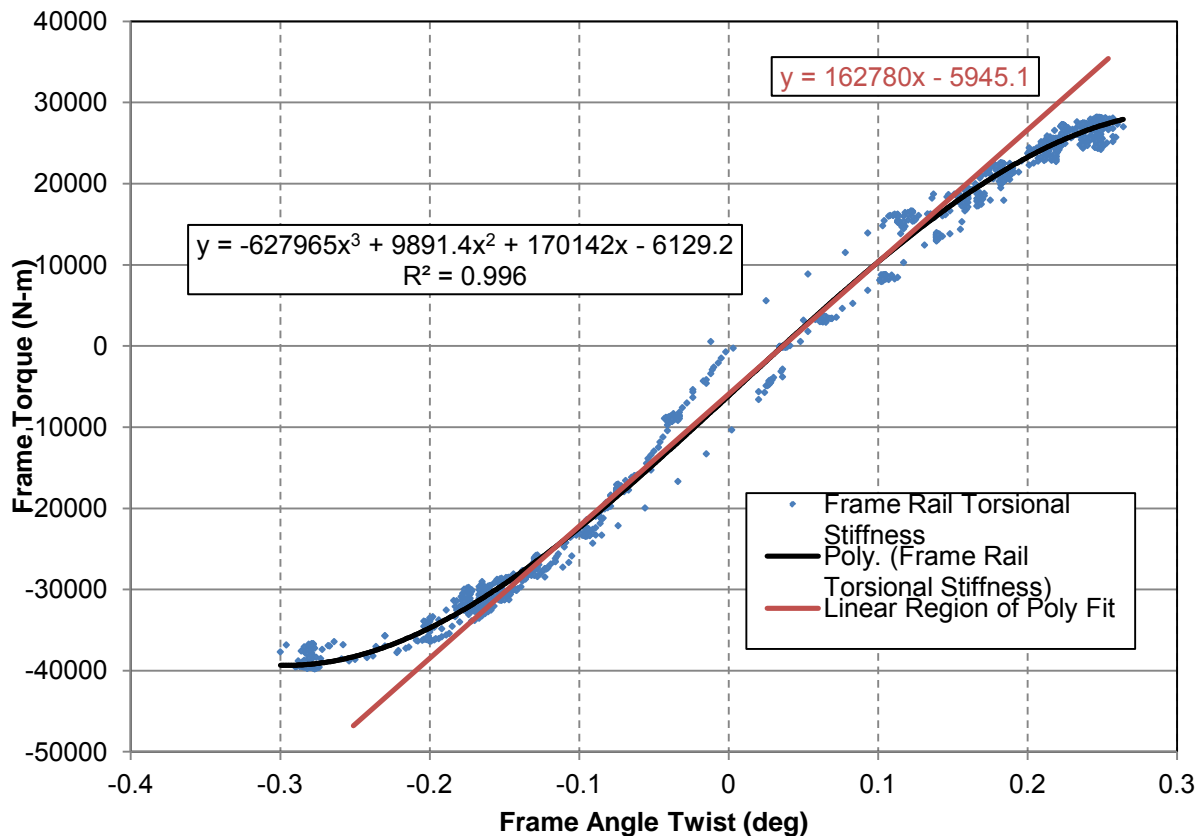


Figure C-81. Graph. Torsional Stiffness, Trailer 2.

Table C-23. Trailer frame and container torsional stiffness.

Cheetah Chassis with Mounted Container Torsional Stiffness Trailer 2		
Torsional stiffness	162780	N-m/deg

C-2.6 Eagle Dolly (NCAT and FedEx)

The Eagle Dolly is characterized by its dual transverse leaf springs, to which the fifth wheel is mounted. The leaf springs provide for vertical compliance between the fifth wheel and the axle, roll compliance of the trailer relative to the dolly axle, and pitch stiffness. The frame structure is rigidly mounted to the dolly axle tube, which in turn implies that the frame structure, axle, and all attached axle components are unsprung weight.

In the NCAT train, as measured, the Eagle dolly was equipped with dual tires. It was connected to the first trailer pintle hook, and the second Cheetah Chassis was mounted to its fifth wheel providing the connection between Trailer 1 and Trailer 2, as shown in Figure C-82 .



Figure C-82. Photo. Eagle dolly in the NCAT train.

Dimensionally the dolly as measured and characterized at the NCAT facility differs from the FedEx dolly measured and characterized at WMU. Differences included the drawbar length, drawbar attachment, length from the pintle eye to the axle centerline, and the main frame section extension forward of the axle centerline as shown in Figure C-83 and Figure C-84.

Table C-24. Dolly (VIN) Vehicle Identification numbers.

Identification Number	
NCAT dolly	F/BC/530/88
FedEx dolly	IU3JX76188BJ17552
Model	VAST20W
GVWR	20,000 lbs

Note: test must be taken with dolly frame from a horizontal (level) position.

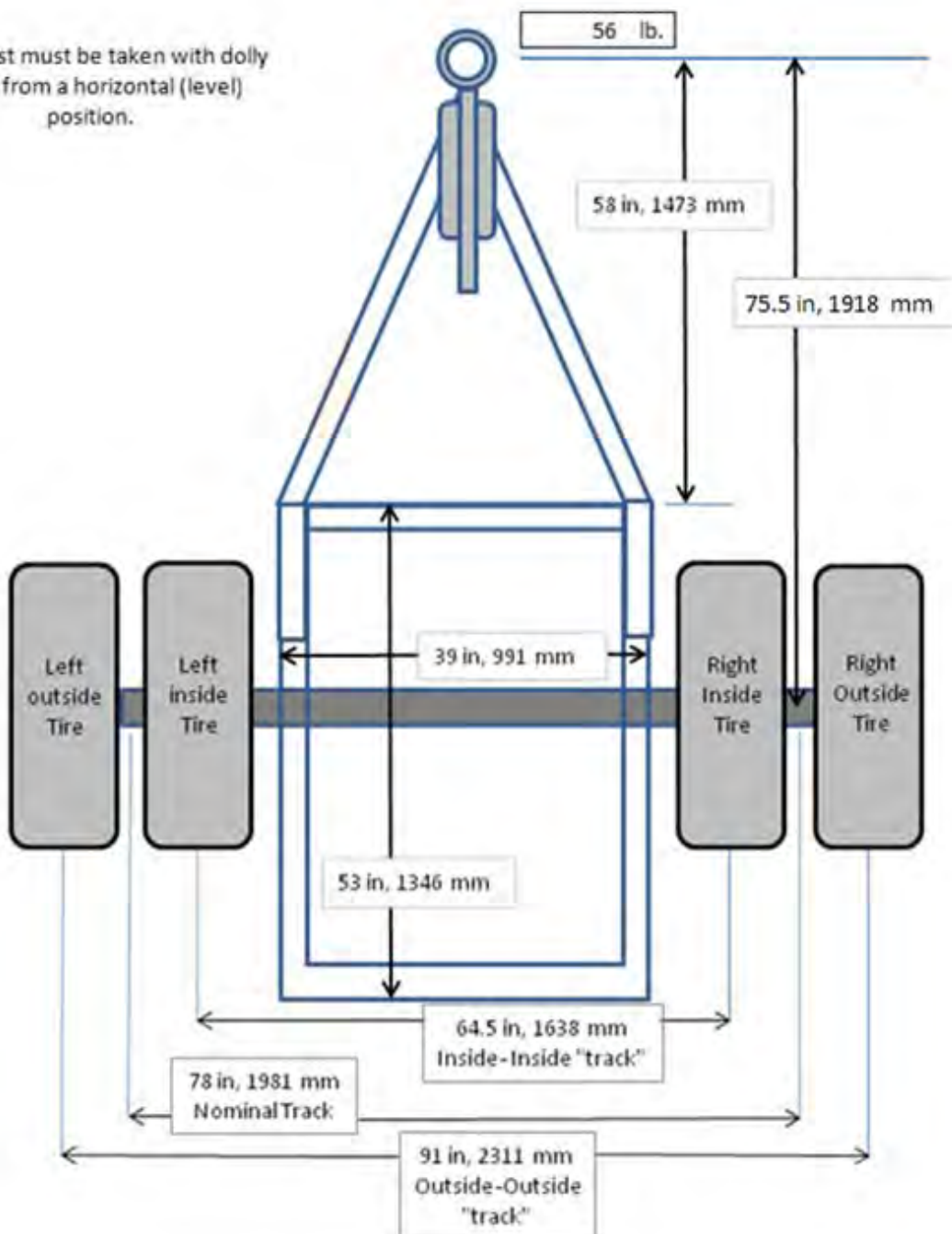


Figure C-83. Diagram. FedEx dolly.

Note: test must be taken with dolly frame from a horizontal (level) position.

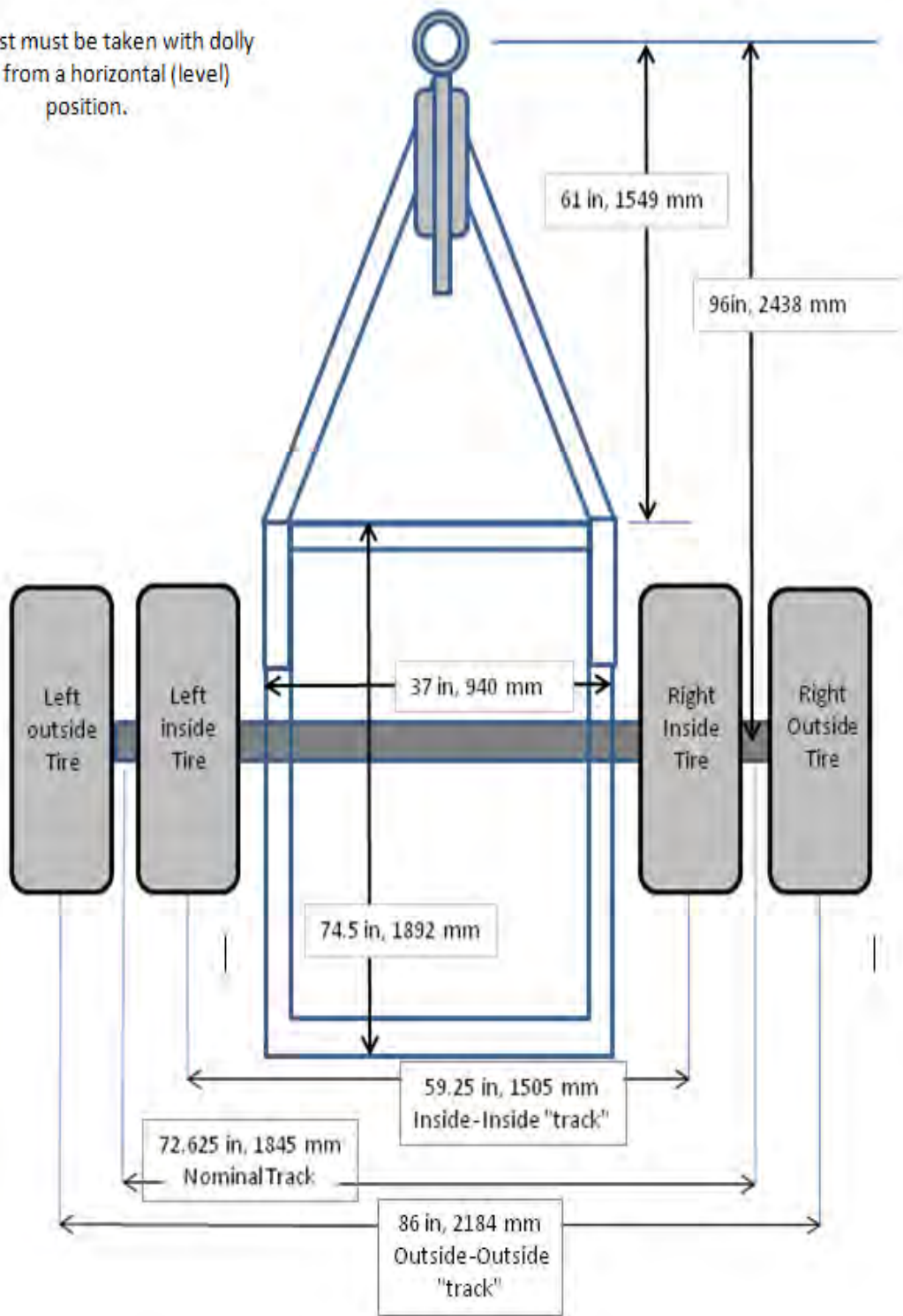


Figure C-84. Diagram. NCAT Eagle Dolly as measured before it was shortened.



Figure C-85. Photo. NCAT dolly drawbar length and attachment.



Figure C-86. Photo. NCAT dolly showing attachment connection.

Table C-25. NCAT (before it was shortened) and FedEx Eagle dolly fundamental measurement differences.

Measured Parameter (with dual tires)	NCAT		FedEx	
	in	mm	in	mm
Pintle eye center to axle centerline	96	2438	75.5	1918
Pintle eye to main frame cross member	61	1549	58	1473
Front cross member to rear cross member	71	1803	53	1346
Axle centerline to rearmost cross member	35.75	908	35.5	902
Inside tire track width	59 1/4	1505	64 3/4	1645
Outside tire track width	86	2184	91	2311
Nominal track width	72 5/8	1845	77 7/8	1978
Outside-to-outside tire dimension	96 1/2	2451	102 1/4	2597

C-2.6.1 Pintle Hook, Eye and Drawbar Assembly

The dolly drawbar, shown in Figure C-87, Figure C-88, and Figure C-89, provides a top surface that is horizontal with the frame structure of the dolly. The lower portion of the drawbar, as shown in Figure C-88, tapers toward the pintle eye.



Figure C-87. Photo. The pintle hook and eye connection (NCAT).



Figure C-88. Photo. Drawbar showing the horizontal orientation of the drawbar and frame (NCAT).



Figure C-89. Photo. Top view of the drawbar of the FedEx dolly.

The pintle eye, which connects to the lead trailer pintle hook, is rubber mounted as shown in Figure C-90, Figure C-91, and Figure C-92. Table C-26 contains the major dimensional characteristics of the eye, eye retention system, and rubber mounting.



Figure C-90. Photo. Rubber mounted pintle eye containment housing with visible retention plates on the FedEx dolly.



Figure C-91. Photo. Retention showing 2.5-in. tubular threaded bolt on the FedEx dolly.



Figure C-92. Photo. Pintle eye retention nut (FedEx).

Table C-26. Pintle eye dimensional characteristics (FedEx).

Dolly Eye Components and Mountings	in.	mm
Eye center to end length	15	381
Eye inside diameter	2 1/4	57.2
Rubber containment housing section width (od)	5	127
Rubber containment housing section height (od)	5 1/2	139.7
Rubber containment housing section length	9 1/2	241.3
Rubber containment housing bolt diameter	7/16	
Pintle rubber mount enclosure wall thickness	1/4	6.35
Rubber free length	11	279.4
Longitudinal dimension to (2) retaining plates from end	3 1/2	88.9
Retaining plate thickness (2 vertical plates)	3/8	9.53
Eye bolt outer dia.(through rubber)	2 1/2	63.5
Tubular Eye bolt ID	1.75	44.45
Dolly drawbar wall thickness	1/4	6.35
Dolly main frame wall thickness	3/8	9.53
Rubber durometer value (Shore A)	88-94	
Rubber elastic modulus (approx @ 92.5)	28.6	Mpa
Number of bolts (4-top, 5-bottom) in containment housing	4 5	

The calculation for the elastic modulus of the rubber was done using an empirical relationship as shown below in Figure C-93.

$$E(MPa) = \frac{0.0981(56 + 7.66S)}{0.137505(254 - 2.54S)}$$

Figure C-93. Equation. Empirical relation for estimating the elastic modulus of rubber.

C-2.6.2 Fifth Wheel, Fifth Wheel Mounting and Transverse Leaf Characteristics

The Eagle dolly fifth wheel, shown in Figure C-94, is a welded steel assembly with a 890-mm (35-in.) diameter contact surface. The fifth wheel is fastened to the two transverse leaf springs by U-bolts with the leaf springs providing compliance for vertical and roll motion. Because the fifth wheel has no pivot bushing, it relies on the transverse springs to absorb any trailer pitch.



Figure C-94. Photo. Fifth wheel on the FedEx dolly.

The compliance between the fifth wheel and the road surface is primarily a function of the transverse leaf spring vertical rates and the radial stiffness of the tires. The tested leaf springs and the attachment to the fifth wheel are shown in Figure C-95, Figure C-96, and Figure C-97. A fractured leaf is identified by the orange paint. Collective judgment was that the crack was in a location that would have an insignificant influence on the vertical stiffness.



Figure C-95. Photo. NCAT Eagle dolly transverse leaf spring.

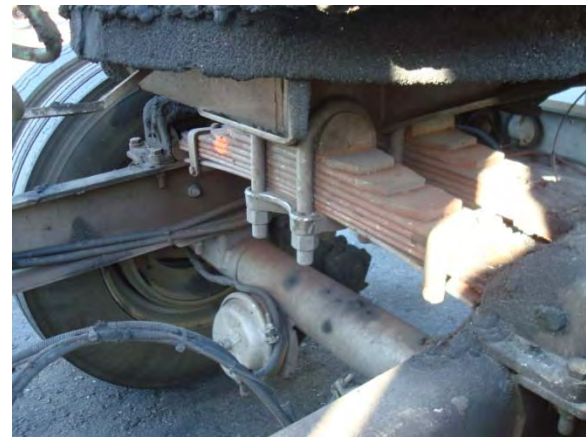


Figure C-96. Photo. NCAT Eagle dolly.



Figure C-97. Photo. Mounting system viewed from beneath the FedEx dolly.

Figure C-98, Figure C-99, and Figure C-100 present the encasement for the transverse leaf spring ends, which are rubber mounted, and the leaf spring spacing. The 4 inch wide leaf spring is centered in the 5 inch wide receiver, which is then bolted to the dolly main frame. The spring center to center distance was measured at 7.5 in. (190.5 mm).

Figure C-99 shows the mounting of the leaf spring receivers and rubber inserts. Figure C-100 clarifies the configuration of the rubber receiver at the leaf spring mounting.



Figure C-98. Photo. Eagle dolly dual transverse leaf spring spacing (NCAT).



Figure C-99. Photo. Leaf Spring rubber end mountings (FedEx).



Figure C-100. Photo. Leaf Spring rubber ends mounting (FedEx).

Figure C-101 presents information from the Silver Eagle web site on spring specifications. The two leaf springs were separated by 8 inches ($7\frac{1}{2}$ inches FedEx). Table C-27 presents the measured specifications for the FedEx and the NCAT dollies.

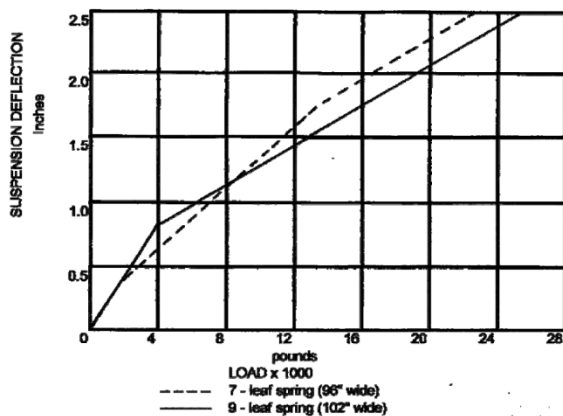


Figure C-101. Graph. Silver Eagle-Eagle Dolly Spring specifications.

Table C-27. Basic Leaf Spring Parameters (NCAT vs. FedEx).

	NCAT		FedEx	
Total leafs in each of two springs	8		8	
Measured arch (very approximate)			2 5/8 inch	
Bolt-bolt spacing in frame mounted hanger			38 ¾	
Frame rail spacing at spring mount			39	
Basic Parameter	mm	inch	mm	inch
Spring to Spring Longitudinal spacing	203	8	190.5	7 ½
Individual Leaf width			101.6	4
Leaf 1 (bottom) (Length, thickness, length is approx.)	756	29 ¾	9.53	0.375
Leaf 2 (encased by rubber boot, length is approx)	1016	40	9.53	0.375
Leaf 3 (encased by rubber boot, length is approx)	1016	40	9.53	0.375
Leaf 4 (above the rubber mounted leafs, length is approx)	826	32 ½	12.70	0.500
Leaf 5 (above the rubber mounted leafs, length is approx)	737	29	12.70	0.500
Leaf 6 (above the rubber mounted leafs, length is approx)	559	22	12.70	0.500
Leaf 7 (above the rubber mounted leafs, length is approx)	432	17	12.70	0.5
Leaf 8 (Top) (length is approx)	305	12	12.70	0.500
Platform block width (leaf attach to the fifth wheel)	178	7	178	7
Spring end mount rubber hardness (durometer)			90	
Approximate rubber elastic modulus			21	Mpa

The rubber surrounding the spring ends was tested with a durometer to ascertain the rubber hardness. A durometer reading of 90 was obtained. The measured durometer reading was translated to an approximate modulus using the empirical relationship in Figure C-93.

Figure C-102 presents a digitized approximation to the Silver Eagle Leaf spring as found on the Silver Eagle website.

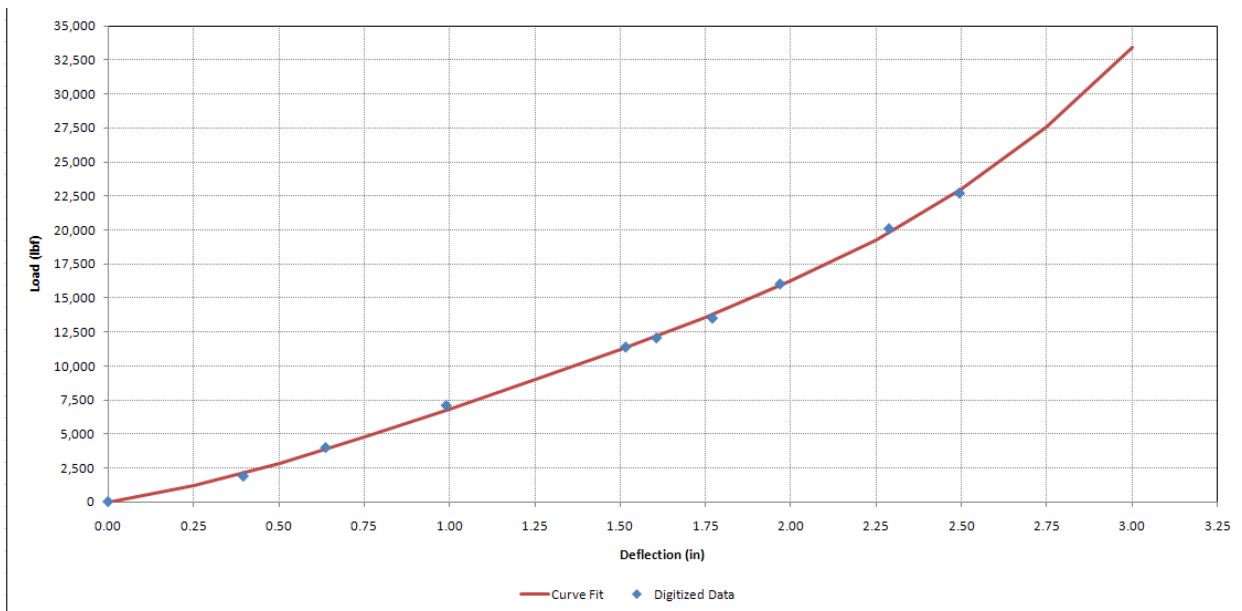


Figure C-102. Graph. Digitized Silver Eagle vertical spring rate.

Figure C-103, Figure C-104, Figure C-105, and Figure C-106 show the U-shaped brackets that fit inside the frame rail of the FedEx dolly. These displayed brackets appear to be installed to directly transfer the spring end loads to the dolly axle assembly. This bracket was on earlier models and the current design does not use these brackets. The NCAT dolly shown in Figure C-96 does not use this bracket.



Figure C-103. Photo. Load transfer bracket (FedEx).



Figure C-104. Photo. Load transfer bracket (FedEx).



Figure C-105. Photo. Load transfer bracket (FedEx).



Figure C-106. Photo. Load transfer bracket assembly bottom (FedEx).

C-2.6.3 Pitch and Roll Stiffness of the Unloaded FedEx Dolly

Response to load was measured independent of the tire stiffness. For the unloaded dolly a kingpin mounted to an I-beam was latched into the fifth wheel. A load was then introduced onto the I-beam, through electronic loads cells, at a specified dimension from the kingpin. The fifth wheel was instrumented with string potentiometers to measure either the pitch or roll displacement between the dolly main frame and the fifth wheel.

In the unloaded state only a limited number of leafs were contributing to the measured stiffness. The values obtained would therefore be expected to be relatively low. The unloaded fifth wheel suspension stiffness, as measured, is shown in Figure C-107 and Figure C-108. Note the hysteresis in the measurement of the pitch torque.

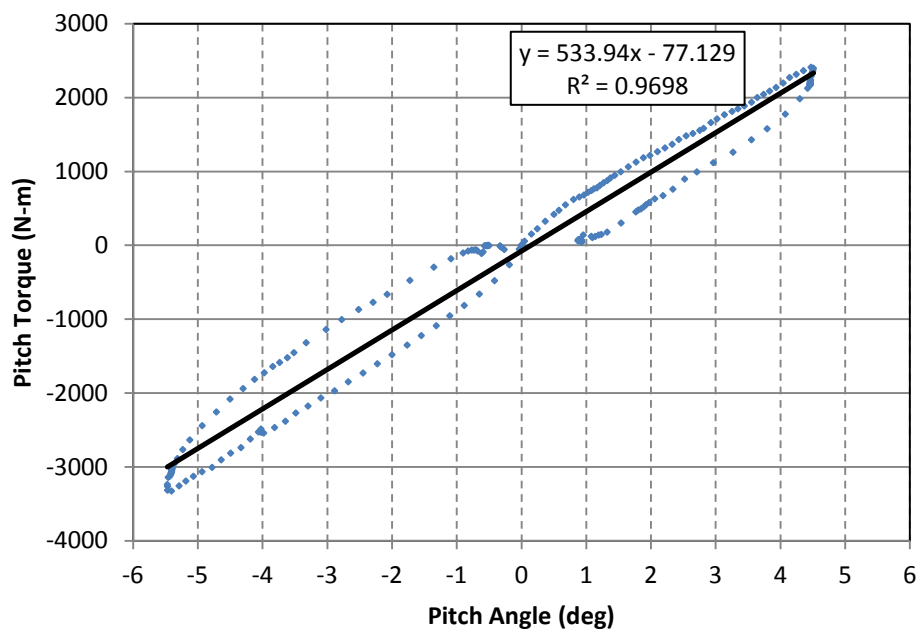


Figure C-107. Graph. Pitch stiffness of the fifth wheel on the unloaded FedEx dolly.

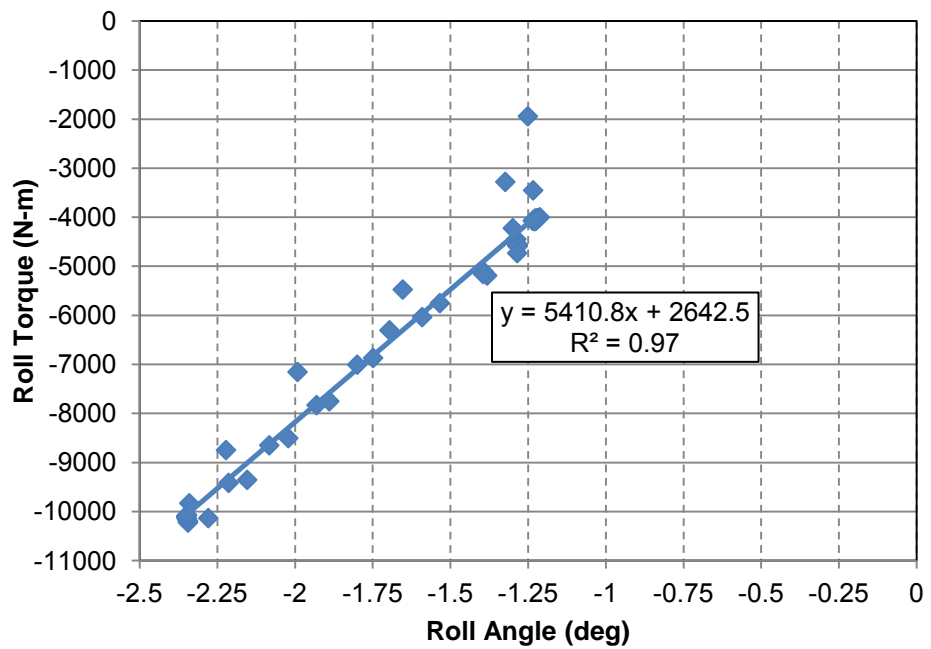


Figure C-108. Graph. Graph. Roll stiffness of the fifth wheel on the unloaded FedEx dolly.

C-2.6.4 Bounce and Roll Stiffness of the Loaded NCAT Eagle Dolly

Figure C-109 and Figure C-110 show the loaded fifth wheel suspension stiffness as measured at NCAT.

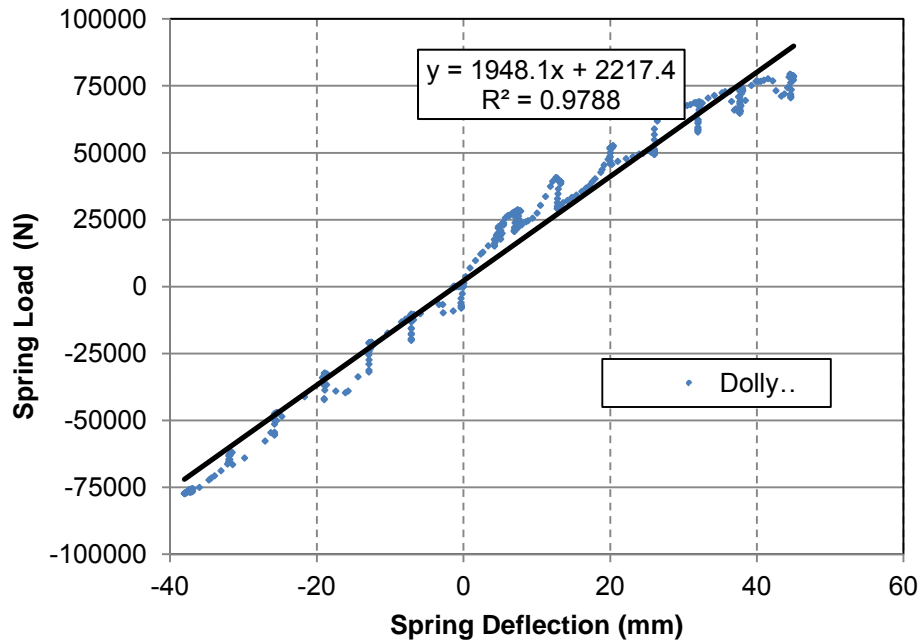


Figure C-109. Graph. Vertical spring rate of the fifth wheel on the NCAT Eagle dolly.

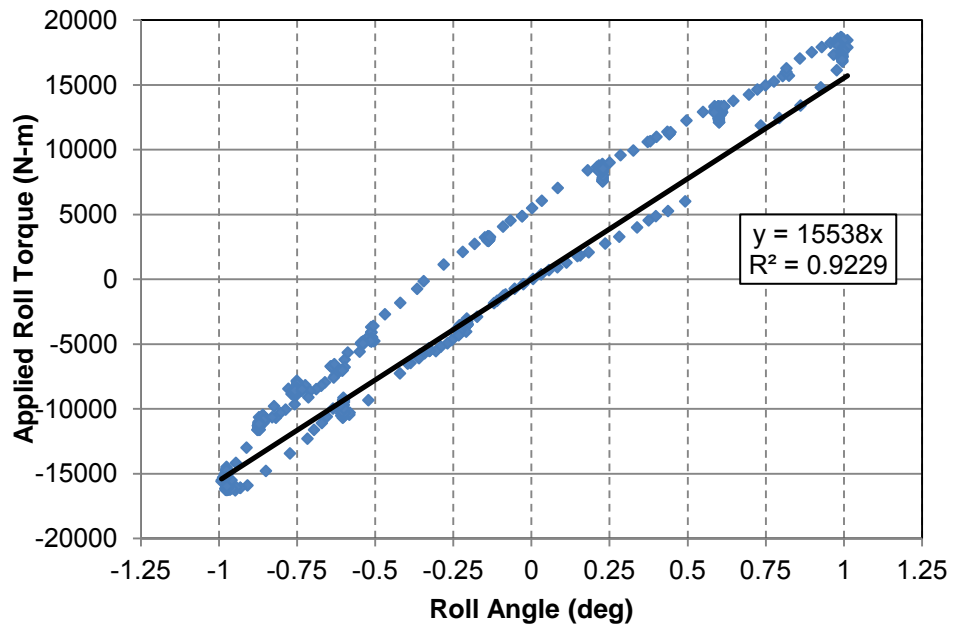


Figure C-110. Graph. Roll stiffness of the fifth wheel on the loaded NCAT Eagle dolly.

Table C-28. Eagle Dolly transverse leaf characteristics.

Parameter	Dolly ID	Value	
Fifth wheel unloaded Pitch stiffness	FedEx	534	N-m/deg
Vertical Spring Rate (2-Springs)	NCAT Dolly	1948	N/mm
Unloaded roll stiffness	FedEx	5410	N-m/deg
Loaded roll stiffness	NCAT Dolly	15538	N-m/deg

C-2.6.5 Weight Distribution WMU FedEx Dolly

The FedEx dolly was weighed to determine its overall weight and the center of gravity location in the X, Y, and Z planes. The dolly incorporates ballast weights rearward of the axle to allow a person to move the dolly easily with little static weight on the Pintle eye. The basic measurements are shown in Figure C-111, with the weights and weight distribution shown in Table C-29 and Table C-30.

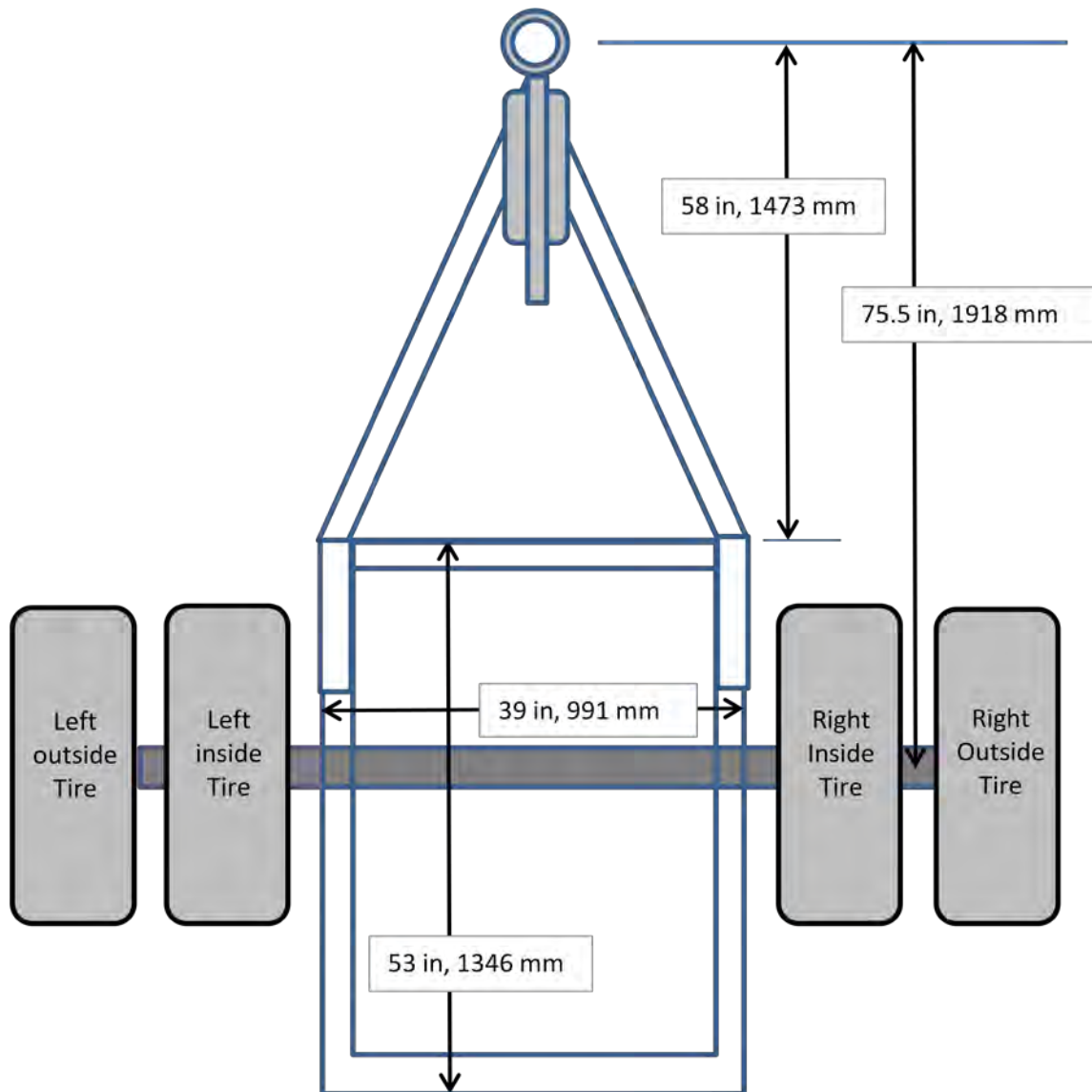


Figure C-111. Diagram. FedEx dolly dimensions.

Table C-29. Calculated weight distributions.

Center of Gravity Locations and Percentages (FedEx) Unloaded					
	in.	mm			
Cgy	0.413	10	right of centerline of dolly	% wt on front eye	1.9%
Cgx	1.095	28	forward of axle centerline	% wt on axle	98.1%
Cgz	5.877	149	above axle centerline	% wt on left duals	48.54%
	26 3/8	670	above ground	% wt on right duals	49.58%

Table C-30. Measured weight properties.

Measured Weights at Specified Locations (FedEx) Unloaded					
	lb	kg		lb	kg
Left outside dual	1071.0	485.8	Right outside dual	649	294.4
Left inside dual	374.0	169.6	Right Inside dual	827	375.1
	1445.0	655.5		1476.0	669.5
Front Pintle eye	56	25.4			
Total Wt	2977.0	1353			

Figure C-112 and Figure C-113 present the steps used to establish the gross weight of the dolly. The four scales were placed under tires and weights recorded. Then the weight under the tongue was taken. These measurements were used to establish the X.Y location of the center of gravity.



Figure C-112. Photo. Weighing the FedEx dolly (axle weights only).



Figure C-113. Photo. Weighing the FedEx dolly (tongue weight only).

The center of gravity of the FedEx dolly in the Z direction was determined by leveling the tongue and establishing its baseline load. The height was measured from the ground to the center of the pintle hook. The pintle hook end was raised until the frame balanced over the axle. At this point, the center of gravity was directly over the axle in all planes. When the system was balanced perfectly, the new height to the center of the hook was measured. Given this difference in heights and the length of the frame from the center of the axle, the angle was found between the level state and the equilibrium state. Based upon these new figures and the calculated C_{gx} distance, the law of triangles was implemented and the height above the centerline of the axle at which the C_{gz} is located was calculated. This height was added to the center of rotation, which is the axle centerline, to find the overall height of the center of gravity in the Z plane, which was established at 670 mm (26 3/8 in.).

C-2.6.6 Dolly Ballast System

Both the NCAT and FedEx dollies carried weights for ballast. The ballast on the FedEx dolly was approximately 552 mm (21.75 in.) behind the axle, with a total weight of 18.6 kg (180 lb). The support system consisted of 127 x 13 mm (5 x 0.5 in.) steel with the center 685 mm (27 in.)

being 279 x 13 mm (11 x 0.5 in.) with two 25 x 152 x 927 mm (1 x 6 x 36.5 in.) steel plates, as shown in Figure C-114 and Figure C-115.

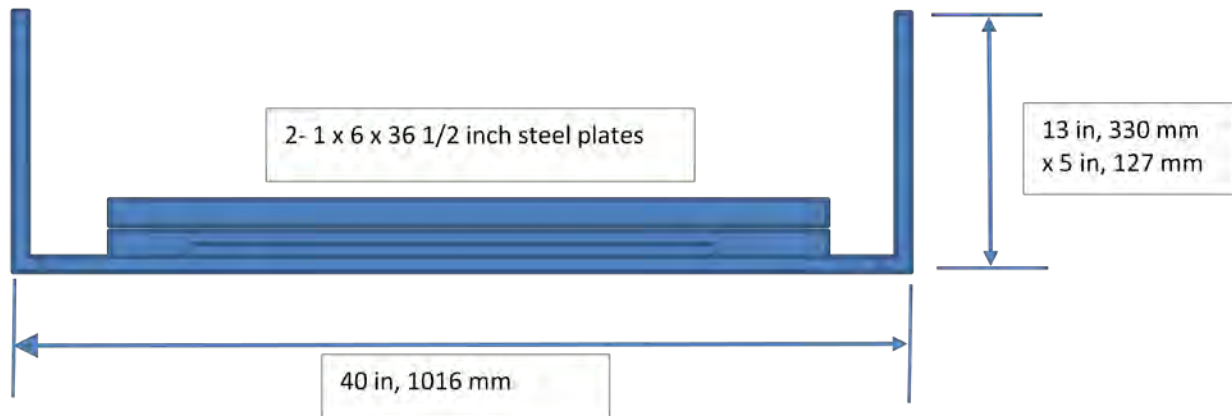


Figure C-114. Diagram. FedEx ballast weight located behind the axle centerline.

As shown in Figure C-115 and Figure C-116 the FedEx dolly had additional ballast over the NCAT dolly. Each of the individual weights was approximately 63 lbs (28.2 kg) on the FedEx dolly; however the NCAT dolly ballast used only one weight, which extended approximately the full width of the frame (37 inches, 940 mm), as shown in Figure C-116. The FedEx dolly weights were 36.5 inches (927 mm) with a 39 inch outside-outside frame width.



Figure C-115. Photo. FedEx dolly ballast system.



Figure C-116. Photo. NCAT Eagle Dolly ballast system.

C-2.7 Falcon Dolly of the NCAT Train (not used in track testing)

VIN: F/BC/477/91

1U3JF801X6BK01018

Only physical measurements were taken of the Falcon dolly in the NCAT train. Characteristics such as roll steer, and roll and bump stiffness, were not collected because this dolly was not used in the track or highway testing. The Falcon dolly, shown in Figure C-117, coupled the third trailer in the NCAT train to the second trailer.



Figure C-117. Photo. Falcon dolly in the NCAT train.

The Falcon dolly differs from the Eagle dolly fundamentally as the axle and related suspension components are unsprung on the Eagle while the frame and fifth wheel assembly are sprung on the Falcon. This dolly utilizes a Hutchens suspension system. The basic dolly dimensions are shown in Table C-31 and in Figure C-118.

Table C-31. Basic Falcon dolly dimensional properties.

Basic configuration		
Longitudinal leaf springs between the axle and the fifth wheel frame with a direct frame mounted pitch pivoting fifth wheel		
	in.	mm
Overall dolly Length	132	3353
Pintle eye to kingpin	104	2642
Pintle eye to axle c/l	103 1/8	2619
Frame width (c-c)	33 1/2	851
Frame width (o-o)	38 1/2	978
Leaf spring span (c-c)	38 1/4	972
Leaf spring width	3	76.2
Inside tire-inside tire track	60	1524
Outside tire-outside tire track	86 1/4	2191

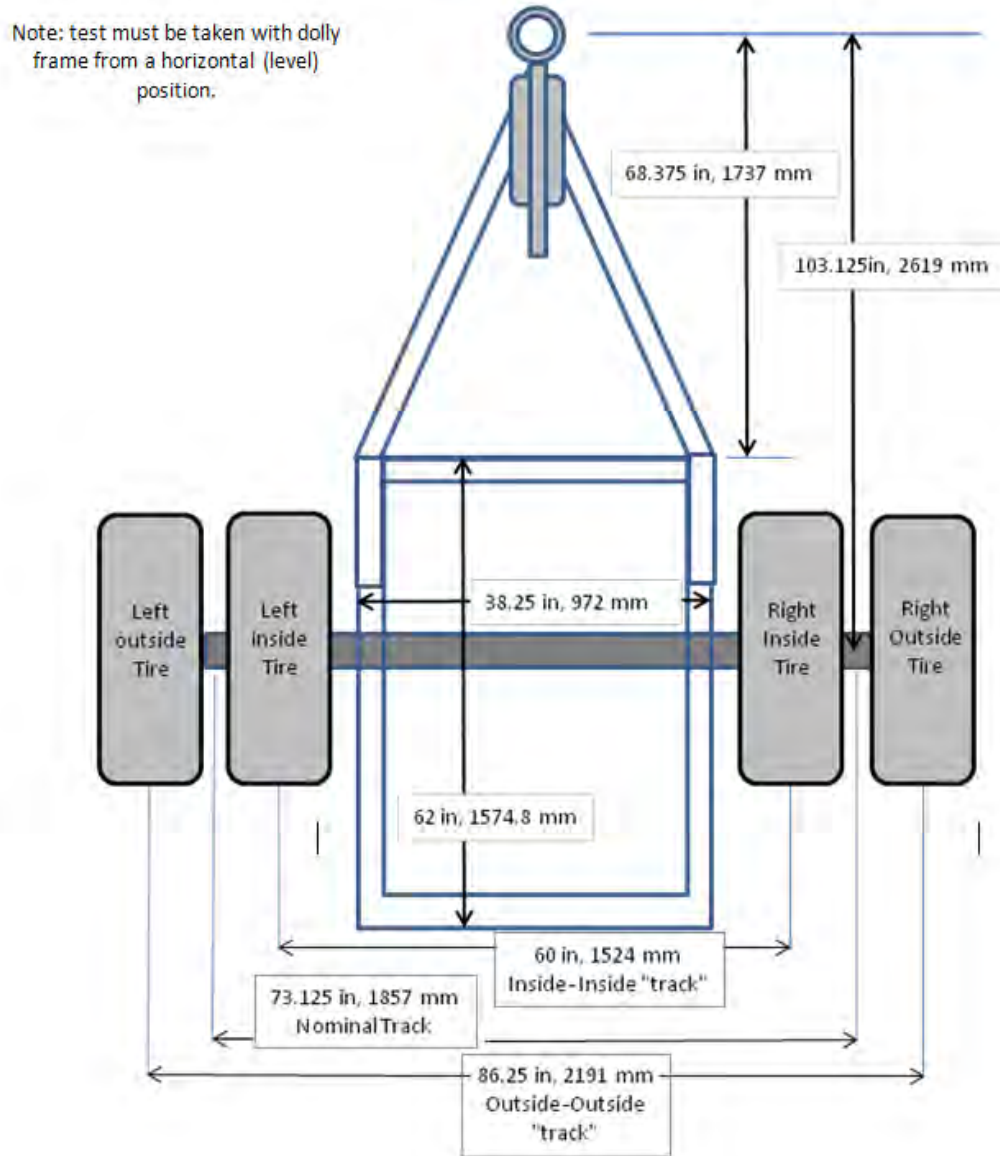


Figure C-118. Diagram. Basic dimensions of Falcon dolly.

The dolly utilizes a larger flange width than the Eagle dolly, as shown in Figure C-119. Also shown in Figure C-119 is the relative location of the fifth wheel on the frame structure. Figure C-120 contains frame outside to outside dimensions as well as frame flange widths.

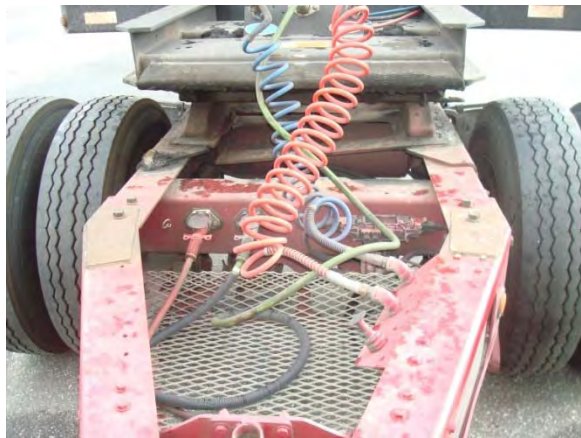


Figure C-119. Photo. Falcon dolly frame showing flange widths.

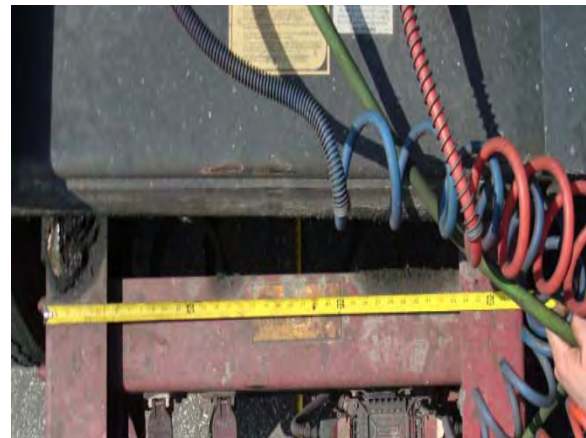


Figure C-120. Photo. Falcon Dolly frame and flange widths.



Figure C-121. Photo. Leaf spring outset from frame rail.



Figure C-122. Photo. Falcon dolly undercarriage (from front).

C-2.7.1 Pintle Hook, Eye and Drawbar Assembly

The dolly drawbar shown in Figure C-87 and Figure C-124 provides a top surface that is horizontal with the frame structure of the dolly. The lower portion of the drawbar, as shown in Figure C-124 and Figure C-125, tapers toward the pintle eye.



Figure C-123. Photo. Falcon drawbar pintle hook and eye connection.



Figure C-124. Photo. Drawbar taper to pintle hook.



Figure C-125. Photo. Top view Falcon pintle and drawbar.

The pintle eye that connects to the lead trailer is welded to a steel drawbar extension as shown in Figure C-126 and Figure C-127. Table C-32 contains the major dimensional characteristics of the eye and eye retention system.



Figure C-126. Photo. Pinto hook and mounting.



Figure C-127. Photo. Pinto drawbar extension location and mounting.

Table C-32. Pinto eye dimensional characteristics (Falcon).

Dolly eye components and mountings	in.	mm
Eye center to end length	24	610
Eye inside diameter	2 ¼	57.2

C-2.7.2 Fifth Wheel, Fifth wheel mounting and Leaf Spring Characteristics

The Falcon dolly fifth wheel pivots on its attachment to the frame. The axle is then connected to two longitudinal leaf springs with U-bolts, with the leaf springs providing vertical bump stiffness, roll stiffness, and to a lesser degree pitch stiffness shown below in Figure C-128, Figure C-129, Figure C-130, and Figure C-131.

Only the right side trailing arm is adjustable as shown in Figure C-129.

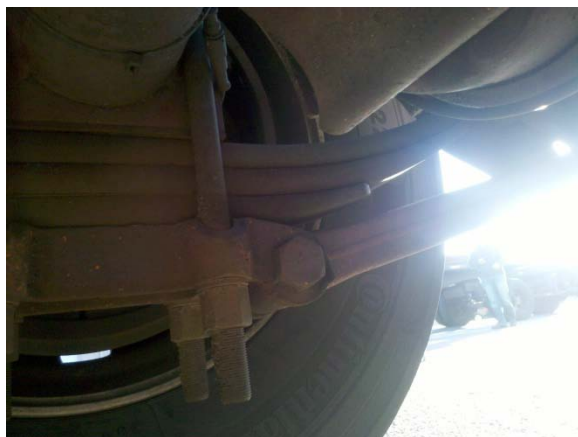


Figure C-128. Photo. Leaf spring and axle assembly.



Figure C-129. Photo. Falcon dolly leaf spring with adjustable trailing arm shown.



Figure C-130. Photo. Falcon dolly leaf spring and axle assembly as viewed from rear.



Figure C-131. Photo. Leaf spring forward end mount with trailing arm.

C-3. Realizing a Solid Model of the FedEx Eagle Dolly

A full scale CAD model of an Eagle converter dolly, manufactured by Silver Eagle Manufacturing Company, was created by means of reverse engineering. Using the Advanced Topometric Sensor (ATOS) 3D digitizer (manufactured by Gesellschaft für Optische Meßtechnik, or GOM mbH), the converter dolly was digitized for precise measurement of individual components. The measurements were used to create and assemble components of a model for dynamic simulation and analysis. The resulting CAD assembly of the converter dolly has been verified against the ATOS data. The CAD model will provide an accurate depiction of forces seen in real-life applications through dynamic simulation software. FedEx provided the dolly to WMU for this work.

C-3.1 Methodology

In large scale applications, optical measurement techniques are the most efficient and precise method to retrieve dimensions. The converter dolly was reverse engineered using the ATOS II 3D digitizer.

The ATOS digitizer consists of two cameras and a projector. A fringe pattern of alternating white light is projected on the object's surface. The 3D coordinates of up to 4 million points are triangulated based on the deformation of light. The digitizer was calibrated for a 476.25 x 400.05 x 400.05 mm measuring volume.

Several scans are required at adjacent perspectives to generate a three dimensional shape. Point markers serve as a reference to link multiple scans into a common coordinate system. Prior to scanning, 5-mm-diameter contrast point markers were adhered to the dolly. Both cameras must see at least three point markers with an ellipse diameter (as a result of seeing the circle at an angle) greater than 3 pixels to register the captured data.

Figure C-132 (left) shows the captured data in grey and reference point markers in green. On the right of Figure C-132, a second scan is automatically transformed into the project using nine of the reference point markers captured in the initial scan (left). The final scan data and reference point markers are shown in Figure C-133.



Figure C-132. Diagram. ATOS scan data automatically transformed into the project using coded reference point markers.

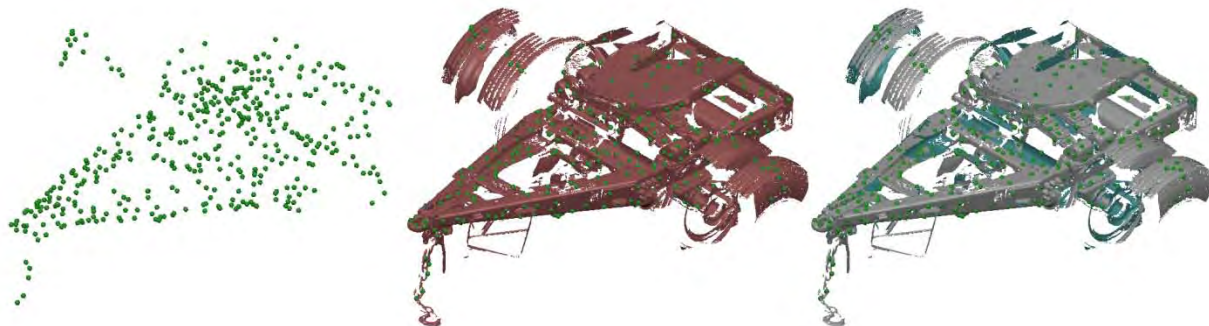


Figure C-133. Diagram. Reference point markers shown in green, scan data in red, positive surfaces in grey, and negative surfaces in teal.

Each scan generates a large collection of points in three dimensional space, called a point cloud. The ATOS system automatically inserts the point cloud data from each scan into the project, given enough reference point markers. When scanning was complete, the project point cloud was transformed into a polygon mesh of non-overlapping triangles to represent a surface, shown in Figure C-134.

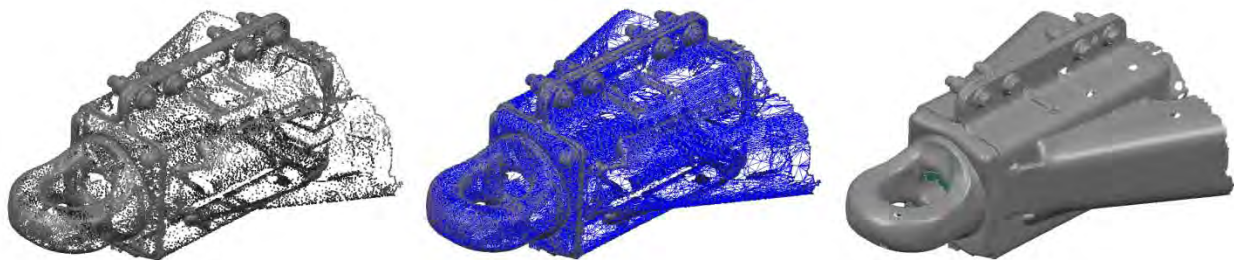


Figure C-134. Diagram. A post processed point cloud is shown on the left. The resulting polygon mesh with blue edges is shown center and the surface representation on the right.

The large size of the project necessitated that the data be meshed and processed in multiple sections. To ensure dimensional accuracy of components spanning the entire project, the sections were merged into one file, requiring file size reduction of each of the sections. To keep detail, each section was thinned and smoothed based on surface tolerance. In the smoothing process, points are moved, and in the thinning process, they are eliminated. The process of removing unnecessary points from the mesh is shown in Figure C-135.

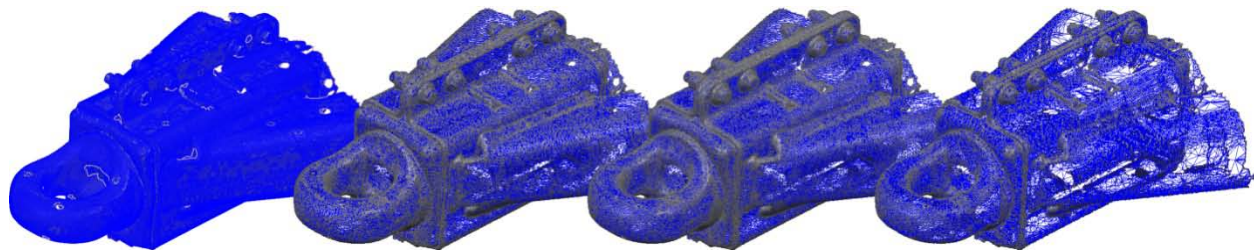


Figure C-135. Diagram. Progressive removal of unnecessary points from the mesh to reduce file size.

Measurements were performed and recorded using geometric primitives in the ATOS software. Commonly used geometric primitives include plane, cylinder, and line. These primitives are generated by the “best fit” criterion using selected elements from the mesh. Best fit point outliers are controlled by using 1 Sigma to 5 Sigma limits in the ATOS software. In general 5 Sigma was used. Due to the weathered condition of the dolly, such as grease on the axle or flaking paint, 3 Sigma was used in some instances. This enabled selection of the entire axle while automatically filtering out the unwanted data, giving an accurate cylindrical diameter.

CAD models were created using Pro/ENGINEER, a parametric solid modeling software. Individual components were modeled and constrained into respective sub-assemblies. The sub-assemblies were constrained into the accurate location, resulting in a full assembly of the Eagle converter dolly shown in Figure C-136. The respective material property was assigned to each component in the assembly for analysis of mass properties, such as center of gravity, and future use in finite element software.



Figure C-136. Illustration. Pro/ENGINEER CAD rendering of the Eagle dolly.

The Eagle CAD assembly was imported into the ATOS project using the Initial Graphics Exchange Specification (IGES) format. The CAD was manually transformed into the ATOS coordinate system to avoid bias. The CAD model (blue) and scan data (grey) are shown in Figure C-137.

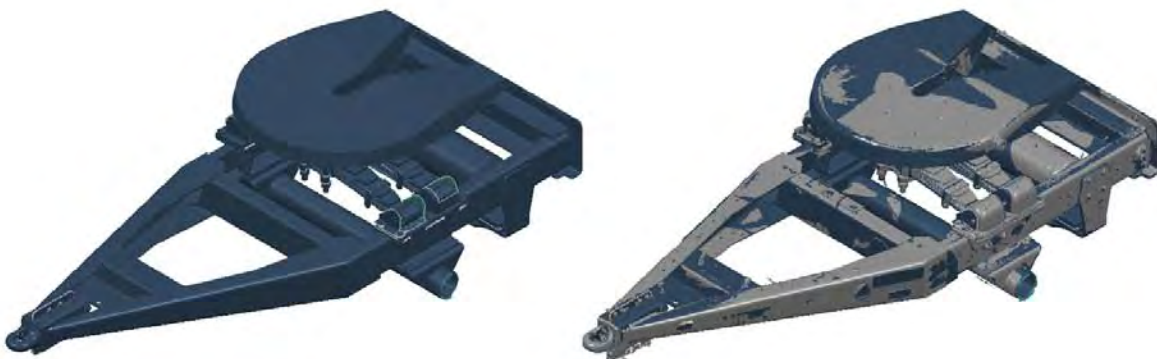


Figure C-137. Diagram. CAD assembly imported into the ATOS scan data for model verification.

The model was verified for dimensional accuracy based on surface deviation to the reference mesh, shown in Figure C-138. Component geometry and placements were corrected such that the CAD model was accurate within 6.35 mm (0.25 in.), which was sufficient for the worn dolly.

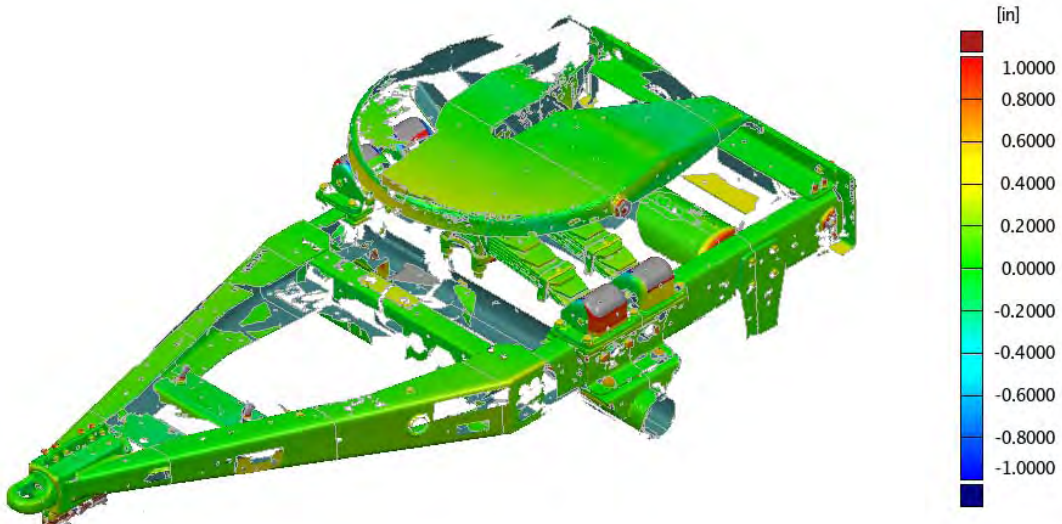


Figure C-138. Diagram. CAD model surface deviation to ATOS scan data.

C-3.2 Bill of Materials

Figure C-139 through Figure C-145 present the bills of material for the various assemblies used to construct the dolly solid model.

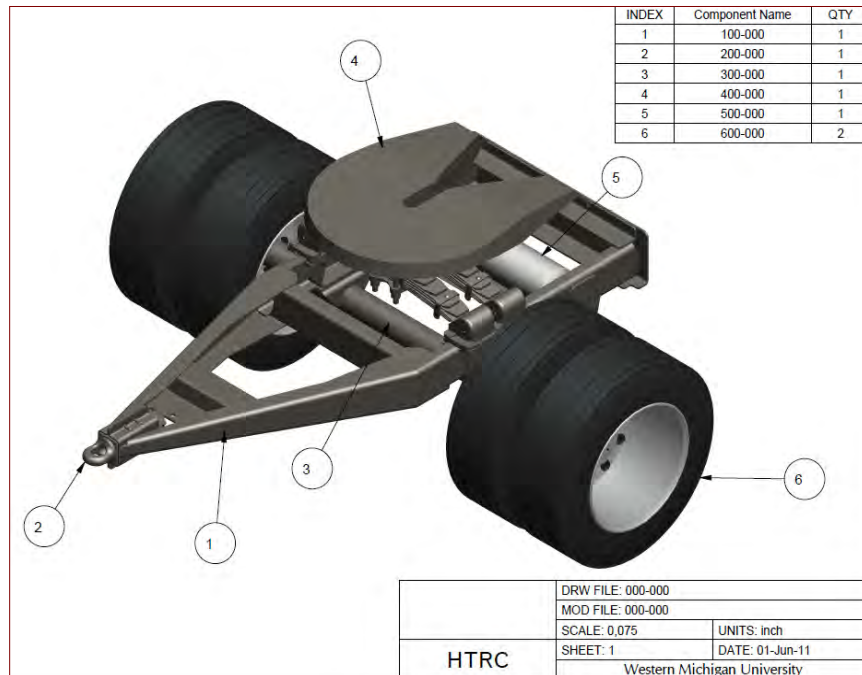


Figure C-139. Diagram. Dolly assembly.

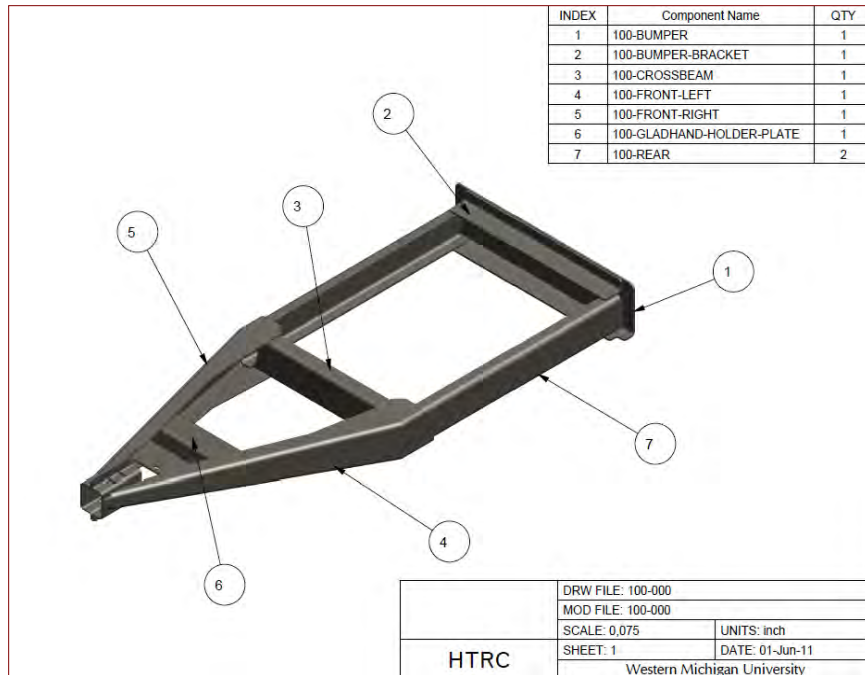


Figure C-140. Diagram. Dolly frame assembly.

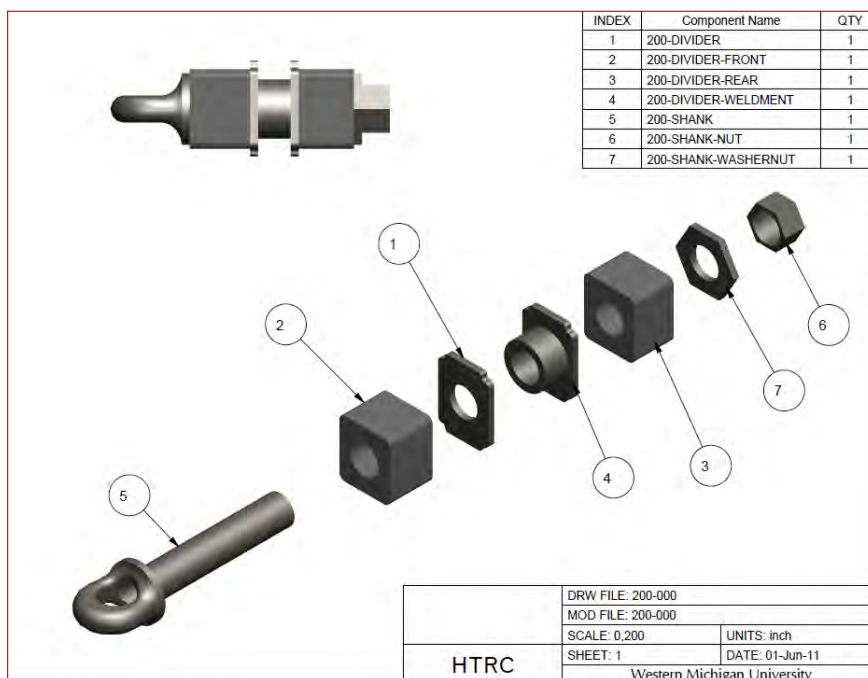


Figure C-141. Diagram. Rotating pintle hook assembly.

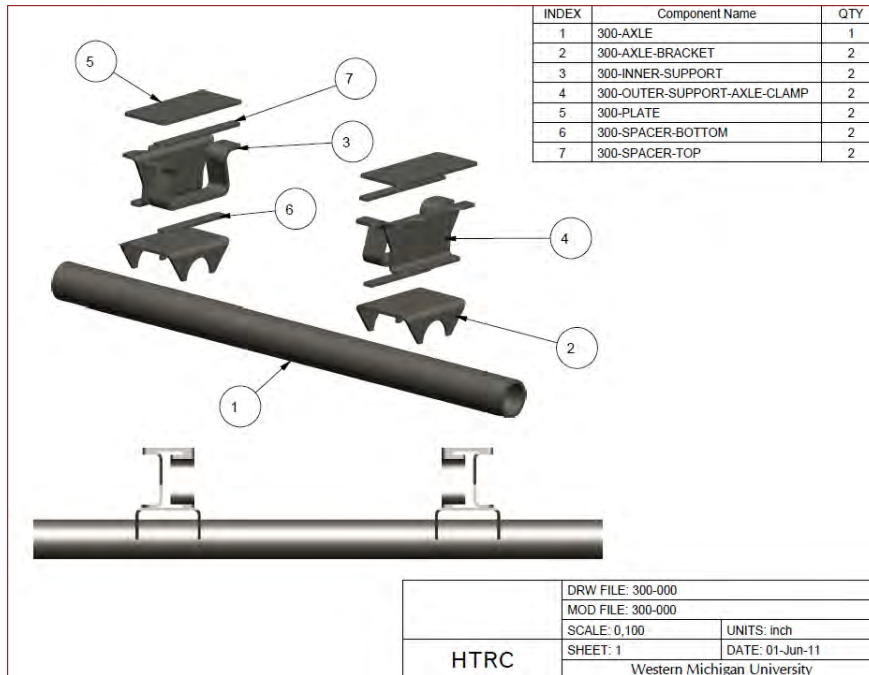


Figure C-142. Diagram. Axle mounting assembly.

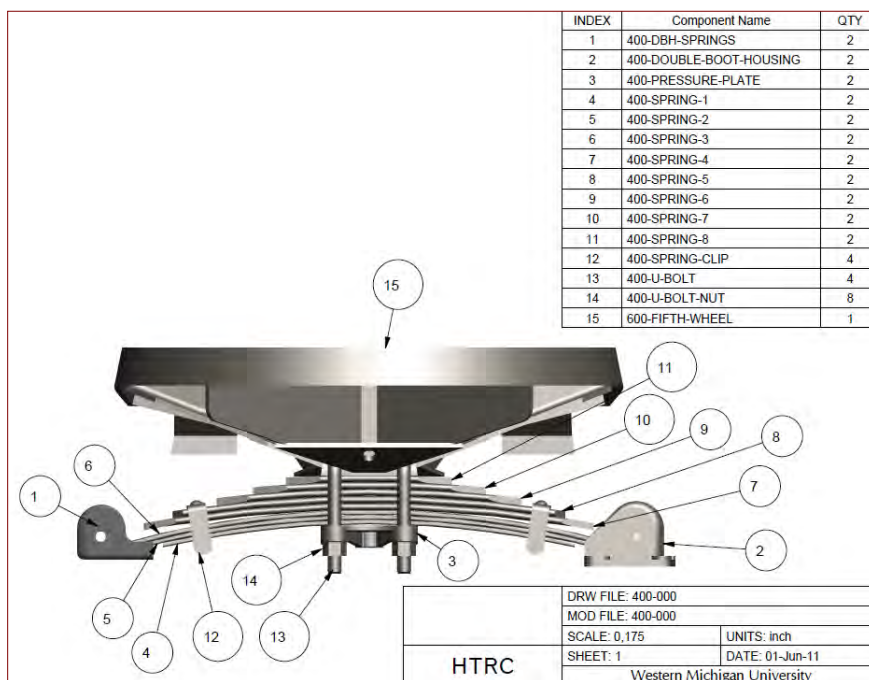


Figure C-143. Diagram. Sprung fifth wheel assembly.

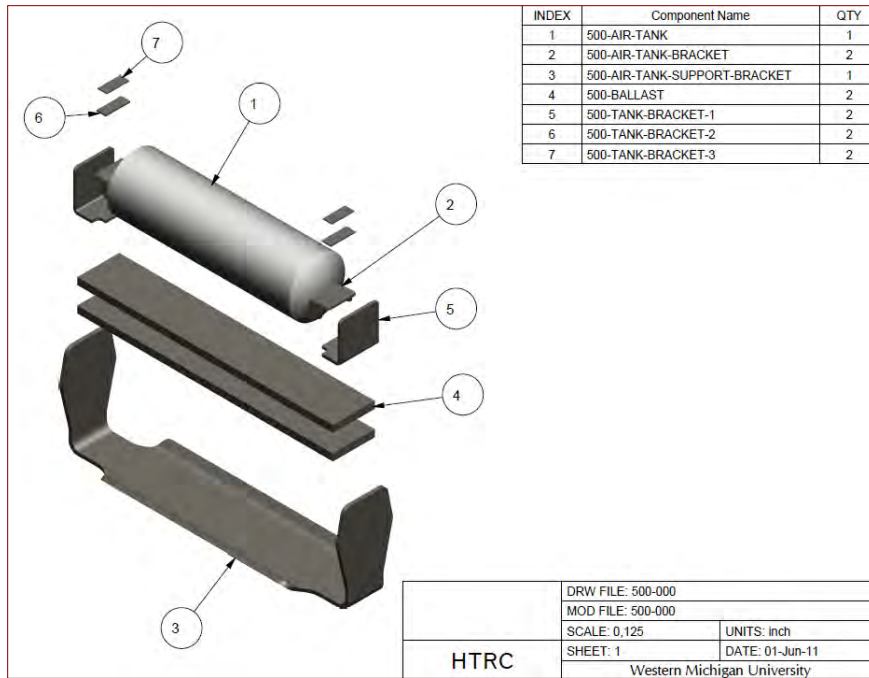


Figure C-144. Diagram. Air tank assembly.

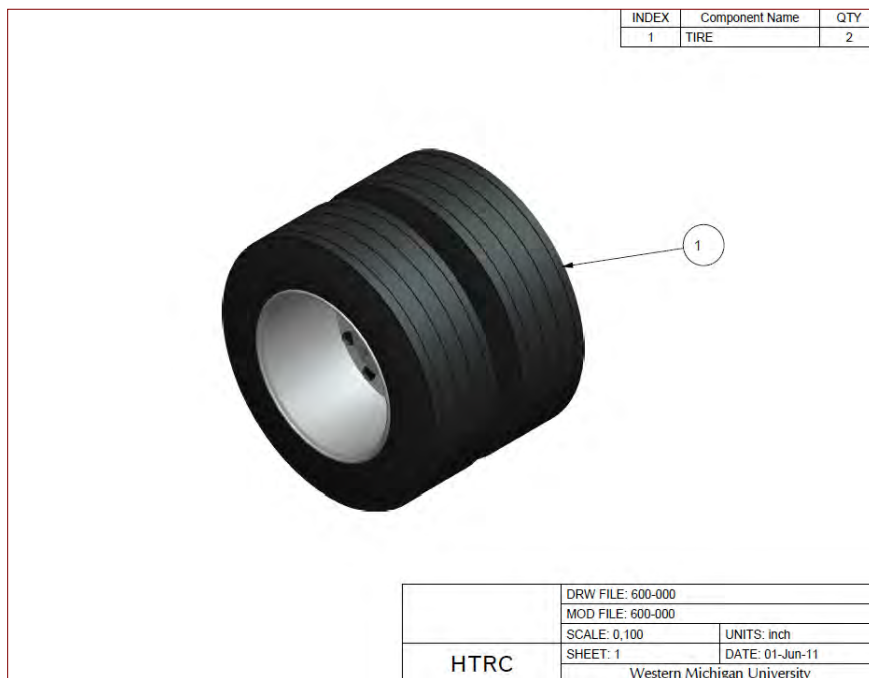


Figure C-145. Diagram. Dual wheel assembly.

C-4. Detailed Dimensions of the Test Vehicle

The dimensions of the complete test vehicle are presented in Table C-33.

Table C-33. Detailed Dimensions.

Freightliner Tractor Detailed Dimensions	*NOTE: Origin in longitudinal axis (X) is at the Front axle Centerline, In lateral axis (Y) is at centerline of truck, and in Vertical axis, at the ground. Use this origin unless dimension specifies point to point locations					
--	---	--	--	--	--	--

<u>Frame</u>							
Measurement	X-axis		Y-axis		Z-axis		Comments
	in	mm	in	mm	in	mm	
Frame Rail Span (CTR-CTR)			31 1/8	791			
Frame Rail Span (OUT-OUT)			34 1/2				
Frame C-Channel Cross-section Dimensions	7/8" x 3 5/8" x 11 1/8" with 1/4" inner C-Channel Reinforcement						
Length of Frame Rail	285 3/4	7258					
Bottom of Frame Rail at Rear Drive Axle					26 1/4		these measurements were taken when loaded, which means that during the LCV loaded state, the frame rails are slightly higher in the rear than in the front of the tractor
Bottom of Frame Rail at Steer Axle							

<u>fifth Wheel</u>							
Fifth Wheel Center	181 1/2	4610			43	1092	Z-direction defines the height of the platform off of the ground
Center to Front Drive Axle	19 3/4	502					front drive axle is located in front of the fifth wheel center
Center to Rear Drive Axle	31 1/2	800					rear drive axle is located behind the fifth wheel center
Loaded fifth Wheel ht					43	1092	
fifth Wheel Platform diameter			35 1/2	902			

Steer Axle (SA-1)

Measurement	X-axis		Y-axis		Z-axis		Comments
	in	mm	in	mm	in	mm	
Axle							
Manufacturer/Model				Dana Spicer E-1200I rated at 12,000 lbs			PAVE Reference Information
Track Width (CNT-CNT)			79 1/2	2019			center point b/t tires on each side is the CNT location
Tires outside to outside			89	2261			
Max Track Width at Rated Load			81 1/2	2070			source: Spicer Steer Axle Info - ONLINE
Beam Drop					3 1/2	89	source: Spicer Steer Axle Info - ONLINE
Center of axle to floor (ride ht)					12 3/4	324	NOTE: z coordinate denotes height
Axle cross section height					4 3/4	121	
Steering Components							
Pitman Arm Length					10 5/8	270	
Kingpin to kingpin			69	1753			
King Pin Location							kingpin is located at the center of the axle
King Pin Lateral Inclination (KPI)							kingpin is vertical
Tie rod center-center	47 1/16	1195	33 7/32	844	8 3/8	213	
Tie rod length			66 7/16	1688			
Tie rod arm length							
Push rod length			31 5/8	803			
Push rod declination angle (with horizontal)	12.0 deg from horizontal						
Steer arm length							NOTE: z coordinates is just length
Steering Wheel Rod diameter	0.995	25					

Measurement	X-axis		Y-axis		Z-axis		Comments
	in	mm	in	mm	in	mm	
Suspension							
Leaf Spring Design							Single leaf that extends from the front mount to rear mount with a reinforcement leaf extending only from the axle to forward mount. Each spring eye is connected to the mount by a link that allows the spring eyes to rotate about the mount center
Leaf Spring Dimensions at point nearest the spring eyes (width x thickness)			3 7/8	98	5/8	16	Both single leaf and reinforcement leaf are same width and thickness, springs taper at the same rate getting thicker as they approach the center of the steer axle from each eye
Leaf Spring Dimensions at Center of Steer Axle (width x thickness)			3 7/8	98	1	25	
Spring-Spring Span (CTR-CTR)			35 1/8	892			
Spring - Spring Span (OUT-OUT)			39	991			NOTE: y coordinate is spring span
Forward Spring Eye to Reward Spring Eye	56 1/2	1435					
Steer Axle Leaf Spring Eye Forward	25 5/8	651	17 1/4	438	21 1/2	546	
Steer Axle Leaf Spring Eye Rearward	30 7/8	784	17 1/4	438	19	483	
Damper Length					17	432	NOTE: z coordinate denotes length
Damper Upper Mount	43 7/8	1114	20 3/4	527	37 1/8	943	
Damper Lower Mount	43 7/8	1114	20 3/4	527	20 1/8	511	
Damper-Damper Span			41 1/2	1054			
Damper mounted length (P-P)					17	432	
Damper Inclination angle (fore-aft)	0.75 deg from vertical (in XZ-plane), tilting aft						
Axle Bump Stop Spacing			34 1/4	870			bump stop plate is clamped to the top of the leaf spring
Tires							
(SA-1) Tire Unloaded Tire Diameter					39	991	

<u>Front Drive Axle (DA-1)</u>							
Measurement	X-axis		Y-axis		Z-axis		Comments
	in	mm	in	mm	in	mm	
Axle							
Manufacturer/Model	Dana Spicer DSH40 rated at 40,000 LB					from PAVE Reference Information	
DA-2 to SA-1	213	5410					
DA-2 Track Width (CNT-CNT)			72 1/4	1835			center point b/t tires on each side is the CNT location
DA-2 Tire Outside to Outside			95	2413			
Drive Axle Spacing	51 1/4	1302					
DA-2 Axle Bump Stop Spacing			46	1168			
Static height b / t bump stop (Max Suspension travel)					2.559	65	
Tires							
(DA-2) Tire Unloaded Rolling Rad.					18 1/2	470	
(DA-2) Tire Width (bulge-bulge)			10 1/2	266 7/10			

Measurement	X-axis		Y-axis		Z-axis		Comments
	in	mm	in	mm	in	mm	
Suspension							
Spring-Spring Span			40 1/2	1028.7			
Forward Leaf spring Mount	31	787			9	229	in front of drive axle C/L (X-axis) and below bottom of frame rail (Z-axis)
Total Spring Length	45 7/8	1165					this is the distance from the spring eye (ahead of axle C/L) to center of airbag
Leaf spring Kick-twist angle	30 degrees towards the airbag center (angling towards center of vehicle)						angle measure from the lateral centerline of the spring at the section above the axle
Lateral distance kick-twist angle extends	4 3/4	121					towards center of tractor
Leaf spring inclination angle	10 degrees upwards towards airbag center						this angle represents the angle the spring inclines at from the damper mount to the airbag center
Height the spring inclination angle extends					2 1/2	64	distance between bottom of leaf and bottom center of the hole through the leaf where airbag is mounted
Upper leaf thickness at section below axle					1.87	47	This leaf continues beyond damper mount to airbag center
Upper leaf thickness at airbag centerline					0.944		
Lower leaf thickness at section below axle					0.63	16	This leaf ends underneath damper mount located behind axle
Spring Width at section below axle		3 1/8	79 3/8				
Airbag ID Number (All)	1115zk-6						
Airbag Dimensions (diameter x height)		8 1/4	210	12 9/16	319		height is from top of airbag to bottom, including mounting plates, when the airbags were not pressurized
Airbag bottom center height				13 15/16	354		Top center is located at the bottom of the frame rail
Airbag spacing (CNT-CNT)		31	787				
DA-2 C/L to Airbag Center	14 7/8	378					Airbag centerline located on bottom leaf spring after the leaf spring had tapered towards the airbag, behind the axle C/L
Damper Length	17 3/4						Dimension defines the full length of damper from eye to eye
Lower Damper Eye Center to DA-2	5	127					lower damper eye is located behind the axle C/L
Damper Inclination Angle	10 degrees						Measure from vertical angling in the aft direction
Damper-Damper Span			41 1/2	1054.1			
Static height b / t bump stop and frame (Max suspension travel)					2.559	65	

Rear Drive Axle (DA-2)

Measurement	X-axis		Y-axis		Z-axis		Comments
	in	mm	in	mm	in	mm	
Axle							
Manufacturer/Model			Dana Spicer DSH40 rated at 40,000 LB				from PAVE Reference Information
DA-2 to SA-1	213	5410					
DA-2 Track Width (CNT-CNT)			72 1/4	1835			center point b/t tires on each side is the CNT location
DA-2 Tire Outside to Outside			95	2413			
Drive Axle Spacing	51 1/4	1302					
DA-2 Axle Bump Stop Spacing			46	1168			
Static height b / t bump stop (Max Suspension travel)					2.559	65	
Tires							
(DA-2) Tire Unloaded Rolling Rad.					18 1/2	470	
(DA-2) Tire Width (bulge-bulge)			10 1/2	266 7/10			

Measurement	X-axis		Y-axis		Z-axis		Comments
	in	mm	in	mm	in	mm	
Suspension							
Spring-Spring Span			40 1/2	1028.7			
Forward Leaf spring Mount	31	787			9	229	in front of drive axle C/L (X-axis) and below bottom of frame rail (Z-axis)
Total Spring Length	45 7/8	1165					this is the distance from the spring eye (ahead of axle C/L) to center of airbag
Leaf spring Kick-twist angle	30 degrees towards the airbag center (angling towards center of vehicle)						angle measure from the lateral centerline of the spring at the section above the axle
Lateral distance kick-twist angle extends	4 3/4	121					towards center of tractor
Leaf spring inclination angle	10 degrees upwards towards airbag center						this angle represents the angle the spring inclines at from the damper mount to the airbag center
Height the spring inclination angle extends					2 1/2	64	distance between bottom of leaf and bottom center of the hole through the leaf where airbag is mounted
Upper leaf thickness at section below axle					1.87	47	This leaf continues beyond damper mount to airbag center
Upper leaf thickness at airbag centerline					0.944		
Lower leaf thickness at section below axle					0.63	16	This leaf ends underneath damper mount located behind axle
Spring Width at section below axle		3 1/8	79 3/8				
Airbag ID Number (All)	1115zk-6						
Airbag Dimensions (diameter x height)		8 1/4	210	12 9/16	319		Taken when airbag was pressurized, height is from top of airbag to bottom, including mounting plates
Airbag bottom center height				13 15/16	354		Top center is located at the bottom of the frame rail
Airbag spacing (CNT-CNT)		31	787				
DA-2 C/L to Airbag Center	14 7/8	378					Airbag centerline located on bottom leaf spring after the leaf spring had tapered towards the airbag, behind the axle C/L
Damper Length	17 3/4						Dimension defines the full length of damper from eye to eye
Lower Damper Eye Center to DA-2	5	127					lower damper eye is located behind the axle C/L
Damper Inclination Angle	10 degrees						Measure from vertical angling in the aft direction
Damper-Damper Span		41 1/2	1054.1				
Static height b / t bump stop and frame (Max suspension travel)					2.559	65	

<u>Drivelines</u>							
Measurement	X-axis		Y-axis		Z-axis		Comments
	in	mm	in	mm	in	mm	
Main Driveline							
Tubing O.D.			5.12	130			source: Axle, Transmission, Driveline info - ONLINE
Wall thickness			0.197	5			source: Axle, Transmission, Driveline info - ONLINE
Inter-axle Driveline							
Tubing O.D.			4.96	126			source: Axle, Transmission, Driveline info - ONLINE
Wall thickness			0.118	3			source: Axle, Transmission, Driveline info - ONLINE

NCAT Cheetah Chassis Trailer System & Component Geometry	*NOTE: Origin in longitudinal axis (X) is at the King Pin Centerline, In lateral axis (Y) is at centerline of trailer, and in Vertical axis at the ground. Use this origin unless dimension specifies point to point location.						
--	--	--	--	--	--	--	--

Measurement	X-axis		Y-axis		Z-axis		Comments
	in	mm	in	mm	in	mm	
Frame							
Main Frame Beam Cross Section Dimensions			4.11	104	12 1/8	308	
Forward Beam Cross Section Dimension			4.11	104	6 5/8	168	the kingpin platform is mounted to this section of frame rail
Main/Forward Frame Beam Web Thickness			0.210	5			
Frame I-beam Thickness (top/bottom flanges)	0.372	9					
Total Frame Rail Length (front to rear bumper)	278.5	7074					
Frame Rail Extension Beyond Kingpin	15	381					towards front of train
Length of Forward Frame Rail Section	75	1905					
Taper Angle of Frame Rail From Forward to Main Beam	tapering 24° downward						frame rail tapers from 6 5/8" to 12 1/8"
Top of Frame to Ground					47 11/16	1211	
Frame Rail Span (CTR-CTR)			36	914			Frame rails have a constant width for the length of the trailer
Frame Rail Span (OUT-OUT)			40 1/4	1022			
Kingpin-Trailer Axle Offset	181 1/8	4601			21 3/4	552	
Kingpin Platform Off Ground					41 1/16	1043	
Trailer Pintle to Kingpin Platform (height)					9 9/16	243	
Landing Gear to Trailer Axle (CNT-CNT)	123 1/2	3137					
Pintle Off Ground					30 1/2	800	
Frame Cross Member Supports	The cross members are C-channels						
Support Cross Sectional Dimensions	3 1/8	79	35 3/4	908	8	203	y-direction denotes the length that the cross section spans
Support Spacing (CNT-CNT)			48 5/8	1235			
Support Spacing (out-out)			51 3/4	1314			

Measurement	X-axis		Y-axis		Z-axis		Comments
	in	mm	in	mm	in	mm	
Suspension	Manufacturer: Hutchens Industries						
Spring-Spring Span (CTR-CTR)			36	914			
Hanger to Hanger Spacing (CNT-CNT)	36 1/2	927					from contact point to contact point
Forward Hanger to Axle C/L	19	483					
Leaf Spring/Hanger Contact Point Below Bottom of Frame Rail					4.83	123	
Number of Leafs	3 leafs						
Combined Leaf Thickness	Total thickness (of three leafs) is 3"						Matches 3-leaf H.D., High Arch, Hutchens Spring 365-00 characteristics
Leaf Spring Leaf Width			3	76			
Trailer Axle	Manufacturer: Dana Corporation						
Track Width (CTR-CTR)			71 1/2	1816			
Track Width (OUT-OUT)			81 1/2	2070			
Axle Ride Ht (GRD-CTR)					19 5/16	491	
Axle O.D.	5	127					Source: Hendrickson Trailer Application Guide
Axle Wall Thickness			1/2	13			Source: Hendrickson Trailer Application Guide
Axle to Bottom of Frame					16	406	
Landing Gear to Axle C/L (CNT-CNT)	123 1/2	3137					
Kingpin Platform-Trailer Axle Offset	181 1/8	4601			21 3/4	552	
Trailer Axle C/L to Pintle C/L	53 1/2	1359			12 3/16	310	
Tires							
Tire Loaded Rolling Radius					19 5/16	491	
Tire Width (bulge-bulge)			10 3/4	273			

Measurement	X-axis		Y-axis		Z-axis		Comments
	in	mm	in	mm	in	mm	
Cargo Container							
Front of Container	26	660					this is the distance from the center of the kingpin to the front of container
Container Dimensions	228	5791	96	2438	102	2591	(length x width x height); length measured outside wall to outside wall
Container Wall Cross Section	All dimension for wall cross section apply to the sides and front of container						
Container Wall Profile	side wall has a repeating chamfer pattern						
Protrusion Face Angle	26 deg - both out and in						
Horizontal Width of Flat Surface of Protrusion	2.87	73					
Length on the Inclined Protrusion Face	2.7	69					
Wall Thickness	.093" metal thickness for both side walls						
Forklift Slot Center from King Pin	106	2692					
Distance Between Fork Lift Holes	51	1295					
Container Under-Body Traverse Supports (ribs)							
Rib Cross Section Dimensions	2		92	2337	4		
Rib Spacing	12	305					
Container Corner Lift Hole Diameter	Oval in shape, with 2" diameter circles spaced 1.68 inches apart						
Corner Lift Hole Metal Thickness	uniform metal thickness of .63" on all 4 corners						

Note: The dolly used in testing had shorter side rails (72 inches vs 96 inches)

NCAT Silver Eagle Dolly 1 Detailed Dimensions	Make:	Silver Eagle		NOTE: Origin in longitudinal axis (X) is at the center of the pintle, In lateral axis (Y) is at centerline of the converter dolly, and in Vertical axis at the ground. Use this origin unless dimension specifies point to point location.							
	Model:	Eagle									
	Dolly ID:	F/BC/530/88									
	Position in Train:	First dolly									
Measurement	X-axis		Y-axis		Z-axis		Comments				
	in	mm	in	mm	in	mm					
Axle											
Track Width			72 5/8	1845							
Tire Width (bulge-bulge)			10 1/2	267							
Center of Axle to Ground					18 5/16	465					
Axle O.D.	5	127									
Suspension											
Center of Pintle to C/L of first Traversed Leaf Spring	89 5/8	2276					leaf springs are lateral across frame refer to pictures for better understanding				
FWD-RWD Leaf Spring Spacing (CNT-CNT)	8	203									
Spring Pin Height					32	813					
Spring Pin to Spring Pin (bushing housing)			38 1/2	978							
Bottom of Lowest Leaf to Top of Frame					1 5/8	41	Taken at center of dolly along the y-axis				
Leaf Dimensions of Traversal Leaf-Springs	width (x-axis)		traverse span (y-axis)		thickness (z-axis)						
spring 1 (bottom spring)	4	101	29 3/4	755	3/8	10					
spring 2	4	101	39	990	3/8	10					
spring 3	4	101	39	990	3/8	10					
spring 4	4	101	32 1/2	825	1/2	13					
spring 5	4	101	28 1/4	717	1/2	13					
spring 6	4	101	22 1/4	565	1/2	13					
spring 7	4	101	17	432	1/2	13					
spring 8	4	101	12	305	1/2	13					

Measurement	X-axis		Y-axis		Z-axis		Comments
	in	mm	in	mm	in	mm	
Tires							
Tire Loaded Rolling Radius					18 5/16	465	
Tire Width (bulge-bulge)			10 1/2	267			

Measurement	X-axis		Y-axis		Z-axis		Comments
	in	mm	in	mm	in	mm	
<u>Frame and Drawbar</u>							
Frame Rail Span (CNT-CNT)			33 1/2	851			
Frame Rail Span (OUT-OUT)			37	940			
Frame Rail C-Channel Cross Section Height	3	76	7	178	0.4	10	width x height x thickness
Frame Height (top of frame to ground)					28 5/8	727	
Frame Height (bottom of frame to ground)					21 5/8	549	
Frame Flange Thickness					0.4	10	
Cross Member C-Channel Cross-Section Dimensions	3	76	7	178	0.4	10	width x height x thickness
Drawbar Length	61	1549					measured perpendicular from the forward face of cross member to pintle center
Drawbar Narrowing Angle	12 deg inward						narrows from the frame rail span width to a width of 3 5/8" at pintle
Drawbar C-Channel Cross Section (nearest pintle hook)			3.56	90			width of each drawbar rail at pintle hook
Drawbar C-Channel Cross Section (nearest frame rail)			7 9/16	192			width of each drawbar rail at main frame connection
Drawbar C-Channel Flange Thickness					0.28	7	
Drawbar Tapering Angle	8 deg upward from the horizontal						Bottom edge of C-channel tapers towards the top edge
Pintle to Rear Bumper	127 7/8	3248					
Pintle Center to Ground Ht					30 1/2	775	
Pintle to Dolly Axle	93 5/8	2378					
Pintle to fifth Wheel Center	93 5/8	2378					
Fifth Wheel Platform to Dolly Axle Center					24	610	
Fifth Wheel Platform to Top of Frame					14 3/8	365	
Rear Bumper Top Flange					0.39	10	
Platform U-bolt Diameter			0.96	24			

NCAT Silver Eagle Falcon Dolly Detailed Dimensions (This dolly was not used in the track or highway tests.)	Make:	Silver Eagle	NOTE: Origin in longitudinal axis (X) is at the center of the pintle, In lateral axis (Y) is at centerline of the converter dolly, and in Vertical axis at the ground. Use this origin unless dimension specifies point to point location.			
	Model:	Falcon				
	Dolly ID:	F/BC/477/91				
	Position in Train:	Second Dolly				

Measurement	X-axis		Y-axis		Z-axis		Comments
	in	mm	in	mm	in	mm	
Frame & Drawbar							
Length of dolly (pintle hook to rear bumper)	130 3/8	3312					
Pintle to Ground Ht					30 1/2	775	
Pintle to Dolly Axle	103 1/8	2619					
Pintle to fifth wheel Center	104 1/4	2648					
Frame Rail Span (CTR-CTR)			33 1/2	851			
Main frame C-channel width			5 5/16	135			
Bottom of frame rail height off of ground					23	584.2	
Length of drawbar	68 3/8	1737					including 24" extension
Drawbar narrowing angle (turns in 20 deg from straight)	20 deg inward, perpendicular length of 44 3/8 "						Drawbar does not taper above or below the frame rails
Drawbar pintle hook straight extension	24	610					This extension is from the front of the drawbar to the pintle eye
Axle & Tires							
Track Width			73 1/8	1857			
Inside tire to inside tire (cnt-cnt)			60	1524			
Outside tire to outside tire (cnt-cnt)			86 1/4	2191			
Tire Width (bulge-bulge)			10 1/2	267			
Axle Ride Ht (to center of axle)					19	483	
Axle O.D.	5	127					

Measurement	X-axis		Y-axis		Z-axis		Comments
	in	mm	in	mm	in	mm	
Suspension							
Forward Hanger/Leaf spring Contact Point	78	1981			19 1/2	495	leaf springs are longitudinal
Reward Hanger/Leaf spring Contact Point	118 1/4	3004			18 15/16	481	
FWD-RWD Leaf spring span	40 1/4	1022					
Leaf spring lateral span (center-center)			38 1/4	972			
Pintle hook to forward leaf spring contact	82 7/8	2105					
Leaf spring bracket width			4.2	107			
Leaf spring arc height from horizontal			7	178			
U-bolts connecting leaf springs to axle	14.75" high with 6" spread, diameter of 0.83"						
Leaf spring width			3	76			
Suspension Range of Motion							

Appendix D:

TruckSim® Release Notes

This page intentionally left blank.

Table of Contents

D-1	THE TRUCKSIM® COORDINATE SYSTEM.....	D-1
D-2	MODEL FORMULATION	D-2
D-2.1	SELECTING THE CONFIGURATION	D-3
D-2.1.1	Steer Axle Compliances (Axle 1).....	D-7
D-2.1.2	Steer Axle Kinematics (Axle 1).....	D-9
D-2.1.3	Drive Axle Compliances (Axles 2 & 3).....	D-10
D-2.1.4	Drive Axle Kinematics (Axles 2 & 3).....	D-13
D-2.2	MODELING THE TRAILERS.....	D-15
D-2.2.1	Trailer Axle Compliance.....	D-17
D-2.2.2	Trailer Axle Kinematics	D-19
D-2.3	MODELING THE DOLLIES.....	D-20
D-2.3.1	Dolly Axle Compliance	D-21
D-2.3.2	Dolly Axle Kinematics.....	D-23
D-2.3.3	Dolly Sprung Mass.....	D-24
D-2.4	MODELING THE PINTLE HITCH	D-25
D-2.5	MODELING THE FIFTH WHEEL.....	D-26
D-2.6	MODELING THE TIRES.....	D-26
D-2.7	SETTING THE MASS PROPERTIES OF THE TEST VEHICLE	D-29
D-3	MANEUVERS AND STEERING INPUT	D-33
D-3.1	THE CONSTANT RADIUS COURSE.....	D-33
D-3.2	THE SINGLE LANE CHANGE	D-35
D-3.3	THE DOUBLE LANE CHANGE.....	D-36
D-3.4	GRADUAL SINGLE LANE CHANGE.....	D-37
D-3.5	SPEED CONTROL FOR ALL MANEUVERS	D-39
D-3.6	FUTURE CONSIDERATIONS FOR BUILDING A TRUCKSIM® MODEL.....	D-39

List of Tables

Table D-1. Steer axle compliance parameters used to characterize the test vehicle in TruckSim®. The table is in the order of the screen capture in Figure D-5.....	D-8
Table D-2. Steer Axle Kinematic Parameters used for modeling the NCAT test vehicle. The table is in the order of the screen capture in Figure D-7.....	D-10
Table D-3. Drive axle compliance parameters used to characterize the test vehicle in TruckSim®. The table is in the order of the screen capture in Figure D-8.....	D-12
Table D-4. Drive axle kinematic parameters used for modeling the NCAT test vehicle. The table is in the order of the screen capture in Figure D-10.....	D-14
Table D-5. Trailer axle compliance parameters used to characterize the test vehicle in TruckSim®. The table is in the order of the screen capture in Figure D-13.....	D-18
Table D-6. Trailer Axle Kinematic Parameters used for modeling the NCAT test vehicle. The table is in the order of the screen capture in Figure D-15.....	D-20
Table D-7. Dolly axle compliance parameters used to characterize the test vehicle in TruckSim®. The table is in the order of the screen capture in Figure D-17.....	D-22
Table D-8. The following table lists the dolly axle kinematic parameters used for modeling the NCAT test vehicle. The table is in the order of the screen capture shown in Figure D-19.....	D-24
Table D-9. The parameters and their source for the tire characterization used for the LCV model.....	D-27
Table D-10. The wheel loads and axle loads at their respective locations in the combination. The “Measured” column refers to wheel loads measured on the test vehicle. The “TruckSim®” column refers to the wheel loads of the modeled vehicle. All values in kg	D-30
Table D-11. Gross weights of the units in the NCAT vehicle.....	D-30
Table D-12. Location of payload CG.....	D-31
Table D-13. The location of the sprung mass CG as entered in TruckSim® for each respective unit of the combination without payloads.....	D-32

List of Figures

Figure D-1. Sketch. The above figure shows the coordinate system used by TruckSim®. (Mechanical Simulation Corporation 2010)	D-2
Figure D-2. Screen Capture. The “TruckSim Run Control Screen” for the model of the LCV test vehicles at NCAT test facility (Mechanical Simulation Corporation 2010).	D-3
Figure D-3. Screen Capture. The “Loaded Combination” screen. From this screen the modeler links the units in the combination together and selects payloads. This screen also allows navigation to the constituent units for parameter modification.	D-4
Figure D-4. Screen Capture. The “Lead Unit” screen. The modeler navigates to lower pages to enter in more detailed kinematic, compliance, and mass property data (Mechanical Simulation Corporation 2010).	D-4
Figure D-5. Screen Capture. The “Suspension: Solid Axle Compliance, Springs, and Dampers” screen allows the modeler to enter data to define the spring and damper characteristics for the vehicle (Mechanical Simulation Corporation 2010).	D-7
Figure D-6. Screen Capture. The “Suspension: Measured Total Roll Stiffness” screen in TruckSim® calculates the auxiliary roll stiffness for the steer axle (Mechanical Simulation Corporation 2010).	D-9
Figure D-7. Screen Capture. The “Suspension: Solid Axle System Kinematics” screen allows the modeler to enter data to define the steer axle kinematic characteristics for the vehicle (Mechanical Simulation Corporation 2010).	D-9
Figure D-8. Screen Capture. The “Solid Axle Compliance, Springs, and Dampers” screen allows the modeler to enter data to define the drive axle spring and damper characteristics for the vehicle (Mechanical Simulation Corporation 2010).....	D-11
Figure D-9. Screen Capture. The “Suspension: Measured Total Roll Stiffness” screen in TruckSim® for the NCAT tractor steer axle (Mechanical Simulation Corporation 2010).....	D-13
Figure D-10. Screen Capture. The “Solid Axle System Kinematics” screen allows the modeler to enter data to define the drive axle spring and damper characteristics for the vehicle (Mechanical Simulation Corporation 2010).....	D-13
Figure D-11. Screen Capture. The “Suspension: Solid Axle Roll Steer” screen (Mechanical Simulation Corporation 2010).	D-14
Figure D-12. Screen Capture. The “Trailer with 1 Axle” screen (Mechanical Simulation Corporation 2010).....	D-15
Figure D-13. Screen Capture. The “Trailer Axle Compliance” screen allows the modeler to enter data to define the trailer axle spring and damper characteristics for the vehicle (Mechanical Simulation Corporation 2010).....	D-17
Figure D-14. Screen Capture. The “Suspension” Measured Total Roll Stiffness” screen in TruckSim® for the NCAT trailer (Mechanical Simulation Corporation 2010).	D-19
Figure D-15. Screen Capture. The “Solid Axle System Kinematics” screen allows the modeler to enter data to define the trailer axle kinematic characteristics for the vehicle (Mechanical Simulation Corporation 2010).....	D-19
Figure D-16. Screen Capture. The “Vehicle: Dolly with 1 Axle” screen (Mechanical Simulation Corporation 2010).	D-21

List of Figures (Continued)

Figure D-17. Screen Capture. The “Solid Axle Compliance, Springs, and Dampers” screen where the modeler defines the dolly compliance (Mechanical Simulation Corporation 2010).....	D-21
Figure D-18. Screen Capture. The “Suspension: Measured Total Roll Stiffness” screen in TruckSim® for the NCAT Dolly (Mechanical Simulation Corporation 2010).....	D-23
Figure D-19. Screen Capture. The “Solid Axle System Kinematics” screen allows the modeler to enter data to define the dolly axle kinematic characteristics for the vehicle (Mechanical Simulation Corporation 2010).....	D-23
Figure D-20. Screen Capture. Sprung Mass definition for Silver Eagle dolly (Mechanical Simulation Corporation 2010)	D-25
Figure D-21. Screen Capture. The “Hitch: Joint Assembly” screen allows the modeler to define the pitch, heave, and yaw moment characteristics that define the pintle hitch (Mechanical Simulation Corporation 2010).....	D-25
Figure D-22. Screen Capture. The “Hitch” screen allows the modeler to define the pitch, heave, and yaw moment characteristics that define the fifth wheel. This model was used at all 3 fifth wheel positions in the NCAT LCV model (Mechanical Simulation Corporation).....	D-26
Figure D-23. Screen Capture. The “Tire” screen allows the modeler to navigate between the different force and moment data sets used to characterize the modeled tire (Mechanical Simulation Corporation 2010)	D-27
Figure D-24. Screen Capture. The “Tire Longitudinal Force” screen allows the modeler to enter in the longitudinal force characteristics in tabular form. THIS IS NOT ACTUAL TIRE DATA (Mechanical Simulation Corporation 2010).....	D-28
Figure D-25. Screen Capture. The “Tire Lateral Force” screen allows the user to enter the lateral force characteristics in tabular form. THIS IS NOT ACTUAL TIRE DATA (Mechanical Simulation Corporation 2010)	D-28
Figure D-26. Screen Capture. The “Tire: Aligning Moment” screen allows the user to enter the aligning moment characterizing data in tabular form. THIS IS NOT ACTUAL TIRE DATA (Mechanical Simulation Corporation 2010).....	D-29
Figure D-27. Screen Capture. The “Payload: Box Shape” shows the point mass payload definition for Trailer 1. This is typical for the three trailers aside from the magnitude of the mass and its location forward and aft (Mechanical Simulation Corporation 2010)	D-31
Figure D-28. Screen Capture. The “Lead Unit Sprung Mass” definition screen allows the modeler to adjust the unsprung mass properties of the tractor (Mechanical Simulation Corporation 2010)	D-32
Figure D-29. Screen Capture. The “Road: X-Y Coordinates of Centerline” screen allows the modeler to set up the course geometry (Mechanical Simulation Corporation 2010).....	D-34
Figure D-30. Screen Capture. Road elevation of 14% corresponding to the 8-deg bank of the NCAT track (Mechanical Simulation Corporation 2010).....	D-34
Figure D-31. Screen Capture. The “Road: Animator Repeated Object” screen allows course set up for the Single Lane Change maneuver (Mechanical Simulation Corporation 2010).....	D-35

List of Figures (Continued)

- Figure D-32. Screen Capture. The “Control: Steering by the Closed-loop Driver Model” screen shows the target path for simulation of the Single Lane Change Maneuver (Mechanical Simulation Corporation 2010). D-36
- Figure D-33. Screen Capture. The “Road: Animator Repeated Object” screen allows the course set up for the double lane change maneuver (Mechanical Simulation Corporation 2010)..... D-36
- Figure D-34. Screen Capture. The “Control: Steering by the Closed-loop Driver Model” screen allows the target path for simulation of the Double Lane Change Maneuver to be defined (Mechanical Simulation Corporation 2010)..... D-37
- Figure D-35. Screen Capture. The “Road: Animator Repeated Object” screen allows the course set up for the gradual single lane change maneuver (Mechanical Simulation Corporation 2010). D-38
- Figure D-36. Screen Capture. The “Control: Steering by the Closed-loop Driver Model” screen allows the target path for simulation of the Gradual Single Lane Change Maneuver to be defined. (Mechanical Simulation Corporation 2010)..... D-39

This page intentionally left blank.

Parameters describing the model of a truck are entered in TruckSim® (Mechanical Simulation Corp., Ann Arbor, MI) through a series of graphic screens. This appendix presents the screens that were used to enter the model of the NCAT triple as described in Chapter 6.

Tables following many of the screens list the values that were put in the fields and the source for those values. Where possible, values were taken from actual measurements of the vehicle; their source is identified as the WMU Vehicle Characterization Report (Appendix C). Parameters listed “As Packaged” were left as the default parameters of TruckSim® because no measurement of the NCAT vehicle was available.

D-1 The TruckSim® Coordinate System

TruckSim® uses the ISO coordinate system. The global coordinate system is right handed and defined in TruckSim as X_E facing forward, Y_E facing to the left and Z_E facing upward. This and the following related coordinates systems are depicted in Figure D-1.

The vehicle coordinate system in TruckSim® is right handed and defined as the positive X_V direction along the longitudinal centerline of the unit pointing in the forward direction, the positive Y_V direction at the CG of the vehicle pointing toward the left side, and the positive Z_V direction at the CG of the vehicle point upward. This coordinate system is used to describe the attitude of the vehicle dynamically and locations within the vehicle. Forward motion is positive in the X_V direction and positive roll is rotation about the X_V axis in the direction from Y_V toward Z_V . Lateral motion is positive in the Y_V direction and positive pitch is rotation about the Y_V axis in the direction from Z_V to X_V . Elevation is positive in the Z_V direction and positive yaw is rotation about the Z_V axis in the direction from X_V to Y_V .

The Intermediate coordinate system is right handed and defined in TruckSim® as Z pointing upward parallel to Z_E , Y is the cross product of X and Z_E and X is in the vertical plane that contains X_V . The intermediate coordinate system is used to transform the yaw rotation from the vehicle coordinate system to the global coordinate system. This coordinate system is included in this description but is of no interest to this research and was included for background.

TruckSim® defines each unit (tractor, trailer, or dolly) in the combination as a separate vehicle. The origin for the tractor is the centerline of the front axle. The sprung mass origin for the trailers and dollies are at the front hitch at zero vertical elevation (ground level). The sprung mass origin for the tractor is longitudinally and laterally at the axle centerline at zero vertical elevation (ground level). The axles are located longitudinally from these origins. It is possible to set back the front axle of the tractor, but the origin remains at the axle. Each dimension that defines the vehicle is in the coordinate system of the unit (tractor, trailer or dolly) that the dimensioned component is attached to.

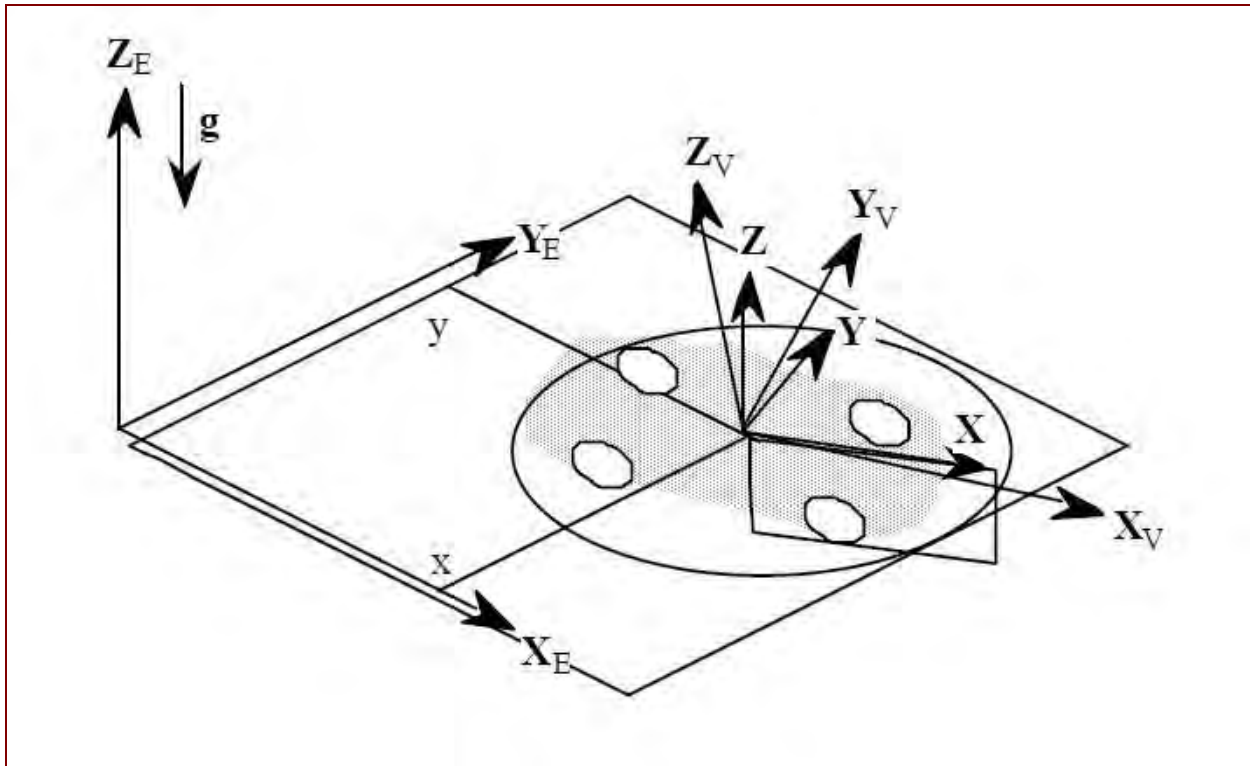


Figure D-1. Sketch. The above figure shows the coordinate system used by TruckSim®.
(Mechanical Simulation Corporation 2010)

D-2 Model Formulation

The first screen the modeler encounters in TruckSim® is the “TruckSim Run Control” screen (Figure D-2). From this screen the modeler accesses all aspects of the model, its simulation, and its output. Vehicle and maneuver selection as well as output format is controlled from this screen.

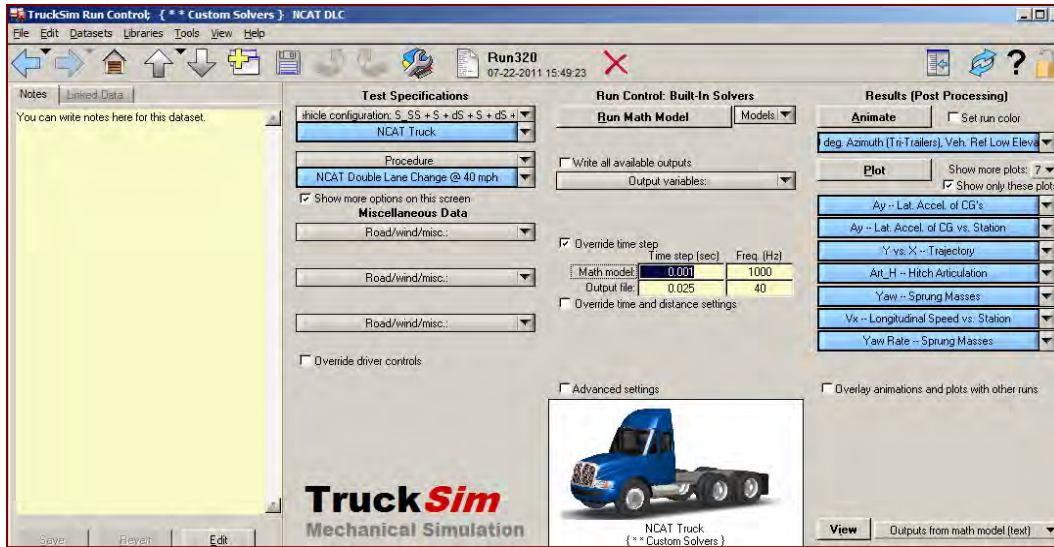


Figure D-2. Screen Capture. The “TruckSim Run Control Screen” for the model of the LCV test vehicles at NCAT test facility (Mechanical Simulation Corporation 2010).

D-2.1 Selecting the Configuration

Modeling the NCAT test vehicle in TruckSim® began with selecting the appropriate vehicle configuration from the list at the top of the “Test Specifications” heading on the Run Control Screen. The configuration chosen for the NCAT vehicle was denoted as S_SS+S+dS+S+dS+S. The “S” in this nomenclature stands for solid suspension. The “dS” stands for 1-axle dolly. The “_” denotes a common frame. The “+” denotes a hitched connection. Hence the selected generic vehicle for this model is a 3-axle tractor hitched to a 1-axle trailer, hitched to a 1-axle dolly, hitched to a second 1-axle trailer, hitched to a second 1-axle dolly, that is finally hitched to a third 1-axle trailer. This was chosen as the configuration for the NCAT test vehicle because it best fit the actual configuration. The preconfigured vehicle configuration was copied and renamed “NCAT Truck.”

To change parameters to model the behavior of the test vehicle, the modeler navigated to the “Loaded Combination Screen” (Figure D-3). This screen contains links to the parameter screens that were used to define the characteristics of the model.

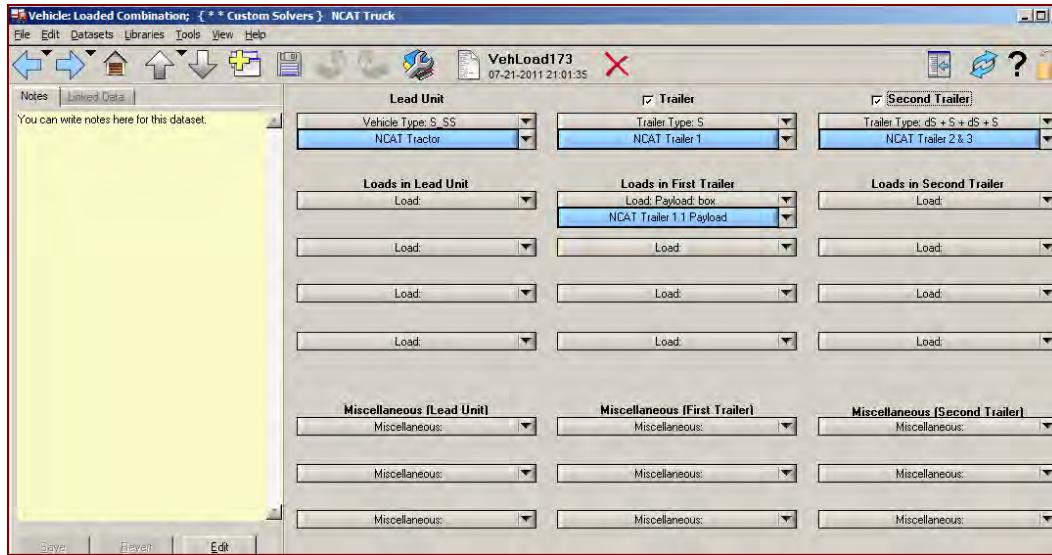


Figure D-3. Screen Capture. The “Loaded Combination” screen. From this screen the modeler links the units in the combination together and selects payloads. This screen also allows navigation to the constituent units for parameter modification.

The modeler navigates from the “Vehicle: Loaded Combination” screen to the “Vehicle: Lead Unit with 3 Axles” screen (Figure D-4). It is here that the modeler can see the options available for characterizing a vehicle.

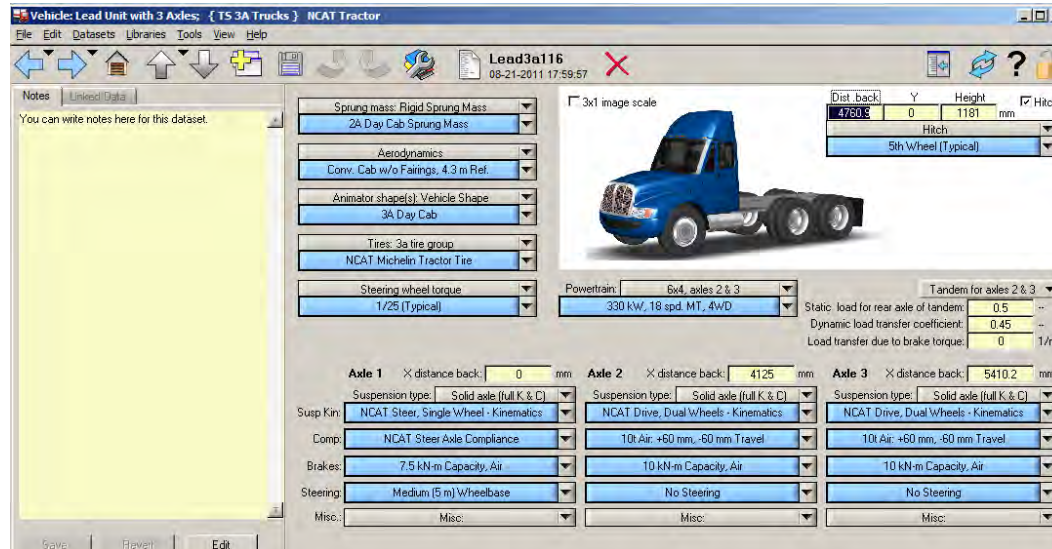


Figure D-4. Screen Capture. The “Lead Unit” screen. The modeler navigates to lower pages to enter in more detailed kinematic, compliance, and mass property data (Mechanical Simulation Corporation 2010).

This screen allows the section of mass properties, kinematics, and compliances for a 3-axle day cab tractor configuration. The gray bars indicate categories to select from, while the blue bars link to tables of data characterizing the categorized model property. For this investigation, the

categories were left as packaged with the TruckSim® custom solvers. The following list explains the selections shown in Figure D-4 (in order from top to bottom and left to right):

- 1) **Sprung mass: Rigid Sprung Mass/2A Day Cab Sprung Mass** – This selection was used because the layout of the sprung mass between a 3-axle day cab and a 2-axle day cab is similar, aside from the different length and overall mass. This category links to a screen that allows the mass properties to be tailored by mass and location. The license of TruckSim® for this research allows only rigid sprung mass modeling.
- 2) **Aerodynamics/Conv. Cab w/o Fairings, 4.3 m Ref** – This selection was left as packaged in the TruckSim® custom solver package, because aerodynamics were not of interest for this investigation. The aerodynamic behavior is described in tables of coefficient of drag per slip angle for each of the three aero forces and three aero moments.
- 3) **Tires: 3a tire group/NCAT Michelin Tractor Tires** – Michelin provided tire data in the form of force-moment per slip angle plots. These data were imported into TruckSim® for modeling purposes.
- 4) **Steering wheel torque/1/25(Typical)** – These data were left as packaged with the software, because the study of the vehicle response for this investigation does not consider driver torque inputs. This would be of use if the steering system were more accurately characterized and the test vehicle outfitted with steering torque sensing instrumentation.
- 5) **Powertrain: 6x4, axles 2 & 3 / 330 kW, 18 spd. MT, 4WD** – This was selected as the powertrain to allow the model power to complete the maneuvers. It is not representative of the actual powertrain of the NCAT test vehicles. The 18-Speed transmission aids in providing the proper gear ratio needed to complete the maneuver at speed.
- 6) **Hitch / Fifth Wheel (Typical)** – This option links to force-moment data that characterize the fifth wheel dynamically. This was left as packaged, because no other value was known for the test vehicle.
 - a. **Dist. back** – This is the distance the fifth wheel is mounted back from the origin (front axle). This was set at 4760.9 mm as was reported by WMU.
 - b. **Y** – The lateral location was left at 0 mm from center as reported by WMU.
 - c. **Height** – The height of the fifth wheel was set to 1181 mm as was reported by WMU.
- 7) **Axle 1: Steer Axle**
 - a. **X distance back** – This is set to zero (the front axle is the origin of the tractor).
 - b. **Suspension type: Solid axle (full kinematics and compliance, or K&C)** – This option was left as packaged because the NCAT tractor has a solid axle front suspension that is typical of this kind of vehicle. The axle motion was characterized in this model by K&C data.

- c. **Susp Kin: NCAT Steer, Single Wheel – Kinematics** – This links the solver to kinematic parameter tables characterizing the test vehicle.
- d. **Comp: NCAT Steer Axle Compliance** – This links to the kinematics of the steer axle as characterized by WMU.
- e. **Brakes: 7.5kN-m Capacity, Air** – This was left as packaged with the software, because braking performance was not of interest in this investigation.
- f. **Steering: Medium (5m) Wheelbase** – This was selected because it sets the steering model for 100% Ackerman steering for a 5 meter wheel base tractor, which is in agreement with WMU Characterization Report.

8) **Axle 2: Forward Drive Axle**

- a. **X distance back** – This value is set to 4125 mm back as measured and reported by WMU.
- b. **Suspension type: Solid axle (full K&C)** – This was left as packaged because the NCAT tractor has solid suspension drive axles typical of this kind of vehicle. The axle motion was characterized by K&C data.
- c. **Comp: 10t Air: +60 mm -60 mm Travel** – As packaged 10 ton air suspension. This was used because no characterization data existed for the drive axles of the NCAT test vehicle.
- d. **Brakes: 10kN-m Capacity, Air** – This was left as packaged because braking performance was not of interest for this investigation.
- e. **Steering: No Steering** – This was left as packaged because the test vehicle was not equipped with drive axle steering.

9) **Axle 3: Rearward Drive Axle (modeled identically to the Forward Drive Axle)**

- a. **X distance back** – This is set to 5410.2 mm as reported in by WMU in their Characterization Report.
- b. **Suspension type:** (modeled identically to the Forward Drive Axle)
- c. **Comp: 10t Air:** (modeled identically to the Forward Drive Axle)
- d. **Brakes:** (modeled identically to the Forward Drive Axle)
- e. **Steering:** (modeled identically to the Forward Drive Axle)

10) **Other options on this page**

- a. **Static load for rear axle of tandem:** Left as packaged at 0.5, because this approximated the actual value from the static axle loads of the test vehicle.
- b. **Dynamics load transfer coefficient:** This was left as packaged at 0.45, because no other value was known for this option that characterized the test vehicle.
- c. **Load Transfer due to break torque:** This value was left as packaged at 0 m^{-1} because no other value was known for this option that characterized the test vehicle.

D-2.1.1 Steer Axle Compliances (Axle 1)

The modeler enters the spring and damper characterization data in the “Suspension: Solid Axle Compliance, Springs, and Dampers” screen (Figure D-5).

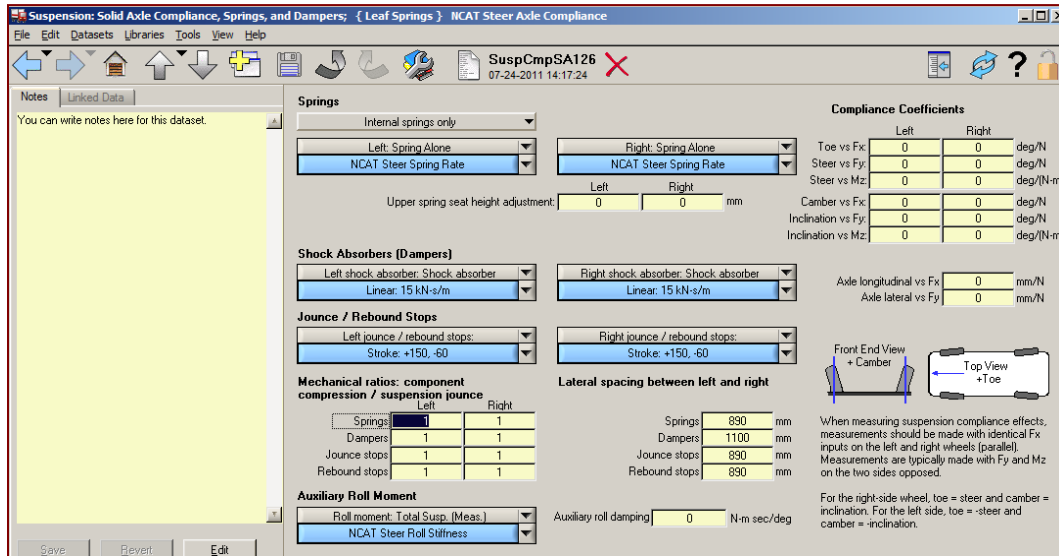


Figure D-5. Screen Capture. The “Suspension: Solid Axle Compliance, Springs, and Dampers” screen allows the modeler to enter data to define the spring and damper characteristics for the vehicle (Mechanical Simulation Corporation 2010).

Table D-1 contains the parameters that were used to define the steer axle compliances of the NCAT test vehicle.

Table D-1. Steer axle compliance parameters used to characterize the test vehicle in TruckSim®.
The table is in the order of the screen capture in Figure D-5.

Model Parameter	Value	Source
Internal springs only	Selected	As Packaged
Left Spring Alone	NCAT Steer Spring Rate 263 N/mm with 2000 N friction	WMU Characterization Report
Right Spring Alone	NCAT Steer Spring Rate 263 N/mm with 2000 N friction	WMU Characterization Report
Left shock absorber: Shock absorber	Linear: 15 kN/m	As Packaged
Right shock absorber: Shock absorber	Linear: 15 kN/m	As Packaged
Left jounce / rebound stops	+150, -60 mm	As Packaged
Right jounce/ rebound stops	+150, -60 mm	As Packaged
Mechanical ratios: component Compression/suspension jounce		
Springs	Left = 1, Right = 1	As Packaged
Dampers	Left = 1, Right = 1	As Packaged
Jounce stops	Left = 1, Right = 1	As Packaged
Rebound stops	Left = 1, Right = 1	As Packaged
Roll moment: Total Suspension (Measured)	NCAT Steer Roll Stiffness, See Figure 6-7 below.	WMU Characterization Report
Lateral spacing between left and right		
Springs	890 mm	WMU Characterization Report
Dampers	1100 mm	WMU Characterization Report
Jounce Stops	890 mm	WMU Characterization Report
Rebound Stops	890 mm	WMU Characterization Report
Auxiliary roll damping	0 N-m-s/deg	As Packaged
Toe vs Fx	Left = 0, Right = 0 deg/N	As Packaged
Steer vs Fy	Left = 0, Right = 0 deg/N	As Packaged
Steer vs Mz	Left = 0, Right = 0 deg/N-m	As Packaged
Camber vs Fx	Left = 0, Right = 0 deg/N	As Packaged
Inclination vs F	Left = 0, Right = 0 deg/N	As Packaged
Inclination vs Mz	Left = 0, Right = 0 deg/N-m	As Packaged
Axle longitudinal vs Fx	0 mm/N	As Packaged
Axle lateral vs Fy	0 mm/N	As Packaged

The screen shown in Figure D-6 calculates and displays the auxiliary roll stiffness. TruckSim® calculates the auxiliary roll stiffness from the roll stiffness provided by the vertical suspension springs and measured roll stiffness of the vehicle. The numbers in the right column are roll moment measured on the test vehicle from the WMU Characterization Report, and they are

plotted in the blue trace. The red trace is the difference, calculated by TruckSim®. This same approach is used to calculate the auxiliary roll stiffness for the drive, trailer, and dolly axles.

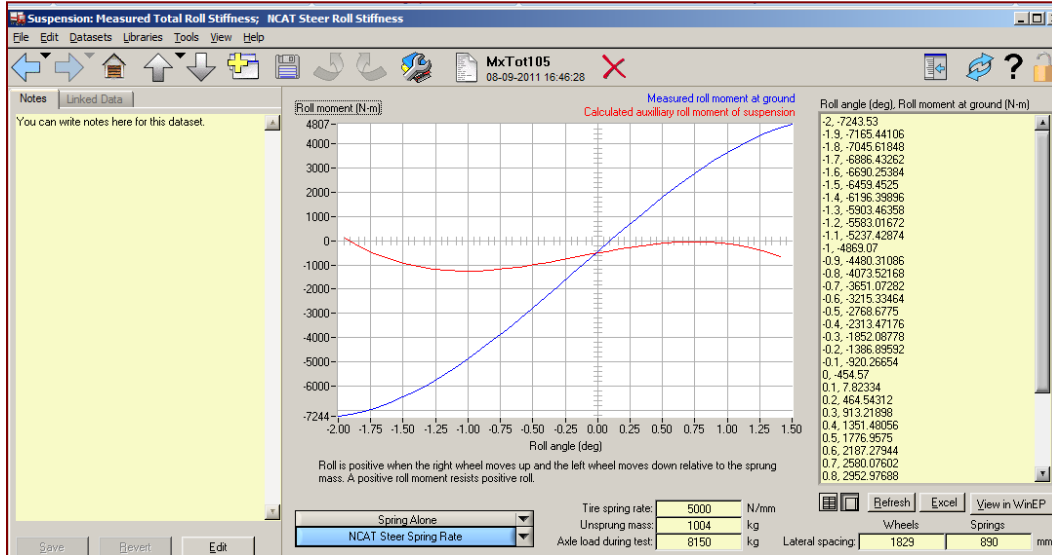


Figure D-6. Screen Capture. The "Suspension: Measured Total Roll Stiffness" screen in TruckSim® calculates the auxiliary roll stiffness for the steer axle (Mechanical Simulation Corporation 2010).

D-2.1.2 Steer Axle Kinematics (Axle 1)

The modeler enters the kinematic characterization data in the “Suspension: Solid Axle System Kinematics” screen (Figure D-7).

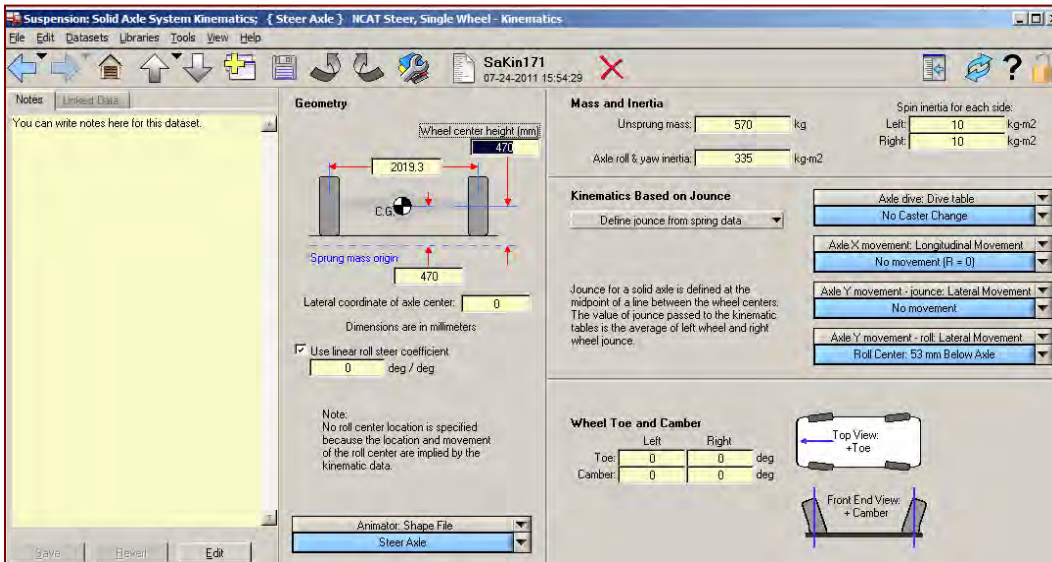


Figure D-7. Screen Capture. The “Suspension: Solid Axle System Kinematics” screen allows the modeler to enter data to define the steer axle kinematic characteristics for the vehicle (Mechanical Simulation Corporation 2010).

Table D-2 contains the parameters that were used to define the steer axle kinematics of the NCAT test vehicle. Parameters listed as sourced from WMU Characterization Report are based on the characterization testing performed and reported by WMU. Parameters listed as sourced from “As Packaged” were left as the default parameters in TruckSim®. This was due to lack of better characterization data. This was thought reasonable, because the default models were stable for the purpose of the research.

Table D-2. Steer Axle Kinematic Parameters used for modeling the NCAT test vehicle.
The table is in the order of the screen capture in Figure D-7.

Model Parameter	Value	Source
Wheel Center Height	470 mm	WMU Characterization Report
Track Width	2019.3 mm	WMU Characterization Report
Sprung Mass Origin	470 mm	WMU Characterization Report
Lateral Coordinate of Axle Center	0 mm	Generic Model as Packaged
Use linear roll steer coefficient	0 deg/deg	WMU Characterization Report
Un sprung Mass	570 kg	Generic Model as Packaged
Axle roll & yaw inertia	335 kg-mm ²	Generic Model as Packaged
Axle dive: Dive table	No Caster Change	Generic Model as Packaged
Axle X movement: Longitudinal Movement	No Movement (R=0)	Generic Model as Packaged
Axle Y movement –jounce: Lateral Movement	No Movement	Generic Model as Packaged
Axle Y movement – roll: Lateral Movement	Roll Center: 53 mm Below Axle	Generic Model as Packaged
Static Toe Left	0 deg	Generic Model as Packaged
Static Camber Left	0 deg	Generic Model as Packaged
Static Toe Right	0 deg	Generic Model as Packaged
Static Camber right	0 deg	Generic Model as Packaged
Spin Inertia Left	10 kg-m ²	Generic Model as Packaged
Spin Inertia Right	10 kg-m ²	Generic Model as Packaged
Define Jounce from spring data	Selected	Assumption*

* The TruckSim® solver was allowed to determine the location where jounce started so that the neutral point of the travel was based on model parameters.

D-2.1.3 Drive Axle Compliances (Axles 2 & 3)

The modeler enters the drive axle compliance characterization data in the “Solid Axle Compliance, Springs, and Dampers” screen (Figure D-8).

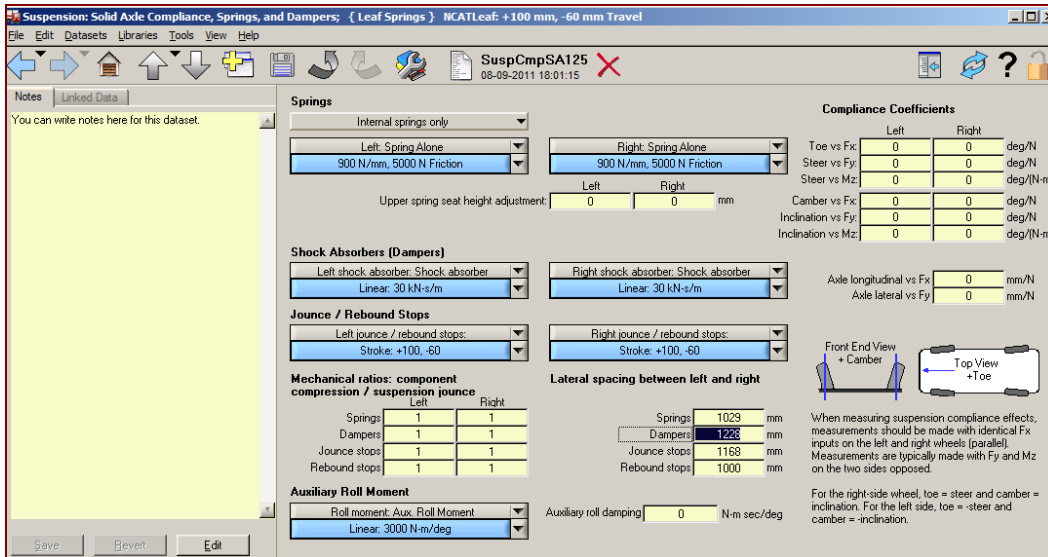


Figure D-8. Screen Capture. The “Solid Axle Compliance, Springs, and Dampers” screen allows the modeler to enter data to define the drive axle spring and damper characteristics for the vehicle (Mechanical Simulation Corporation 2010).

Table D-3 contains the parameters that were used to define the drive axle compliances of the NCAT test vehicle. Parameters listed as sourced from WMU Characterization Report are based on the characterization testing performed and reported by WMU. Parameters listed as sourced from “As Packaged” were left as the default parameters in TruckSim®. This was due to lack of better characterization data. This was thought reasonable because the default models were stable for the purpose of the research.

Table D-3. Drive axle compliance parameters used to characterize the test vehicle in TruckSim®.
The table is in the order of the screen capture in Figure D-8.

Model Parameter	Value	Source
Internal springs only	Selected	As Packaged
Left Spring Alone	900 N/mm, 5000 N Friction	As Packaged
Right Spring Alone	900 N/mm, 5000 N Friction	As Packaged
Left shock absorber: Shock absorber	Linear: 30 kN/m	As Packaged
Right shock absorber: Shock absorber	Linear: 30 kN/m	As Packaged
Left bounce / rebound stops	+100, -60 mm	As Packaged
Right bounce/ rebound stops	+100, -60 mm	As Packaged
Roll moment: Total Susp (Measured)	NCAT Steer Roll Stiffness, See Figure D-9.	WMU Characterization Report
Mechanical ratios: component Compression/suspension jounce		
Springs	Left = 1, Right = 1	As Packaged
Dampers	Left = 1, Right = 1	As Packaged
Jounce stops	Left = 1, Right = 1	As Packaged
Rebound stops	Left = 1, Right = 1	As Packaged
Roll moment: Total Susp (Measured)	Linear 3000 N-m/deg	As Packaged
Lateral spacing between left and right		
Springs	1029 mm	As Packaged
Dampers	1100 mm	As Packaged
Jounce Stops	890 mm	As Packaged
Rebound Stops	890 mm	As Packaged
Auxiliary roll damping	0 N-ms/deg	As Packaged
Toe vs Fx	Left = 0, Right = 0 deg/N	As Packaged
Steer vs Fy	Left = 0, Right = 0 deg/N	As Packaged
Steer vs Mz	Left = 0, Right = 0 deg/N-m	As Packaged
Camber vs Fx	Left = 0, Right = 0 deg/N	As Packaged
Inclination vs Fy	Left = 0, Right = 0 deg/N	As Packaged
Inclination vs Mz	Left = 0, Right = 0 deg/N-m	As Packaged
Axle longitudinal vs Fx	0 mm/N	As Packaged
Axle lateral vs Fy	0 mm/N	As Packaged

The roll stiffness for the axle was calculated by the screen in Figure D-9.

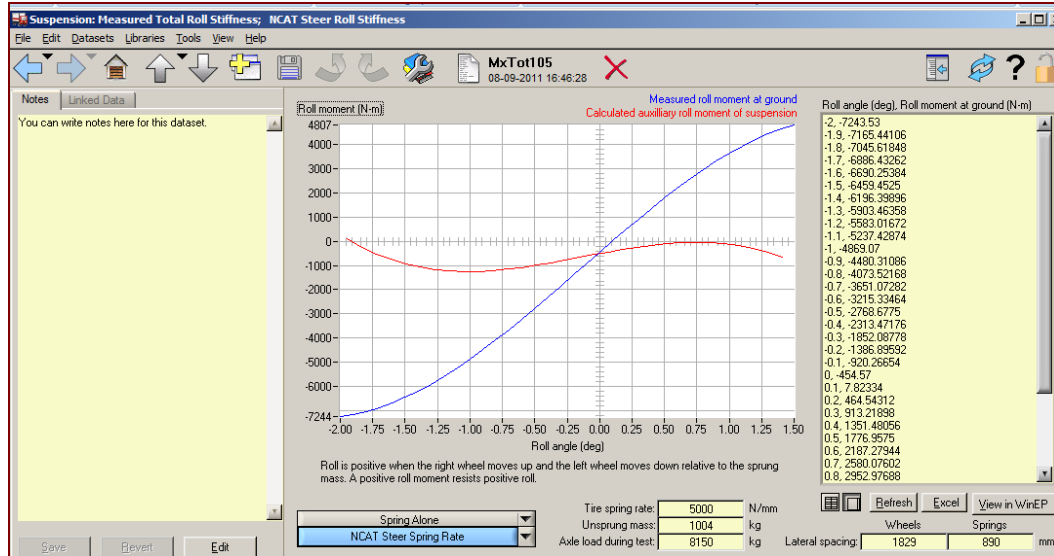


Figure D-9. Screen Capture. The “Suspension: Measured Total Roll Stiffness” screen in TruckSim® for the NCAT tractor steer axle (Mechanical Simulation Corporation 2010).

D-2.1.4 Drive Axle Kinematics (Axles 2 & 3)

The modeler enters the drive axle kinematics in the “Solid Axle System Kinematics” screen (Figure D-10).

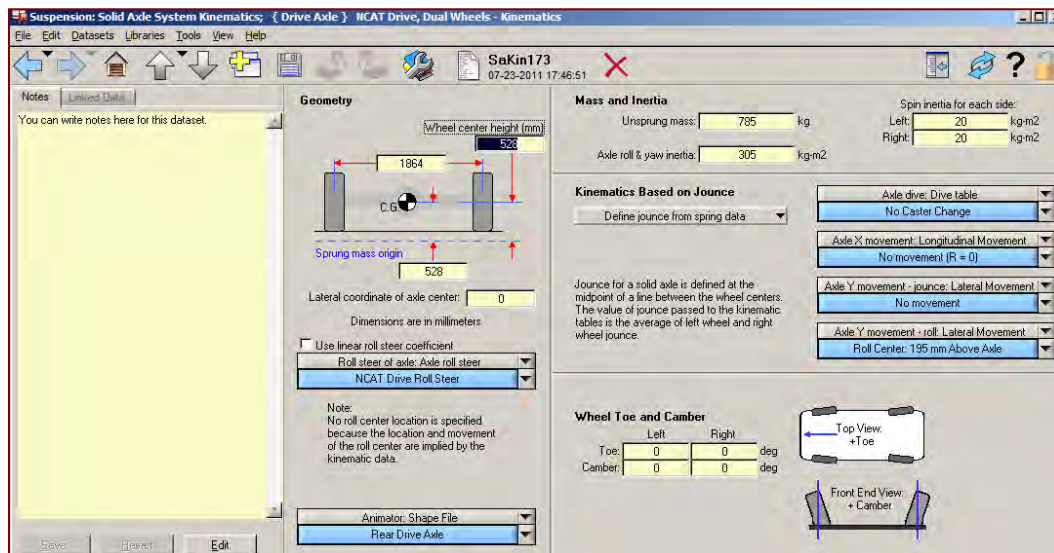


Figure D-10. Screen Capture. The “Solid Axle System Kinematics” screen allows the modeler to enter data to define the drive axle spring and damper characteristics for the vehicle (Mechanical Simulation Corporation 2010).

Table D-4 contains the parameters that were used to define the drive axle kinematics of the NCAT test vehicle.

Table D-4. Drive axle kinematic parameters used for modeling the NCAT test vehicle.
The table is in the order of the screen capture in Figure D-10.

Model Parameter	Value	Source
Wheel Center Height	528 mm	WMU Characterization Report
Track Width	1864 mm	WMU Characterization Report
Sprung Mass Origin	528 mm	Assumption
Lateral Coordinate of Axle Center	0 mm	Assumption
Roll steer of axle: Axle roll steer	See Figure D-11	WMU Characterization Report
Un sprung Mass	785 kg	Generic Model as Packaged
Axle roll & yaw inertia	305 kg-mm ²	Generic Model as Packaged
Axle dive: Dive table	No Caster Change	Generic Model as Packaged
Axle X movement: Longitudinal Movement	No Movement (R=0)	Generic Model as Packaged
Axle Y movement – jounce: Lateral Movement	No Movement	Generic Model as Packaged
Axle Y movement – roll: Lateral Movement	Roll Center: 53 mm Below Axle	Generic Model as Packaged
Static Toe Left	0 deg	Generic Model as Packaged
Static Camber Left	0 deg	Generic Model as Packaged
Static Toe Right	0 deg	Generic Model as Packaged
Static Camber right	0 deg	Generic Model as Packaged
Spin Inertia Left	20 kg-m ²	Generic Model as Packaged
Spin Inertia Right	20 kg-m ²	Generic Model as Packaged
Define Jounce from spring data	Selected	Assumption. See Table D-2.

In Figure D-11, the tabular values in the right column are from the WMU Characterization Report. The red plot of Axle steer versus Axle relative roll is a linear interpolation of the tabular data.

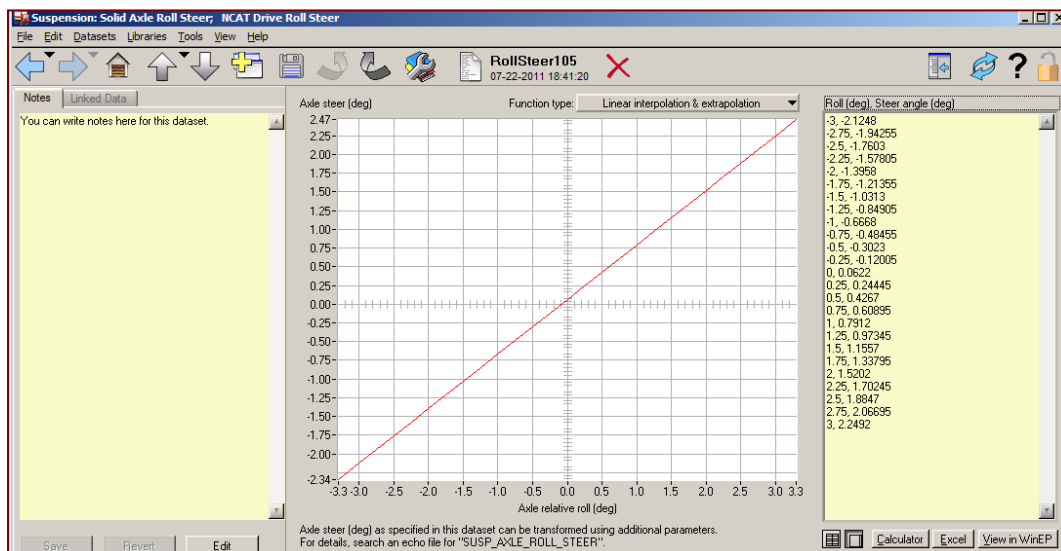


Figure D-11. Screen Capture. The "Suspension: Solid Axle Roll Steer" screen (Mechanical Simulation Corporation 2010).

D-2.2 Modeling the Trailers

Each of the three trailers was characterized as having similar kinematics, so all trailers were given the same kinematic and compliance definition in the TruckSim® model. As the trailers for the test vehicle were modeled in TruckSim®, the only difference was in mass properties. Trailer Payload was moved to adjust the mass distribution in each trailer model. Trailer definition varied slightly due to the configuration for its location in the vehicle. Trailer 1 is different in definition from Trailer 2, because Trailer 1 requires no dolly to attach to the combination.

Trailer 2 varies from Trailer 1 only by the addition of a pintle hitch for a dolly. Trailer 3 varies from Trailer 2 by the omission of a pintle hitch, because there is no additional dolly to attach to the rear of Trailer 3. To access Trailer 1 and characterize it in the model, the modeler navigates away from the “Vehicle Loaded Combination” screen (Figure D-3) to the “Vehicle: Trailer with 1 Axle” screen (Figure D-12). Trailers 2 and 3 are combined into one screen as an additional single unit. In the “Loaded Combination” screen (Figure D-3), this unit is listed under the category of Second Trailer. With the Special Solver data set, the modeler navigates to a page that allows definition of the extra units just as Trailer 1 was defined from the “Loaded Combination” page.

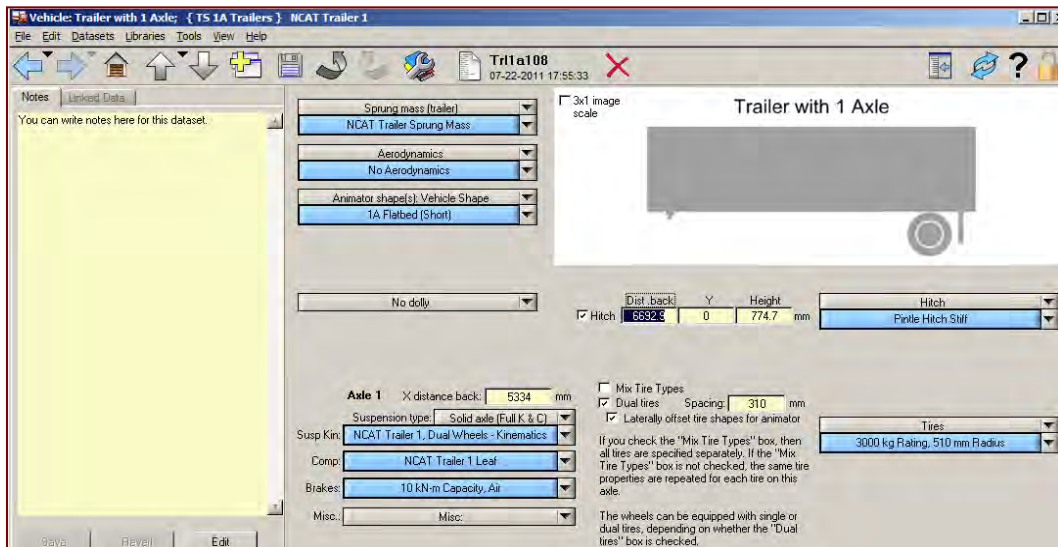


Figure D-12. Screen Capture. The “Trailer with 1 Axe” screen (Mechanical Simulation Corporation 2010).

This is the beginning page for definition of the trailer. The modeler navigates to lower pages to enter in more detailed kinematic, compliance, and mass property data for a single-axle trailer. The gray bars indicate categories to select from, while the blue bars link to tables of data characterizing the categorized model property. For this investigation, the categories were left as packaged with the TruckSim® custom solvers. The following list explains the selections shown in Figure D-12 (in order from top to bottom and left to right):

- 1) **Sprung mass (trailer) / NCAT Trailer Sprung Mass** – This links to the definition of the sprung mass of the typical NCAT trailer. The sprung mass of the vehicles varied significantly per modifications to the shipping containers and payload. Because the trailers were permanently loaded, the sprung mass of the trailer could not be measured easily, so for this investigation the sprung mass model for each trailer was left as it came packaged in TruckSim®. The mass properties of the vehicle were adjusted by shifting the location of the payload.
- 2) **Aerodynamics / No Aerodynamics** – This was left as packaged. For this research, the aerodynamics of the trailers was not of interest.
- 3) **Animator shape(s): Vehicle Shape / 1A Flatbed (short)** – The color of the truck body was changed to white to resemble the NCAT test vehicle tractor.
- 4) **No dolly** – This was left as packaged, because no dolly was necessary for Trailer 1.
- 5) **Hitch (Check Box)** – This was left checked to include the connection from Trailer 1 to Dolly 1
 - a. **Dist. back** – This was set to 6692.9 mm to reflect the distance as reported by WMU, of the hitch from the origin of the trailer.
 - b. **Y** – This was left as packaged at 0 mm off center to reflect the lateral location of the hitch reported by WMU.
 - c. **Height** – This was set to 774.7 mm to reflect the height of the hitch above ground as reported by WMU.
- 6) **Hitch (Bar) / Pintle Hitch Stiff** – This links to the definition of the pintle hitch based on characterization data reported by WMU.
- 7) **Axle 1**
 - a. **X distance back** – This was set to 5334 mm to reflect the location from the vehicle origin as reported by WMU.
 - b. **Suspension type: Solid Axle (full K&C)** – This was left as packaged because Trailer 1 has a solid drive axle suspension typical of this kind of vehicle. The axle motion was characterized by K&C data.
 - c. **Comp: NCAT Trailer 1 Leaf** – The Trailer 1 NCAT leaf was created from the as packaged 15.5 ton leaf definition with the same travel.
 - d. **Brakes: 10 kN-m Capacity, Air** – This was left as packaged because brake performance was not of interest to this research.
 - e. **Tires / Michelin 275/80R22.5 XT1** – Michelin supplied tire characterization data in the form of force-moment per slip angle plots.
 - f. **Other fields** – Unmixed, Dual tires are specified with a center to center spacing of 310 mm. This was left as packaged, because the tires were not mixed on the test vehicle and the spacing was unknown. The tire shapes were laterally offset for the animator.

D-2.2.1 Trailer Axle Compliance

The modeler enters the trailer axle compliance characterization data in the “Solid Axle Compliance, Springs, Dampers” screen (Figure D-13).

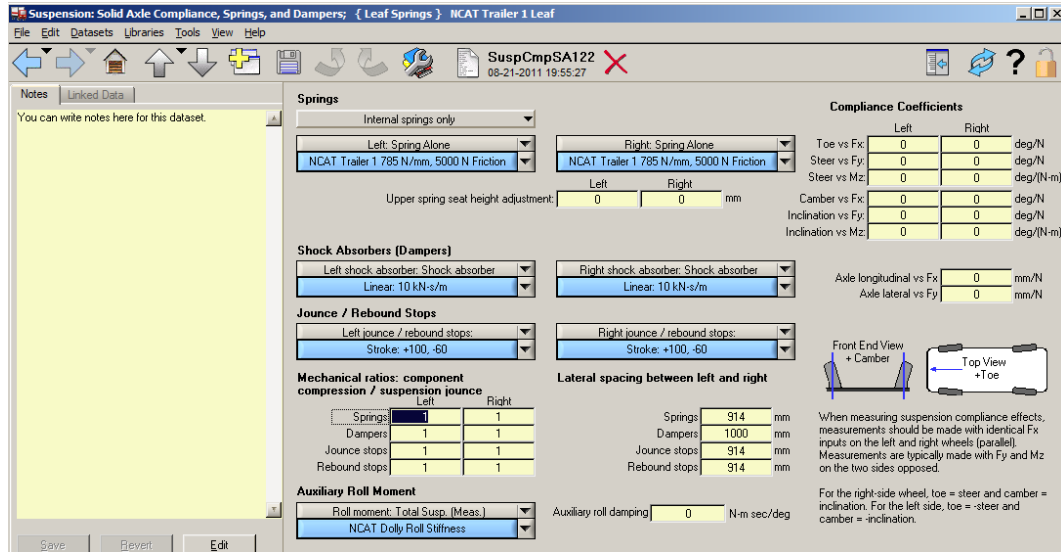


Figure D-13. Screen Capture. The “Trailer Axle Compliance” screen allows the modeler to enter data to define the trailer axle spring and damper characteristics for the vehicle (Mechanical Simulation Corporation 2010).

Table D-5 contains the parameters that were used to define the trailer axle compliances of the NCAT test vehicle. Parameters listed as sourced from WMU Characterization Report are based on the characterization testing performed and reported by WMU. Parameters listed as sourced from “As Packaged” were left as the default parameters in TruckSim®. This was due to lack of better characterization data. This was thought reasonable because the default models were stable for the purpose of the research.

Table D-5. Trailer axle compliance parameters used to characterize the test vehicle in TruckSim®.
The table is in the order of the screen capture in Figure D-13.

Model Parameter	Value	Source
Internal springs only	Selected	Generic Model as Packaged
Left Spring Alone	900 N/mm, 5000 N Friction	Generic Model as Packaged
Right Spring Alone	900 N/mm, 5000 N Friction	Generic Model as Packaged
Left shock absorber: Shock absorber	Linear: 10 kN-s/m*	Generic Model as Packaged
Right shock absorber: Shock absorber	Linear: 10 kN-s/m*	Generic Model as Packaged
Left jounce / rebound stops	+100, -60 mm	Generic Model as Packaged
Right jounce/ rebound stops	+100, -60 mm	Generic Model as Packaged
Roll moment: Total Susp (Measured)	NCAT Steer Roll Stiffness, See Figure 6-7 below.	WMU Characterization Report
Mechanical ratios: component Compression/suspension jounce		
Springs	Left = 1, Right = 1	Generic Model as Packaged
Dampers	Left = 1, Right = 1	Generic Model as Packaged
Jounce stops	Left = 1, Right = 1	Generic Model as Packaged
Rebound stops	Left = 1, Right = 1	Generic Model as Packaged
Roll moment: Total Susp (Measured)	Linear 3000N-m/deg	Generic Model as Packaged
Lateral spacing between left and right		
Springs	1029 mm	Generic Model as Packaged
Dampers	1100 mm	Generic Model as Packaged
Jounce Stops	890 mm	Generic Model as Packaged
Rebound Stops	890 mm	Generic Model as Packaged
Auxiliary roll damping	0 N-m-s/deg	Generic Model as Packaged
Toe vs Fx	Left = 0, Right = 0 deg/N	Generic Model as Packaged
Steer vs Fy	Left = 0, Right = 0 deg/N	Generic Model as Packaged
Steer vs Mz	Left = 0, Right = 0 deg/N-m	Generic Model as Packaged
Camber vs Fx	Left = 0, Right = 0 deg/N	Generic Model as Packaged
Inclination vs Fy	Left = 0, Right = 0 deg/N	Generic Model as Packaged
Inclination vs Mz	Left = 0, Right = 0 deg/N-m	Generic Model as Packaged
Axle longitudinal vs Fx	0 mm/N	Generic Model as Packaged
Axle lateral vs Fy	0 mm/N	Generic Model as Packaged

* Note: 10 kN-s/m dampers added to the trailer suspension for numerical stability.

Figure D-14 displays the calculation of the auxiliary roll stiffness.

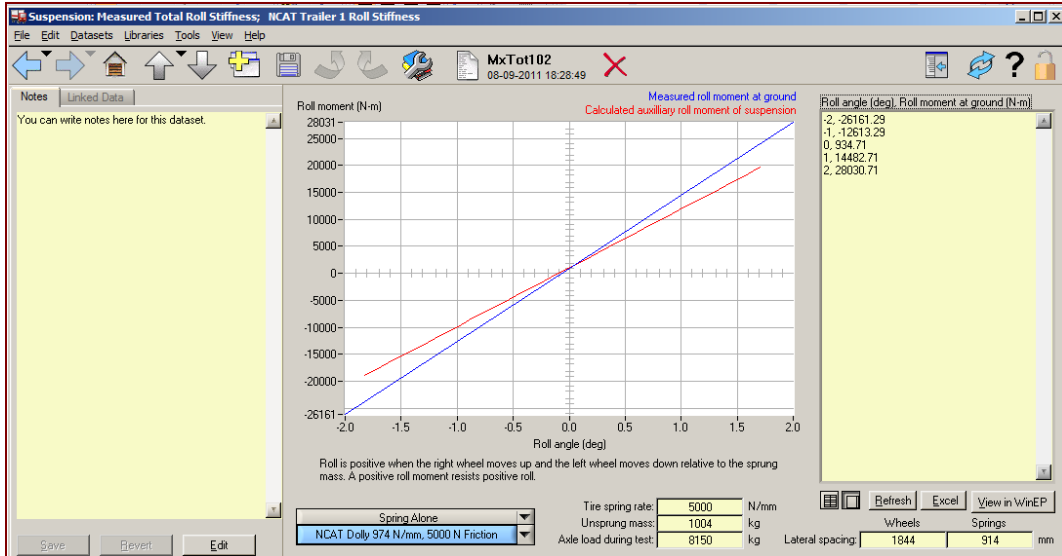


Figure D-14. Screen Capture. The “Suspension” Measured Total Roll Stiffness” screen in TruckSim® for the NCAT trailer (Mechanical Simulation Corporation 2010).

D-2.2.2 Trailer Axle Kinematics

The modeler enters the trailer kinematics characterization data in the “Solid Axle System Kinematics” screen (Figure D-15).

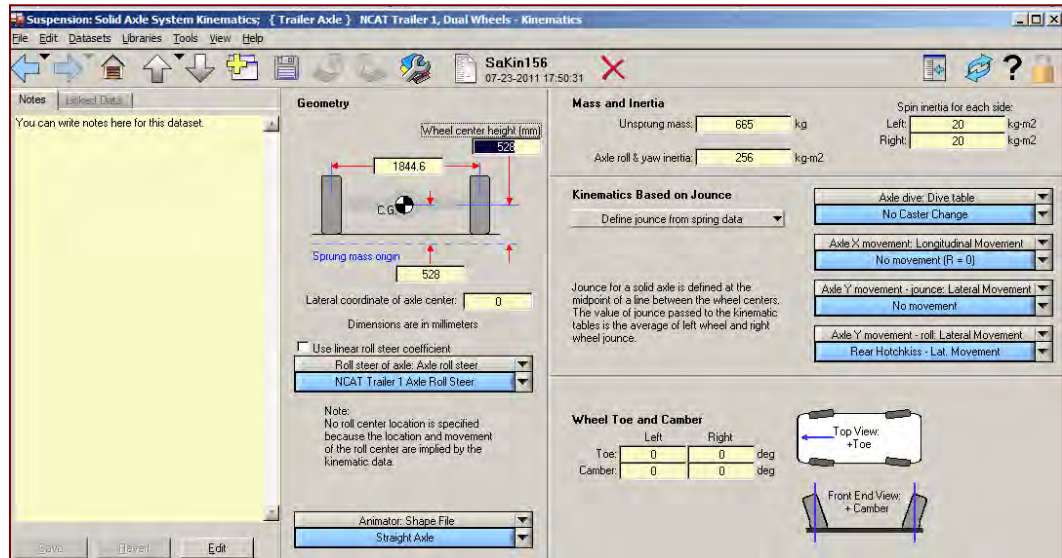


Figure D-15. Screen Capture. The “Solid Axle System Kinematics” screen allows the modeler to enter data to define the trailer axle kinematic characteristics for the vehicle (Mechanical Simulation Corporation 2010).

Table D-6 contains the parameters that were used to define the trailer axle kinematics of the NCAT test vehicle. Parameters listed as sourced from WMU Characterization Report are based on the characterization testing performed and reported by WMU. Parameters listed as sourced

from “As Packaged” were left as the default parameters in TruckSim®. This was due to lack of better characterization data. This was thought reasonable because the default models were stable for the purpose of the research.

Table D-6. Trailer Axle Kinematic Parameters used for modeling the NCAT test vehicle.
The table is in the order of the screen capture in Figure D-15.

Model Parameter	Value	Source
Wheel Center Height	528	WMU characterization
Track Width	1844.6 mm	WMU characterization
Sprung Mass Origin	528 mm	Assumption
Lateral Coordinate of Axle Center	0 mm	Assumption
Use linear roll steer coefficient	0.2607deg/deg	WMU characterization
Un sprung Mass	665 kg	Generic Model as Packaged
Axle roll & yaw inertia	256 kg-mm ²	Generic Model as Packaged
Axle dive: Dive table	No Caster Change	Generic Model as Packaged
Axle X movement: Longitudinal Movement	No Movement (R=0)	Generic Model as Packaged
Axle Y movement –jounce: Lateral Movement	No Movement	Generic Model as Packaged
Axle Y movement – roll: Lateral Movement	Roll Center: 53 mm Below Axle	Generic Model as Packaged
Static Toe Left	0 deg	Generic Model as Packaged
Static Camber Left	0 deg	Generic Model as Packaged
Static Toe Right	0 deg	Generic Model as Packaged
Static Camber right	0 deg	Generic Model as Packaged
Spin Inertia Left	20 kg-m ²	Generic Model as Packaged
Spin Inertia Right	20 kg-m ²	Generic Model as Packaged
Define Jounce from spring data	Selected	Assumption. See Table D-2.

D-2.3 Modeling the Dollies

TruckSim® treats the dolly as its own unit with a separate screen for its definition. The standard one-axle dolly packaged with TruckSim® is different from the dollies that were used in the test vehicle. The NCAT test vehicle was equipped with sprung fifth wheel dollies. The fifth wheel was attached to the dolly frame with transverse leaf springs. The dolly axle was mounted rigidly to the frame. The dolly frame, axle, brakes, and other hardware all contribute to the unsprung mass of the dolly. To define this in TruckSim®, the sprung mass, consisting of the fifth wheel and its mechanism, was estimated to have a mass of 200 kg. The balance of the mass measured for the dolly, 1250 kg, was attributed to unsprung mass. This configuration also affected the kinematic definition of the dolly. The transverse leaf sprung fifth wheel, when attached to the dolly frame, allowed no roll steer of the axle. This was defined in TruckSim® by setting the linear coefficient of roll steer to 0 deg/deg. The modeler can access all characterization data from the “Dolly with 1 Axle Screen” shown in Figure D-16. This is the beginning page for

definition of the dolly. The modeler navigates to lower pages to enter in more detailed kinematic, compliance, and mass property data.

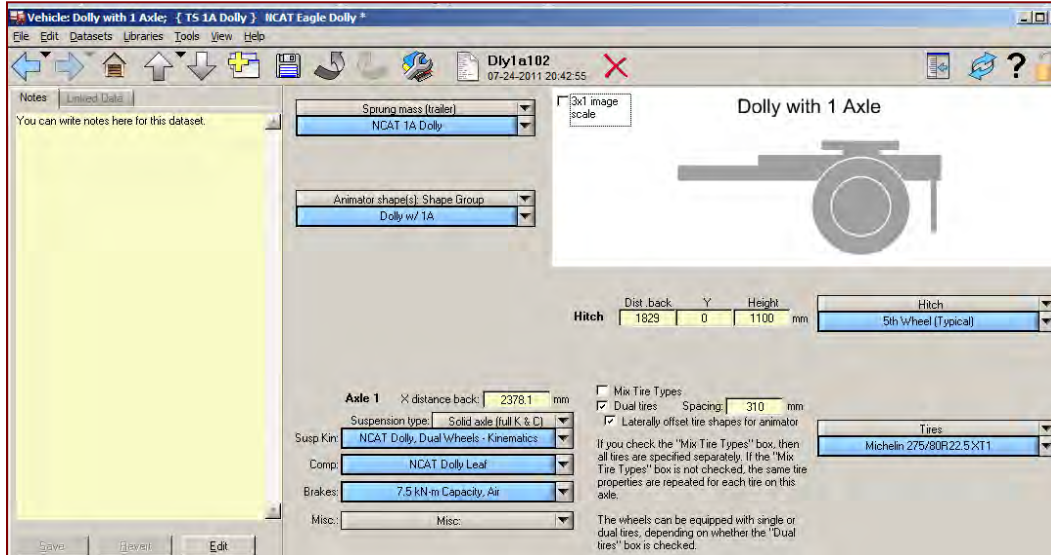


Figure D-16. Screen Capture. The “Vehicle: Dolly with 1 Axle” screen (Mechanical Simulation Corporation 2010).

D-2.3.1 Dolly Axle Compliance

The modeler enters the dolly compliance characterization data in the “Solid Axle Compliance, Springs, and Dampers” screen (Figure D-17).

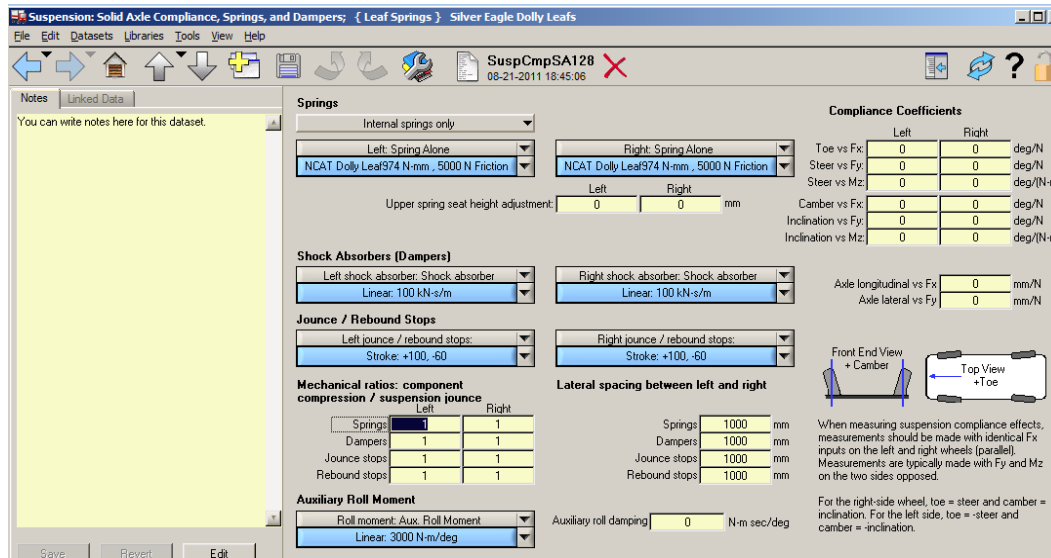


Figure D-17. Screen Capture. The “Solid Axle Compliance, Springs, and Dampers” screen where the modeler defines the dolly compliance (Mechanical Simulation Corporation 2010).

Table D-7 contains the parameters that were used to define the dolly axle compliances of the NCAT test vehicle.

Table D-7. Dolly axle compliance parameters used to characterize the test vehicle in TruckSim®.
The table is in the order of the screen capture in Figure D-17.

Model Parameter	Value	Source
Internal springs only	Selected	Generic Model as Packaged
Left Spring Alone	NCAT Dolly 974 N/mm, 5000 N Friction	WMU Characterization Report
Right Spring Alone	NCAT Dolly 974 N/mm, 5000 N Friction	WMU Characterization Report
Left shock absorber: Shock absorber	*100 kN-s/mm	Test vehicle was not equipped
Right shock absorber: Shock absorber	*100 kN-s/m	Test vehicle was not equipped
Left bounce / rebound stops	+100, -60 mm	Generic Model as Packaged
Right bounce/ rebound stops	+100, -60 mm	Generic Model as Packaged
Mechanical ratios: component Compression/suspension jounce		
Springs	Left = 1, Right = 1	Generic Model as Packaged
Dampers	Left = 1, Right = 1	Generic Model as Packaged
Jounce stops	Left = 1, Right = 1	Generic Model as Packaged
Rebound stops	Left = 1, Right = 1	Generic Model as Packaged
Roll moment: Total Susp (Measured)	NCAT Dolly Roll Stiffness, See Figure 6-18	WMU Characterization Report
Lateral spacing between left and right		
Springs(mm)	914 mm	WMU Characterization Report
Dampers(mm)	1000 mm	Generic Model as Packaged
Jounce Stops(mm)	914 mm	Assumption
Rebound Stops(mm)	914 mm	Assumption
Auxiliary roll damping	0 (N-m s/deg)	Generic Model as Packaged
Toe vs Fx	Left = 0, Right = 0 deg/N	Generic Model as Packaged
Steer vs Fy	Left = 0, Right = 0 deg/N	Generic Model as Packaged
Steer vs Mz	Left = 0, Right = 0 deg/N	Generic Model as Packaged
Camber vs Fx	Left = 0, Right = 0 deg/N	Generic Model as Packaged
Inclination vs Fy	Left = 0, Right = 0 deg/N	Generic Model as Packaged
Inclination vs Mz	Left = 0, Right = 0 deg/N	Generic Model as Packaged
Axle longitudinal vs Fx	0 mm/N	Generic Model as Packaged
Axle lateral vs Fy	0 mm/N	Generic Model as Packaged

**100 kN-s/mm damping was added to dolly compliance due to the unknown hysteretic nature of the sprung fifth wheel dolly configuration. It is thought that better characterized suspension friction would lead to less additional damping. Without damping the model becomes numerically unstable leading to wild fluctuation in several responses.

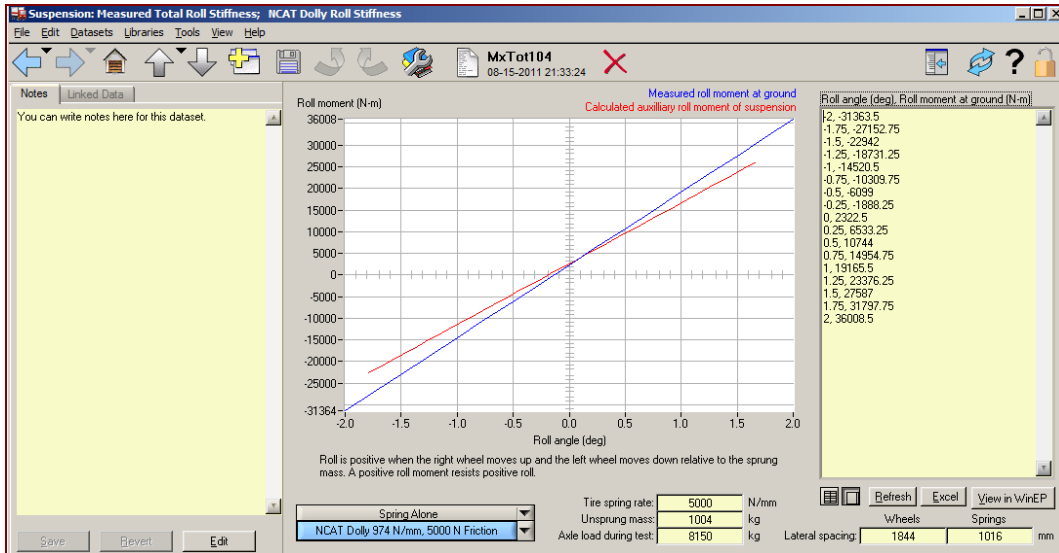


Figure D-18. Screen Capture. The “Suspension: Measured Total Roll Stiffness” screen in TruckSim® for the NCAT Dolly (Mechanical Simulation Corporation 2010).

D-2.3.2 Dolly Axle Kinematics

The modeler enters the dolly kinematic characterization data into the “Suspension: Solid Axle System Kinematics” screen (Figure D-19).

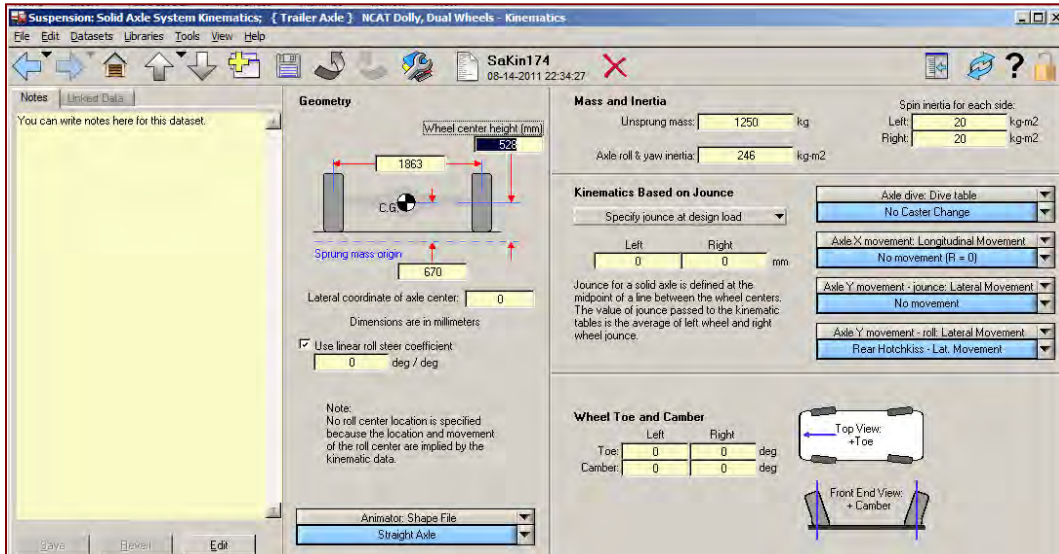


Figure D-19. Screen Capture. The “Solid Axle System Kinematics” screen allows the modeler to enter data to define the dolly axle kinematic characteristics for the vehicle (Mechanical Simulation Corporation 2010).

Table D-8 contains the parameters that were used to define the dolly axle kinematics of the NCAT test vehicle. Parameters listed as sourced from the WMU Characterization Report are based on the characterization testing performed and reported by WMU. Parameters listed as sourced from “As Packaged” were left as the default parameters in TruckSim®. This was due to

lack of better characterization data. This was thought reasonable because the default models were stable for the purpose of the research.

Table D-8. The following table lists the dolly axle kinematic parameters used for modeling the NCAT test vehicle. The table is in the order of the screen capture shown in Figure D-19.

Model Parameter	Value	Source
Wheel Center Height (mm)	528	WMU Characterization Report
Track Width (mm)	1844.6	WMU Characterization Report
Sprung Mass Origin (mm)	528	Assumption
Lateral Coordinate of Axle Center (mm)	0	Assumption
Use linear roll steer coefficient (deg/deg)	0.2607	WMU Characterization Report
Un sprung Mass (kg)	665	Generic Model as Packaged
Axle roll & yaw inertia (kg-mm ²)	256	Generic Model as Packaged
Axle dive: Dive table	No Caster Change	Generic Model as Packaged
Axle X movement: Longitudinal Movement	No Movement (R=0)	Generic Model as Packaged
Axle Y movement – jounce: Lateral Movement	No Movement	Generic Model as Packaged
Axle Y movement – roll: Lateral Movement	Roll Center: 53 mm Below Axle	Generic Model as Packaged
Static Toe Left (deg)	0	Generic Model as Packaged
Static Camber Left (deg)	0	Generic Model as Packaged
Static Toe Right (deg)	0	Generic Model as Packaged
Static Camber right (deg)	0	Generic Model as Packaged
Spin Inertia Left (kg-m ²)	20	Generic Model as Packaged
Spin Inertia Right (kg-m ²)	20	Generic Model as Packaged
Define Jounce from spring data	Selected	Assumption. See Table D-2.

D-2.3.3 Dolly Sprung Mass

The sprung mass of the Silver Eagle, Eagle model dolly is small in comparison to the dolly mass. In a typical dolly the axle and tires are sprung to the frame of the dolly. For this analysis, 200 kg is an estimate in the mass of the fifth wheel. The 1100 mm height of the sprung mass places the CG at the dolly. The balance of the mass of the dolly is taken up in the axle mass located in the K&C definition in Figure D-20.

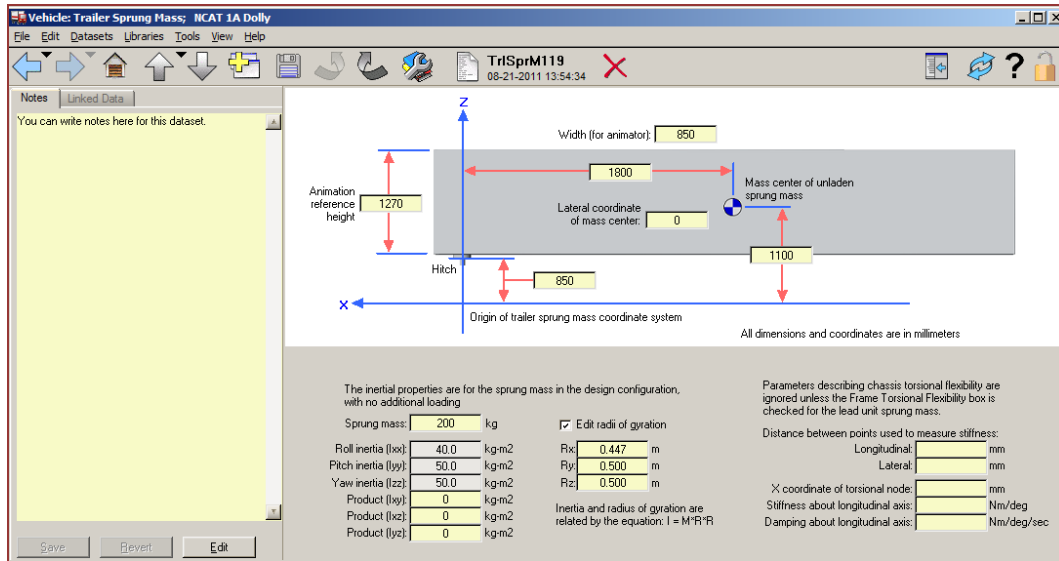


Figure D-20. Screen Capture. Sprung Mass definition for Silver Eagle dolly (Mechanical Simulation Corporation 2010).

D-2.4 Modeling the Pintle Hitch

The pintle hitch was left as the generic model as packaged, because no data were available to characterize it any differently. The sub-limit nature of the testing and subsequent modeling does not require any more detailed characterization of the hitch. The pintle hitch is defined by pitch, heave, and yaw moment data in tabular form. The “Hitch” screen (Figure D-21) allows the modeler to define the pintle hitch. As this was unchanged from the generic model as packaged, no detailed description of this component will be included in this report.

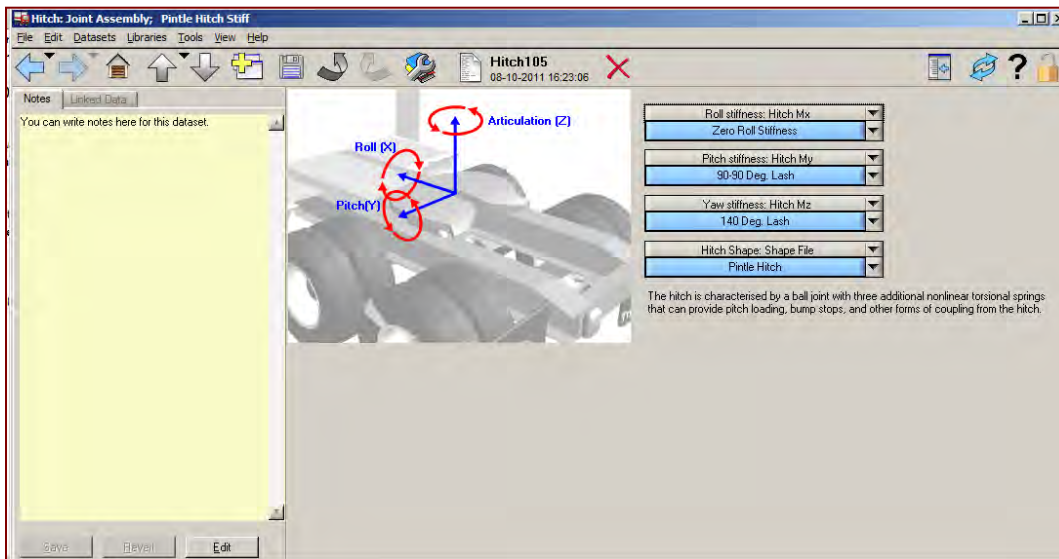


Figure D-21. Screen Capture. The “Hitch: Joint Assembly” screen allows the modeler to define the pitch, heave, and yaw moment characteristics that define the pintle hitch (Mechanical Simulation Corporation 2010).

This hitch model was used at both pintle hitch positions in the NCAT LCV model. The graphic does not resemble the pintle hitch, because all internal hitches in TruckSim® are modeled in the same user screen.

D-2.5 Modeling the Fifth Wheel

The fifth wheel was left as the generic model as packaged, because no data were available to characterize it any differently. The fifth wheel is defined by pitch, heave, and yaw moment data in tabular form. The “Hitch” screen shown in Figure D-22 allows the modeler to define the fifth wheel. Because this was unchanged from the generic model as packaged, no detailed description of this component will be included in this report.

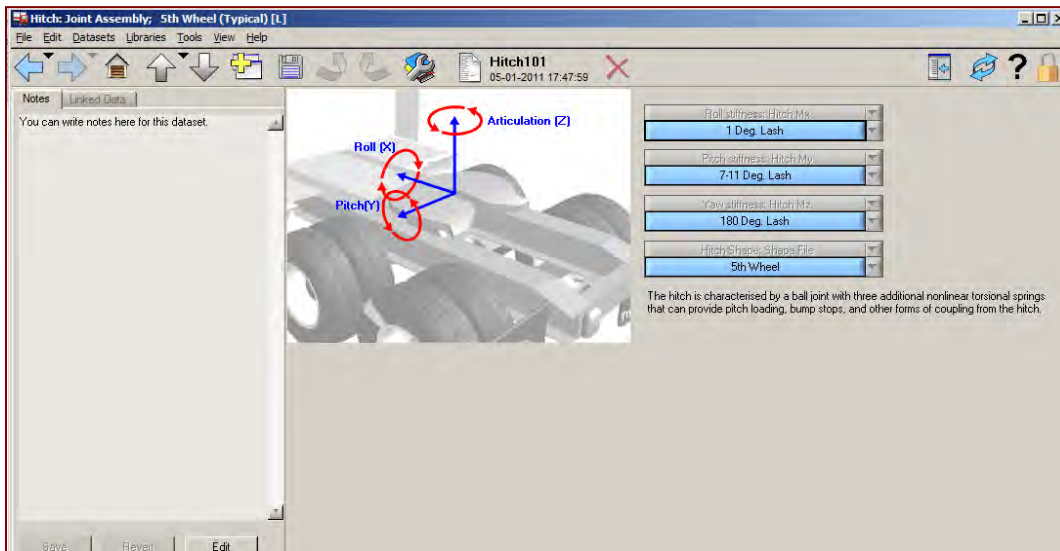


Figure D-22. Screen Capture. The “Hitch” screen allows the modeler to define the pitch, heave, and yaw moment characteristics that define the fifth wheel. This model was used at all 3 fifth wheel positions in the NCAT LCV model (Mechanical Simulation Corporation).

D-2.6 Modeling the Tires

Michelin Americas Research Company provided a full set of tires for the NCAT test vehicle for testing. The tires were size 275/80R22.5 for all positions. The steer axle was outfit with Michelin XZA tires, the drive axle was outfit with Michelin XDA tires, and the trailer and dolly axles were all outfit with Michelin XT1 tires. Michelin provided the tire characterization data in tables containing lateral force per normal load and slip angle, longitudinal force per normal load and slip ratio, and aligning moment per normal load and slip angle to use in the model (by CU-ICAR).

The modeler enters the tire characterization data in the “Tire” screen shown in Figure D-23 through Figure D-26. (The tire properties shown in these figures are illustrations only, and are not the actual data used in the simulation, which is proprietary.) Table D-9 shows that some of

the tire properties were “as packaged” in TruckSim®, and that some were provided by Michelin for the particular tires used in this project.

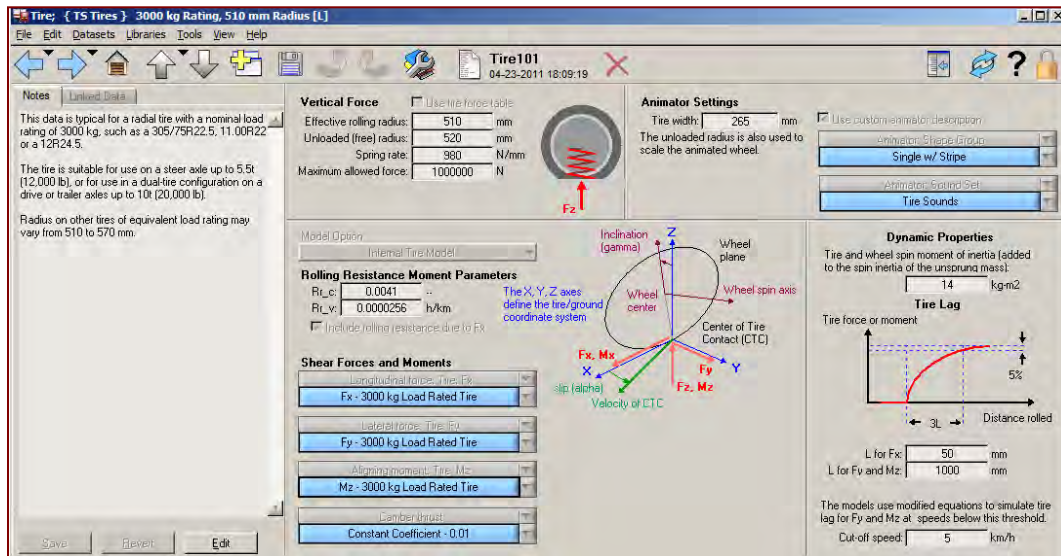


Figure D-23. Screen Capture. The “Tire” screen allows the modeler to navigate between the different force and moment data sets used to characterize the modeled tire (Mechanical Simulation Corporation 2010).

Table D-9. The parameters and their source for the tire characterization used for the LCV model

Model Parameter	Value	Source
Vertical Force		
Effective Rolling Radius	510 mm	As Packaged
Unloaded (free) Radius	520 mm	As Packaged
Spring Rate	980 N/mm	As Packaged
Maximum allowed force	1000000 N	As Packaged
Model Option	Internal Tire Model	As Packaged
Rolling Resistance Parameters		
Rr_c	0.0041	As Packaged
Rr_v	0.0000256 h/km	As Packaged
Shear Force and Moments		
Longitudinal force: Tire Fx	Fx -3000 kg Load Rated Tire	As Packaged
Lateral force: Tire Fy	Fy Michelin 275/80R22.5 XZA	Model Developed from Michelin Data
Aligning Moment: Tire Mz	Mz Michelin 275/80R22.5 XZA	Model Developed from Michelin Data
Camber Thrust	Constant Coefficient- 0.01	As Packaged
Animator: Shape Group	Single w/Stripe	As Packaged
Animator: Sound Set	Tire Sounds	As Packaged
Dynamic Properties		
Spin Inertia	14 kg·m²	As Packaged
Lag for Fx	50 mm	As Packaged
Lag for Fy and Mz	1000 mm	As Packaged
Cut-off speed	5 km/h	As Packaged

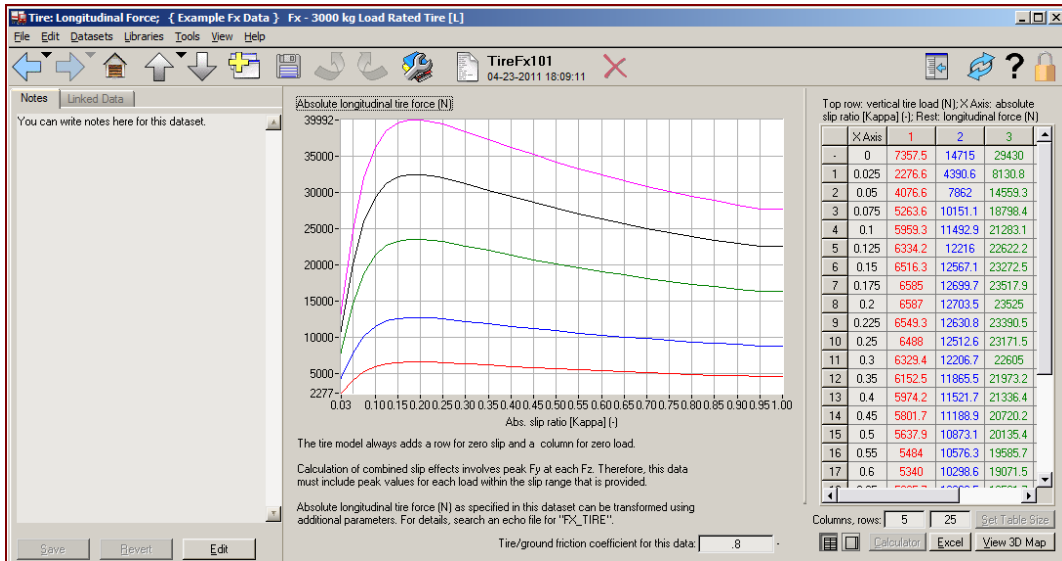


Figure D-24. Screen Capture. The “Tire Longitudinal Force” screen allows the modeler to enter in the longitudinal force characteristics in tabular form.
THIS IS NOT ACTUAL TIRE DATA (Mechanical Simulation Corporation 2010).

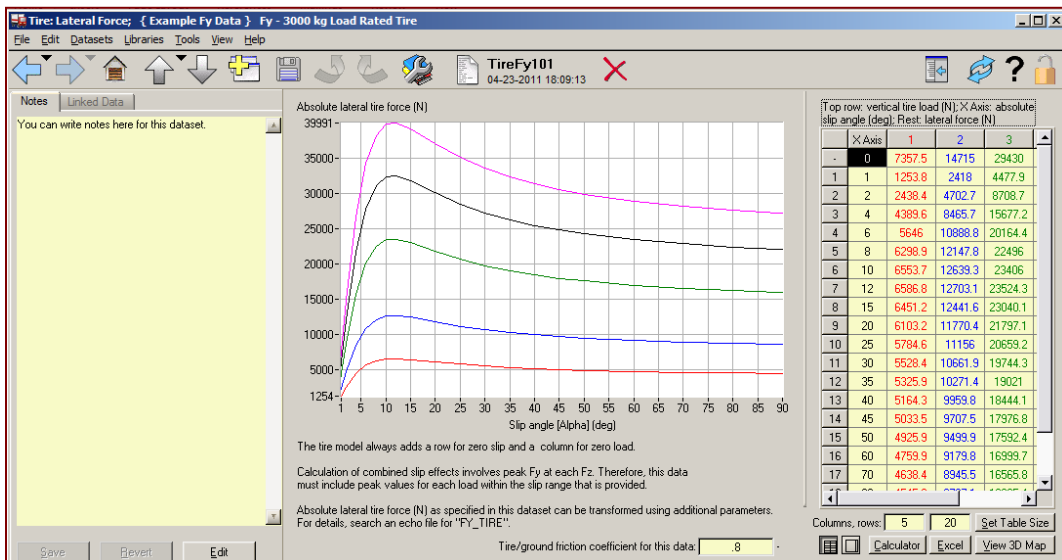


Figure D-25. Screen Capture. The “Tire Lateral Force” screen allows the user to enter the lateral force characteristics in tabular form. THIS IS NOT ACTUAL TIRE DATA (Mechanical Simulation Corporation 2010).

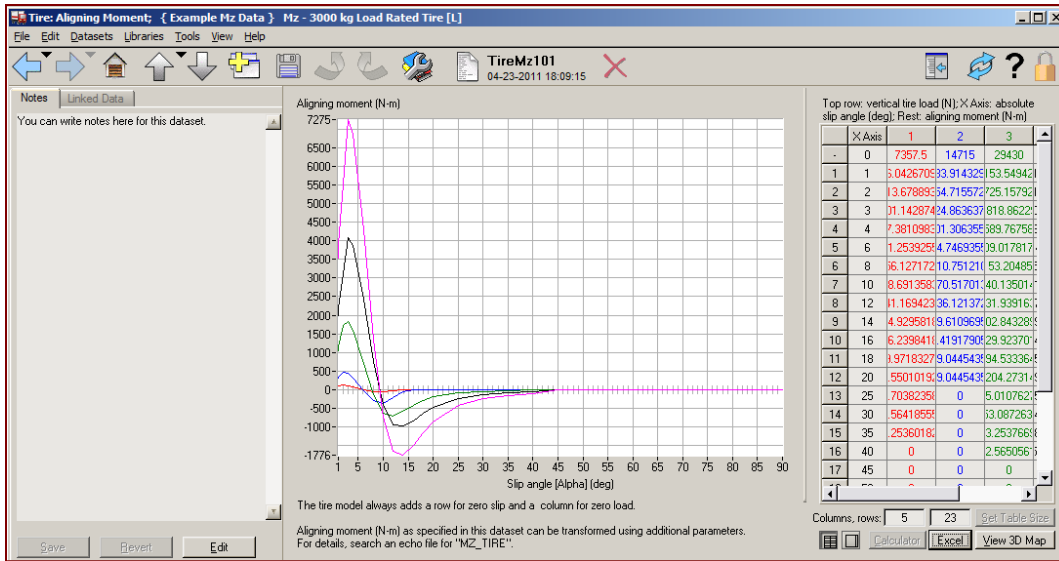


Figure D-26. Screen Capture. The “Tire: Aligning Moment” screen allows the user to enter the aligning moment characterizing data in tabular form.

THIS IS NOT ACTUAL TIRE DATA (Mechanical Simulation Corporation 2010).

D-2.7 Setting the Mass Properties of the Test Vehicle

The mass properties of the NCAT vehicle were set by effectively scaling out the vehicle as a driver would in real life. A test procedure was set up in TruckSim® to provide a quasi-static condition for the wheel loads to be measured. This quasi-static test was to allow the vehicle to roll forward at 5 km/h with no engine power. This was necessary to eliminate any brake holding torque effects from the output of the simulation. The test procedure was allowed to run for 10 s. This was to allow any starting transients of the solver (minute oscillations at the beginning of the run) to dissipate. The wheel loads were reported by TruckSim® at each contact location. A MATLAB™ script was written in conjunction with Simulink software to obtain the wheel load data and provide convenient test control. The output from the MATLAB™ script was total gross vehicle weight, wheel loads, axle loads, and hitch loads. Table 10-11 lists the mass wheel loading that was measured on the NCAT test vehicle and modeled in TruckSim®. Table 10-12 shows the gross mass and weight of the units in the NCAT test vehicle.

Table D-10. The wheel loads and axle loads at their respective locations in the combination. The “Measured” column refers to wheel loads measured on the test vehicle. The “TruckSim®” column refers to the wheel loads of the modeled vehicle. All values in kg.

Location	Left		Right		Whole Axle	
	Measured	TruckSim®	Measured	TruckSim®	Measured	TruckSim®
Steer Axle	2624	2530	2760	2489	5385	5019
1 st Drive Axle	4457	4769	5068	4795	9525	9563
2 nd Drive Axle	4661	4795	4615	4819	9276	9615
Trailer 1 Axle	4118	4433	4683	4399	8801	8832
Dolly 1 Axle	5045	4885	4457	4873	9502	9758
Trailer 2 Axle	4299	4641	5385	4614	9683	9255
Dolly 2 Axle	4683	4636	4434	4625	9118	9261
Trailer 3 Axle	4412	4679	5023	4648	9434	9327
TOTAL	34,299	35,368	36,425	35,262	70,724	70,630

Table D-11. Gross weights of the units in the NCAT vehicle.

	Measured	TruckSim®	Measured	TruckSim®
Unit	kg	kg	lb	lb
Tractor and Trailer 1	32,986	33,029	72,900	72,994
Trailer 2	19,186	19,013	42,400	42,019
Trailer 3	18,552	18,588	41,000	41,080
Whole Vehicle	70,724	70,630	156,300	156,093

To ease the wheel load tuning, a unique trailer payload was created for each trailer by copying the standard TruckSim® trailer payload for doubles and renaming them accordingly. The representational size of the payload was reduced to a point mass allowing simple adjustment of location and magnitude to obtain the measured wheel loads and gross weight from the test vehicle. The point mass reduction was assumed based on the thought that size of the payload would have no effect on a rigid body model and that the responses would be based on the location and the magnitude of the mass. Figure D-27 shows the payload definition for Trailer 1. Table D-12 lists the location of the payloads used to adjust the overall weight distribution of the modeled trailers.

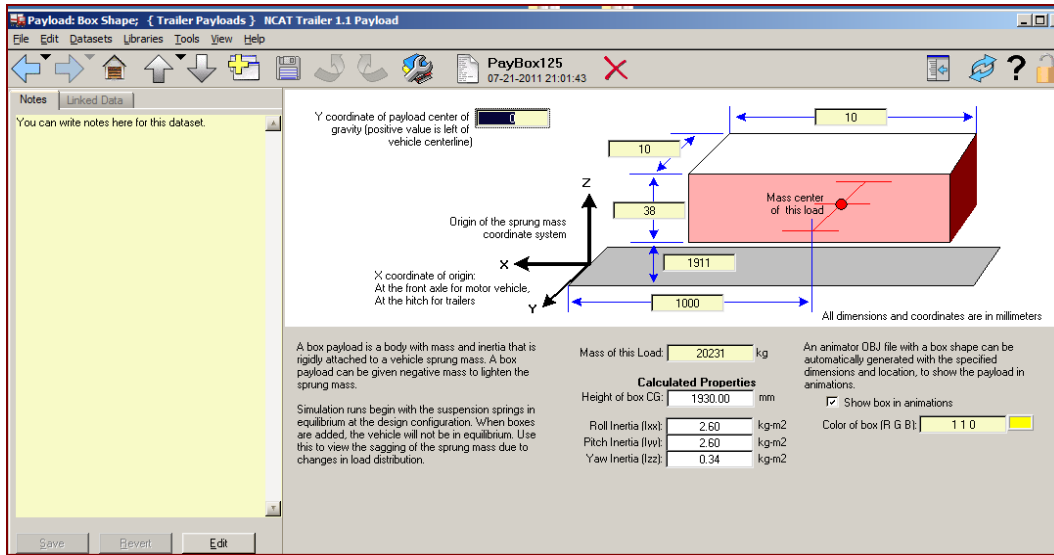


Figure D-27. Screen Capture. The “Payload: Box Shape” shows the point mass payload definition for Trailer 1. This is typical for the three trailers aside from the magnitude of the mass and its location forward and aft (Mechanical Simulation Corporation 2010).

Table D-12. Location of payload CG.

Unit	X _v	Y _v	Z _v
Trailer 1	1000 mm	0 mm	1911 mm
Trailer 2	1732 mm	0 mm	1911 mm
Trailer 3	2582 mm	0 mm	1911 mm

The NCAT tractor has no payload of its own, but due to the fifth wheel connection to Trailer 1, the mass properties of both had to be considered simultaneously. This was performed by adjusting the location and size of the payload modeled for Trailer 1 to approach the fifth wheel load estimated by WMU, then adjusting the location of the Tractor sprung mass to approach the wheel loads measured from the test vehicle. Figure D-28 shows the Tractor sprung mass definition. Table D-13 lists the location of the sprung mass for each unit in the model of the NCAT test vehicle.

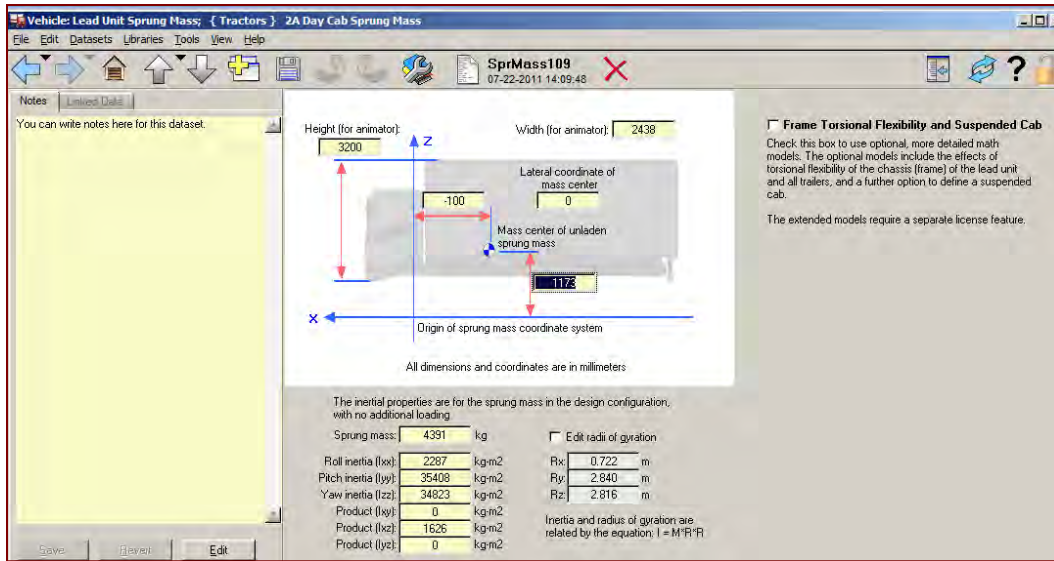


Figure D-28. Screen Capture. The “Lead Unit Sprung Mass” definition screen allows the modeler to adjust the unsprung mass properties of the tractor (Mechanical Simulation Corporation 2010).

Table D-13. The location of the sprung mass CG as entered in TruckSim® for each respective unit of the combination without payloads.

Unit	X _v	Y _v	Z _v	Source
Tractor	-100 mm	0 mm	1173 mm	Mass Property Adjustment
Trailer 1		0 mm	1819 mm	As Packaged
Dolly 1	1800 mm	0 mm	850 mm	Estimate
Trailer 2		0 mm	1819 mm	As Packaged
Dolly 2	1800 mm	0 mm	850 mm	Estimate
Trailer 3		0 mm	1819 mm	As Packaged

There is a significant difference between the TruckSim® model and actual measured wheel loads. This is due to the unknown empty weights of the test vehicle. By using standard TruckSim® unit weights then tailoring the overall combination wheel loads and gross weight by shifting payload position and magnitude, critical mass distribution information is lost. The modeler can only attempt to replicate wheel loads as measured. In an ideal situation, the primary procedure for adjusting the mass properties should only be a “sanity” check for the modeler. Tuning of the mass properties of the model in this fashion lead to unexpected results to minute changes.

To allow the TruckSim® modeler to better characterize the mass properties of the test vehicle, the following mass properties for each unit must be known:

1. Unsprung mass: magnitude and location within each unit and the entire combination
2. Sprung mass: magnitude and distribution in all three planes (x, y, and z)

3. Payload: size, shape, mass, and location for each test configuration
4. Unladen wheel loads
5. Laden wheel loads for each test configuration.

This information will allow the modeler to “build” each unit of the combination unloaded according to the mass properties and dimensions of each unit, and then tune the combination and finally the test configurations with the addition and placement of the payloads.

D-3 Maneuvers and Steering Input

The hand wheel angle measured during the maneuvers was used in open loop fashion to guide the simulation through the maneuvers where the simulation was compared with measurements, as described in Chapter 6. The driver model required no additional tuning for this method, because the simulation was controlled directly from imported steer data. This avoided the driver model completely.

Idealized maneuvers were modeled with closed-loop steering. Sections of the NCAT test facility were modeled in TruckSim® to aid model verification and analysis. The track was modeled in sections to simplify the modeling procedure and to facilitate analysis by generating maneuver- and location-specific simulation data. The test facility was modeled by modifying pre-packaged simulated test roads. TruckSim® lane change and circle track models were modified to resemble the test facility. Driver path and course set up are maneuver-specific and are presented as such.

A third way to steer the model, not used in this study, is for the TruckSim® path following model to steer along the test vehicle’s actual path as recorded by GPS. The driver model optimizes the steering input required to pass the centerline of the front axle over the designed target path throughout the maneuver. Driver model parameters are transport lag and preview time. Transport lag is the pure delay from determining the optimized steer angle to implementation of steer angle into the model. This is used to model the reaction time of the driver. The driver model transport lag was set to 0 s and the preview time to 1 s in developing this approach. This is to allow the use of GPS data to plot the vehicle path for analysis and verification. The GPS data likely includes driver response based on the individual’s actual physical characteristics and driving style.

D-3.1 The Constant Radius Course

The constant radius turn was simulated by creating a model of a circular track with the centerline radius of the NCAT test facility. This was accomplished by scaling a prepackaged TruckSim® model of a banked 500-ft-radius circle track to match the path of radius 479 ft using the “Calculator” button in the lower left corner of the “Road X-Y Coordinates of Centerline” screen (Figure D-29).

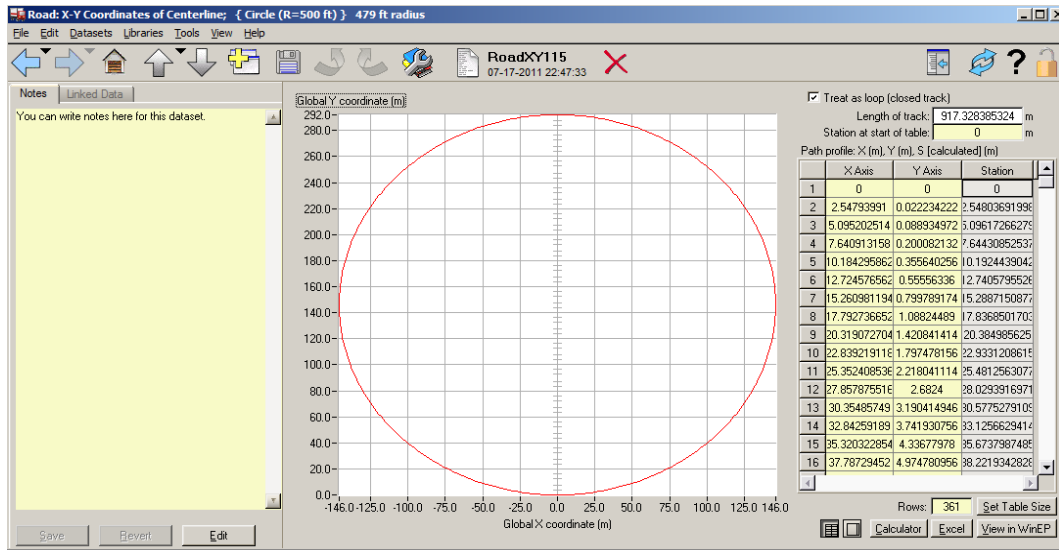


Figure D-29. Screen Capture. The “Road: X-Y Coordinates of Centerline” screen allows the modeler to set up the course geometry (Mechanical Simulation Corporation 2010).

The bank was set to 14% in accordance with the 8-deg bank in the curves at the NCAT track by setting the parameter in the “Off Center Elevation” category on the “Road: 3D Surface” screen (Figure D-30). The spiral-bank sections of the track were not modeled due to lack of planned maneuvers for this area. The driver model is set to follow the centerline of this course with no offset.

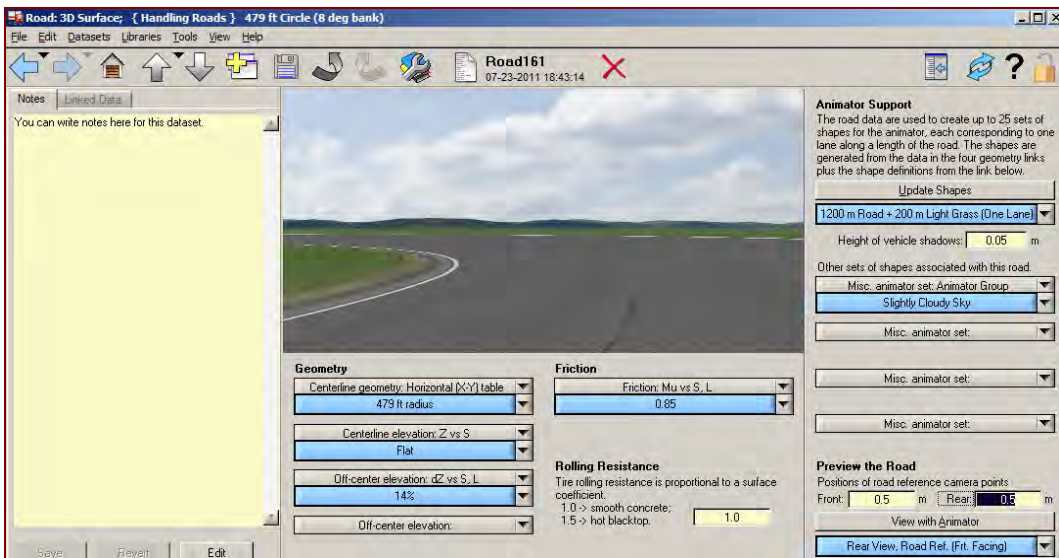


Figure D-30. Screen Capture. Road elevation of 14% corresponding to the 8-deg bank of the NCAT track (Mechanical Simulation Corporation 2010).

D-3.2 The Single Lane Change

The existing TruckSim® single lane change course was modified to resemble the test course as configured for test week at NCAT. The test area is delineated with cones in TruckSim® and laid out by entering coordinates into the table at the lower right side of the “Road: Animator Repeated Object Screen” (Figure D-31).

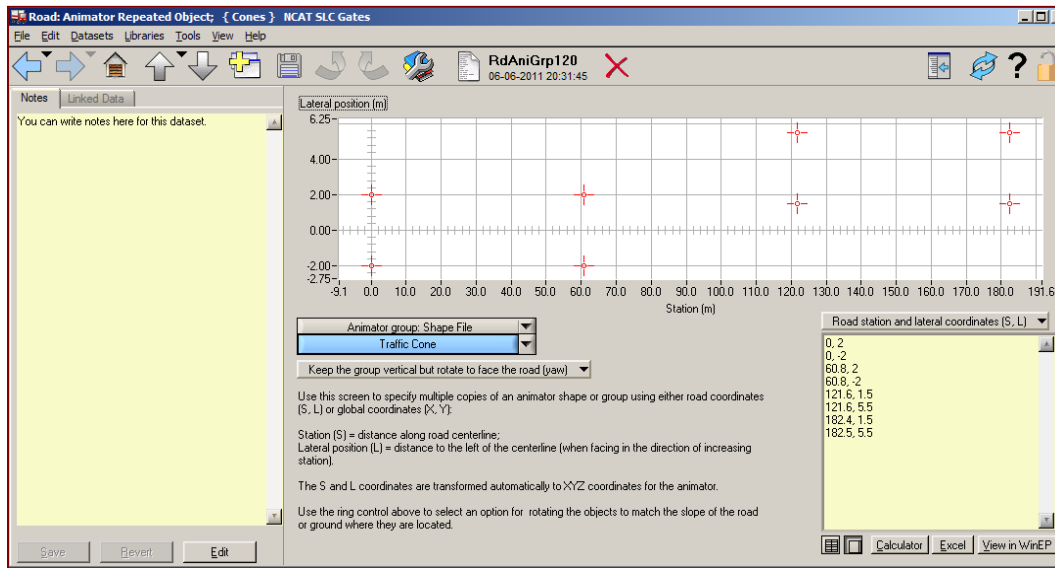


Figure D-31. Screen Capture. The “Road: Animator Repeated Object” screen allows course set up for the Single Lane Change maneuver (Mechanical Simulation Corporation 2010).

The simulated driver path for the single lane change was established through trial and error to resemble the path planned for the maneuver outlined in the test plan. The maneuver was then changed to resemble the maneuver performed during testing. As the maneuver was performed at NCAT, the truck was steered toward the left lane as the tractor exited the entrance (Gate 1 in Figure 4-17) and aimed at the next set of cones (Gate 2) in the left lane 61 m (200 ft) down track. Upon clearing the gates, the driver model was to maintain lateral position in the center of the left lane for the duration of the maneuver. Figure D-32 shows the TruckSim® plot of the designed target path for the single lane change.

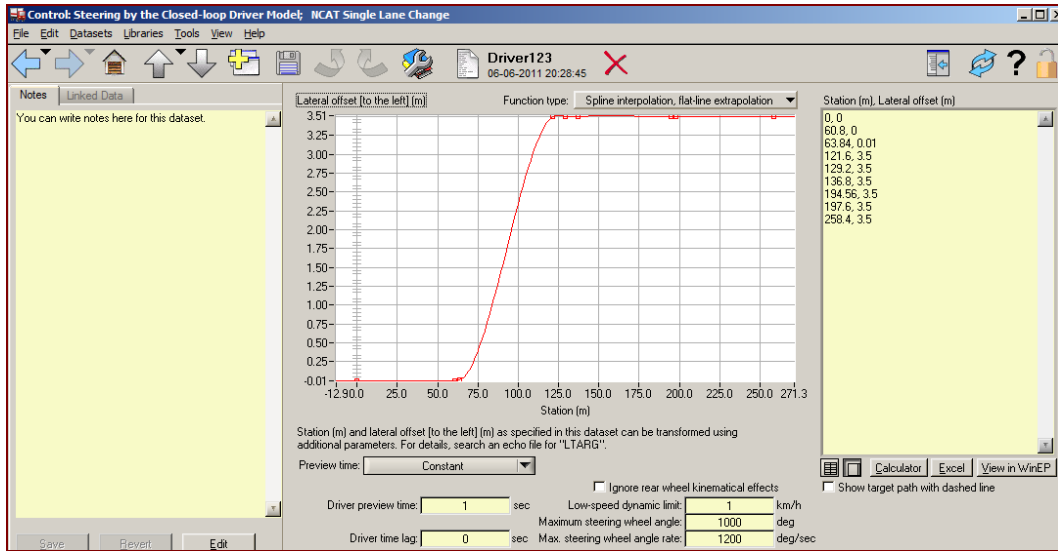


Figure D-32. Screen Capture. The “Control: Steering by the Closed-loop Driver Model” screen shows the target path for simulation of the Single Lane Change Maneuver (Mechanical Simulation Corporation 2010).

D-3.3 The Double Lane Change

The existing TruckSim® double lane change course was modified to resemble the test course as configured for test week at NCAT. The test area is delineated with cones in TruckSim® and laid out by entering coordinates into the table at the lower left side of the “Road: Animator Repeated Object Screen” (Figure D-33).

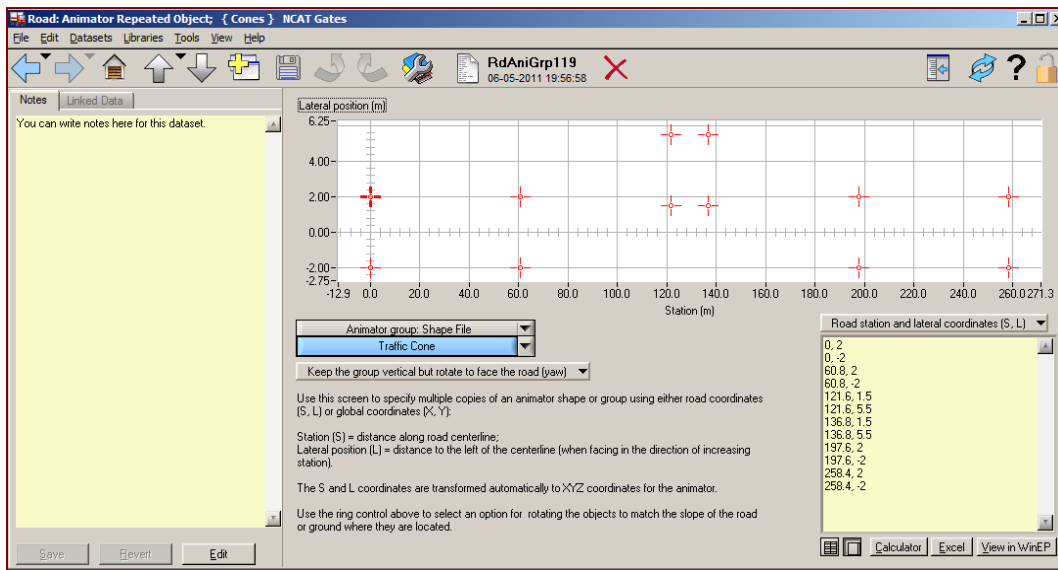


Figure D-33. Screen Capture. The “Road: Animator Repeated Object” screen allows the course set up for the double lane change maneuver (Mechanical Simulation Corporation 2010).

The simulated driver path for the double lane change was established through trial and error to resemble the path planned for the maneuver outlined in the test plan. The maneuver was then

changed to resemble the maneuver performed during testing. As the maneuver was performed at NCAT, the truck was steered toward the left lane out of the entrance (Gate 1 in Figure 4 and aimed at the next set of gates (Gate 20) in the left lane 61 m (200 ft) down track. The tractor was then aimed at the next gate (Gate 2 or 3) 50 ft farther down the left lane. When the front axle cleared the next gate, the tractor was then steered back to the right lane and aimed at the final gate (Gate 3 or 4) 200 ft down track in the right lane. Upon clearing the final gate the truck was to continue in the right lane for the duration of the maneuver. Figure D-34 shows the TruckSim® plot of the designed target path for the double lane change.

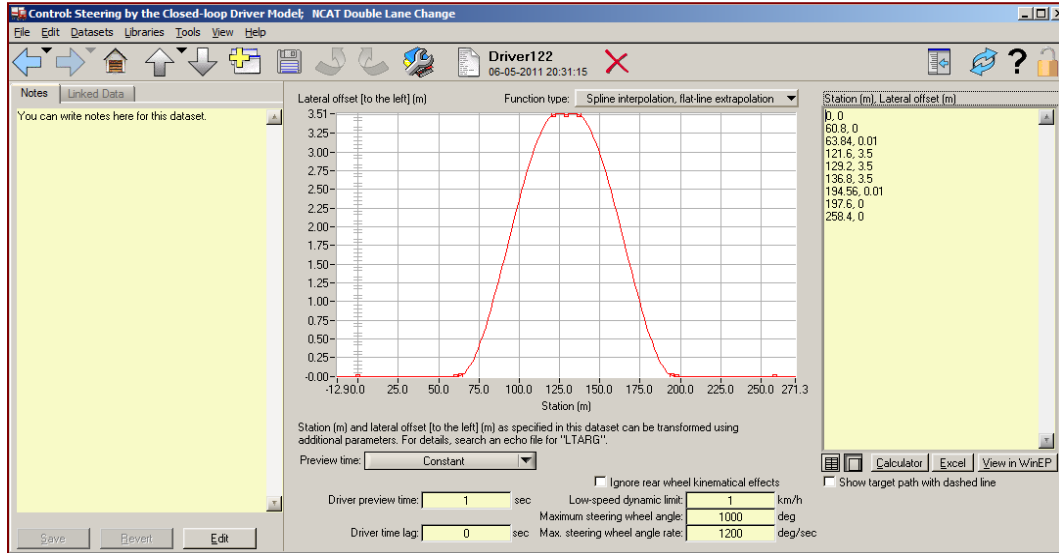


Figure D-34. Screen Capture. The “Control: Steering by the Closed-loop Driver Model” screen allows the target path for simulation of the Double Lane Change Maneuver to be defined (Mechanical Simulation Corporation 2010).

D-3.4 Gradual Single Lane Change

The existing TruckSim® single lane change course was modified to resemble the test course as configured for test week at NCAT. The test area is delineated with cones in TruckSim® and laid out by entering coordinates into the table at the lower left side of the “Road: Animator Repeated Object Screen” (Figure D-35).

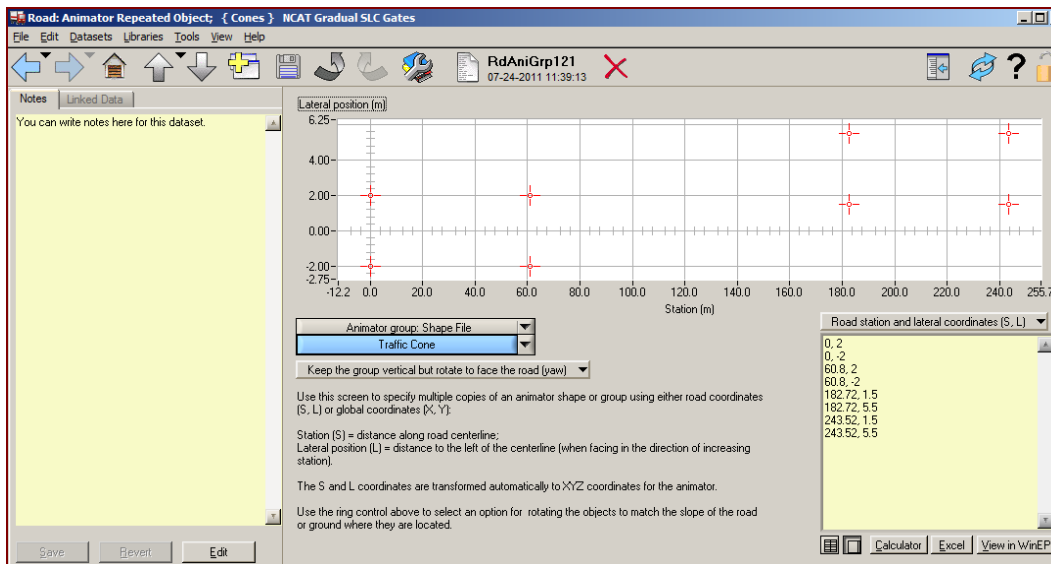


Figure D-35. Screen Capture. The “Road: Animator Repeated Object” screen allows the course set up for the gradual single lane change maneuver (Mechanical Simulation Corporation 2010).

The simulated driver path for the gradual lane change was established through trial and error to resemble the path planned for the maneuver outlined in the test plan. The maneuver was then changed to resemble the maneuver performed during testing. As the maneuver was performed at NCAT, the truck was steered toward the left lane out of the entrance gate (Gate 1) and aimed at the next set of gates (Gate 2 and 3) in the left lane 400 ft down track. Upon clearing the gates the Truck was to maintain lateral position in the center of the left lane for the duration of the maneuver.

The modeler enters coordinates for the path of the vehicle into the table in the lower left corner of Figure D-36. The data are interpolated and extrapolated in the driver path for the maneuver. TruckSim® gives the modeler several choices as to how to interpolate and extrapolate the data into the shape for the driver model to follow. For this maneuver, “Spline interpolation, flat-line extrapolation” was selected. Figure D-36 shows the TruckSim® plot of the designed target path for the double lane change.

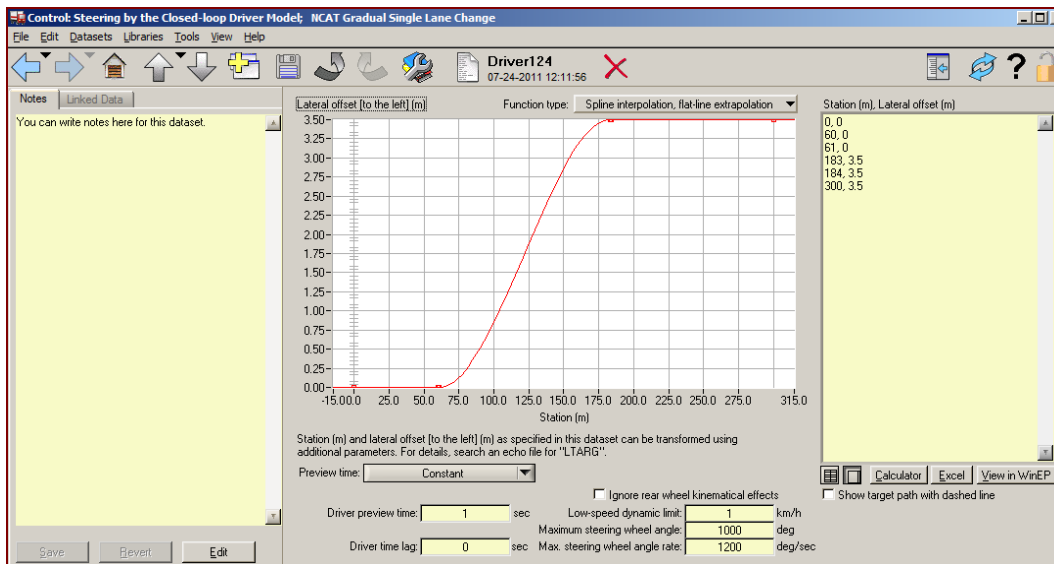


Figure D-36. Screen Capture. The “Control: Steering by the Closed-loop Driver Model” screen allows the target path for simulation of the Gradual Single Lane Change Maneuver to be defined. (Mechanical Simulation Corporation 2010).

D-3.5 Speed Control for All Maneuvers

The speed is controlled in the TruckSim® simulations by essentially setting a target speed and allowing the speed controller to maintain the speed. The model’s ability to maintain the test speed throughout the maneuver depends upon the drive train selection and transmission control as well. For the purposes of this investigation, the test vehicle was outfitted with a 300 kW engine and an 18-speed transmission. The transmission was set to shift automatically per vehicle speed needs. This setup allowed the test speed to be changed by simply entering the desired speed into a field.

D-3.6 Future Considerations for Building a TruckSim® Model

The best information available during this project was used to build and validate this TruckSim® model. It was obtained primarily through the WMU vehicle characterization reported in Appendix C. More resources are necessary to improve this model. The primary changes made to the as packaged model to create the model of the NCAT test vehicle were in mass properties and axle location. Much of the measured data for compliance were linearized and expressed as a single coefficient, with values similar to what was packaged with TruckSim®.

Building a potentially higher fidelity TruckSim® model should start with vehicle characterization data collected on a kinematics and compliance measurement machine such as the one at Michelin Americas Research Company (Warfford 2004). Many aspects of this model were left as packaged because of the lack of available resources to make vehicle measurements. Certain K&C data were omitted from this model.

K&C testing will supply the TruckSim® modeler with the following vehicle characteristics missing from the current model:

- Hysteretic vertical suspension force
- Suspension frictional force
- Kinematic changes for lateral and longitudinal suspension deflections
- Range of motion and bump stop locations
- Bump stop force-deflection data.

Some data missing from this model are not available from K&C testing. Unsprung mass properties of the axles and suspensions can be measured with the components removed from the vehicle. Longitudinal and lateral center of gravity can be better estimated if the vehicle is weighed both loaded and unloaded. A tilt table would also be beneficial to find the height of the CG and potentially improve the fidelity of the model.

Accurate damper force-velocity plots can be used in TruckSim® to characterize the dampers. These data can be obtained by using a shock dynamometer.

Appendix E:

Adams Model Release Notes

This page intentionally left blank.

Table of Contents

E-1	OVERVIEW.....	E-1
E-2	MODEL SETUP AND USE	E-1
E-2.1	CONFIGURATION AND INITIAL CONDITIONS	E-2
E-2.2	SIMULATING EVENTS	E-2
E-2.3	POST PROCESSING	E-3

This page intentionally left blank.

E-1 Overview

This portion of the document is intended to accompany the model of the longer combination vehicle (LCV) that was developed in the Adams multi-body dynamics package (MSC Software, Santa Ana, CA). This appendix provides instructions for running the model and information regarding the various command files used to manipulate the model. Chapter 7 of the main text describes the different units of the model in detail. Researchers at The University of Akron were responsible for leading the model creation phase of the project, with significant contributions from other consortium members.

Some of the Adams program's advanced capability, applied in the subject LCV model, allows body flexibility, intermittent contact, and nonlinear entities. Due to the application of these advanced techniques, in addition to the general complexity of the system, it is advisable to develop familiarity with the Adams program before attempting to manipulate this model. There are tutorials and training courses available from MSC, the provider of Adams, which will help a new user become familiar with the program by starting with simple systems.

Adams also is available with many advanced graphical interface options, which are designed to facilitate the creation and analysis of specific types of systems. To allow for the most flexibility, among other reasons, this model was developed in the basic module of Adams known as "Adams/View."

The model was created using Imperial units. This was the unit system familiar to the researchers at the University of Akron, and also the form in which much of the vehicle data were supplied. The global Cartesian coordinate system used in the model has the positive x-axis directed along the longitudinal axis of the vehicle pointed rearward. The positive y-axis is directed from the driver side of the vehicle toward the curb side. The positive z-axis is directed "up," opposite the direction of the acceleration due to gravity.

E-2 Model Setup and Use

The commands to build the LCV model are stored in an ASCII text file named "AU_NCAT_LCV.cmd." By selecting "File>Open" from the menu, and specifying "command file" as the type, this file may be selected and opened in Adams/View. For an experienced user, direct manipulation of model entities is possible by editing this text file.

Once the model is loaded, Adams contains several powerful methods of examining the system details. These are found through the "info" capability. Right-clicking on any Adams entity will provide an option to show important information about its parameters and connectivity in a text window. Selecting any other entities that are listed in the window allows for their detailed examination. In addition, a "graphical topology" option will generate a picture showing a basic representation of the construction of the model.

E-2.1 Configuration and Initial Conditions

In order to set the model to the correct initial conditions, some preloads may be required. This is of particular importance to maintain the correct ride height for air suspensions, where the correct initial airbag force is needed. The model was initially set for the default preloads required for the system as tested at AU-NCAT. If the user requires a different loading configuration, new preloads will need to be determined. This can be an iterative process, although engineering-based initial estimates can minimize the number of iterations required. The velocity of the vehicle is another example of an initial condition that can be changed, but is currently specified to match one of the as-tested conditions.

Each tire element in the model requires a tire definition file. This is an ASCII text file containing information regarding which tire algorithm will be used by the model, as well as the supporting tire property data. Individual tires may reference separate tire files as needed, such as steer, drive, or trailer tires. Each tire will also reference a road definition file. All of the tires in this model reference the same simple, flat road.

E-2.2 Simulating Events

The primary goal of building this model is to be able to have it execute specific simulated test track maneuvers. These events are differentiated by the intended path of the vehicle, as well as the vehicle velocity. The intended path of the vehicle is stored as a “spline” element. This is a two-dimensional array of x-y coordinates that are offset from the vehicle origin to allow a one-second settling time before the event begins. An Excel spreadsheet is provided, which demonstrates the generation of this data serves as a means of developing new events. An Adams “polyline”, which is a simple curve entity, has been generated for each path and velocity, providing graphical feedback during animations of results. The initial velocity of each body in the model is assigned at the beginning of each simulation. Both the velocity and path are maintained using simple controllers.

In general, a sequence of simulations is performed for a particular event. The first event is a static equilibrium solution. This step is useful for removing large initial transients, which can be generated at the beginning of a simulation as tires develop loads and contact elements engage. In some instances, additional Adams modeling elements, such as bushings or fixed joints, may be added to assist the model in finding equilibrium. These “static locks” are useful in keeping tires from rotating and having other unwanted motion. They are subsequently deactivated for the remaining solutions. The next step is to execute a dynamic analysis of short time duration with a very small time step. This allows the numerical integration algorithm to “get started,” and also resolve any transient effects that occur despite the static equilibrium solution. Finally, the full dynamic analysis is performed for the amount of time required by the event and velocity. The model has successfully performed straight driving, constant radius cornering, and single- and double-lane change events.

For convenience, the event command sequences are stored in ASCII text files. These files can be read into Adams, and the program will automatically make any configuration settings, and perform the complete simulation. An example file name would be “AU_NCAT_DLC_35mph.cmd”. This file would set the vehicle velocity to 35 mph, and run the double-lane change event. The sequence of events performed by the commands in this file would be as follows:

- Generate an Adams simulation control file, which specifies the sequence and options for the simulations, including the duration.
 - AU_NCAT_DLC_35mph.acf
- Generate an Adams data set file, which contains the model defined as required by the solver.
 - AU_NCAT_DLC_35mph.adm
- Generate an executable file to call the external Adams solver.
 - AU_NCAT_DLC_35mph.bat
- Begin the solution, generating the following files in the working directory.
 - AU_NCAT_DLC_35mph.res
 - AU_NCAT_DLC_35mph.req
 - AU_NCAT_DLC_35mph.gra
 - AU_NCAT_DLC_35mph.msg
- Read the results into Adams/View.
- Run the output macro, “Export_Data_To_File_LCV.cmd,” generating the ASCII text file.
 - AU_NCAT_DLC_35mph.csv

The user may then perform post-processing on the results in Adams or Excel.

If Adams is executed outside the graphical interface in this manner, command files to run a series of events may be created and called, generating results for many maneuvers. Being text files, they can also be directly modified to perform variations of the specified maneuver. It also proves convenient to store the results outside of the Adams graphical user interface, since this prevents the database from becoming too large.

E-2.3 Post Processing

Each simulation will generate data for every element within the model, which can result in a large quantity of information, not all of which may be of interest. The analyst may use the normal Adams post-processing tool to examine these results. However, an ASCII text file, “Export_Results_To_File_LCV.cmd,” contains commands that will export quantities deemed important to this phase of the project to an external file. This file may also be modified to meet

specific needs. The text result file, generated in comma delimited format, may be opened in Excel or any other plotting program. If the Excel spreadsheet is used, the user will have the ability to report results in Imperial or metric units.

	A	B	C	D	E	F	G	H
1	Model Name	.model_1				Units		
2	Analysis Name	AU_NCAT_DLC_35mph				mm		
3								
4	Data generated by macro	Export_Results_to_Text_Files_LCV.cmd						
5	Data Filename	AU_NCAT_DLC_35mph.csv						
6	Time Stamp	2011/09/02	12:36:22			2011/09/02 @ 12:36:22		
7								
8	AU NCAT DLC 35mph							
9								
10	Velocity	35	MPH					
11		56.3	KPH					
12								
13	0.00	0.00	0.00	0.00	0.00	0.00	0.00	0.00
14	0.00	-0.066	-0.062	-0.062	-0.061	-0.019	-0.054	-0.056
15	14.97	0.066	0.062	0.063	0.063	0.018	0.054	0.055
16								
17	Simulation Data (1524 Rows)							
18	Data Conversion Factor ->	1	1	1	1	1	1	1
19	Time	Tractor	Trailer1	Trailer2	Trailer3	Tractor	Trailer1	Trailer2
20		0	0	0	0	0	0	0
21		Yaw	Yaw	Yaw	Yaw	Roll	Roll	Roll
22		Rate	Rate	Rate	Rate	Rate	Rate	Rate
23	(s)	(deg/sec)	(deg/sec)	(deg/sec)	(deg/sec)	(deg/sec)	(deg/sec)	(deg/sec)
24								
25	0.000	0.000	0.000	0.000	0.000	0.000	0.000	0.000
26	0.004	0.000	-0.001	0.000	0.000	0.002	0.000	0.000
27	0.009	0.001	-0.001	0.000	0.000	0.001	0.002	0.000
28	0.045	0.007	-0.002	0.000	0.000	-0.016	0.003	0.000
29	0.062	0.009	-0.003	0.000	0.001	0.003	0.005	0.000
30	0.110	0.012	-0.004	0.001	0.001	-0.001	0.003	0.000
31	0.160	0.010	-0.003	0.002	0.001	0.002	0.000	-0.001
32	0.210	0.007	-0.001	0.002	0.001	0.002	-0.003	-0.002
33	0.260	0.005	0.000	0.002	0.000	0.001	-0.004	-0.002
34	0.310	0.003	0.001	0.001	0.000	0.001	-0.004	-0.001

Figure E-1. Screen Shot. Post-Processing with Excel

The model results may also be examined directly within Adams, which has a capable post processing tool. The primary use is to generate animations of the results, or to examine quantities not exported to the text file.